



3 1176 00162 7588

NASA CR- 159,253

NASA-CR-159253  
19800024886

## NASA Contractor Report 159253

# Evaluation of Laminar Flow Control System Concepts for Subsonic Commercial Transport Aircraft

LOCKHEED-GEORGIA COMPANY  
Marietta, Georgia 30063

CONTRACT NAS 1-14631  
SEPTEMBER 1980

LIBRARY COPY

OCT 23 1980

LANGLEY RESEARCH CENTER  
LIBRARY, NASA  
HAMPTON, VIRGINIA



National Aeronautics and  
Space Administration

Langley Research Center  
Hampton, Virginia 23665



NF01073

## FOREWORD

Contract NAS 1-14631 between the National Aeronautics and Space Administration and the Lockheed-Georgia Company, effective October 1976, provided for the evaluation of laminar-flow-control system concepts for subsonic commercial transport aircraft. The contract was sponsored by the Aircraft Energy Efficiency (ACEE) Project Office of the Langley Research Center with D. B. Snow, A. L. Braslow, and M. C. Fischer serving as NASA Technical Monitors. This document, submitted in fulfillment of DRL-004 of the subject contract, constitutes the final study report.

At the Lockheed-Georgia Company, the study was performed under the cognizance of R. H. Lange, Manager of the Advanced Concepts Department, with R. F. Sturgeon serving as study manager. Principal contributors to the study include the following:

J. A. Bennett	Aerodynamics Task Leader
L. B. Brandt	Aerodynamics
A. E. Holmes	Aerodynamics
W. F. LaBozzetta	Aerodynamics
F. R. Etchberger	Design Task Leader
H. J. Abbey	Design
L. B. Lineberger	Structures and Materials Task Leader
R. T. Beall	Manufacturing
R. E. Barrie	Composite Design
W. R. Roberts	Weights
R. S. Ferrill	LFC Systems Task Leader
B. I. Reynolds	LFC Ducting
J. G. Tibbetts	Surface Configuration
H. Young	Surface Configuration
J. C. Muehlbauer	Leading-Edge Cleaning
G. Swift	Acoustics
R. D. O'Brien	Production Costs
S. G. Thompson	Operating Costs
W. J. Keese	Maintainability

N80-33394



## TABLE OF CONTENTS

<u>Section</u>	<u>Title</u>	<u>Page</u>
	FOREWORD	ii
	LIST OF FIGURES	vi
	LIST OF TABLES	xvi
1.0	SUMMMARY	1
2.0	INTRODUCTION	5
3.0	SYMBOLS AND ABBREVIATIONS	6
4.0	STUDY APPROACH	10
4.1	Study Objectives	10
4.2	Study Plan	10
4.3	Life Cycle	12
4.4	Design Criteria	12
4.5	Reference Technology Level	13
4.5.1	Aerodynamics	13
4.5.2	Flight Controls	16
4.5.3	Propulsion Systems	17
4.5.4	Structures and Materials	19
4.5.5	LFC Systems	19
4.5.6	Aircraft Systems	21
4.6	Costing Assumptions	22
5.0	BASELINE CONFIGURATION DEVELOPMENT	23
5.1	Mission Definition	23
5.1.1	Assumptions and Methodology	23
5.1.2	Mission Parameters	28
5.1.3	LFC Mission Profile	28
5.2	Parametric Configuration Analyses	29
5.2.1	Procedures	29
5.2.2	Parametric Results	30
5.2.3	Configuration Selection	35
5.3	Configuration Definition	38

TABLE OF CONTENTS (CONT'D)

<u>Section</u>	<u>Title</u>	<u>Page</u>
6.0	CONCEPT EVALUATION	42
6.1	Aerodynamics	42
6.1.1	Design Objectives	42
6.1.2	Airfoil/Boundary-Layer Analysis	42
6.1.3	Wing Analysis and Design	54
6.1.4	High-Lift System Development	66
6.1.5	Stability and Control	78
6.2	Structures and Materials	80
6.2.1	Design Objectives	80
6.2.2	LFC Surface Panel Development	81
6.2.3	Leading-Edge Development	118
6.3	LFC Suction System	138
6.3.1	Design Objectives	138
6.3.2	Surface Configuration	138
6.3.3	Suction Ducting System	152
6.3.4	Suction Units	176
6.3.5	Controls	182
6.4	Leading-Edge Region Cleaning	185
6.4.1	Design Objectives	185
6.4.2	Concept Evaluation	186
6.4.3	Testing	190
6.5	Auxiliary Systems Integration	216
7.0	CONFIGURATION SELECTION AND ASSESSMENT	218
7.1	Operational Considerations	218
7.1.1	Airline Recommendations	218
7.1.2	Ground Operations	220
7.1.3	Flight Operations	220
7.2	Configuration Development	223
7.2.1	Configuration Variations	223
7.2.2	Configuration Selection	225
7.2.3	Configuration Definition	225
7.2.4	Configuration Performance	237
7.3	Turbulent Configuration	242
7.3.1	Configuration Definition	242
7.3.2	Configuration Performance	244

TABLE OF CONTENTS (CONT'D)

<u>Section</u>	<u>Title</u>	<u>Page</u>
7.4	Configuration Comparison	248
7.4.1	General Characteristics	248
7.4.2	Weight	248
7.4.3	Economics	248
7.4.4	Fuel Efficiency	250
8.0	RECOMMENDED SUBSYSTEM DEVELOPMENT	255
8.1	LFC Test Bed Development	255
8.1.1	Objectives	255
8.1.2	Configuration Description	256
8.1.3	Leading-Edge Test Section	258
8.1.4	Aerodynamic Configuration	262
8.1.5	Structural Analysis	264
8.1.6	Performance Evaluation	266
8.1.7	Flight Test Program	268
8.1.8	Conclusions	269
8.2	Validator Aircraft Development	270
8.2.1	Validator Program Objectives	270
8.2.2	General Arrangement	270
8.2.3	Aerodynamic Configuration	272
8.2.4	Structural Configuration	279
8.2.5	Aircraft Systems	282
8.2.6	LFC Systems	285
8.2.7	Instrumentation	286
8.2.8	Validator Performance	287
8.2.9	Program Planning	289
8.2.10	ROM Cost Estimates	289
8.2.11	Conclusions	290
8.3	Advanced Development Requirements	291
8.3.1	Aerodynamics	291
8.3.2	Structures and Materials	292
8.3.3	LFC Systems	292
8.3.4	Leading-Edge Region Cleaning	294
8.3.5	Aircraft Design	294
	REFERENCES	296

## LIST OF FIGURES

<u>Figure</u>	<u>Title</u>	<u>Page</u>
1	Study Plan	11
2	Life Cycle	11
3	LFC Aerodynamics Criteria	14
4	Wing Section Design Curves	15
5	Example of Secondary Active Trailing-Edge Flaps	15
6	International Flight Profile	28
7	Basic Matrix Fuel Volume Ratios	31
8	FAA Field Lengths for Initial Configuration Basic Matrix	31
9	Basic Matrix DOC Values	32
10	Field Length Variation With Engine Cruise Power Setting and Bypass Ratio	33
11	DOC Variation With Engine Cruise Power Setting and Bypass Ratio	33
12	DOC Sensitivity to Change in Aspect Ratio	34
13	Block Fuel Sensitivity to Aspect Ratio	35
14	Variation of DOC with Cruise M	37
15	DOC Variation With Altitude	38
16	General Arrangement	39
17	Inboard Profile	40
18	Original Baseline Airfoil Pressure Distribution	44
19	Interim Baseline Airfoil Pressure Distribution	45
20	Parametric Mass Flow Suction Level	46
21	Upper Surface Pressure Distributions	47
22	Upper Surface Crossflow Disturbance N Factors	48
23	Lower Surface Pressure Distributions	49

LIST OF FIGURES (CONT'D)

<u>Figure</u>	<u>Title</u>	<u>Page</u>
24	Lower Surface Disturbance N Factors	49
25	Interim Airfoil Pressure Distribution	50
26	Mass Flow Suction Level	51
27	Crossflow Disturbance N Factors	51
28	Tollmien-Schlichting Instability Envelope	53
29	LFC 2-D Wind Tunnel Model	53
30	LFC Airfoil AF11-12	55
31	AF11-12 Viscous Pressure Distribution at Mach = 0.745, $C_L = 0.750$	56
32	Revised Suction Distribution	56
33	Final Baseline LFC Airfoil Lower Surface N Factors	57
34	Final Baseline LFC Airfoil Upper Surface Crossflow N Factors	57
35	Wing Loft Regions	58
36	WPRESS Root Section Pressure Distribution for Interim Wing	59
37	Span Lift Coefficient Distribution and Flap Schedule	60
38	Transonic Wing Program Span Load Distribution	61
39	Transonic Wing Program Span Lift Distribution	62
40	Transonic Wing Program Root Pressure Distribution	63
41	TAP Wing Root Pressure Distribution	64
42	LFC Baseline Wing Twist Schedule	65
43	LFC Baseline Wing Aft Flap Deflection Schedule	65
44	LFC Baseline Wing Span Loading Distribution	66



## LIST OF FIGURES (CONT'D)

<u>Figure</u>	<u>Title</u>	<u>Page</u>
45	LFC Baseline Wing Spanwise Variation of Lift Coefficient	66
46	3-D Isometric Pressure Distribution for LFC Baseline Wing	67
47	High Lift Characteristics - Clean Wing and Effect of Aileron Droop With Takeoff Flaps	68
48	Comparison of Span Loading for Clean Wing and Varying Aileron Droop With Takeoff Flaps, = 10	70
49	Clean Wing Span Load Distribution at Stall	71
50	Span Load Distribution at Stall, Takeoff Flaps, Aileron Undelected	72
51	Span Load Distribution at Initial Lift Curve Break, Takeoff Flaps, Aileron Droop	73
52	Span Load Distribution at Stall, Takeoff Flaps and Aileron Droop	74
53	High Lift Characteristics - Refined Takeoff Flap Schedule	75
54	High Lift Characteristics - Landing Flaps, Moderate Aileron Droop	76
55	High Lift Characteristics - Landing Flaps, Full Aileron Droop	77
56	Span Load Distribution - Lift Off and Approach Conditions	79
57	Plan for LFC Surface Development	82
58	LFC Surface Smoothness Criteria	83
59	LFC Surface Waviness Criteria	84
60	Wing Box Structure for Non-Structural Concepts	85
61	Non-Structural Concepts	86
62	Structural Concepts	89

LIST OF FIGURES (CONT'D)

<u>Figure</u>	<u>Title</u>	<u>Page</u>
63	Combination Concepts	92
64	Selected Surface Concept	92
65	Surface Design	94
66	Surface Materials and Sizing	96
67	Sawed Slot With Slot Duct	99
68	Sawed Slot	99
69	Structural Skin	100
70	Hat Section Stiffeners	100
71	Surface Panel No. 3 - Upper Surface	102
72	Surface Panel No. 3 - Lower Surface	102
73	Test Specimens - LFC Surface Panel No. 1	104
74	Test Specimens - LFC Surface Panel No. 2	105
75	Temperature Test Arrangement	106
76	Icing Test Specimen	107
77	Corrosion/Bending Test Arrangement	107
78	Impact Test Arrangement	108
79	Impact Test Specimen	109
80	Repairability Test Specimen	110
81	Lightning Test Specimen	111
82	Compression Panel Test - 1.334 MN (300 000 lb)	113
83	Compression Panel Test - 2.224 MN (500 000 lb)	113
84	Compression Panel Test - Failure Mode	114
85	LFC Surface Panel No. 3 With Impact Gun	115
86	Delaminated Area Indicated by Ultrasonic Inspection After Residual Strength Test	117

LIST OF FIGURES (CONT'D)

<u>Figure</u>	<u>Title</u>	<u>Page</u>
87	Concept No. 1 - Graphite/Epoxy Skin, Duct and Aluminum Honeycomb	120
88	Concept No. 2 - Graphite/Epoxy Spanwise Ducts With Titanium Face Sheets	120
89	Concept No. 3 - Corrugated Graphite/Epoxy Skins and Ducts	121
90	Concept No. 4 - Titanium Skin, Graphite/Epoxy Duct Bonded in Honeycomb, on Stiffeners	121
91	Concept No. 5 - Honeycomb Panel With External Ducts	122
92	Concept No. 6 - Graphite/Epoxy Corrugated Panel Support on G/E Stiffener	123
93	Leading-Edge Structural Concept	124
94	Leading-Edge Structure	125
95	Leading-Edge Design Details	125
96	Collector Duct Tools	127
97	Collector Duct Prototype Tool Try	127
98	Slot-Duct Former Tool With the First Ply of Fiberglass Prepreg in Place	128
99	Graphite/Epoxy Fabric Outer Face Sheet Being Formed to Tool	128
100	Outer Face Sheet and Slot Former Tool Molded into the Leading-Edge Tool	129
101	Leading-Edge Tool and Part Showing Air Duct and Honeycomb Core Installation	129
102	Four-Legged Upper Surface Attach Angle Tool and Molded Part	130
103	Leading-Edge Structure and Formed Titanium Skin Ready for Bonding	132
104	Slotting of Leading-Edge Test Article	132

LIST OF FIGURES (CONT'D)

<u>Figure</u>	<u>Title</u>	<u>Page</u>
105	Hinge Angle Shear Test Failure Mode	133
106	Arrangement for Hinge Angle Tension Test	133
107	Hinge Angle Tension Test Failure Mode	134
108	Four-Leg Angle Tension Test Failure Mode	135
109	LFC Leading-Edge Proof Test Load Distribution	136
110	Loading Arrangement Details	137
111	Typical Criteria Limit Envelope	140
112	Upper Wing Surface Design Envelope	142
113	Lower Wing Surface Design Envelope	143
114	Production Oriented Wing Surface Design	147
115	Performance Oriented Wing Surface Design	147
116	Surface Design	152
117	Leading-Edge Ducting and Metering Schematic	153
118	Wing-Box Ducting and Metering Schematic	154
119	Wing-Box Ducting System	155
120	Surface Pressure Loss Characteristics	158
121	Surface Duct/Metering Hole Geometry Effects on Slot Velocity Variation	159
122	Slot/Hole Tolerance Effects Comparison - Percent Dimensional Deviations	160
123	Slot/Hole Tolerance Effects - Criteria Parameters	161
124	Effect of Hat-Section Duct Outlet Design on Sensitivity to Slot Tolerances	163
125	Spanwise Hat-Section Pressure Effects	164
126	Test Duct Laboratory Arrangement	170
127	Effect of Baseline Metering Configuration	171

# LIST OF FIGURES (CONT'D)

<u>Figure</u>	<u>Title</u>	<u>Page</u>
128	Effect of Metering Hole Spacing on Slot Flow Variations	172
129	Slot Flow Variation Summary	173
130	Pressure Loss - Comparison of Slot/Metering Combination with Summation of Individual Components	174
131	Duct Internal and External Octave Band Noise Levels	176
132	Suction Requirement Profile	178
133	Suction Pump	181
134	Schematic of Suction System	184
135	Subscale Cleaning Test Configuration	192
136	Subscale Cleaning Test Installation	193
137	Fluid Composition Tests	195
138	Surface Test Samples	199
139	Effects of Stagnation Location	201
140	Slot Suction System Schematic	205
141	Cleaning Slot Configuration	206
142	Slot Cleaning System Schematic	207
143	Model Assembly	209
144	Installed Wind Tunnel Model	210
145	Insect Injector	211
146	Dry Leading Edge Accretion-Insect Ratio = 16 Run No. 34	212
147	Dry Leading Edge Accretion-Insect Ratio = 16 Run No. 34 Closeup	213
148	Test Run No. 41 - $q = 239 \text{ N/m}^2$ ( $5 \text{ lb/ft}^2$ ), = $0.262 \text{ rad}$ ( $15^\circ$ )	214



LIST OF FIGURES (CONT'D)

<u>Figure</u>	<u>Title</u>	<u>Page</u>
149	Test Run No. 41 - $q = 3735 \text{ N/m}^2$ (78 lb/ft <sup>2</sup> ), = 0.262 rad (15°)	215
150	DOC Comparison - Configuration Variations	225
151	General Arrangement	227
152	Inboard Profile	228
153	Ducting Arrangement for Fuselage-Mounted LFC Suction Units	228
154	Ducting Arrangement Section Cuts	229
155	Wing Structural Arrangement	229
156	Trailing-Edge Flaps and Spoiler Arrangement	230
157	Wing Cross-Section	231
158	Empennage Structural Arrangement	232
159	Power Plant Installation	232
160	Wing-Mounted Main Landing Gear	234
161	Fuselage-Mounted Main Landing Gear	235
162	Schematic of Hydraulic Supply System	236
163	Schematic of Hydraulic Distribution	236
164	Schematic of Aircraft Fuel System	238
165	Airport Performance	239
166	Payload/Range	240
167	Range Variation With Loss of LFC System	242
168	Turbulent Transport	243
169	Turbulent Baseline Airport Performance	245
170	Turbulent Baseline Payload/Range	246
171	Configuration Comparison	249

LIST OF FIGURES (CONT'D)

<u>Figure</u>	<u>Title</u>	<u>Page</u>
172	Interior Arrangement	250
173	DOC vs Fuel Price	253
174	Fuel Efficiency Comparison	254
175	Plan View of Modified JetStar	256
176	Structural Design of Leading-Edge Test Section	257
177	Schematic of Slot Suction System	259
178	Schematic of Cleaning System	261
179	JetStar Upper Wing Surface Loft Regions	262
180	Streamwise Airfoil Sections	263
181	Structural Design Airspeeds vs Altitude	265
182	Maximum Speed Capability - Modified JetStar	267
183	General Arrangement - LFC Validator/DC-9	271
184	Schematic, LFC Pump Installation	272
185	DC-9 Validator Root Section Development	273
186	DC-9 Validator Outer Wing Section Development	274
187	Wing Planform	275
188	DC-9 LFC Validator Wing Twist Schedule	276
189	DC-9 LFC Validator Wing Aft Flap Schedule	276
190	Transonic Wing Program Isometric Wing Pressure Distributions	277
191	Baseline LFC Suction Distribution	278
192	Current LFC Validator Lower Surface Crossflow Disturbance N Factors	278
193	Wing Structural Arrangement	279
194	Leading Edge	280

LIST OF FIGURES (CONT'D)

<u>Figure</u>	<u>Title</u>	<u>Page</u>
195	Structural Design Airspeeds vs Altitude	281
196	Center of Gravity Travel	284
197	Takeoff Field Length Comparison	287
198	Payload-Range Comparison of DC-9-15 With Various Validator Cases	288
199	Program Schedule - LFC Validator Aircraft	289

## LIST OF TABLES

<u>Table</u>	<u>Title</u>	<u>Page</u>
1	Characteristics of Pratt & Whitney Aircraft STF 477 Turbofan Engine	18
2	Selection of Advanced Materials for Wing	20
3	Weight Technology Factors	21
4	Distribution of 2000 ICAO World Traffic Over 3000 Miles One-Way Daily Average Passengers	25
5	Total Long-Haul Aircraft Requirements for the Year 2000 Based on Daily Service at 60% Load Factor	26
6	Potential Long Range Market	27
7	Baseline Candidates	36
8	Baseline Configuration Characteristics	41
9	Effect of $C_{L_{MAX}}$ on Configuration Sizing	79
10	Comparison - Non-Structural Concepts	88
11	Comparison - Structural Concepts	91
12	Comparison - Combination Concepts	93
13	Wing Internal Loads	94
14	Comparison of Slotting Procedures	98
15	Test Specimens	106
16	Test Summary - Corrosion/Bending	107
17	Test Summary - Foreign Object Damage	108
18	Test Results - Lightning Strike	111
19	LFC Leading-Edge Concept Evaluation	123
20	Slot and Metering Hole Dimensions for Leading-Edge Section	126
21	Cruise Envelope Perturbations	144
22	Fixed Design Point Margin Sensitivity Trend	146

LIST OF TABLES (CONT'D)

<u>Table</u>	<u>Title</u>	<u>Page</u>
23	Upper Surface Production Design Data	148
24	Lower Surface Production Design Data	149
25	Upper Surface Performance Design Data	149
26	Lower Surface Performance Design Data	150
27	Tolerance Study Configuratiton	157
28	Leading-Edge Metering System	166
29	Summary of Measured Noise Levels, dB(C)	175
30	Suction Unit Comparison	179
31	Weight Comparisons - Candidate Leading- Edge Cleaning Concepts	191
32	Cleaning Fluid Composition	194
33	Surface Test Configuration	198
34	Nominal Leading-Edge Slot Geometry - Upper Surface	203
35	Nominal Leading-Edge Slot Geometry - Lower Surface	204
36	Suction System Instrumentation	204
37	Leading-Edge slot Geometry - Cleaning System	206
38	Cleaning System Instrumentation	208
39	Surface Instrumentation	210
40	LFC Maintenance Requirements	221
41	Configuration Variations	224
42	Performance for Typical Missions - LFC Transport	241
43	Weight Summary-Turbulent Airplane	244
44	Performance for Typical Missions - Turbulent Transport	247



LIST OF TABLES (CONT'D)

<u>Table</u>	<u>Title</u>	<u>Page</u>
45	General Characteristics Comparison	251
46	Weight Comparison	252
47	Economic Comparison	253
48	Structural Design Criteria	264
49	Estimated Weight Empty	266
50	Weight Statement	283
51	ROM Cost Estimates - LFC Validator Program	290

## 1.0 SUMMARY

This report summarizes the results of a study conducted in the October 1976 - June 1980 period under NASA Contract NAS 1-14631 to evaluate laminar flow control system concepts for subsonic commercial transport aircraft. The ultimate objective of the LFC program is to demonstrate that the technology is available to permit incorporation of LFC into long-range commercial jet transports in the post-1990 period. The specific objectives of the study reported herein support this program objective and include:

- (1) The evaluation of alternatives in the design of laminar-flow-control subsonic commercial transports for operation in the 1990 time period.
- (2) The definition of requirements for detailed subsystem development in subsequent program phases.

In satisfying these objectives, the study was organized into major tasks devoted to the definition of an initial study baseline configuration, the use of the baseline as a vehicle for the evaluation of alternative system concepts, the integration of selected concepts into the baseline to form the final study configuration, and the comparison of this configuration to an advanced technology turbulent transport optimized for the same mission.

As the initial task in the study, titled Mission Definition and Baseline Configuration, an extensive evaluation of traffic projections and market analyses was conducted to define probable missions for commercial transports entering service in the post-1990 period. The selected mission is characterized by a passenger payload of 400 and a range of 12 038 km (6500 n mi). At reduced ranges, the aircraft has the capability of transporting the full passenger payload and 16 874 kg (37 200 lb) of belly cargo. Average state length was estimated to be 6112 km (3300 n mi). A cruise speed of  $M = 0.80$  was selected for the study aircraft. Airport performance is compatible with projected international airports, with a FAR field length of 3048 m (10 000 ft) and maximum approach speed of 269 km/hr (145 kn).

The baseline LFC transport incorporates laminarization of both wing surfaces to the 75% chord location and all empennage surfaces to the 65% chord location.

The major portion of the study effort was devoted to a series of tasks conducted under the heading of Concepts Evaluation. Included in these tasks were analytical investigations, design studies, and subsystem testing conducted to evaluate alternative concepts in the following areas:

- (1) Aerodynamics
- (2) Structures and materials
- (3) Suction Systems
- (4) Leading-edge region cleaning

#### (5) Integration of auxiliary systems

In aerodynamics, primary efforts were devoted to the development of solutions to the basic problems of LFC wing design. Included were extensive analyses of alternative airfoil sections as required to minimize both suction system requirements and the complexity of the suction surface design. For selected airfoil sections, three-dimensional analyses were conducted and conceptual LFC wings were defined. Studies were conducted as required to develop conceptual high-lift systems compatible with both specified airport performance requirements and the peculiar constraints imposed by the integration of LFC surfaces into the wing. The final LFC wing design, based on a supercritical pressure distribution, is compatible with both operational requirements and systems requirements of the final study configuration.

A central problem in the definition of a feasible production configuration for LFC transports is the development of LFC surface designs which satisfy aerodynamic requirements without imposing unacceptable structural weight penalties, manufacturing costs, and operational requirements. Consequently, extensive investigations were conducted in the development of structural concepts for both the wing-box and the leading-edge regions of the wing of the baseline LFC transport. As a part of the development, alternative structural concepts were evaluated, detailed designs were developed for selected concepts, manufacturing procedures were established, and fullscale structural specimens were fabricated and tested.

The selected LFC surface design for the wing-box region is a structural skin and hat-section stiffener configuration with LFC ducting and metering integrated into the structure. The structural elements are fabricated of graphite/epoxy composites, with a titanium outer face sheet for lightning protection and resistance to erosion and corrosion. Three 0.91 m x 1.52 m (3 ft x 5 ft) LFC surface panels were fabricated and subjected to extensive environmental and structural testing which validated the design concept.

The selected leading-edge design employs components of sandwich construction with graphite/epoxy face sheets and corrosion resistant aluminum honeycomb core. A thin gauge titanium skin, bonded to the surface panel outer face sheet, contains the required suction slots and provides environmental protection for the composite structure. A fully functional 1.83 m (6 ft) section of the leading edge, representative of the baseline aircraft wing at the 98% semispan location, was fabricated and structurally tested to validate the design.

Suction system studies were conducted with the goal of developing a slotted surface suction system for airfoil laminarization which considers not only the basic design requirements and criteria but also provides allowances for deviations from an ideal design and for off-design conditions that exist for a production aircraft. The suction system selected for the study aircraft is based on the integration of suction ducting and metering into the structure of the wings and empennage. Suction flow from the wing surface progresses through the slot into a slot duct and the first level of metering before entering ducts formed by the hat-section stiffeners in the wing structure. Flow from the hat-sections is collected by



chordwise ribs at 76.2 cm (30-in.) intervals, and transferred through trunk ducts in the leading edge to suction units in the wing-root region of the fuselage. A limited experimental evaluation of the slot/metering system was conducted to evaluate the selected configuration. Within the limits established by uncertainties in LFC surface design criteria, the selected configuration is compatible with the requirements of the study aircraft.

In the task devoted to leading-edge region cleaning, the evaluation of candidate concepts resulted in the selection of a fluid dispersal system integrated into the leading edge to counter potential insect contamination and provide icing protection for LFC aircraft proposed for the 1990 period. Wind-tunnel testing of a sub-scale leading-edge section was conducted to evaluate alternative configurations for fluid dispersal and the effectiveness of the fluid film in preventing insect accretion. This testing facilitated the selection of a conceptual design for the leading-edge section and demonstrated the effectiveness of the concept in preventing insect accretion at low speeds. Based on the results of this testing, a full-scale leading-edge section, sized for the mid semispan region of aircraft in the JetStar/DC9-10 class, was designed and fabricated. This test section, incorporating functional cleaning and suction systems, was tested in the Lockheed-Georgia Company low-speed wind-tunnel and demonstrated the effectiveness of the cleaning system design in preventing leading-edge contamination at speeds representative of the takeoff-climb profile for LFC aircraft.

In the investigation of integrating the LFC systems with existing auxiliary aircraft systems, it was determined that there is no benefit to be realized in attempting to integrate the suction system with airplane pneumatic or auxiliary power systems. The only advantageous integration of systems is that fundamental to the selected leading-edge concept which integrates the insect protection and deicing systems.

In the configuration selection and assessment task, the final LFC configuration incorporating selected system concepts was compared to an advanced technology turbulent configuration. Although there are configurational differences, both aircraft represent near-optimum configurations for the defined mission and a valid comparison of the benefits provided by LFC is possible. The turbulent airplane is configured in the traditional form of current passenger transports with wing-mounted engines and a low-horizontal tail. High-lift devices for the turbulent airplane include leading-edge slats and modified Fowler trailing-edge flaps. To provide a clean wing for maximum LFC efficiency, engines on the LFC configuration are mounted on the aft fuselage and the horizontal tail is in a T configuration. There are no leading-edge devices included on this configuration to minimize wing surface discontinuities. LFC suction pumps are housed in pods beneath and extending forward of the wing roots. The aft fuselage of the LFC configuration is extended by 4.27 m (14 ft) to structurally accommodate the pylons which support the propulsion engines.

The gross weight of the LFC transport is 8.2% less than that of the turbulent configuration. This is achieved in part by the integration of suction system elements with the aircraft structure with the result that the LFC surface penalty is only 2.4% of empty weight. The total weight of the LFC system represents 4.4% of empty weight. It is significant to note

that mission fuel for the LFC configuration is 21.7% less than that of the turbulent transport. For a fuel price of \$0.19/l (\$0.45/gal), the 21.7% block fuel advantage offsets a 13% maintenance advantage and a 2% advantage in depreciation accruing to the turbulent aircraft with the result that direct operating costs are equal for a 6112 km (3300 n mi) stage length. Similar cost computations for a 12 038 km (6500 n mi) flight shift the comparison in favor of the LFC aircraft, reflecting the greater advantage of LFC with increasing range.

In early 1980, the price of jet fuel was almost \$0.26/l (\$1.00/gal). At this price, LFC provides a 4% DOC advantage. As fuel costs rise to \$0.52/l (\$2.00/gal), a DOC advantage of 10% results from the application of LFC. In terms of fuel efficiency, at the average stage length of 6112 km (3800 s mi), the LFC transport demonstrates an advantage in fuel efficiency of 91% and 28%, respectively, compared to the best of the current transports and the advanced technology turbulent aircraft. At 9100 km (6500 s mi), the fuel efficiency of the LFC transport is greater than that of current transports by 255%. These data illustrate the dramatic potential offered by a fleet of LFC transports in the 1990 time period.

As a part of the task devoted to the identification of future development requirements, studies were conducted which demonstrated the feasibility of using the NASA JetStar aircraft as a test bed for the evaluation of leading-edge LFC concepts. An additional task in this area established the feasibility of integrating the Lockheed LFC wing design into a DC-9-10 aircraft to form a LFC validator configuration. Further requirements for future development include the validation of current concepts, the continued development of manufacturing procedures, the investigation of operational characteristics in flight, and the refinement of design criteria and methodology. To a great extent, these requirements can be satisfied by the major programs currently included in the NASA LFC program plan. These programs are:

- (1) The NASA high-speed wind-tunnel program;
- (2) The JetStar leading-edge flight test program;
- (3) The LFC wing panel structural design and development program; and
- (4) The LFC validator flight test program.

These programs are logical steps toward the ultimate goal of verifying the credibility of LFC as a viable candidate for incorporation into commercial transports for the 1990's.



## 2.0 INTRODUCTION

The recognition of potential long-term shortages of petroleum-based fuel, evidenced by dramatic increases in costs and periods of limited availability since 1973, has emphasized the need for improving the fuel efficiency of long-range transport aircraft. In 1976, in response to this need, the NASA established the Aircraft Energy Efficiency (ACEE) program with the objective of maintaining the U. S. competitive advantage through the development of new technology for fuel efficiency. Of all advanced technology concepts currently under consideration for application during the next two decades, Laminar Flow Control (LFC) offers the greatest potential for improving the fuel efficiency of transport aircraft. Consequently, LFC is included as one element of the ACEE program and the NASA has formulated a three-phase program with the goal of developing LFC technology to permit application to aircraft in the 1990 period.

Both the theoretical methods and engineering and design techniques requisite to the application of LFC have been reasonably well-known since the mid-1940's. The validity of this background and the potential of LFC were partially evaluated in the 1960-1966 period by Northrop as a part of the X21A LFC Demonstration Program (Ref. 1-4). More recent studies, described in Reference 5, have evaluated the potential economic advantages of LFC in the projected airline environment. However, a conclusion common to all previous evaluations is that significant advances are required in both the operational verification and the development of basic design criteria for LFC prior to the incorporation of this technology on a production transport.

This report summarizes the work accomplished by Lockheed during the first phase of the program directed toward the satisfaction of these requirements. Section 4.0 of this report provides background information defining the overall study plan, assumptions basic to all study tasks, and the technology level appropriate to long-range commercial transport aircraft entering service in 1993. Section 5.0 describes the analyses conducted to select mission parameters, the parametric analyses conducted to define optimum aircraft configurational parameters and the resultant baseline configuration. The baseline aircraft defined in this section was used as a vehicle for the evaluation and development of alternative LFC system concepts described in Section 6.0. In this section, alternatives are evaluated in the general areas of aerodynamics, structures and materials, LFC systems, leading-edge region cleaning, and integration of auxiliary systems. Based on these evaluations, concepts in each area are selected for further development and testing and ultimate incorporation in the final study aircraft. The integration of selected system concepts into the final LFC configuration and the economic and operational characteristics of this configuration relative to a similarly-optimized advanced technology turbulent transport are described in Section 7.0. Investigations devoted to the definition of requirements for future LFC system development are summarized in Section 8.0.

Use of commercial products or names of manufacturers in this report does not constitute official endorsement of such products or manufacturers, either expressed or implied, by the National Aeronautics and Space Administration.

### 3.0 SYMBOLS AND ABBREVIATIONS

#### Symbols

a	speed of sound, m/s (ft/s)
b	wing span, m(ft)
c	local wing chord, m(ft)
$C_D$	drag coefficient
$c_f$	skin friction coefficient
$C_L$	lift coefficient
$C_P$	pressure coefficient
$c_s$	slot spacing, cm(in)
e	span efficiency factor
$F_n$	net thrust, N(lb)
H	cruise altitude, m(ft)
k	height of three-dimensional surface roughness, m(ft)
M	Mach number
m	mass, kg(lb)
N	natural logarithm of the ratio of a boundary-layer disturbance amplitude to its amplitude at neutral stability
n	crossflow velocity, m/s(ft/s)
P	absolute pressure, $N/m^2$ (lb/in <sup>2</sup> )
R	Reynolds number
$R_c$	wing chord Reynolds number
$R_e$	boundary-layer tangential-flow Reynolds number
$R_k$	roughness Reynolds number
$R_s$	length Reynolds number
$R_n$	boundary layer crossflow Reynolds number
$R_\theta$	boundary layer momentum thickness Reynolds number

S	area, $m^2(ft^2)$
s	surface distance, m(ft)
t	thickness, m (ft)
t/c	wing thickness-to-chord ratio, measured streamwise
T	temperature, $^{\circ}C(^{\circ}F)$
U	potential flow velocity, m/s(ft/s)
$U_o$	free stream velocity, m/s(ft/s)
$U_e$	velocity at edge of boundary layer, m/s(ft/s)
$v_s$	area suction velocity, m/s(ft/s)
$V_D$	design dive speed
$W_A$	engine airflow, kg/s(lb/s)
$w_n$	boundary layer crossflow velocity component in the direction normal to the potential flow streamline, m/s(ft/s)
w	slot width, mm(in)
x/c	chord location
$(x/c)_L$	chordwise extent of laminarization
x	streamwise coordinate, m(ft)
y	spanwise coordinate, m(ft)
z	coordinate normal to surface, m(ft)
$\alpha$	angle of attack, rad (deg)
$\beta$	slot design parameter, $(\beta = \frac{t}{w R_w})$
$\gamma$	ratio of specific heats
$\delta$	boundary-layer thickness, m(ft)
$\delta'$	boundary-layer displacement thickness, m(ft)
$\eta$	cruise power ratio, wing semispan location
$\theta$	boundary-layer momentum loss thickness, m(ft)
$\Lambda$	wing sweep angle, rad (deg)

$\mu$	absolute viscosity, $\text{Ns/m}^2$ ( $\text{lb s/ft}^2$ )
$\nu$	kinematic viscosity, $\text{M}^2/\text{s}$ ( $\text{ft}^2/\text{s}$ )
$\rho$	density, $\text{kg/m}^3$ ( $\text{lb/ft}^3$ )
$\sigma$	slot design parameter
$\tau$	slot design parameter

#### Subscripts

o	free-stream
s	slot
k	roughness
e	edge of boundary layer
z	sucked height of boundary layer

#### Abbreviations

APU	auxiliary power unit
AR	aspect ratio
ATA	Air Transport Association
ATC	air traffic control
ATT	advanced technology transport
BPR	bypass ratio
DOC	direct operating cost, $\text{\$/skm}(\text{\$/ssm})$
ECS	environmental control system
EPNdB	effective perceived noise level, decibels
FBW	fly-by-wire
FPR	fan pressure ratio
FS	wing front spar, fuselage station
LE	leading edge
L/D	lift to drag ratio
LFC	laminar flow control



MAC	mean aerodynamic chord, m(ft)
MLG	main landing gear
NDI	non destructive inspection
OEW	operating empty weight, kg(lb)
OPR	overall pressure ratio
PL	payload, kg(lb)
P&WA	Pratt & Whitney Aircraft
R&T	research and technology
RS	wing rear spar
RSS	relaxed static stability
SAS	stability <sup>1</sup> augmentation system
SFC	specific fuel consumption, $\frac{\text{mg/s}}{\text{N}} \left( \frac{\text{lb/hr}}{\text{lb}} \right)$
SLS	sea level standard
SSM	statute mile
TE	trailing edge
TF	turbulent flow
TIT	turbine inlet temperature, °C(°F)
TOGW	takeoff gross weight, kg(lb)
TRL	transition location on lower surface
TRU	transition location on upper surface
T/W	thrust-to-weight ratio
VPF	variable pitch fan
W/S	aircraft wing loading, $\text{kg/m}^2(\text{lb/ft}^2)$
WS	wing station



#### 4.0 STUDY APPROACH

This section outlines the basic assumptions and criteria which are fundamental to all aspects of the study. Included is a definition of study objectives, the overall plan employed to achieve study objectives, design criteria, and the assumed technology level.

#### 4.1 STUDY OBJECTIVES

The study described in this report has two primary objectives:

- (1) The evaluation of alternatives in the design of laminar-flow-control subsonic commercial transports for operation in the 1990's time period.
- (2) The definition of requirements for detailed subsystem development in subsequent program phases.

#### 4.2 STUDY PLAN

The general approach used in conducting the study is illustrated in the flow chart of Figure 1. Section numbers of this report corresponding to activities outlined in the study plan are included in the figure.

The existing technology data base was used in conjunction with airline inputs and independent mission analyses to define requirements for a 1993 commercial transport and establish a reference baseline configuration for subsequent use in evaluating advanced system concepts. In the Concept Evaluation Phase, analytical investigations, design studies, and subsystem testing, were conducted to evaluate alternative concepts in the following areas:

- (1) Aerodynamics
- (2) Structures and materials
- (3) Suction systems
- (4) Leading-edge region cleaning
- (5) Integration of auxiliary systems

Upon completion of the concept evaluations and test programs, the optimum LFC system elements were integrated into the baseline configuration as a part of the Configuration Selection and Assessment task. To assess the relative advantages of LFC, the LFC transport configuration selected in this process was compared to an advanced technology turbulent configuration optimized for the same mission.

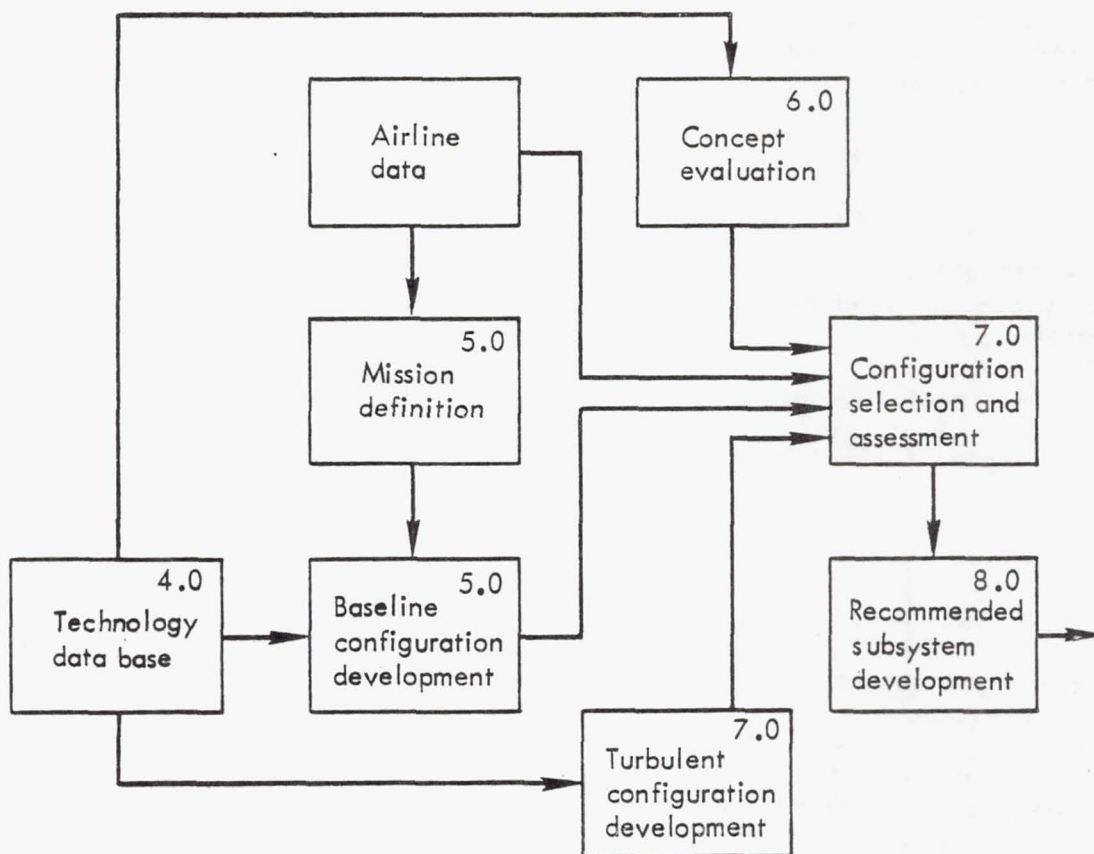


Figure 1. Study plan

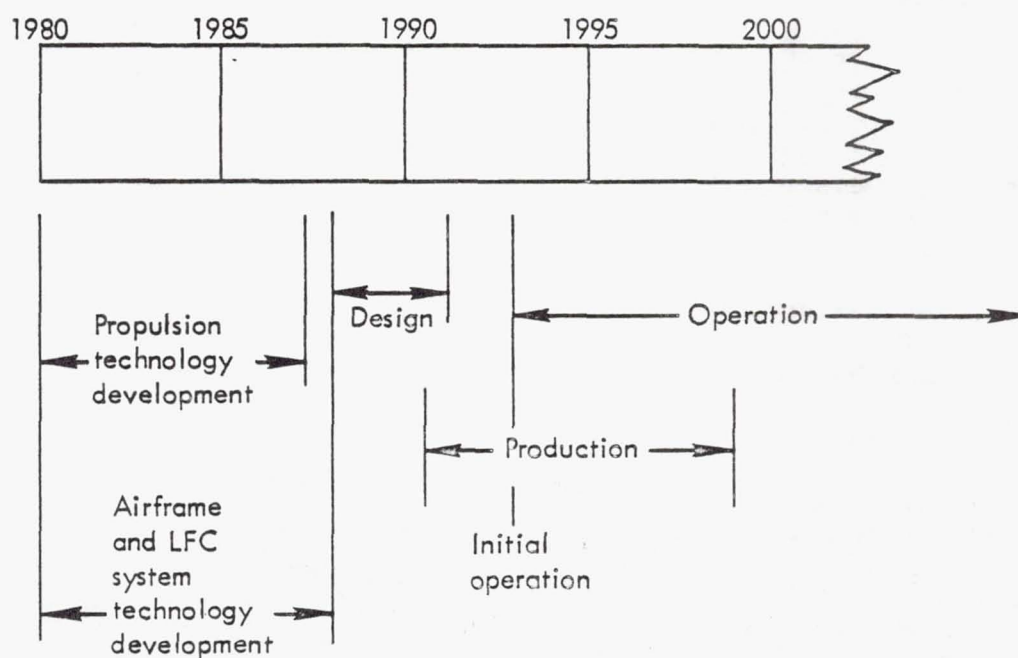


Figure 2. Life cycle

The concept evaluations, subsystem tests, and configuration assessment activities provide a sound basis for the definition of requirements for subsystem development in subsequent phases of the NASA LFC Program.

#### 4.3 LIFE CYCLE

The assumed life cycle for study aircraft is shown in Figure 2. For initial passenger operation in 1993, the following technology levels are appropriate:

Airframe technology level - 1988

Engine technology level - 1987

#### 4.4 DESIGN CRITERIA

Recent projections of the IATA Technical Committee indicate that airlines will expect a minimum design life objective of 90 000 flight hours for long-range aircraft entering service in the post-1990 period. The airlines do not expect a crack-free structure for this length of service but do expect an airframe which can be maintained economically. Previous widebody jet experience indicates that the airlines will expect a service life warranty contract of approximately one-half of the design life objective. Therefore, a warranty service life of 45 000 flight hours was used to establish the wing ultimate tension cutoff stress level for the baseline airplane.

The study aircraft satisfy the requirements for type certification in the transport category under Federal Aviation Regulations - Part 25, and are capable of operating under pertinent FAA rules.

Based on realistic estimates of achievable progress for the technology readiness date assumed for the study aircraft, the following noise criteria were selected:

- |   |                  |                   |
|---|------------------|-------------------|
| o | Takeoff sideline | FAR 36 -10 EPN dB |
| o | Takeoff flyover  | FAR 36 -6 EPN dB  |
| o | Approach flyover | FAR 36 -5 EPN dB  |

These levels are 2 EPNdb below the standards currently proposed as a part of NPRM 75-37C in Reference 6.

The study aircraft are provided with fuel reserves in accordance with the requirements of FAR 121.645. In addition to the fuel reserve allowances specified in this regulation, the final LFC study aircraft are designed with adequate reserve fuel to accommodate loss of the LFC system due to weather phenomena during three percent of the mission cruise time.



The basic design criteria for LFC systems developed as a part of the X-21 Program represent the most comprehensive set of guidelines currently available. Therefore, the criteria established by this program and reported in Reference 7 form the basis for the definition of LFC systems for the study aircraft.

#### 4.5 REFERENCE TECHNOLOGY LEVEL

As a preliminary to the parametric configuration analyses and subsequent configuration optimization activities leading to the definition of final study aircraft, the level of technology likely to be available for application in the early-1990 period was established. This section summarizes the reference technology level assumed for all configuration development activities.

##### 4.5.1 Aerodynamics

###### 4.5.1.1 Aerodynamics Criteria

The most complete set of criteria for the development of external aerodynamic configurations compatible with LFC systems requirements was developed as a part of the X-21 program described in Reference 7. The criteria of this document were updated to include results of pertinent recent investigations. This updating included a critical review of LFC suction requirements and dual use of active trailing-edge control flaps for gust alleviation and minimization of LFC suction flow rates in varying operational conditions. Advances in near-field acoustics predictive technology were examined to determine if aerodynamic configuration constraints should be increased or relaxed. Acoustic effects on suction requirements were addressed by inclusion of an excess suction system capacity similar to the approach used for the X-21. As a result of improvements in aerodynamics design and analysis methods, aerodynamics criteria were updated to the status depicted in Figure 3.

###### 4.5.1.2 Airfoil Technology

The aircraft configurations developed in this study incorporate advanced technology supercritical airfoil sections characterized by an extensive region of supercritical flow terminated by a moderate-strength shock located fairly far aft. Typical wing section design curves, which define the technology level of the airfoil type, are shown in Figure 4. Subsequent design perturbations included supercritical versus shock-free and roof-top sections, while recognizing relative LFC suction requirements and changes in structural weight due to thickness and shape differences. Some variation in airfoil thickness and form were also examined to maximize internal volume for fuel and ducting and improve leading-edge boundary layer characteristics.

Advanced technology secondary active trailing-edge flaps of the type shown in Figure 5 were adopted as a means of automatically maintaining desired pressure gradients, controlling shock position, and minimizing LFC suction requirements over a moderate range of operating conditions.

#### BOUNDARY LAYER STABILITY CRITERIA WITH NO SOUND DISTURBANCES

CALCULATED WAVE AMPLITUDE GROWTH FACTORS (N FACTORS) BELOW A PRESCRIBED VALUE.

LOWER FREQUENCY WAVES (NEAR 0 HZ) DUE TO CROSSFLOW INSTABILITIES HAVE  $N < 10.5$ . INCOMPRESSIBLE LOCALLY PARALLEL THEORY, (SALLY), USED FOR CALCULATIONS.

HIGHER FREQUENCY (0 - 8 KHZ) WAVES DUE TO VISCOUS INSTABILITY (TOLLMIE-SCHLICHTING) HAVE  $N < 11$ .

STAGNATION ZONE MOMENTUM THICKNESS REYNOLDS NO.  $< 100$ .

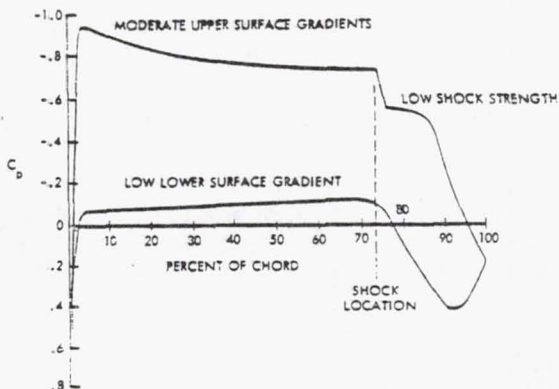
LOW UNIT REYNOLDS NO. AND/OR CHORD REYNOLDS NO.

#### LAYOUT REQUIREMENTS

- SMALL SIZED NACELLE AND SUCTION PUMP PODS
- HIGH WING LOCATION PREFERENCE
- LOCAL CONTOURING OF NACELLES, PODS, AND FUSELAGE INTERSECTIONS WITH FLYING SURFACES TO MAXIMIZE EXTENT OF STRAIGHT ISOBARS
- AFT LOCATION OF WING-MOUNTED PODS OR NACELLES TO MINIMIZE PRESSURE INTERFERENCE AND ACOUSTIC DISTURBANCES
- MINIMUM SWEEP AND MAXIMUM ASPECT RATIO

#### POTENTIAL FLOW PRESSURES

- STRAIGHT ISOBARS BOTH UPPER AND LOWER SURFACES (IMPLIES SIMILAR CHORDWISE PRESSURES AT ALL SPAN STATIONS)
- LARGE EXTENT OF LOW PRESSURE GRADIENT IN CHORD DIRECTION AND INITIAL RAPID ACCELERATION OF VELOCITY AT LEADING EDGE AS INDICATED IN ILLUSTRATION
- PRESSURES COMPATIBLE WITH LOCAL EFFECTIVE MACH NO.  $\leq 1.17$
- TRAILING EDGE PRESSURE COEFFICIENT 0.20 MINIMUM



#### SMOOTHNESS CRITERIA

CHORD REYNOLDS NO.  $= 80 \times 10^6$   
CHORD = 13.7 M (45 FT)

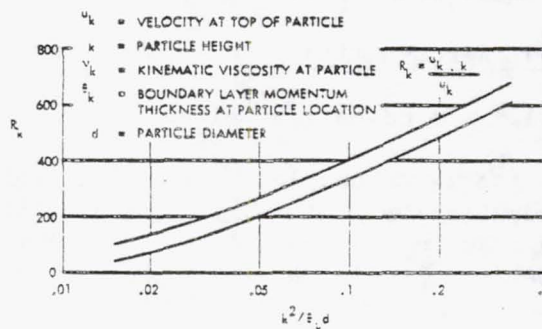
- FOR TWO-DIMENSIONAL SURFACE WAVES (SINGLE WAVES), THE ALLOWABLE WAVE AMPLITUDE RATIO IS GIVEN BY THE FORMULA

$$\frac{a_1}{\lambda} \approx \left( \frac{59000 C_{\text{opt}}^2}{\lambda (Re)^{1.5}} \right)^{1/2}$$

WHERE  $a_1$  = DOUBLE WAVE AMPLITUDE  $\lambda$  = WAVE-LENGTH AND  $C$  = CHORD. FOR MULTIPLE WAVES, ONE-THIRD OF THE VALUE, SHOULD BE USED

- FOR FORWARD-FACING STEPS, THE ALLOWABLE STEP HEIGHT IS GIVEN BY  $(Re/h) \cdot (h) \approx 1800$ ,  $h$  = STEP HEIGHT. FOR AFT-FACING STEPS, ONE-HALF OF THIS VALUE IS ALLOWED.
- FOR GAPS, THE ALLOWABLE GAP WIDTH IS EXPRESSED BY  $(Re/h) \cdot (g) \approx 15000$  WHERE  $g$  IS THE GAP WIDTH.

#### ALLOWABLE THREE-DIMENSIONAL ROUGHNESS FOR LAMINAR FLOW



#### ACOUSTIC DISTURBANCE

- ALLOW 10% ADDITION TO TOTAL SUCTION REQUIREMENT TO AVOID CROSSFLOW DESTABILIZATION OF STRONG SOUND ENVIRONMENT
- USE LOW NOISE LEVEL ENGINE CYCLES
- QUANTITATIVE X-21A RESULTS AS ILLUSTRATED BELOW

#### CRITICAL DISTURBANCE LEVELS WITH NOMINAL SUCTION

THE DESIGN-CRITERIA LINE REPRESENTS THE ALLOWABLE SOUND-PARTICLE VELOCITY WITH NOMINAL SUCTION. INCREASED SUCTION PERMITS HIGHER LEVELS

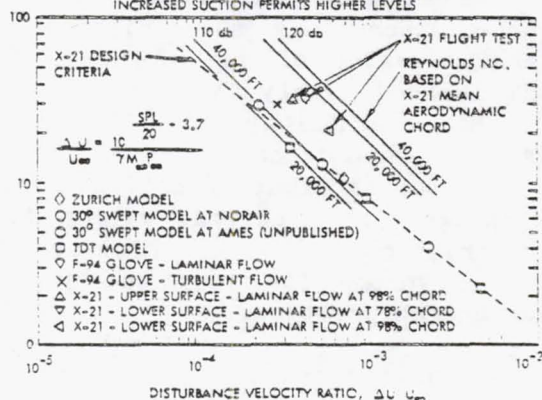


Figure 3. LFC aerodynamics criteria



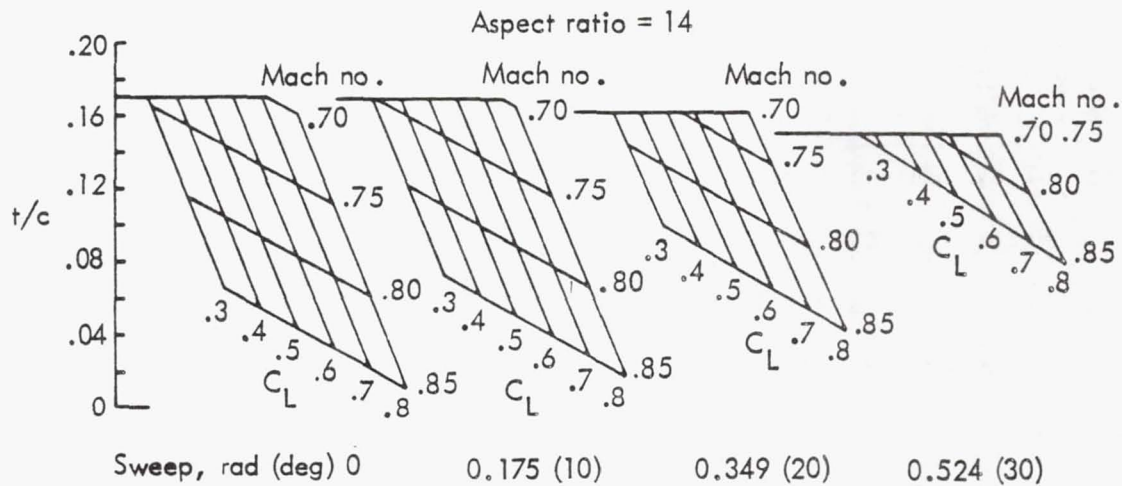


Figure 4. Wing section design curves

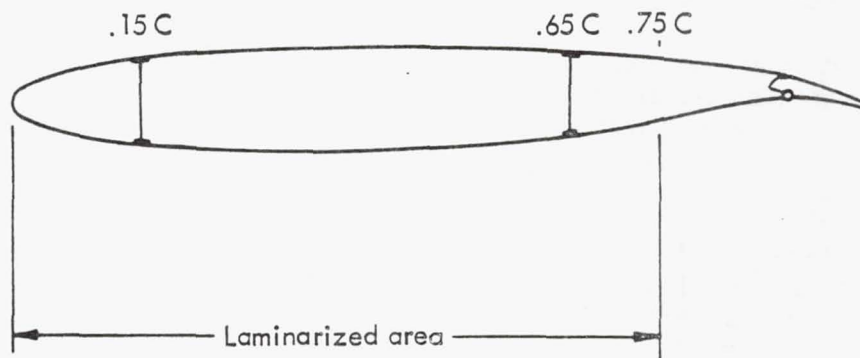


Figure 5. Example of secondary active trailing edge flaps

#### 4.5.1.3 High-Lift Device Technology

Design and analysis studies performed were compatible with a current-technology mechanical flap system which provides the required airport performance with the smallest penalty to direct operating cost. Single- and multiple-slotted flaps and appropriate leading-edge devices were assessed in the study from the standpoint of chordwise and spanwise extent, lift and drag effectiveness, relative weight penalty, and high-lift compatibility with airfoil section shapes desirable for LFC. Studies considered leading-edge surfaces designed to protect the leading-edge from insects, which also function as normal aerodynamic leading-edge devices.

#### 4.5.2 Flight Controls

The flight control system incorporates the elements of active control technology (ACT) which promise significant improvements in the efficiency of large transport aircraft.

The ACT system encompasses the following modes of control:

- o Relaxed Static Stability
- o Stability Augmentation System
- o Maneuver Load Control
- o Gust Load Alleviation
- o Flutter Mode Control
- o Ride Control

The major improvements offered by the above systems are: minimization of airframe weight, incorporation of automatic trouble-shooting, and improved ride characteristics.

The four channel fly-by-wire (FBW) system is controlled on each channel by an on-board digital computer. A digital system is mandated by the extensive complex signal processing, the flexibility required to accommodate the multi-mode control logic laws, and the redundancy required by an FBW system.

Geared elevators driven by the stabilizer, a double hinged rudder, and outboard ailerons provide low speed control. Ground-operable-only spoilers are provided for deployment during ground rollout or rejected takeoff. All controls and instrumentation required for the operation of the airplane in the air and on the ground are located in the flight station. The on-board computers provide feedback for two hydro-mechanical units which provide the pilots with artificial feel in all three control axes.

The following paragraphs provide brief descriptions of the multi-modes of the ACT system.

##### 4.5.2.1 Relaxed Static Stability (RSS)

Relaxing the static stability requirements in the pitch and yaw axes reduces horizontal and vertical tail sizes significantly. These size reductions thus reduce drag and airframe weight which requires less fuel or provides a tradeoff for increased range. These augmented systems are critical for certain portions of the high-speed flight envelope. However, cruise and landing control are not dependent on the RSS system.

##### 4.5.2.2 Stability Augmentation System (SAS)

The three axis SAS, a dual system with full time monitoring, provides pitch and yaw damping and turn coordination. This system improves the air-

plane handling characteristics, making the pilot's task easier and improving the ride qualities. As discussed under the RSS, the augmented stability in the pitch axis allows the tail sizes to be smaller than without augmentation while allowing the aft center-of-gravity limit to be extended into the unstable region with the horizontal tail flying near the zero lift point.

#### 4.5.2.3 Maneuver Load Control (MLC)

The MLC system reduces bending loads on the wing. As the wing is loaded to some pre-determined level, the full-span trailing edge secondary flaps operate to reduce wing bending moments and to restrict torsional loading to specified limits.

#### 4.5.2.4 Gust Load Alleviation (GLA)

The GLA system reduces gust loads on the wing through the use of accelerometers which respond to wing motion. Much as in the MLC system, signals from the on-board computers activate the trailing-edge secondary flaps to limit wing bending and torsional loads to preset limits. Pitch damping is provided by the elevator to damp airplane oscillations.

#### 4.5.2.5 Flutter Mode Control (FMC)

The FMC system capability can be provided if more detailed analyses of the LFC transport indicate that it is necessary. All the required system logic, sensors, and control hardware are on board to provide other modes of ACT. If required, an automatic mode of flutter speed "increase" would raise the wing flutter limit from  $V_D$  to  $1.2 V_D$ .

#### 4.5.2.6 Ride Control (RC)

Like the FMC system, the equipment to provide RC is on-board. Thus through proper programming of system sensor anticipation, a smoother ride would be provided.

### 4.5.3 Propulsion Systems

#### 4.5.3.1 Propulsion Engine Definition

The Pratt & Whitney Aircraft STF-477 study engine was chosen as the primary propulsion unit for the study aircraft. This engine cycle was the end product of Tasks II and III of a P&WA study performed under contract to the NASA Lewis Research Center and reported in Reference 8. The objective of these tasks was to evaluate low energy consumption engines and technology requirements for in-service operation in the post-1990 period. P&WA provided an uninstalled performance spectrum for this engine in Reference 9. These data include a range of engine power settings, Mach ranges, and altitudes covering a realistic flight spectrum with and without engine power and bleed air extraction. A summary of engine characteristics is presented in Table 1.



TABLE 1. CHARACTERISTICS OF PRATT & WHITNEY  
AIRCRAFT STF 477 TURBOFAN ENGINE

<u>Parameter</u>	<u>Performance</u>	<u>Increment from 1976 Technology</u>
Thrust	118 100 N (26 550 lb)	
TSFC	$0.793 \frac{\text{mg } W_f}{\text{sec N}}$ ( $0.280 \frac{\text{lb } W_f}{\text{hr lbf}}$ )	-12.5%
FPR	1.7 nominal	
BPR	8.0 nominal	
OPR	45 nominal	
TIT (Max)	1427°C (2600°F)	
$W_{at}$	472 kg/sec (1040 lb/sec)	
Weight	1787 kg (3940 lb)	-22%
Diameter	1.92 m (75.6 in)	
Length	2.88 m (113.2 in)	

The low-pressure spool consists of a one-stage fan and three low-pressure compressor stages. These components include advanced blading aerodynamics and seals for better component efficiency and lower noise while maintaining good component life and performance retention. The low-pressure spool is driven by a five-stage uncooled turbine, incorporating higher loading and advanced aerodynamics and seals. The high-pressure spool incorporates a ten-stage compressor driven by a two-stage highly-loaded turbine, both incorporating technology advances similar to the low-pressure spool. The high-pressure turbine also includes advanced metallurgy, cooling, and coating technologies.

The basic engine data of Reference 9 are sized for an uninstalled rated thrust of 118 100 N (26 500 lb) but scaling data are provided to cover a range of 71 200 - 178 000 N (16 000 - 40 000 lb). The study airplane requires a thrust of 149 193 N (33 540 lb) which is well within this range of scaling data.

The basic uninstalled STF-477 data were modified to incorporate installation losses for an engine nacelle with a three-quarter length fan

duct. Allowance was made in the installation losses for the inlet duct wall, fan duct inner and outer wall, and primary exhaust duct outer wall acoustic treatment of advanced technology low-loss configurations as described in Reference 10. Since the STF-477 engine was basically configured to meet FAR 36 - 10 EPNdB noise criteria, this type of treatment should be adequate to meet the noise criteria of this study.

#### 4.5.4 Structures and Materials

The selection of materials for the major structural components of the study configuration was based on the results reported in the studies of References 11 and 12. Candidate materials and structural concepts were examined for each element of the structure. Materials and concepts were selected on the basis of the lowest cost per pound of weight saved. The weight technology factors were developed for a constant-size airplane by substituting different materials and structural concepts and computing the weights of structural elements for identical structural requirements. A weight factor of 1.00 was assigned to the conventional aluminum structure, and the ratio of the weight of the advanced material and concept to that of aluminum was defined as the weight factor. The full benefits of advanced materials were realized by sizing the total airplane, including the power plant and other systems, to take advantage of the lower structural weights. The selection of advanced materials for wing, are depicted in Table 2.

Table 3 describes the distribution of advanced materials among the airframe components and lists the corresponding weight technology factors. Utilization of advanced materials for 66% of the airframe weight results in study aircraft which weigh about 67% of that of comparable current transports. Advanced materials are used in both primary and secondary structure.

#### 4.5.5 LFC Systems

The basic design technology for LFC suction surface and metering systems was developed as a part of the X-21 Program in the early 1960's and represents the most comprehensive set of guidelines currently available. Therefore, the criteria and limits established by that program and reported in Reference 7 were used as the basis for the definition of slot and metering configurations. These criteria were augmented by a limited amount of static testing of slot/metering configurations and a Lockheed-funded low-speed wind-tunnel test of the laminarizing characteristics of the full-scale leading-edge test panel fabricated under this contract.

A leading-edge cleaning system to prevent insect accretion was developed by both subscale and full-scale low-speed wind-tunnel testing under this contract. The subscale model was fabricated by Lockheed funding while the full-scale tests were conducted on the leading-edge test panel fabricated under this contract.

The internal suction ducting system is essentially state-of-the-art for low velocity air ducting, although analyses of system tolerance effects were conducted under this contract.



TABLE 2. SELECTION OF ADVANCED MATERIALS FOR WING

<u>Structure</u>	<u>Material &amp; Concept</u>	<u>Weight Factor</u>
Outer Wing Box Structure		
Interspar Covers	Graphite/Epoxy Panels	0.60
Root Joint Increment	Titanium Straps	0.65
Joints, Splices & Fasteners	Reduction in Splices & Fasteners	0.50
Spar Caps	Molded Graphite/Epoxy	0.49
Spar Webs	Molded Graphite/Epoxy	0.51
Interspar Ribs	Molded Graphite/Epoxy Truss Type	0.57
Center Wing Box Structure		
Interspar Covers	Graphite/Epoxy Panels	0.64
Root Joint Increment	Titanium Straps	0.64
Joints, Splices & Fasteners	Reduction in Splices & Fasteners	0.48
Spar Caps	Molded Graphite/Epoxy	0.54
Spar Webs	Molded Graphite/Epoxy	0.53
Interspar Ribs	Molded Graphite/Epoxy Truss Type	0.57
Secondary Structure		
Trailing Edge Flaps	Graphite/Epoxy Skins & Ribs	0.64
Ailerons	Graphite/Epoxy	0.64
Fixed Trailing Edge	Graphite/Epoxy Skins & Ribs	0.64
Leading Edge	Molded Graphite/Epoxy Skins & Top Hat Formers	0.65
Tips	Graphite/Epoxy	0.54
Misc. Doors, Root Fairing	Kevlar 49	0.60
TOTAL WING		0.61

TABLE 3. WEIGHT TECHNOLOGY FACTORS

<u>Component</u>	<u>Advanced Material Weight (%)</u>	<u>Weight Technology Factor</u>
Wing	85	0.61
Fuselage	71	0.66
Horizontal Tail	67	0.74
Vertical Tail	67	0.74
Nacelle and Pylon	35	0.79
Landing Gear	23	0.84
Weighted Average	66	0.67

The suction units were uniquely configured and sized for this study employing an advanced engine technology base with recognition of restrictions imposed by the nature and requirements of the LFC suction system.

#### 4.5.6 Aircraft Systems

The normal aircraft systems presumed to be used in the study aircraft are those generally accepted by industry as being viable candidates for improvement or upgrading during the next decade. Examples of such improvement may be further miniaturization of electronic systems, higher pressure hydraulic systems to reduce hydraulic actuator sizes, and the major changes involving fly-by-wire flight control systems incorporating active controls.

#### 4.6 COSTING ASSUMPTIONS

The following assumptions were employed for the generation of aircraft price and direct operating cost data for both the LFC and turbulent study aircraft.

- (1) All cost are expressed in January 1, 1979, dollars
- (2) Total production: 350 units
- (3) Production span: 10 years
- (4) Production rate: 1.5 - 4 units/month
- (5) Learning curve
  - o Labor: 75%
  - o Materials: 89%
- (6) Spares
  - o Airframe: 6%
  - o Engine: 30%
- (7) Utilization: 4200 hr/year
- (8) Depreciation: 14 years to 10%
- (9) Fuel price: All economic comparisons assumed a fuel price of \$0.12/l (\$0.45/gal). Additional economic data were generated for fuel prices of:
  - o \$0.06/l (\$0.225/gal)
  - o \$0.24/l (\$0.90/gal)
  - o \$0.58/l (\$2.25/gal)

## 5.0 BASELINE CONFIGURATION DEVELOPMENT

The plan developed for the realization of contract objectives requires the development of a study baseline aircraft to be used as a vehicle for the evaluation of alternative LFC system concepts during subsequent study phases. This section summarizes the analyses conducted in the process of developing the baseline configuration. Included as a part of these analyses is a definition of the study mission requirements, the parametric configuration analyses conducted in the selection of aircraft geometry, engine, and operational parameters, and the characteristics of the selected configuration.

### 5.1 MISSION DEFINITION

#### 5.1.1. Assumptions and Methodology

As the first phase in the development of a study baseline, the Lockheed-California Company performed analyses to determine the size and mission characteristics for LFC aircraft to be introduced in the 1993 time period. These analyses were based on three assumptions:

- (1) The LFC transport will be primarily a long-range aircraft, since the major benefit promised by LFC technology is potential fuel savings. These savings occur during cruise, and thus increase with increasing range. Consequently, this market analysis focuses on distances greater than 4800 km (3000 s mi). Virtually all U. S. domestic traffic is thus excluded. North Atlantic traffic, the world's largest international market, is included.
- (2) No second generation SST will be in service in the time frame under consideration. Therefore, subsonic transports will satisfy international traffic demands. The present Concorde, or a minor derivative thereof, would have no effect on the LFC transport due to its high seat mile costs of operation and ownership.
- (3) Fossil fuels will still be the primary source of aircraft energy in the year 2000. As a result, it is not necessary to consider alternative fuels for the study aircraft.

Regarding economic growth, no specific projections were made to year 2000, except that current relative growth rates will continue and that world travel status of the USSR and PRC will not change. If these two areas become major markets, demand for an LFC transport will increase.

The basis of these analyses was the development of estimates of present geographical traffic distribution i.e., a "top down" approach. Every available source of data was examined, such as Immigration and Naturalization Service reports, published flight schedules, origin-destination data from major international carriers, and traffic reports published by foreign government agencies. A product of this research was a traffic distribution matrix describing estimated traffic volumes between major world areas distributed among 805 km (500 s mi) increments.



Total demand was projected to year 2000. This forecast, based on 1975 relative distributions, was divided into major market areas. Within these areas, the traffic was further divided into mileage blocks for the traffic over 4800 km (3000 s mi). The results of this projection are shown in Table 4.

With each element of the matrix considered as a discrete market, calculations were made to determine the number of aircraft of various sizes required to satisfy projected demand in the year 2000. Each traffic figure was converted from annual to an average one-way daily average format, assuming each aircraft would operate at a 60% load factor, fleet sizes for 200, 300, 400, 500, and 600 passenger aircraft were determined.

Examining the discrete market data in 805 km (500 s mi) blocks, aircraft fleet requirements were determined. A summary of these data is given in Table 5.

Perhaps the most striking feature of this table is the fact that for each of the five aircraft, the total fleet requirements drop sharply beyond 11 260 km (7000 s mi). However, in view of the fact that Pan American is already providing scheduled nonstop service using a 747 SP under restricted load conditions in a 11 900 km (7 400 s mi) market (Sydney to San Francisco), it was decided to examine more closely those markets involving distances of between 9650 and 12 870 km (6000 and 8000 s mi).

At least eight major markets exist which involve distances slightly greater than 11 260 km (7000 s mi). Combined with the information contained in Table 5, this provides sufficient grounds for selecting a specific LFC aircraft range requirement. Table 5 clearly shows that the aircraft should be capable of scheduled flights (including appropriate reserves) of at least 11 260 km (7000 s mi). The precise range figure should in fact be several hundred miles greater. The conclusion of this study is that the market requires a range of 12 038 km (7500 s mi).

As shown in Table 6, projections of traffic in 2000 indicate that there will be 28 major markets involving distance between 9170 and 12 870 km (5700 and 8000 s mi). Assuming a 60% load factor, all 28 markets would support at least one daily flight of a 200-passenger aircraft, 27 (96 percent) would support a 300-passenger aircraft, (86 percent) would support a 400-passenger aircraft, 19 (68 percent) a 500-passenger aircraft, and 17 (61 percent) would support a 600-passenger aircraft.

The above figures clearly justify an aircraft with a capacity of at least 300 passengers. Considering the incentives to make the aircraft as large as practicable, a 400-passenger aircraft seems justified and is the recommendation of this study.

TABLE 4. DISTRIBUTION OF 2000 ICAO WORLD\* TRAFFIC OVER 4800 km (3000 s mi)  
ONE-WAY DAILY AVERAGE PASSENGERS

	DISTANCE BLOCKS IN km (s mi) × 100															
	48-56 (30-35)	56-64 (35-40)	64-72 (40-45)	72-80 (45-50)	80-89 (50-55)	89-97 (55-60)	97-105 (60-65)	105-113 (65-70)	113-121 (70-75)	121-129 (75-80)	129-137 (80-85)	137-145 (85-90)	145-153 (90-95)	153+ (95+)	TOTAL	
U. S. Domestic	444	222	666	889	0	0	0	0	0	0	0	0	0	0	2 221	
U. S./Can.-L./S. Am.	273	0	1 084	4 337	4 610	538	513	935	124	17	33	0	0	6	12 470	
N. Am.-Europe	9 192	18 726	16 359	4 088	6 539	2 974	388	799	202	28	0	0	0	0	59 295	
N. Am.-Asia/Oceania	0	808	1 077	0	6 461	4 307	3 904	8 076	1 010	437	883	883	883	84	28 813	
Europe-S. America	0	464	2 558	2 318	2 326	2 318	1 035	1 871	372	166	166	0	0	16	13 610	
Europe-Africa	5 413	0	3 294	2 351	2 351	0	1 788	3 253	422	207	174	0	0	26	19 279	
Europe-Asia/Oceania	0	1 086	3 148	2 284	0	11 949	5 630	1 499	0	595	16	698	0	5 376	32 281	
Other	14 613	16 861	2 248	6 745	4 496	0	0	0	0	0	0	0	0	0	44 963	
Total	29 935	38 167	30 434	23 012	26 873	22 086	13 258	16 433	2 130	1 450	1 272	1 581	883	5 508	212 932	
Percent	14.1	17.9	14.3	10.8	12.6	10.4	6.2	7.7	1.0	0.7	0.6	0.7	0.4	2.6	100.0	

\*EXCLUDING USSR

TABLE 5. TOTAL LONG-HAUL AIRCRAFT REQUIREMENTS FOR THE YEAR 2000  
BASED ON DAILY SERVICE AT 60% LOAD FACTOR

Kilometers(00) (Statute Miles)	Aircraft Seating Capacity				
	<u>200</u>	<u>300</u>	<u>400</u>	<u>500</u>	<u>600</u>
48-56 (3000-3500)	247	165	122	97	81
56-64 (3500-4000)	315	210	156	124	104
64-72 (4000-4500)	250	165	123	97	81
72-80 (4500-5000)	190	124	93	72	61
80-89 (5000-5500)	220	145	108	85	71
89-97 (5500-6000)	181	119	89	70	59
97-105 (6000-6500)	107	70	53	41	33
105-113 (6500-7000)	134	89	65	51	44
113-121 (7000-7500)	16	10	6	5	4
121-129 (7500-8000)	9	6	3	2	2
129-137 (8000-8500)	9	4	3	2	2
137-145 (8500-9000)	12	7	5	4	3
145-153 (9000-9500)	7	4	3	2	2
153+ (9500+)	44	29	22	17	14
TOTAL	1 741	1 147	851	669	561

TABLE 6. POTENTIAL LONG RANGE MARKETS

<u>City-Pair</u>	<u>km</u>	<u>n.mi.</u>
BOM-NYC	12 525	6 763
SYD-YVR	12 492	6 745
LAX-SYD	12 053	6 508
SFO-SYD	11 940	6 447
DEL-NYD	11 747	6 343
LAX-MNL	11 732	6 335
HKG-LAX	11 638	6 284
MEX-TYO	11 306	6 105
MNL-SFO	11 219	6 058
HKG-SFO	11 099	5 993
NYC-TYO	10 869	5 869
LON-SIN	10 869	5 869
HNL-SIN	10 790	5 826
MAD-TYO	10 762	5 811
BKK-HNL	10 590	5 718
LON-KUL	10 543	5 693
AKL-LAX	10 479	5 658
HKG-YVR	10 249	5 534
CHI-TYO	10 117	5 463
BUE-MAD	10 047	5 425
LAX-SAO	9 910	5 351
ROM-TYO	9 886	5 338
BUE-LAX	9 842	5 314
NYC-TEH	9 840	5 313
GVA-TYO	9 801	5 292
OSA-ROM	9 714	5 245
PAR-TYO	9 699	5 237
LON-HKG	9 638	5 204



To further verify these size and range requirements, a "bottom-up" approach was employed in which a list of city-pairs involving distances at or near the range figures described above was compiled. Using all available sources of data, city-pair traffic volume estimates were made for 1975 and 2000. A final LFC aircraft range requirement was selected and an aircraft size was chosen based on the projected traffic volume in the various city-pair markets at or near the selected maximum range.

### 5.1.2 Mission Parameters

Following is a summary of the results of the mission analysis:

Design Range	12 038 km (7500 s mi, 6500 n mi)
Cruise Speed	M = 0.80 - 0.85
Capacity	400 passengers
Production Quantity	350

Having determined the basic mission parameters for the 1990 LFC transport, the average stage length to be expected for actual airline operation was calculated using historical data for currently operational aircraft. The average stage length predicted for actual airline operation is 6112 km (3300 n mi).

### 5.1.3 LFC Mission Profile

The recommended mission profile to be used in the design and analyses of the LFC airplane is the standard international flight profile for maximum range and minimum fuel. This profile is depicted in Figure 6.

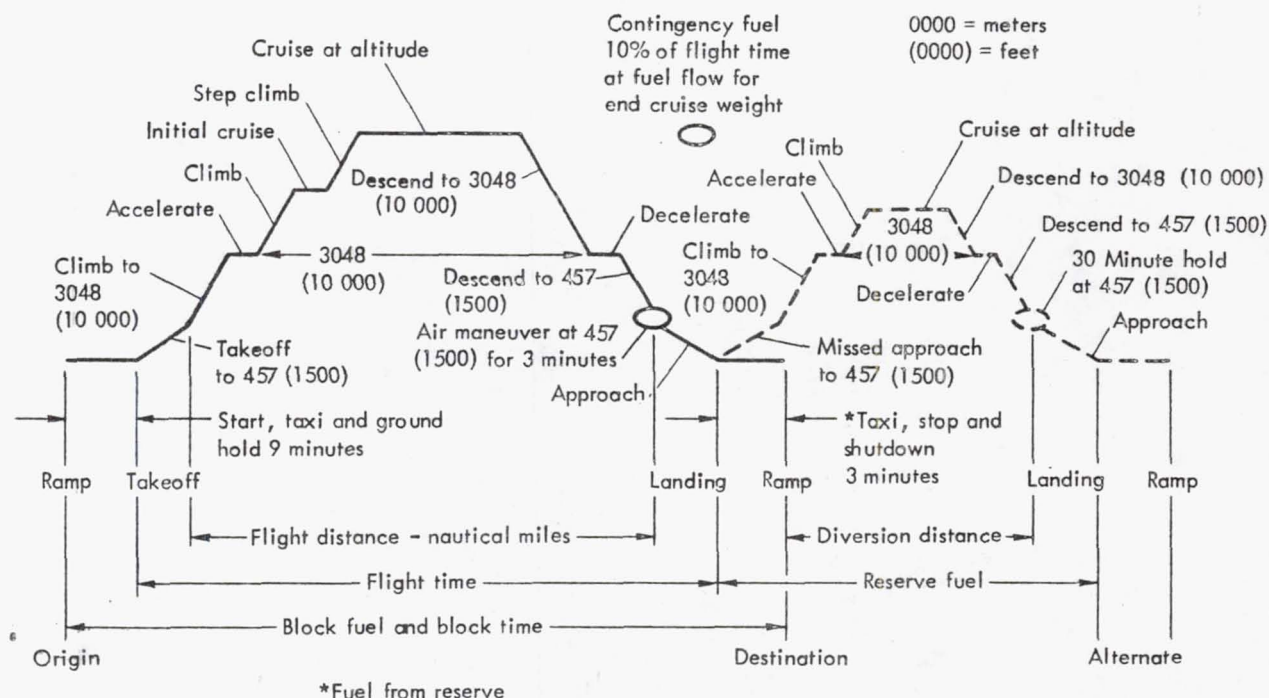


Figure 6. International flight profile

## 5.2 PARAMETRIC CONFIGURATION ANALYSES

A conventional wide-body fuselage configuration, sized for 400 passengers and 16 874 kg (37 200 pounds) of belly cargo, was used for all parametric analyses. The parametric configurations use two LFC suction units mounted in the fuselage near the wing root. A weight penalty of 6.786 kg/m<sup>2</sup> (1.39 lb/ft<sup>2</sup>) in addition to the basic structural weight is assumed for the areas where LFC suction is applied. Laminarized areas are approximately 75% of the exposed wing area and 65% of the exposed empennage area. Four fuselage-mounted engines are assumed for the parametric configurations.

The following sweep/Mach number schedule was used for the basic study:

Mach No.	0.70	0.75	0.80	0.85
Sweep - rad (deg)	0	.258 (14.8)	.436 (25.0)	.549 (31.5)

The results of the studies reported in Reference 5 were considered adequate for use in design decisions for an LFC configuration satisfying the mission requirements of this study. Consequently, these analyses were not repeated.

### 5.2.1 Procedures

The Lockheed Generalized Aircraft Sizing Program (GASP) was employed for all parametric configuration analyses. As the initial step in the analysis, eleven cruise-altitude/cruise-Mach number combinations were defined with cruise altitudes ranging from 10 973 to 13 411 m (36 000 to 44 000 ft) and Mach numbers ranging from 0.70 to 0.85.

Two phases were required to develop optimum configuration parameters for each cruise-altitude/cruise-M combination. In the first phase, wing loading was varied from 415 to 610 kg/m<sup>2</sup> (85 to 125 lb/ft<sup>2</sup>) and aspect ratio was varied from 10 to 14, to establish optimum configuration geometry independent of airport performance constraints. In the second phase, engine bypass ratio, cruise power ratio, and aspect ratio were varied parametrically to optimize airport performance for each configuration geometry. Engine bypass ratios ranging from 6.0 to 13.0 and cruise power ratios ranging from 0.70 to 0.90 were considered. The maximum cruise power setting was constrained to a value of 0.90 to assure satisfactory climb performance with LFC off to an altitude approaching the initial cruise altitude.

Following are the primary criteria for selecting baseline candidates:

- (1) Near minimum direct operating cost for a 6112 km (3300 n mi) mission.
- (2) Moderate aspect ratio to assure sufficient LFC duct volume and provide adequate design flexibility.
- (3) Use of fuel volume in wing and wing center section.



- (4) A moderate block fuel penalty at the basic design range of 12 038 km (6500 n mi).

### 5.2.2 Parametric Results

#### 5.2.2.1 Wing Geometry

The important constraints for aircraft sized in this phase of the studies proved to be:

- (1) Wing volume available for fuel and LFC ducting.
- (2) The FAA field length limit of 3048 m (10 000 ft).

Adequacy of the available fuel volume is best judged by examining the parameter "fuel volume ratio" for each aircraft sized. This parameter is the ratio of available fuel volume to that required to fly the 12 038 km (6500 n mi) mission with fuel reserves at constant altitude carrying 400 passengers. Since the LFC duct volume required was not precisely known at the time the parametric studies were begun, a FVR (fuel volume ratio) of 1.1 was chosen as a constraint to allow for a possible increase of required suction duct volume after more detailed analysis. Figure 7 gives FVR results for the basic matrix of aircraft sized for a cruise altitude of 12 192 m (40 000 ft) and a cruise Mach number of 0.80. The FAA field length limit is superimposed to complete delineation of a boundary which defines wing loading/aspect ratio combinations which are excluded from consideration because of FVR and field length constraints. High wing loading and high aspect ratio are usually desirable for long-range aircraft from both a fuel usage and DOC standpoint. The optimum aircraft from this matrix thus might be expected to lie somewhere on the combined constraint boundary line.

Figure 8 presents matrix results for FAA field lengths which were used in determining the field length constraint line for Figure 7. Note that for the constant cruise power ratio of 0.85 shown for the basic matrix, almost all aircraft not constrained by the fuel volume limit have field lengths less than the constraint of 3048 m (10 000 ft). Further refinement might therefore indicate that engine size could be slightly reduced, thus increasing cruise power setting to higher than 85%.

Figure 9 shows that the best DOC point does lie along the fuel/field length limit line at the intersection of the two limits. This intersection defines a tentative baseline selection with the following parameters:

Cruise power ratio, $\eta_{CR}$	= 0.85
Engine bypass ratio	= 8.4
DOC	= .922 ¢/skm (1.485 ¢/ssm)
Aspect ratio	= 12.7
Wing loading	= 552 kg/m <sup>2</sup> (113 lb/ft <sup>2</sup> )

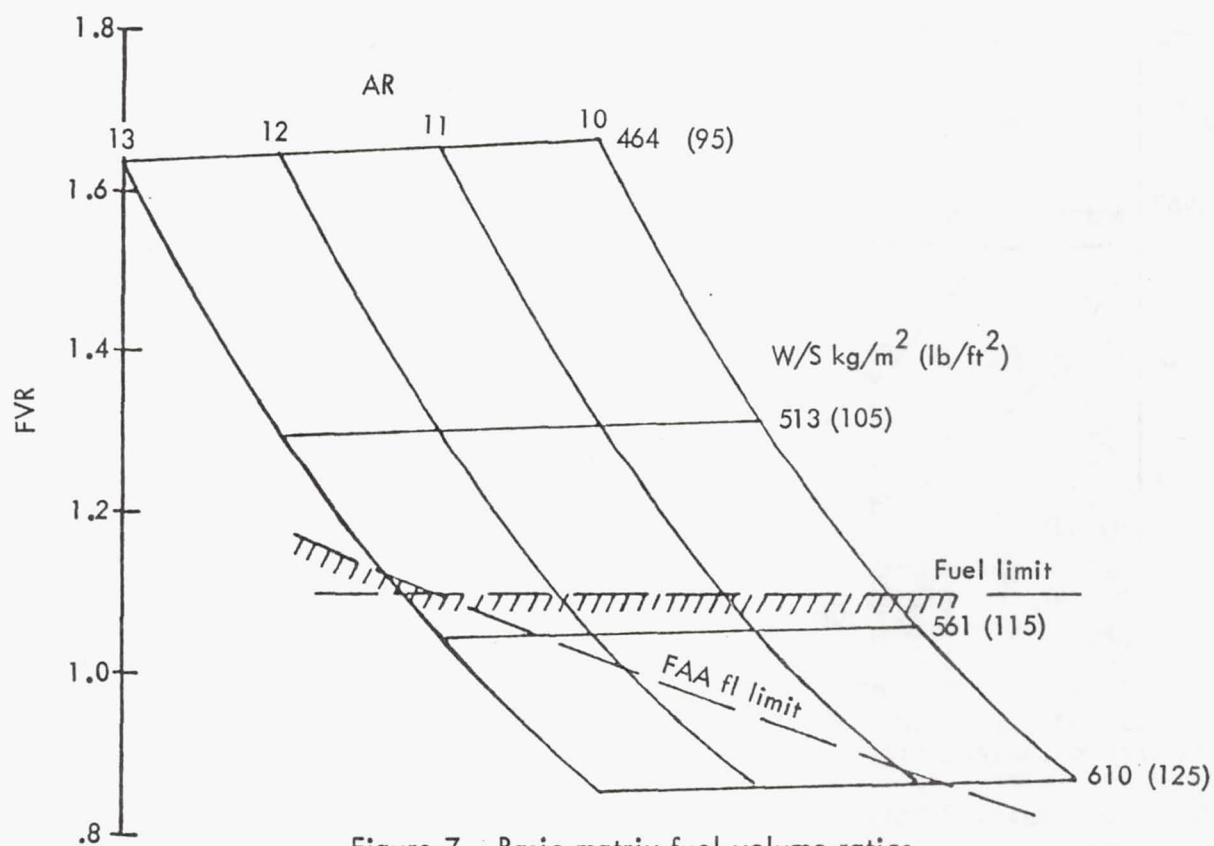


Figure 7. Basic matrix fuel volume ratios

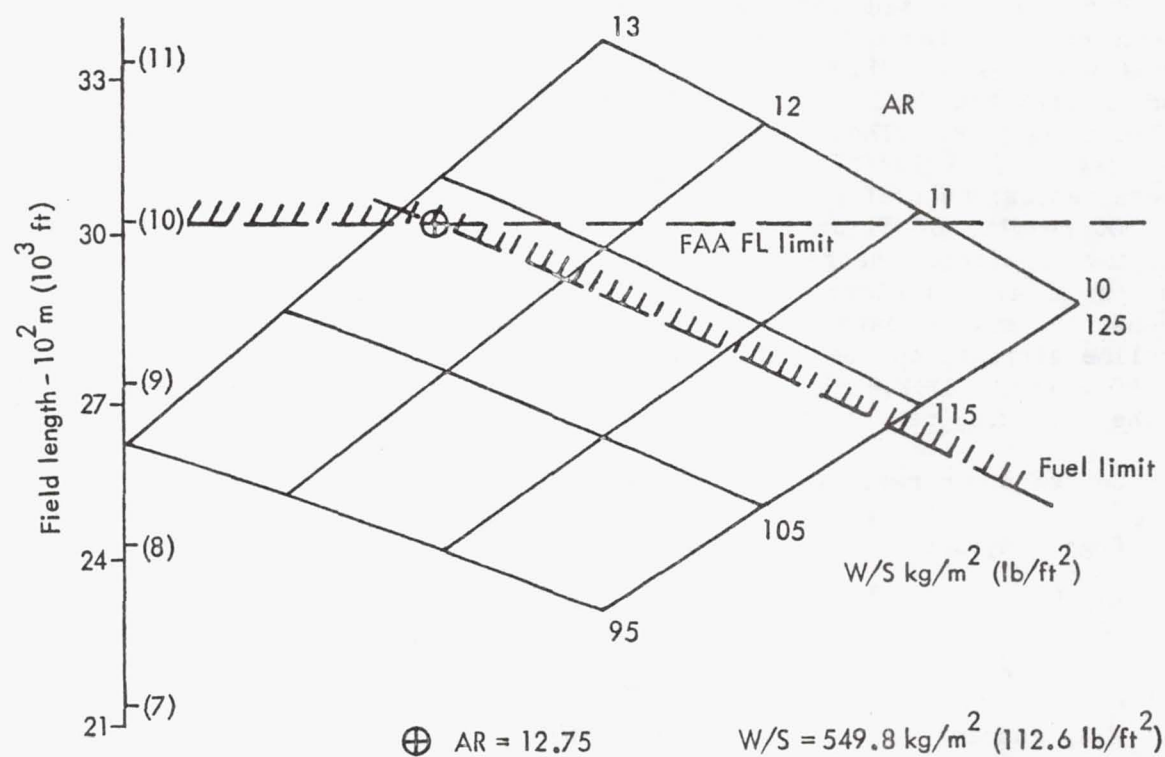


Figure 8. FAA field lengths for initial configuration basic matrix



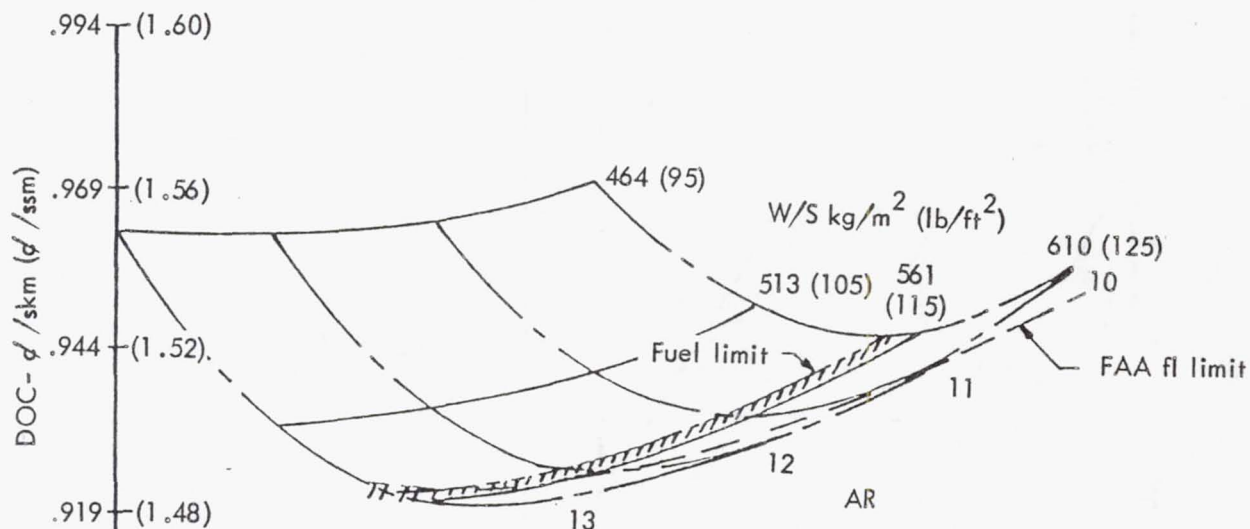


Figure 9. Basic matrix DOC values

Figure 9 also shows that only small penalties in DOC occur at lower aspect ratio to 11.6. Therefore, 11.6 was chosen as the aspect ratio for further baseline refinement.

#### 5.2.2.2 Engine Parameters

For the selected geometry, parametric configuration variations were conducted to evaluate changes in engine bypass ratio, cruise power ratio, and aspect ratio. Figure 10 presents FAA field length data for these studies with the fuel volume limit line superimposed to define the area of excluded options. These studies were run at a constant wing loading of  $551.7 \text{ kg/m}^2$  ( $113 \text{ lb/ft}^2$ ) and aspect ratio of 11.6. Note that the higher bypass ratios are preferred for this wing loading/aspect ratio combination. The DOC results of Figure 11 indicate that if the fuel line were ignored, implying a slight change in wing loading, a bypass ratio of 8.4 would produce a near minimum DOC. Since the engine for generation of all parametric engine data has this bypass ratio, it was chosen for the baseline aircraft in the example case. A slight adjustment of wing loading to  $549.2 \text{ kg/m}^2$  ( $112.5 \text{ lb/ft}^2$ ) produced sufficient fuel volume and results in the following new parameters for the tentative baseline:

Cruise power ratio, $\eta_{CR}$	= 0.88
Engine bypass ratio	= 8.4
DOC	= .922 d/skm (1.485 d/ssm)
Aspect ratio	= 11.6
Wing loading	= $549.2 \text{ kg/m}^2$ ( $112.5 \text{ lb/ft}^2$ )

The DOC value is equal to the value previously determined for an aircraft with an aspect ratio of 12.7.

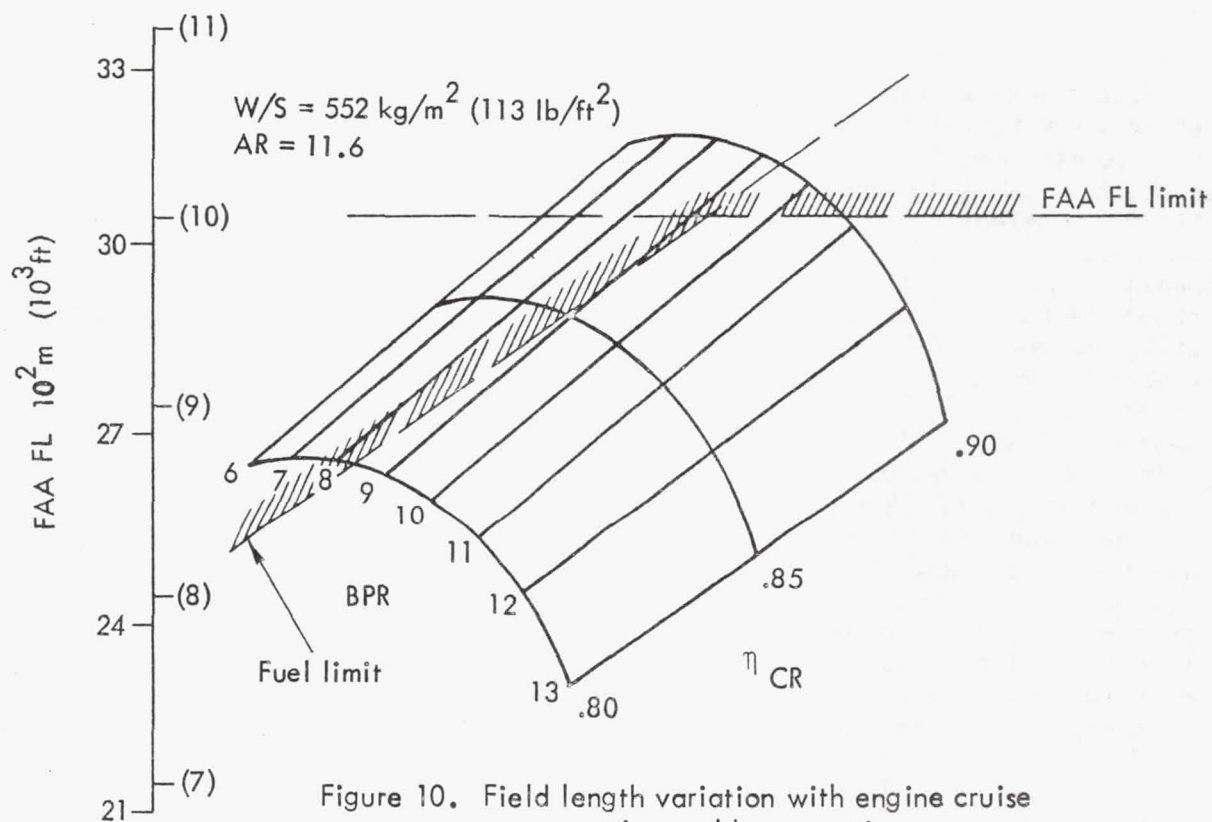


Figure 10. Field length variation with engine cruise power setting and bypass ratio

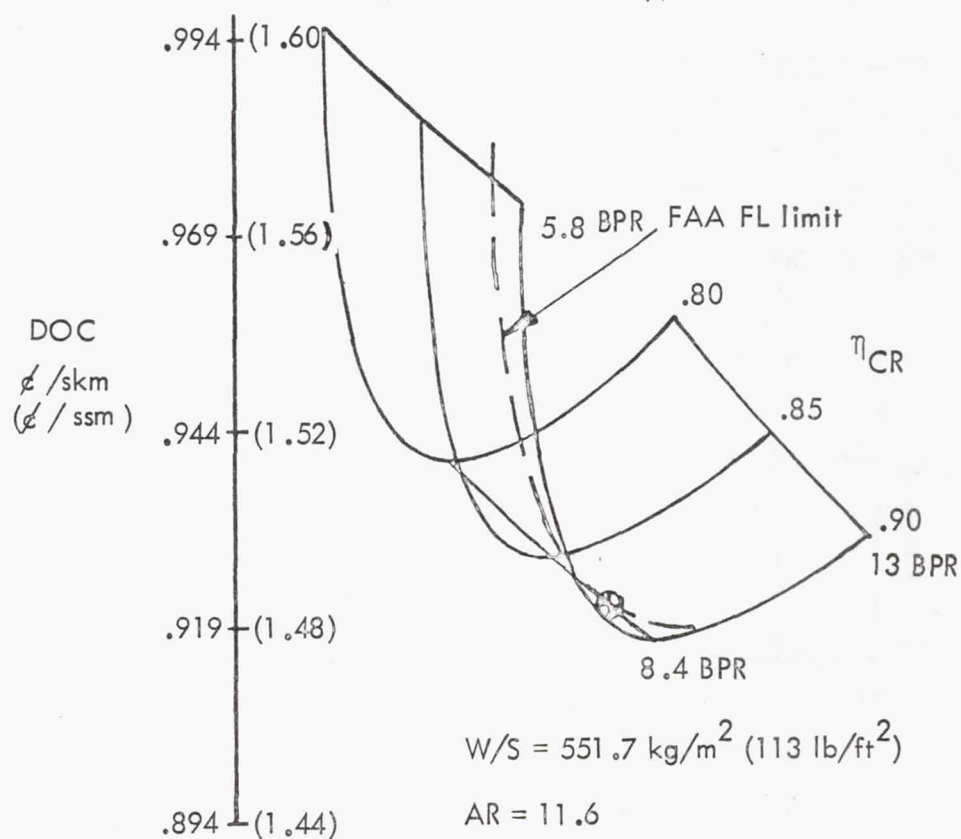


Figure 11. DOC variation with engine cruise power setting and bypass ratio

With the new tentative baseline, wing loading, aspect ratio and power setting were varied to define configurations meeting both fuel volume and field length requirements. Bypass ratio was held constant for these variations. Results presented in Figure 12 demonstrate that the aspect ratio 11.6 selection is a near-optimum choice for the DOC criterion and also meets the criterion for moderate aspect ratio. Note that at approximately  $AR = 11$  the cruise power ratio limit of 0.90 is reached and further reductions in aspect ratio are now accompanied by engine power setting increases. This factor is significant in the increase of DOC noted for aspect ratios less than 11. The wing-fuel-only criterion has obviously been satisfied leaving only the question of block fuel performance to be answered. Figure 13 shows that, as might be suspected, the optimum DOC choice is not the optimum choice from a fuel usage viewpoint. Selection of an aspect ratio of 14 rather than 11.6 would result in a fuel savings of 6%. The technical risks of such a choice would be considerably greater, however, and the small portion of total flights to be flown at the maximum range with full passenger payload does not in itself justify choosing aspect ratio = 14. At least for initial phases of the present studies, it was considered best to start with a lower-risk baseline choice of moderate aspect ratio and determine by future baseline perturbations if the higher aspect ratios are feasible. The tentative baseline selection noted by the

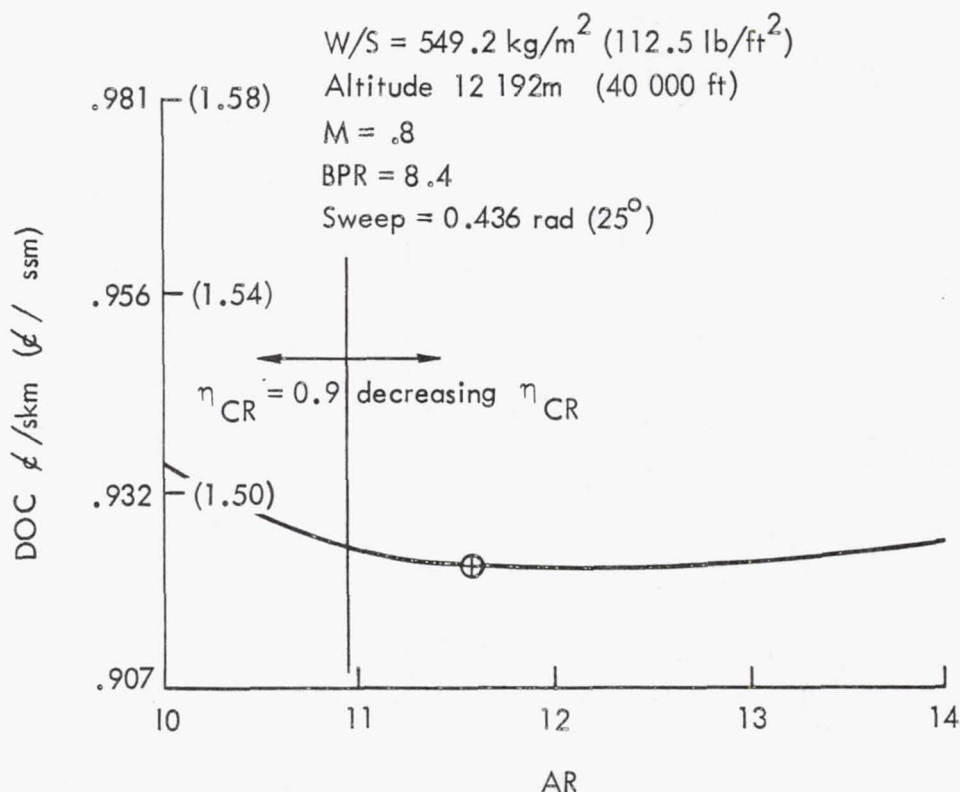


Figure 12. DOC sensitivity to change in aspect ratio

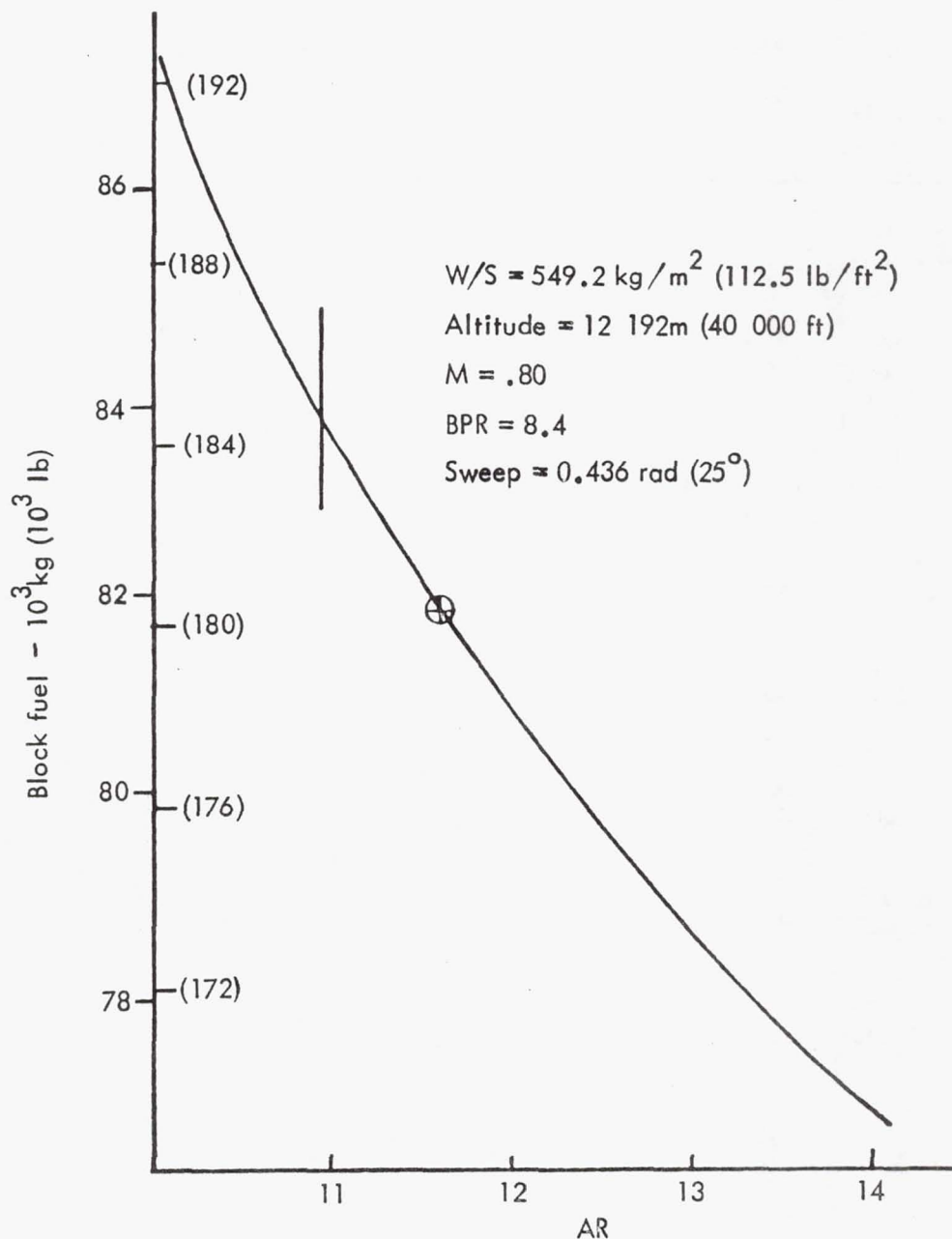


Figure 13. Block fuel sensitivity to aspect ratio

symbol in Figures 12 and 13 was confirmed as the baseline candidate for a cruise Mach number of 0.80 and altitude of 12 192 m (40 000 ft).

### 5.2.3 Configuration Selection

The process just described was conducted for ten other cruise Mach number/altitude combinations selected from the baseline matrix. The summary results of optimization for all eleven combinations is presented in Table 7.



TABLE 7. BASELINE CANDIDATES

Set	Altitude m (ft)	M	$\eta_{CR}$	BPR	DOC $\phi/skm$ ( $\phi/ssm$ )	AR	W/S $kg/m^2$ ( $lb/ft^2$ )
1	12 192 (40 000)	.70	.90	8.40	.961 (1.547)	13.00	571.2 (117.0)
2	12 192 (40,000)	.75	.90	8.40	.936 (1.508)	12.30	556.5 (114.0)
3	12 192 (40 000)	.80	.88	8.40	.922 (1.485)	11.60	549.2 (112.5)
4	12 192 (40 000)	.85	.89	8.40	.916 (1.475)	10.50	541.4 (110.9)
5	10 973 (36 000)	.70	.71	8.40	.936 (1.508)	13.00	610.2 (125.0)
6	10 973 (36 000)	.75	.71	8.40	.920 (1.482)	11.80	585.8 (120.0)
7	10 973 (36 000)	.80	.71	8.40	.911 (1.467)	10.90	576.1 (118.0)
8	10 973 (36 000)	.85	.73	8.40	.905 (1.458)	9.50	571.2 (117.0)
9	13 411 (44 000)	.75	.90	8.40	.999 (1.608)	14.00	524.8 (107.5)
10	13 411 (44 000)	.80	.90	8.40	.990 (1.594)	14.00	518.3 (106.2)
11	13 411 (44 000)	.85	.90	8.40	.997 (1.606)	13.00	516.0 (105.7)

In order to provide better visualization of the results of Table 7, DOC was plotted versus cruise Mach number for various altitudes and is presented in Figure 14, which shows that between  $M = 0.75$  and  $M = 0.85$ , DOC varies less than  $0.019 \phi/skm$  ( $0.03 \phi/ssm$ ) for the two lowest altitudes.

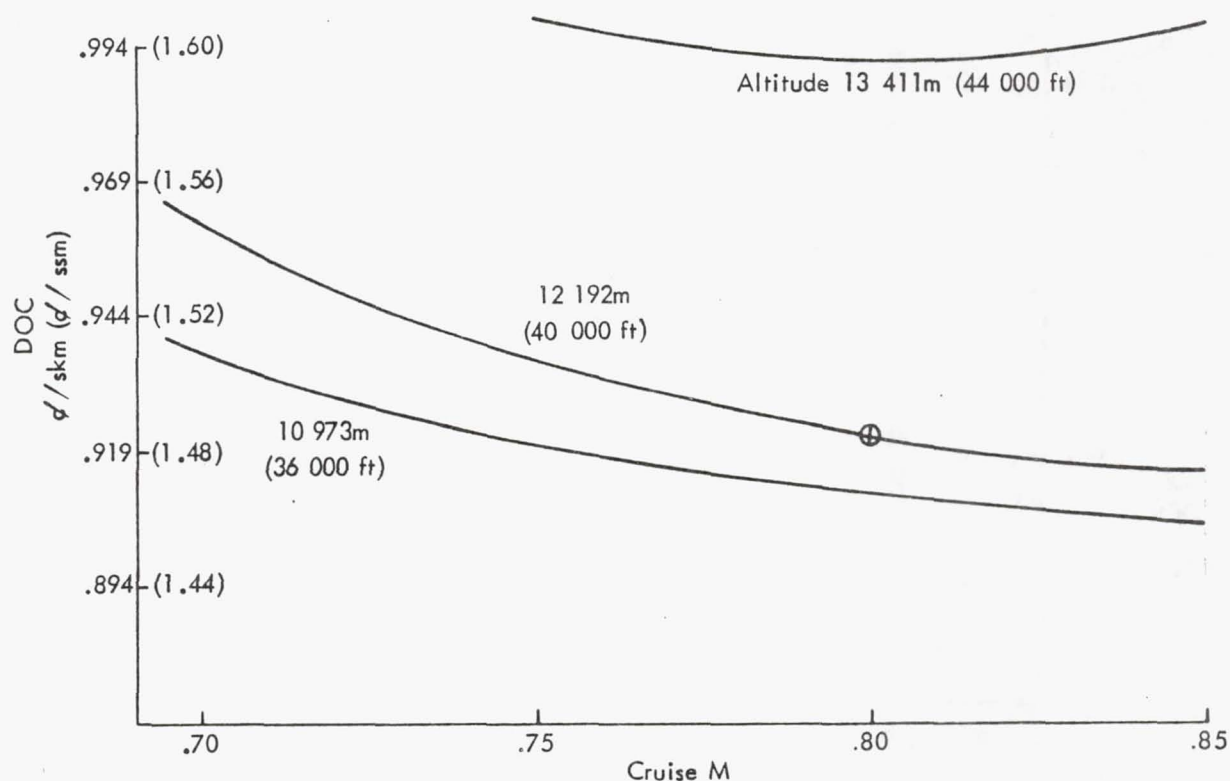


Figure 14. Variation of DOC with cruise M

The leading-edge sweep angle of 0.436 rad (25 deg) associated with  $M = 0.80$  is less critical from a leading-edge contamination standpoint than the sweep of .549 rad (31.5 deg) associated with  $M = 0.85$ . For this reason and others associated with the more severe design problems associated with compressibility effects, a cruise  $M = 0.80$  appears to be a good choice for the baseline aircraft.

The DOC advantage of the 10 973 m (36 000 ft) cruise altitude is also less than 0.019 d/skm (0.03 d/ssm) as compared to the 12 192 m (40 000 ft) cruise altitude for the range of cruise M considered. However, as illustrated by Figure 15, higher altitudes suffer progressively greater DOC penalties. Since the lower unit Reynolds number associated with increasing altitude is beneficial to LFC because of its influence in reducing sensitivity to surface imperfections, an altitude of 12 192 m (40 000 ft) appears to be a reasonable compromise choice of altitude for the baseline aircraft.

The final selected baseline is thus the case previously described in detail and summarized by the row of data labeled Set 3 in Table 7.

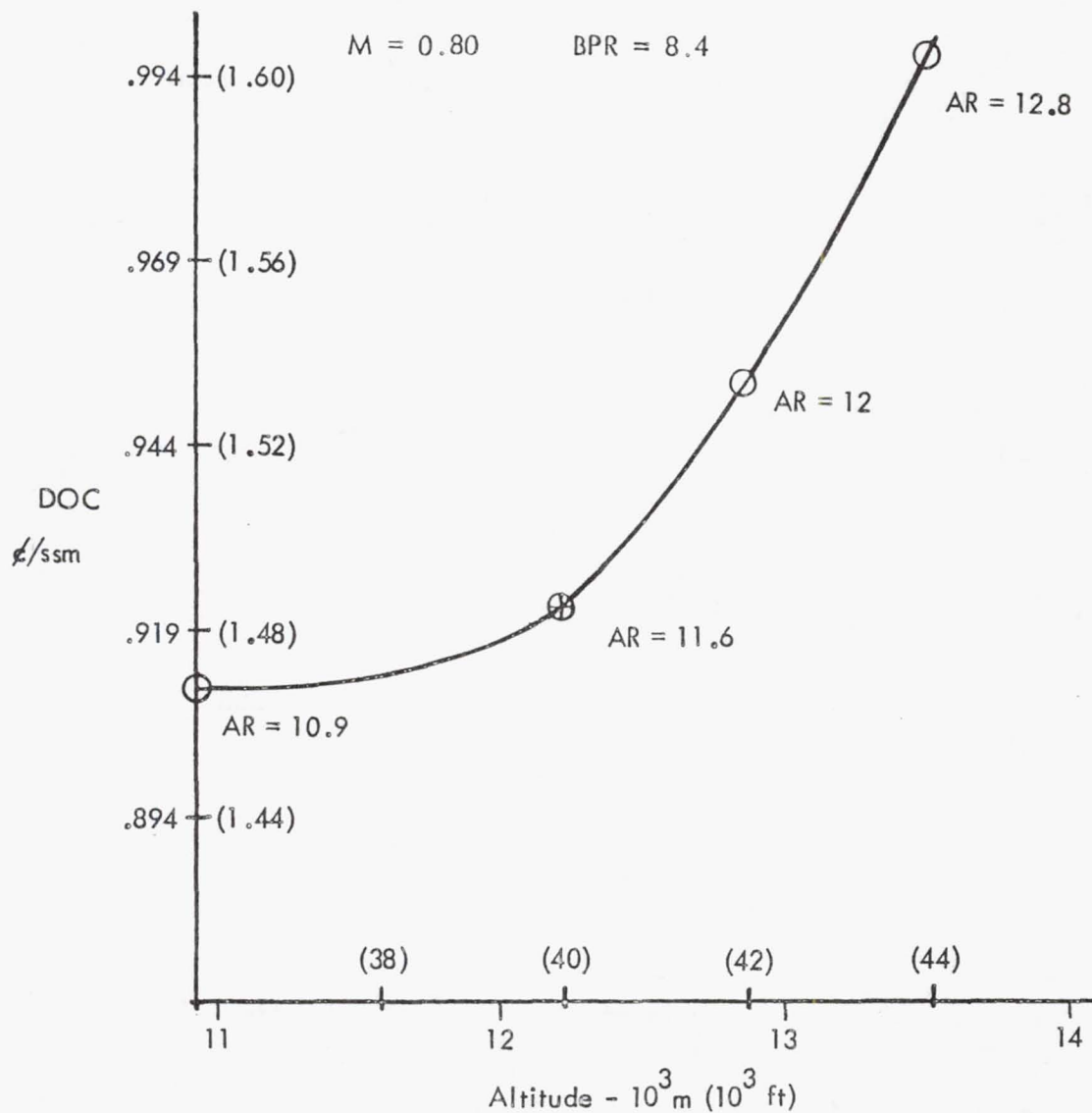
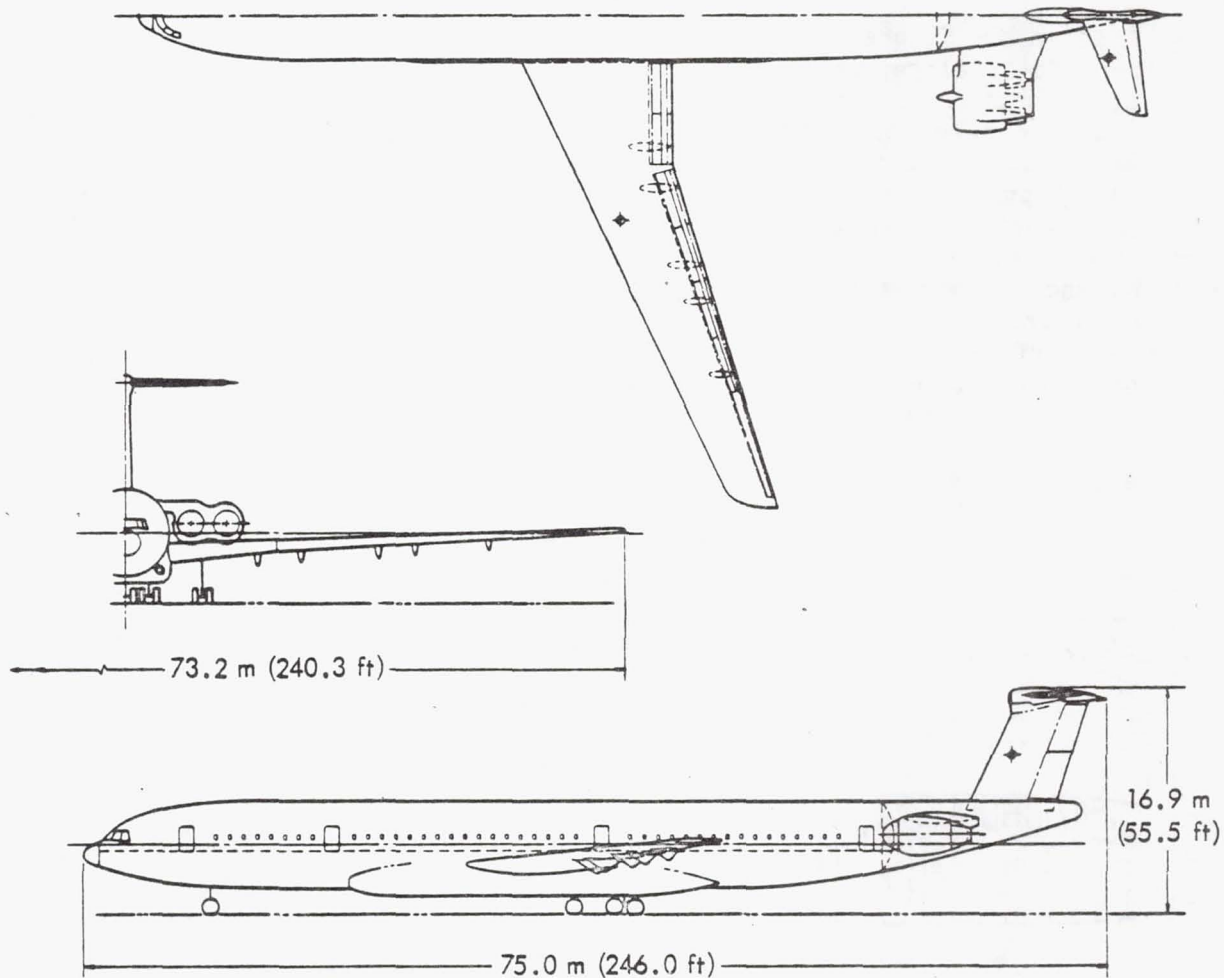


Figure 15. DOC variation with altitude

### 5.3 CONFIGURATION DEFINITION

The parametric configuration analyses of the preceding section establish a basis for the detailed development of a baseline LFC configuration and supporting systems. The baseline configuration described in this section was established as a point of departure for the evaluation of alternative LFC system concepts leading to the final study aircraft configuration.

The baseline LFC configuration is shown in Figure 16. This airplane is a wide-body configuration designed to carry 402 passengers and baggage over an intercontinental range of 12 038 km (6500 n mi) at  $M = 0.80$  with adequate fuel to account for adverse winds, intermittent LFC disruptions due to atmospheric conditions at cruise altitude, and normal international fuel reserves.



	Area	AR	Sweep	Taper
Wing (base)	$452.8 \text{ m}^2$ (4874.4 $\text{ft}^2$ )	11.60	L.E. .436 rad ( $25^\circ$ )	.350
Horizontal	$41.2 \text{ m}^2$ (443.9 $\text{ft}^2$ )	5.00	1/4 Ch .349 rad ( $20^\circ$ )	.400
Vertical	$50.0 \text{ m}^2$ (538.5 $\text{ft}^2$ )	1.50	1/4 Ch .436 rad ( $25^\circ$ )	.800
TOGW	257 174 kg (566 961 lb)			
Engine	151 kN (33 978 lb)			

Figure 16. General arrangement



A typical cabin arrangement, shown in Figure 17, was developed for the purpose of sizing the fuselage. This arrangement accommodates a 10/90 passenger mix, with 40 in first class and 362 in tourist class cabins. Space allowances are made for galleys, lavatories, closets, cabin crew provisions, and rest areas for flight crews as dictated by FAR Part 121.485 for flights of more than 12 hours duration. Space for LD-3 cargo containers is provided forward of the wing box and aft of the main landing gear bay. A bulk cargo bay is also provided at the rear of the pressurized belly. These cargo bays accommodate 16 874 kg (37 000 lb) of cargo.

As shown in Figure 16, the baseline is a low-wing T-tail monoplane with four aft-fuselage mounted propulsion engines. An independently-driven LFC suction unit is located in a fairing under each wing root. The wing has a moderate sweep of  $0.436 \text{ rad}$  ( $25^\circ$ ) at the leading edge with an aspect ratio of 11.6. Full-span flaps, including drooped ailerons, provide the required airport performance. Leading-edge high-lift devices are not required. Partial span spoilers are incorporated. Small-chord secondary flaps incorporated into the main flaps provide upper-surface pressure gradient and shock position control for off-design operation and serve as active controls to minimize structural requirements. The wing and empennage surfaces are laminarized to 75% and 65% chord, respectively. A combination cleaning/deicing system is incorporated in the leading-edge region of laminarized surfaces.

Table 8 summarizes the characteristics of the baseline configuration.

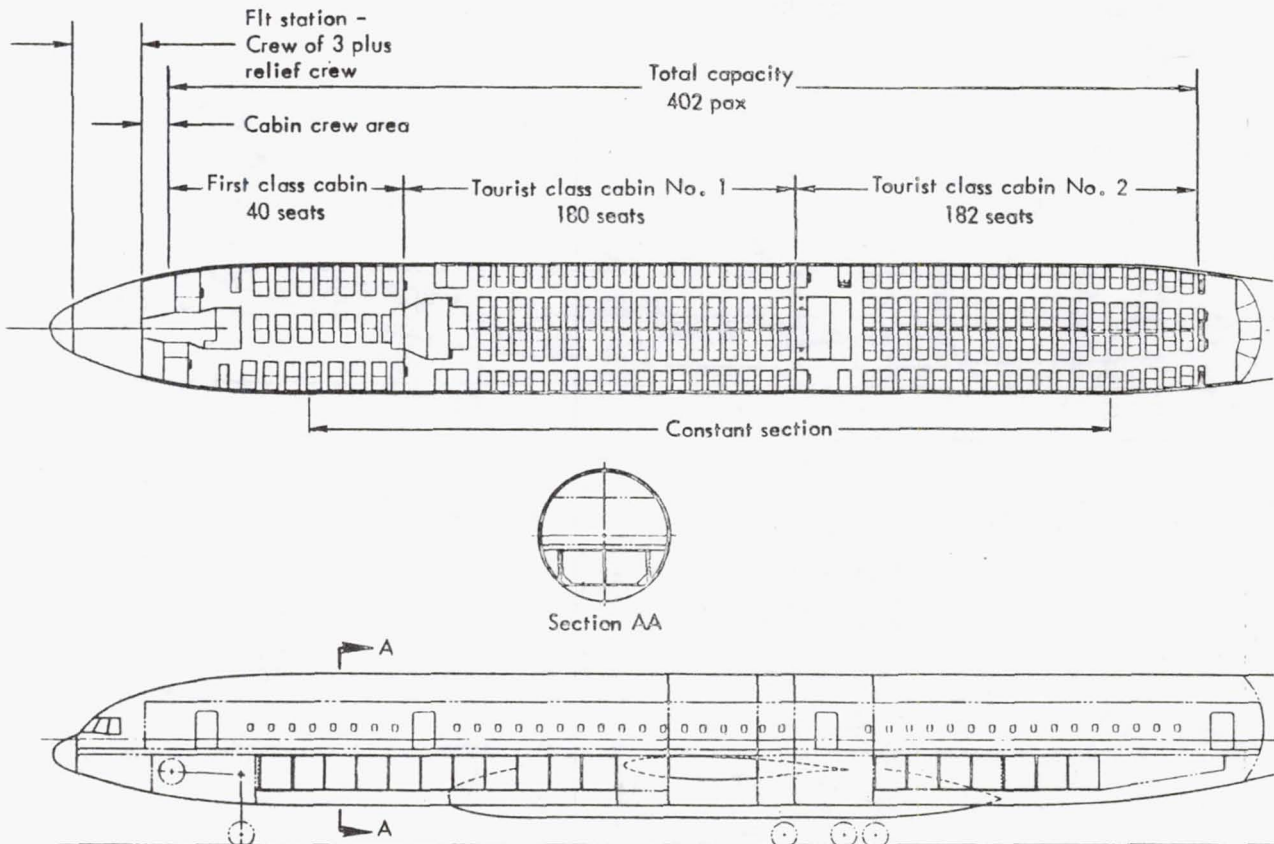


Figure 17. Inboard profile

TABLE 8. BASELINE CONFIGURATION CHARACTERISTICS

<u>Item</u>	<u>Value</u>	
Gross Weight	257 174 kg	(566 961 lb)
Operating Weight	124 054 kg	(273 488 lb)
Block Fuel	80 213 kg	(176 837 lb)
Reserve Fuel	14 441 kg	( 31 836 lb)
Wing Area	452.8m <sup>2</sup>	(4874 ft <sup>2</sup> )
Aspect Ratio		11.6
Thickness Ratio		0.122
L. E. Sweep	.436 rad	(25°)
Horizontal Tail Area	41.2m <sup>2</sup>	(444 ft <sup>2</sup> )
Vertical Tail Area	50.0m <sup>2</sup>	(539 ft <sup>2</sup> )
Body Length/Diameter	75.0m/6.45m	(246 ft/254 in)
Engines (4-STF477)-SLST	151 kN	( 33 978 lb)
OW/GW		0.482
Payload/GW		0.150
T/W		0.230
W/S	566.3 kg/m <sup>2</sup>	(116 lb/ft <sup>2</sup> )
TOFL	3046.5m	(9995 ft)
V <sub>APP</sub>	264.8 km/hr	(143 kn)

## 6.0 CONCEPT EVALUATION

The predominant effort in this study was devoted to the evaluation of options available for the design and development of future LFC commercial transport aircraft. The evaluation of these options included analytical investigations, design studies, and subsystem testing to evaluate alternative concepts in the following areas:

- (1) Aerodynamics
- (2) Structures and materials
- (3) Suction systems
- (4) Leading-edge region cleaning
- (5) Integration of auxiliary systems

This section summarizes the results of these concept evaluation activities and defines the characteristics of systems selected for integration into the final study configuration.

### 6.1 AERODYNAMICS

#### 6.1.1 Design Objectives

The aerodynamic design objectives for the LFC aircraft wing were:

- (1) Low shock loss and minimum drag
- (2) Straight isobars for wing
- (3) Low cross-flow except near wing leading edge
- (4) Low attachment line Reynolds number ( $R_{\theta_{a.l.}}$ ) values
- (5) Minimum overall suction level
- (6) Good off-design performance
- (7) Good LFC-off performance
- (8) Adequate aircraft maneuverability
- (9) Adequate high-lift performance without leading-edge devices.

#### 6.1.2 Airfoil/Boundary Layer Analysis

Initially, this section on airfoil analysis and design describes the baseline airfoil developed as a part of the previous systems study of Reference 5. Subsequently, the initial design variations and problems encountered in the selection of an interim baseline airfoil are detailed. Next, crossflow stability studies which led to further airfoil changes are detailed. In conclusion, selection of the final baseline airfoil, designated AF11-12, is summarized.



#### 6.1.2.1 Definition of Original Baseline Airfoil

Design of an airfoil section for LFC application was initiated in the system study reported in Reference 5. This original airfoil and pressure distribution shown in Figure 18 exhibited some characteristics which were less than optimum, but formed an initial baseline for further development.

The original baseline airfoil was derived using totally subsonic theory and design point pressure distribution checked for the design point Mach number and lift using the transonic airfoil program (TAP) described in Reference 13. From these data, the following potential improvements were identified:

- (1) Aft movement of shock position and reduction of shock strength. Aft movement of the shock was essential since presence of the shock in a laminarized region might cause transition. Laminarization to at least 75% chord was desired, therefore a shock forward of this location would be undesirable, if not unacceptable. A reduction in shock strength on the initial airfoil was also required because the supercritical pressure and distribution on the baseline airfoil upper surface terminated in too strong a shock, particularly at the higher lift coefficients and higher Mach numbers. A reduction in shock strength also provided a more favorable distribution for the initially proposed chordwise ducting arrangement.
- (2) Refinement of secondary flap. Refinement of the active control secondary flap to provide pressure gradient and shock position control for off-design operation is an essential item to provide relatively stable laminar flow control during off-design operation over a range of altitudes, Mach numbers, and lift coefficients while providing good lift control capability for load alleviation and correction of adverse stability effects due to sudden de-laminarization.
- (3) Favorable pressure gradients for chordwise ducting.
- (4) Reduction of non-dimensional leading-edge radius.
- (5) Simplification of airfoil shape.

#### 6.1.2.2 Interim Baseline Airfoil

Considerable design and analysis effort was devoted toward establishing an interim airfoil which would incorporate the desired potential improvements identified for the original baseline airfoil. A number of design pressure distributions and wake profiles were tried in the Carlson design program (Ref. 14). The resulting airfoils generally exhibited undesirably thick trailing edges. Analyses required to decrease the trailing-edge thickness were performed and the resulting pressure distributions were calculated using the transonic airfoil program (TAP). Changes to the contour in the region of the shock were investigated, the airfoil was thinned by factoring the lower surface ordinates back to 90% chord and fairing into the existing airfoil contour, and finally, the upper surface leading edge was refaired. The airfoil, AF7C6-3B4, was chosen as the interim baseline LFC airfoil since it approximated the design pressure distribution and exhibited a fairly low shock strength. Figure 19 shows this interim airfoil and the resulting pressure distribution.



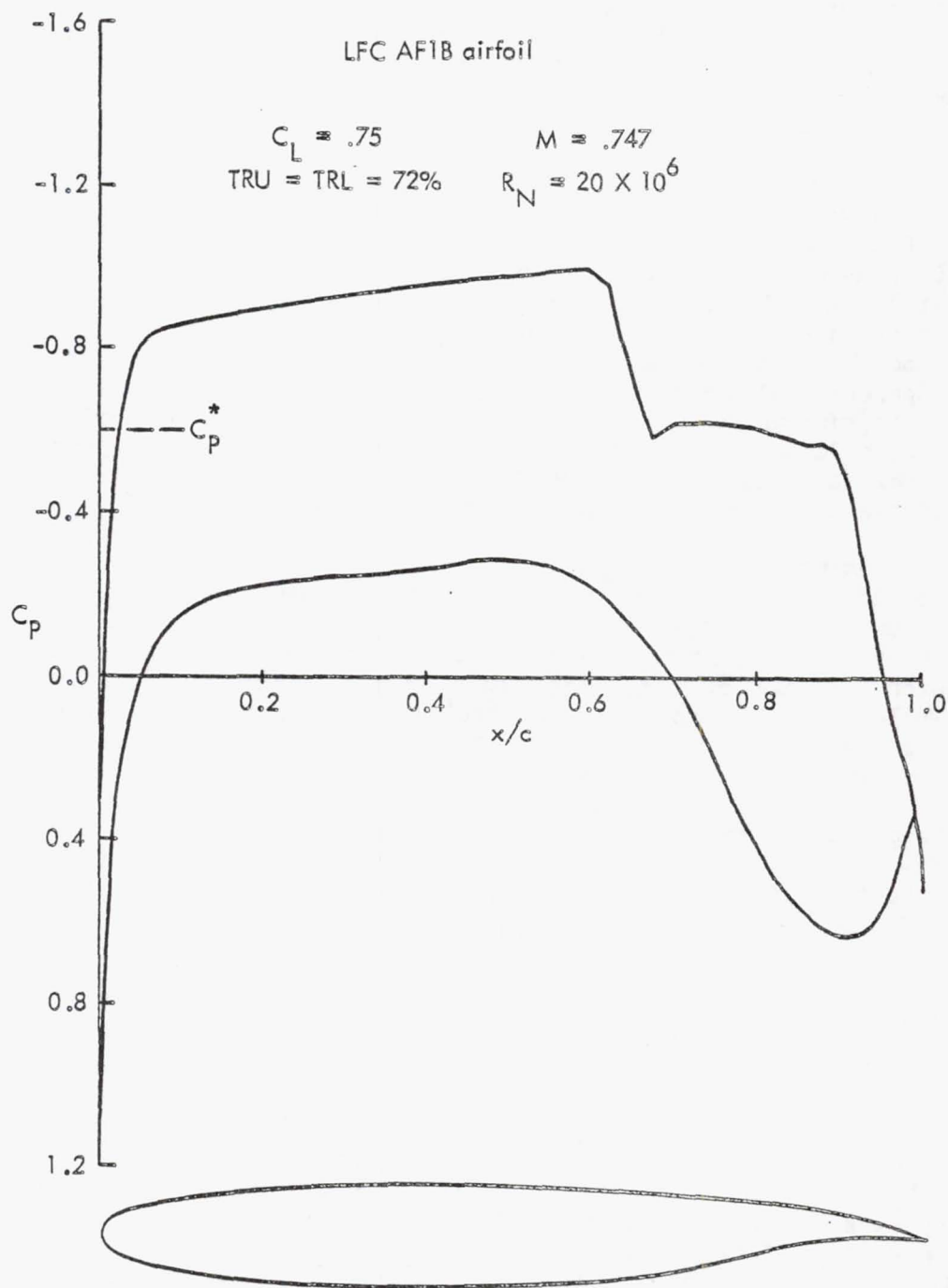


Figure 18. Original baseline Airfoil pressure distribution

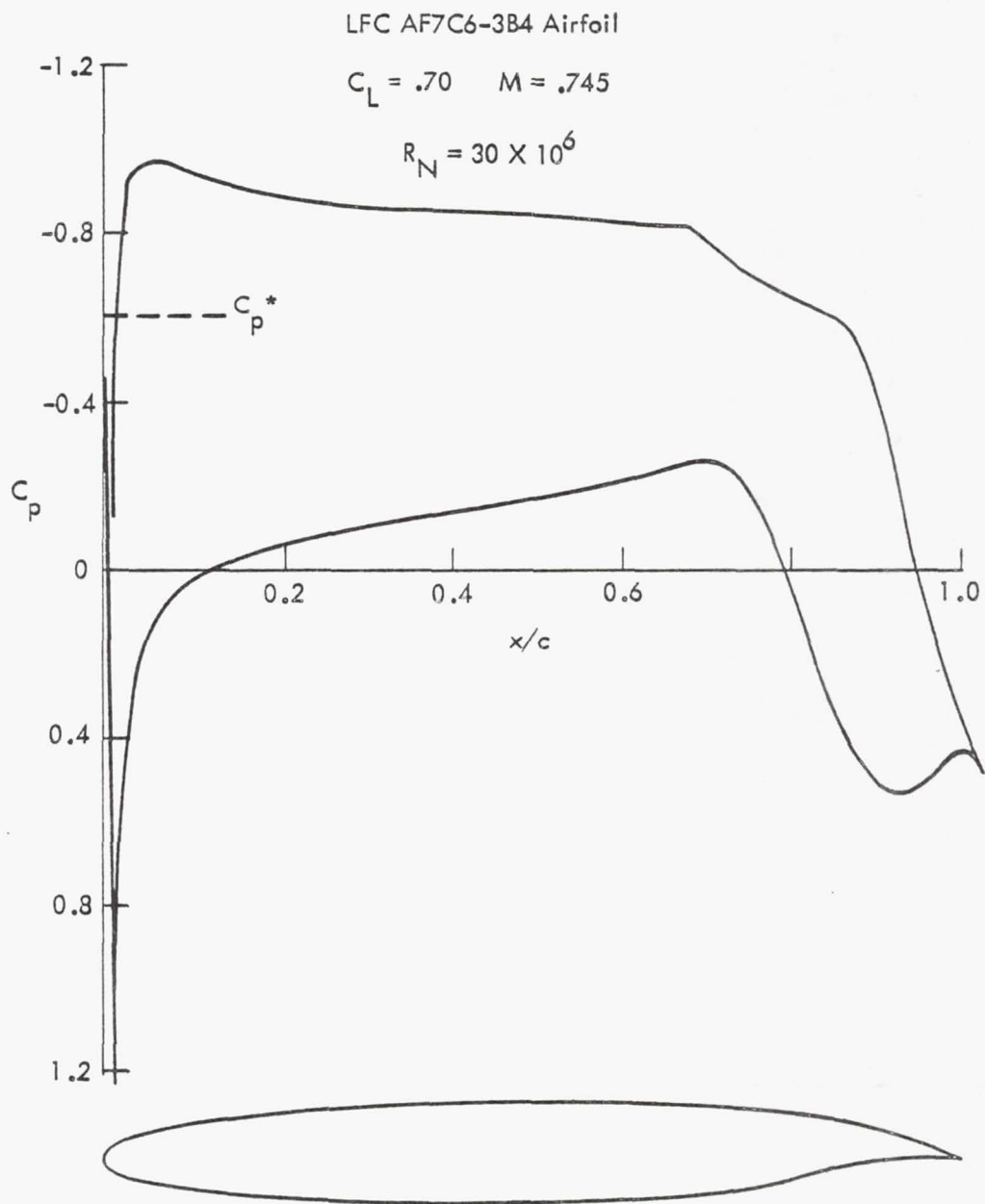


Figure 19. Interim baseline Airfoil pressure distribution

### 6.1.2.3 Boundary Layer Analysis on Interim Baseline Airfoil

With the development of airfoil AF7C6-3B4, which produced the desired design pressure distribution, boundary layer studies were initiated. These studies utilized the Kaups/Cebeci boundary layer code of Reference 15 and the original Srokowski and Orszag stability code, "SALLY," Reference 16. The prime investigation concentrated on the effect of crossflow, but final checks were also made for Tollmien-Schlichting instability. Tollmien-Schlichting calculations were made using a stability code developed under Lockheed funding. All the calculations for the crossflow N factor were done for a frequency of 0.5 Hz. Calculations for Tollmien-Schlichting instability were done for frequencies ranging from 1000 to 8000 Hz.

The parametric mass flow distribution shown in Figure 20 was used in these calculations. The TAP 2-D pressure distributions and the effective airfoil contour were factored, using a modified simple sweep theory, for input into the boundary layer program.

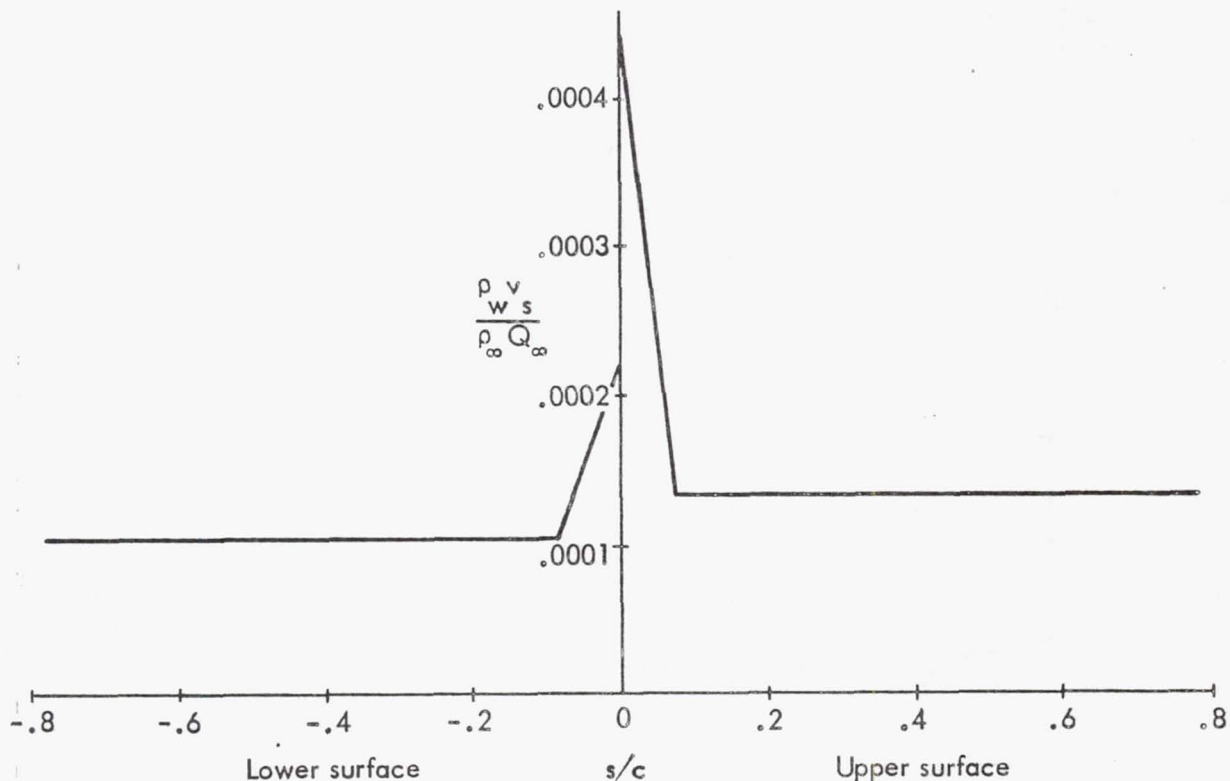


Figure 20. Parametric mass flow suction level

Shown in Figure 21 are three representative upper-surface pressure distributions for airfoil AF7C6-3B4. They are:

- (1) Basic distribution for  $C_L = 0.75$  at the nominal secondary flap setting of  $.035$  rad ( $2^\circ$ ).
- (2) The basic distribution altered to an unfavorable gradient over most of the chord while maintaining approximately the same lift.
- (3) A distribution for  $C_L = 0.40$  with a secondary flap setting of  $-.070$  rad ( $-4^\circ$ ). This is representative of an end-of-cruise condition.

As seen in Figure 22, none of these distributions exceed the acceptable disturbance N factor level of 11. A major effect noted is the correlation between the location on the airfoil where the pressure gradient reduces from the initial extremely negative gradient and the location where the disturbance N factor begins to level off from the initial steep rise. Thus the location at which the airfoil initial negative gradient is alleviated is a prime factor in determining where the rapid increase in the N factor is alleviated. This observation leads to the conclusion that very high initial flow acceleration from the stagnation point is particularly favorable for the baseline pressure distribution, a conclusion which appears to be true in the general case.

#### LFC AF7C6-3B4 Airfoil

$$M = .745$$

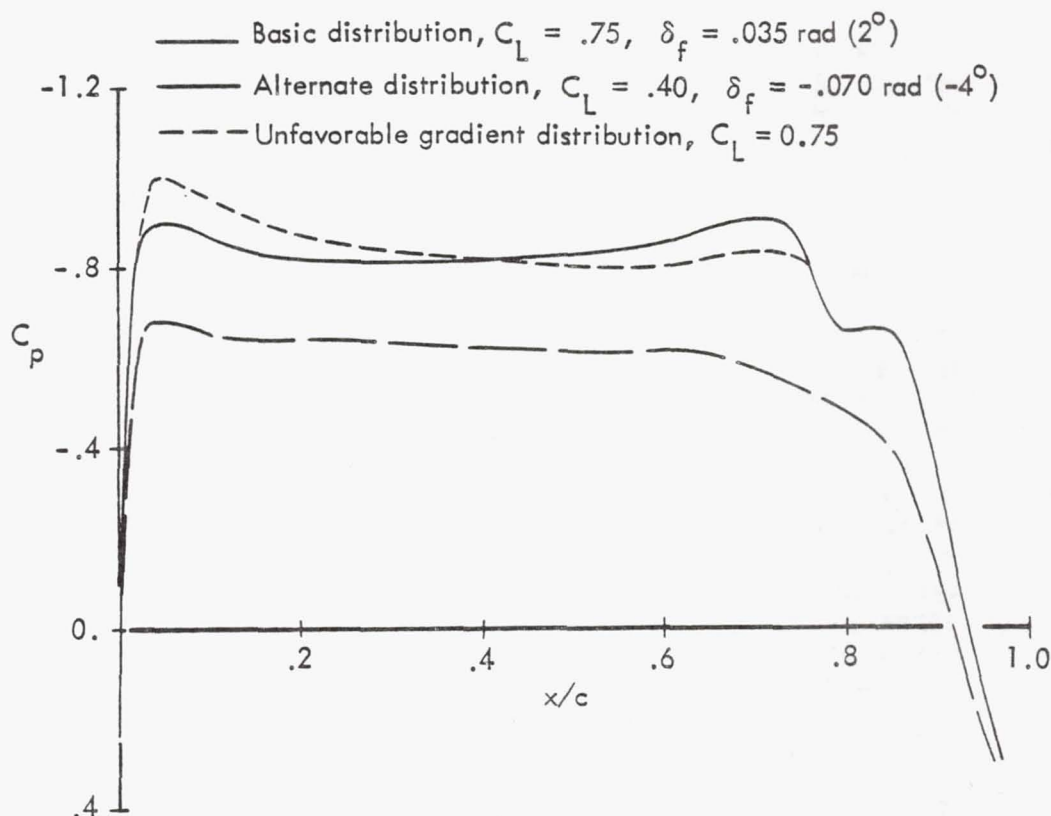


Figure 21. Upper surface pressure distribution



# LFC AF7C6-3B4 Airfoil

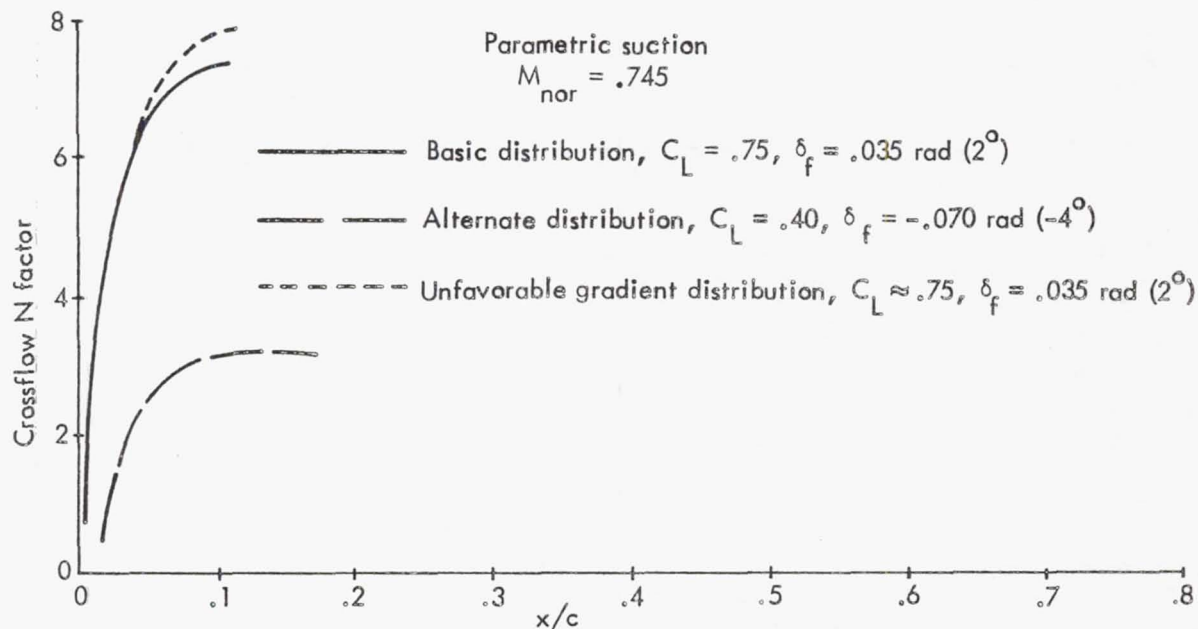


Figure 22. Upper surface disturbance crossflow N factors

When the sensitivity study on the lower surface began, it was immediately evident that the disturbance N factor level was far too high. The basic lower surface pressure distribution for  $C_L = 0.75$  and an alternate distribution for  $C_L = 0.40$  are presented in Figure 23. Figure 24 presents the N factors for both pressure distributions for parametric suction levels. The basic  $C_L = 0.75$  distribution has extremely high N factors, while the  $C_L = 0.40$  distribution is just above the acceptable level. This again demonstrates the trend observed on the upper surface that the sooner the leading edge negative pressure gradient is alleviated, the lower the N factor will be.

In order to prevent lower surface boundary layer instabilities from developing, it was necessary to find a way of reducing the lower surface disturbance N factor to an acceptable level, therefore a Lockheed computer program based on "a" mean-line theory was utilized to alter the lower surface contour. This airfoil, AF10-3, and the resulting surface pressure distributions are presented in Figure 25. The AF10-3 airfoil and pressure distribution, when analyzed with parametric suction levels, decreased the disturbance N factor from that for the AF7C6-3B4 airfoil, but a further decrease was needed. In order to decrease the N factor below the maximum acceptable level of 11, the lower-surface suction was increased as indicated in Figure 26. Sensitivity studies provided very acceptable guidelines in establishing the new suction distribution. The resulting crossflow disturbance N factor, for the upper and lower surfaces of airfoil AF10-3, are presented in Figure 27. These calculations were done for a frequency of 0.5 Hz, which has been shown to be critical for crossflow instabilities.

A study of Tollmien-Schlichting type instabilities for airfoil AF10-3 was performed using a stability code, similar to SALLY, developed at Lock-

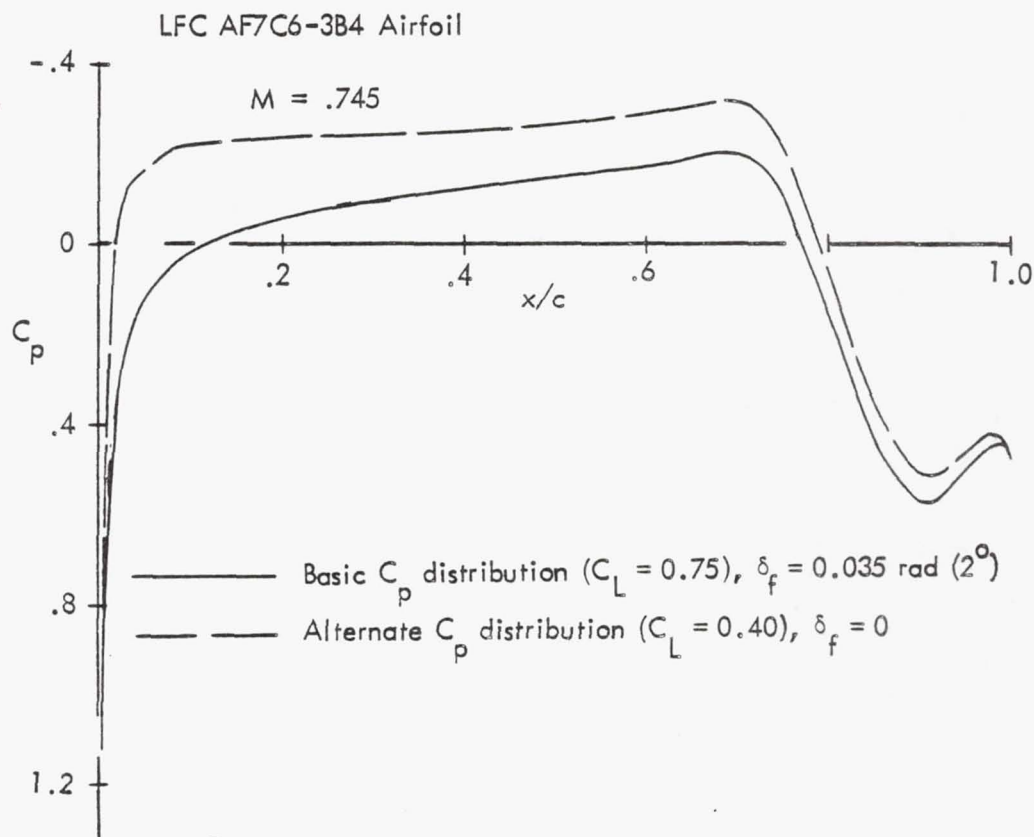


Figure 23. Lower surface pressure distributions

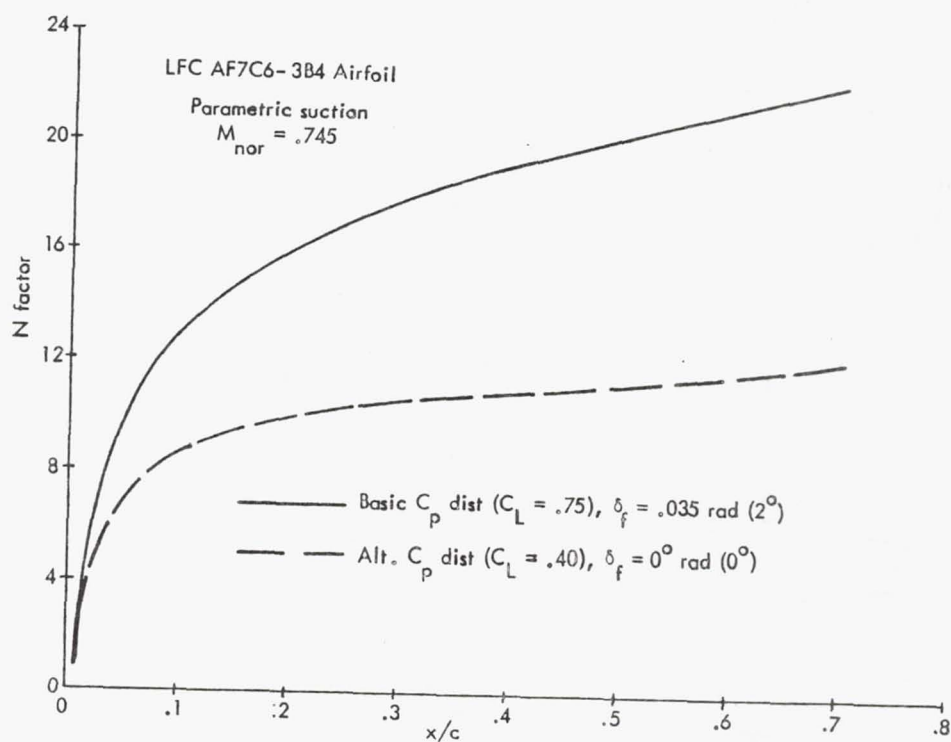


Figure 24. Lower surface disturbance N factors

LFC AF10-3 Airfoil

$$\delta_f = .035 \text{ rad } (2^\circ)$$

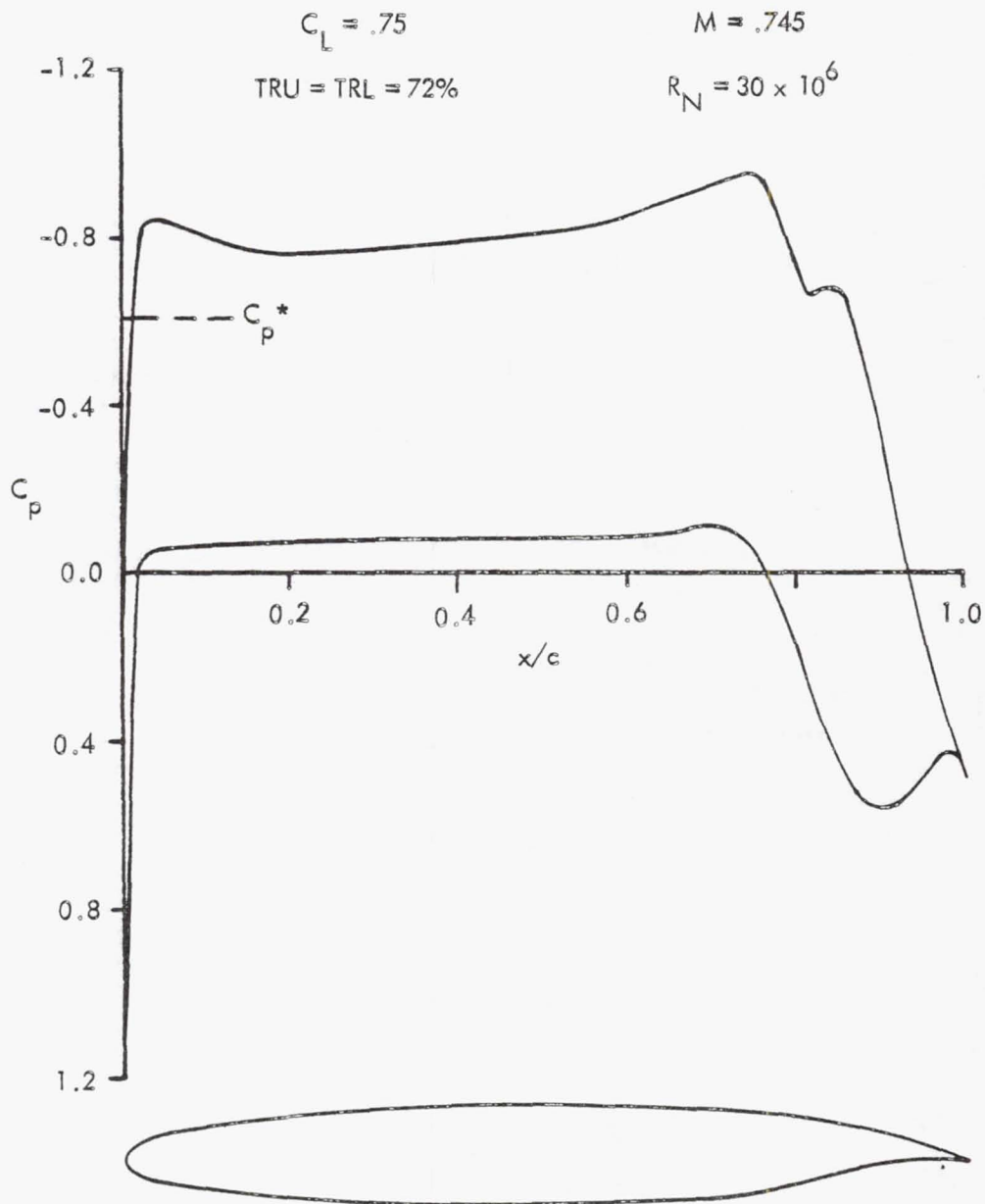


Figure 25. Interim Airfoil pressure distribution

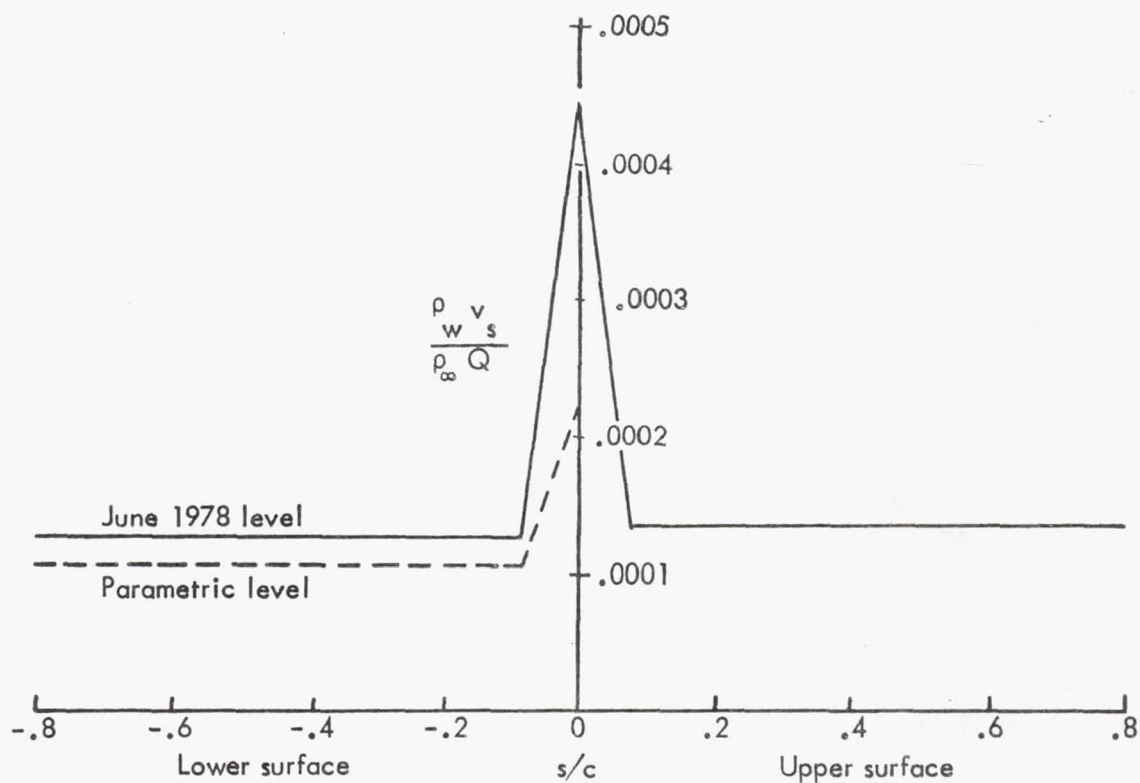


Figure 26. Mass flow suction level

LFC AF10-3 Airfoil

$$\delta_f = .035 \text{ rad } (2^\circ)$$

$$M_{\text{nor}} = 0.745 \quad R_N = 35 \times 10^6$$

June 1978 suction level

Disturbance frequency =  $0.5 \text{ Hz}$

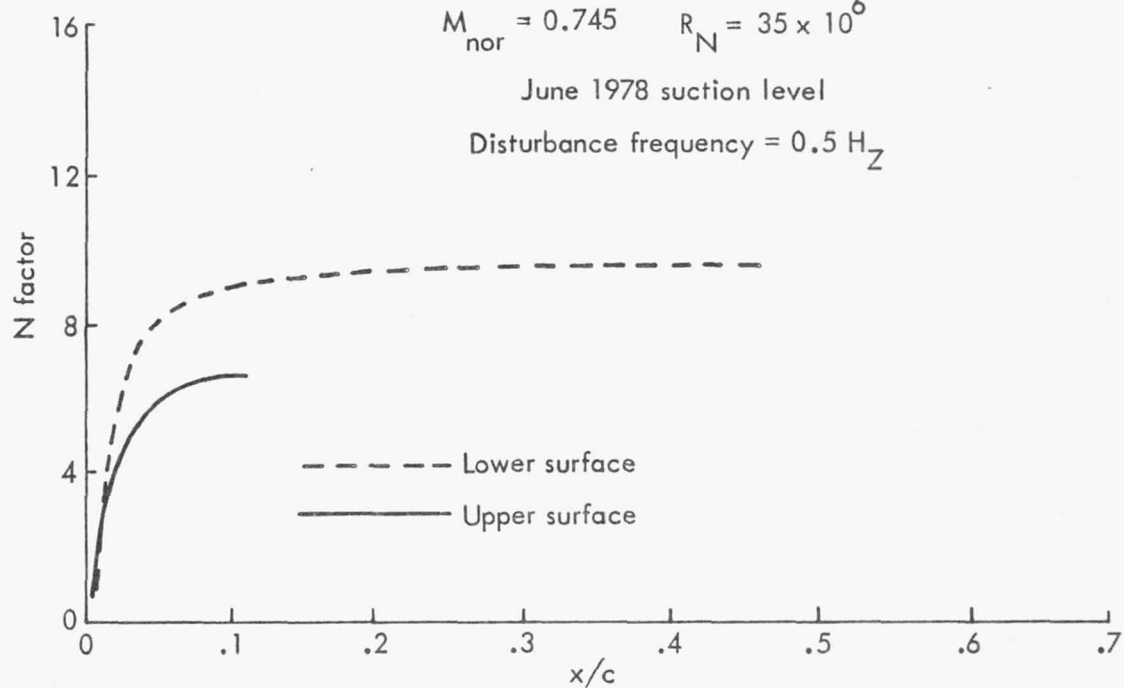


Figure 27. Crossflow disturbance N factor



heed. The results of this study indicated that there are no areas of instability over the lower surface for disturbance frequencies ranging from 1000 Hz to 8000 Hz. On the upper surface, for the same range of frequencies, only minimal effects were found. The largest N factor calculated was 2.6 at a frequency of 4500 Hz. Figure 28 presents the envelope of disturbance frequency influence for Tollmien-Schlichting instabilities.

AF10-3 airfoil thus has an acceptable pressure distribution and a moderate shock strength. This airfoil would have been chosen as the final baseline airfoil, but results from the LFC high-speed wind tunnel test, discussed in the next section, indicated that the aft pressure gradient should be reduced.

#### 6.1.2.4 Airfoil High-Speed Wind-Tunnel Testing

As part of Lockheed-funded research and development, a 2-D airfoil model was built and tested at high subsonic speeds in the Lockheed Compressible Flow Wind Tunnel. Model geometry was that of the LFC AF7C6-3B4 Airfoil described in Section 6.1.2.2. Although the airfoil was designed for the use of suction to maintain a laminar boundary layer, no provision for applying suction to the model was made. The model had a 17.78 cm (7 in) chord. Upper and lower surface pressure orifices were included to record pressure distributions. The 10% chord secondary flap had brackets to set deflections of 0, .035, .105, and  $-.070$  rad (0, 2, 6 and  $-4$  degrees). Figure 29 shows the model mounted in the tunnel.

The test objectives were to:

- (1) Obtain initial data on an advanced supercritical airfoil designed for laminar flow control.
- (2) Verify theoretical estimates of pressure distributions.
- (3) Establish whether steep adverse pressure gradients on the aft portion of the airfoil can be attained without causing excessive boundary layer thickness or flow separation problems.
- (4) Determine secondary control flap effectiveness.
- (5) Establish initial drag levels in the turbulent condition.

Test results indicated that:

- (1) TAP needs improvement for design work in the treatment of the relation of the 2-D section on an unswept, untapered planform to a more realistic case of flow over a 2-D section with an approximation of sweep and taper effects.
- (2) The airfoil trailing edge boundary layer is too thick.
- (3) Model contour problems exist at the joints.
- (4) The airfoil aft contour may need revision.

LFC AF10-3 Airfoil

Upper surface

$$\delta_f = .035 \text{ rad } (2^\circ)$$

Parametric suction

$$M_{\text{nor}} = .745$$

$$R_N = 35 \times 10^6$$

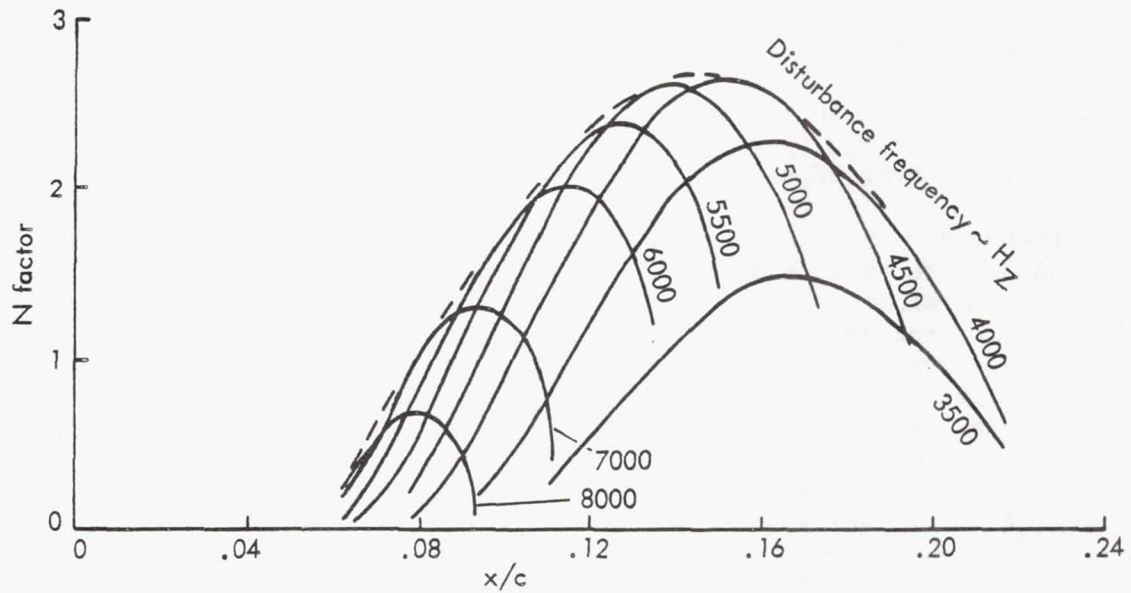


Figure 28. Tollmien-Schlichting instability envelope

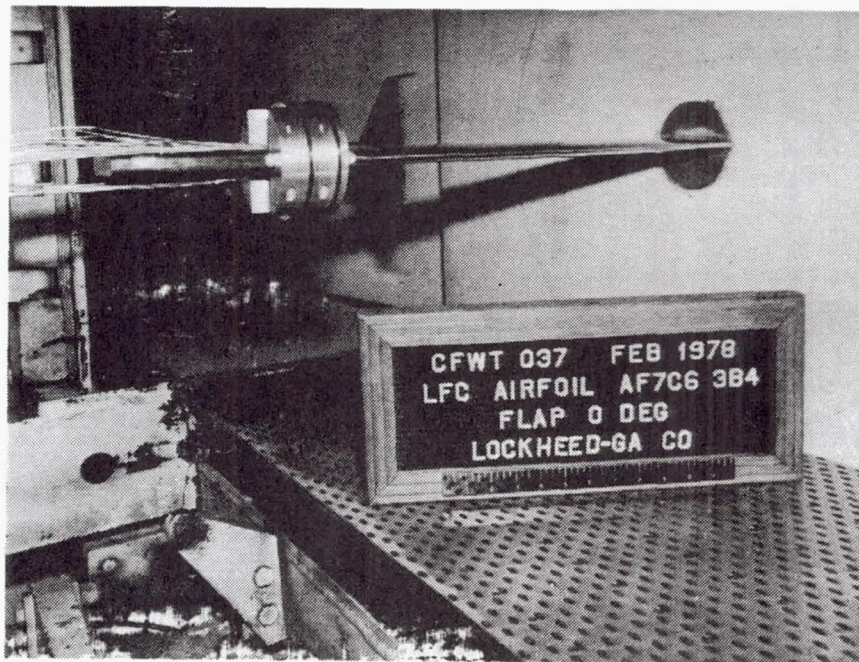


Figure 29. LFC 2-D wind tunnel model



#### 6.1.2.5 Final Baseline Airfoil Design and Boundary Layer Analysis

As a result of wind tunnel test results and additional analytical work, the following goals were established for the design of the final baseline airfoil:

- (1) Elimination of stagnation zone suction.
- (2) Adjustment of trailing edge pressure recovery.
- (3) Reduction of shock strength.
- (4) Refinement of secondary flap.
- (5) Adjustment of section shapes for 3-D wing design.

Stratford incipient separation pressure distributions (Ref. 17) were used as a guide to determine a reasonable design pressure distribution with a reduced gradient over the aft portion of the airfoil. Changes to the airfoil to produce the desired pressures were calculated using the "a" mean-line theory program. The deflection of the aft flap was then changed to alter the shock position and strength. These design changes were conducted with some doubt still remaining concerning the theoretical calculation of the boundary layer and pressure characteristics near the airfoil trailing edge. These design perturbations resulted in the final baseline airfoil AF11-12, which is shown in Figure 30. The design pressure distribution for this airfoil is shown in Figure 31. This pressure distribution does show some relief of the aft gradient and a reduction in the shock strength when compared to the interim airfoil pressure distribution shown in Figure 25.

For the boundary layer analysis calculations on the final baseline airfoil, the suction distribution was revised to eliminate suction near the airfoil nose. This revision was made to accommodate the leading-edge cleaning system. The revised suction distribution, referred to as the January 1979 suction, is compared to the June 1978 suction in Figure 32. Figure 33 presents a comparison of the lower surface N factors for the January 1979 suction with the N factors for the June 1978 suction and zero suction levels. It is evident that the January 1979 suction level results in an acceptable N factor level. The upper surface N factors for the January 1979 suction, which are shown in Figure 34, also have an acceptable level. Airfoil AF11-12 was thus chosen for the LFC baseline airfoil and meets the revised design goals listed in Section 6.1.2.5.

#### 6.1.3 Wing Analysis and Design

This section presents the design and analyses of the interim and final baseline LFC wing. Inviscid transonic solutions were obtained for the interim wing using the Bailey-Ballhaus 3 Transonic Wing Program (TWP)(Ref. 18). To approximate viscous effects, the final baseline wing was lofted using "fluid" sections. A "fluid airfoil" is formed by the addition of the boundary-layer displacement thickness to the basic airfoil ordinates. This loft was based on airfoil AF10-3, since the AF11-12 section was developed subsequent to the time at which the final baseline wing was analyzed. The

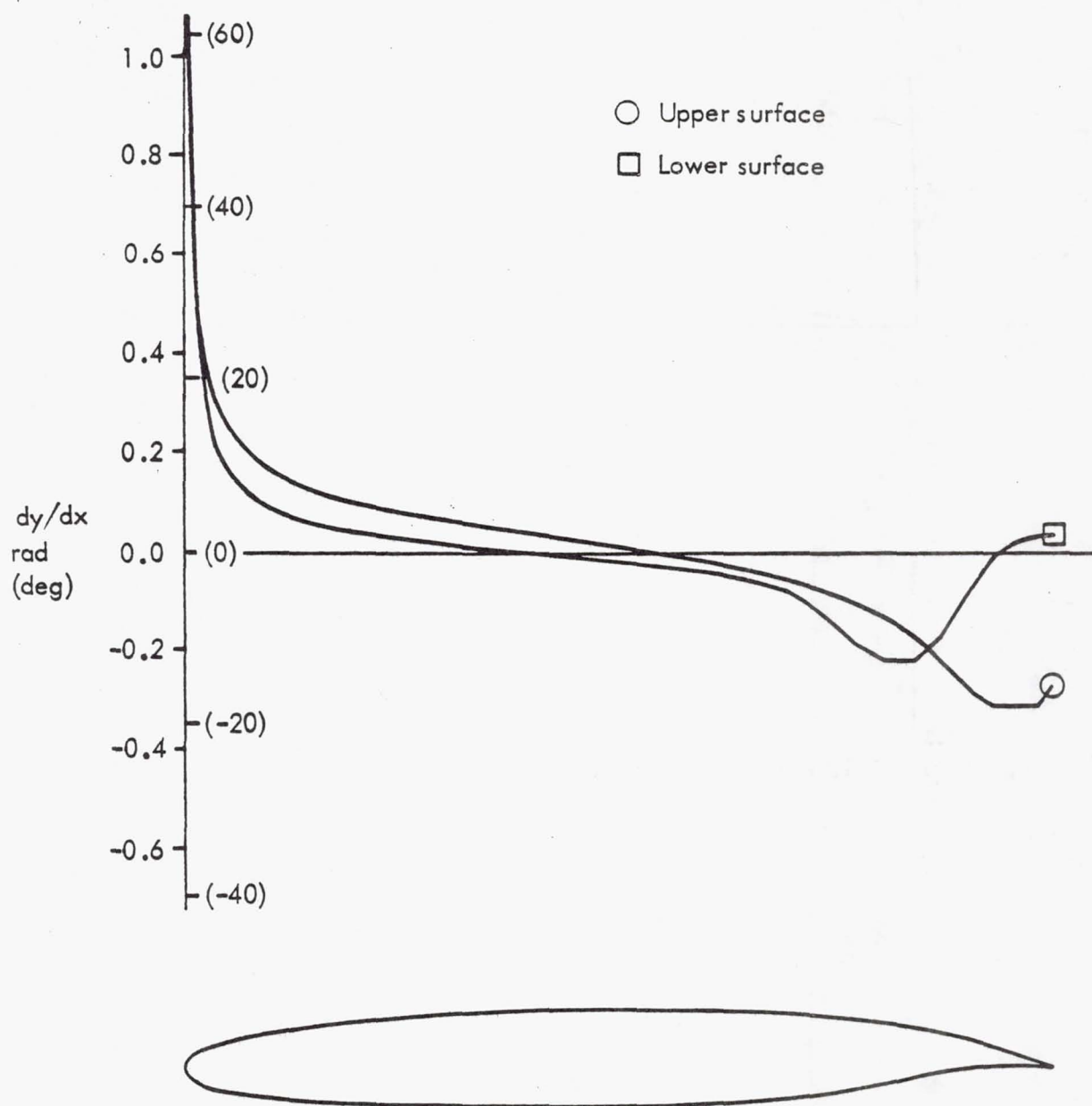


Figure 30. LFC Airfoil AF11-12



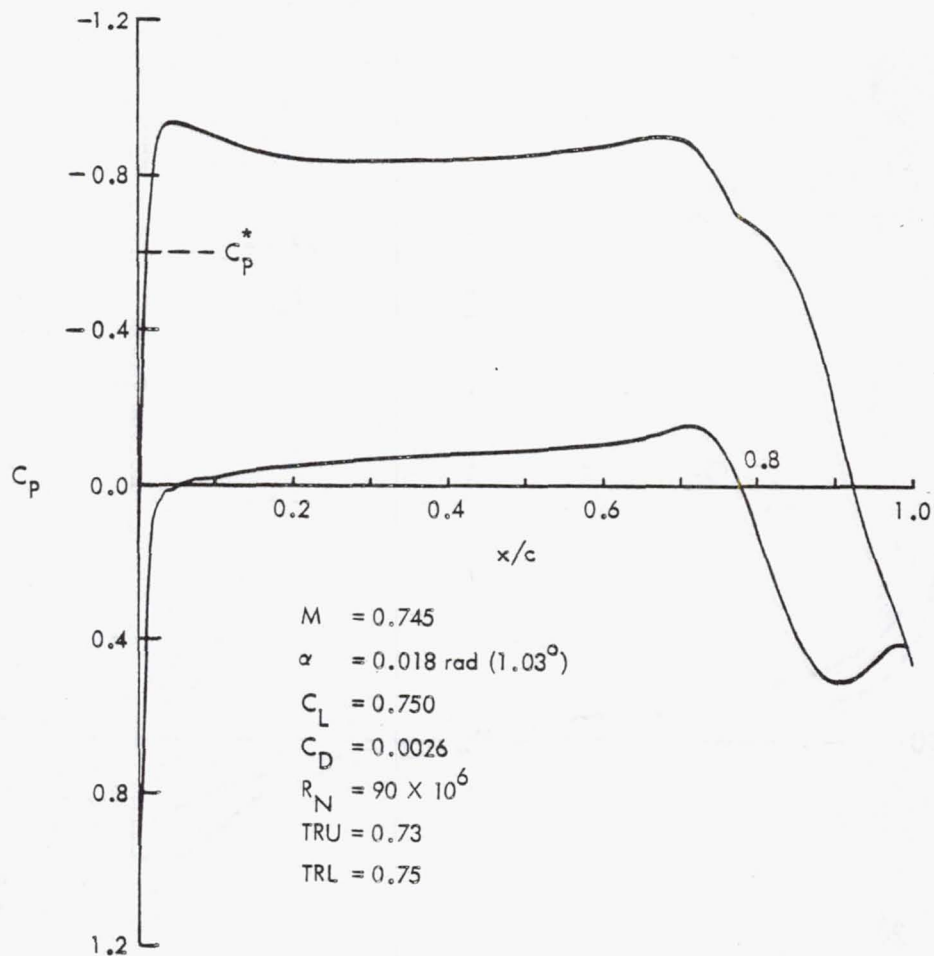


Figure 31. AF11-12 viscous pressure distribution at mach = 0.745,  $C_L = 0.750$

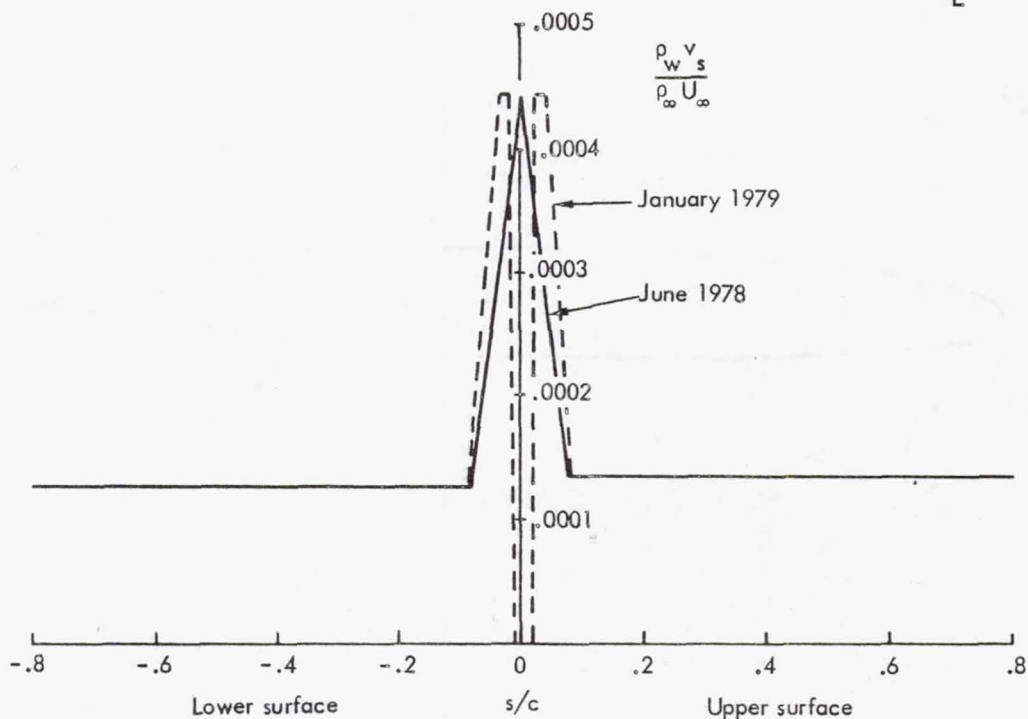


Figure 32. Revised suction distribution

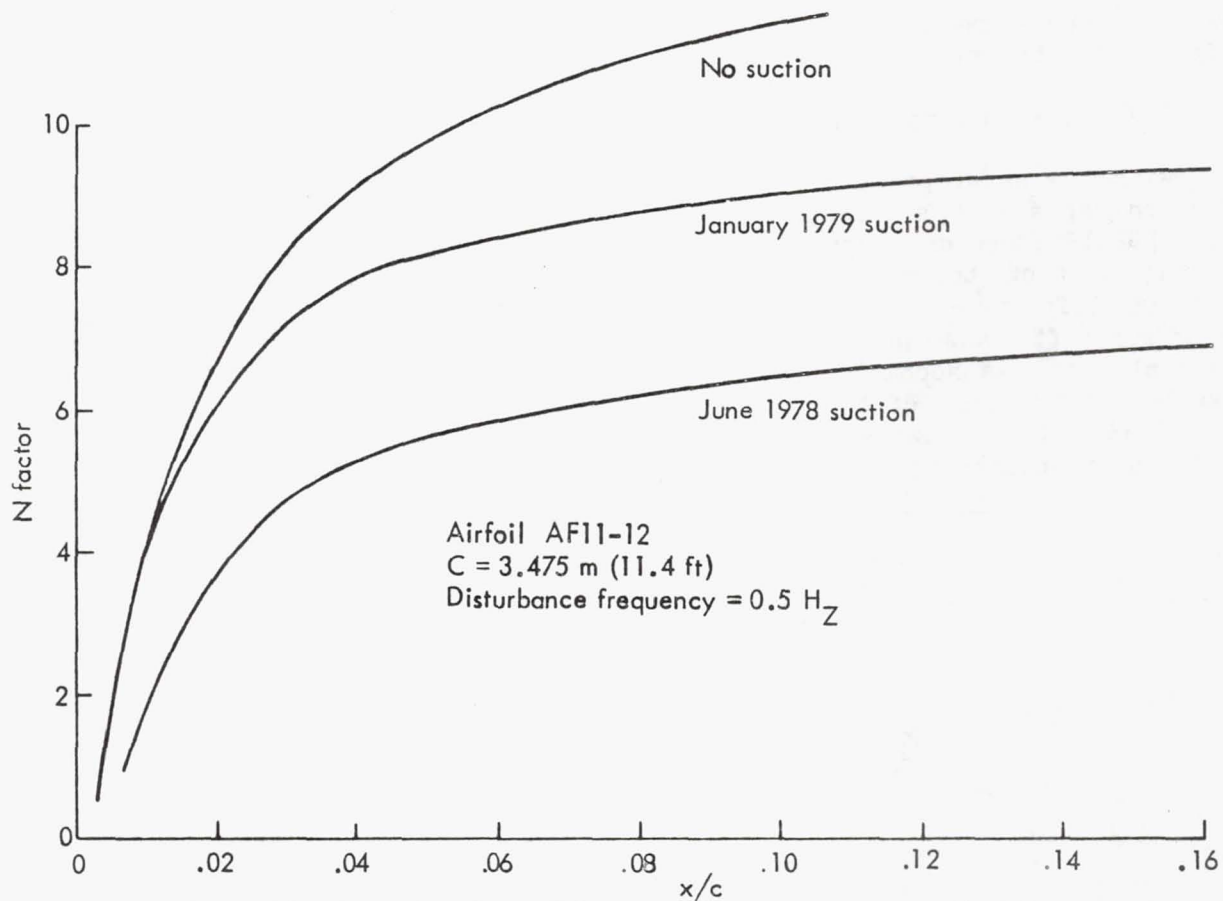


Figure 33. Final baseline LFC Airfoil lower surface crossflow N factors

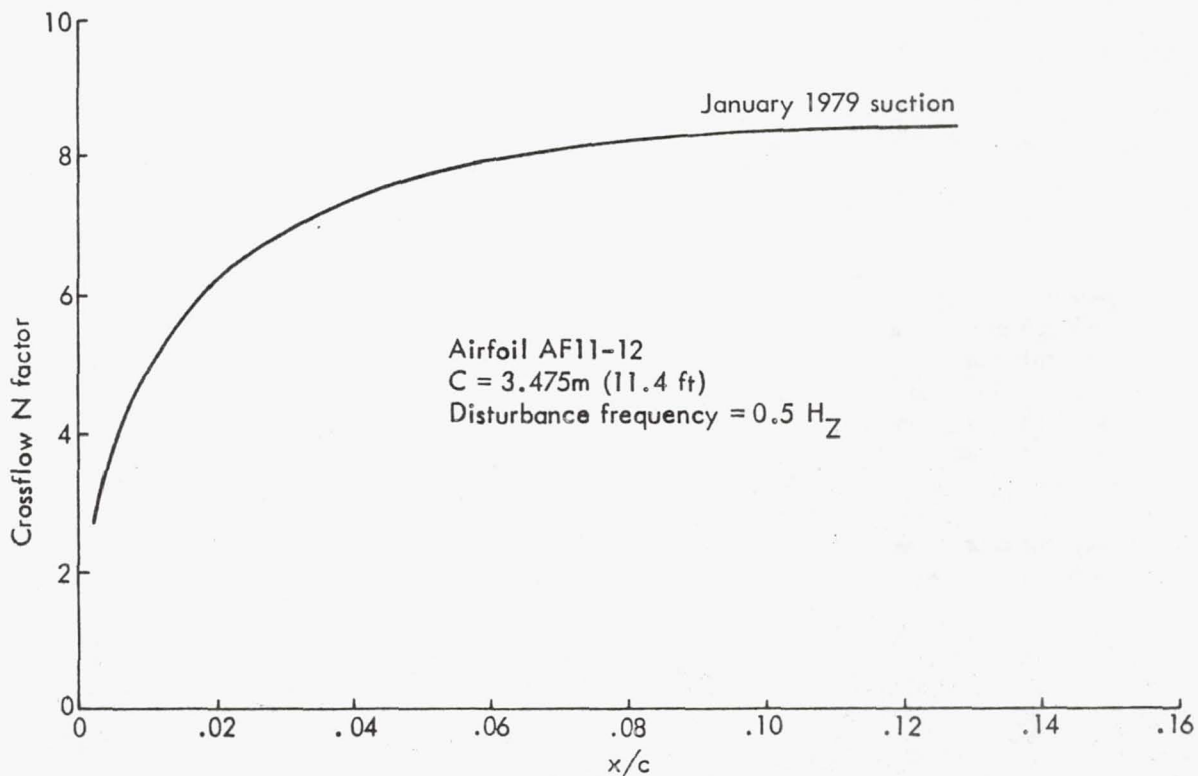
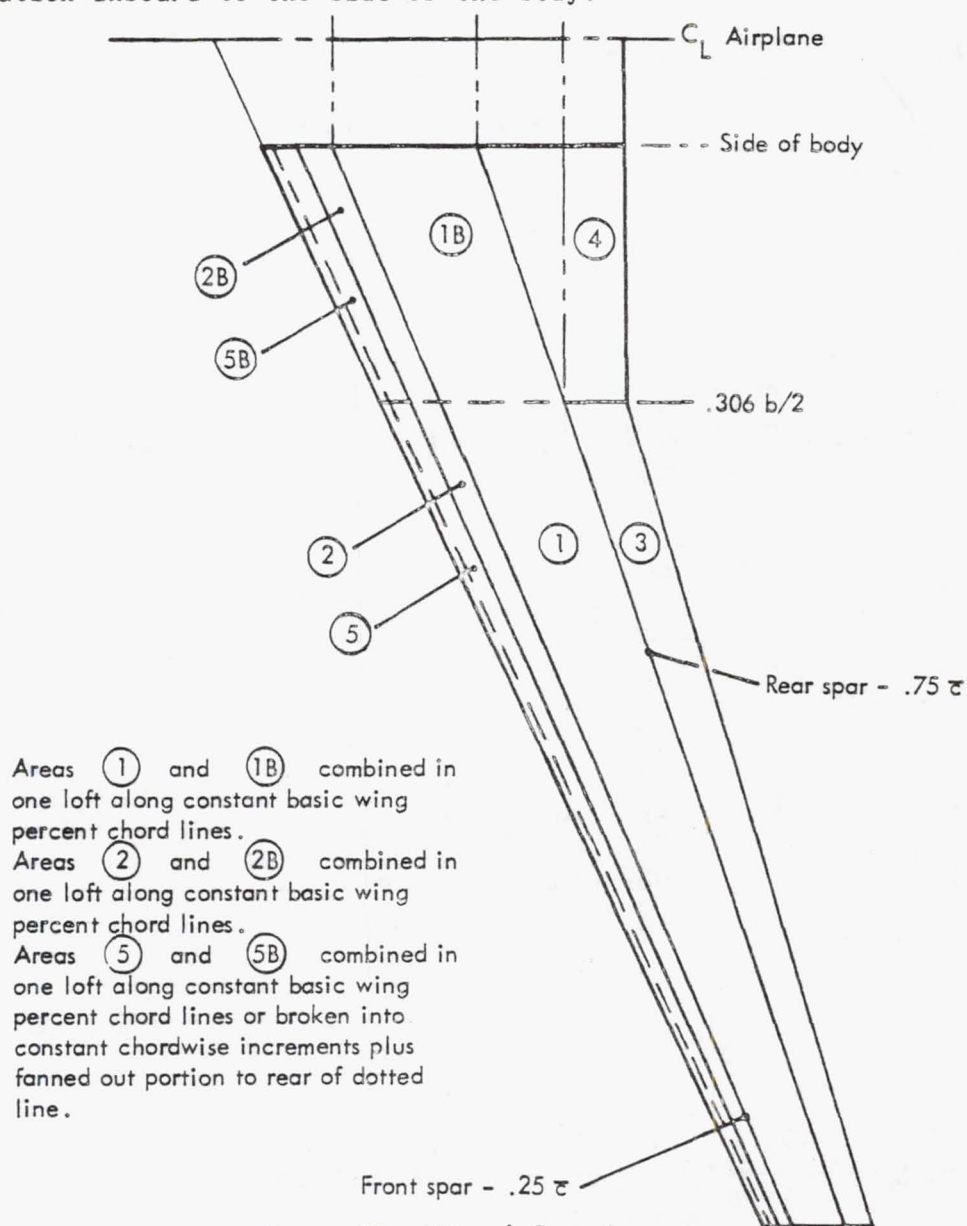


Figure 34. Final baseline LFC Airfoil upper surface crossflow N factors

overall three-dimensional effects under study were known to be not greatly affected by the slight changes to the airfoil sections.

### 6.1.3.1 Interim Wing Design

With the development of the interim airfoil, AF7C6-3B4, and a modified version for a root section, the interim wing loft was made using the Lockheed LSPREP computer program. The LFC wing may require somewhat unconventional lofting techniques. In determining interim wing geometry, the various loft panels under consideration are illustrated in Figure 35. Separate loft techniques need not be applied to each individual panel. The initial loft was accomplished using a linear element loft along constant-percent chord lines of the unbatted wing over the regions 1, 1B, 2, 2B, 3, 5 and 5B. In the batted region, 4, the elements are fanned out from the break station inboard to the side of the body.



The interactive effects of the fuselage and wheelwell fairing on the wing root required initial analysis by the Lockheed 2-D wing root analysis program WPRESS. This analysis program considers the subsonic effects of body overpressures and the unsweeping of isobars near the fuselage to predict the root pressure distribution for subsonic flows. Fuselage and wheelwell fairing overpressures were calculated using the Lockheed version of the Hess Aerodynamic Interference Program (AIP) and a Lockheed distributed surface vorticity program. These fuselage overpressures, root airfoil ordinates, and planform characteristics are then input into the WPRESS program to obtain root pressure distributions. The predicted interim wing root section pressure distribution is shown in Figure 36. The loft program, LSPREP, was modified to output data in the form required for direct input to the Lockheed lifting surface program, L7. The span loading and span efficiency calculations of L7 provided feedback into the twist distribution and aft control flap distribution for wing lofting by LSPREP. Typical results of this process are shown for span lift coefficient in Figure 37.

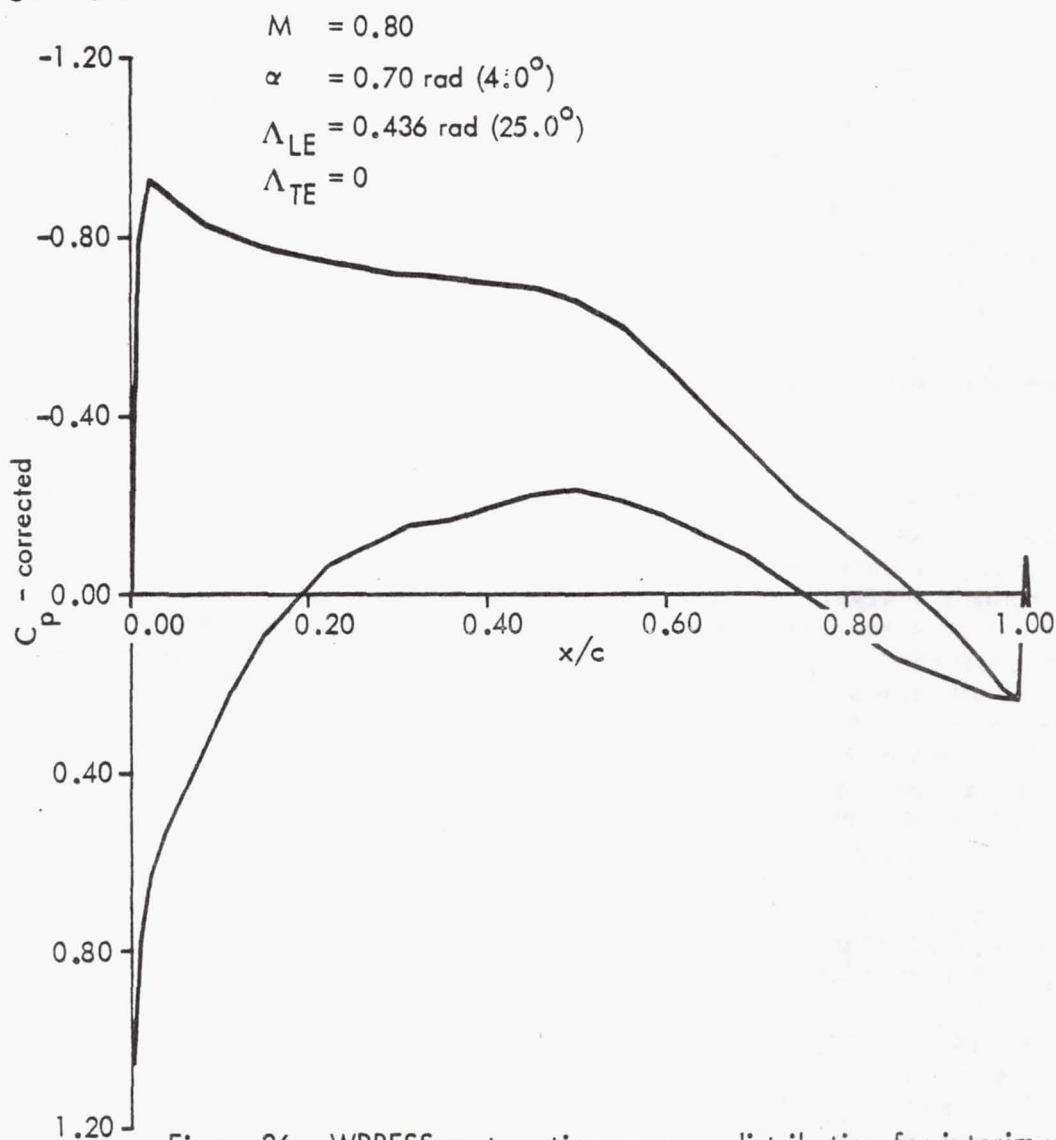


Figure 36. WPRESS root section pressure distribution for interim wing



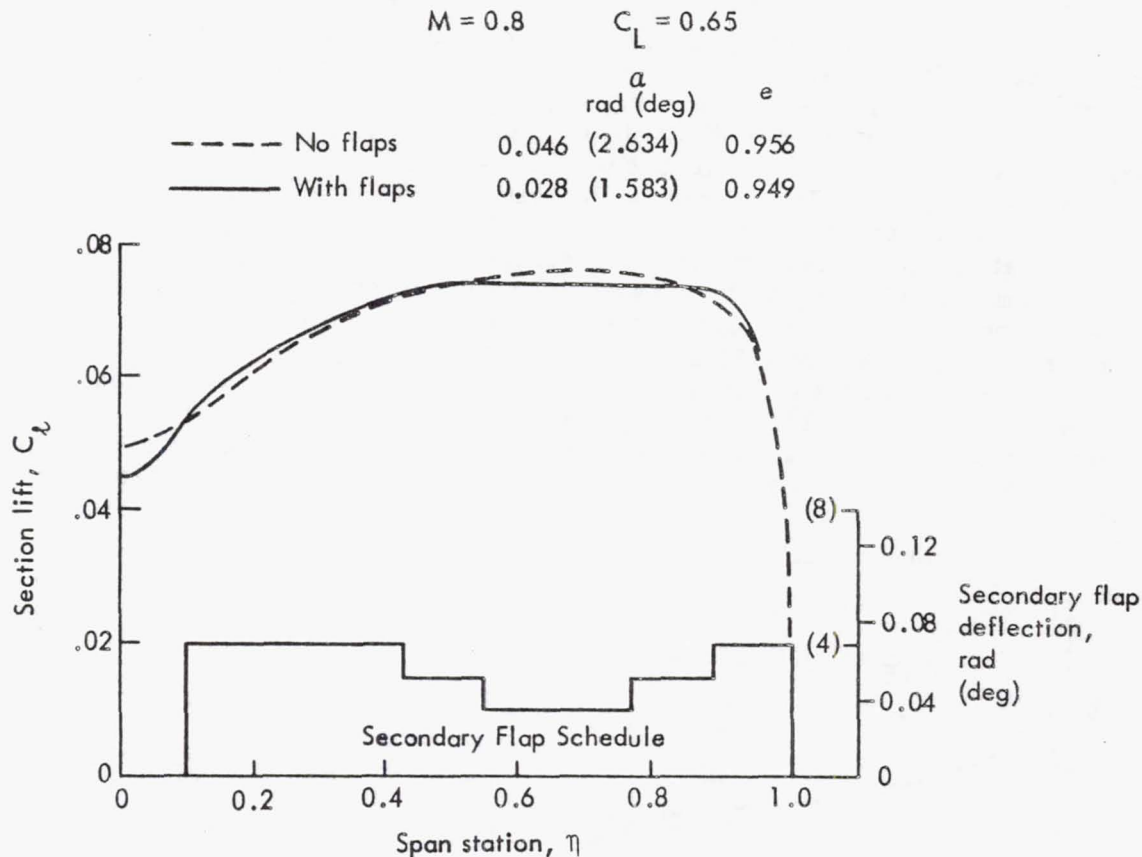


Figure 37. Span lift coefficient distribution and flap schedule

After the effects of most of the wing design variables were quantified using available low-cost analysis tools, preparations for full 3-D transonic wing analysis were begun. The Bailey-Ballhaus 3 code, was selected for the transonic analysis of the interim wing with geometry determined by the initial loft techniques described. The input deck was prepared as a direct output of the loft program, LSPREP. This allows the best geometric representation of wings which may have a somewhat unusual loft due to the various concessions for suction system and manufacturing simplicity. The results reflect several runs in which the computational grid was successively modified to improve convergence and accuracy. The span load distribution for the cruise condition, as predicted by the Transonic Wing Program, is shown in Figure 38. The two fluctuations in the distribution near 20% and 60% chord probably occur because the transonic solution is not fully converged at 300 iterations, but appear fairly well smoothed out by 400 iterations. Similar data are presented in Figure 39 for the spanwise distribution of lift coefficient.

The transonic pressure distributions obtained from the 3-D solution were based on inviscid flow with an unconservative assumption relating to conservation of mass. A first order correction for boundary layer effects

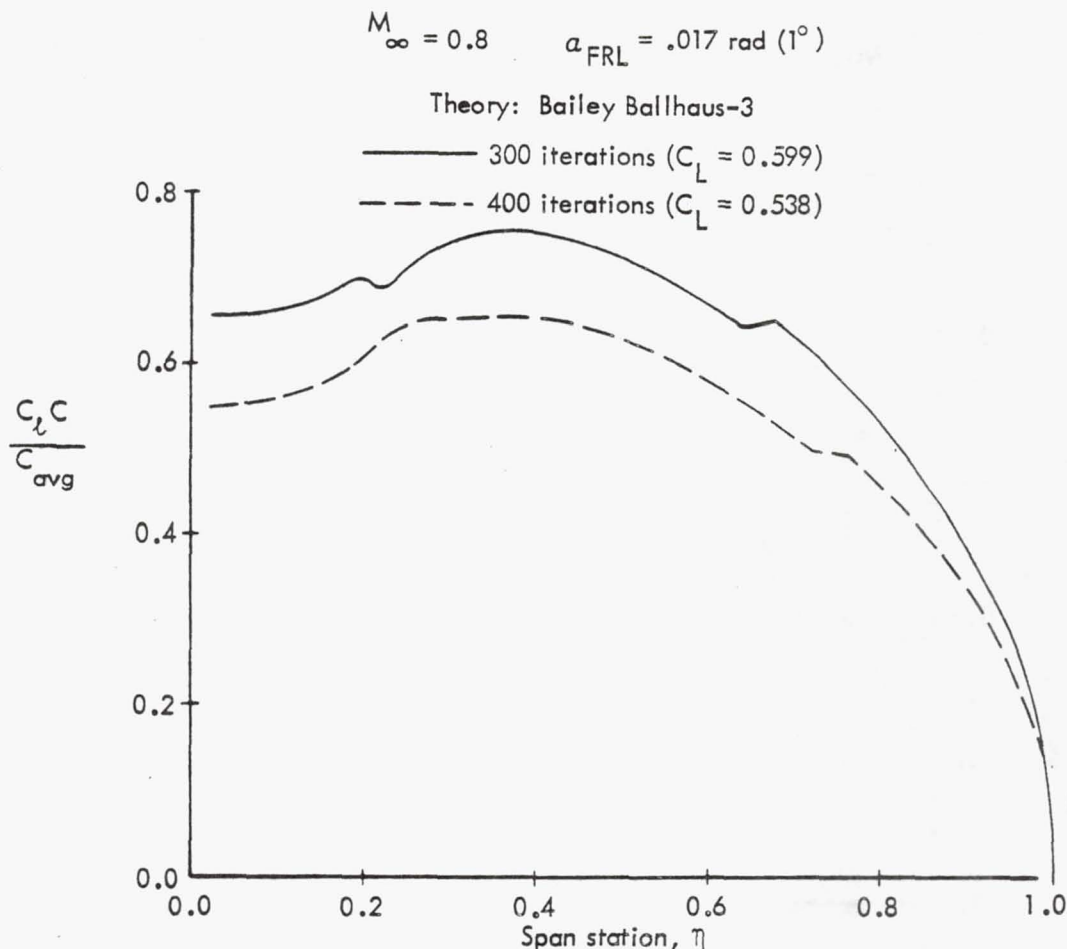


Figure 38. Transonic wing program span load distribution was included, however, in the 3-D solution by deflecting the aft flap up  $.035 \text{ rad } (2^\circ)$  for the entire outboard wing. This correction is a good approximation of the predicted boundary layer effect except in the region immediately aft of the shock. The calculated root pressure distribution is shown in Figure 40.

The analysis indicated the following changes should be incorporated into the next wing loft:

- (1) Increase root twist angle relative to outboard wing twist angles to pick up inboard loading slightly.
- (2) Modify the root upper surface to reduce the indicated shock strength, and produce better isobar patterns for the inboard wing region.
- (3) Include the boundary layer obtained from 2-D solutions to obtain an equivalent fluid airfoil input for the 3-D inviscid transonic program.
- (4) Define a preliminary swept tip to straighten tip isobars.
- (5) Include an aft flap deflection schedule to tailor the span load distributions as required.

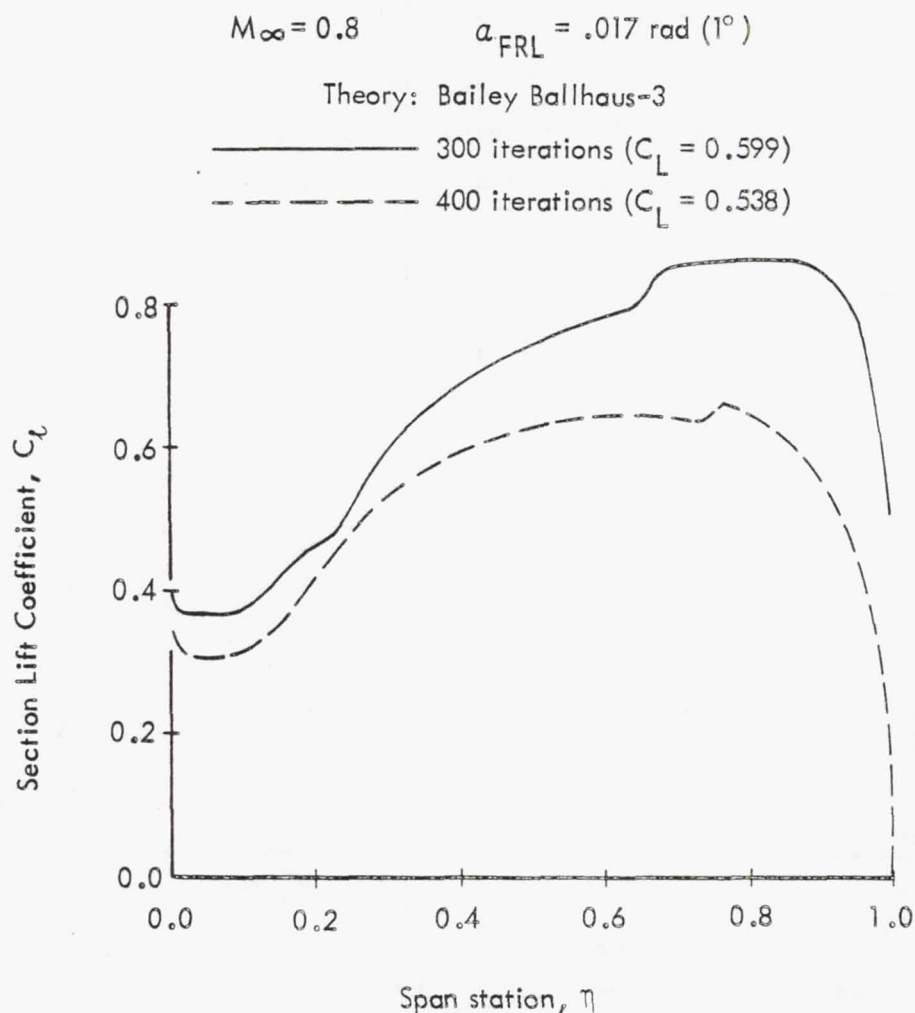


Figure 39. Transonic wing program span lift distribution

#### 6.1.3.2 Baseline Wing Design

A series of modifications to the root section were made to produce the desired pressure distribution. The modifications were performed using the Lockheed "a" mean-line program and the 2-D Transonic Airfoil Program (TAP). Previous Lockheed efforts have demonstrated the validity of this approach by showing the excellent correlation between 2-D and 3-D pressure distributions. Modifications to reduce the shock resulted in the baseline root section, Root 3-30. The design point pressure distribution for this section is illustrated in Figure 41.

Because the Bailey-Ballhaus Transonic Wing Program (TWP) uses inviscid theory, TAP was used to calculate boundary layer thicknesses at the design cruise point for the root, break, and tip sections. These boundary layer thicknesses were added to the Root 3-30 root section, and to the AF10-3 sections at the break and tip stations to produce fluid sections, which were then factored to streamwise ordinates. The fluid airfoils computed at the root, break station and tip were subsequently lofted to obtain a fluid wing referred to as the fluid loft 8 wing. By examination of pre-

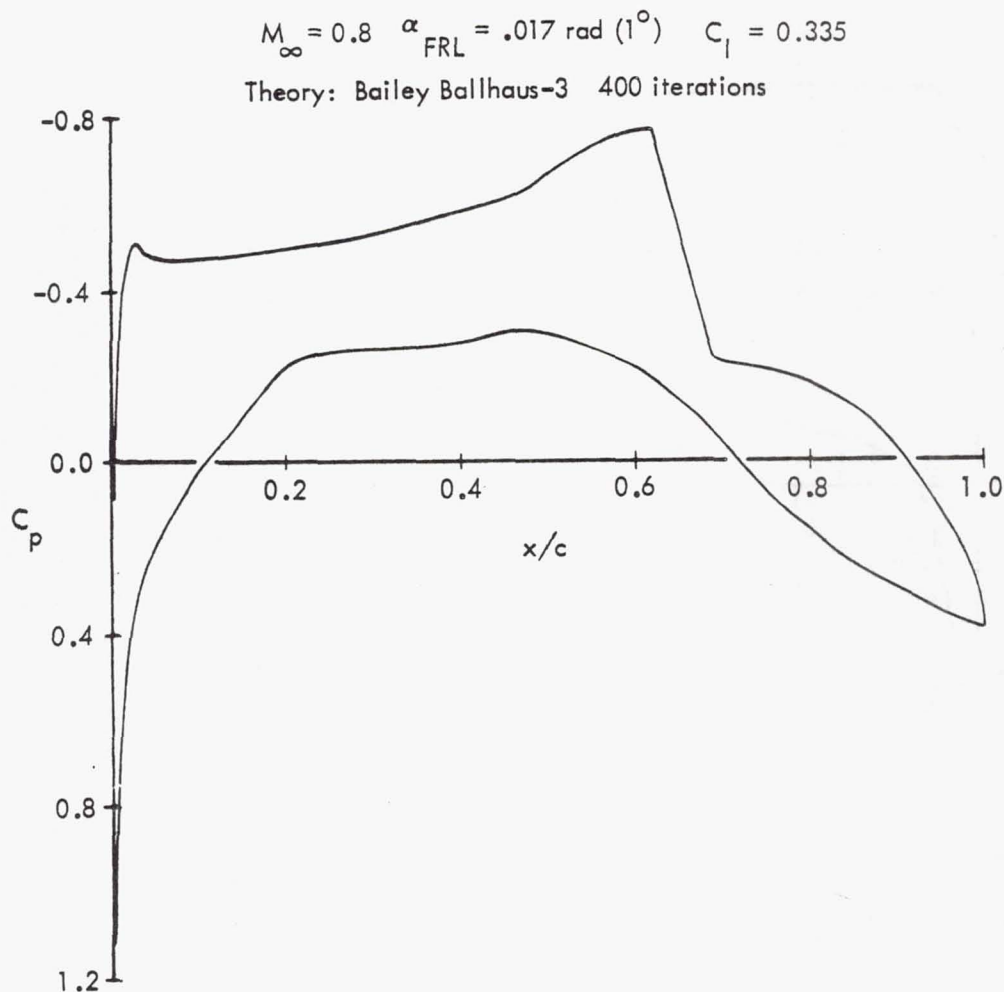


Figure 40. Transonic wing program root pressure distribution

vious data and additional estimations of the aft flap effectiveness, a new wing definition was developed. The resultant twist schedule is given in Figure 42. A new spanwise schedule for aft flap deflection to tailor the span load distribution is shown in Figure 43. Figures 44 through 46 illustrate span loading, span lift coefficient, and pressure distribution results from TWP for the fluid LFC final baseline wing. The results indicate that the changes in aft flap schedule and twist schedule are effective in altering span-load distribution, shock strength and location. The overall wing isobar pattern is thus significantly altered. Additional design perturbations would be required, however, to produce a more satisfactory wing.



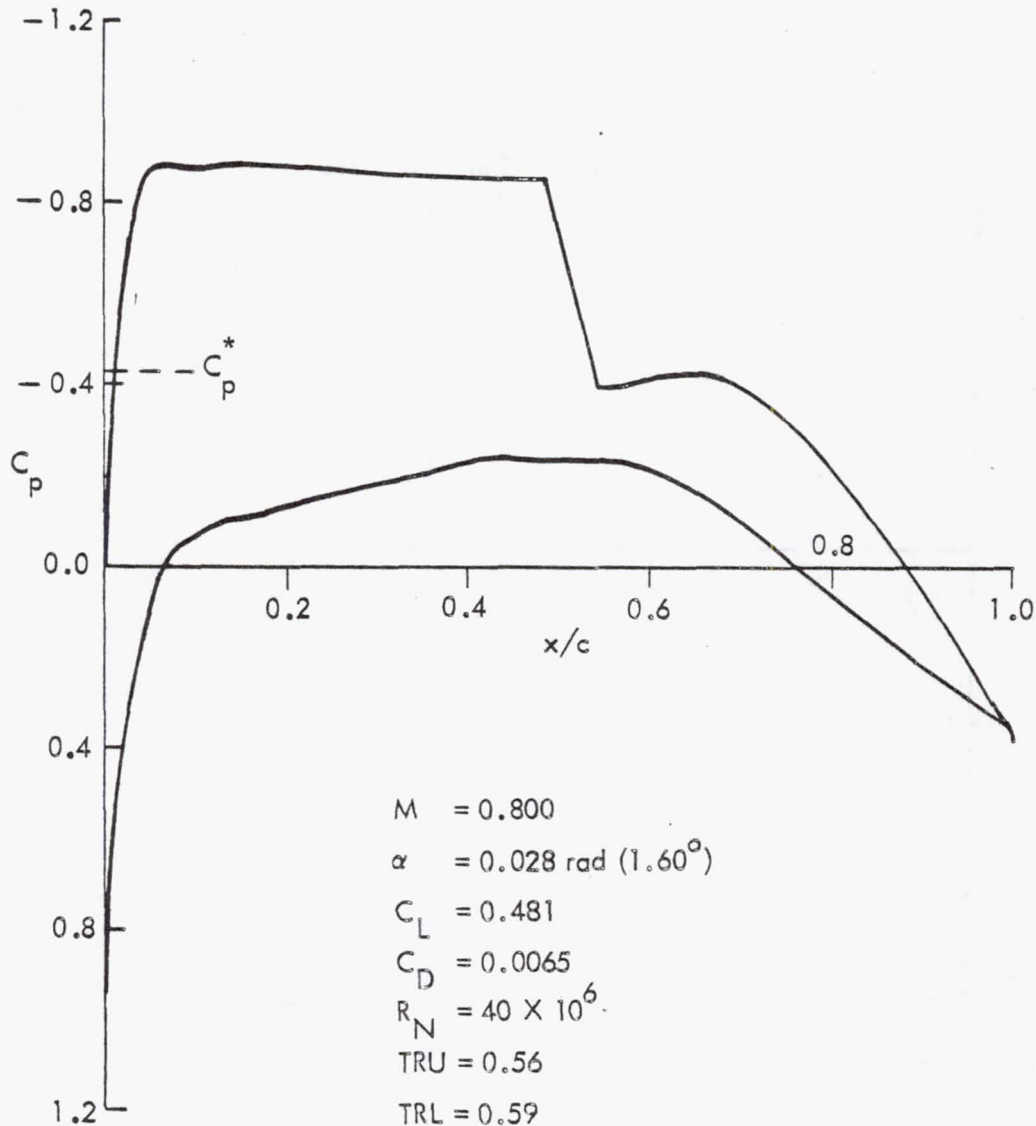


Figure 41. TAP wing root pressure distribution

Note in Figure 46, for example, that design problems still exist in the mid-semi-span region of the wing because of the aft position of existing shocks. This aft position would result in excessive shock wave drag and also would probably cause boundary layer separation problems in the trailing edge region because of resultant high pressure gradients. It should be pointed out, however, that the 3-D wing definition always tends to lag in time the 2-D airfoil definition exercises. In this case, the airfoil AF10-3 used in LFC Fluid Wing Loft 8 had been superseded by AF11-12, as discussed in Section 6.1.2. Changes to the twist schedule and flap schedule of Fluid Wing Loft 8 were included in a new wing loft incorporating AF11-12, accomplished as part of the DC-9 validator study, which is detailed in Section 8.2.

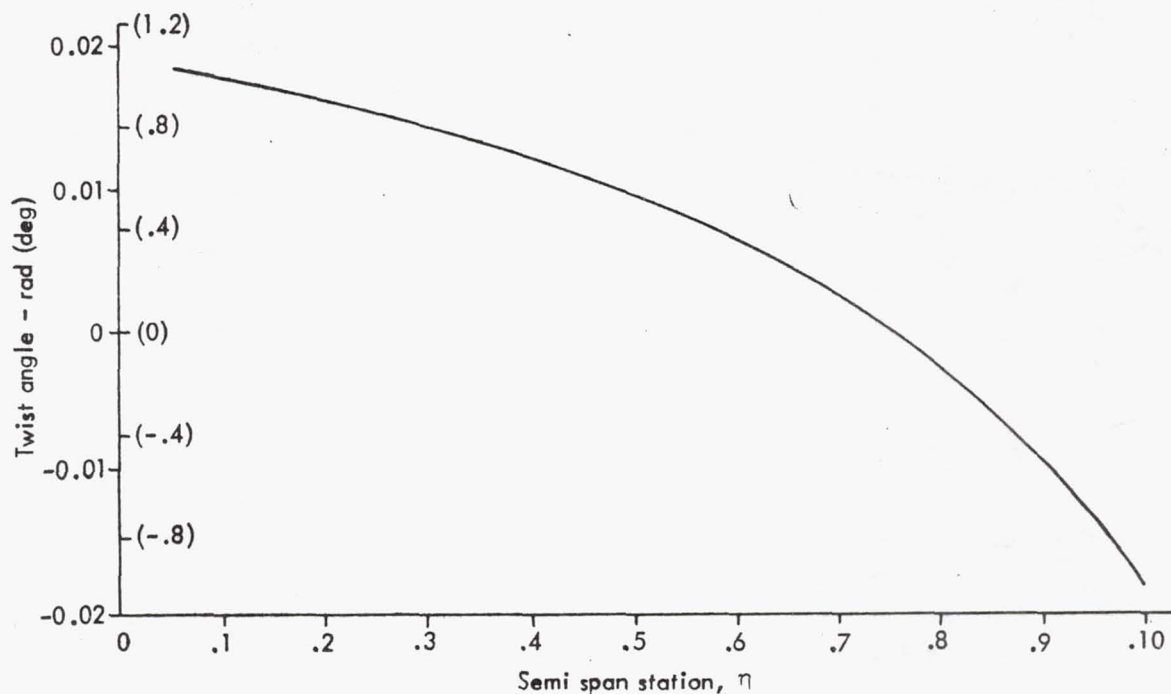


Figure 42. LFC baseline wing twist schedule

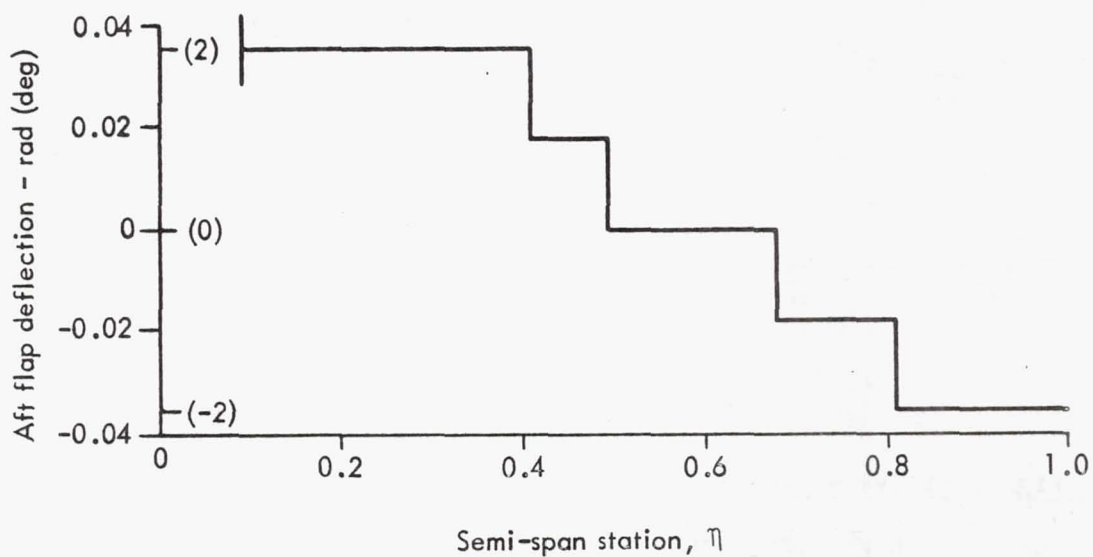


Figure 43. LFC baseline wing aft flap deflection schedule

This validator wing reduces the shock problems in the mid-span region of the Fluid Loft 8 wing. Although the DC-9 validator wing is smaller than the 1993 aircraft wing, the changes made to the Fluid Loft 8 wing to produce the DC-9 validator wing illustrate that a satisfactory 1993 aircraft wing can be designed using the Fluid Loft 8 wing as a starting point.

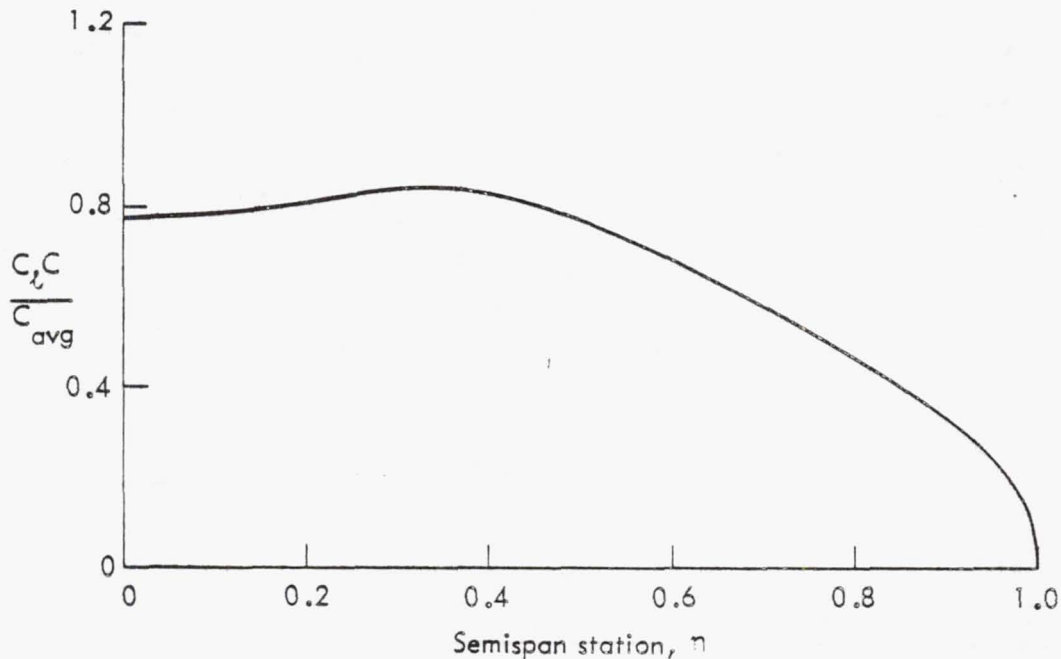


Figure 44. LFC baseline wing span loading distribution

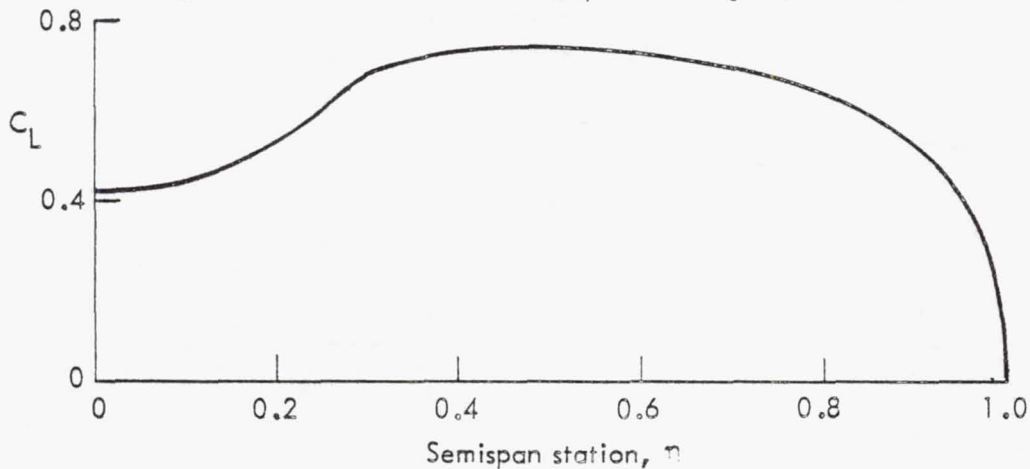


Figure 45. LFC baseline wing spanwise variation of lift coefficient

#### 6.1.4 High-Lift System Development

The baseline high-lift system was analyzed to:

- (1) Verify that parametric program aerodynamic characteristics estimates for the high-lift system were sufficiently accurate for baseline configuration optimizations.
- (2) Provide data for baseline configuration optimization corrections, if necessary.
- (3) Define the scheduling of deflections of the high-lift devices which best satisfies both performance and stability and control requirements.

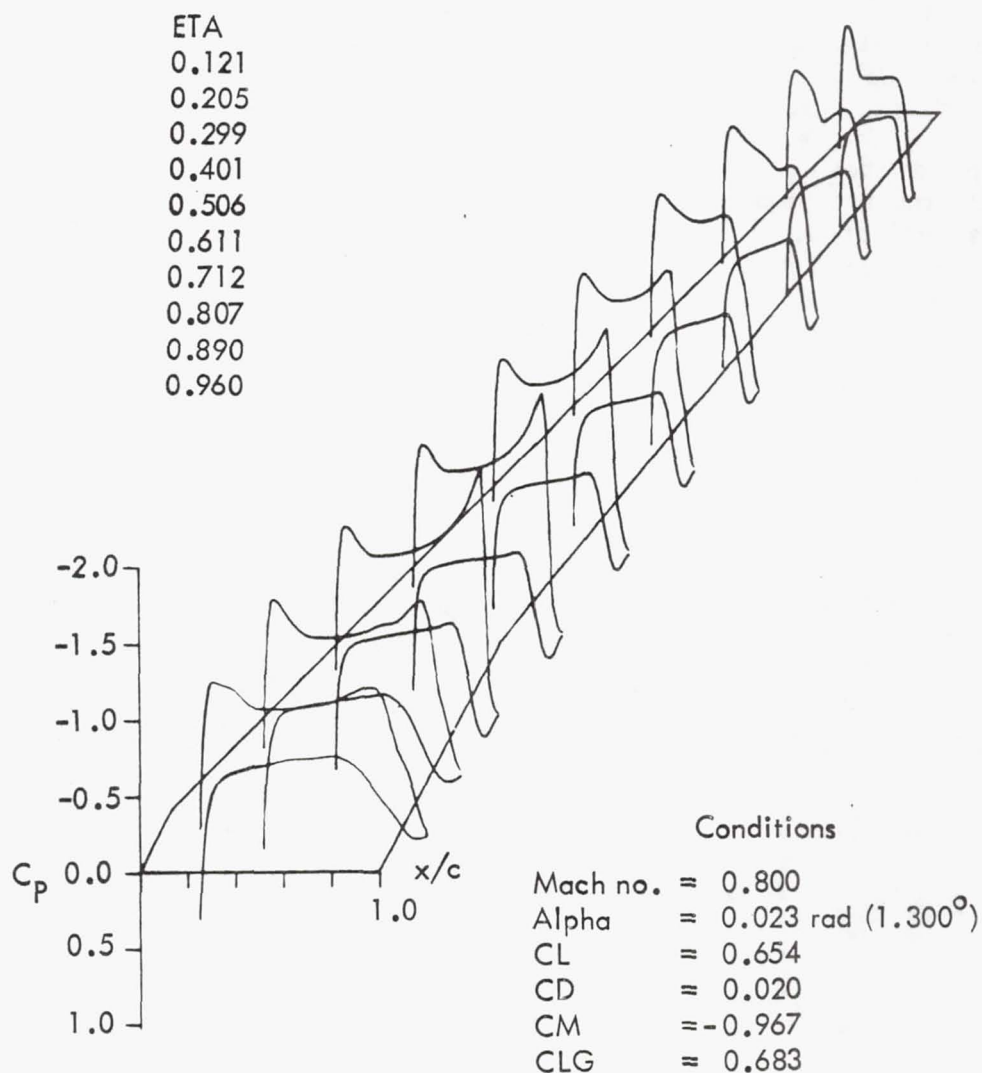


Figure 46. 3-D isometric pressure distribution for LFC baseline wing

The analyses of the baseline takeoff and landing high-lift system verified the predicted levels of the parametric sizing program, GASP. As a consequence, it was verified that the baseline airplane can operate from a 3048 m (10 000 ft) field without a leading-edge device. The final baseline airplane uses .052 rad (3°) higher flap deflections for takeoff than described in Section 6.1.4.1 as the takeoff flap configuration. This adjustment was necessary because of small configuration changes to the final baseline.



#### 6.1.4.1 Clean Wing and Takeoff Flaps

The predicted clean wing lift characteristics through stall are shown in Figure 47. Also illustrated in Figure 47 are the lift characteristics with takeoff flaps, nominally  $.436$  rad ( $25^\circ$ ), and varying amounts of aileron droop. The effect of deflecting the two-segment aileron or outboard flap is shown for three possible cases: (1) both segments not deflected, (2) inboard segment deflected with outboard undeflected, and (3) both segments deflected. In the last case of full-span flap deflection, the two flap segments inboard on the battened portion of wing were deflected an additional  $.087$  rad ( $5^\circ$ ).

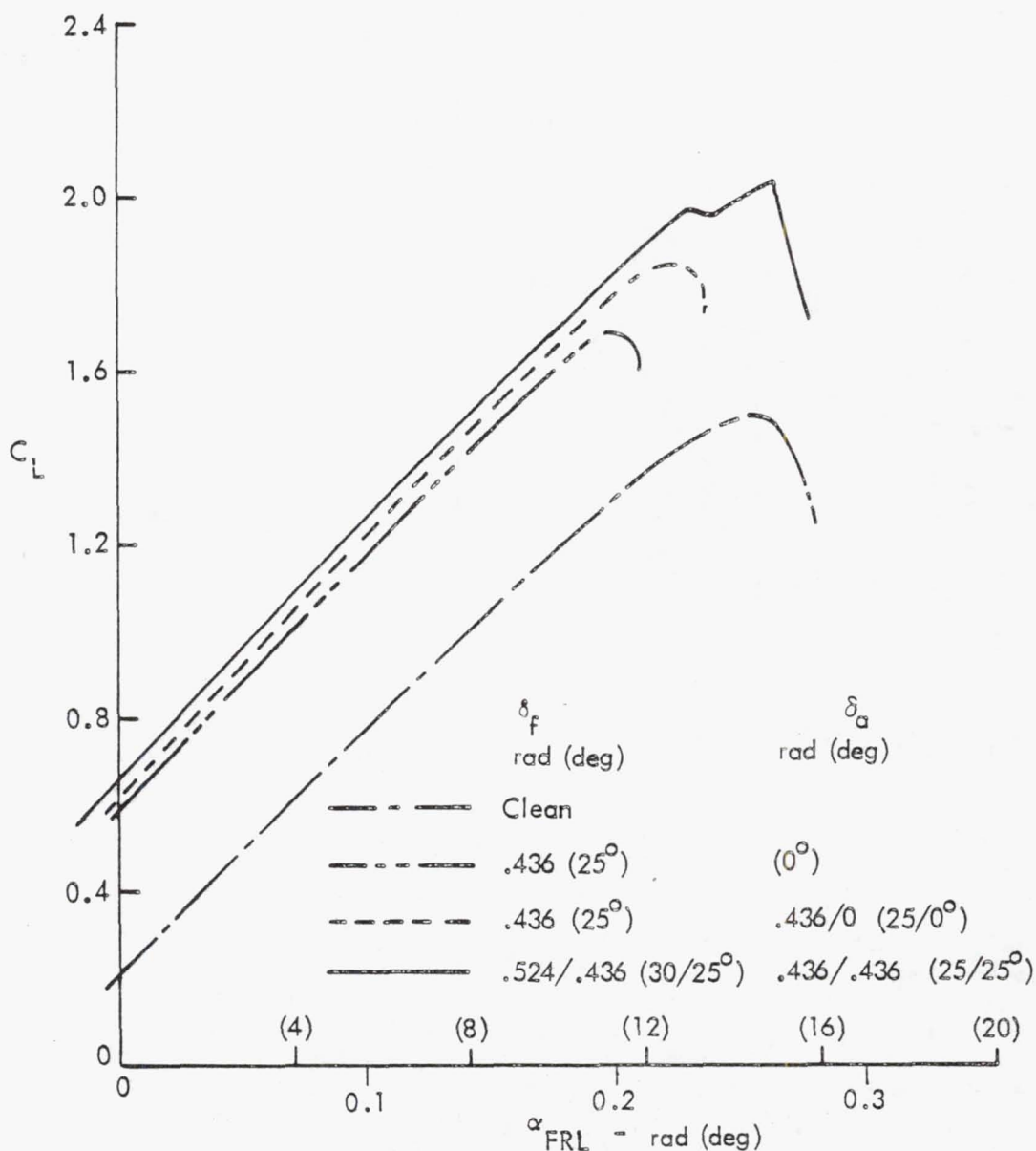


Figure 47. High lift characteristics - clean wing and effect of aileron droop with takeoff flaps

The span-load distributions for each of the above conditions are shown in Figure 48 at  $.175 \text{ rad } (10^\circ)$  angle of attack to illustrate the effects of aileron droop. This angle of attack is representative of the lift-off and climb-out phases of takeoff.

The clean-wing load distributions through stall are given in Figure 49. Note that the stall begins near mid-semi-span and progresses outboard. Similar data are presented in Figure 50 for the configuration with takeoff flaps and undeflected ailerons. The span-load distributions indicate an outboard initiation of stall. Such a characteristic is undesirable both from the standpoints of maximum lift achievable and undesirable stability and control near stall.

For the case of full-span takeoff flaps, the lift curve slope given in Figure 47 indicates a break between  $.227 \text{ rad } (13^\circ)$  and  $.244 \text{ rad } (14^\circ)$  angle of attack, prior to the wing stall at about  $.262 \text{ rad } (15^\circ)$ . The span-load distributions through this break are shown in Figure 51. These data indicate an initial stall near the 70% semi-span station. This initial stall alters the loading, but allows the inboard flap to continue to build up load to the point of an inboard stall over the battened region of the wing, as shown in Figure 52. Note that the outboard flap/aileron segment (approximately 81% to 95% semi-span) appears to maintain attached flow well into the stall. Based on the above observations and theoretical force and moment results, this configuration should be less likely to exhibit undesirable pitch-up or roll-off near  $C_{L\text{Max}}$ .

Further refinement of the takeoff flap schedule was made to eliminate the break in the lift curve prior to full wing stall, as depicted in Figure 53. The outboard slotted flap segment (approximately 58% to 68% semi-span) was retracted slightly to  $.384 \text{ rad } (22^\circ)$  deflection to blend aerodynamically with the unslotted simple-hinge flap/aileron of the outboard two segments. The resultant smoothing of the lift curve is shown by comparison of Figure 53 with Figure 47. A small increase in maximum lift is also indicated and any pitch-up or roll-off tendencies near stall are further reduced.

#### 6.1.4.2 Landing Flaps

A brief study was also conducted to determine the effectiveness of the landing flaps. The initial flap schedule consisted of  $.873 \text{ rad } (50^\circ)$  deflection for the two segments on the battened portion of the wing,  $.698 \text{ rad } (40^\circ)$  deflection for the three segments from the break station at 30% semi-span out to 58% semi-span,  $.524 \text{ rad } (30^\circ)$  deflection for the next slotted flap segment, and  $.262 \text{ rad } (15^\circ)$  deflection for the two outboard simple-hinge plain flap segments. The lift curve for this initial schedule, shown in Figure 54, indicates two breaks prior to stall where local stall and resultant load relief result. Three-dimensional viscous effects, not fully considered in the theory, would tend to smooth the curve as indicated by the dashed line. Lift data with a refined flap schedule for the landing configuration, shown in Figure 55, indicate that the pre-stall lift breaks can be eliminated without loss in maximum lift.

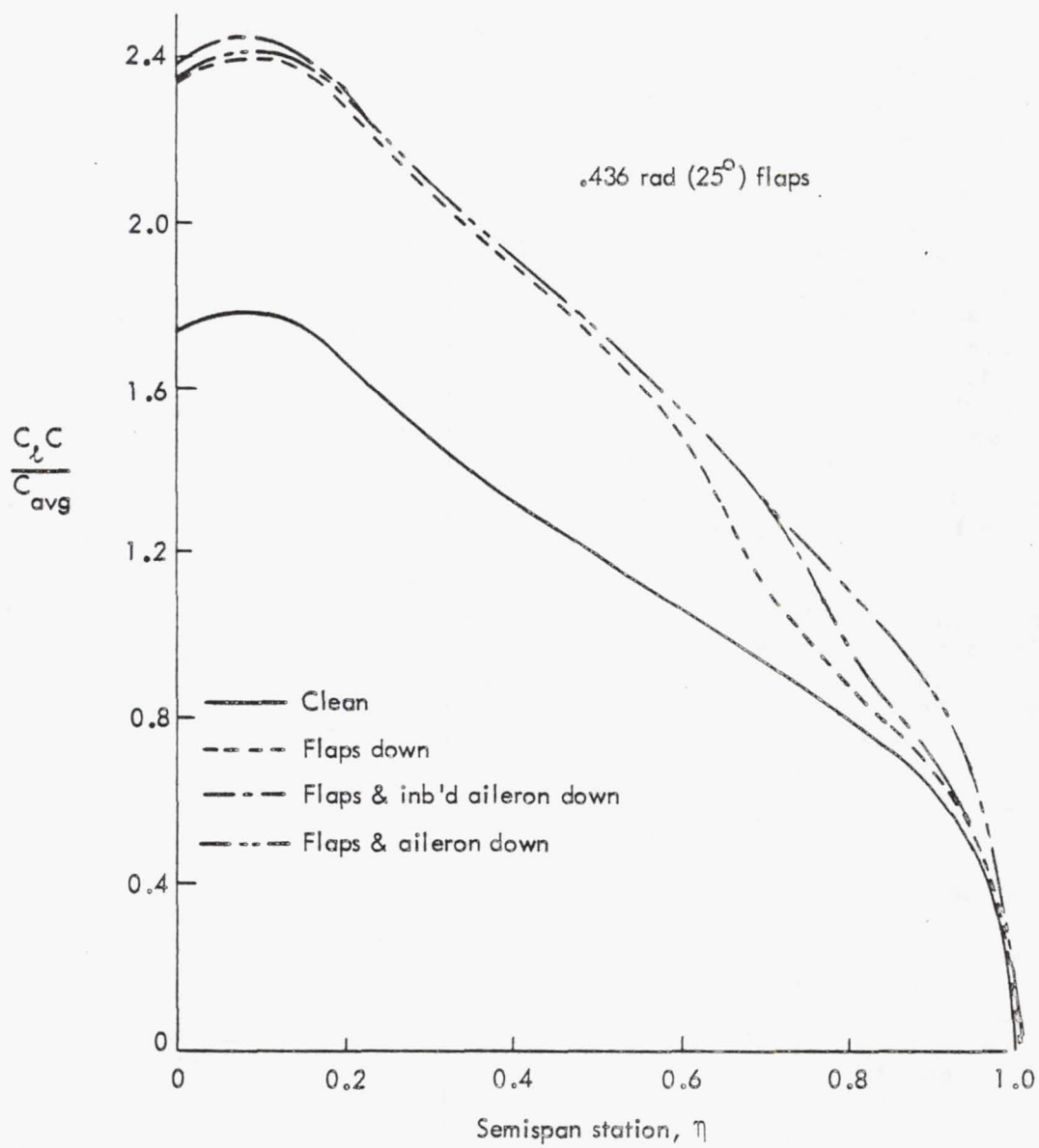


Figure 48. Comparison of span loading for clean wing and varying aileron droop with takeoff flaps,  $\delta = 10^\circ$

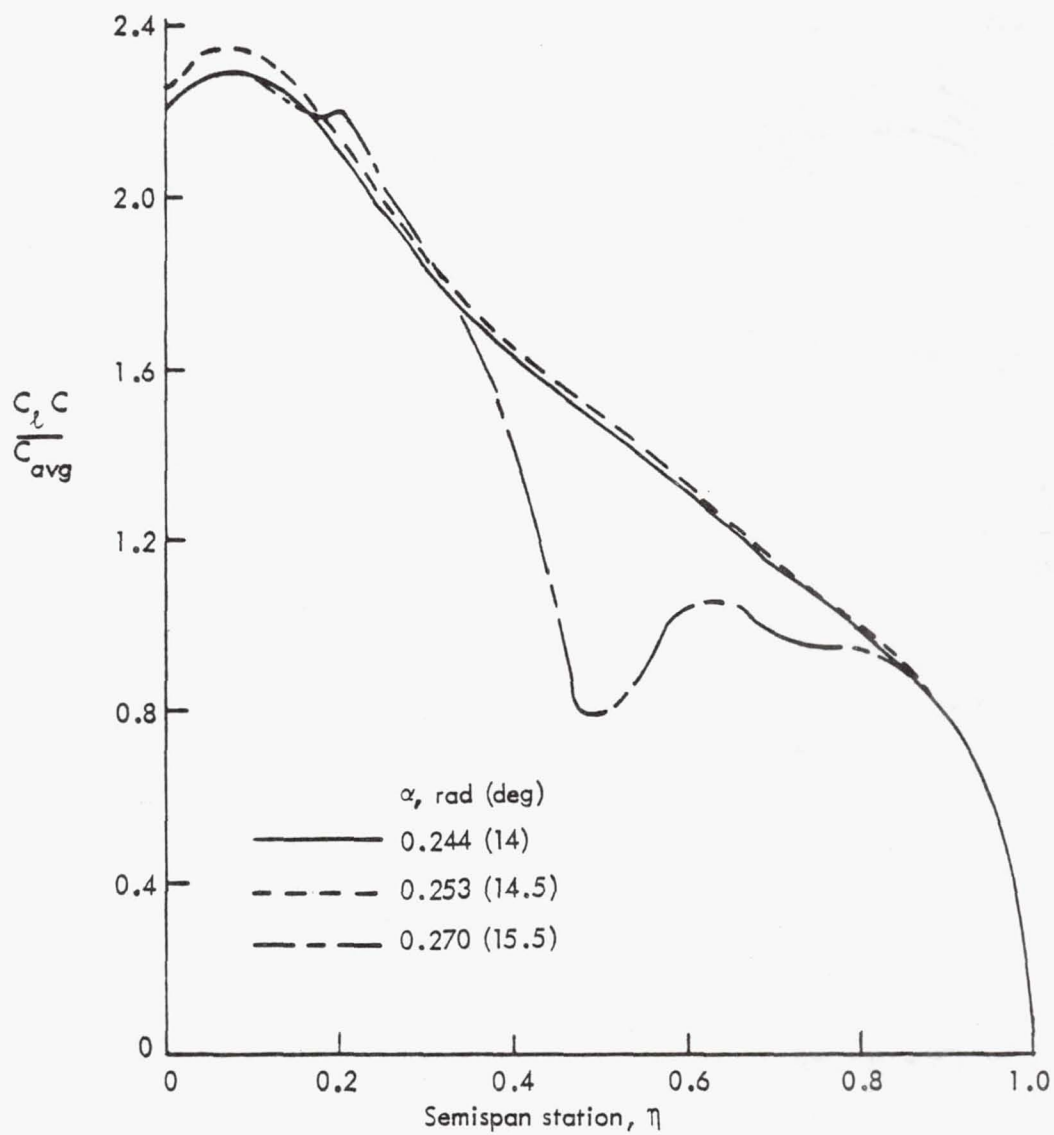


Figure 49. Clean wing span load distribution at stall



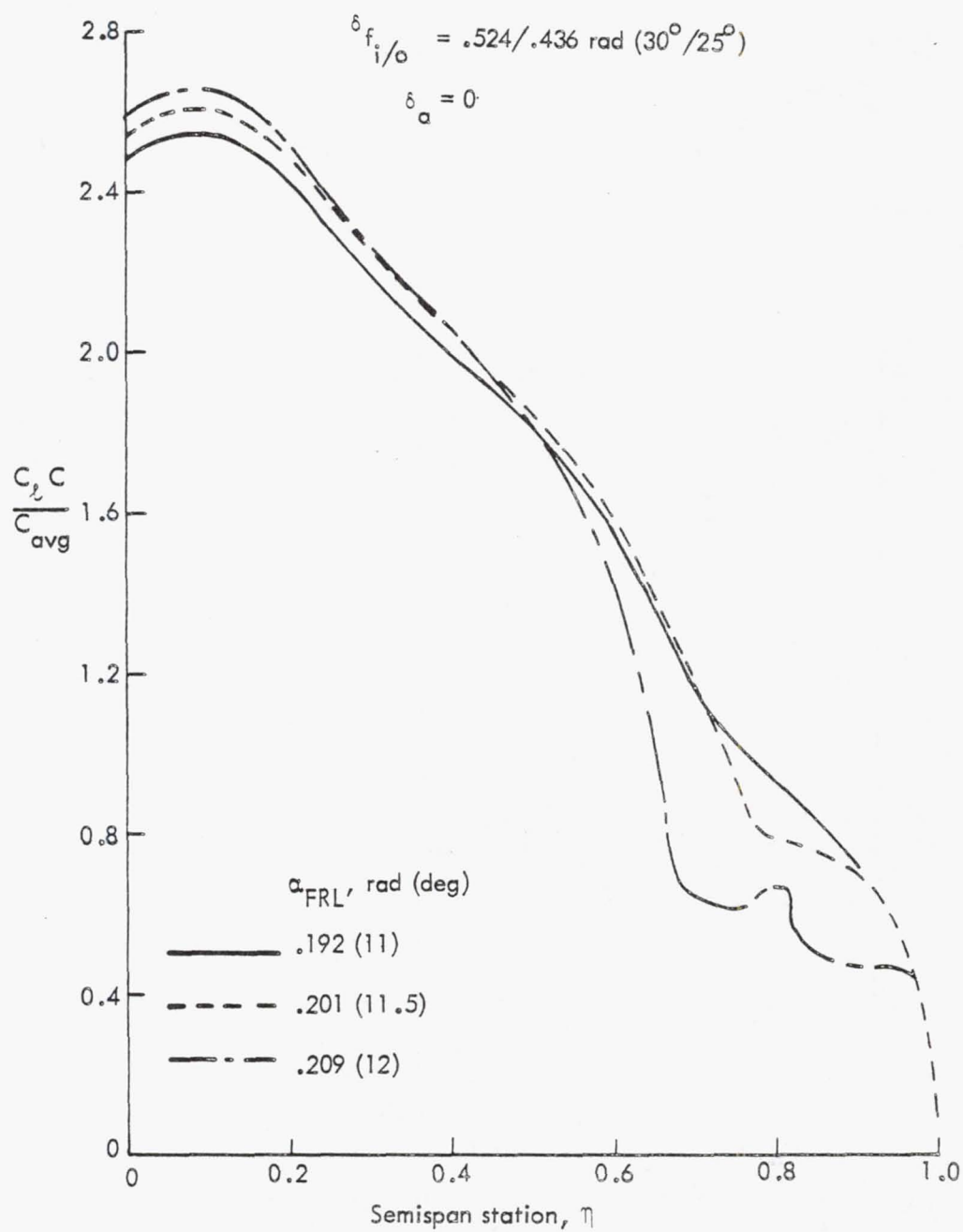


Figure 50. Span load distribution at stall, takeoff flaps, aileron undeflected

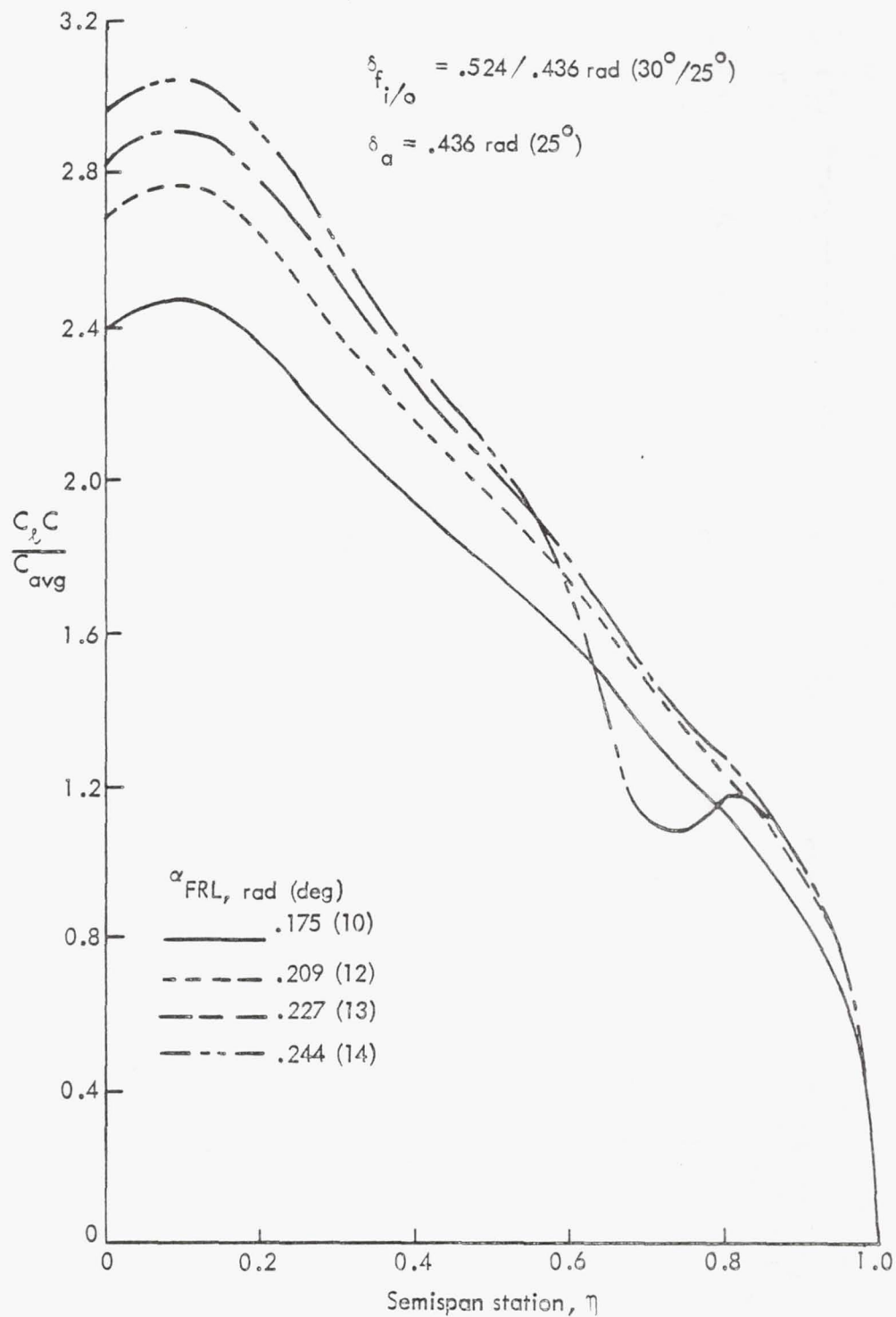


Figure 51. Span load distribution at initial lift curve brake, takeoff flaps, aileron droop

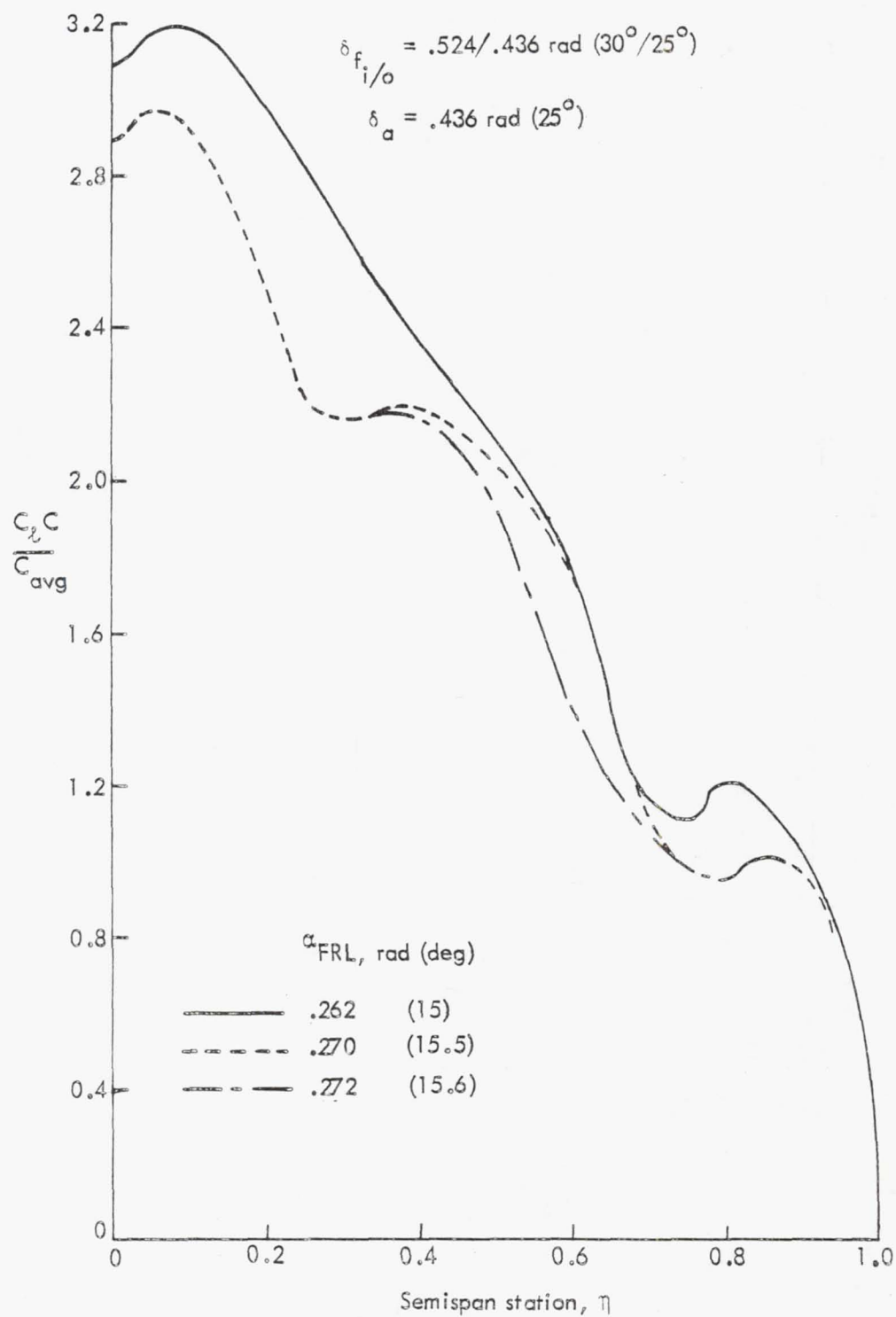


Figure 52. Span load distribution at stall, takeoff flaps and aileron droop

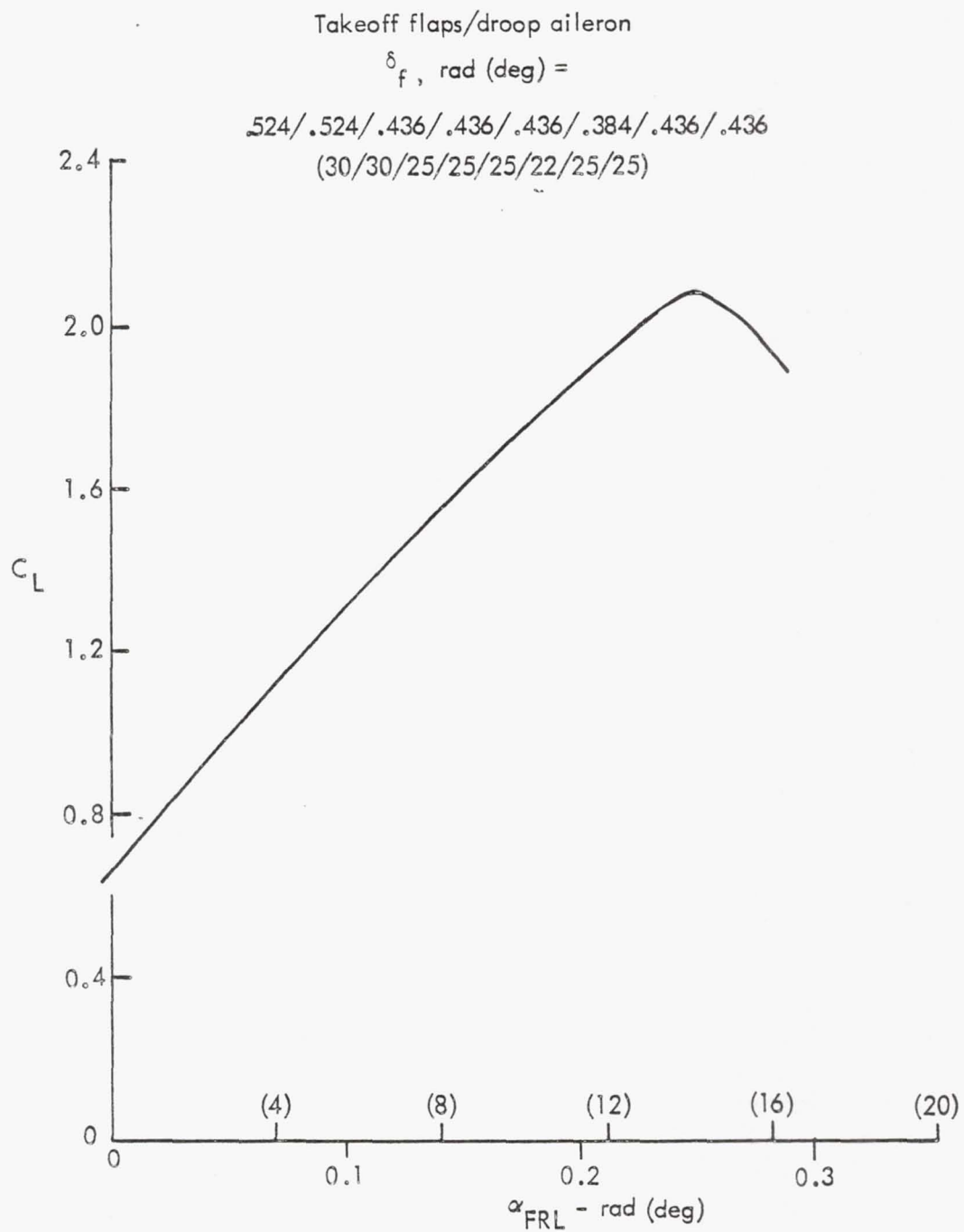


Figure 53. High lift characteristics - refined takeoff flap schedule



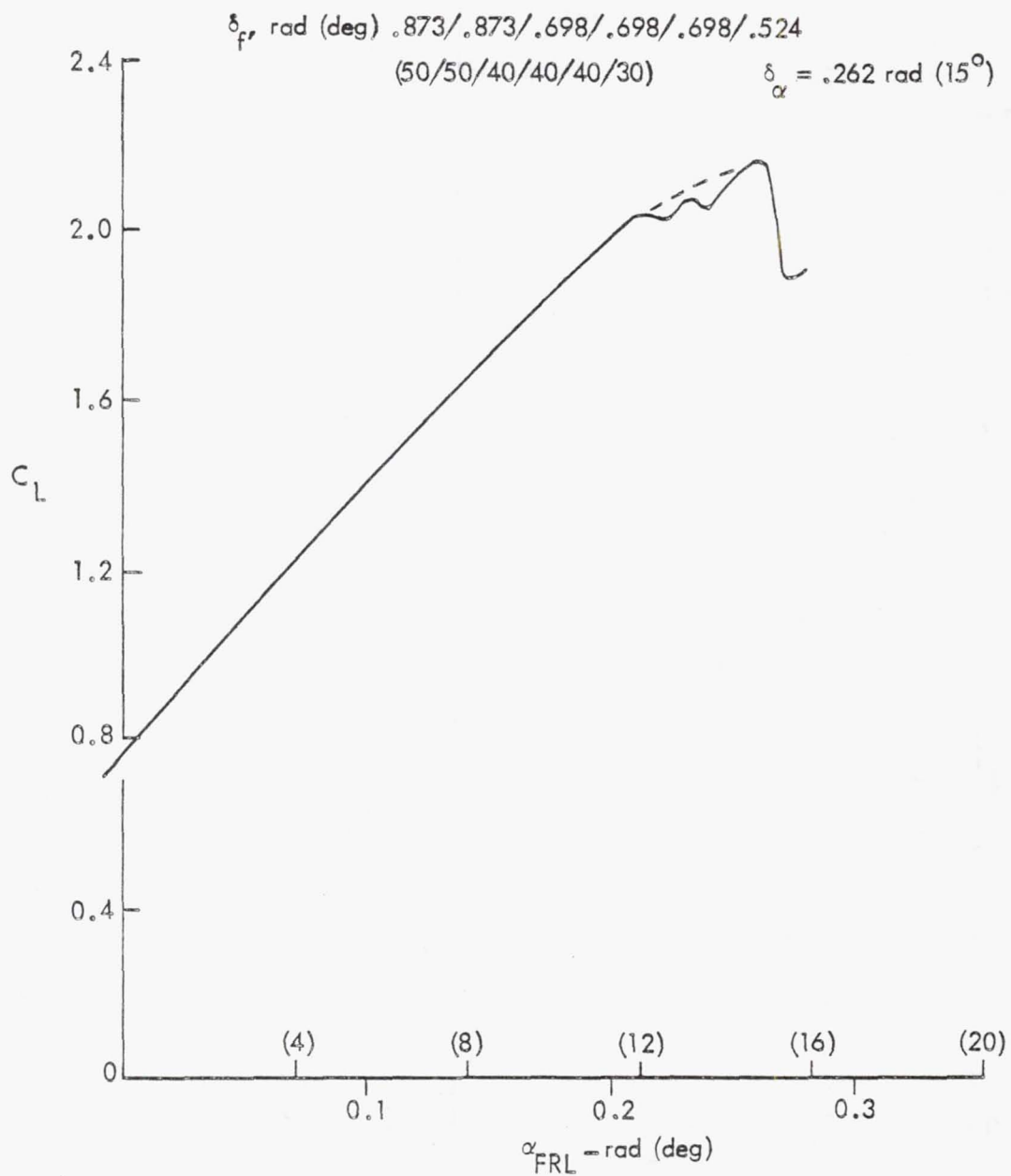


Figure 54. High lift characteristics - landing flaps, moderate aileron droop

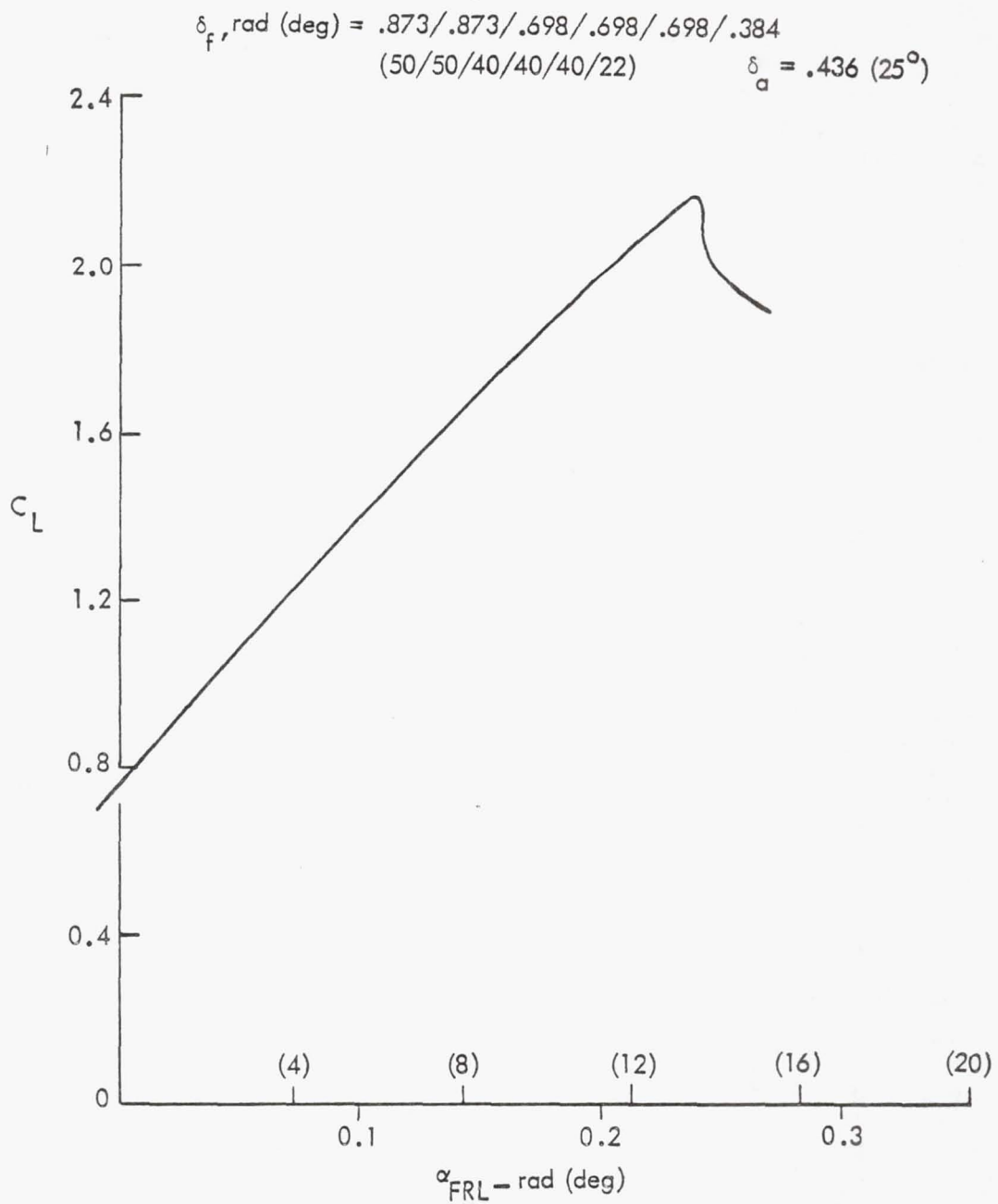


Figure 55. High lift characteristics - landing flaps, full aileron droop

#### 6.1.4.3 Sensitivity of Study Configurations to High-Lift System Technology Level

The selection of a high-lift system without leading-edge devices may appear to be dependent upon achievement of  $C_{L \text{ Max}}$  levels which are questionably high, based on rational analysis of leading-edge flow conditions near stall. Present levels of two-dimensional and three dimensional  $C_{L \text{ Max}}$  have been derived on the basis of sound engineering analysis. However, failure to achieve the predicted  $C_{L \text{ Max}}$  levels does not preclude the selection of a configuration without leading-edge devices. Table 9 shows the results of a study of the effect of  $C_{L \text{ Max}}$  level on configuration sizing and parameter selection for the following cases:

Configuration (1) - Baseline Case

Configuration (2) - Baseline Case with  $\Delta C_{L \text{ Max}} = -0.30$  ( $C_{L \text{ Max}} = 1.89$ )

Configuration (3) - Baseline Case with  $\Delta C_{L \text{ Max}} = -0.15$  ( $C_{L \text{ Max}} = 1.94$ ),  
and increased engine thrust

Configuration (4) - Baseline Case with  $\Delta C_{L \text{ Max}} = -0.15$  ( $C_{L \text{ Max}} = 2.02$ ),  
and increased wing area

Configuration (5) - Baseline Case with  $\Delta C_{L \text{ Max}} = -0.30$  ( $C_{L \text{ Max}} = 1.85$ ),  
and increased engine thrust

With the exception of configuration (2), which has a field length requirement of 3727 m (12 230 ft), all of these configurations satisfy the 3048 m (10 000 ft) field length requirement. Note that alternative thrust and wing area combinations can be easily found for substantially lower  $C_{L \text{ Max}}$  levels which cause only relatively minor block fuel penalties. D.O.C. penalties would be correspondingly small. Configuration (5) is considered to be a very pessimistic assessment; however, achievement of the lower level of high-lift system performance indicated in the study would not result in the need for a major configuration change and choice of no leading-edge devices is not invalidated by moderately lower  $C_{L \text{ Max}}$  levels.

#### 6.1.4.4 Summary of High-Lift Analysis

The span load distributions for the operational lift levels at lift-off and approach conditions are given in Figure 56. Predicted vortex drag efficiency factors, "e", are also indicated.  $C_{L \text{ Max}}$  and drag predictions for these configurations verify that initial GASP predictions for a high-lift system with no leading-edge devices can be achieved with the baseline high-lift system. Further study of the baseline high-lift system performance or stability and control characteristics would be justified only when an experimental development program is initiated.

#### 6.1.5 Stability and Control

Stability and control for the LFC baseline aircraft has been studied sufficiently to ensure that technical problems peculiar to the use of LFC will be amenable to solution using technology available by 1990. In deriving the basic design concepts for both the LFC baseline and the compara-

TABLE 9. EFFECT OF  $C_{L_{Max}}$  ON CONFIGURATION SIZING

Configuration	Basic $C_{L_{Max}}$	$C_{L_{Max}}$ to	$\delta_{to}$ rad (deg)	Take-off Weight kg (lb)	Wing Area $m^2$ ( $ft^2$ )	Thrust Engine N (lb)	Block Fuel kg (lb)	% Change In Block Fuel	Approach Speed km/hr (kn)
(1)	0	2.15	0.576	271 192	495	155 430	83 137	-	256
			(33)	(597 867)	(5333)	(34 944)	(183 283)	-	(138)
(2)	-0.30	1.89	0.611	271 192	495	155 430	83 137	-	272
			(35)	(597 867)	(5333)	(34 944)	(183 283)		(147)
(3)	-0.15	1.94	0.524	273 900	501	166 698	83 794		263
			(30)	(603 836)	(5391)	(37 477)	(184 731)	+0.80	(142)
(4)	-0.15	2.02	0.576	276 954	551	155 067	84 536		250
			(33)	(610 569)	(5931)	(34 862)	(186 366)	+1.68	(135)
(5)	-0.30	1.85	0.576	276 873	506	178 925	84 544		272
			(33)	(610 391)	(5452)	(40 226)	(186 385)	+1.69	(147)

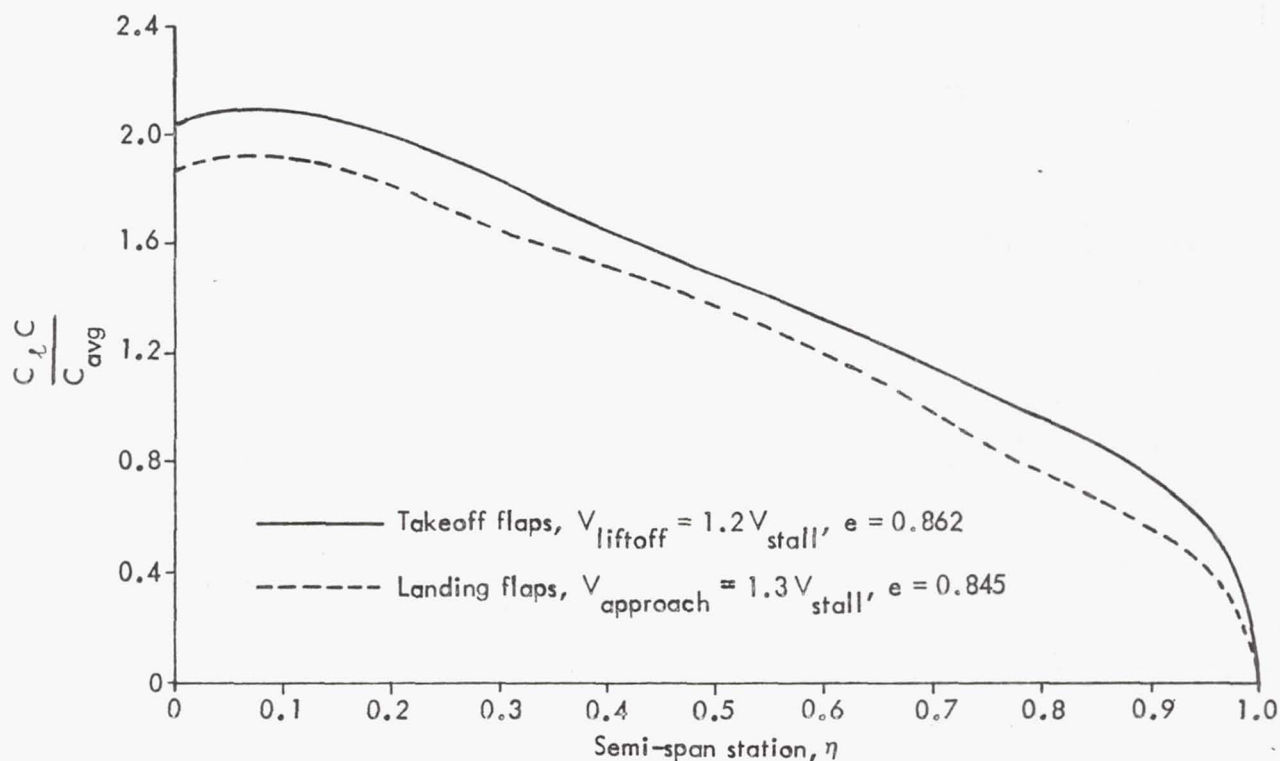


Figure 56. Span load distribution - lift off and approach conditions



tive turbulent baseline, the full predicted 1990 technology level for flight controls has been assumed, as outlined previously in Section 4.5.2. Various aspects of stability and control are discussed in the following sub-sections. Note that the control algorithm complexities of the sophisticated flight controls system required are beyond the scope of the present discussion.

#### 6.1.5.1 Longitudinal Stability and Control

Satisfactory longitudinal stability and control was provided for the LFC baseline by sizing the horizontal tail and control surfaces to provide stability levels and control response consistent with aircraft of the L-1011 and C-5 weight class. The GASP aircraft sizing program automatically defines a sufficient horizontal tail area matched to the aircraft size. The comparative turbulent aircraft horizontal tail and controls are sized in GASP consistent with a low-tail effectiveness and the same controls technology level employed for the LFC baseline. For both aircraft baselines an unusually small horizontal tail will furnish adequate stability and control.

#### 6.1.5.2 Lateral/Directional Stability and Control

As in the longitudinal case, lateral/directional stability and control was provided through parametric sizing in GASP. Differences in vertical tail sizing because of engine placement and the LFC baseline T-tail configuration have been recognized. Stability augmentation allows the small vertical tails used on both baselines. The lateral control system for both baselines provided rates of roll, through concept and sizes of roll control devices, which are comparable to C-5 roll performance, which is excellent for a large aircraft. Again, precise control algorithms were not developed and should be the subject for future flight controls and aerodynamics stability and control work. The modes of operation of the aft secondary flap and load alleviation device are of particular concern in the case of future LFC aircraft. However, criteria, control algorithms, and precise operational characteristics of the secondary flap were beyond the scope of the current study.

### 6.2 STRUCTURES AND MATERIALS

A central problem in the definition of a feasible production configuration for LFC transports is the development of LFC surface designs which satisfy aerodynamic requirements without imposing unacceptable structural weight penalties, manufacturing costs, and operational requirements. Consequently, extensive investigations were conducted in the development of structural concepts for both the wing-box and the leading-edge regions of the wing of the baseline LFC transports. As a part of the development, alternative structural concepts were evaluated, detailed designs were developed for selected concepts, manufacturing procedures were established, and full-scale structural specimens were fabricated and tested.

#### 6.2.1 Design Objectives

The laminarization of the boundary layer begins on the wing surface from which small quantities of the boundary layer are removed to stabilize

the flow over the surface. Thus, the selection of an optimum surface configuration is of primary importance in the development of a production LFC transport. The design objectives pertinent to the development of LFC structure include the following:

- (1) Satisfaction of the stringent requirements for surface smoothness and waviness.
- (2) Compatibility with manufacturing procedures adaptable to a production environment.
- (3) compatibility with in-service inspection, maintenance, and repair, while providing a high degree of reliability.
- (4) Imposition of minimum weight and cost penalties on the airframe.

#### 6.2.2 LFC Surface Panel Development

##### 6.2.2.1 Concept Evaluation and Selection

The following methods of providing the required surface configuration are available to the designer:

- o Non-structural covers
- o Structural surfaces
- o Combination of the first two methods

The plan for development and evaluation of alternative surfaces is shown in the flow diagram of Figure 57.

Concept design entailed the identification of alternative candidate concepts. The preliminary design effort included the development of consistent weight and cost factors for comparison during the evaluation. To develop weight and cost data, the preliminary design effort included the estimation of loads for the baseline LFC aircraft wing, selection of materials, and the sizing of surface/wing elements. For study purposes, the evaluation was restricted to the portions of the LFC upper and lower surfaces forming the main structural elements between the wing front and rear spars.

In addition to the above, the following were accomplished:

- o Manufacturing procedures were developed for each concept.
- o Estimates of manufacturing costs were completed for each concept.
- o The maintainability and reliability of each concept were assessed.
- o Procedures for repairing damaged surfaces were developed for each concept.
- o The compatibility of each surface concept with surface design criteria and other elements of the LFC system was evaluated.

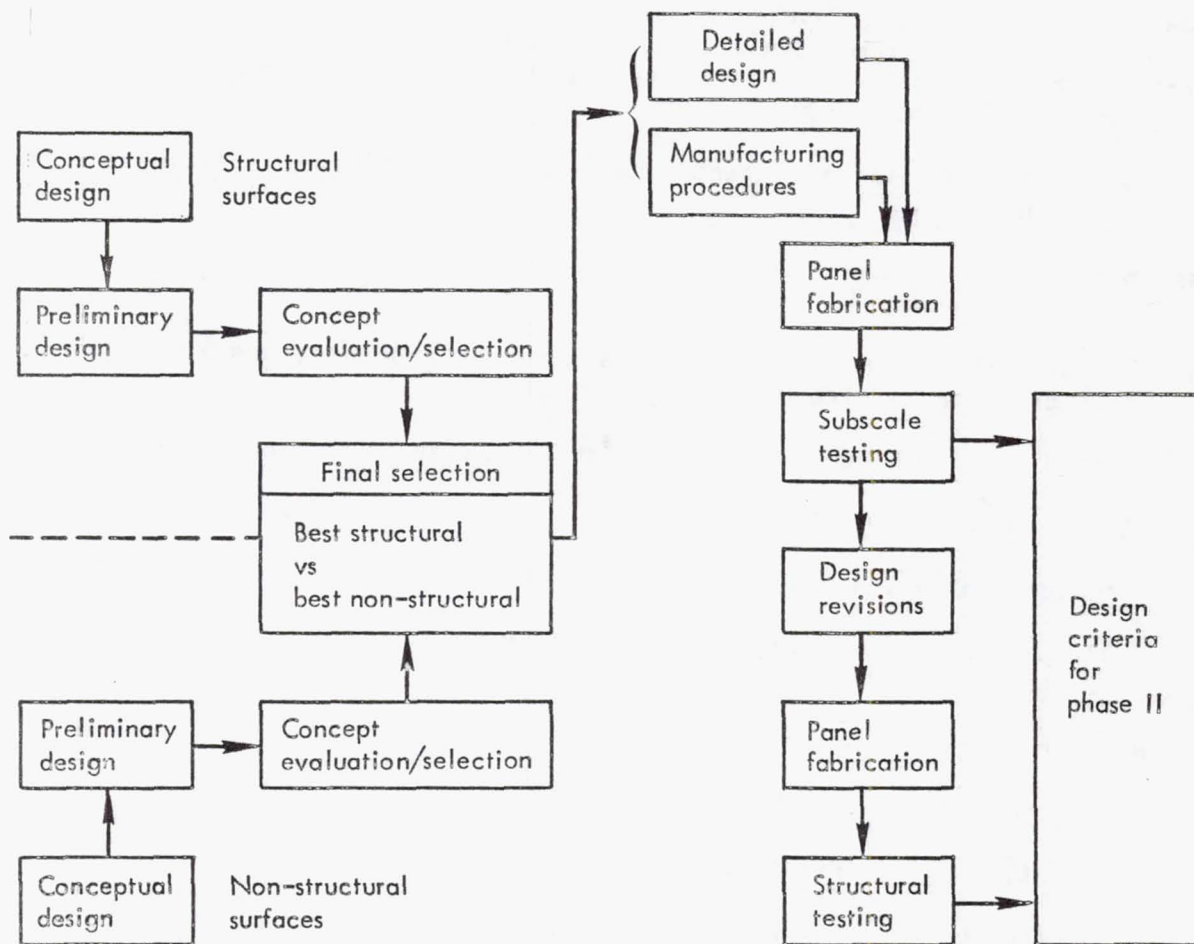


Figure 57. Plan for LFC surface development

Upon completion of this procedure for each of the candidate concepts, recommended non-structural, structural, and combination concepts were selected. These concepts were subsequently compared to permit selection of a single concept for future development.

Design guidelines were prepared for both structural and non-structural surfaces to assist designers and evaluators in their efforts to identify the recommended surface configuration.

The important criteria are:

- o Minimize external fasteners
- o Minimize external joints
- o Minimize steps, gaps, and surface waviness
- o Minimize duct intrusion into fuel cells
- o Provide for inspection of primary structure
- o Consider repair characteristics



- o Maintain required aero contour under 1g flight deflection
- o Satisfy service life goals

Figure 58 outlines the smoothness requirements for LFC surfaces as a function of cruise altitude. At the selected cruise altitude of 12 192 m (40 000 ft), only the 0.015 cm (0.006 in) down step requirement is expected to present significant manufacturing problems.

The maximum permissible amplitudes for LFC surface waves are shown in Figure 59 as a function of wavelength for three chord lengths.

The ideal LFC surface would be an infinitely smooth aerodynamic shape with no seams, joints, or surface fasteners. Since such a surface is unattainable in the context of a high production article, it is necessary from the outset of concept design to make a series of compromises in the form of judgments to define a practical approach to the problems of manufacturing, repair, and maintenance. The requirements for close tolerance slots and surface ducting, along with the requirements imposed by smoothness and waviness criteria, appear to be amenable with the manufacturing techniques envisioned for the 1990 time frame. Thus, it is assumed that all concepts described herein can be made to perform their required functions.

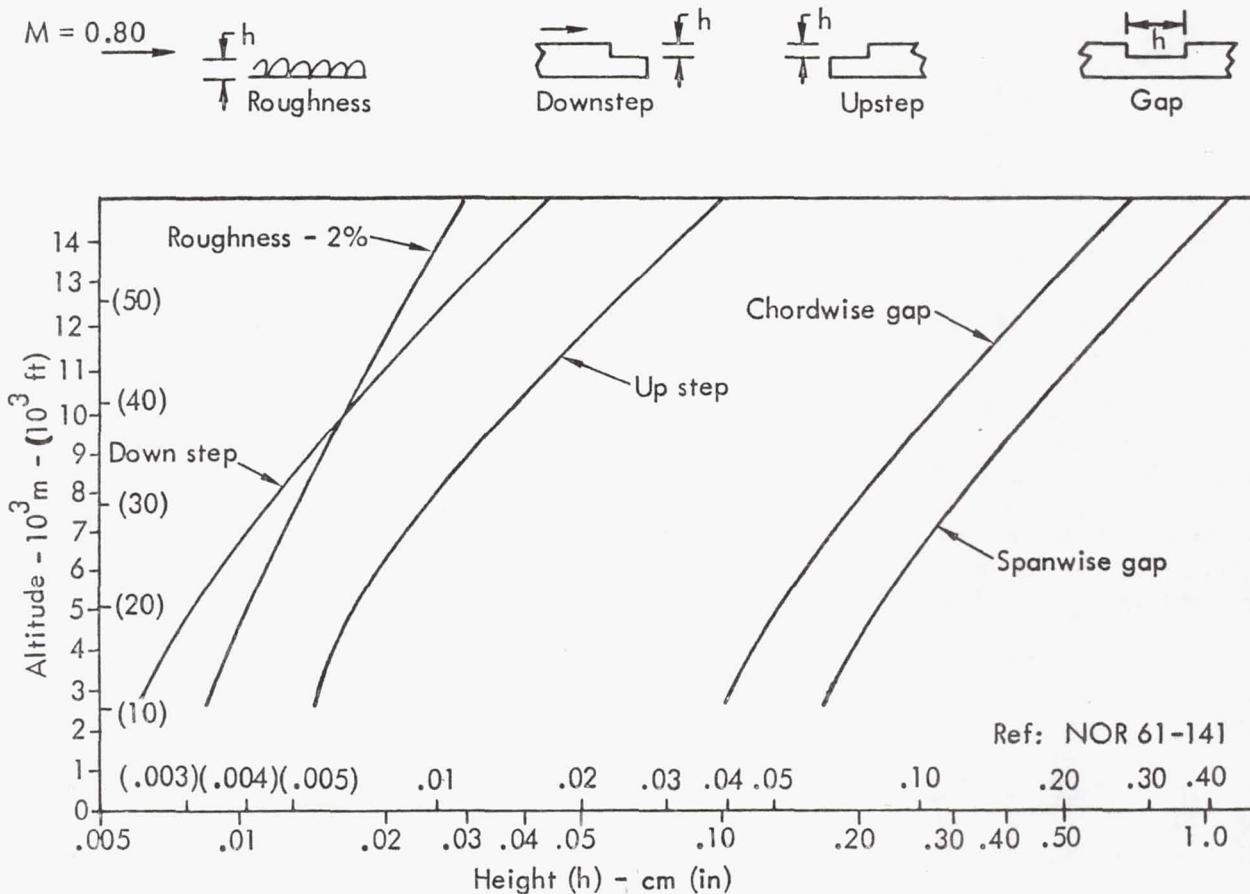


Figure 58. LFC surface smoothness criteria



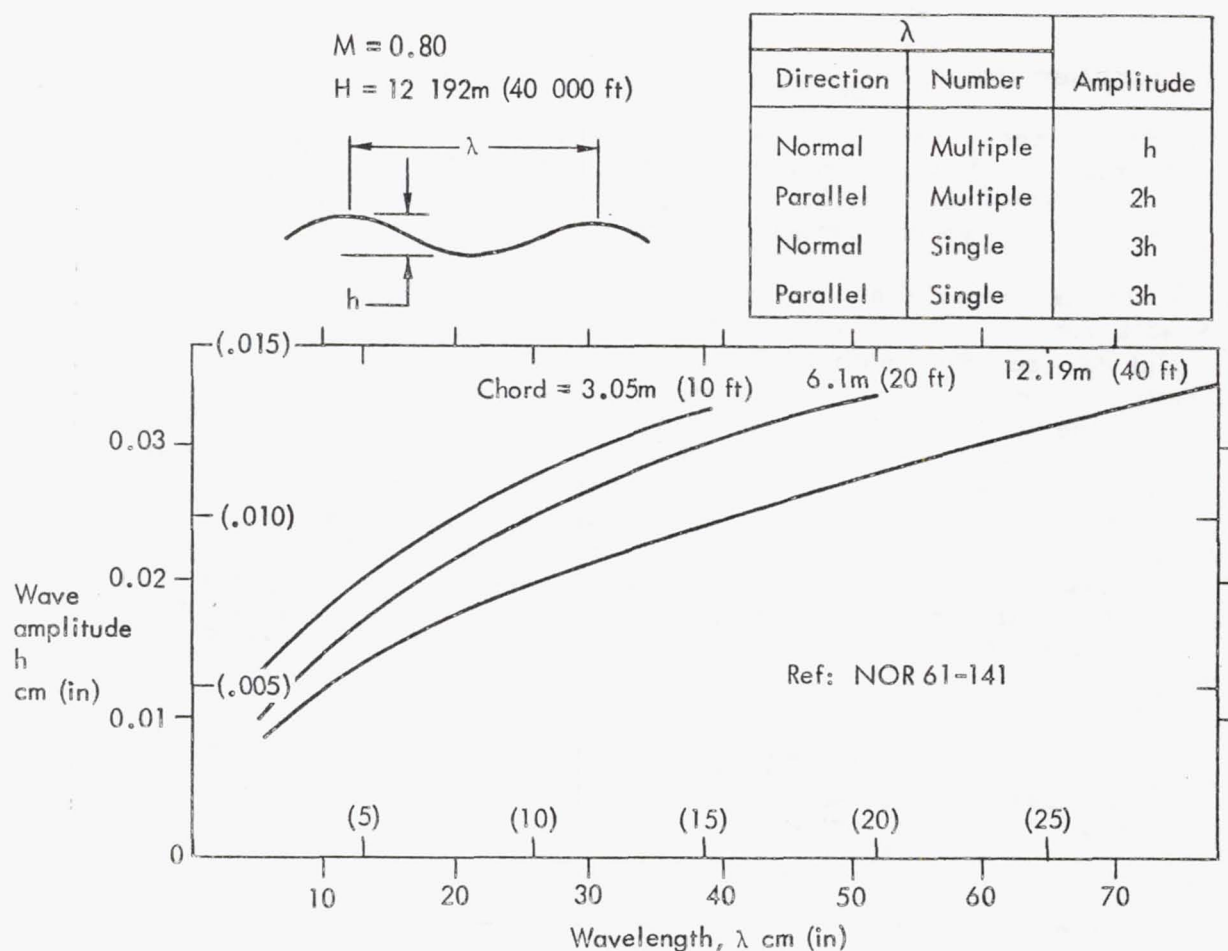


Figure 59. LFC surface waviness criteria

The obvious task for the designer is to identify concepts offering the highest probability of success or the lowest degree of compromise at the lowest possible weight and cost penalties to the airframe. Each of the concepts developed in this study offer some advantages in that each satisfies some if not all of the design guidelines. In many cases, the meeting of one guideline necessitates compromise in another area. In order to proceed with the concept, the designer must rationalize the accepted deficiency by assuming that good detail design and advanced manufacturing and maintenance techniques available by 1990 will minimize adverse effects of the compromise, and further, that testing will prove broader tolerances to be acceptable, thus reducing system sensitivity.

This section includes descriptions of each of the thirteen LFC surface concepts considered as candidates for further development and for use on the final 1993 LFC transport configuration.

#### Non-Structural Surface Concepts

Wing Box Structure - The basic wing box structure selected to support the non-structural panels under consideration is the hat-stiffened configuration shown in Figure 60.

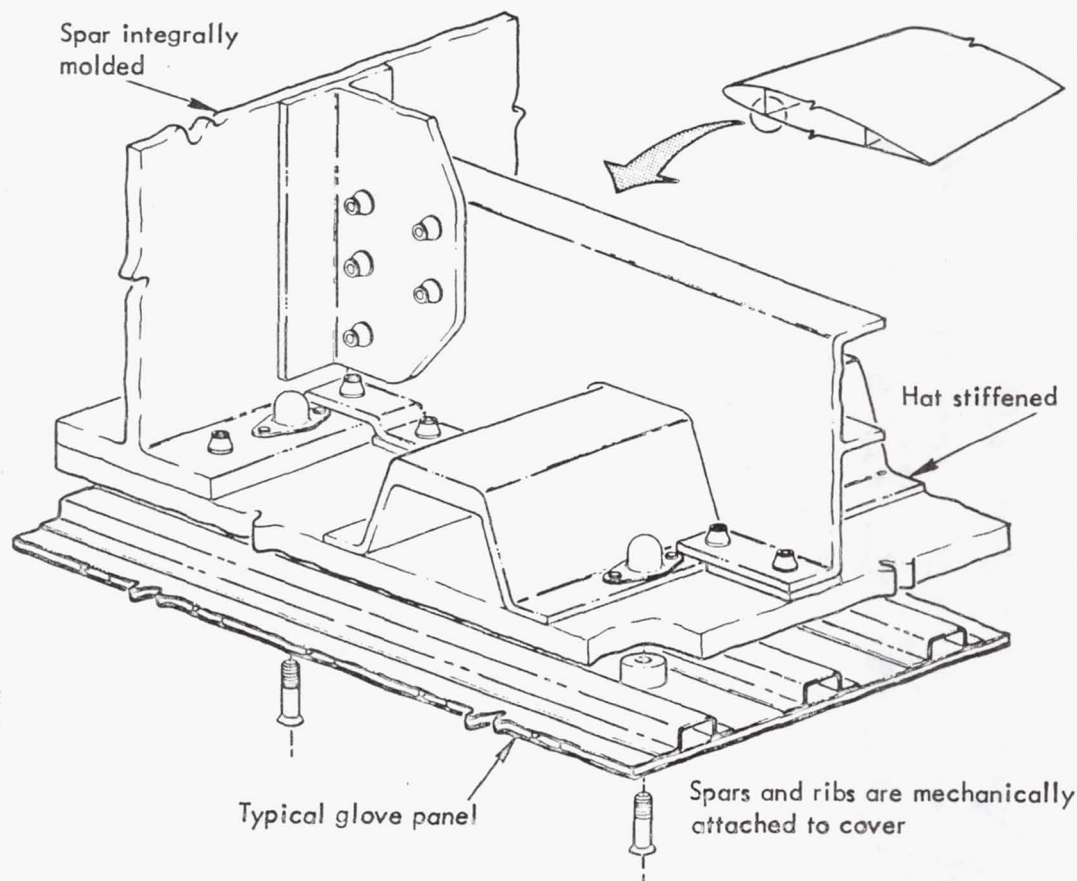


Figure 60. Wing box structure for non-structural concepts

All major components are fabricated from graphite/epoxy material and wherever possible are one-piece bonded assemblies. The cover assemblies consist of precured skins and hat-section stiffeners which are joined in a second stage bonding operation. Several methods of glove panel attachment require some penetration of the cover panels. Where cover penetration is required, dome nuts are utilized to prevent fuel leakage.

The rib design is a truss arrangement comprised of integrally molded caps to which pultruded diagonals are mechanically attached.

Front and rear spars are integrally molded assemblies and are continuous from root to tip.

Penetration of the cover panels does not present a potential aerodynamic problem as with the various integral designs. Therefore mechanical fasteners are used for substructure to cover attachment.

Floating Panel, Blind-Stud Mounted - This LFC surface panel concept, shown in Figure 61 is a glove-type panel which is allowed to float on the basic wing structure. The panel is installed with the wing in the 1g

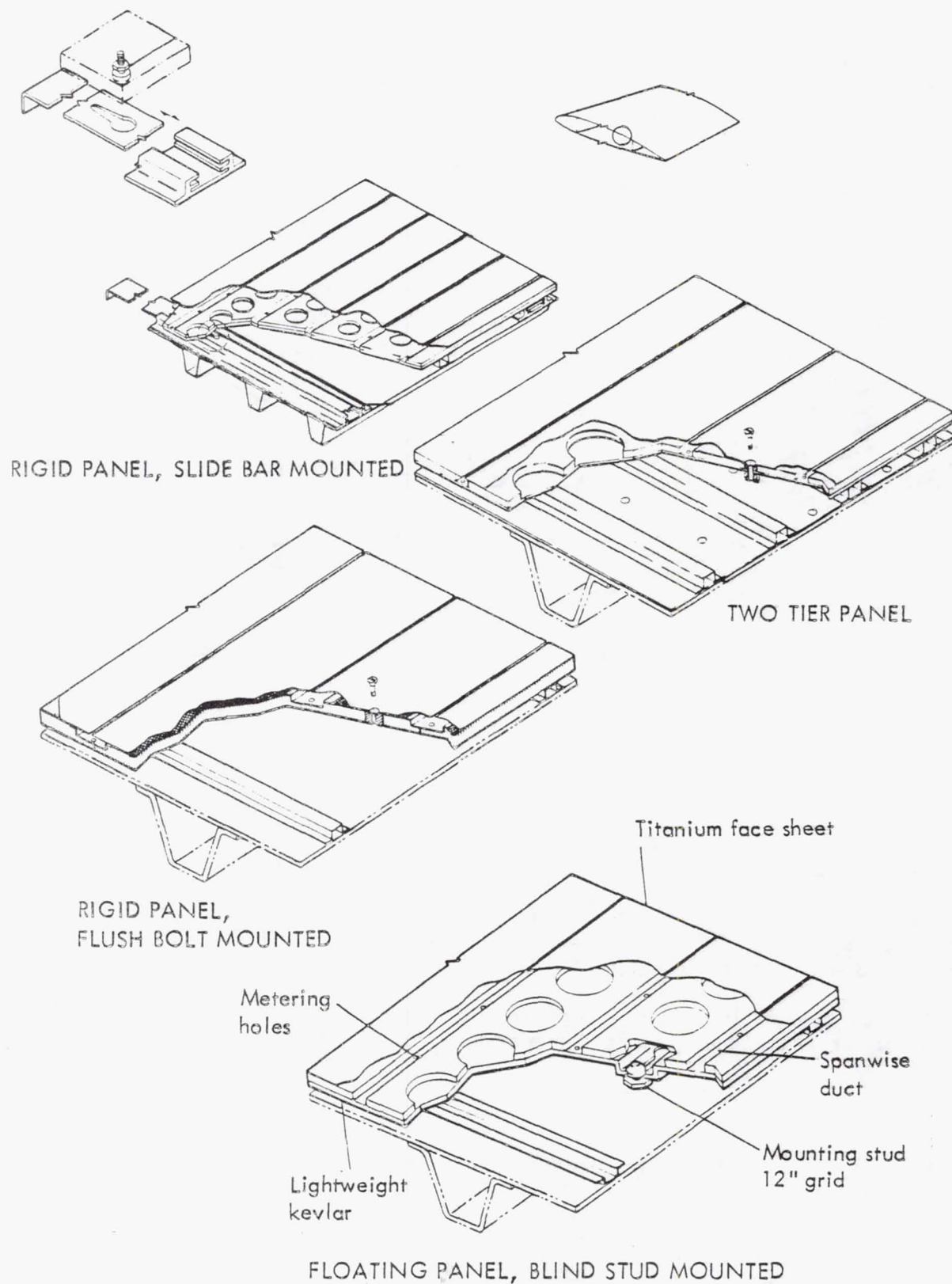


Figure 61. Non-structural concepts



cruise condition in order to attain the required contour and smoothness in operation. Each panel is approximately 381 cm (150 in) in span by the local chord length from 6% to 75%.

Rigid Panel, Flush-Bolt Mounted - This LFC surface concept, shown in Figure 61 is a glove type panel rigidly fastened to the basic wing with bolts, and is designed to resist the strain induced by wing bending. Since it is rigidly attached, it may provide a small increment of wing bending strength. Each panel is approximately 381 cm (150 in) in span by the local length from 6% to 75%. The panel rests on formers attached to the basic wing structure.

Two-Tier Panel - Also shown in Figure 61 is a glove-type panel rigidly fastened to the basic wing with bolts. Thus, it is designed to resist the strain induced by wing bending. This panel may provide a small increment to total required wing strength. Each panel is approximately 381 cm (150 in) in span by the local chord lengths from 6% to 75%. The chordwise formers in this case are incorporated into the 2-tier panel.

Rigid Panel, Slide-Bar Mounted - This LFC surface panel concept is a non-structural panel similar to the first concept described above. As shown in Figure 61, this panel is rigidly fastened to the basic wing by slide bars instead of floating keyholes. The slide bars are restrained after assembly by a removable nose cap.

The comparison of non-structural LFC surface panel concepts shown in Table 10 provides the basis for the selection of the "rigid panel, flush bolt" concept for further evaluation.

#### Structural Surface Concepts

Honeycomb - The honeycomb cover shown on Figure 62 features inner and outer face sheets of graphite/epoxy material separated by a honeycomb core approximately 3.81 cm (1.5 in) thick. Several core materials were considered including aluminum, fiberglass and nomex, with preference being given to the non-metallic materials to obviate potential corrosion problems. An alternative honeycomb cover arrangement was also developed in which the chordwise duct is introduced to transfer the air flow from the spanwise ducts into the main leading edge trunk duct.

Hat Stiffener - In the configuration shown on Figure 62, structural elements of the covers and substructure are utilized for ducting purposes. With this dual purpose approach, no parasitic ducting weight is introduced and substantial weight savings is realized. The cover panel is comprised of a graphite/epoxy skin containing integrally molded spanwise ducts and hat-section stiffeners running parallel to the front beam. An alternate version employing a different system of chordwise ducts was also developed.

Blade Riser - An efficient method of stiffening highly-loaded wing panels, particularly the tension surface, is the blade riser configuration shown on Figure 62. The cover panel assembly consists of an outer skin containing recesses for spanwise ducts to which a blade riser of predominantly uni-axial material is secondary bonded. In this design, a thin gauge inner skin is required to form the inside spanwise duct.



TABLE 10. COMPARISON - NON-STRUCTURAL CONCEPTS

	<u>Floating Panel Blind Stud</u>	<u>Rigid Panel Flush Bolt</u>	<u>Two-Tier Panel</u>	<u>Rigid Panel Slide Bar</u>
<u>Characteristics</u>				
Laminar Efficiency (%)	85	85	85	85
Chordwise Joints	7	7	7	7
Spanwise Joints	1	1	1	1
External Fasteners				
no/m <sup>2</sup>	6.5	10.8	8.6	2.2
(no/ft <sup>2</sup> )	(0.6)	(1)	(0.8)	(0.2)
<u>Weight</u>				
Non-Structural				
kg/m <sup>2</sup>	0.68	0.49	0.57	0.97
(lb/ft <sup>2</sup> )	(1.50)	(1.09)	(1.25)	(2.13)
Wing Structure				
kg/m <sup>2</sup>	0.25	0.25	0.20	0.25
(lb/ft <sup>2</sup> )	(0.55)	(0.55)	(0.44)	(0.55)
kg/m <sup>2</sup>	0.93	0.74	0.77	1.22
TOTAL (lb/ft <sup>2</sup> )	(2.05)	(1.64)	(1.69)	(2.68)
<u>Manufacturing</u>				
Procedures	3	1	2	4
\$/m <sup>2</sup>	2583	2164	2497	2551
Cost (\$/ft <sup>2</sup> )	(240)	(201)	(232)	(237)

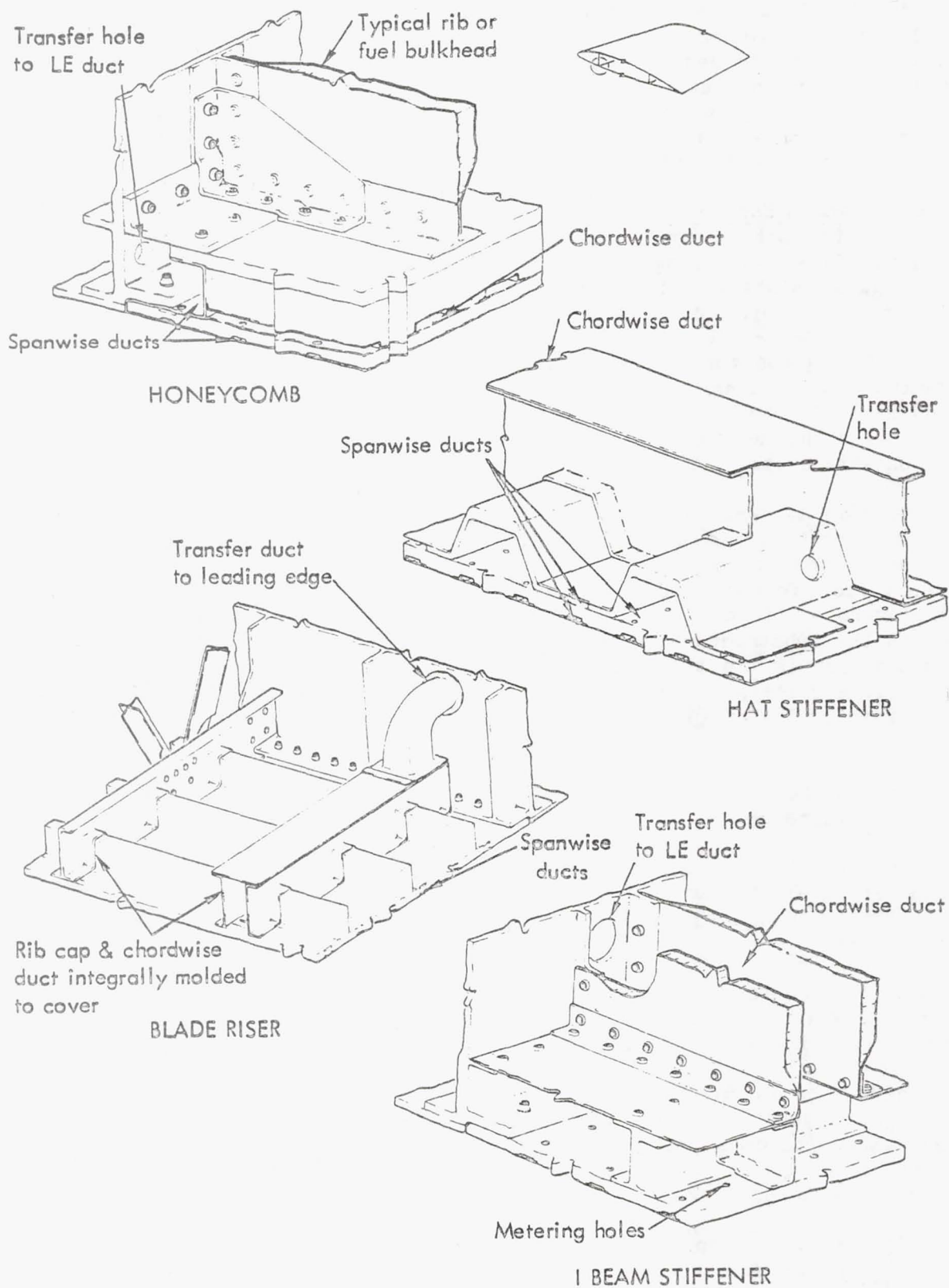


Figure 62. Structural concepts

I-Section Stiffener - This cover panel shown on Figure 62 is similar to that for the blade riser except that I-section stiffeners are used instead of blades. A predominant feature of this design is the large spanwise ducts which are formed by attaching an inner skin to the flange of the I-beams and running between ribs and from front to rear spar.

The data shown in Table 11 provide the basis for selecting the "hat stiffener" concept for further evaluation.

Combination Surface Concepts - The panel concept shown in Figure 63 endeavors to combine some of the advantages of both glove and integral concepts while minimizing the respective disadvantages. In this concept, the spanwise slots and ducts are contained in a removable surface panel while the chordwise ducting is molded into the composite sandwich substructure. The removable outer surface panel is fabricated by bonding a layer of lightweight Kevlar syntactic tape between an outer skin of titanium and an inner skin of Kevlar 49. The titanium outer sheet has spanwise suction slots. The light-weight Kevlar syntactic tape core with the inner skin, metering holes are drilled as required along the length of the spanwise ducts.

The main load-carrying substructure is comprised of an aluminum honeycomb core sandwiched between 2 layers of graphite/epoxy. Kevlar hat-sections embedded into the honeycomb core form chordwise ducts to carry suction flow forward and aft to leading- and trailing-edge trunk ducts. Metering holes, to match those drilled in the thin outer panel, are drilled through the substructure graphite/epoxy outer layer to provide a flow path from the spanwise to the chordwise ducts. The substructure is designed as a one-piece semispan structure while the removable outer surface panels are approximately 381 cm (150 in) in span by the local chord length from 3% to 75%.

Three methods of attaching the thin outer panel to the substructure are shown on Figure 63.

The data shown in Table 12 provide a basis for selecting the "bonded" method of panel attachment for further study.

#### Concept Selection

In addition to the weight and cost data presented previously, the three final concepts were evaluated relative to maintenance requirements, inherent reliability, repair procedures, and compatibility with ducting.

On the basis of these evaluations, the hat-section stiffened panel shown in Figure 64 was selected for further development. Both the quantitative concept characteristics and the qualitative rankings provide justification for this selection. Following are the most significant considerations in this choice:

- (1) Of primary importance is the uncertainty associated with satisfying surface smoothness and waviness criteria with any removable panel configuration. While subsequent testing may show such configurations to be feasible, it is not reasonable to select such a configuration for development in the current study.

TABLE 11. COMPARISON - STRUCTURAL CONCEPTS

	<u>Honeycomb</u>	<u>Honeycomb Alt</u>	<u>Hat Stiffener</u>	<u>Hat Stiffener Alt</u>	<u>Blade Riser</u>	<u>I-Section Stiffener</u>
<u>Characteristics</u>						
Laminar Efficiency (%)	100	100	100	100	100	100
Chordwise Joints	0	0	0	0	0	0
Spanwise Joints	2	2	2	2	2	2
External Fasteners	0	0	0	0	0	0
<u>Weight</u>						
Non-Structural						
kg/m <sup>2</sup>	-	-	-	-	-	-
(lb/ft <sup>2</sup> )	-	-	-	-	-	-
Wing Structure						
kg/m <sup>2</sup>	0.69	0.72	0.22	0.22	0.24	0.24
(lb/ft <sup>2</sup> )	(1.53)	(1.58)	(0.49)	(0.49)	(0.53)	(0.53)
TOTAL kg/m <sup>2</sup>	0.69	0.72	0.22	0.22	0.22	0.22
(lb/ft <sup>2</sup> )	(1.53)	(1.58)	(0.49)	(0.49)	(0.53)	(0.53)
<u>Manufacturing</u>						
Procedures	4	4	1	2	3	2
Cost \$/m <sup>2</sup>	2745	2831	506	506	635	958
(\$/ft <sup>2</sup> )	(255)	(263)	(47)	(47)	(59)	(89)



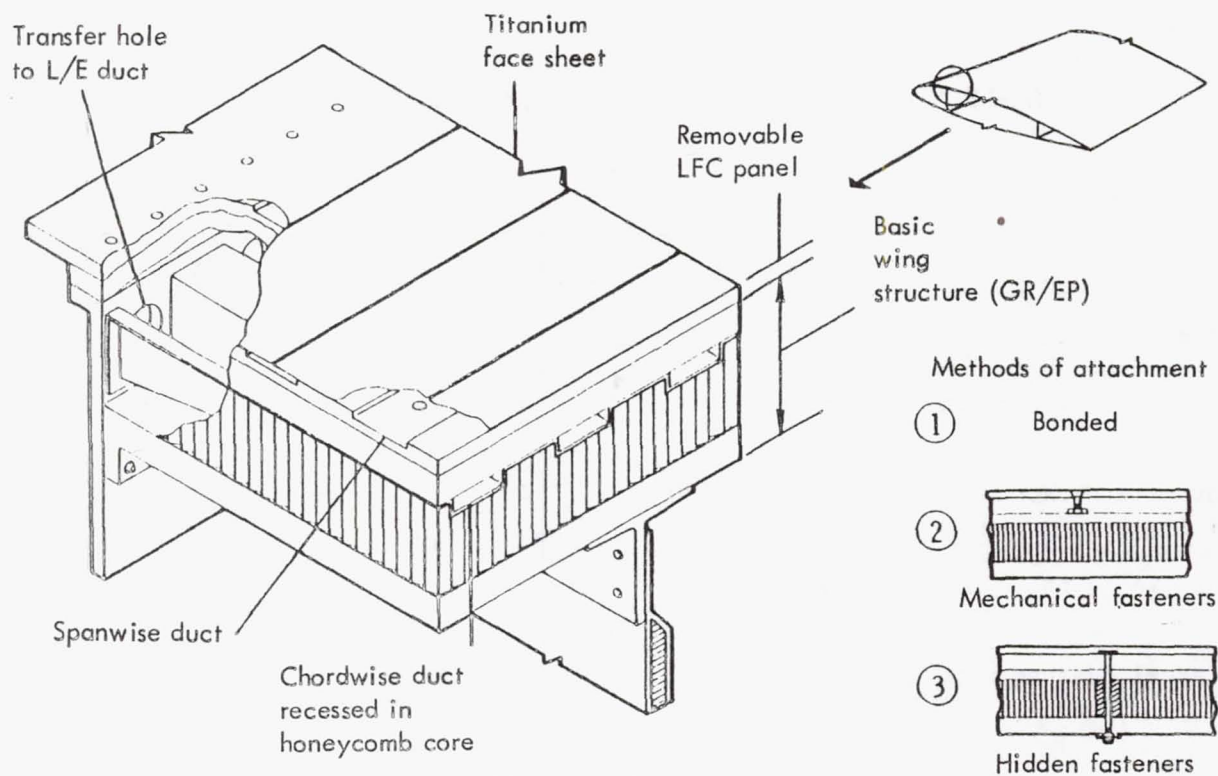


Figure 63. Combination concepts

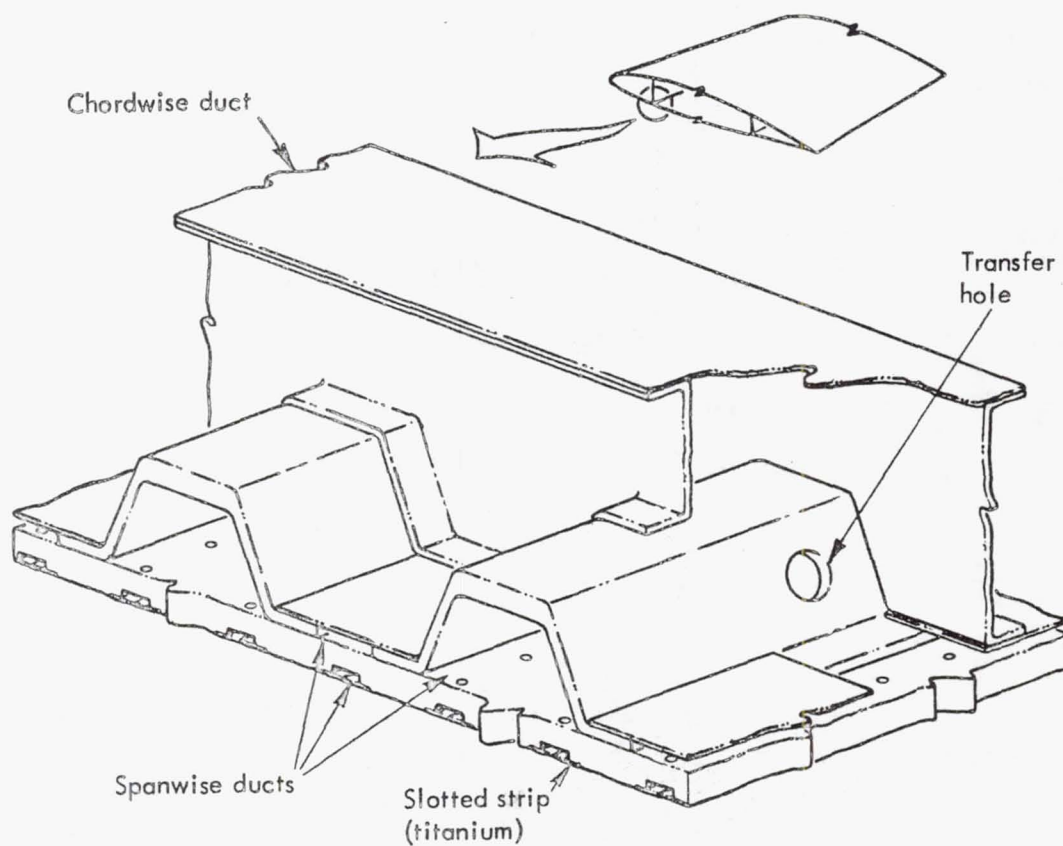


Figure 64. Selected surface concept

TABLE 12. COMPARISON - COMBINATION CONCEPTS

	<u>Removable Panel- Bonded</u>	<u>Removable Panel- Mech Fasteners</u>	<u>Removable Panel- Hidden Fasteners</u>
<u>Characteristics</u>			
Laminar Efficiency (%)	85	85	85
Chordwise Joints	7	7	7
Spanwise Joints	1	1	1
External Fasteners no/m <sup>2</sup> (no/ft <sup>2</sup> )	0	10.8 1	0
<u>Weight</u>			
Non-Structural kg/m <sup>2</sup> (lb/ft <sup>2</sup> )	0.41 (0.90)	0.68 (1.51)	0.74 (1.63)
Wing Structure kg/m <sup>2</sup> (lb/ft <sup>2</sup> )	0.57 (1.26)	0.64 (1.40)	0.64 (1.40)
TOTAL kg/m <sup>2</sup> (lb/ft <sup>2</sup> )	0.98 (2.16)	1.32 (2.91)	1.37 (3.03)
<u>Manufacturing</u>			
Procedures	2	3	4
Cost \$/m <sup>2</sup> (\$/ft <sup>2</sup> )	3888 (360)	4298 (398)	4298 (398)

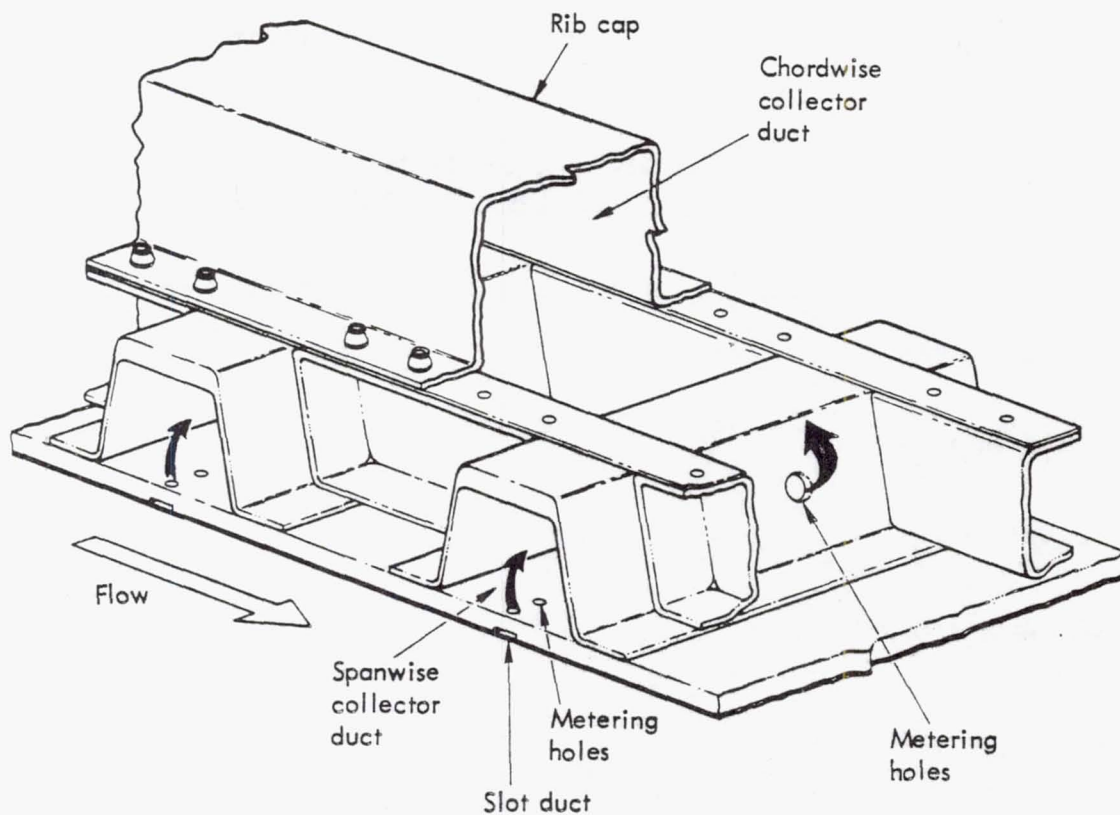


Figure 65. Surface design

TABLE 13. WING INTERNAL LOADS

% Semispan	Cover				Spar Shear	
	$N_x$		$Q$		$Q$	
	$10^3$ N/cm	(KIPS/in)	$10^3$ N/cm	(KIPS/in)	$10^3$ N/cm	(KIPS/in)
0.09	73.9	(42.2)	4.4	(2.5)	7.9	(4.5)
0.30	66.4	(37.9)	5.4	(3.1)	11.2	(6.4)
0.55	39.4	(22.5)	3.8	(2.2)	10.5	(6.0)
0.75	16.1	( 9.2)	2.3	(1.3)	6.7	(3.8)
0.85	6.7	( 3.8)	1.4	(0.8)	4.2	(2.4)

- (2) The selected structural concept provides the potential of greater laminarization efficiency by minimizing chordwise joints and external fasteners.
- (3) The weight increment of the alternatives is greater than that of the selected structural concept by factors of 3.3 and 5.9.
- (4) The cost increment of the alternatives is greater than that of the selected structural concept by factors of 4.3 and 8.5.
- (5) The alternative non-structural and combination concepts tend to aggravate many of the maintenance problems they were intended to solve. The selected structural concept appears to be superior in every maintenance area evaluated. Inspection of the surface is readily accomplished through a combination of visual and NDI techniques.
- (6) The major deficiencies of the selected concept are the potential reliability problems created by secondary ducting within fuel tanks and the relatively limited flexibility provided for slot spacing. It is anticipated that compromises can be incorporated to minimize the impact of both of these deficiencies.

#### 6.2.2.2 Design

Figure 65 illustrates the selected LFC surface configuration with suction flow denoted by arrows. Boundary layer air is pulled through spanwise surface slots into spanwise capillaries, then through metering holes into the structural hat stiffeners. Suction flow is carried spanwise until it reaches the chordwise collector duct which is formed by hollow rib caps located on alternate ribs. Details of the internal ducting and metering are given in Section 6.3.2. Designs based on this surface configuration were completed as a part of the development and testing of three 0.91 m x 1.52 m (3 ft x 5 ft) panels.

The LFC surface is constructed of graphite/epoxy. Each element is bonded in place with mechanical fasteners used at rib caps. The entire surface is covered by a sheet of titanium. The surface is designed to accommodate slot spacings, of 5.08, 7.62, and 10.15 cm (2, 3, and 4 in) or multiples thereof.

When the up-bending loads are applied to the sectional geometries, the critical internal loads shown in Table 13 result. The test loads for the 0.91 m x 1.52 m (3 ft x 5 ft) LFC surface panel are those corresponding to the 30% semispan location.

Details of the surface concept, including the selection of materials and number and orientation of the 5208/T300 graphite/epoxy plies, are shown in Figure 66.

The outer surface material is 6AL-4V annealed titanium. Thickness is in the range 0.041 cm to 0.051 cm (.016 in to 0.20 in). The selection of titanium for the outer face sheet was primarily based on corrosion consideration along the slots. A sawed slot in aluminum sheet could not be



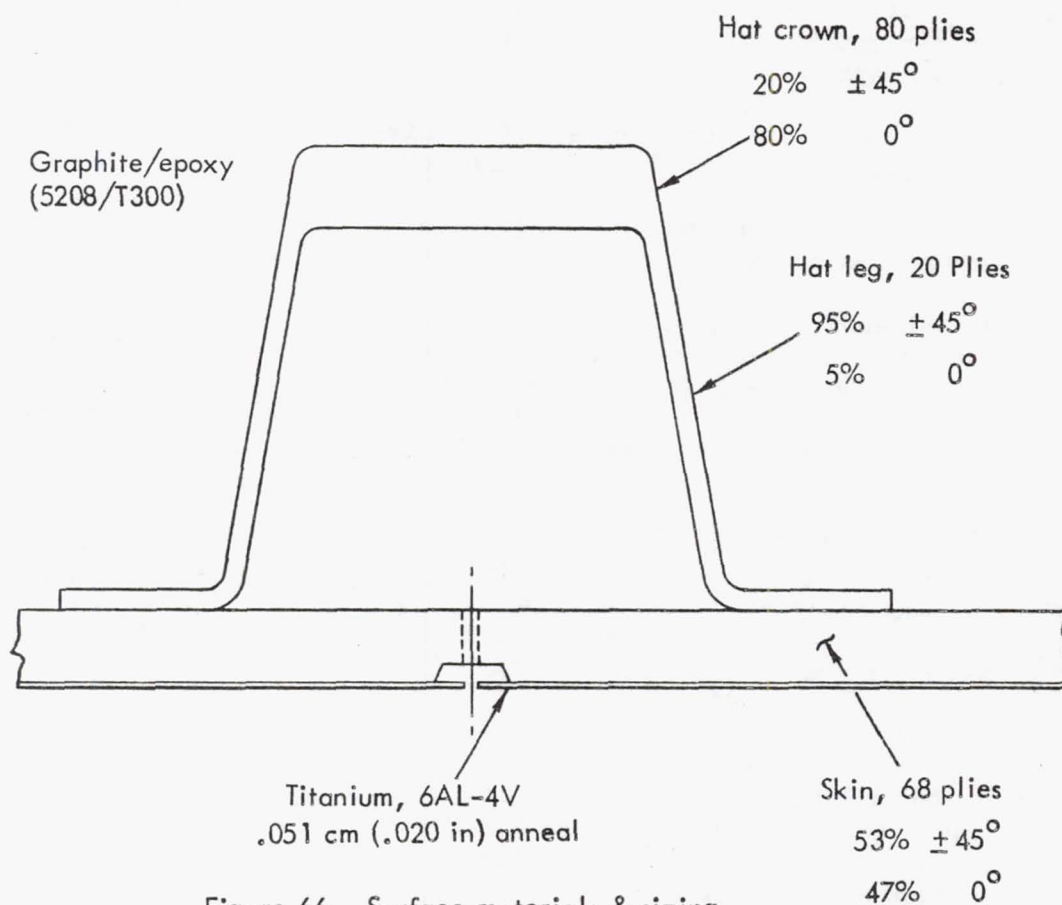


Figure 66. Surface materials & sizing

suitably protected against corrosion. The titanium sheet provides protection against:

- o FOD and other impact damage to the substructure graphite/epoxy skin
- o Lightning
- o Sand/rain erosion
- o Ultraviolet radiation

Note that the titanium sheet is used to carry primary wing loads. Therefore, no weight penalty results from the use of titanium instead of aluminum. In the mid-chord region, the suction slots with widths ranging from 0.020 cm to 0.030 cm (0.008 in to 0.012 in) are spaced at 15.2 cm and 27.9 cm (6 in and 11 in) for the upper and lower surfaces, respectively. The titanium is structurally bonded to the skin with FM123-4 adhesive. This bond is cured at 79.1°C (200°F) to reduce the impact of thermal mismatch of the titanium and the graphite/epoxy skin. This FM123-4 bond was selected because of its low flow to preclude filling the slot duct with the excess resin bleed.

The wing skin material, 5208/T300 graphite/epoxy, was selected due to:

- o The potential weight saving up to 40% relative to current metals
- o The capability of molding to a tool to meet LFC smoothness criteria
- o The reduced notch sensitivity for metering holes relative to current metals.

The graphite/epoxy skin is pre-bled in stacks of 16-20 plies. The 0.20 cm (0.08 in) deep by 0.76 cm (0.30 in) wide slot ducts are molded into the skin during cure cycle. The typical skin thickness varies from 0.25 cm (0.10 in) up to 1.09 cm (0.43 in) for the tip and root, respectively. In some padded areas the thickness reaches 2.54 cm (1.0 in).

The hat material is also 5208/T300 graphite/epoxy. The thickness of the hat crown varies from 0.25 cm to 1.27 cm (0.1 in to 0.50 in) from the tip to the root. The hat is structurally bonded to the skin using American Cyanamid FM73 adhesive cured at 106.9°C (250°F) in an autoclave using vacuum bag pressure. The rib clips, shown in Figure 65, are fabricated from 5208/T300 graphite/epoxy to permit curing at the same temperature as the hats. Four titanium fasteners are installed at each rib clip to each hat leg to carry the rib tension load into the skin. These fasteners were found to be necessary because of the low allowable interlayer tension stress of graphite/epoxy.

#### 6.2.2.3 Manufacturing Procedures

The manufacturing procedures evaluated during this phase of the study were directed toward the development of three 0.91m x 1.52m (3 ft x 5 ft) LFC surface panels to be employed in subscale testing. To permit fabrication of the selected LFC surface design, manufacturing development was required to economically produce acceptable slots in titanium and fabricate basic hat-stiffened wing-box structure from graphite-epoxy composite material in sections thicker than had previously been fabricated. A variety of slotting procedures and graphite/epoxy structure fabrication and assembly procedures were evaluated in the selection of manufacturing procedures providing a high-quality, dimensionally accurate LFC wing panel structure. Following is a brief discussion of the investigations conducted.

#### Surface Slotting

The following criteria were established for slots in the titanium LFC surface:

- (1) A slot width range of 0.076 mm to 0.228 mm (0.003 in to 0.009 in).
- (2) A slot width tolerance of  $\pm 10\%$ .
- (3) The slot entrance equal to or thinner than the slot exit to minimize slot contamination.
- (4) Sharp slot edges to facilitate control of air flow through the slots.

Table 14 summarizes the results of investigations conducted in the evaluation of candidate slotting procedures. Of the eight procedures evaluated, including both pre-assembly and post-assembly techniques, the sawing technique was judged to be most compatible with requirements for the slotting of titanium in a production environment. Slots can cut at rates ranging from 7.52 cm/min (3 in/min) for 0.008 cm (0.003 in) slots to 25.4 cm/min (10 in/min) for slots greater than 0.015 cm (0.006 in).

Figure 67 shows a photo of a sawed slot in titanium. Note the corner fillets formed by the FM123-4 adhesive bond. Figure 68 shows the cross-section of a 0.018 cm (0.007 in) saw cut slot in 0.051 cm (0.020 in) titanium.

### Structural Skin

A major problem in the development of thick sections of 5208 graphite/epoxy was the ply thickness distribution through the skin. Bleeding from one side yielded plies against the bleeder which were too thin and plies away from the bleeder which were too thick. A 20-ply stack which was pre-

TABLE 14. COMPARISON OF SLOTTING PROCEDURES

<u>Slotting</u>	<u>Verified Production Potential</u>	<u>Comments</u>
Electro-discharge machining	Yes	Further work required to get slot width to .008 cm (.003 in)
Joining machined strips		
Bonding	No	Slot tolerance exceeded $\pm .003$ cm ( $\pm .001$ in)
Welding	No	Slot tolerance exceeded $\pm .003$ cm ( $\pm .001$ in)
Electron Beam	No	Failed to produce slots consistently
Water Jet	No	Maximum rate of 2.54 cm/min (1 in/min)
Laser	No	Unacceptable slots
Planer	No	Minimum slot width of .020 cm (.008 in)
Saw	Yes	Provides most consistent slots
Chem-milling	No	Failed to provide square corners



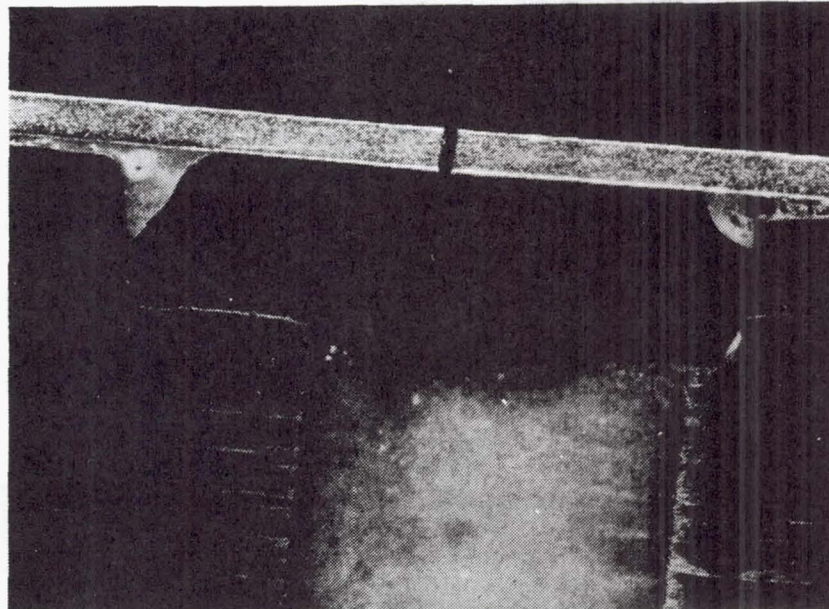


Figure 67. Sawed slot with slot duct

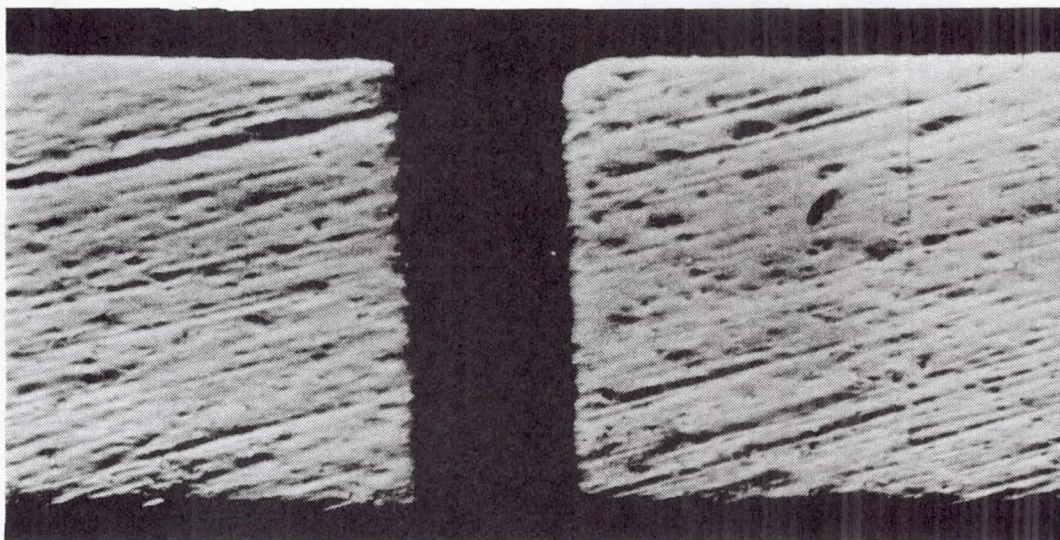


Figure 68. Sawed slot

bled yielded uniform ply thickness. Thus, pre-bleed was selected as the preferred process for thick 5208 graphite/epoxy sections.

Slot ducts were formed by aluminum strips tack riveted to the skin tool with 16-ply graphite/epoxy between the aluminum strips. An aluminum foil backing sheet was used to prevent splintering during drilling of the metering holes. Figure 69 is a photograph of the completed structural skin.

#### Hat-Section Stiffeners

The hat-section stiffeners were produced in a female mold. A 0.61m (24 in) long prototype tool was made of aluminum, and an attempt was made to



let the vacuum bag mold the inside of the part. While the part was generally acceptable, there were wrinkles caused by bag folds. Cracking also occurred in the 20-ply 0 stacks in the hat crown. The four-ply (+45/-45/-45/+45) modules were pre-bled prior to forming into the mold. Pre-bled modules were found to be much easier to form since they were well compacted.

A rubber plug was made to mold the center of the hat and was used on additional prototype runs. Cracking of the 0 plies in the crown was not resolved. One try placed a ply of graphite fabric in the center of each of the 20-ply 0 stacks but failed to alleviate the cracking. Some changes to the cure cycle were also made, but neither helped the cracking problem or completely eliminated voids. Crack-free structural components were achieved by reducing the number of 0 plies in the crown to ten. Completed hat-section stiffeners are shown in the photograph of Figure 70.

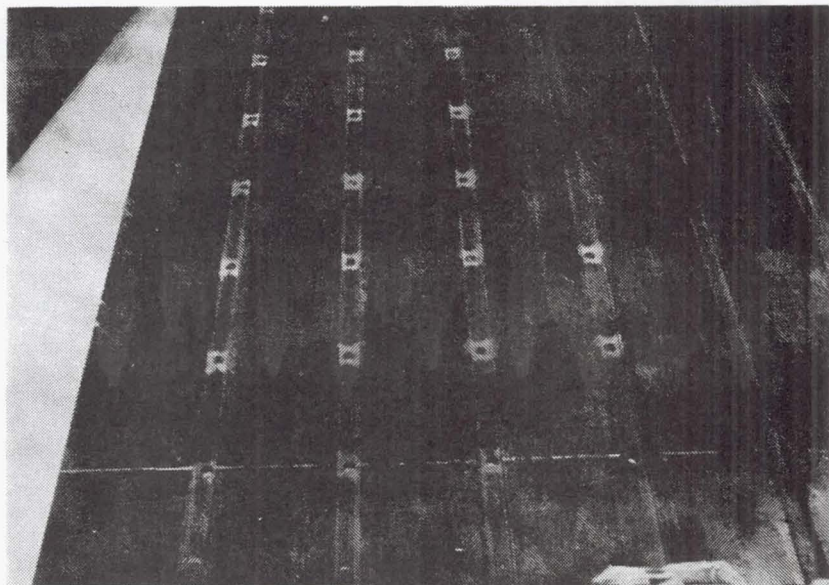


Figure 69. Structural skin

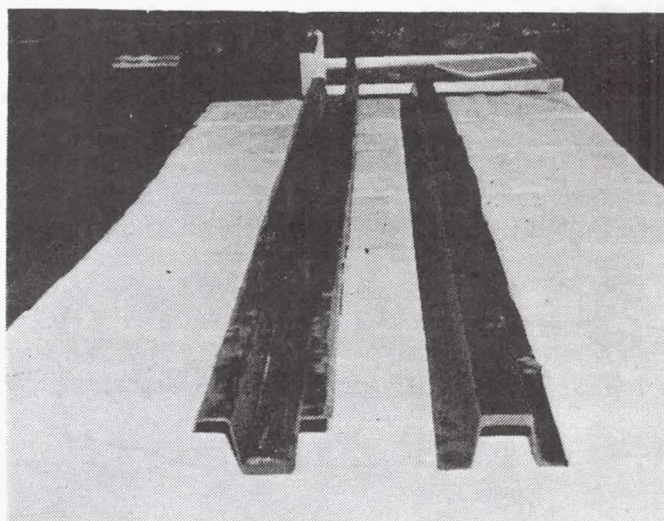


Figure 70. Hat section stiffeners

## Panel Assembly

In the bonding of the hat-section stiffeners to the structural skin, the web flange stiffness of the hat sections was found to be adequate to withstand light autoclave pressure. Therefore verification bond runs with the adhesive encapsulated in 0.013 mm (0.0005 in) Teflon were conducted at 68.94 kN/m<sup>2</sup> and 137.88 kN/m<sup>2</sup> (10 psi and 20 psi) autoclave pressures. After the adhesive cured, the hat was stripped from the skin and a replica of the bond line was removed from between the Teflon. Both cure pressures produced a good bond with adhesive thicknesses from 0.051 mm to 0.152 mm (0.002 in to 0.006 in).

In bonding the titanium skin to the structural skin, the initial attempt used a 121°C (250°F) curing adhesive, American Cyanamid FM73.1. A demonstration panel was made by bonding strip to slotted titanium to a part of the first 96-ply panel. Warpage of 0.101 cm (0.040 in) in 61 cm (24 in) was experienced, which precluded using an elevated temperature bonding procedure for attaching the titanium skin to the surface panel. A room-temperature curing adhesive was tried which had been used previously for bonding titanium doublers to aluminum structure on aircraft. Both Hysol EA 9309.1 and Mil-S-8802 polysulfide sealant were evaluated as room-temperature curing adhesives. The panel with MIL-S-8802 resulted in non-uniform bond lines and a step at the slot edges; therefore, Hysol EA 9309.1 was selected.

In subsequent compression testing of the panel bonded with EA 9309.1 adhesive, the titanium skin began buckling and disbonding at approximately 50% of the failure load. In solving this problem, three alternative adhesives, designated FM123-4, FM73, and MB1113, were evaluated. The FM73 and MB1113 adhesives had excessive flow, which partly blocked the slot ducts. Flow of FM123-4 was acceptable. As illustrated by Figure 67, a small fillet was formed, but no blockage of the slot duct occurred. During subsequent impact/compression testing, the titanium skin did not buckle or disbond before the total section failed. Upon failure, graphite layers were pulled apart. Therefore, the FM123-4 bond withstood ultimate load. The final LFC surface panel was fabricated using sawed titanium, bonded with FM123-4. This panel satisfied all surface criteria. Maximum values of 0.007 cm and 0.013 cm (0.003 in and 0.005 in) were measured for steps at slots, and 7.62 cm (3 in) waves, respectively, compared to allowable values of 0.015 cm (0.006 in) and 0.013 cm (0.005 in). The completed surface panel is shown in Figures 71 and 72.

## Summary of Manufacturing Procedures

The following summarizes the manufacturing procedures developed for fabrication of LFC surface panels:

- (1) The outer skin, inner skin, and hat stiffeners are separately cured and subsequently joined by structural adhesive bonding.
- (2) During the final bonding cycle, the shear clips are integrally molded in place.
- (3) The titanium face sheet is bonded to the outer skin with FM123-4 adhesive.



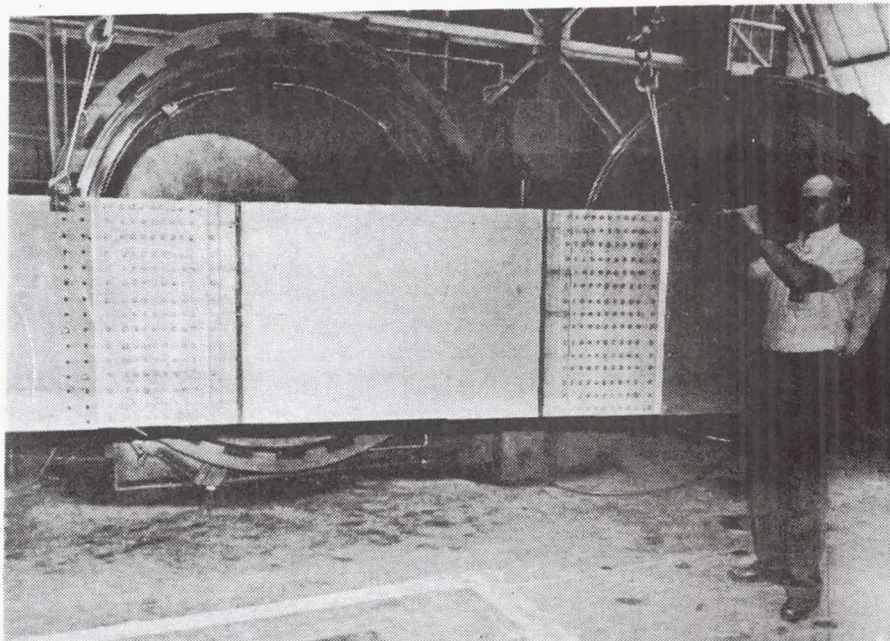


Figure 71. Surface panel No. 3 - upper surface

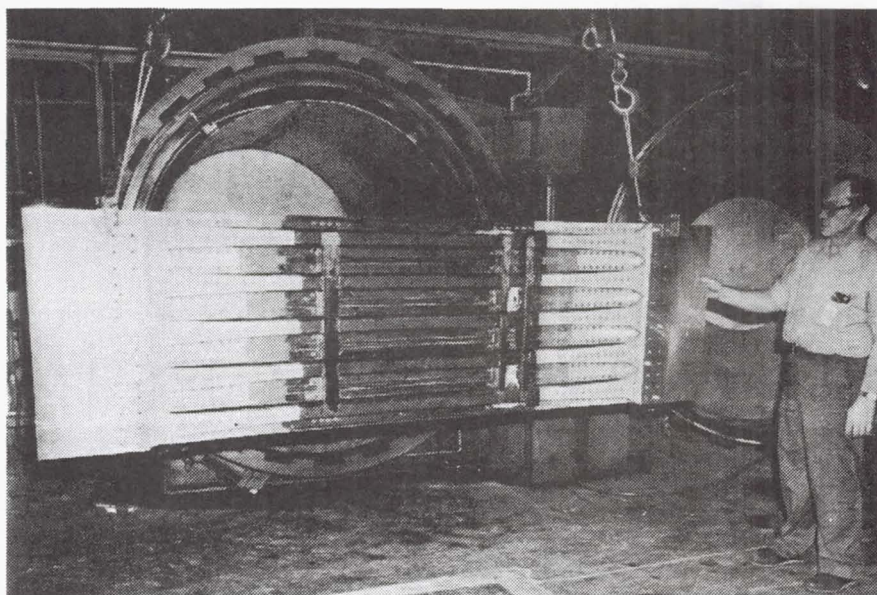


Figure 72. Surface panel No. 3 - lower surface

(4) The titanium face sheet is slotted using a jeweler's saw.

#### 6.2.2.4 Testing

Subscale testing of LFC surface panels was conducted in the following areas:

- (1) Environmental
  - o Temperature

- o Icing
  - o Corrosion
  - o Foreign object damage
  - o Repairability
  - o Lightning
- (2) Structural component tests
- o Rib clip tension
  - o Rib clip shear
  - o Compression

### (3) Fatigue

Test specimens were cut from the three 0.91 m x 1.52 m (3 ft x 5 ft) LFC surface panels described in the preceding section. A photograph of the first surface panel illustrating the allocation of test specimens is presented in Figure 73. The sectioning of the second surface panel to acquire the large specimens for the compression tests is illustrated by Figure 74. The number and characteristics of test specimens is outlined in Table 15.

The narrative which follows summarizes pertinent results of selected tests.

### Temperature

Thermal testing was conducted to evaluate the effect of temperature changes on the width of slots in the LFC surface panel and to verify handbook values for the thermal coefficient of expansion for the thick composite structural skin. The thermal test panel and instrumentation are illustrated by Figure 75. In the temperature range from  $-51^{\circ}\text{C}$  ( $-60^{\circ}\text{F}$ ) to  $82^{\circ}\text{C}$  ( $180^{\circ}\text{F}$ ), the maximum variation in slot width ranged from  $+6.35$  and  $-6.10 \times 10^{-4}$  mm ( $+25$  and  $-24 \times 10^{-6}$  in). Thus, slot width variations due to temperature changes are considered to be insignificant. An acceptable comparison of measured and handbook values for the coefficient of expansion for the composite structure was obtained.

### Icing

Icing tests were conducted to evaluate the effect of entrapped water in the hat section stiffeners and in the surface ducts and metering holes.

As shown by Figure 76, a specimen was cut from the panel for icing tests, and the ends of the hats were closed by clamping aluminum plates with a rubber seal to each end. A stand-pipe was attached to one end and filled with water. The specimen was placed in a low-temperature chamber and frozen at  $-18^{\circ}\text{C}$  ( $0^{\circ}\text{F}$ ). One hat flange separated from the skin. As



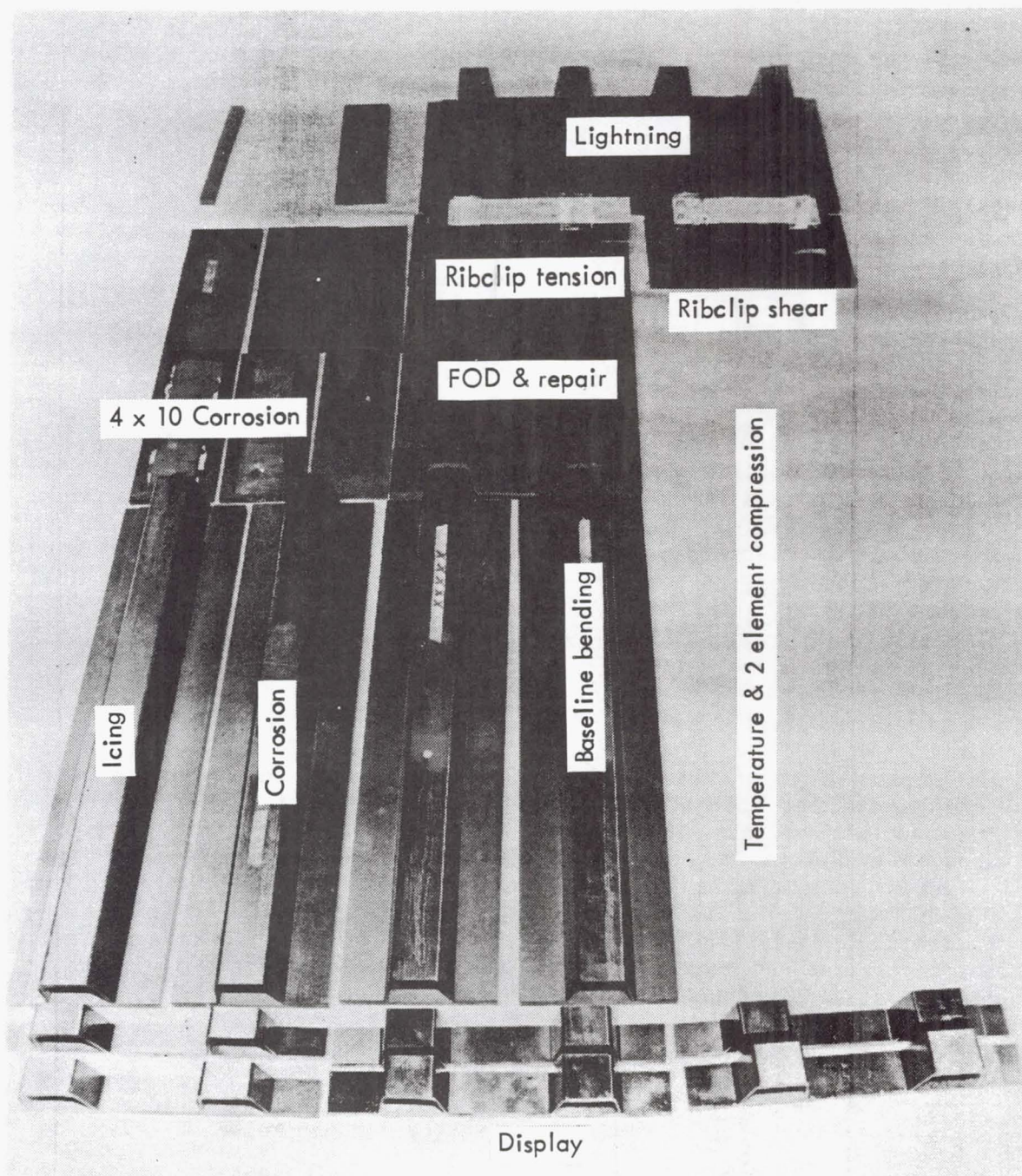


Figure 73. Test specimens - LFC surface panel No. 1



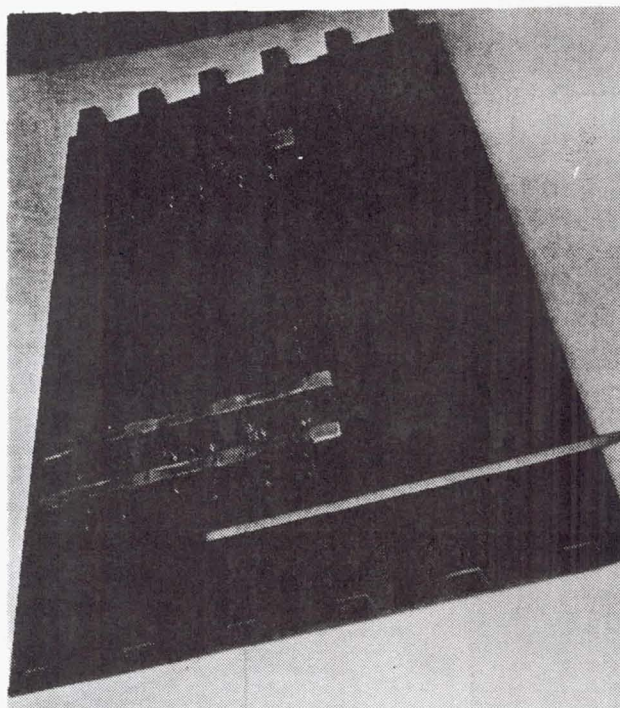


Figure 74. Test specimens - LFC surface panel No. 2

illustrated by Figure 76, failure was within the composite hat flange. The flange separation emphasizes the need to keep water out of the hat sections during low temperature operation.

For the evaluation of icing in the surface ducts and metering holes, the ducts and holes were filled with water through the skin slots. The specimen was exposed to 15 freeze-thaw cycles, after which there was no visually detectable damage. Removal of the titanium skin did not reveal any hidden damage. A section was cut through a metering hole, and the specimen was mounted and polished. Microscopic examination up to 200X showed no delamination or cracking.

#### Corrosion

Tests were conducted to evaluate the effect of environments representative of those encountered in airline operations on the bending strength of the LFC surface panel.

Three 10.16 x 25.40 cm (4 x 10 in) panel specimens were exposed to 30 days of salt fog, 30 days of high humidity, and 30 days of Weather-O-Meter, respectively. In addition, a 0.15 x 0.61 m (6 x 24 in) specimen was exposed to 30 days in the Weather-O-Meter environment. Weather-O-meter exposure simulates outdoor weathering. The test machine exposes the specimens to sunshine (zenon arc) and rain (water spray). A test cycle of 17 minutes of sunshine and 3 minutes of sunshine and rain was used. After exposure, the specimens were static tested in a four-point bending test, as

TABLE 15. TEST SPECIMENS

Type of Test	Panel No.	Number of Specimens	Dimensions	
			cm	(in)
Temperature	1	1	30.5 x 91.4	(12 x 36)
Icing	1	1	15.2 x 30.5	(6 x 24)
Corrosion (4 pt bending)				
Skin	1	4	10.2 x 25.4	(4 x 10)
Panel	1	2	15.2 x 61.0	(6 x 24)
Foreign object damage and repairability	1	1	30.5 x 30.5	(12 x 12)
Lightning	1	2	30.5 x 30.5	(12 x 12)
Rib clip				
Tension	1	1	15.2 x 30.5	(6 x 12)
Shear	1	1	15.2 x 30.5	(6 x 12)
Compression				
2 elements	1	1	30.5 x 91.4	(12 x 36)
4 elements	2	1	61.0 x 152	(24 x 60)
Fatigue	3	1	76.2 x 188	(30 x 74)

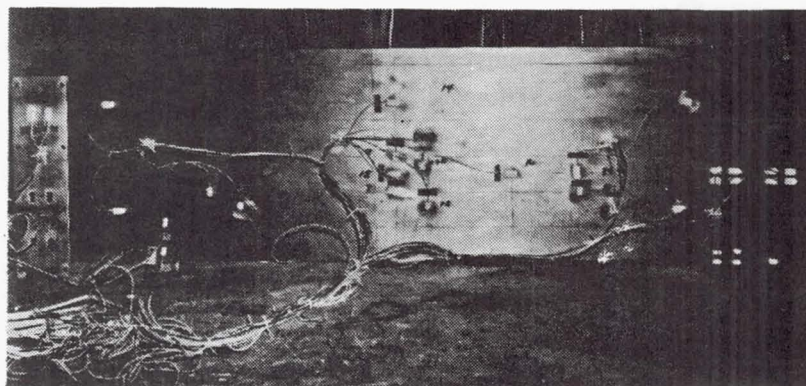


Figure 75. Temperature test arrangement



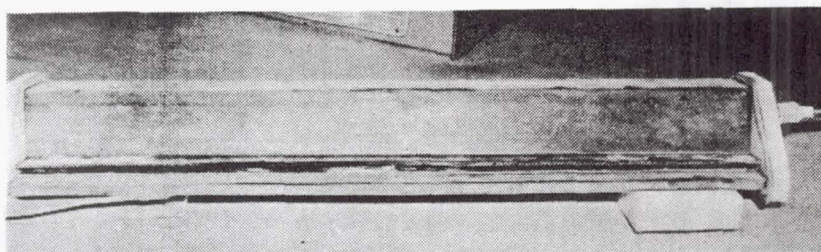


Figure 76. Icing test specimen

illustrated by Figure 77. As shown in Table 16, the maximum reduction in bending strength was 18% for the smaller specimen subjected to the Weather-O-Meter environment. The larger specimen showed a 7% reduction. The environmental effect was accounted for in the structural design.

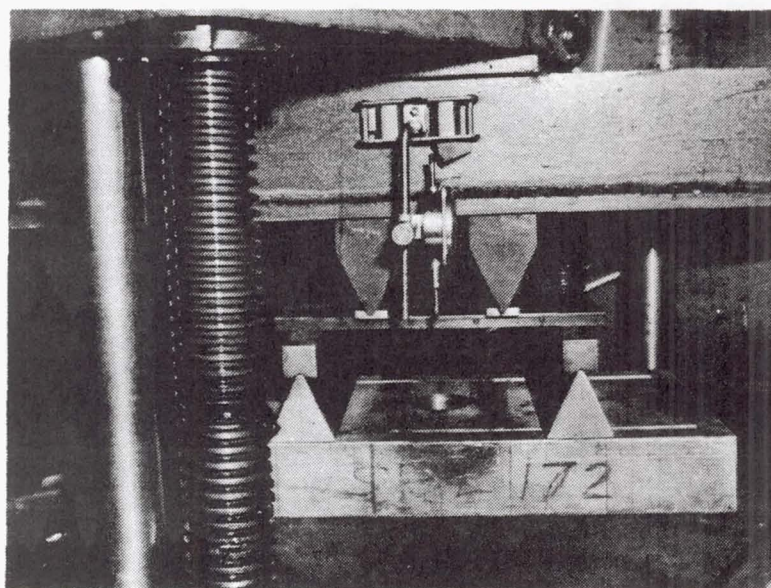


Figure 77. Corrosion/bending test arrangement

TABLE 16. TEST SUMMARY - CORROSION/BENDING

<u>Environment</u>	<u>Specimen</u>		<u>Reduction in Bending Strength - %</u>
	<u>cm</u>	<u>in</u>	
Salt fog	10.2 x 25.4	(4 x 10)	11
Humidity	10.2 x 25.4	(4 x 10)	13
Weather-O-Meter	10.2 x 25.4	(4 x 10)	18
Weather-O-Meter	15.2 x 61.0	(6 x 24)	7



## Foreign Object Damage

The objective of this test was to determine the resistance of an LFC surface panel to foreign object damage.

Using the experimental arrangement shown in Figure 78, the LFC surface panel was impacted over the slotted surface duct and over the composite-supported titanium at energy levels of 5.76, 11.52, 23.04, 46.08, and 92.16 m-kg (5, 10, 20, 40 and 80 in-lb). The depth of the maximum indentation at each impact point was measured with a depth micrometer and is reported in Table 17. Figure 79 shows the result of a 92.16 m-kg (80 in-lb) impact over a surface duct. Removal of the titanium skin revealed little visual damage to the composite over the plenum and none over solid laminate.

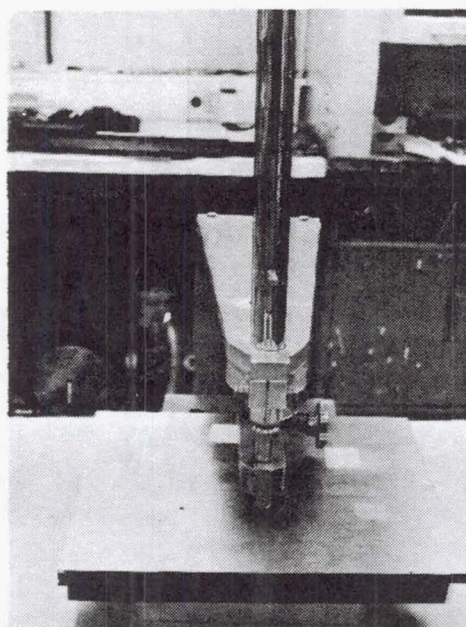


Figure 78. Impact test arrangement

TABLE 17. TEST SUMMARY - FOREIGN OBJECT DAMAGE

Impact Load		Over Duct		Over Laminate		Ply Damage
m-kg	(in-lb)	mm	(in)	mm	(in)	
5.76	(5)	0.025	(0.001)	0	(0)	0
11.52	(10)	0.152	(0.006)	0.025	(0.001)	0
23.04	(20)	0.457	(0.018)	0.050	(0.002)	0
46.08	(40)	0.508	(0.020)	0.075	(0.003)	0
92.16	(80)	0.813	(0.032)	0.101	(0.004)	10

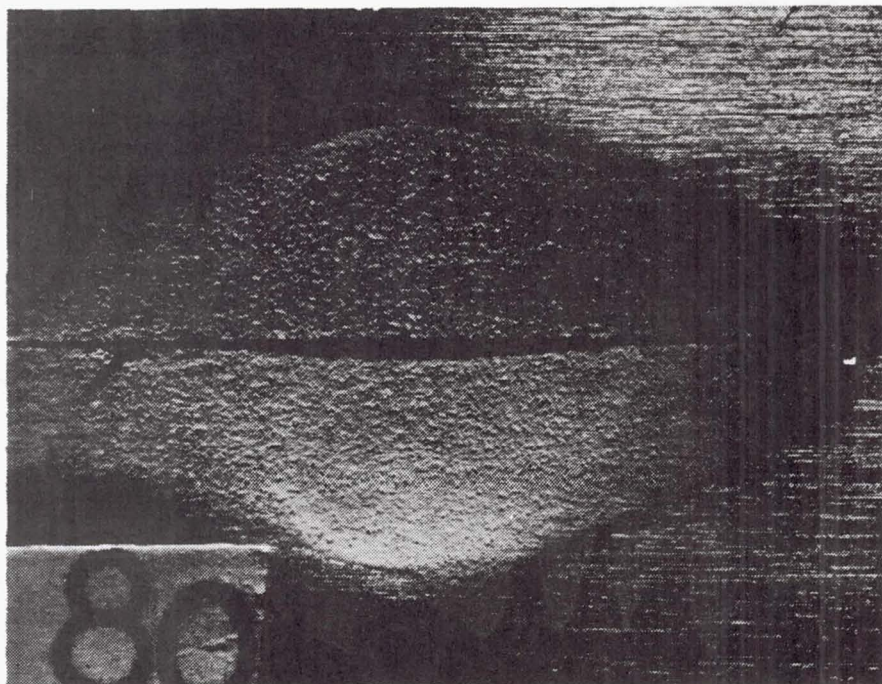


Figure 79. Impact test specimen

The data of Table 17 indicate that none of the impacts in the range tested would create a surface indentation sufficiently deep to cause transition of the laminar boundary layer if the impact occurred over titanium supported by composite. However, depending on chord location, impacts in the range of 11.52 - 23.04 m-kg (10 - 20 in-lb) over a surface plenum would result in an unacceptable surface discontinuity. For purposes of comparison, a 1.27 cm (0.5 in) diameter stone at a relative velocity of 222.2 km/hr (120 kn) is equivalent to a 57.6 m-kg (50 in-lb) impact energy level.

#### Repairability

The objective of this investigation was to demonstrate that typical damage to the slotted titanium LFC surface can be repaired by methods usable in-service by fleet operators.

The LFC surface panel specimen of the foreign object damage test described in the preceding section was used as the test specimen. Repairs were made to the dents produced by the 23.04 m-kg (20 in-lb) to 92.16 m-kg (80 in-lb) impacts in the titanium over the surface ducts.

Removal of the damaged titanium surface with a hole saw was considered to be partially successful. A pilot hole was drilled in the center of the damaged area and allowed to penetrate the composite for approximately 0.63 cm (0.25 in). Additional control of the cutting tool was accomplished with a guide. Removal of the titanium skin was readily accomplished with the hole saw but it was not possible to stop the cut precisely in the adhesive layer and slight scoring of the composite occurred each time.

The second method attempted was the use of a counterbore, chucked in a low-speed, hand-held, drill motor. A pilot hole and cutting guide were



used. The cut was terminated in the adhesive layer with no damage to the composite substrate. No problem was experienced with overheating. However, the edge of the cut in the titanium was not square due to the normal radius on a counterbore. A special counterbore was prepared with a square edge and a grind more suited to titanium cutting. Excellent results were obtained. Control of the cut using the hand-held drill was easily accomplished.

A patch was prepared from electro-discharge-machine-slotted titanium sheet with a connecting tang in the center of the patch, as illustrated by Figure 80. Preparation for bonding was by conventional procedures. The composite surface was prepared by light sanding followed by an acetone wash. Both surfaces were lightly coated with Hysol EA 9309 adhesive and the patch was placed in position. Small strips of shim stock were used to align the slots, light pressure was applied, and the adhesive was allowed to cure at room temperature. The connecting tang was removed using a hand-held jeweler's saw.

Step profile measurements were made on several patches to determine smoothness. A typical patch had a total surface variation within a 5.08 cm (2 in) circle of only 0.063 mm (0.0025 in) and a maximum step of 0.038 mm (0.0015 in) which is well within the requirements established in Figures 58 and 59.

It was demonstrated that a damaged slot can be returned to the original configuration using hand-held tools. While the tests were conducted on a bench, the entire operation could have been conducted either on the upper or lower surface of an aircraft wing. Repairs of this nature could be performed within a time span of four to six hours by using heat lamps to accelerate the adhesive cure.

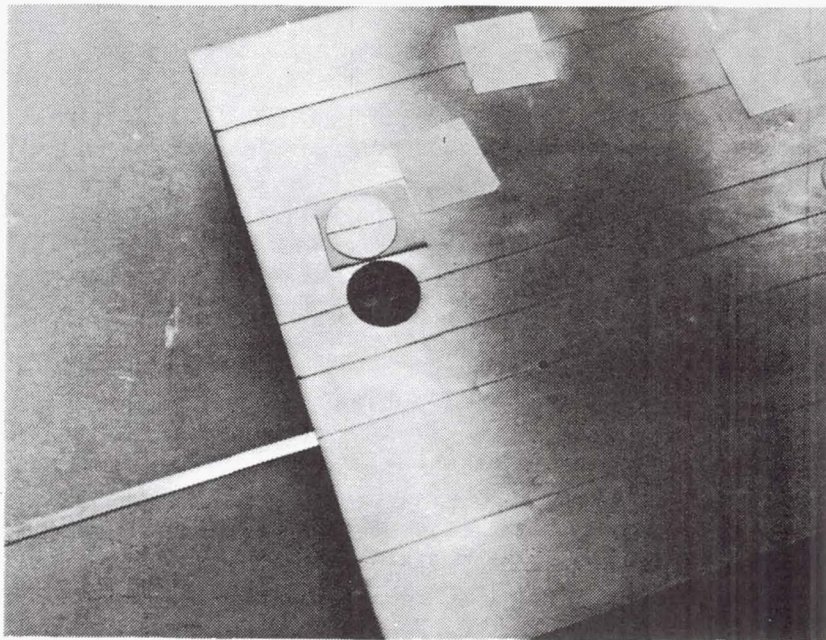


Figure 80. Repairability test specimen

## Lightning

Preliminary tests were performed to ensure that the structural arrangement of the LFC surface panel is resistant to lightning strike. The test specimen shown in Figure 81 was tested by NASA personnel in the NASA LRC lightning strike test facility.

Three specimens were tested. One panel was tested for baseline data and the second was subjected to 260 thermal-humidity cycles. Test conditions are outlined in Table 18. The third specimen was tested for internal arcing.

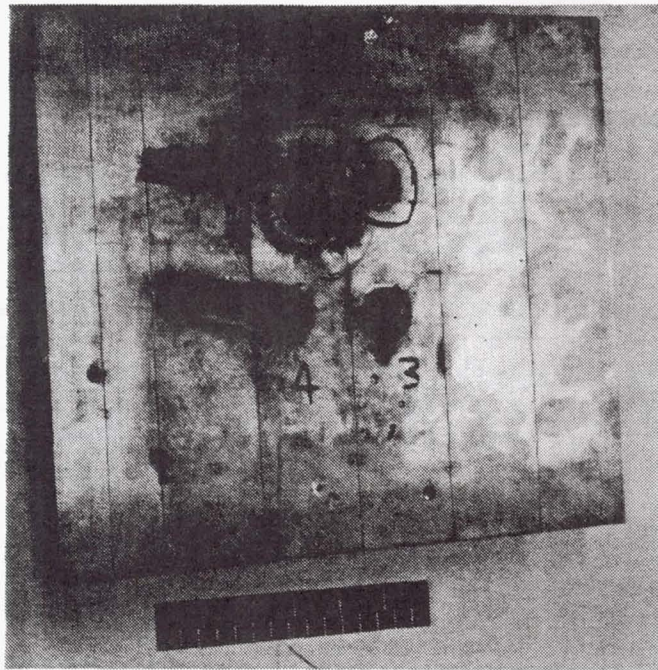


Figure 81. Lightning test specimen

TABLE 18. TEST RESULTS - LIGHTNING STRIKE

Number	High Voltage Spike	Continuing amp	Current msec	Edges Grounded	Burn Thru	Disbond
	kV					
1	25	0	0	All	No	No
2	42.5	0	0	All	No	Some
3	25	500	200	All	Yes	Yes
4	25	500	200	One	Yes	Yes
5	25	500	200	All	Yes	Yes
6	45	0	0	All	No	Yes



In all six tests, the titanium face sheet was effective in preventing the current from penetrating the composite. The panel after four lightning strikes is shown in Figure 81. The extent of disbonding between the face sheets and composite was examined using ultrasonic techniques. The results of this effort and the physical appearance of the panels suggest the possibility that aerodynamic forces encountered after a lightning strike might cause additional delamination. These aerodynamic forces might become more intense due to irregularities in the wing surface, but even the loss of titanium strips between slots would not result in a catastrophic failure.

The third 30 x 30 cm (1 x 1 ft) lightning strike panel specimen included:

- o Rib clips bonded between hats
- o Rib clip fasteners installed through skin and hat legs
- o A simulated rib bolted to the rib clip cap

The cap attachment was grounded with all other surfaces insulated with mylar. A 45 kV discharge to the titanium skin resulted in no apparent internal arcing. The graphite/epoxy composite appeared to provide an electrical path for the charge. These tests established that lightning strikes to wing panels would not cause a catastrophic bond failure.

### Compression

The objective of the panel compression test was to obtain design data for a four-element compression panel. The acceptable criterion for the compression panel was a design ultimate load of 6.49 MN/m (37.08 kips/in) without failure.

A 0.61 m x 1.52 m (24 in x 60 in) compression panel was removed from the second LFC wing surface panel shown in Figure 74. The specimen ends were potted using Magnabond 69-9 tooling plastic and machined as required for the test configuration. The specimen was instrumented with thirty-four axial strain gauges and seventeen deflection transducers. Aluminum "T" sections, simulating rib caps, were attached to the rib clips. All strain gauge and deflection transducer readings were recorded by a B&F Model SY 156 data acquisition system.

The specimen was loaded in .445 MN (100 000 lb) increments. While loading between .890 MN (200 000 lb) and 1.334 MN (300 000 lb), it was noted that the titanium skin was buckling at the top and the bottom edge of the panel, including areas that had previously been determined to have some disbonding. This was documented by the photograph shown in Figure 82. Loading was continued to 2.224 MN (500 000 lb) and buckling of the titanium strips progressed over the length of the panel, as shown in Figure 83. The specimen withstood 3.959 MN (890 000 lb), the design ultimate load, when failure occurred by delamination of the hats and skin, as shown in Figure 84.

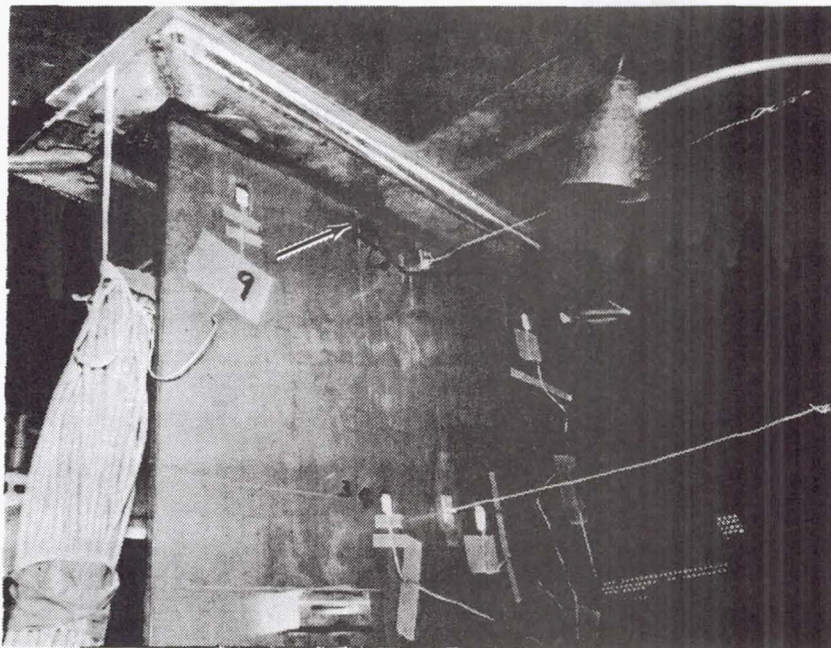


Figure 82. Compression panel test - 1.334 MN (300 000 lb)

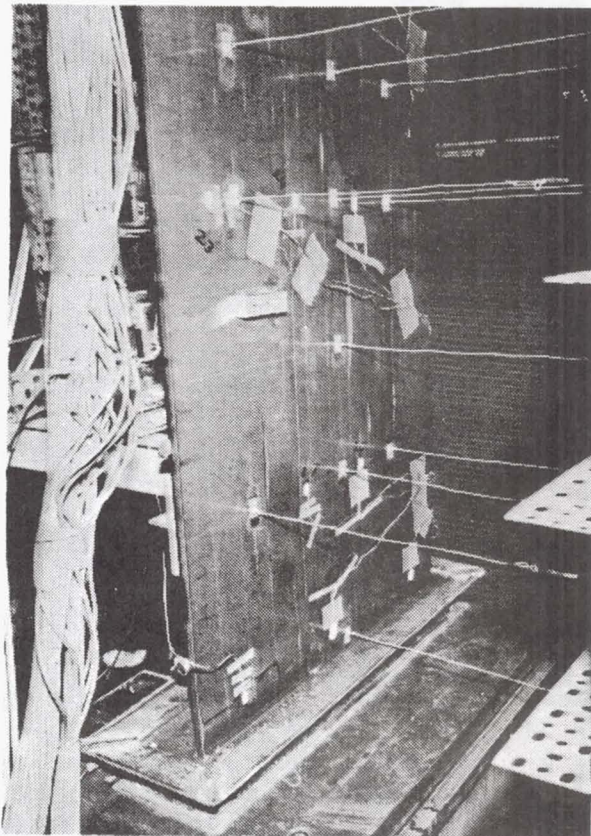


Figure 83. Compression panel test - 2.224 MN (500 000 lb)



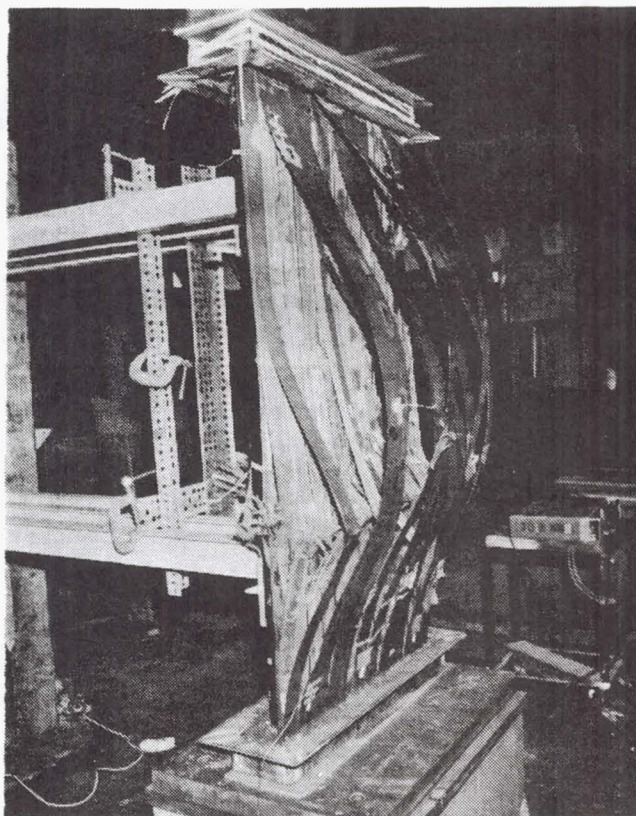


Figure 84. Compression panel test - failure mode

Following is a summary of significant events during the test:

MN	<u>Load</u> (10 <sup>3</sup> lb)	<u>Maximum Strain</u>	<u>Equivalent G Force</u>	
.890	(200)	.0012	.84	Audible noises
1.334	(300)	.0019	1.26	Titanium skin began buckling
3.959	(890)	.007*	3.75	Panel failed at 100% ultimate load

\*Extrapolated value. No strain data were obtained at failure.

Investigations conducted after this test and described in Section 6.2.2.3 resulted in the selection of an alternative adhesive to prevent premature buckling of the titanium skin. Both the environmental testing and the structural testing conducted in this phase of the study provided results demonstrating the compatibility of the selected LFC surface panel design with the anticipated operational environment for future LFC transports.

## Fatigue

The objective of this test was to investigate the durability of a typical section of the LFC wing panel, including effects of foreign object damage and a large simulated crack. The test specimen was the third LFC surface panel, shown in Figures 71 and 72. The panel was instrumented with 50 axial strain gauges. Acoustic emission (AE) transducers were mounted on the panel and monitored throughout the test.

After assembly of the panel and end fittings, the panel was exposed for 100 days to 95% relative humidity at 68°C (180°F). This exposure resulted in a moisture level of over 1%. A strain survey showed good load distribution.

Before beginning the fatigue test, the panel was subjected to foreign object damage. The panel was loaded to 2.22 MN (500 000 lb) in tension and impacted with a 1.27 CM (0.5 in) diameter aluminum ball traveling at 61 m/sec (200 ft/sec). The test arrangement with the impact gun in place is shown in Figure 85.

The surface panel was subjected to the equivalent of two lifetimes using a loading spectrum based on the L-1011 lower wing surface. Each lifetime includes 18 000 simulated flights applied as flight-by-flight type loading. Each lifetime includes 218,000 cycles with the panel subjected to the limit stress level of 229.6 MN/m<sup>2</sup> (33.3 KSI).

After the second lifetime, a 15.2 cm (6 in) slot perpendicular to the centerline of the hat was cut completely through the center of the panel to

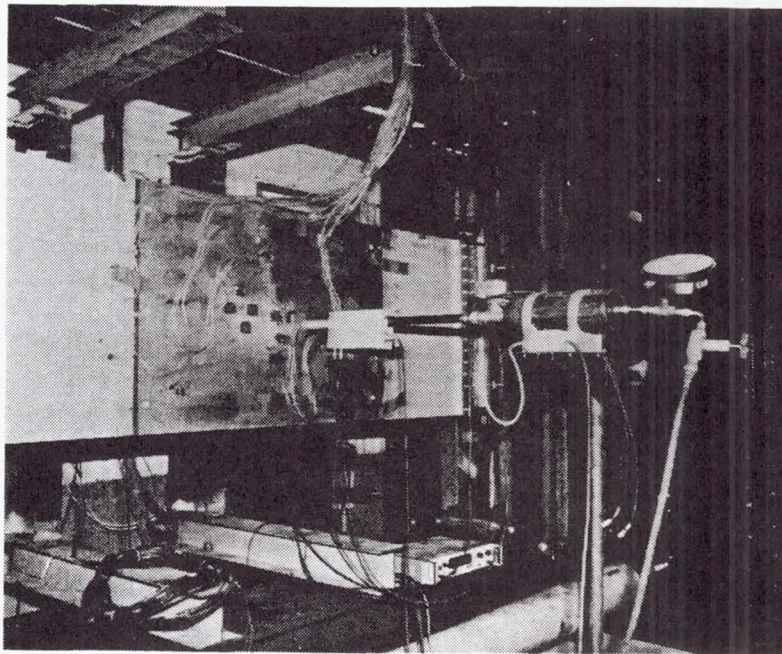


Figure 85. LFC surface panel No. 3 with impact gun



simulate a crack. The panel was fatigue tested for an additional 1440 flights and tested for residual strength.

During fatigue testing, visual, ultrasonic, and enhanced radiography inspections were conducted at the following intervals:

- (1) Initial strain survey
- (2) 3600 flights
- (3) 9000 flights
- (4) 18,000 flights
- (5) 27,000 flights
- (6) 36,000 flights
- (7) Strain survey after damage
- (8) 720 flights after damage
- (9) 1440 flights after damage

In addition, the specimen was visually inspected while cycling. No damage was detected at any time up to 36 000 flights (2 lifetimes). After approximately the first half-life of cycling, an increase in minor acoustic events was detected in the rib clip area. Thereafter, a detailed inspection was conducted in this area at each inspection cycle. No damage was detected by any of the above procedures.

Inspection by enhanced X-ray after the strain survey following the saw cut revealed some matrix cracking at each end of the saw cut. It was generally limited to a few of the 45° fiber bundles and did not extend more than 1.91 cm (0.75 in). No delamination was detected by either X-ray or ultrasonic inspection. Visual inspection showed a fracture forming in the titanium skin at the saw cut tip after only 100 flights. Ultrasonic inspection after 720 flights revealed two small areas of suspected delamination. Neither was over 1.91 cm (0.75 in) in diameter. One was adjacent to the center of the cut at the slot duct, the other adjacent to the lower saw cut tip but not in the crack extension area. Enhanced X-ray did not confirm either suspected delamination. After 1440 flights, the crack in the titanium skin extended to 2.16 cm (0.85 in) at the lower tip and 1.47 cm (0.58 in) at the upper tip. Neither X-ray or ultrasonic inspection indicated any delamination under the crack extension. Matrix cracking along fiber bundles continued slightly in front of the crack tip in the titanium.

After completion of the fatigue testing, a tension load of 1.92 MN (430 000 lb) was applied to the panel in a residual strength test. This loading produces a stress level of  $269.6 \text{ MN/m}^2$  (39.1 KSI), which compares to a maximum stress level of  $229.6 \text{ MN/m}^2$  (33.3 KSI) at limit load. The test was monitored with both strain gauges and AE equipment.

The graphite/epoxy outer skin crack grew from the saw cut damage of 15.2 cm (6 in) to approximately 35.6 cm (14 in). Hats two and four inboard legs disbonded from the outer skin for a range of 15.2 cm to 30.5 cm (6 to 12 in). The titanium surface cracked for about 7.6 cm (3 in) on each side of the saw cut with some associated disbonding. Figure 86 illustrates both crack growth and areas of delamination resulting from the test.

The loading cycle for 1440 flights equals 7200 flight hours, or 1.8 years, of simulated airline service. That the crack did not grow in the graphite/epoxy during this cycling and the crack in the titanium skin grew less than 2.54 (1 in), verified that this is a controlled slow-crack-growth type of structure. In addition, the higher-modulus titanium surface cracked ahead of the graphite, therefore, a visual inspection would show local hot spots in the substructure. No cracks started in other areas of potential concern, such as the metering holes, the impact area, and the rib clip fasteners.

The residual strength test verified that the crack did arrest, the remaining structure would still possess appreciable load-carrying ability, and that design features such as low-modulus crack-arrestment strips are not necessary for the LFC wing surface design to satisfy FAA damage tolerance criteria.

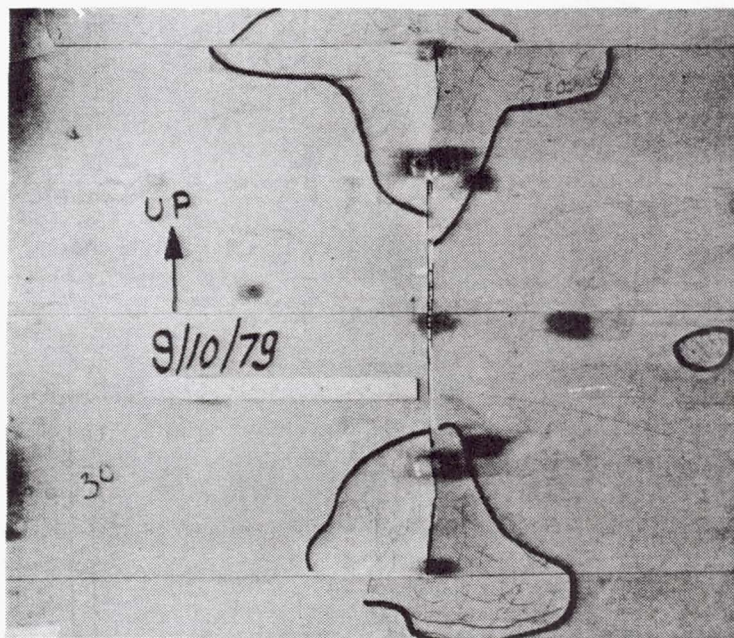


Figure 86. Delaminated area indicated by ultrasonic inspection after residual strength test



### 6.2.3 Leading-Edge Development

There is general concurrence that the design and fabrication of the leading-edge region represents one of the most challenging problems attending the development of operational LFC aircraft. Investigations summarized in the preceding section were directed toward the development of LFC surface panels representative of the mid-chord region of LFC wings, with little attention devoted to the solution of problems peculiar to the leading edge. The activities summarized in this section had the dual objectives of:

- (1) Performing the design, manufacturing development, fabrication and test activities required to define procedures for LFC leading-edge development, and
- (2) Providing a fully functional leading-edge test section for subsequent evaluation of cleaning and suction systems in low-speed wind-tunnel tests.

This section is limited to a description of leading-edge section development. Wind-tunnel testing of the resultant leading-edge section is described in Section 6.4.4.

The configuration of the leading-edge selected for development is based on the wing defined for the 1993 LFC transport and described in Section 6.1. The leading edge is a constant-chord section, representative of the baseline wing at 98% semi-span. The chord of the leading-edge specimen is 41.4 cm (16.3 in), with an airfoil thickness at the front spar of 25.4 cm (10 in).

#### 6.2.3.1 Concept Evaluation

At the first phase in the development of an LFC leading-edge section alternative design concepts were evaluated. For the purpose of the concept evaluation and selection procedure, it was not necessary to design the complete leading-edge section. Rather, only the upper surface panel of the leading edge was used for the evaluations. This element was selected for the following reasons:

- (1) This panel has the most stringent slot spacing requirements in the leading-edge region.
- (2) This panel is subjected to the highest air loads.
- (3) This panel is the largest of those in the leading-edge section.
- (4) Smoothness criteria are most critical in the region of this panel.

Following are the major guidelines established for the concept evaluation procedure:

- (1) Use the airfoil developed for the 1993 baseline configuration and described in Section 6.1.
- (2) The panel must be compatible with two levels of suction flow metering.



- (3) Slots in the panel are parallel to the 0.5% chord line.
- (4) The panel must accommodate slot pitch variations from 1.57 cm (0.62 in) to 12.7 cm (5.0 in).
- (5) The panel must accommodate slot width variations from 0.008 cm (0.003 in) to 0.025 cm (0.010 in).
- (6) The panel must accommodate a slot duct depth of 0.20 cm (0.08 in) and slot duct widths ranging from 0.38 cm to 0.76 cm (0.15 in to 0.30 in).
- (7) The maximum pressure differential across the panel was assumed to be 20.7 kN/m<sup>2</sup> (3 psi).
- (8) The upper surface panel must attach to the front spar.

#### Evaluation Procedure

The conceptual panel designs were evaluated relative to the following criteria:

- (1) Surface smoothness
- (2) Suction duct efficiency
- (3) Weight
- (4) Cost
- (5) Integrity and reliability
- (6) Manufacturing
- (7) Repairability

The concept evaluation was conducted in two phases. During a preliminary phase, nine design concepts were evaluated. On the basis of this preliminary evaluation three of the concepts were eliminated. The remaining six concepts were redesigned in an attempt to minimize the design deficiencies revealed by the evaluation.

#### Concept Descriptions

Figures 87 through 92 show the conceptual designs subjected to the final phase of the evaluation. Following is a brief description of each concept.

Concept No. 1 - This concept, shown in Figure 87, uses graphite/epoxy inner and outer skins and collector ducts, sandwiching aluminum honeycomb core. Filler material of lightweight Kevlar (syntactic tape) forms the slot ducts. The outer face sheet is titanium.

Concept No. 2 - This concept is shown in Figure 88. This concept employs titanium inner and outer face sheets, supported by spanwise graphite/epoxy ducts.

Concept No. 3 - Figure 89 shows that this concept employs graphite/epoxy woven fabric for the inner skin and corrugated inner and outer ducts. The outer face sheet is titanium.

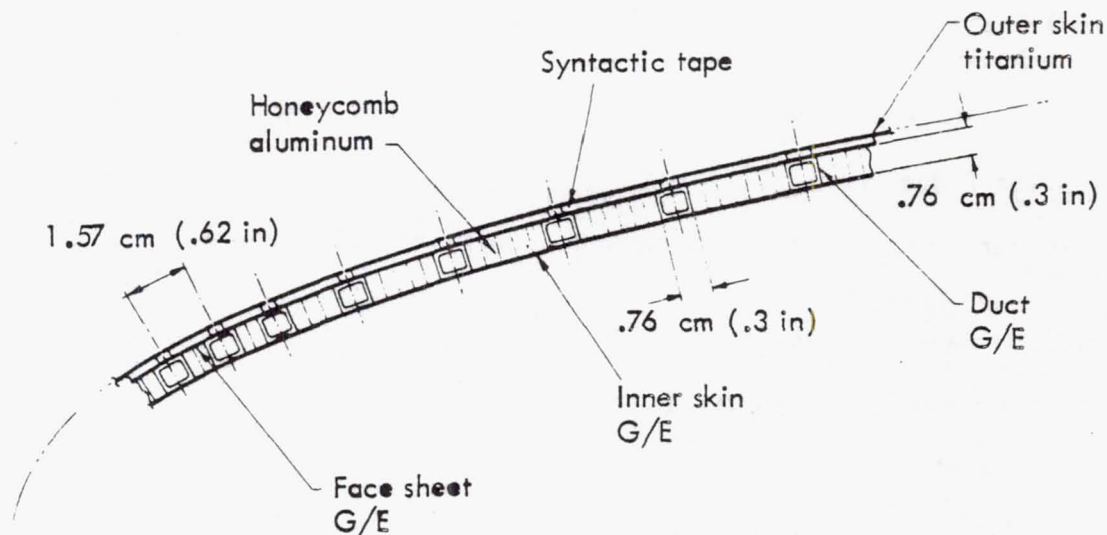


Figure 87. Concept No. 1 - graphite/epoxy skin, duct and aluminum honeycomb

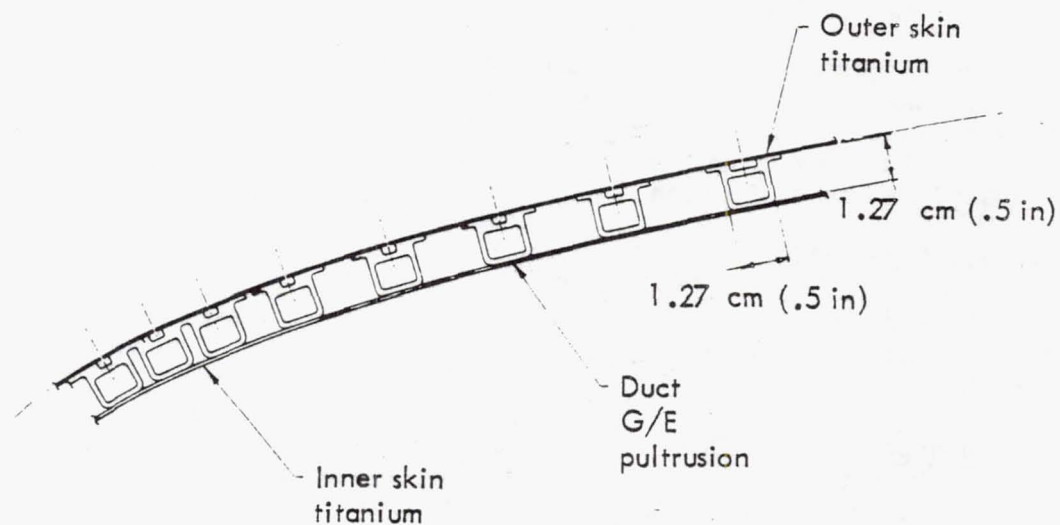


Figure 88. Concept No. 2 - graphite/epoxy spanwise ducts with titanium face sheets

**Concept No. 4** - As shown in Figure 90, this concept uses inner and outer face sheets of titanium. The slot ducts and collector ducts are formed by graphite/epoxy pultrusions. Face sheets and ducts are bonded into the outer panel with aluminum honeycomb core between the ducts. This thin panel is supported by chordwise stiffeners of graphite/epoxy.

**Concept No. 5** - For this concept, graphite/epoxy face sheets are bonded to aluminum honeycomb core, as shown in Figure 91. Slot ducts are formed by syntactic tape used as filler material. The collector ducts are formed by rounded hats made of graphite/epoxy bonded to the inside of the honeycomb panel. The honeycomb core is potted at all metering holes. The outer face sheet is titanium.

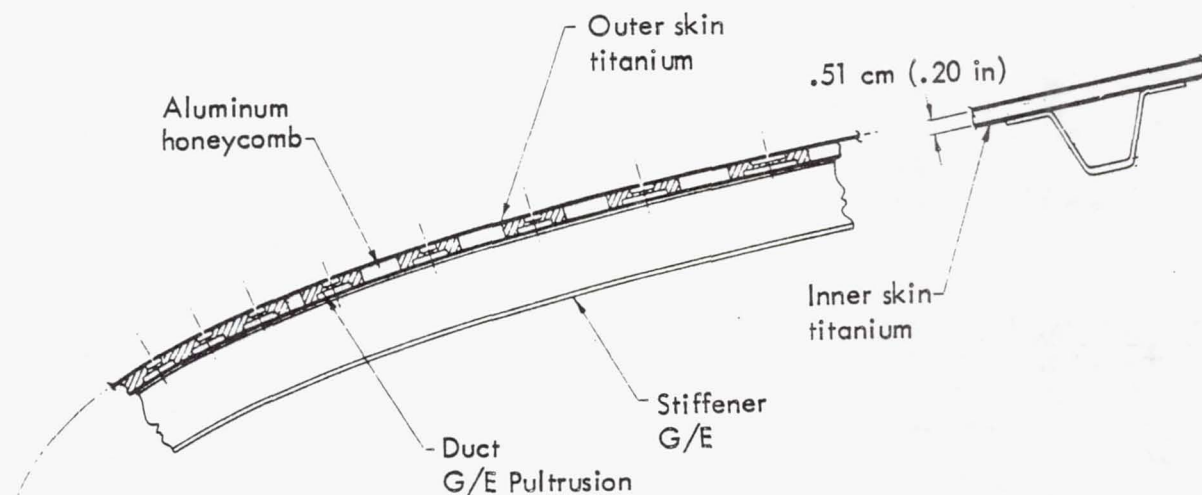


Figure 89. Concept No. 3 - corrugated graphite/epoxy skins and ducts

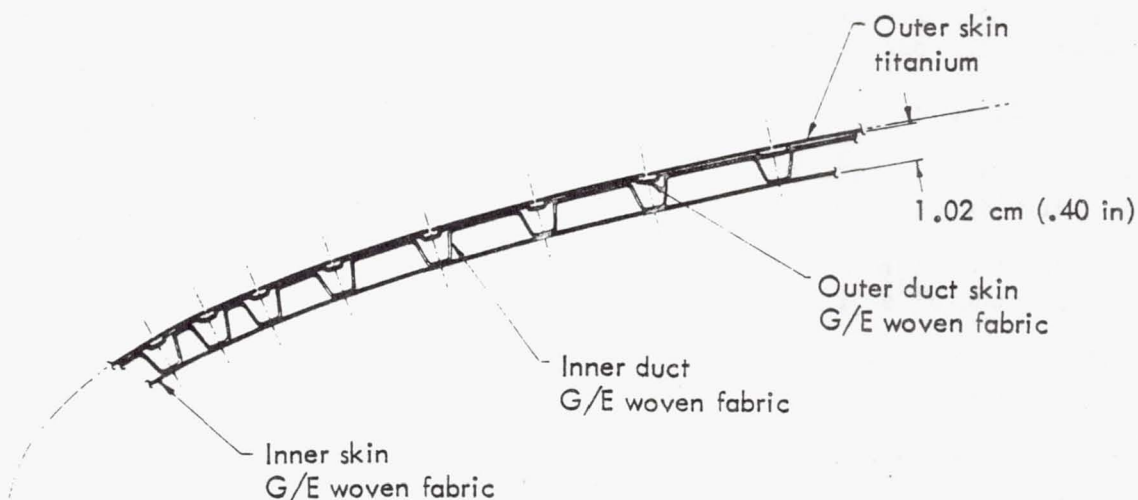


Figure 90. Concept No. 4 - titanium skin, graphite/epoxy duct bonded in honeycomb, on stiffeners



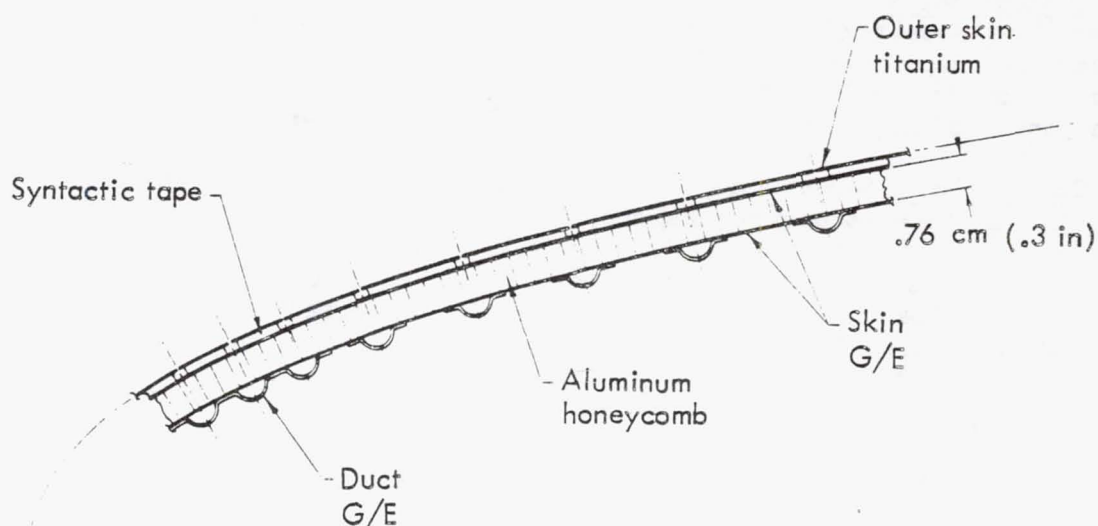


Figure 91. Concept No. 5 - honeycomb panel with external ducts

**Concept No. 6** - The graphite/epoxy outer skin is supported by a corrugated graphite/epoxy inner duct skin, as shown in Figure 92. The panel is supported by chordwise graphite/epoxy hat stiffeners. The slot ducts are formed by syntactic tape used as a filler material. The outer skin is titanium.

### Concept Selection

In the final evaluation of the six candidate concepts and selection of a single concept for further development, each concept was evaluated relative to the previously defined criteria by appropriate evaluators in each area. All concepts were given a score ranging from 0 to 10. Each evaluator was required to comment on any scores between 0 and 3 and between 7 and 10. The purpose of this requirement was twofold:

- (1) For the low scores, to ensure that a simple redesign would not eliminate the problem areas.
- (2) For the high scores, to investigate the possibility of incorporating these features into other designs.

Table 19 gives the results of the final evaluation. As shown in this table, concept no. 1, the graphite/epoxy, aluminum honeycomb design, received the highest total score by a significant margin. This concept ranked first in every area except "duct efficiency" and "surface smoothness," and had high scores in those areas. Therefore, this leading-edge design concept was selected for further development.

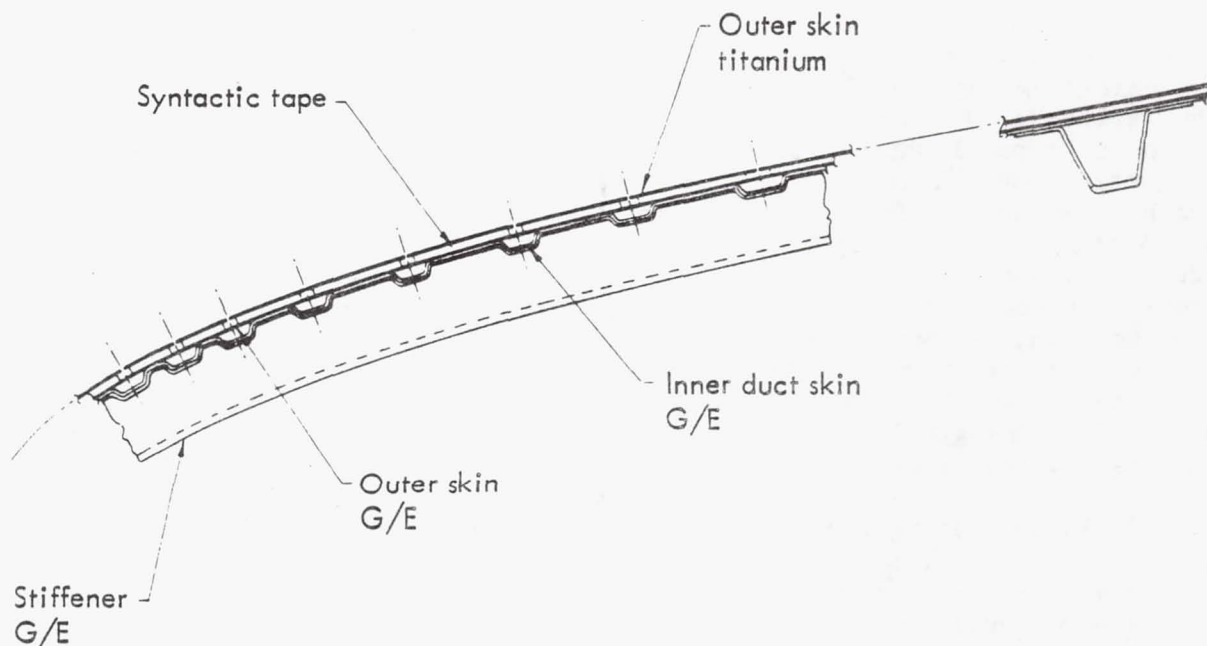


Figure 92. Concept No. 6 - graphite/epoxy corrugated panel support on G/E stiffener

TABLE 19. LFC LEADING-EDGE CONCEPT EVALUATION

Concept	<u>1</u>	<u>2</u>	<u>3</u>	<u>4</u>	<u>5</u>	<u>6</u>
Weight	8	2	5	5	5	6
Cost	9	8	3	5	7	4
Integrity	8	5	4	5	7	7
Manufacturing	7	7	5	6	4	5
Repairability	6	4	4	6	5	6
Duct Efficiency	8	10	9	4	5	3
Surface Smoothness	7.5	6.5	7	5	8	5.5
Total Score	53.5	42.5	37	36	41	36.5
Rank	1	2	4	6	3	5

### 6.2.3.2 Design

Figure 93 is a perspective drawing showing the structural arrangement of the leading-edge section and the method of attachment to the front spar.

The section is fabricated in two panels, a fixed upper/nose panel and a hinged lower panel which provides access for maintenance and adjustment of the suction and washing systems. The substructure consists of two full-length diaphragms. These members provide support for the covers and form the boundaries of the upper and lower surface trunk ducts. All leading-edge components are of sandwich construction with graphite/epoxy face sheets and corrosion resistant aluminum honeycomb core. A thin gauge titanium skin, bonded to the surface panel outer face sheet, contains the required suction slots and also provides environmental protection for the composite structure. Details of the leading-edge section and a single suction duct are given in Figures 94 and 95. Table 20 gives pertinent slot and metering hole dimensions.

### 6.2.3.3 Manufacturing Procedures

Figure 93 identifies the following structural components of the leading-edge section:

- (1) Collector ducts
- (2) Upper/nose and lower surface panels
- (3) Forward and aft diaphragms
- (4) Diaphragm attachment fitting.

The discussion which follows summarizes the final procedures developed for the fabrication of these components.

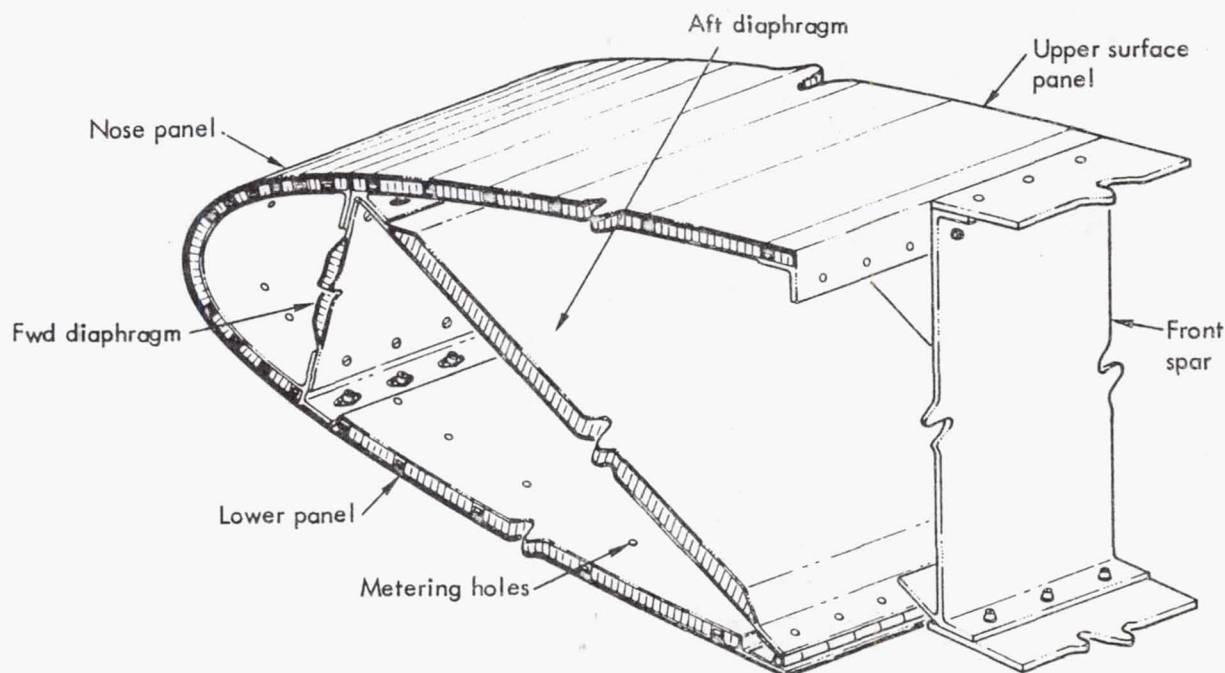


Figure 93. Leading-edge structural concept



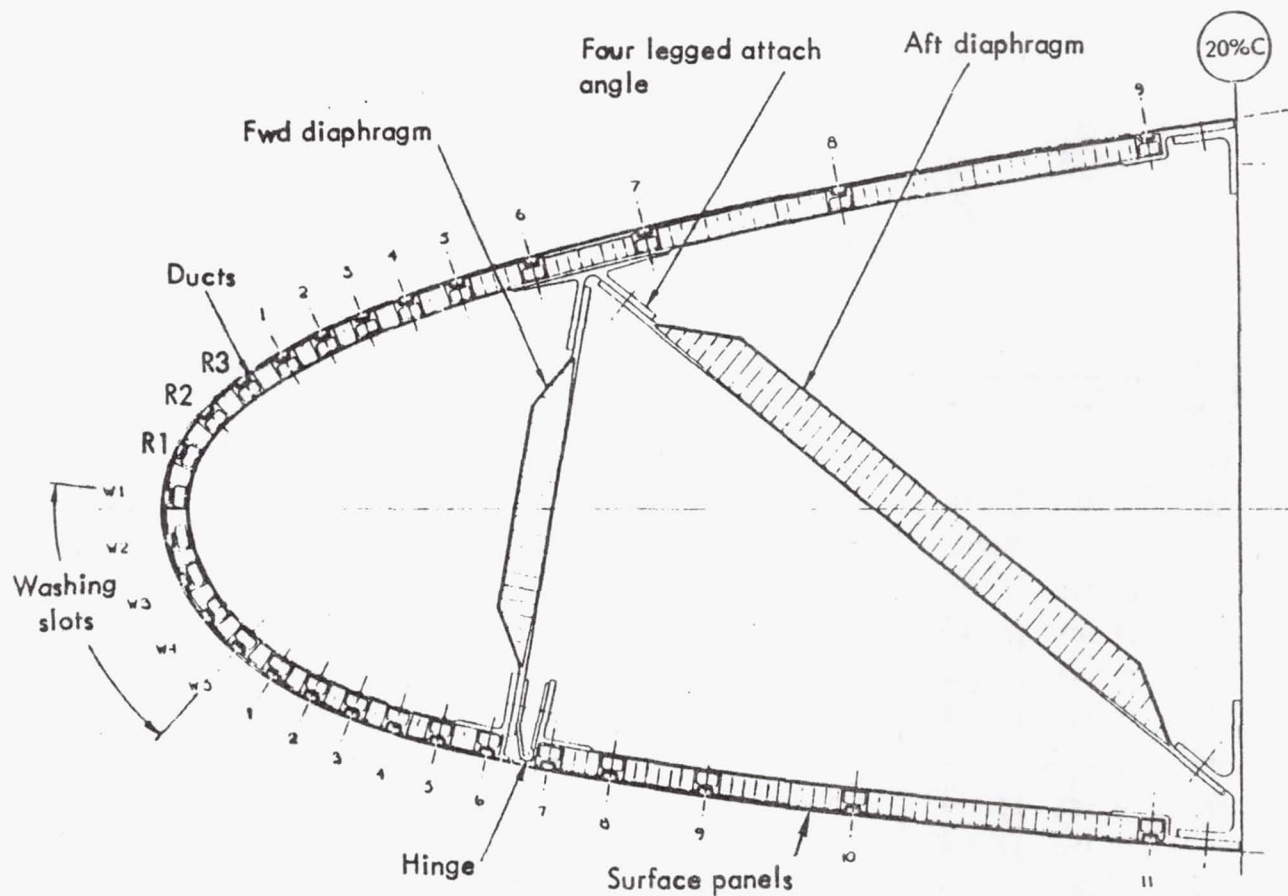


Figure 94. Leading-edge structure

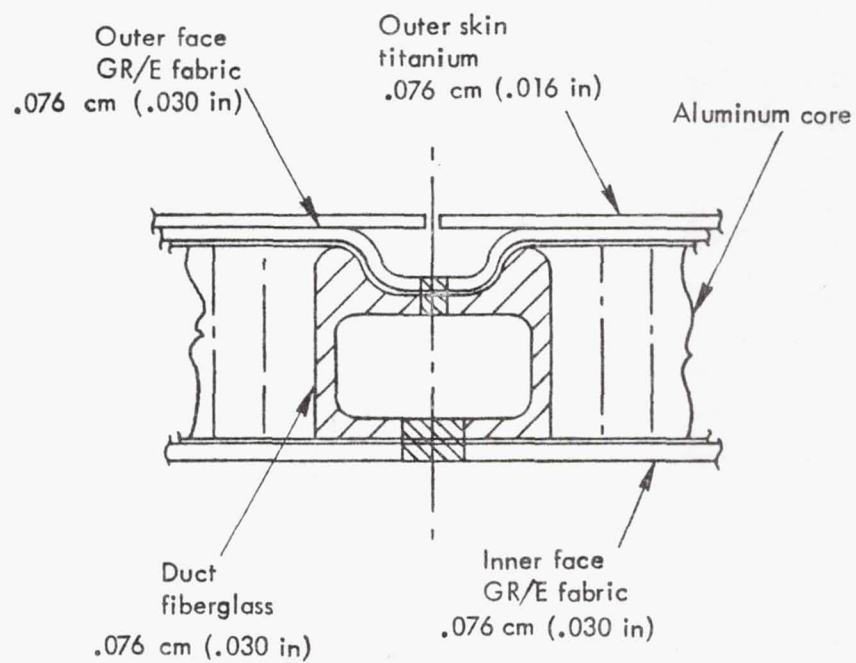


Figure 95. Leading-edge design details

TABLE 20. SLOT AND METERING HOLE DIMENSIONS  
FOR LEADING-EDGE SECTION

Slot No.	S		Slot Width		Metering Hole Diameter		Metering Hole Spacing	
	cm	in	cm	in	cm	in	cm	in
U9	3.165	1.246	0.0145	0.0057	0.102	0.040	0.64	0.25
U8	17.527	5.538	0.0107	0.0042	0.102	0.040	0.64	0.25
U7	20.985	8.262	0.0094	0.0037	0.089	0.035	0.51	0.20
U6	25.090	9.878	0.0081	0.0032	0.089	0.035	0.51	0.20
U5	27.795	10.943	0.0069	0.0027	0.089	0.035	0.51	0.20
U4	29.688	11.688	0.0069	0.0027	0.089	0.035	0.51	0.20
U3	31.341	12.339	0.0069	0.0027	0.089	0.035	0.51	0.20
U2	32.916	12.959	0.0069	0.0027	0.089	0.035	0.51	0.20
U1	34.491	13.579	0.0069	0.0027	0.089	0.035	0.51	0.20
R3	36.180	14.244	--	--	0.089	0.035	0.51	0.20
R2	37.869	14.909	--	--	0.089	0.035	0.51	0.20
R1	39.558	15.574	--	--	0.089	0.035	0.51	0.20
W1	41.247	16.239	0.0069	0.0027	0.089	0.035	0.51	0.20
W2	40.790	16.059	0.0069	0.0027	0.089	0.035	0.51	0.20
W3	38.250	15.059	0.0069	0.0027	0.089	0.035	0.51	0.20
W4	37.640	14.819	0.0069	0.0027	0.089	0.035	0.51	0.20
W5	36.065	14.199	0.0069	0.0027	0.089	0.035	0.51	0.20
L1	34.491	13.579	0.0069	0.0027	0.089	0.035	0.51	0.20
L2	32.916	12.959	0.0069	0.0027	0.089	0.035	0.51	0.20
L3	31.341	12.339	0.0069	0.0027	0.089	0.035	0.51	0.20
L4	29.766	11.719	0.0069	0.0027	0.089	0.035	0.51	0.20
L5	28.191	11.099	0.0069	0.0027	0.089	0.035	0.51	0.20
L6	26.543	10.450	0.0081	0.0032	0.089	0.035	0.51	0.20
L7	24.270	9.555	0.0081	0.0032	0.089	0.035	0.51	0.20
L8	22.032	8.674	0.0081	0.0032	0.089	0.035	0.51	0.20
L9	18.687	7.357	0.0094	0.0037	0.089	0.035	0.51	0.20
L10	13.508	5.318	0.0107	0.0042	0.102	0.040	0.64	0.25
L11	3.142	1.237	0.0145	0.0057	0.102	0.040	0.64	0.25

### Collector Ducts

The collector ducts are 0.76 cm (0.30 in) square tubes. In the fabrication of these ducts, Ferro E293/120 fiberglass prepreg was wrapped around small rubber mandrels, loaded into a machined cavity, and cured. Expansion of the rubber provided the cure pressure. The ducts were cut into sections and plastic slugs were inserted to form dams at the desired intervals. Collector duct segments were bonded into full-span lengths prior to layup in the part. Figures 96 and 97 illustrate the collector duct tooling and wrapping of fiberglass prepreg.

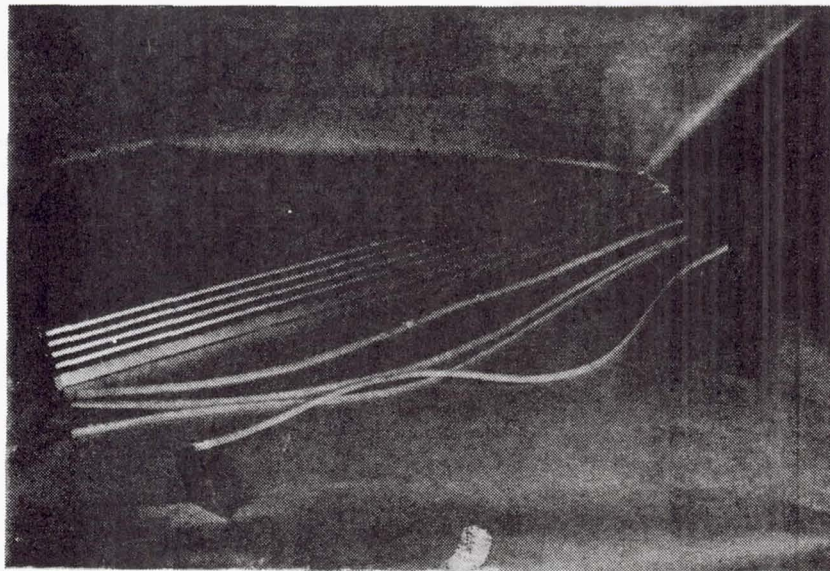


Figure 96. Collector duct tools



Figure 97. Collector duct prototype tool try



## Surface Panels

The major problem encountered in fabrication of the leading-edge surface panels was the development of tooling to produce the small slot ducts required in the panel. Due to the extremely small size of the duct, the slot duct form cannot be readily machined or fixed into the tool. A unique method was devised to handle the offset and the slot duct former. A reverse image of the slot duct is machined in a 0.318 cm (0.125-in) sheet of 6061-T6 aluminum alloy. Only 0.051 cm (0.020 in) thickness is left between the slot ducts. Placement of the slot ducts is extremely accurate, since they are located by the machine. After the entire outer surface is machined, the aluminum sheet is removed and annealed. Figure 98 shows the slot duct former sheet with the first glass ply laid up to the tool.

Fabrication of the leading-edge surface panels begins by laying up one ply of a high tack fiberglass prepreg (Cordo E293/120) to the slot duct former tool. The four plies of graphite fabric were positioned on the tool ensuring that no voids were formed at the slot duct edges. Figure 99

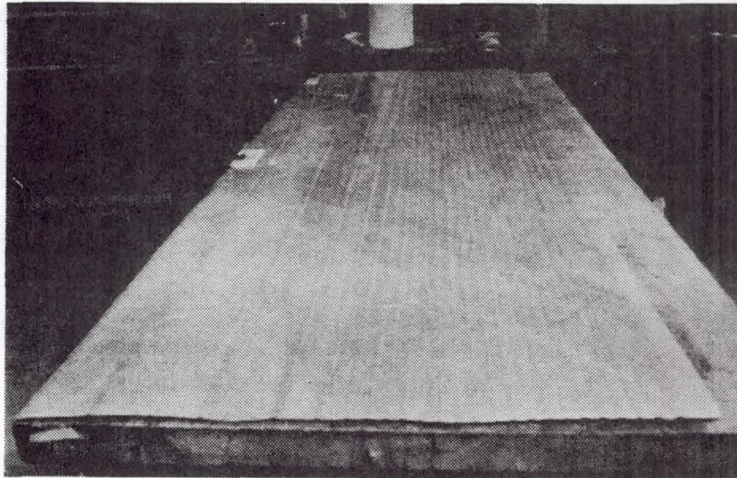


Figure 98. Slot-duct former tool with the first ply of fiberglass prepreg in place

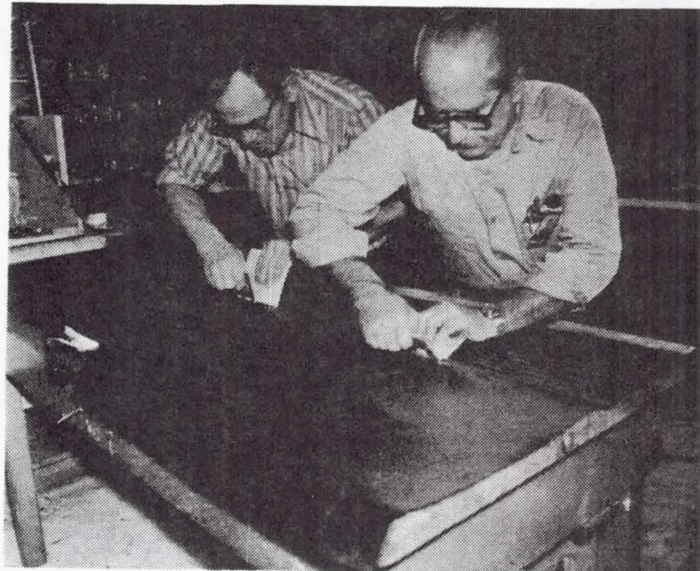


Figure 99. Graphite/epoxy fabric outer face sheet being formed to tool

illustrates the procedure. It should be noted that the graphite fabric was laid up in a  $+45^\circ$  orientation. The slot-duct former tool with the outer skin was then folded into the leading edge mold as shown in Figure 100, which was possible due to the annealed condition of the former sheet. It was positioned into the tool and pinned to prevent slippage. Figure 101 shows installation of the air ducts and core. Following this, the outer face sheet was laid up over the core and the part was bagged for autoclave cure. The entire assembly was cocured in one step. Fabrication of the lower surface was accomplished in a similar manner.

### Diaphragms

Diaphragms were produced by cocuring graphite/epoxy fabric over honeycomb core blankets which were machined to detail dimensions. After cure, the detail parts were trimmed to size for assembly.



Figure 100. Outer face sheet and slot former tool molded into the leading-edge tool

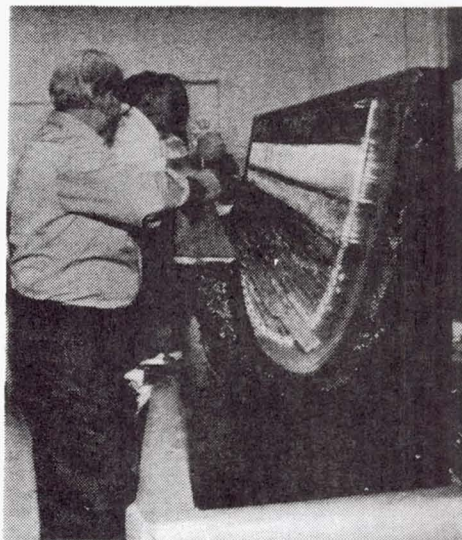


Figure 101. Leading-edge tool and part showing air duct and honeycomb core installation



### Diaphragm Attachment Fittings

The four-legged attachment angle tool consisted of a machined female aluminum plate representing the inner surface of the leading edge at the attach point. Two aluminum form blocks were used to form the outer angles, while a center rubber plug formed the center angle. Graphite/epoxy fabric was laid up over the tool details, the tool assembled, and the part auto-clave cured. Figure 102 shows the tool and the resultant fitting.

### Leading Edge Assembly

Prior to assembly it was necessary to drill approximately 7000 metering holes from the slot ducts into the collector plenum. Extremely clean holes were required with no fraying or splintering. These holes were from 0.089 cm (0.035-in) diameter to 0.127 cm (0.050-in) diameter, spaced on 0.51 cm (0.20 in) centers. Solid carbide circuit board drills were used in both a high-speed modeler's drill press and a hand-held portable drill. Drill speed was 8000 to 10 000 rpm. On a larger article, automatic drilling equipment would be used. For a single article, it was faster to drill manually using a template.

After drilling the metering holes in the slot duct, the four-legged angle was attached and the outer surface prepared for bonding by vacublasting. The vacublast operation removed any fuzz from the metering holes. The titanium skin was rolled to shape and cleaned.

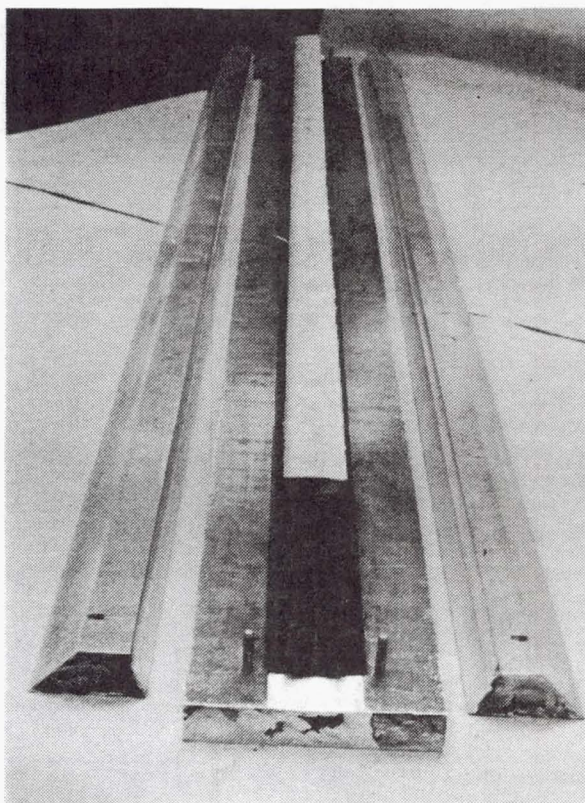


Figure 102. Four-legged upper surface attach angle tool and molded part



The leading edge and roll-formed titanium ready for bonding are shown in Figure 103. Bonding was accomplished in the same tool in which the part was originally molded with the slip sheet deleted.

### Slotting

After bonding, the upper surface/nose panel was attached to an assembly jig representing the front beam. Internal diaphragms and the lower surface were installed. The entire assembly was mounted on a rotary table for positioning during slotting. Slotting was accomplished with 0.008 cm to 0.013 cm (0.003 in to 0.005 in) high-speed steel jewelers saws. Figure 104 shows the setup used. After the slots were cut, the unit was removed from the assembly jig and cleaned.

For the test article, the maximum measured slot down step was 0.0091 cm (0.0036 in), which compares to an allowable downstep of 0.0173 cm (0.0070 in). Some slot closure was observed. This closure is a result of relieving residual stresses. These residual stresses could be produced by:

- o The rolling process used for the titanium skin
- o The procedure used for bonding the titanium skin to the leading edge
- o The graphite/epoxy bonding/tooling/bagging process

Further manufacturing development in subsequent programs will address this slot closure problem.

### Summary of Manufacturing Procedures

- (1) The collector ducts and outer panel skin are cured separately.
- (2) The outer skin, collector ducts, honeycomb core, and inner skin are laid up in the contour tool and cocured.
- (3) The diaphragms and diaphragm attachment fittings are cured separately.
- (4) Metering holes are drilled in the slot ducts, the diaphragms are installed, and the titanium face sheet is bonded to the surface panel.
- (5) The titanium face sheet is slotted using a jeweler's saw.

### 6.2.3.4 Testing

#### Component Testing

As a part of the development of the leading-edge test section, component tests were conducted as required to verify selected elements of the design.

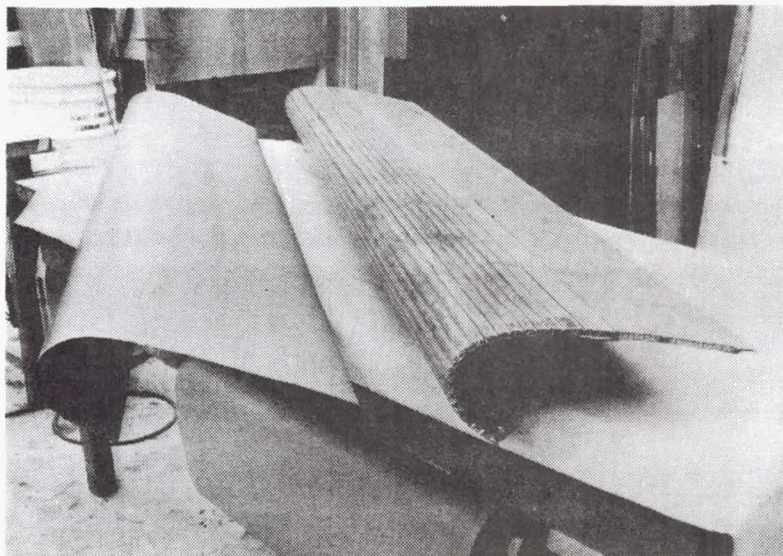


Figure 103. Leading-edge structure and formed titanium skin ready for bonding

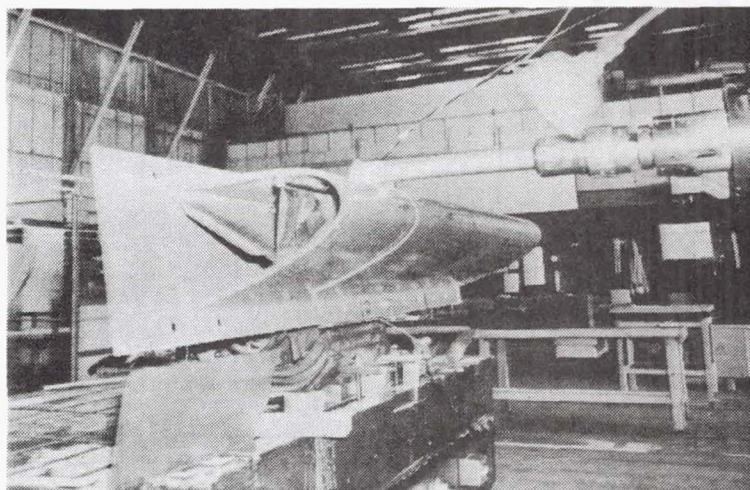


Figure 104. Slotting of leading-edge test article

**Hinge Angle Shear Test** - A portion of a tool-trial specimen of the lower surface panel of the leading-edge test section was tested in shear. Failure occurred by buckling of the honeycomb core at the edge of the tie down support as shown in Figure 105.

The failure load of  $2.41 \text{ kN}$  ( $542 \text{ lb}$ ) is equivalent to a surface pressure load of over  $214 \text{ kN/m}^2$  ( $31 \text{ lb/in}^2$ ), compared to the maximum lower surface design pressure of  $13.8 \text{ kN/m}^2$  ( $2 \text{ lb/in}^2$ ).

**Hinge Angle Tension Test** - A portion of a tool-trial specimen of the lower surface panel was tested in tension. The test objective was to verify the structural capability of the hinge angle and panel joint. The specimen was tested in the Universal Test Machine using the arrangement shown in Figure 106. Failure occurred at  $4.78 \text{ kN}$  ( $1075 \text{ lb}$ ) by buckling of the honeycomb core below the first duct, as shown in Figure 107. The failure load was approximately eight times the maximum design load.



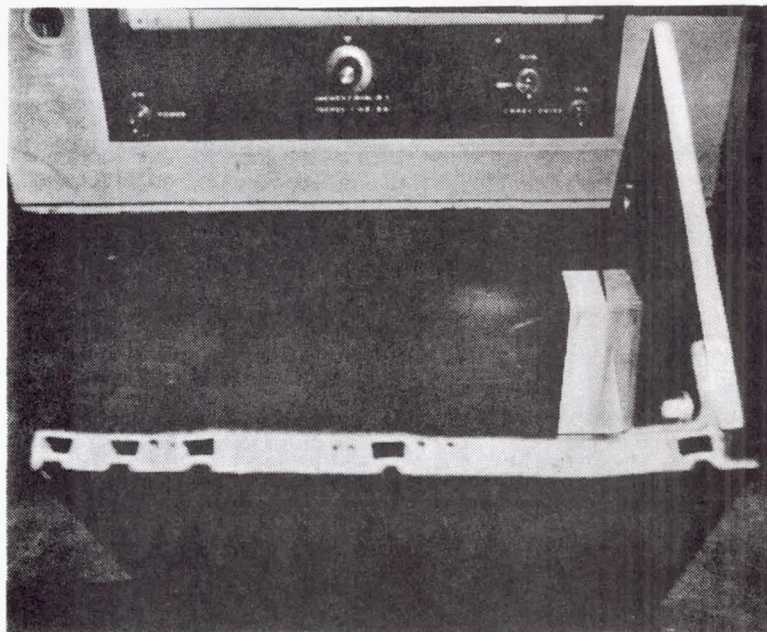


Figure 105. Hinge angle shear test failure mode

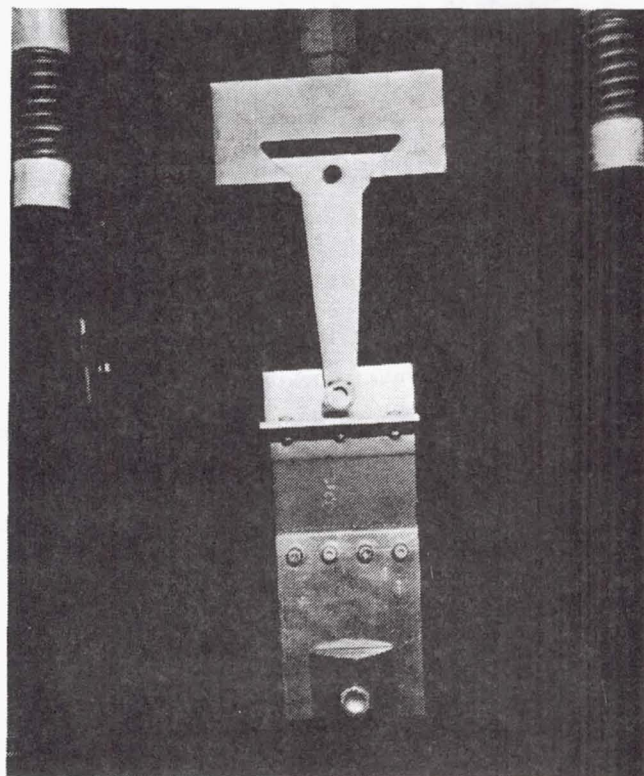


Figure 106. Arrangement for hinge angle tension test



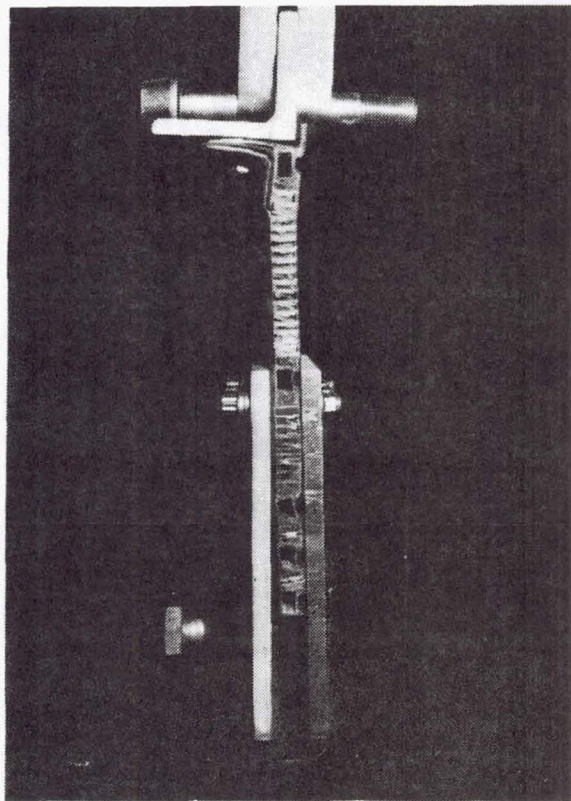


Figure 107. Hinge angle tension test failure mode

**Four-Leg Attach Angle Test** - The four-leg attach angle fitting used to attach the upper surface of the leading-edge test section to internal diaphragms was tested in tension. The objectives of this test were to determine the structural integrity of the fitting and the tension strength of the bond between the fitting and the upper surface panel.

The test specimen was the end of the four-leg angle attached/bonded to a simulated upper surface panel. The simulated panel was an early manufacturing development part. Failure occurred at 5.6 kN (1260 lb) at the duct in the skin panel at the support tiedown, as shown in Figure 108.

The four-leg angle withstood more load than the upper surface panel can apply. The failure load of 5.6 kN (1260 lb) is equivalent to an upper surface pressure loading of  $620.5 \text{ kN/m}^2$  ( $90 \text{ lb/in}^2$ ).

#### Leading-Edge Proof Test

The leading-edge section was loaded to simulate upper and lower surface pressures three times greater than the maximum expected during wind-tunnel testing. The chordwise pressure distributions applied are shown in Figure 109. The distributions were uniform in the spanwise direction. No damage was detected during or after loading.

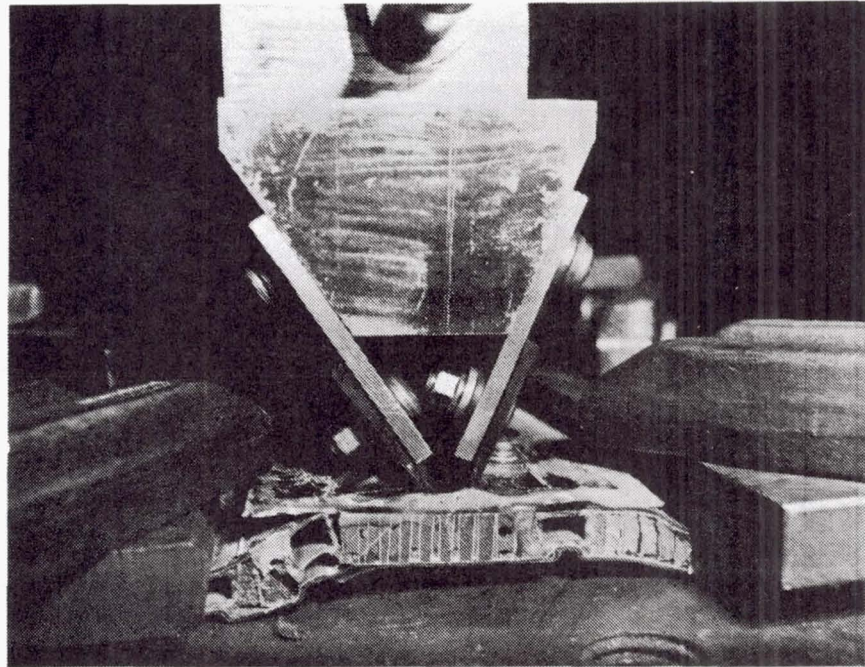


Figure 108. Four-leg angle tension test failure mode

The leading-edge section was attached to an aluminum plate which was bolted to the vertical wall of the universal test frame. Attachment was such that the leading-edge section was in an inverted position. This allowed the lower surface to be loaded with lead shot and lead pigs. Pads were bonded to the upper surface, and loads were applied by three hydraulic actuators through linkage designed to provide the desired distribution. Part of the upper surface loading was applied by lead shot in the aft bay of the leading edge panel. Overall views of the test arrangement are shown in Figure 110.

Acoustic emission (AE) techniques were used to monitor the test article to locate any damage that might occur during proof loading. The test article was monitored continuously during loading. Some general resin matrix cracking occurred, but the signal level was very low, indicating that microscopic size cracking occurred. No resin matrix microcracking of the type associated with delamination and splitting parallel to the fiber direction was detected. No fiber fracture was detected.

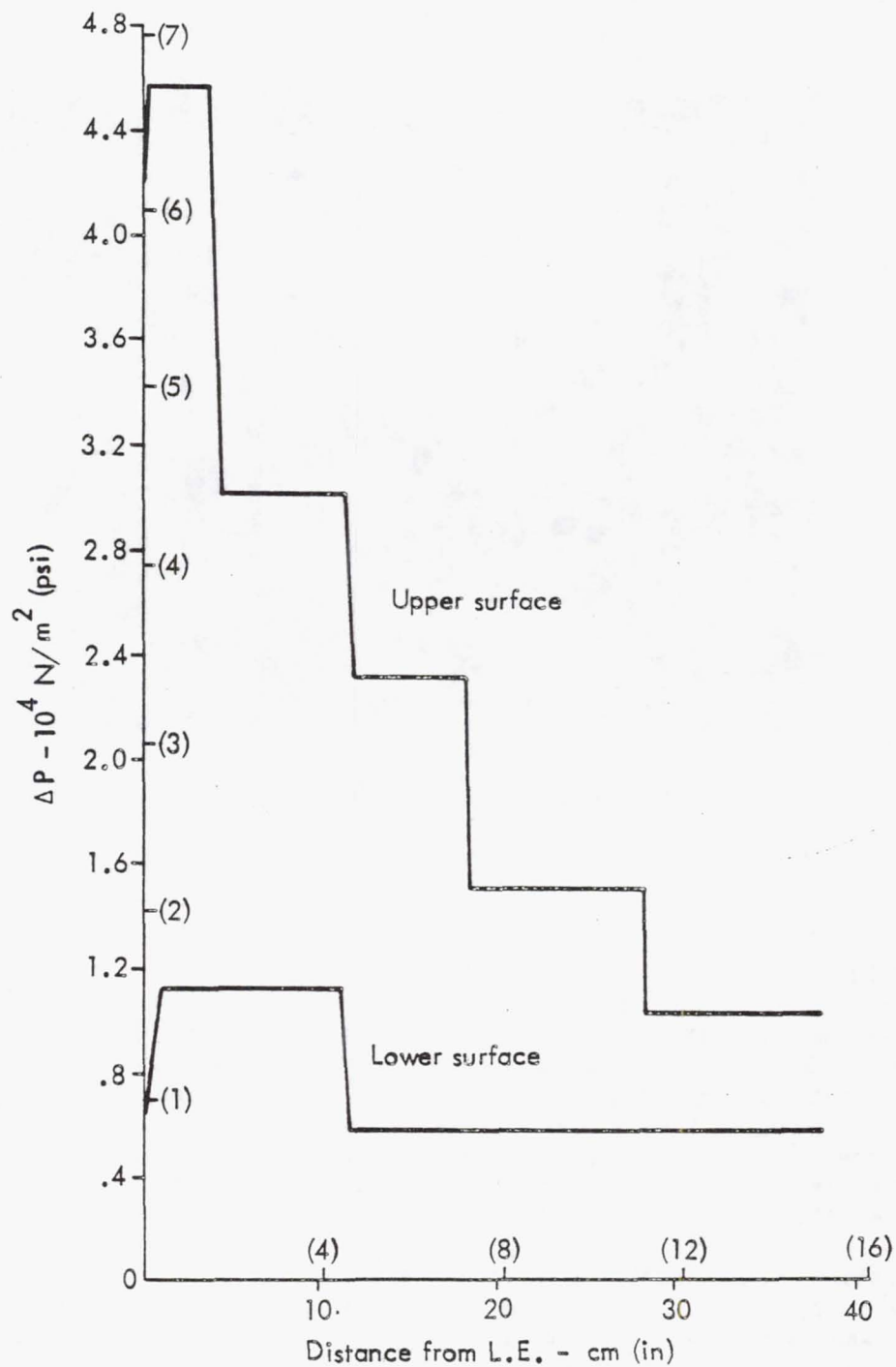


Figure 109. LFC leading-edge proof test load distribution



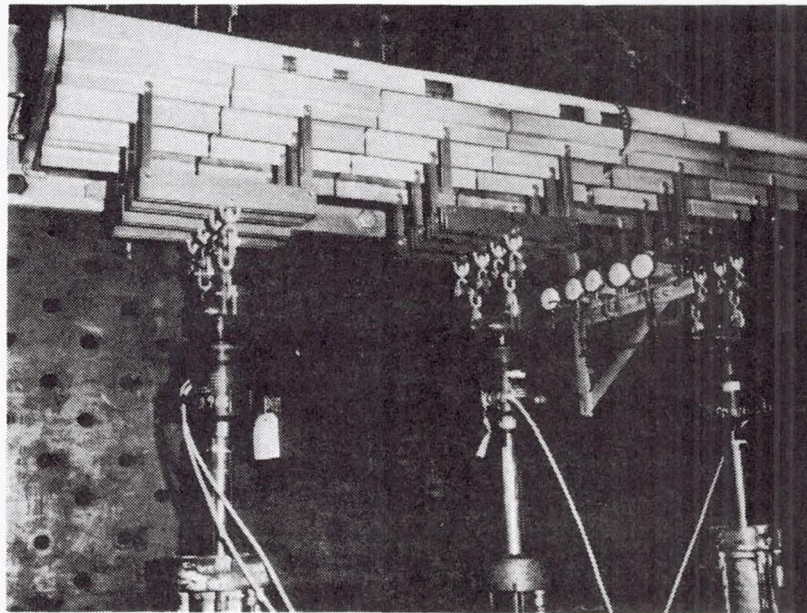
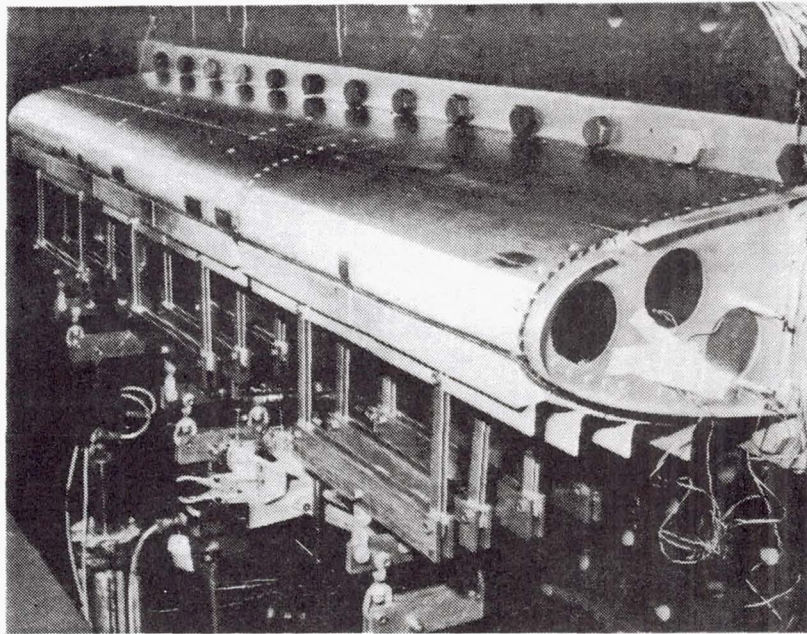


Figure 110. Loading arrangement details

## 6.3 LFC SUCTION SYSTEM

### 6.3.1 Design Objectives

The primary objective of the suction system design is to achieve efficient removal of the low-energy boundary layer air from the airfoil surfaces as required to maintain laminar flow over the surface. A secondary, but equally important, objective is to design a system which is compatible with the structural design, manufacturing techniques and capabilities, low manufacturing cost, high reliability, and good maintainability. Accomplishment of the primary objective is dependent on removal of boundary layer air in a selective manner to prevent boundary layer transition. The required inflow of suction air is not uniform over the surface and the variation in local pressure over the airfoil surface necessitates various levels of suction pressure differentials in order to achieve the required local levels of suction. These constraints dictate that the suction surface and internal ducting be the subject of a careful design analysis in order to achieve the primary objective while maintaining compatibility with the secondary objective.

### 6.3.2 Surface Configuration

#### 6.3.2.1 Sensitivity Studies

Prior to initiation of the suction surface slot configuration design, a better understanding of the slot performance sensitivities to the slot configuration was necessary. This required a method of assessing the slot design criteria as a function of slot configuration, wing geometry, and flight variables. Slot design envelopes were defined to aid in selecting slot configuration and were incorporated into wing surface design charts. Sensitivities of these design envelopes and design charts were assessed against variations in wing chord and cruise flight conditions.

#### Design Criteria

The suction slot design must provide slots having flow characteristics that are predictable, stable, uniform along the length of the slot, and free from surface flow disturbances. Criteria and limits for slot design were developed to meet these requirements during the X-21 program in the early 1960's by NORAIR and are summarized in Reference 7. Unfortunately, supporting data are not well documented in the literature. When these criteria and limits are applied to the design of slots for the current airfoil requirements, mutually exclusive conflicts exist between the criteria. A strict application of the criteria and limits to define the surface slot configuration results in slot widths and spacings in the leading-edge region that are impractical, if not impossible, to manufacture on a production airplane. For these reasons, it is necessary to accept some compromises in these criteria and limits. However, the lack of sufficient supporting data precludes a sound and confident judgement of these compromises.

These criteria are listed below with a brief description. The limits indicated are used as goals in the current study and are in general agreement with those of Reference 7.



- o  $\beta_w = \frac{t}{wRw}$ ; Limit:  $\beta_w \geq 0.0075$

This is a slot geometry/flow parameter. The limit is indicative of the extent of predictability of the slot flow characteristics.

- o  $w/z$ ; Limit:  $1.0 \leq w/z \leq 1.4$

This parameter is the ratio of the slot width to the sucked height. The criteria limits are indicative of slot flow stability. For purposes of this study, an attempt was made to hold the value in the middle of the acceptable range (i.e.,  $w/z = 1.2$ ) insofar as practicable.

- o  $C_{ps} = \frac{\Delta P_{\text{slot}}}{q_o}$ ; Limit  $\geq 0.02$

This parameter is defined by the slot pressure loss divided by the free stream dynamic pressure and is indicative of slot flow uniformity, stability and slot pressure loss.

- o  $U_z/U_e$ ; Limit  $\leq 0.30$

This parameter is the ratio of the velocity of the boundary layer flow at the sucked height to the velocity at the edge of the boundary layer. The upper limit was selected to limit the influence of suction on the stream flow outside the sucked boundary layer. It is desirable to maintain the value of this parameter as low as practicable.

- o  $R_w$ ; Limit  $\leq 100$

The slot Reynolds number is based on the slot width and flow conditions and is indicative of slot flow stability. In the leading-edge region, where the boundary layer is quite thin, other criteria, notably  $U_z/U_e$  dictate slot Reynolds numbers well below this limit. In the higher  $x/c$  regions, other criteria were consistent with an  $R_w$  above 100. It was concluded that the limit of 100 would be observed as far as practical, but  $R_w$  would be allowed to exceed 100 where other criteria precluded reaching that limit.

#### Design Envelope Derivation

As a result of the complexities and interactive effects of the design criteria and the possibility of aircraft operation at other than basic design cruise conditions, a surface configuration sensitivity study was conducted to permit development of a design that would allow for off-design conditions. The basic approach adopted for this effort was to determine a design based on commonality of slot spacing and slot width over as much of the wing span as possible without violating any of the design criteria at off-design conditions.



An analytical evaluation of the governing equations for the  $\beta_w$ ,  $w/z$ ,  $C_{ps}$  and  $U_z/U_e$  slot design criteria showed that they may all be expressed in terms of  $R_w$  slot Reynolds number,  $R_w$ , and slot width,  $w$ , for given airfoil surface boundary layer, airflow  $w$  conditions, and distributed suction flow requirements. Similarly, the slot spacing,  $\Delta C_n$ , is defined solely by slot Reynolds number,  $R_w$ , at these same surface aerodynamic conditions. An upper limit of  $R_w$  may, in turn, be defined by the upper limit of the boundary layer sucked height velocity ratio  $U_z/U_e$  and the local boundary layer conditions. Thus, for a given location on an airfoil surface with defined surface aerodynamic conditions and suction rate, specific limiting value lines may be plotted for each of the slot design criteria as a function of  $R_w$  vs  $w$ , or, in the case of slot spacing, simply as a function of  $R_w$ . An example of such a plot is shown on Figure 111.

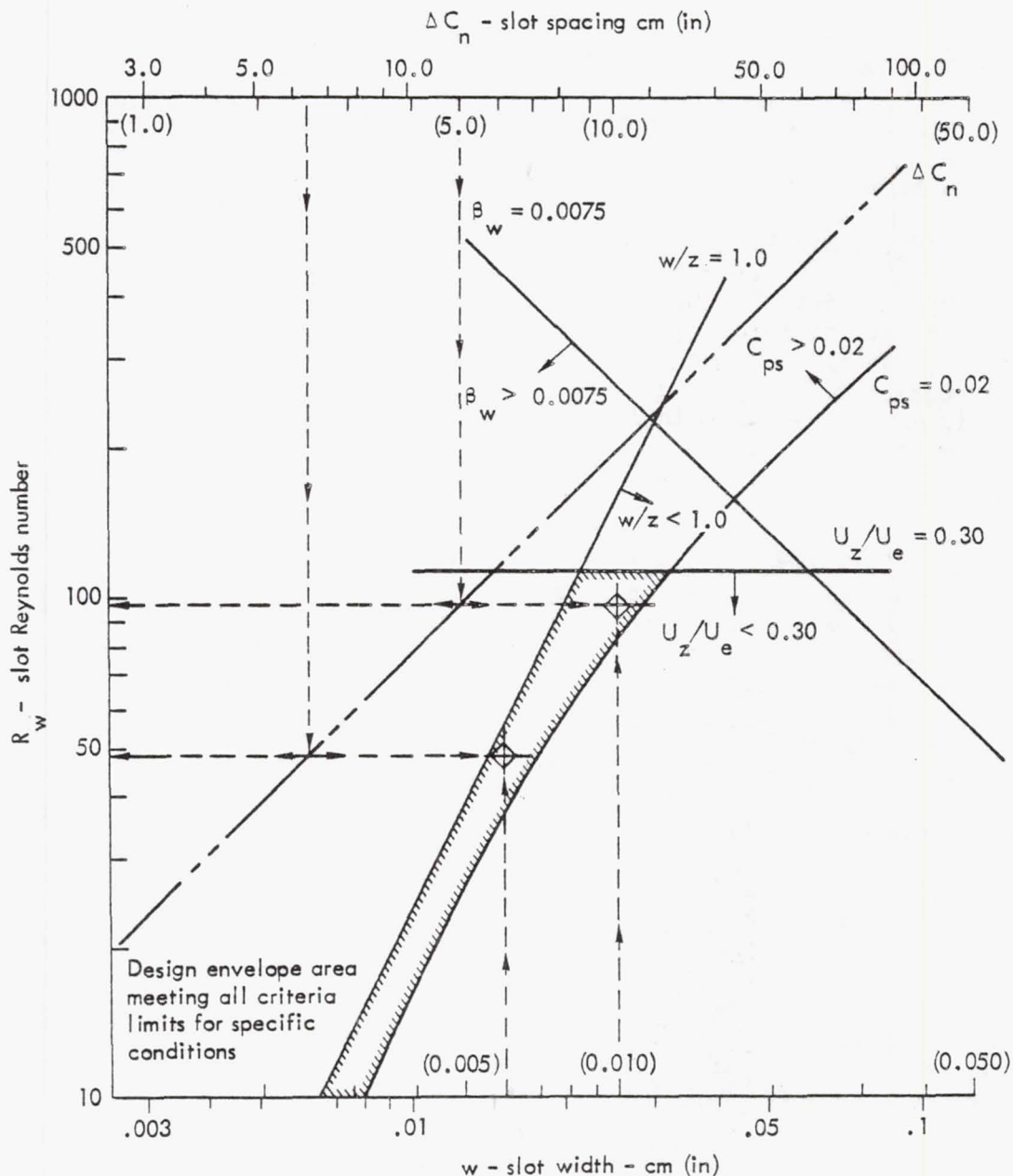


Figure 111. Typical criteria limit envelope

The limiting values of these criteria in terms of  $R_w$  as a function of  $w$  are shown as solid lines with the direction of acceptable criteria variations indicated by arrows. The intersection of the areas of acceptable criteria values is indicated by heavier lines and cross hatching on the figure. This area is referred to herein as a "Design Envelope" and is defined as the area on a criteria limit plot, or design chart, within whose boundaries all the criteria limits are satisfied for a specific surface location, airfoil geometry, flight condition, and distributed suction rate. The relationship between  $\Delta C_n$  and  $R_w$  for these same conditions is shown as a phantom line on the figure.

The design chart may be used to select a design configuration by choosing a slot spacing or a slot width that is compatible with structural or manufacturing requirements. The examples shown on Figure 111 reflect selection of convenient values for slot width and spacing. Selection of the higher point reflects a larger slot spacing, thereby requiring fewer slots on the airfoil. It also requires a wider slot, which is easier to manufacture and would be less sensitive to manufacturing tolerances and contamination. However, this point is very close to the  $U_z/U_e$  limit. The lower point is more desirable from a performance standpoint, but requires twice as many smaller slots, which are undesirable from a manufacturing standpoint. For convenience, the upper point indicated by the open symbol on Figure 111 is referred to as a "production configuration". The lower solid point is referred to as a "performance configuration".

#### Wing Surface Design Charts

The design charts for the upper and lower wing surfaces for the mid-semispan location and design cruise condition are shown in Figures 112 and 113. Only the design envelopes are shown for five chordwise locations from  $x/c = 0.01$  to  $x/c = 0.70$  with the other lines omitted for clarity. The performance and production design points, shown as shaded and open points respectively, are located for each of the  $x/c$ 's indicated. Although there are much larger design envelopes available, design points were chosen with emphasis placed on:

- (1) Commonality of design
- (2)  $w/z$  values from 1.0 to 1.4
- (3)  $C_{ps}$  values as great as possible
- (4)  $U_z/U_e$  values from 0.2 to 0.3
- (5) In the case of the production oriented design, large slot widths and slot spacings but without minimum dimensional limits.

It will be observed that nearly all of the design envelope for  $x/c$  of 0.012 on the upper surface and all of the design envelope for  $x/c$  of 0.011 on the lower surface are below reasonable slot width production manufacturing capabilities. An upper  $R_w$  limit of 100 may only be achieved over a portion of the design envelopes beyond an  $x/c$  of 0.20 on the upper surface and none at the design envelopes above  $x/c$  of 0.20 on the lower surface. These mutual exclusions of slot designs by the existing criteria or manu-

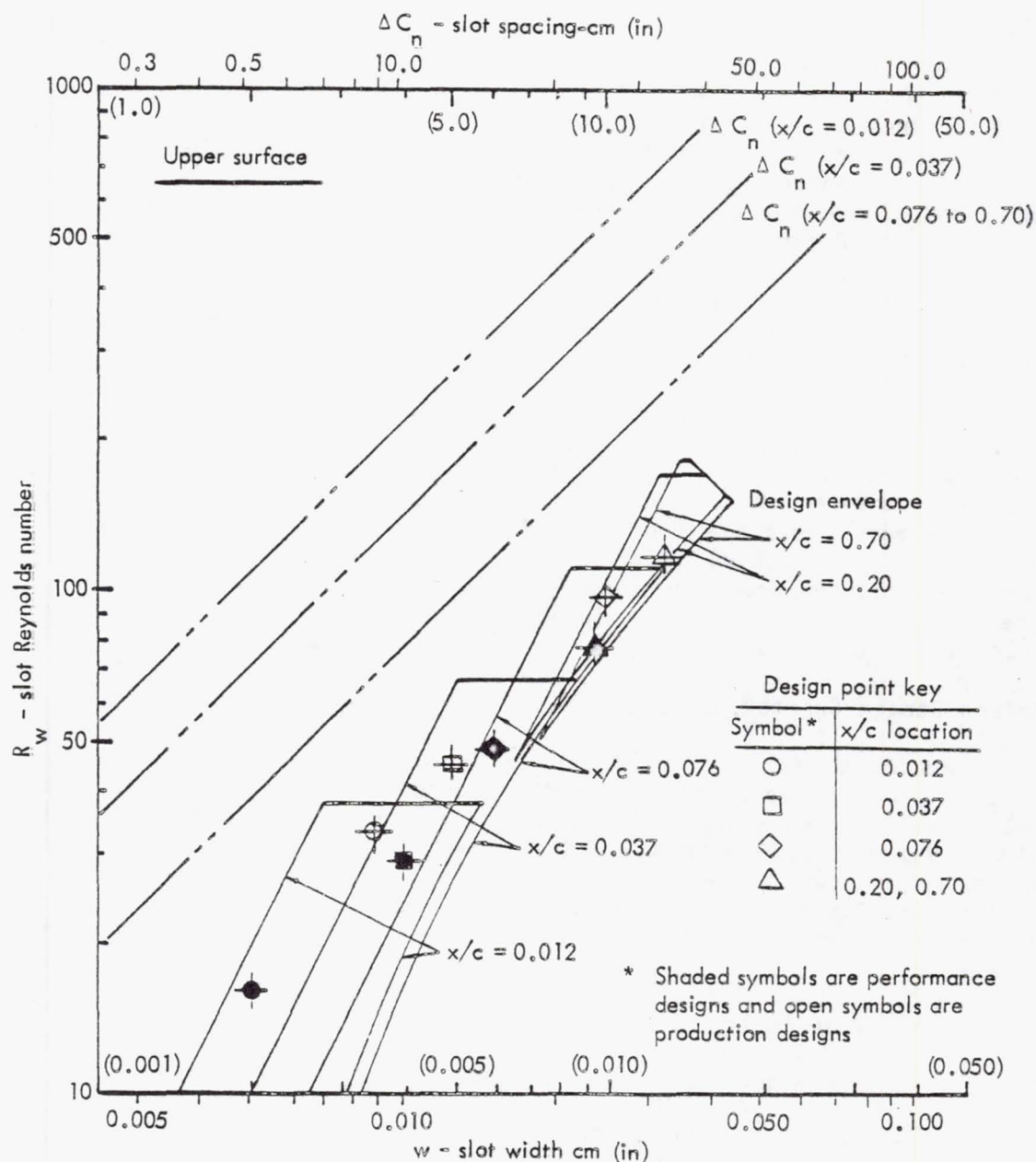


Figure 112. Upper wing surface design envelope

facturing capabilities is one of the deficiencies of the existing criteria. In this case, the other criteria were allowed to take precedence over the  $R_w$  limit, and the sensitivity studies were conducted without manufacturing constraints.

The design charts are unique to a given flight condition, airfoil, boundary layer, and suction flow. It follows that they are sensitive to variations within the cruise flight envelope and to various wing stations. This sensitivity defines the slot performance design margin for a given design at various spanwise locations and cruise flight conditions.



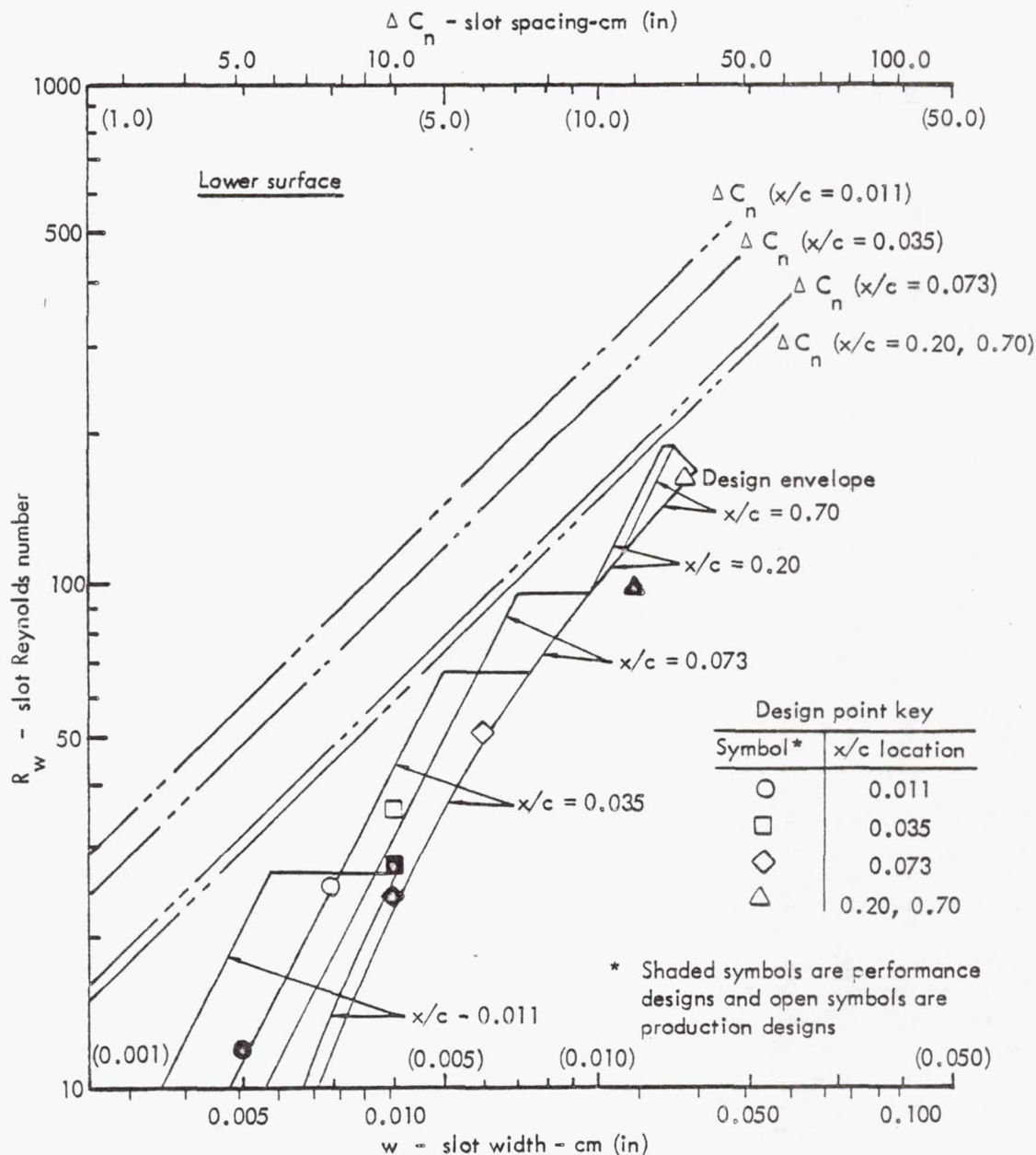


Figure 113. Lower wing surface design envelope

The range of flight conditions evaluated in this study are presented in Table 21 and represent the range over which the aircraft might operate during cruise. Evaluations included consideration of the  $C_p$  characteristics and level changes and boundary layer characteristic changes for a fixed airfoil shape and distributed suction level. Data for spanwise variations in airfoil shape and  $C_p$  were unavailable at the time of the sensitivity study. In order to achieve maximum simplicity in a production airplane, the suction system will be optimized for cruise conditions and no provision will be made for differentially controlling the section distribution. Therefore, a fixed distributed suction level was considered appropriate for this sensitivity study.

TABLE 21. CRUISE ENVELOPE PERTURBATIONS

Altitude		Mach	Chord Length	
m	(ft)		m	(ft)
12 192	(40 000)	0.80	6.953	(22.813)
12 192	(40 000)	0.80	7.416	(24.330)
12 192	(40 000)	0.80	3.859	(12.660)
10 668	(35 000)	0.80	6.953	(22.813)
13 716	(45 000)	0.80	6.953	(22.813)
12 192	(40 000)	0.75	6.953	(22.813)
12 192	(40 000)*	0.80	6.953	(22.813)

\* End cruise pressure distribution

From these data, the following four conditions were generated for use as a "cause" to which the sensitivity trend "effect" was evaluated.

- (1) Spanwise location: This is a geometry variable consisting of movement outboard along the wing from 30% to 85% semispan locations, 7.416m and 3.859m (24.33 and 12.66 ft) chords, respectively. Care should be exercised in applying the trends indicated by this variable since the properties were independently evaluated for each spanwise location. In an actual airplane design, spanwise compromises in slot width, spacing, and slot runout would be necessary to achieve some degree of continuity, both aerodynamically and structurally, between various spanwise locations.
- (2) Altitude: The perturbation involved increasing flight altitude from 10 668m to 13 716m (35 000 ft to 45 000 ft) at a constant Mach number of 0.80.
- (3) Mach number: This variation evaluated the trend as a result of decreasing the cruise Mach number from 0.80 to 0.75 at a constant altitude of 12 192m (40 000 ft).
- (4) Start to end cruise: This perturbation was included to investigate the trends due to mission progression from start to end cruise condition at 12 192m (40 000 ft) and 0.80 Mach number.

These variations were considered in designing the slot configuration for the basic design cruise condition by evaluating the configuration for the changes in criteria. Through this approach, the slot configuration design was modified to equalize the compromises to the various criteria. The relative change in the actual values of the criteria parameters for a fixed design point due to the flight perturbations is of major interest.

The fixed design point trend presented in Table 22 is in the form of percentage change in the actual criteria parameter ( $C_{ps}$ ,  $w/z$ ,  $U_z/U_e$ ,  $R_w$ ) values due to the previously defined variables. The percentage change was calculated by the difference in the final and initial values divided by the initial value. Upper and lower surfaces are listed separately for  $C_{ps}$ ,  $w/z$ , and  $U_z/U_e$ . However, the change in  $R_w$  is the same for both upper and lower surface and are combined in the table under the heading of "Both." It should be remembered that the criteria values were evaluated for constant slot width, slot spacing, and  $x/c$  location.

Relative to the defined limits, increasing values of  $C_{ps}$  and  $w/z$  and decreasing values of  $U_z/U_e$  and  $R_w$  are desirable. Using these ground rules, evaluation of Table 22 and the indicated figures show the following trends:

- (1) Due to the complexity of slot position as a function of  $x/c$  location as spanwise movement is encountered, the trends toward acceptable/unacceptable criteria margins due to spanwise movement is uncertain and additional analysis is needed to define these trends.

However, if this geometry perturbation is considered as the criteria margin trend due to a change in chord length of 7.415m down to 3.840m (24.33 ft down to 12.6 ft), or approximately 2 to 1, some interesting trends, or lack of trends, are observed. Preliminary observations indicate a change of only 11% to 13% in criteria margins for  $w/z$  and  $U_z/U_e$  with no change in criteria margins for  $R_w$ ,  $\beta_w$ , and  $C_{ps}$ . This trend of negligible changes in criteria values for a fixed-design condition with reducing chord length indicates that a short-chord validator might be feasible in the selection of a flight vehicle for that phase of the program.

- (2) Increasing altitude offered improved  $C_{ps}$ ,  $U_z/U_e$ , and  $R_w$  margins, but reduced the  $w/z$  margin. Conversely, decreasing altitude reduced  $C_{ps}$ ,  $U_z/U_e$ , and  $R_w$  margins, while improving the  $w/z$  margin.
- (3) The percentage changes due to decreasing Mach number are so slight on all four criteria that variation of this flight condition will probably have negligible effects on the overall performance of the LFC system.
- (4) Criteria margins from start to end cruise appear to vary differently, even over the upper and lower surfaces. The changes in  $w/z$ ,  $U_z/U_e$ , and  $R_w$  are very slight, and probably will not significantly change during the mission. The  $C_{ps}$  margin, however, appears to increase on the lower wing surface while decreasing at a faster rate on the upper wing surface. Indications are that, at the end of cruise,  $C_{ps}$  values on the upper wing surface could become critical.



TABLE 22. FIXED DESIGN POINT MARGIN SENSITIVITY TREND

	$C_{ps}$		$w/z$		$U_z/U_e$		$R_w$
Surface	Upper	Lower	Upper	Lower	Upper	Lower	Both
Spanwise location (Decreasing Chord)	N/C	N/C	+11	+13	+11	+13	N/C
Increasing Altitude	+27	+22	-18	-13	-6	-13	-37
Decreasing Mach number	-2	+3	+2	-2	-4	-2	-5
Start to end cruise	-16	+9	+4	-5	N/C	-3	N/C

#### 6.3.2.2 Surface Designs

As a result of the previous sensitivity study and the design points determined on Figures 112 and 113, Figures 114 and 115 were developed to graphically illustrate both the production and performance oriented designs. The mid-span chord location with a chord length of 6.953m (22.813 ft) was considered. The chordwise design region for both the upper and lower wing surfaces start at the first slot aft of the leading-edge cleaning/deicing system region located at  $x/c = 0.01$ . The design region terminates on the upper and lower surfaces at about  $x/c = 0.70$  due to the standing shock wave and adverse pressure gradients located in this vicinity. The other spanwise locations considered in the sensitivity study are not included due primarily to the need for additional analysis to determine the best locations for terminating unnecessary slots. The formats of Figures 114 and 115 includes an  $x/c$  scale which is appropriate for approximating slot widths, spacings and criteria at other spanwise stations. However, spanwise airfoil and  $C_p$  variations are not considered.

#### Production Oriented Design

The production design illustrated by Figure 114 shows the outline of the airfoil shape as a function of both  $x/c$  and chord distance  $x$ . The suction slots are represented by marks internal to the airfoil outline. The external divisions signify different zones, an alpha character describing a major zone distinguished by a constant slot width throughout, and the numeric character describing a sub-zone region of each major zone. The combined alpha-numeric zone corresponds to a line of slot performance data in the associated tables which follow. Each line of slot performance data in these tables corresponds to a specific  $x/c$  location, while the alpha-numeric zone represents a range of  $x/c$  locations. For analysis purposes, it was assumed that all slots located in a zone performed in a manner such that the table values reflect the average slot performance for that zone.

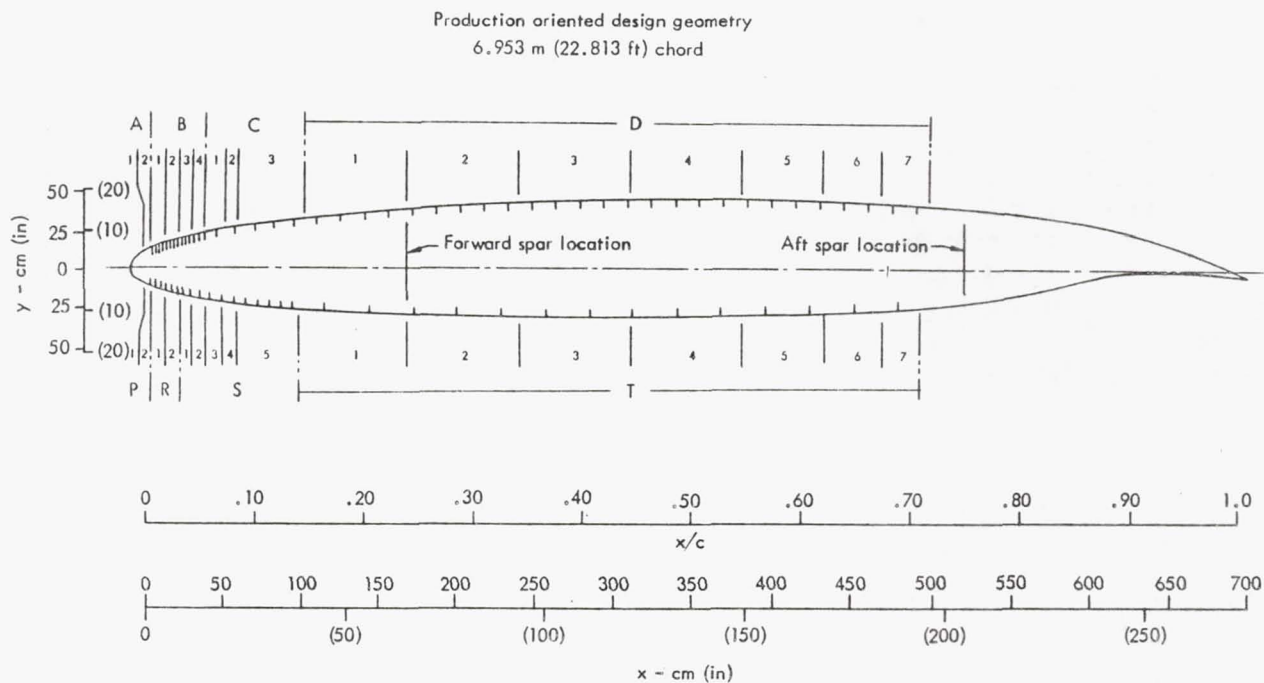


Figure 114. Production oriented wing surface design

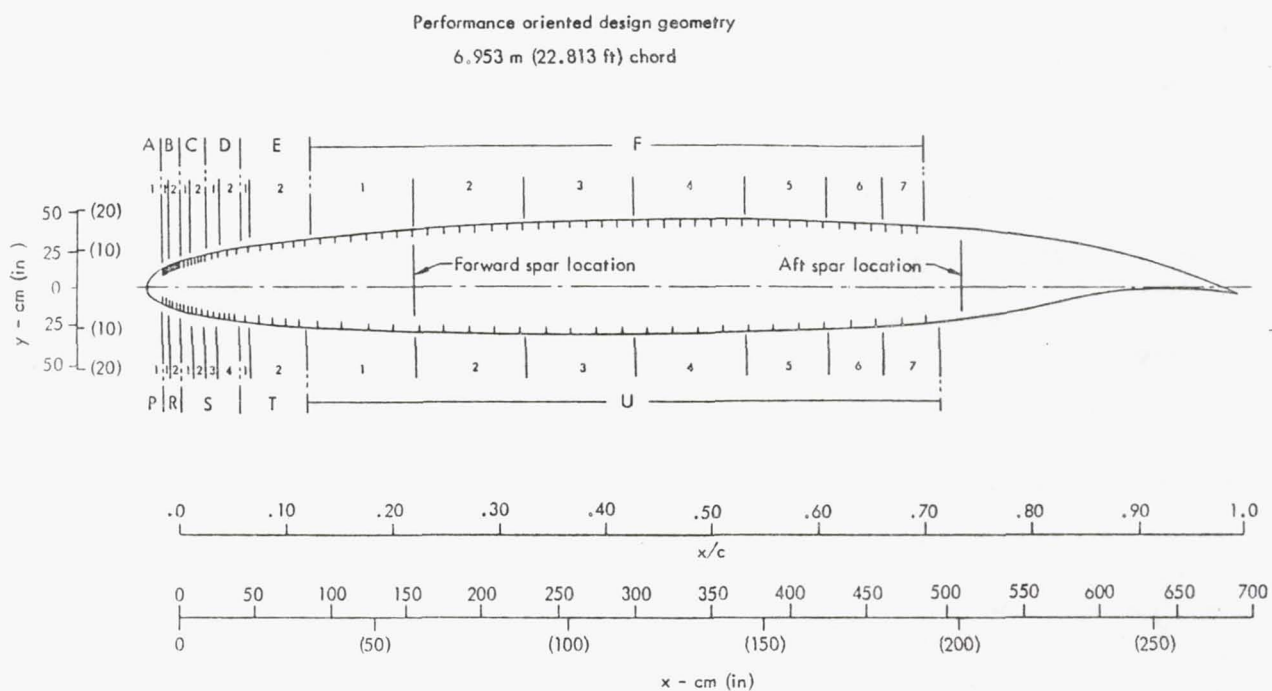


Figure 115. Performance oriented wing surface design

Slot locations are not shown in zones A and P due to very small spacing in those regions. Table 23 lists both the geometry and performance of the upper surface for the 12 192m (40 000 ft), 0.80 Mach number cruise condition. The column headings correspond to an alpha-numeric zone location (ZONE), chordwise (X/C) location, slot width (W) in inches, slot spacing ( $\Delta$  CN) in inches, slot Reynolds number (RW), the ratio of slot width to boundary layer sucked height (W/Z), the ratio of sucked-height velocity to boundary-layer edge velocity (UZ/UE), slot geometry and flow parameter (BETA), and slot pressure loss coefficient (CPS). Similar data were generated for all of the variations in spanwise location and cruise flight variations discussed in Section 6.3.2.1. The lower surface geometry and performance are similarly illustrated on Figure 114 and listed for the design cruise condition on Table 24.

TABLE 23. UPPER SURFACE PRODUCTION DESIGN DATA

Altitude = 12 192 m (40 000 ft)			Mach No. = 0.80			Chord = 6.953 m (22.813 ft)		
ZONE	X/C	W	CN	RW	W/Z	UZ/UE	BETA	CPS
A1	.1200-01	.3500-02	.6200+00	.3393+02	.1351+01	.2830+00	.1684+00	.6069-01
A2	.1800-01	.3500-02	.6200+00	.3074+02	.1328+01	.2583+00	.1859+00	.5821-01
B1	.2700-01	.5000-02	.1120+01	.4847+02	.1295+01	.2839+00	.8252-01	.4537-01
B2	.3700-01	.5000-02	.1250+01	.4480+02	.1204+01	.2452+00	.8929-01	.4100-01
B3	.4800-01	.5000-02	.1250+01	.3979+02	.1180+01	.2133+00	.1005+00	.3456-01
B4	.6200-01	.5000-02	.1750+01	.3386+02	.1165+01	.1790+00	.1181+00	.2750-01
C1	.7600-01	.1000-01	.5000+01	.9675+02	.1270+01	.2783+00	.2067-01	.2772-01
C2	.9200-01	.1000-01	.5000+01	.9675+02	.1226+01	.2678+00	.2067-01	.2756-01
C3	.1000+00	.1000-01	.5000+01	.9675+02	.1202+01	.2624+00	.2067-01	.2752-01
D1	.2000+00	.1300-01	.6000+01	.1161+03	.1249+01	.2480+00	.1325-01	.2105-01
D2	.3000+00	.1300-01	.6000+01	.1161+03	.1213+01	.2404+00	.1325-01	.2108-01
D3	.4000+00	.1300-01	.6000+01	.1161+03	.1195+01	.2364+00	.1325-01	.2129-01
D4	.5000+00	.1300-01	.6000+01	.1161+03	.1168+01	.2318+00	.1325-01	.2166-01
D5	.6000+00	.1300-01	.6000+01	.1161+03	.1170+01	.2331+00	.1325-01	.2202-01
D6	.6500+00	.1300-01	.6000+01	.1161+03	.1188+01	.2385+00	.1325-01	.2250-01
D7	.7000+00	.1300-01	.6000+01	.1161+03	.1183+01	.2397+00	.1325-01	.2299-01

### Performance Oriented Design

The performance oriented design is illustrated in Figure 115 in the same manner as the previous production configuration. Note the increased number of major zones corresponding to an increased variety of slot widths and the reduced slot spacing on both the upper and lower surfaces. The slots are not indicated in Zones A and P due to the very small spacing in those regions. Tables 25 and 26 list both the geometry and performance of the performance oriented upper and lower surface designs respectively for the 12 192m (40 000 ft) altitude, 0.80 Mach number cruise condition.



TABLE 24. LOWER SURFACE PRODUCTION DESIGN DATA

Altitude = 12 192 m  
(40 000 ft)

Mach No. = 0.80

Chord = 6.953 m  
(22.813 ft)

ZONE	X/C	W	CN	RW	W/Z	UZ/UE	BETA	CPS
P1	.1106-01	.3000-02	.8750+00	.2555+02	.1363+01	.2925+00	.2610+00	.4233-01
P2	.1760-01	.3000-02	.9200+00	.2560+02	.1215+01	.2393+00	.2604+00	.4546-01
R1	.2560-01	.4000-02	.1500+01	.3916+02	.1296+01	.2803+00	.1277+00	.3832-01
R2	.3510-01	.4000-02	.1500+01	.3607+02	.1109+01	.2185+00	.1386+00	.3502-01
S1	.4640-01	.6000-02	.2300+01	.4977+02	.1352+01	.2436+00	.6697-01	.1994-01
S2	.5910-01	.6000-02	.2650+01	.5006+02	.1249+01	.2249+00	.6658-01	.2047-01
S3	.7340-01	.6000-02	.3250+01	.5135+02	.1186+01	.2178+00	.6491-01	.2159-01
S4	.8910-01	.6000-02	.3250+01	.4875+02	.1107+01	.1925+00	.6838-01	.2007-01
S5	.1000+00	.6000-02	.3250+01	.4875+02	.1077+01	.1871+00	.6838-01	.2008-01
T1	.2000+00	.1500-01	.1100+02	.1650+03	.1198+01	.2799+00	.8081-02	.2145-01
T2	.3000+00	.1500-01	.1100+02	.1650+03	.1186+01	.2752+00	.8081-02	.2153-01
T3	.4000+00	.1500-01	.1100+02	.1650+03	.1094+01	.2526+00	.8081-02	.2155-01
T4	.5000+00	.1500-01	.1100+02	.1650+03	.1092+01	.2507+00	.8081-02	.2158-01
T5	.6000+00	.1500-01	.1100+02	.1650+03	.1056+01	.2411+00	.8081-02	.2163-01
T6	.6500+00	.1500-01	.1100+02	.1650+03	.1076+01	.2449+00	.8081-02	.2168-01
T7	.7000+00	.1500-01	.1100+02	.1650+03	.1141+01	.2465+00	.8081-02	.2087-01

TABLE 25. UPPER SURFACE PERFORMANCE DESIGN DATA

Altitude = 12 192 m  
(40 000 ft)

Mach No. = 0.80

Chord = 6.953 m  
(22.813 ft)

ZONE	X/C	W	CN	RW	W/Z	UZ/UE	BETA	CPS
A1	.1200-01	.2000-02	.3000+00	.1642+02	.1110+01	.1969+00	.6091+00	.1223+00
B1	.1800-01	.3000-02	.3700+00	.1834+02	.1473+01	.1996+00	.3634+00	.4742-01
B2	.2700-01	.3000-02	.5600+00	.2424+02	.1099+01	.2007+00	.2751+00	.7002-01
C1	.3700-01	.4000-02	.8300+00	.2975+02	.1182+01	.1998+00	.1681+00	.4179-01
C2	.4800-01	.4000-02	.1100+01	.3501+02	.1006+01	.2001+00	.1428+00	.5189-01
D1	.6200-01	.6000-02	.2180+01	.4218+02	.1252+01	.1998+00	.7902-01	.2364-01
D2	.7600-01	.6000-02	.2500+01	.4838+02	.1077+01	.1968+00	.6891-01	.2896-01
E1	.9200-01	.7000-02	.2800+01	.5418+02	.1146+01	.2004+00	.5273-01	.2355-01
E2	.1000+00	.7000-02	.2900+01	.5612+02	.1105+01	.1998+00	.5092-01	.2486-01
F1	.2000+00	.9500-02	.4000+01	.7740+02	.1118+01	.2025+00	.2720-01	.2029-01
F2	.3000+00	.9500-02	.4000+01	.7740+02	.1086+01	.1963+00	.2720-01	.2041-01
F3	.4000+00	.9500-02	.4000+01	.7740+02	.1069+01	.1930+00	.2720-01	.2052-01
F4	.5000+00	.9500-02	.4000+01	.7740+02	.1045+01	.1893+00	.2720-01	.2087-01
F5	.6000+00	.9500-02	.4000+01	.7740+02	.1047+01	.1904+00	.2720-01	.2123-01
F6	.6500+00	.9500-02	.4000+01	.7740+02	.1063+01	.1948+00	.2720-01	.2168-01
F7	.7000+00	.9500-02	.4000+01	.7740+02	.1059+01	.1957+00	.2720-01	.2216-01

TABLE 26. LOWER SURFACE PERFORMANCE DESIGN DATA

Altitude = 12 192 m  
(40 000 ft)

Mach No. = 0.80

Chord = 6.953 m  
(22.813 ft)

ZONE	X/C	W	CN	RW	W/Z	UZ/UE	BETA	CPS
P1	.1106-01	.2000-02	.4100+00	.1197+02	.1327+01	.2002+00	.8354+00	.5667-01
R1	.1760-01	.3000-02	.9200+00	.2560+02	.1215+01	.2393+00	.2604+00	.4546-01
R2	.2560-01	.3000-02	.1000+01	.2611+02	.1190+01	.2289+00	.2554+00	.4936-01
S1	.3510-01	.4000-02	.1160+01	.2789+02	.1261+01	.1921+00	.1793+00	.2492-01
S2	.4640-01	.4000-02	.1290+01	.2792+02	.1203+01	.1824+00	.1791+00	.2526-01
S3	.5910-01	.4000-02	.1480+01	.2796+02	.1114+01	.1680+00	.1788+00	.2575-01
S4	.7340-01	.4000-02	.1500+01	.2370+02	.1164+01	.1480+00	.2110+00	.2115-01
T1	.8910-01	.6500-02	.3500+01	.5250+02	.1156+01	.1998+00	.5861-01	.1848-01
T2	.1000+00	.6500-02	.3500+01	.5250+02	.1124+01	.1942+00	.5861-01	.1849-01
U1	.2000+00	.1175-01	.6670+01	.1000+03	.1206+00	.2180+00	.1701-01	.1423-01
U2	.3000+00	.1175-01	.6670+01	.1000+03	.1193+01	.2143+00	.1701-01	.1429-01
U3	.4000+00	.1175-01	.6670+01	.1000+03	.1101+01	.1967+00	.1701-01	.1430-01
U4	.5000+00	.1175-01	.6670+01	.1000+03	.1099+01	.1952+00	.1701-01	.1432-01
U5	.6000+00	.1175-01	.6670+01	.1000+03	.1062+01	.1877+00	.1701-01	.1435-01
U6	.6500+00	.1175-01	.6670+01	.1000+03	.1082+01	.1907+00	.1701-01	.1439-01
U7	.7000+00	.1175-01	.6670+01	.1000+03	.1148+01	.1920+00	.1701-01	.1385-01

## Surface Design Comparison

It was recognized that the combination of the multiple design criteria available and the two design philosophies might result in conflicts whereby all the criteria could not be met concurrently. This incompatibility did occur in two instances and compromises between the conflicting criteria limits were implemented. One compromise occurred in the production oriented design concept where the slot Reynolds number was allowed to exceed the limit of 100 in order to hold  $C_{ps}$  above 0.02 on both upper and lower wing surfaces from x/c of 20% to 70%. This trend toward a higher  $R_w$  resulted directly from the production design philosophy of larger slot spacing. The other compromise occurred on the lower surface of the performance oriented design concept where  $C_{ps}$  fell below 0.02 from x/c of 9% to 70% in order to hold  $R_w$  equal to or less than the limit of 100. This was consistent with the performance design concept of maintaining a more conservative  $R_w$  margin.

These two cases represent the extremes of the required range of compromise. An ultimate selection would necessitate a tradeoff involving the magnitudes of performance penalties and production and maintenance costs associated with each. Presently there are no known data defining performance penalty or risk associated with  $R_w$  values in excess of 100 or  $C_{ps}$  values below 0.02. Consequently, no meaningful tradeoff can be made. As pointed out earlier, both  $R_w$  and  $C_{ps}$  appear to be primarily associated with local spanwise slot velocity distribution and conservative or unconventional slot duct and metering design could possibly eliminate the necessity for any compromise. In any event, data are not available which would invalidate either design.



Comparison of the resultant criteria parameter values listed in Tables 23 through 26 and the previously defined criteria limits indicates reasonable agreement. The parameter margins relative to the criteria limits imply the degree of insensitivity to deviations from the design cruise point of 12 192m (40 000) ft and 0.8 Mach number. Both designs show reasonable insensitivity to deviations at altitudes from 10 668m to 13 716m (35 000 ft to 45 000 ft) and Mach number variations down to 0.75. They are both relatively insensitive to changing conditions between start cruise and end cruise. The performance oriented design showed a higher degree of insensitivity than the production design. These observations are consistent with the philosophies of these two designs.

The performance oriented design has generally smaller slots than the production design and is therefore more sensitive to slot tolerances. A nominal slot tolerance of  $\pm 0.00127$  cm ( $\pm 0.0005$  in) is anticipated to be a relatively ambitious goal for production airplanes in the 1990 time period. The effects of such considerations as flexure, Poisson's ratio and thermal growth are expected to be quite low compared to the  $\pm 0.00127$  cm ( $\pm 0.0005$  in) nominal slot tolerance assumed. These effects will generally be uniform over large areas of the surface with gradual transitions. Therefore, highly localized effects are unlikely and analytical evaluations for cruise conditions should permit their accommodation by designing the slot and metering system for the cruise conditions. However, isolated manufacturing variations, contamination, erosion, and other operational considerations may exceed this value. If the nominal  $\pm 0.00127$  cm ( $\pm 0.0005$  in) tolerance is applied to all slots and converted to slot suction flow variations for both the performance and production configurations, the performance oriented configuration reflects a 40% higher flow sensitivity to this tolerance over the upper wing surface from approximately 10% to 70% x/c, as shown on Figure 116. This in itself is not of great concern, since the percentage of flow variation is small, but the isolated larger variations could be of concern, both because they are local in nature and they are of larger magnitude. These isolated larger variations are therefore more likely to cause delaminarizing slot flow disturbances on the performance design. The figure indicates that the small slots in the region forward of 10% x/c are likely to be a problem for both configurations because of the high-tolerance induced slot flow variations. The performance design suction flows reflect a substantially higher sensitivity. The potential problem in this leading-edge region is increased by its vulnerability to contamination and damage, which could greatly amplify the flow variations over those shown on the figure. This leads to the observation that the performance design should be compromised toward the production design in this leading-edge region.

In addition to the high sensitivity of the slots in the leading edge region to tolerances, the close spacing and small slot suction flows dictate that the metering system would similarly be scaled down from that of the 10% to 70% x/c region. Small slot ducts and metering holes will add their own increased production tolerance sensitivity, which will be greater for the performance design.

The production oriented design requires a total of 82 slots over the upper and lower surfaces as compared to 122 total slots for the performance design. This represents nearly a 50% increase in the number of slots to



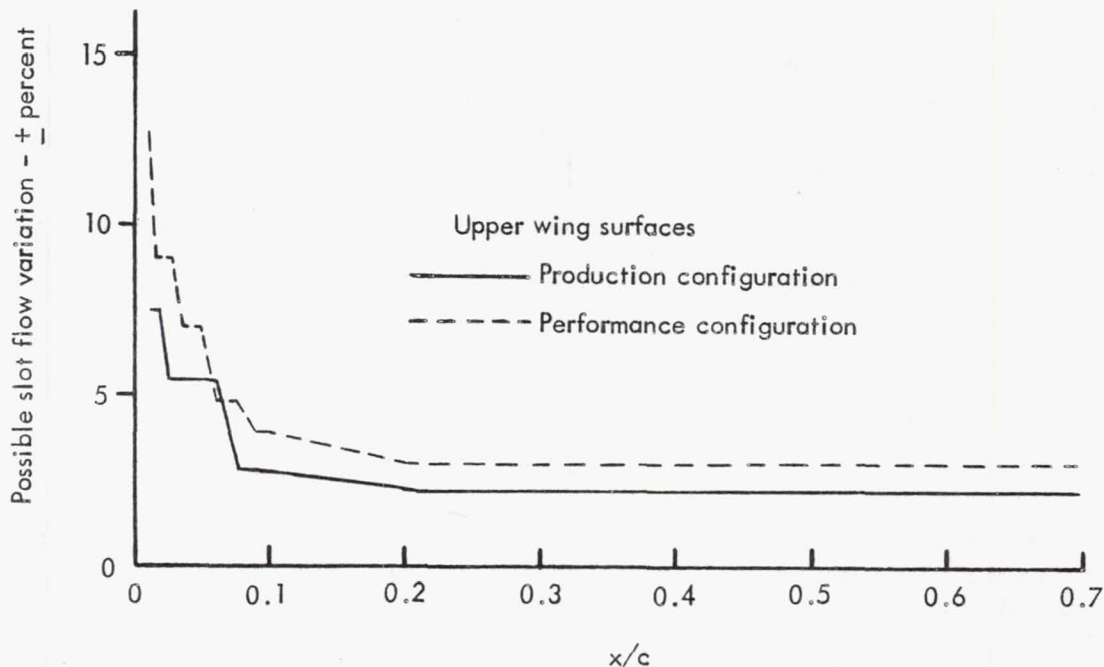


Figure 116. Surface design sensitivity

attain the greater margins of the performance oriented design. Some obvious drawbacks of this trend are that each slot will require a slot duct, metering system, and collector ducts, all of which contribute to a more costly and complex design.

### 6.3.3 Suction Ducting System

The suction ducting system is composed of a matrix of ducts to meter, collect and transport the suction flow from each surface slot to the suction pump. Desired distribution of suction flow over the wing surfaces is primarily controlled by the metering system contained within the airfoil surface structure. Further metering is included in collector ducting integral with the structural members of the wing, with final collection occurring in the trunk ducts formed by the wing leading-edge cavity. Trunk ducts convey the suction flow to the wing root, where additional ducting features provide necessary suction pump control capability. Ducting provisions for the suction pump are included in the discussion of suction system controls in Section 6.3.5.

#### 6.3.3.1 Ducting Concept

The ducting system for the baseline airplane has evolved over the course of this study based on both LFC system requirements and structural considerations. The resulting system concepts are compatible with both disciplines with relatively few compromises to either. The requirements of both disciplines divide naturally into leading-edge requirements and wing-box requirements. Somewhat different, although conceptually similar, configurations were developed for the mutual benefit of both disciplines. Thus, two basic types of configurations have been developed, one for the leading-edge region and the other for the wing-box region.

## Leading-Edge Ducting

The suction surface of the leading-edge region provides the entire metering system for the suction flow, as illustrated in Figure 117. The surface described in Section 6.2.3 consists of a slotted titanium skin bonded to a contoured continuous graphite composite structural skin with inner slot ducts pre-formed into the surface, the closing side of the duct being formed by the titanium skin. A pre-formed fiberglass collector duct is bonded to the underside of the graphite and another continuous graphite sheet forms the inner skin.

Metering holes connect the slot duct to the collector duct and serve to distribute the slot flow uniformly along the slot. This metering prevents excessive slot flow variations that might otherwise occur as a result of slot width manufacturing tolerances and variations in external aerodynamic parameters. The diameter,  $d_s$ , and spacing  $S_s$ , of these metering holes must be selected to result in suction flow pressure losses approximating those of the slots. They must provide stable flow and controlled pressure distribution in the slot duct that will limit slot flow variations to less than 1% across the slot lengths between metering holes.

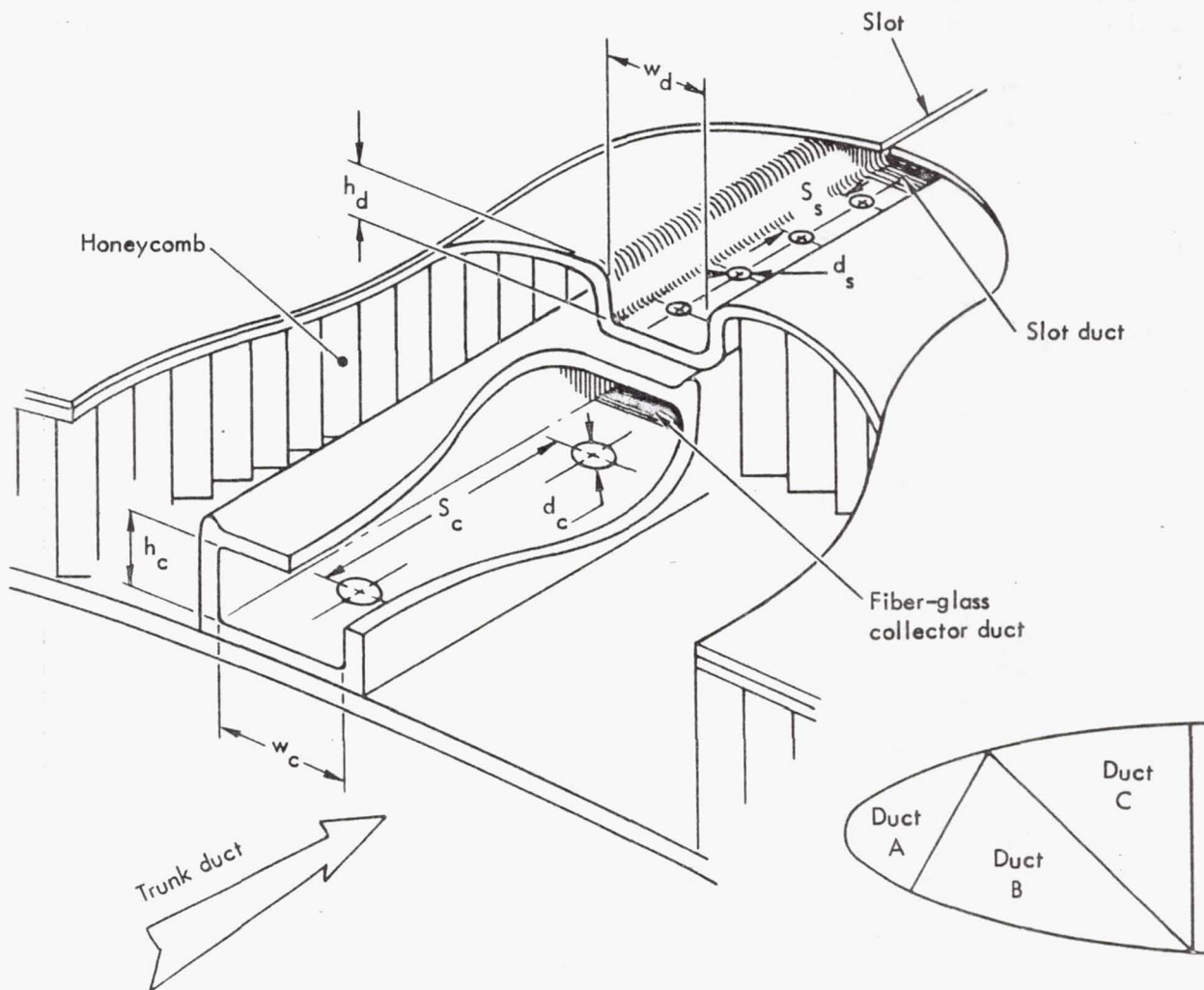


Figure 117. Leading-edge ducting and metering schematic

A second and final level of leading-edge suction metering is provided by metering holes from the collector duct to the leading edge trunk duct immediately inside the skin as illustrated schematically by the inset in Figure 117. This metering is provided to meet two requirements: the collector cavity pressure must be maintained at a uniform level to provide the proper discharge environment for the upstream slot metering holes, and proper flow metering must be provided downstream to match the local pressures within the respective trunk ducts.

### Wing-Box Ducting

The slot suction metering concept in the wing-box region is essentially the same as that of the leading-edge region, although the actual configuration differs in several respects. For this surface, discussed in detail in Section 6.2.2, the titanium skin is bonded directly to a graphite composite structural skin. The structural requirements for this skin are such that the skin is relatively thick and therefore does not incorporate collector ducts in the same manner as the leading edge. The slot ducts are formed into the surface as shown in Figure 118, and the structural hat members bonded to the inner surface of the skin serve as slot collector ducts. The relatively large cross-sectional area contained within the hat-section cavity serves as a duct to carry the flow spanwise to a rib location where the flow is metered through orifices into chordwise ducts which are integral with the wing rib caps. These chordwise ducts are located at inter-

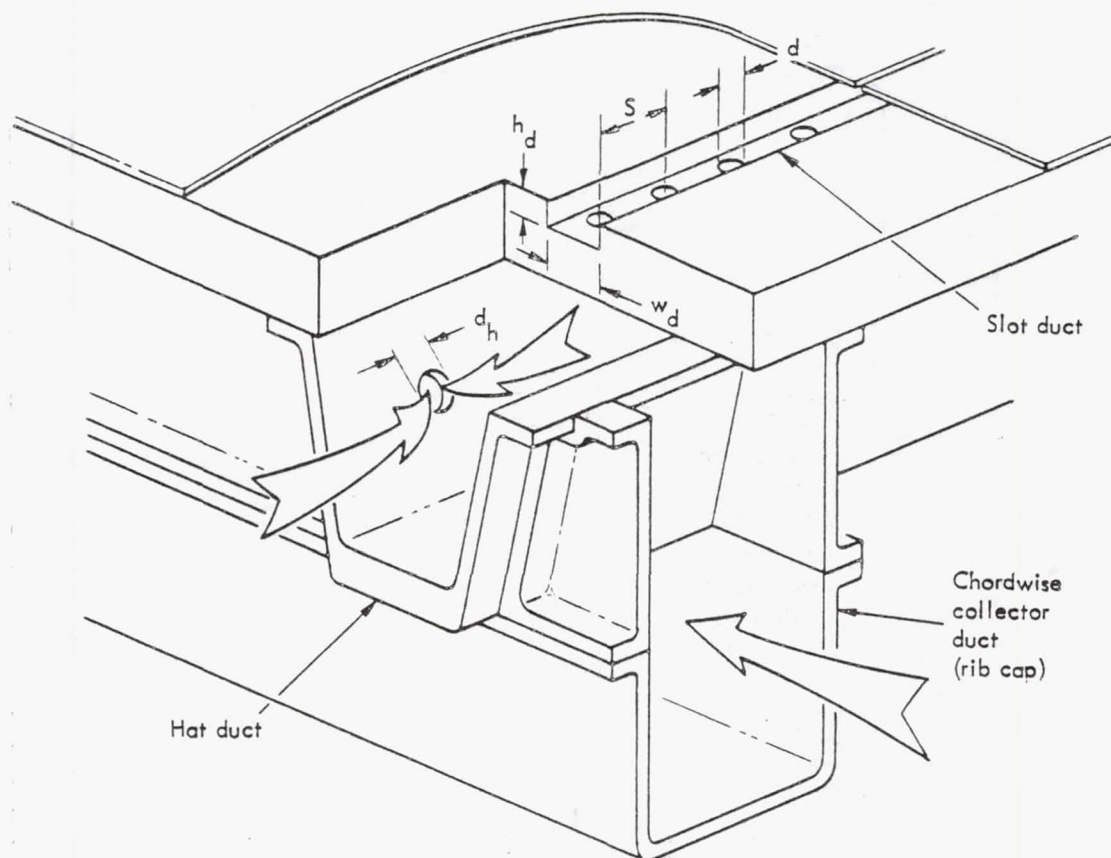


Figure 118. Wing-box ducting and metering schematic



vals along the wing. The hat ducts flow either inboard or outboard to the nearest chordwise duct as shown in Figure 119. The chordwise ducts convey the suction flow forward to a trunk duct, where the flows are metered to match the pressure existing locally in the appropriate trunk duct.

Metering holes are drilled from the slot ducts into the hat-section collector ducts through the structural skin and serve the same function as those in the leading-edge region. Orifices through the forward leg of the hat section meter the flow from the hat duct into the chordwise ducts integral with the rib caps. These metering holes serve to regulate the flow from spanwise segments of slot relative to that of other slots located within the same spanwise segment of the upper or lower box surface. Separate chordwise ducts are included for the upper and lower surfaces, permitting different pressures in the two chordwise ducts at any wing station. Metering of the hat-duct flow into the chordwise duct for either the upper or lower surface is thus independent of the significant pressure differentials that exist between the two surfaces.

The final level of wing-box suction flow metering is provided at the junction of the chordwise collector ducts with the leading-edge trunk ducts. Metering at this point maintains additional spanwise control and matching of upper and lower surface flows with the leading-edge flows. However, the primary requirements for the metering is to match the suction flow and the pressures within the collector duct to the pressures existing in the trunk ducts. Upper surface air flows into trunk duct C, shown schematically on Figure 117, while lower surface air flows into trunk duct B. The pressures within these trunk ducts are dictated by the requirements of the lowest-pressure suction flows entering them. The upper-surface leading-edge flows are metered directly into the trunk ducts. The surface pressures over the leading-edge region, therefore, dictate the pressures in these trunk ducts.

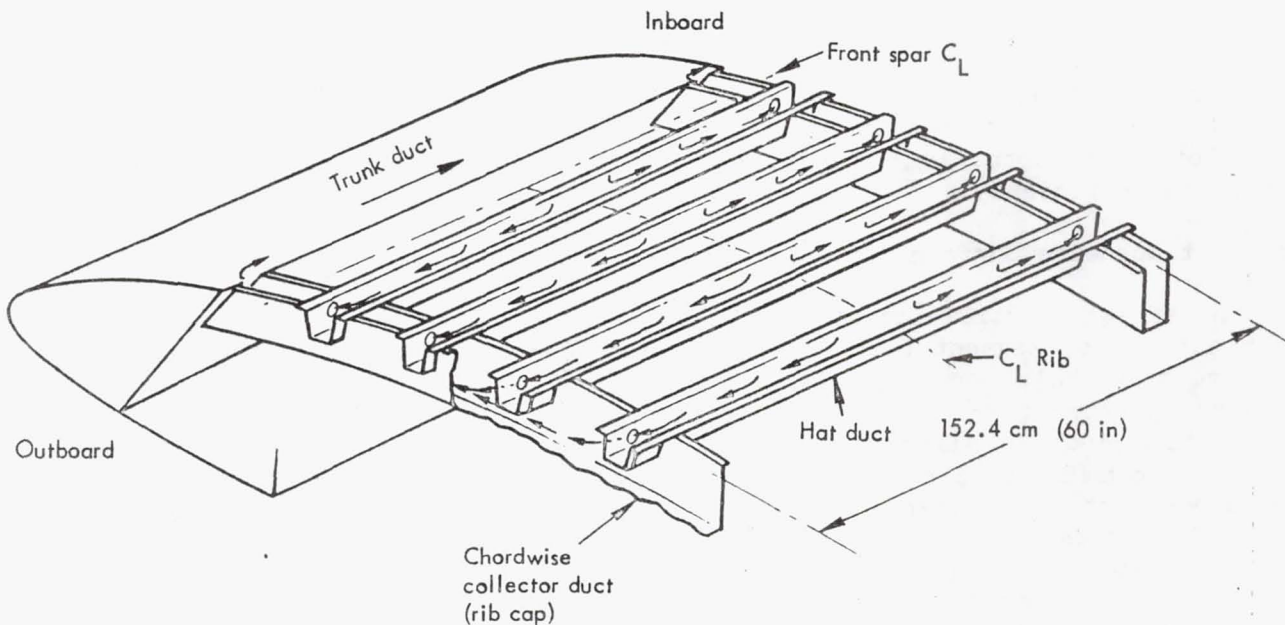


Figure 119. Wing-box ducting system

### 6.3.3.2 Sensitivity Study

An evaluation of the baseline system was accomplished to examine the sensitivities of the suction system performance to production and operational tolerances. The objective was to quantify the influence of those variables predicted to be most critical and most likely to reveal any serious deficiencies in the baseline concept or identify potential design/fabrication problem areas. The studies were centered around the effects which would most strongly influence the local suction flow at the wing surface, i.e., at the suction slots, since the magnitude and character of the flow into and through the slots represents a basic measure of the system viability.

#### Sensitivity Study Geometry

The system reference geometry upon which the sensitivity studies are based is defined in Table 27 and is representative of the baseline airplane upper wing-box surface, with the slot configuration representative of those in Section 6.3.2.

To maintain acceptable flow control with the metering holes, it is necessary that the metering hole pressure losses be at least as high as the slot losses. Otherwise more control is allotted to the slots than to the metering holes. For use as a reference in the present sensitivity studies, the hole geometry was adjusted as indicated in Table 27 and Figure 120. The geometry provides holes of 0.21 cm (0.083 in) diameter spaced at 1.27 cm (0.5 in) intervals. These dimensions meet the maximum spacing-to-diameter ratio criteria for sharp-edged holes ( $s/d \leq 6.0$ ), as recommended in Reference 7. As shown in the figure, the total surface pressure loss with this geometry is 358.53 N/m<sup>2</sup> (0.052 psi), representing a total slot/hole pressure loss equal to approximately 3.25% of the wing surface local pressure.

The effect of this slot metering hole geometry upon the slot flow velocity variation is favorable, as shown by Figure 121. This shows that the hole geometry appears to provide some possible margin for reduction of the slot duct depth, which would likely have a favorable effect on wing structural efficiency.

#### Constant Spanwise Surface Effects

The effect of utilizing constant slot width and metering hole diameters over a spanwise segment between chordwise collectors was analyzed for the slot metering hole geometry of Table 27. The analysis showed that, proceeding downstream from the most upstream metering hole into the spanwise hat-section duct, a slight progressive decrease in hole diameter would be required to maintain a constant slot flow spanwise. The effect of utilizing a constant hole diameter resulted in maximum slot suction flow deviation of less than 0.1%, occurring at the downstream exit end of a 76.2 cm (30 in) flow run in the hat-section duct. Although these flow variations are exceedingly small, the characteristics indicate that these variations would rapidly increase with increasing spanwise flow distance and become significant in tradeoffs establishing the best spacing between chordwise collectors. This indicates that if hat-duct flow lengths greatly exceed



76.2 cm (30 in), increases in metering hole diameters would be required at the locations farther from the collector duct.

#### Dimensional Tolerance Effects

Evaluations of the effects of dimensional tolerances were confined primarily to surface slot and metering hole deviations for a single slot and were assumed independently of any other deviations on the wing surface in either flow or pressure loss. In actuality, any change in slot flow resulting from dimensional deviations would be accompanied by a change in back pressure at the affected slots, tending to compensate to a degree for the dimensional deviation. Therefore, the dimensional deviation effects determined for single spanwise runs presented in this report are conservatively high relative to multiple-slot effects. Acceptability of single slot effects, especially if considered as affecting the total wing, would imply acceptability of multiple-slot effects.

TABLE 27. TOLERANCE STUDY CONFIGURATION

##### Slot configuration

- o Slot spacing = 15.24 cm (6 in)
- o Slot width = 0.0279 cm (0.011 in)
- o Skin thickness at slot = 0.0508 cm (.02 in)

##### Metering configuration

- o Surface duct width = 0.3302 cm (0.13 in)
- o Height = 0.254 cm (0.01 in)
- o Metering hole spacing = 1.27 cm (0.5 in)
- o Diameter = 0.2108 cm (0.083 in)
- o Hole spacing to diameter ratio = 6
- o All holes same diameter at maximum offset from slot

##### Internal Ducting

- o Subsurface spanwise flow is through structural hat sections
- o Hat section spacing = slot spacing = 15.24 cm (6 in)
- o Chordwise ducts located at alternate wing ribs -  
spacing = 152.4 cm (60 in)
- o Spanwise flow distance before chordwise collection =  
75.2 cm (30 in)



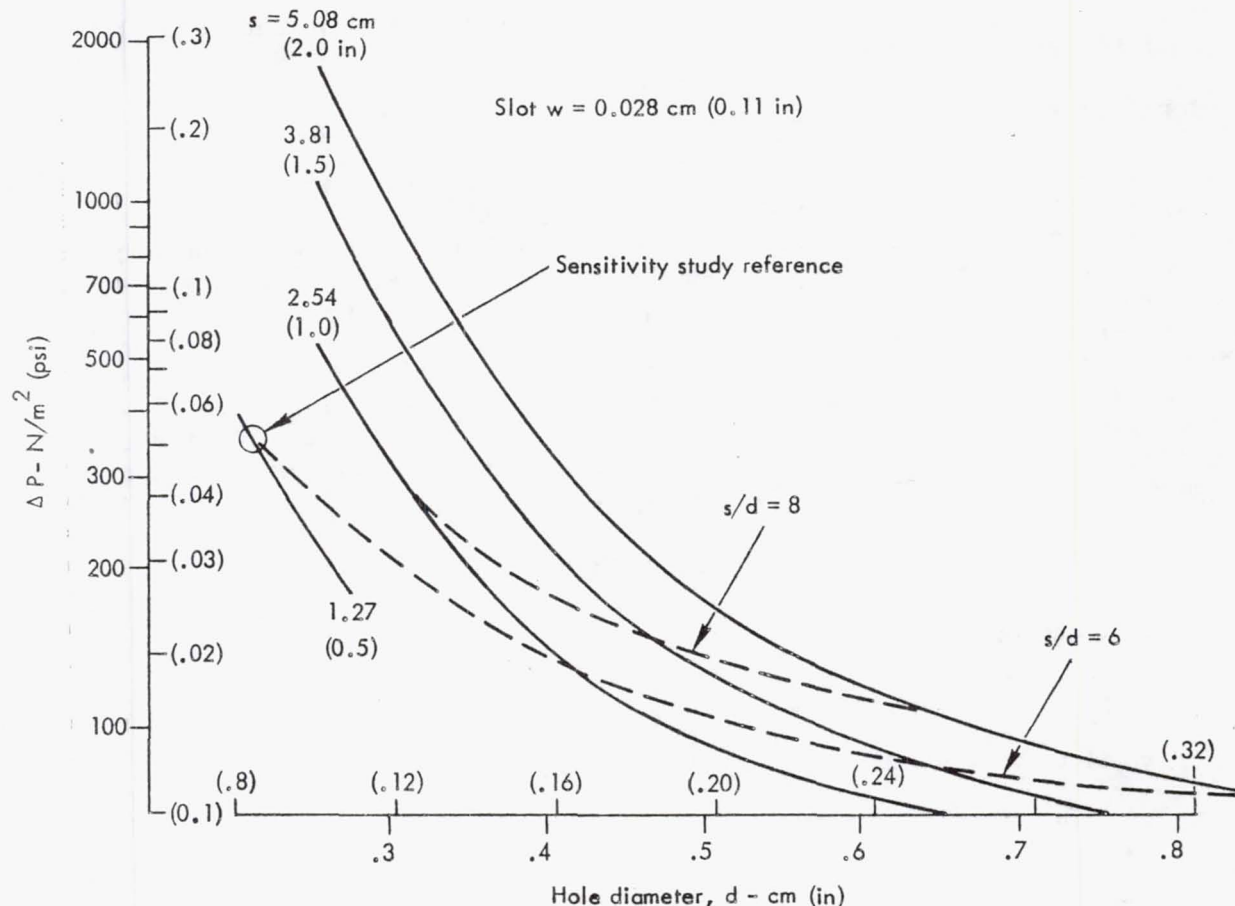


Figure 120. Surface pressure loss characteristics

The deviation effects of other ducting components, including the hat, chordwise, and trunk ducts, plus the hat and chordwise duct metering outlets, are also expected to be less than for the single-run slot/holes. Because of the relatively larger dimensions of these other components, the feasible tolerance ranges should represent a considerably smaller percentage of the design nominal area per unit flow than would the tolerance ranges for the surface slot/holes. The slot back pressure deviations resulting from the accumulation of dimensional tolerances downstream of the spanwise hat section ducts could have significant effects upon the slot performance.

**Slot/Hole Tolerance Effects on Slot Flow** - The evaluations assumed the slot/hole deviations to be constant between chordwise collectors and are summarized in Figure 122. Slot flow deviation data are presented for the separate effects of deviations in the slot and hole dimensions singly, while the other remains at the reference nominal. Although data are presented for a range of slot/hole tolerances of  $\pm 30\%$ , it is anticipated that the feasible tolerance ranges for the 0.0279 cm (0.011 in) nominal slots would be of much smaller magnitude. The  $\pm 30\%$  range is covered only to show the tolerance effect trends and to provide added emphasis that the tolerances must be closely controlled. Section 6.3.3.2 indicated that slot widths of 0.00508 to 0.00762 cm (0.002 to 0.003 in) were desirable in satisfying the slot criteria in the leading-edge region and a 30% deviation in these slots would only be 0.00152 to .00229 cm (0.0006 to 0.0009 in).

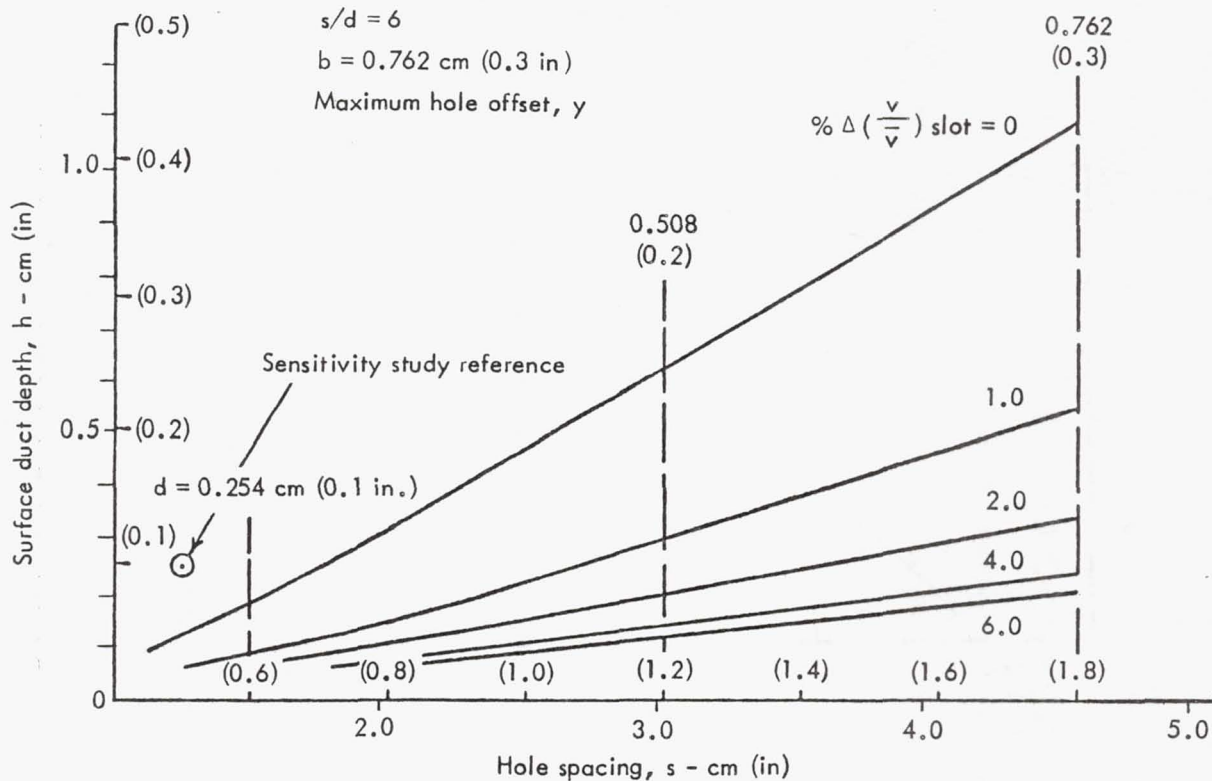


Figure 121. Surface duct/metering hole geometry effects on slot velocity variation

Figure 122(B) shows that the slot flow is quite sensitive to slot width tolerances. A 20% deviation in slot width results in an approximate 10% change in slot flow. Consequently, a  $\pm 20\%$  slot tolerance alone, excluding all other system effects, would require the wing surface boundary layer to be capable of tolerating a suction flow range of approximately 20% of design flow. For a given dimensional deviation, the hole effects are considerably less than the slot effects. A dimensional deviation that produces a  $\pm 20\%$  change in slot width would only produce a  $\pm 2\%$  change in metering hole diameter due to the larger dimension of the hole. This metering hole deviation would produce approximately a  $\pm 2.5\%$  deviation in slot flow or about 25% of the change for the same dimensional slot deviation. Comparison of the effects of negative tolerances and positive tolerances for both the slots and holes shows, as would be expected, that the flow is more sensitive to negative tolerances, though the difference between the negative and positive effects appear negligible for the holes. The effect of area deviations, shown in Figure 122(A), is essentially the same for slots and holes. The slot and hole dimensional tolerances are likely to be of the same order of magnitude. Consequently, slot width tolerances will be more critical than will hole diameter tolerances for

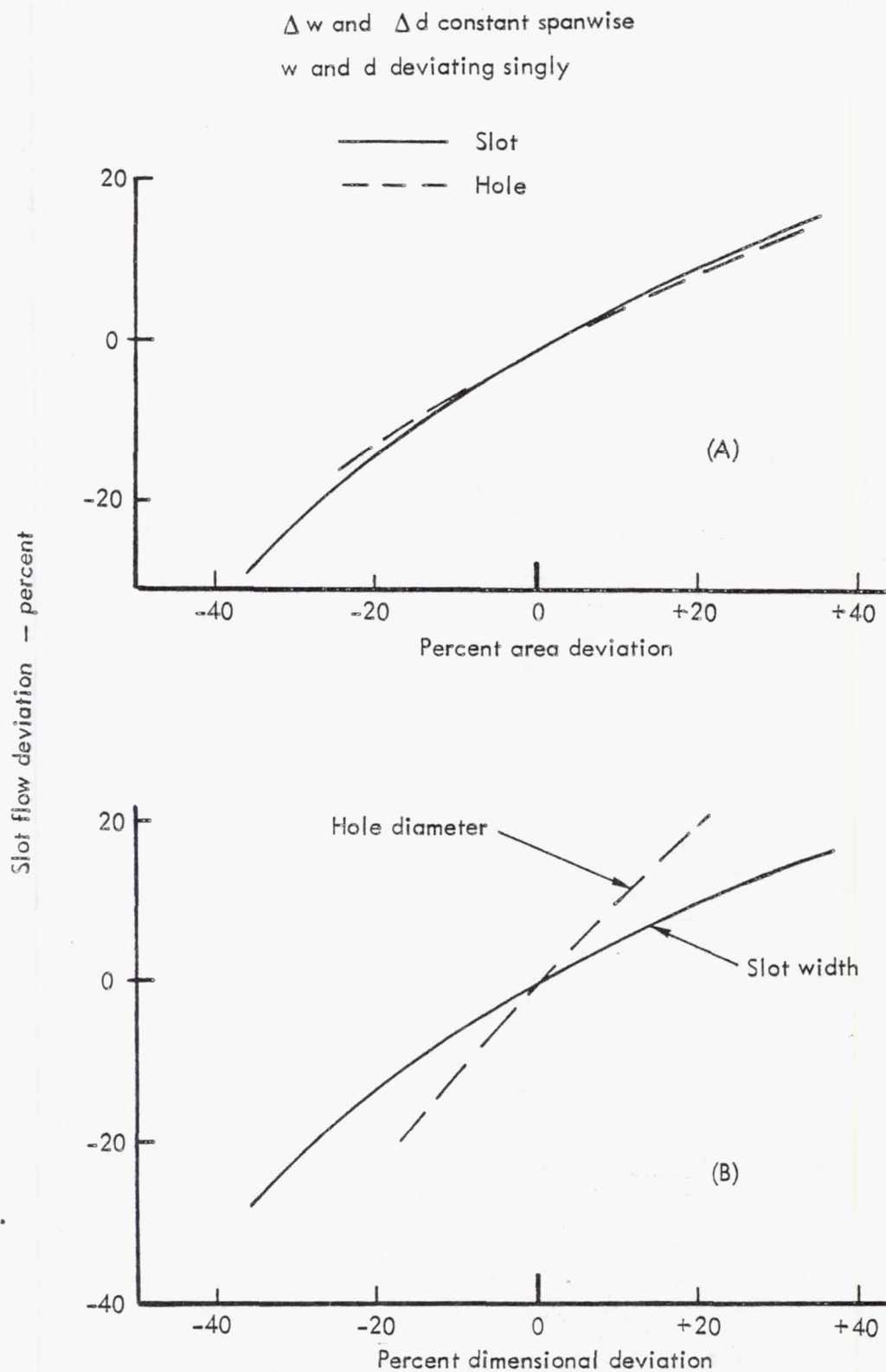


Figure 122. Slot/hole tolerance effects comparison - percent dimensional deviations



feasible slot/hole geometries. This observation is based on the flow sensitivities for a reference geometry which produces equal pressure losses across the slot and the holes at nominal design flow. Any change in the relative slot and hole pressure drops would also result in a change in the relative flow sensitivities although further analysis showed that this afforded little relief to the high sensitivity to slot width deviations. The slot/hole tolerance effects on spanwise slot flow distribution were also investigated. It was found that the tolerances had little effect on the spanwise distribution discussed earlier. This characteristic is due primarily to the near plenum flow within the spanwise hat-section duct. Integration of the flow into the structural hat section is a major advantage in this respect.

Slot/Hole Tolerance Effects on Slot Design Parameters - The combined effects of slot and hole tolerances on the slot design criteria parameters are shown in Figure 123. In this plot the 30% slot width tolerance is equivalent dimensionally to the 6% metering hole tolerance, thus putting equivalent tolerances into perspective for the study reference configuration. The slot design parameters are appreciably more sensitive to slot tolerances than to comparable hole tolerances. Of the parameters shown,  $\beta_w$  is clearly the parameter most sensitive to slot tolerances. With the exception of  $w/z$ , all slot parameters are more sensitive to negative tolerances than to positive tolerances. It is interesting to note that negative deviations in slot width would have a favorable effect upon  $R_w$ ,  $\beta_w$ , and  $C_{ps}$ . If deviations in slot width are less than the full distance between collector ducts, there is an amplifying effect on the sensitivities of both

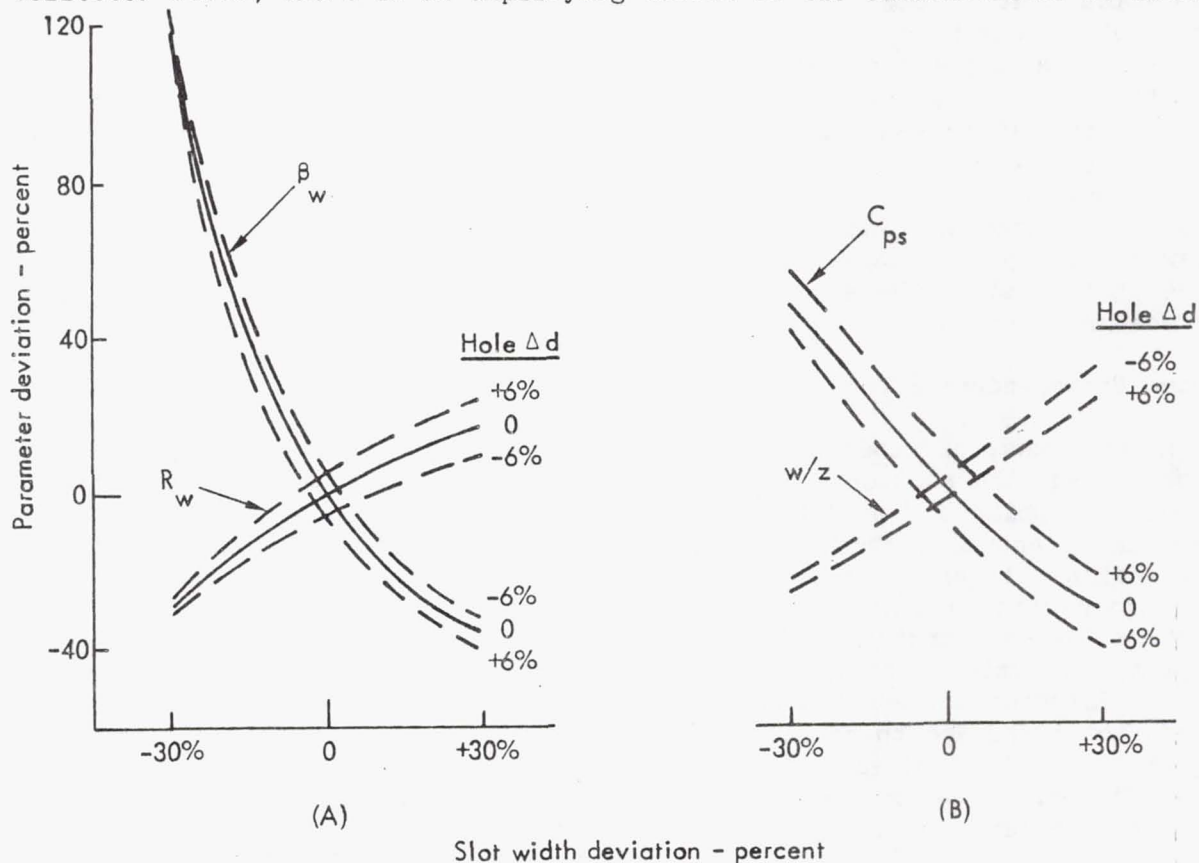


Figure 123. Slot/hole tolerance effects - criteria parameters

the local slot flow and the slot design parameters. This results from spanwise flow in the slot duct. The actual percent deviation in local slot flow may exceed the local percent deviation in slot width for short spans of deviating slot. This underscores the need to maintain uniformity in slot width.

Hat Duct Exit Orifice Tolerance Effects - The tolerance effects presented previously excluded the effects of pressure loss at the transition of the flow from the spanwise hat-section duct into the chordwise duct. The deviation data presented thus far assumed the pressure loss at this location to be zero. Some pressure loss does occur here and, considering the plenum characteristics of the hat-section duct and the consequent flat spanwise distribution of the slot flow, the utilization of a spanwise duct exit orifice for secondary flow control provides advantages. The flow for an entire hat-section flow run can be calibrated/adjusted with this orifice. For this study, a hat-section exit orifice loss of approximately 0.75% of wing surface pressure was assumed.

Effects of the hat-duct exit orifice upon the sensitivities resulting from  $\pm 30\%$  surface slot width deviations are shown in Figure 124. Since the exit geometry has not been defined, and could be any one of several configurations, the effects are presented as a function of selected design pressure loss at the exit orifice. From these data it appears that some advantage might be gained from increasing the design exit orifice pressure loss above that of the baseline. An increase in the design loss would reduce slot flow and  $R_w$  sensitivity to slot width deviations.  $C_{ps}$  sensitivity would be increased but, for negative slot width deviations, the  $C_{ps}$  effects would be favorable;  $w/z$  sensitivity would increase slightly. The desirability of increasing the design loss at the spanwise exit orifice depends upon a tradeoff between these sensitivities and other factors such as pressure loss effect on airplane performance, orifice configuration and envelope constraints, and orifice tolerance effects. In no case does it appear that any advantage would be derived from increasing the design loss above that equal to the surface slot/hole loss, or approximately 3% of wing surface pressure for the reference geometry used for this study.

#### System Backpressure Effects

A study was conducted to evaluate the effect of hat-section duct backpressure upon the suction flow into the surface slots. The results of this evaluation, which are presented in Figure 125 for a range of surface slot and hole tolerances, show that the suction flow is extremely sensitive to hat-section pressure. Any variation in this pressure, which could result from inaccurate pressure loss predictions, tolerance buildup effects on pressure losses downstream of the hat-section flow exist, or instability of the pumping system pressure, could have serious effects upon suction flow rates. Therefore, the suction pump pressure must be accurately controlled. Access to second and third level metering at the spanwise hat-section exits and the chordwise collector exits to allow flow adjustments would be very advantageous. The design flow should be selected at some appropriate intermediate level within the allowable range.

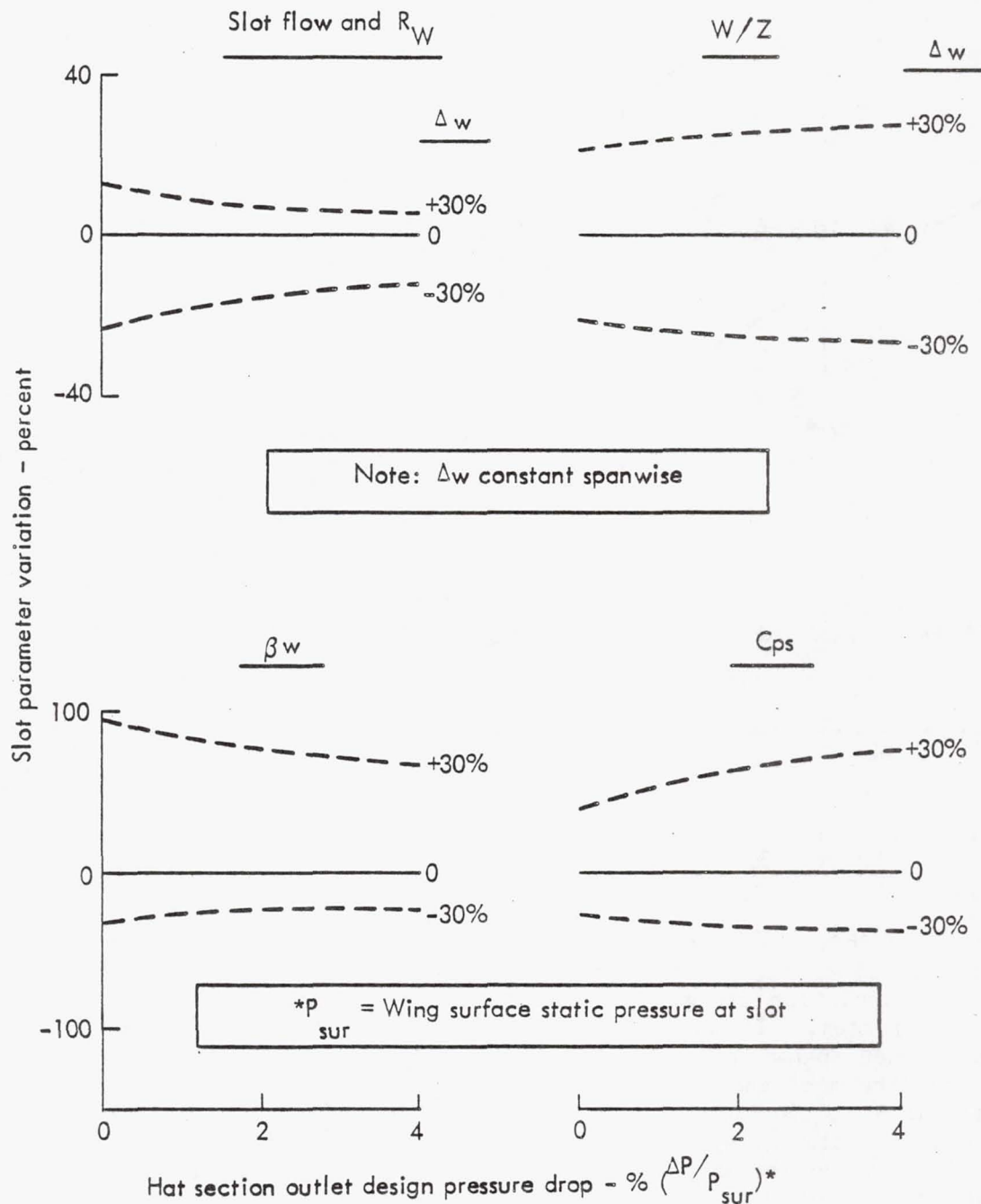


Figure 124. Effects of hat-section duct outlet design on sensitivity to slot tolerances

#### Wing Surface Local Pressure Effects

Deviation of wing surface  $C_p$  from the design values may be either highly local, as in the case of surface waviness, or may be extensive over an entire segment of spanwise slot length, such as might result from an angle of attack or airfoil contour deviation from the design. An analysis of these effects was conducted to evaluate the effect on slot flow.  $C_p$  deviations of  $\pm 1\%$  from design were assumed to affect varying lengths of a slot



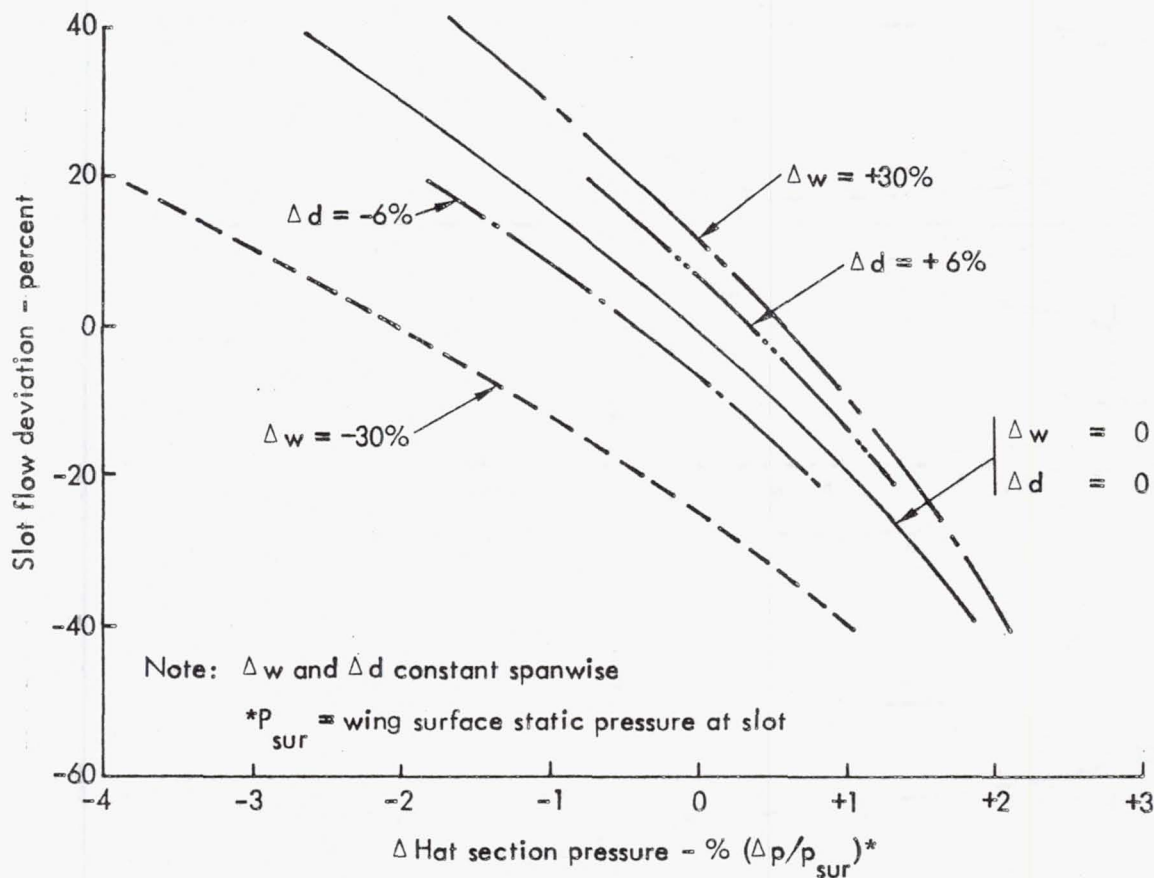


Figure 125. Spanwise hat-section pressure effects

segment from an infinitely small length to a total slot segment length. It was found that local slot flows were much more adversely affected by short lengths of  $C_p$  deviation along the slot than by  $C_p$  deviations over a total slot segment length. It was also found that the slot flow effects were much greater when spanwise flow in the slot duct was considered. Slot flow metering downstream of the slot duct controls the total slot flow such that an increase in slot flow of a portion of the slot segment length is accompanied by a reduction in slot flow through the remainder of the slot length. Thus, where the  $C_p$  deviation exists, the percentage deviation in slot flow or criteria is quite large. If spanwise slot duct flow is unrestricted, the slot parameter deviations are much larger, particularly for very short or very long exposures to deviating  $C_p$ . The portion of slot that is not exposed to the  $C_p$  deviation is most affected when most of the slot is exposed to the  $C_p$  deviation.

From these data it is clear that the wing  $C_p$  levels must be well defined, the surface contours must be closely defined, and the tolerances must be accurately controlled. The surface must be designed with due consideration of slot warpage and misalignment and surface roughness in the region of the slots. Maintenance procedures and intervals for removing wing contamination are important considerations.

### 6.3.3.3 Metering and Ducting Design

The metering and ducting system concept involved for the baseline airplane is described and illustrated in Section 6.3.3.1. The surface metering and ducting is divided logically into different but basically similar configurations for the leading-edge section forward of the front spar and for the wing-box section. These regions and the trunk ducting are described in this section. The fuselage and suction pump ducting is included with controls in Section 6.3.5.

It was not the intention of this design to precisely evaluate and size the myriad of ducts and metering holes in the system that would be required for a production aircraft. Nor was it intended to conduct the trades necessary to optimize the numerous considerations evident from the foregoing sensitivity study. The objective of this effort was to size all components of the system sufficiently to assure suction system compatibility with other airplane considerations and structure and to assure that no significant problems exist in the system concept.

#### Leading Edge

The leading-edge metering system configuration is illustrated in Figure 117. The slot duct dimensions are  $W_d = 0.381$  cm (0.15 in) and  $h_d = 0.203$  cm (0.08 in). Typical slot duct metering hole diameters and spacings are shown on Table 28. Some of these metering configurations do not entirely satisfy all of the independent criteria discussed in Section 6.3.3.2 and References 7 and 19. However, these criteria were derived for a rather restrictive range of configurations and therefore are not completely general. There are indications in the literature that the very low Reynolds number characteristics of the leading-edge slots, together with a very favorable ratio of metering hole spacing to slot duct depth permits some relaxation of the criteria without any penalties to performance. If any deficiencies are found through tests of these configurations prior to final design selection, there are a number of metering system alternatives available for relieving the criteria constraints.

The collector ducts into which the slot duct flow is metered, shown in Figure 117, have a nominal depth,  $h_c$ , of 0.406 cm (0.16 in) and a width  $w_c$ , of 0.330 cm (0.13 in). The flow is metered from these ducts directly into the trunk ducts. Representative spacings,  $S_c$ , and diameters,  $d_c$ , for these metering holes are included in Table 28. The spacing of these holes is primarily dictated by the requirement to maintain a uniform pressure along the collector duct. The diameters of the metering holes are primarily determined by the requirement to control the pressure within the collector duct to a predetermined level, while matching the required flow to the local pressures within the appropriate trunk duct. Since this is the final level at leading-edge slot flow metering, it is very critical to meeting the leading-edge slot flow requirements.

The 15.24 cm (6-in) metering hole spacing,  $S_c$ , in Table 28, is satisfactory for all leading-edge suction slots. Metering hole diameters,  $d_c$ , included in the table, were sized for this spacing and are only representative values. There is considerable flexibility available in designing the collector duct metering in that both the metering hole diameters and



TABLE 28. LEADING-EDGE METERING SYSTEM

## Conceptual Configuration

## Typical Nominal Dimensions

Surface	x/c	Trunk Duct	Slot Duct Metering				Collector Duct Metering			
			Spacing		Diameter		Spacing		Diameter	
			cm	(in)	cm	(in)	cm	(in)	cm	(in)
Upper	0.014	A	0.635	(0.25)	0.066	(0.026)	15.24	(6.0)	0.163	(0.064)
	0.066				0.071	(0.028)			0.254	(0.100)
	0.097	C	0.635	(0.25)	0.094	(0.037)	15.24	(6.0)	0.254	(0.100)
	0.147				0.117	(0.046)			0.295	(0.116)
Lower	0.015	A	0.635	(0.25)	0.069	(0.027)	15.24	(6.0)	0.099	(0.039)
	0.029				0.074	(0.029)			0.119	(0.047)
	0.037	B	0.635	(0.25)	0.071	(0.028)	15.24	(6.0)	0.168	(0.066)
	0.162				0.084	(0.033)			0.183	(0.072)

spacings may be selectively varied for any of the slots. In some cases, the available pressure in the collector ducts significantly exceed the trunk duct pressures. Ejectors could be employed to recover some of this pressure in the trunk duct; however, the increased manufacturing cost and complexity would probably outweigh the limited benefits.

## Wing Box

The suction surface and ducting in the wing-box region was described and illustrated in Section 6.3.3.1 and is generally similar in concept to that of the leading edge. The nominal baseline dimensions of the slot duct illustrated in Figure 118 are  $h_d = 0.254$  cm (0.1 in) and  $W_d = 0.762$  cm (0.3 in). The hat ducts were sized by structural requirements. The resulting duct has an approximate depth of 4.699 cm (1.85 in) and the width varies from approximately 6.096 cm (2.4 in) at the base and 4.064 cm (1.6 in) at the crown, for an average width of 5.08 cm (2.0 in.) Hat-duct spanwise velocities are in the order of 0.01 Mach number and Section 6.3.3.2 showed that hat-duct flow length less than about 76.2 cm (30 in) had virtually no adverse effect on slot flow, but the adverse effects increased rapidly as hat-duct flow length was increased above 76.2 cm (30 in). The baseline



configuration selection was made on the basis that the nominal hat-duct flow length would be 76.2 cm (30 in) and flow lengths greater than this would be individually considered for possible slot duct metering hole adjustment. Since a chordwise collector duct can receive hat-duct flow from both the inboard and outboard directions, each chordwise collector duct collects the flow from a 152.4 cm (60 in) segment of the span, as shown in Figure 119.

A diameter of 0.127 cm (0.05 in) on a 0.762 cm (0.30 in) spacing are typical dimensions for the slot-duct metering holes for both the upper and lower surfaces. Unlike the slot-duct metering holes in the leading-edge region, the slot-duct metering holes in the wing box fall within the available criteria limits contained in the literature. This is due to differences in suction requirements, external aerodynamic differences, and the differences in the configuration. Very little variation in these metering hole diameters is required for any slots on the upper or lower wing-box surface, except as may be required for special cases of hat-duct flow lengths above 76.2 cm (30 in). The 0.762 cm (0.30 in) spacing is adequate for all slot-duct metering holes in the wing box. However, it may be desirable to alter the spacing as an alternative to small diameter variations.

The uniformity of surface pressures and suction flows over both the upper and lower wing-box surface allows use of essentially constant metering hole diameters and spacings between the hat and chordwise ducts. The diameter of these holes is approximately 1.245 and 1.143 cm (0.49 and 0.45 in) for the upper and lower surfaces, respectively. Chordwise variations in these metering hole diameters may be required if significant pressure losses occur in the chordwise ducts.

Each chordwise duct carries the total flow from a 152.4 cm (60 in) span of upper or lower wing-box surface between about 18 and 70% of the chord. Obviously, the total flow through the chordwise ducts increases from the tip ducts to the root ducts. If there is to be low and consistent pressure losses in these ducts, they must all reflect approximately equal duct velocities. This is accomplished by selecting a low maximum Mach number for all chordwise ducts and by varying the duct areas accordingly. Upper wing surface chordwise duct areas vary from 34.2 cm<sup>2</sup> (5.3 in<sup>2</sup>) for the duct nearest the wing tip to 107.7 cm<sup>2</sup> (16.7 in<sup>2</sup>) for the wing root duct. Corresponding duct areas for the lower surface range from 26.4 to 93.5 cm<sup>2</sup> (4.1 to 14.5 in<sup>2</sup>). The differences in required collector duct area between the upper and lower surfaces result from the differences in their respective surface pressures.

The metering of the upper surface chordwise duct flow requires a significant pressure differential to match the trunk duct pressure dictated by the leading-edge suction requirements. The resultant metering orifices are relatively small, ranging from about 2.9 cm (1.15 in) diameter at the wing tip to 5.4 cm (2.1 in) at the wing root. The large metering pressure differential required for the upper surface cannot logically be recovered without altering the trunk ducting configuration, since recovery would tend to raise the trunk duct pressure above the level required for the leading-edge suction flow. In contrast, the lowest pressures occurring on the leading-edge lower surface are nearly the same as the lowest pressure occurring on the lower wing box surface. The requirement for the large

metering pressure differential does not exist and the metering holes may be appreciably larger, ranging from 4.5 cm (1.8 in) at the tip to 8.2 cm (3.2 in) at the wing root.

### Trunk Ducts

The trunk ducts are formed by the leading-edge cavity, which is divided into three separate ducts by two rigid structural diaphragms shown schematically as an inset to Figure 117. These ducts occupy the entire wing leading-edge volume forward of the front spar, which is located at approximately 18% x/c. Both diaphragms attach to the outer skin at a common location on the upper surface, with the forward diaphragm attached at the lower leading-edge surface and the aft diaphragm attached to the lower surface at the front spar. The three ducts taper with the wing chord. Progressing inboard, additions of suction flow to the trunk ducts and pressure losses within the ducts results in the highest duct Mach numbers at the wing root. The highest Mach number occurs in the forward duct as the result of the high suction flow levels from both upper and lower leading-edge surfaces entering this duct. All duct Mach numbers are well below the 0.2 maximum duct Mach number. Wing root Mach numbers of the other ducts were found to be below 0.1. Further refinements of the configuration during a final design process could alter the location of the diaphragms to equalize the Mach numbers and resulting pressure losses. These values do not reflect the presence of leading edge section splices which cause some local disturbances in the ducts, thereby increasing Mach numbers and pressure losses slightly.

The foregoing analysis of the suction metering and ducting system is in keeping with a conceptual evaluation and is not as rigorous as would be involved in the final design of a production aircraft. However, parameters and dimensions are quantified with sufficient accuracy to justify the conclusions that the ducting and metering concept is free of any major or insurmountable problems, is compatible with the structural configuration and manufacturing capabilities, and has potentially satisfactory performance.

#### 6.3.3.4 Testing

Historical data on the interaction effects of a slot and metering system on slot flow spanwise variations are limited to very small slot ducts and large slot widths, both of which are incompatible with the baseline design configuration. Additionally, no data exist on the slot flow variations induced by fabrication tolerances either for a slot alone or a slot in combination with a metering system. Therefore, to gain insight into these and other related slot/metering system flow phenomena, tests on a representative baseline slot/metering/duct configuration were conducted. The primary objective of this testing was to verify the acceptability of the slot spanwise flow variation of the baseline slot duct and metering system design. Secondary objectives were to investigate the theoretical vs actual pressure loss characteristics and performance of the slot, metering system, and slot/metering combination in the presence of a static surface flow field.

All slot flow variation studies described in the literature were conducted by either using a set of static pressure taps or a single hot wire



at a fixed slot spanwise location. The subsurface metering system was adjusted relative to this fixed test location. The limits of adjustment spanwise along the slot appears to have been limited to a few metering orifice pitches. This test procedure gave good results of the effects of the metering system geometry on the slot flow variation through an ideal slot within the limits tested. Both methods of measurement are oriented to determining slot velocity and are only indicative of slot flow if the slot width remains fixed or is accurately known. While the recommended limit for slot flow variation is defined as a  $\pm 1\%$  spanwise variation in slot velocity over the length of metering hole spacing, this is only indicative of the impact on slot flow and slot criteria if the slot width is constant spanwise and of known value. The local slot flow and not velocity determines the value of all of the slot criteria. Spanwise variations are known to exist in slot width due to manufacturing limitations. A direct measurement of slot flow is more indicative of slot and metering system quality and capability than slot velocity.

The approach selected for this testing utilizes a slotted skin that is fixed relative to a subsurface metering and ducting system with a probe traveling along the slot to directly measure local flow variations. Not only does this technique have the capability of examining the effects of metering system geometry on the slot flow variation, but it also has the capability of studying the effect of a metering system on flow variations along a slot that result from manufacturing tolerances. A limit of  $\pm 1\%$  spanwise variation in slot flow was selected as the target and, although it is significantly more restrictive than the recommended  $\pm 1\%$  spanwise variation in velocity, it is a more realistic limit.

## Test Description

**Test Fixture Geometry** - To satisfy the primary objective of the test, a slot/metering/ducting configuration compatible with the baseline design was chosen. A single slot/metering system was attached to a duct of about equal cross-section and half the total length of a spanwise hat section duct, with a single suction source located at one end of the duct. The initial slot width and metering orifice diameter were based on the preliminary suction surface configuration design. The slotted surface was fabricated from 0.051 cm (0.02 in) aluminum sheet and the slot was sawed with a 0.015 cm (0.006 in) nominal thickness saw. The slot was considered to be representative of a slot that would be cut in manufacturing a prototype and had representative variations in slot width which ranged from approximately 0.0152 to 0.0178 cm (0.006 to 0.007 in).

The metering plate was machined from a 1.27 cm (0.5 in) Lucite sheet. The slot duct was milled into the surface and the metering holes were drilled with a 0.2383 cm (0.0938 in) nominal diameter drill. In addition to the baseline metering orifice pitch of 1.27 cm (0.5 in), pitch configurations of 5.08 and 2.54 cm (2 and 1 in) were tested to give a wide enough range of data to permit the development of performance curves. Figure 126 illustrates the basic geometric configuration of the test fixture and the typical test setup.

Local flow through the slot at locations directly over and half-way between each metering orifice were measured to determine spanwise variation



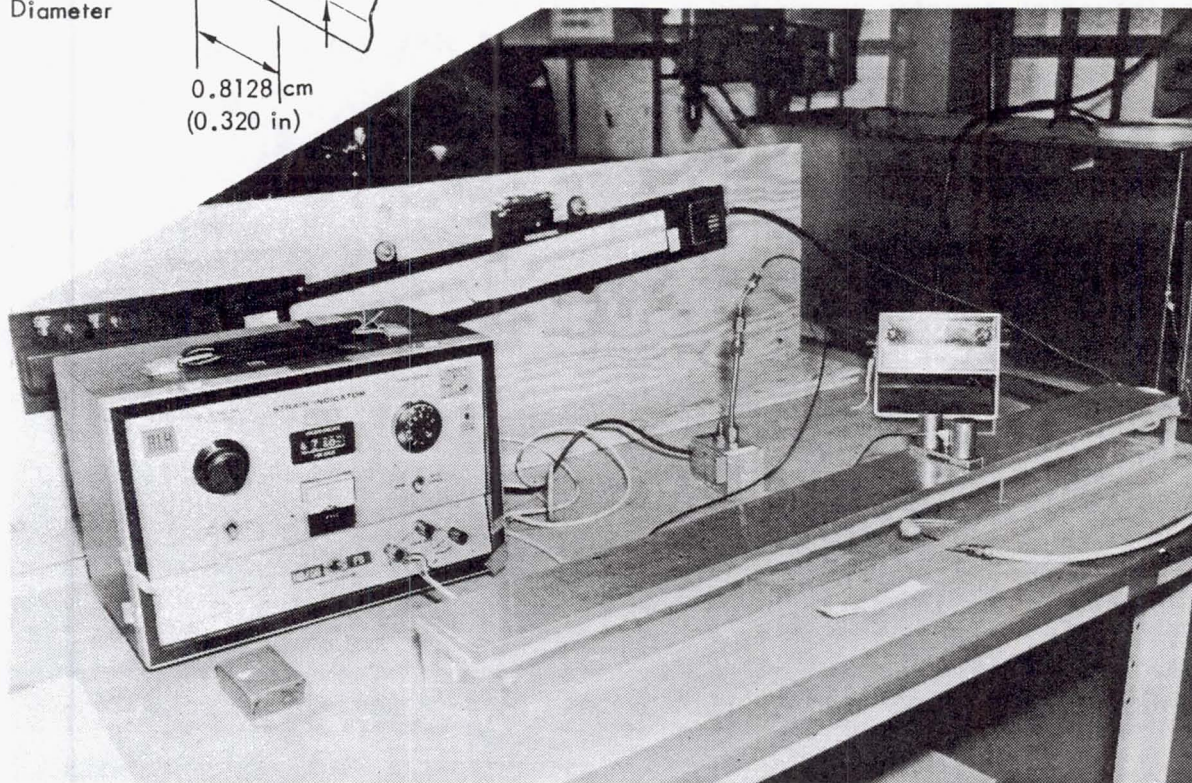
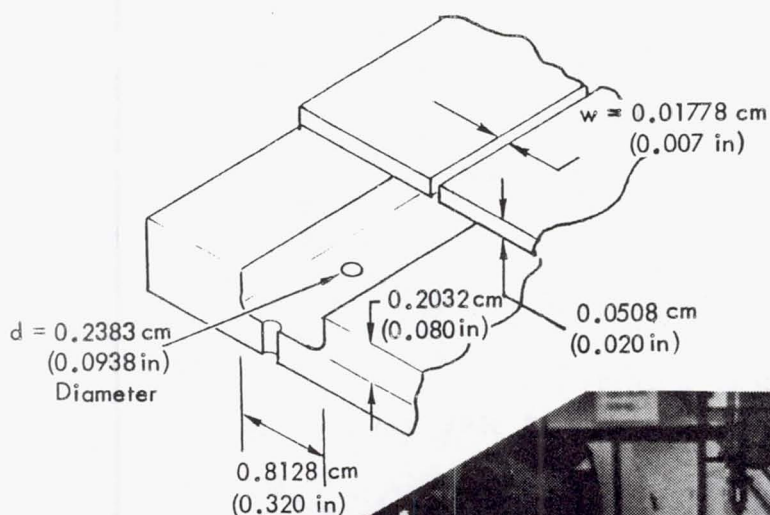


Figure 126. Test duct laboratory arrangement

in slot flow. The pressure loss across the test configuration was measured over a range of representative slot suction flows.

The slot flow variations were measured at slot Reynolds numbers of 50, 80 and 110 for all configurations, with selected specimens evaluated for slot flows up to Reynolds numbers of 290. The local mass flows were measured using a small venturi flow meter which was calibrated against a thin plate orifice. A flexible tube with a knife edge was installed on the downstream end of the venturi to provide a seal on the slotted surface and isolate a 0.3175 cm (0.125 in) segment of the slot. A weighted carrier assembly was used to maintain constant sealing pressure on the flexible tube. The venturi throat pressure measurements were made using a pressure transducer and Wheatstone Bridge with a minimum pressure sensitivity equivalent to 0.0051 cm (0.002 in) of water.

Pressure loss as a function of flow rate was measured for each configuration for equivalent slot Reynolds numbers ranging from 15 to 110. Selected configurations were evaluated at higher flows ranging up to slot Reynolds numbers of about 290. In all cases, total duct suction flow rate was recorded using a rotameter. The combined slot/metering total pressure loss was recorded using the pressure transducer and Wheatstone Bridge combination previously described.

## Results and Analysis

The local slot flow measurements taken using the venturi were averaged and the ratio of local-to-average flow was calculated for each spanwise location. Over twenty plots of these slot flow spanwise variation data were generated illustrating both the flow variations between metering orifices and the general flow variation along the slot span. The effect of a well designed subsurface metering system on reducing random spanwise slot flow variations is shown in Figure 127 by the comparison of flow through a slot without metering and a slot with the baseline metering system.

In the slot alone testing illustrated by this figure, the slot flow passed without obstruction into a relatively large plenum which may be considered representative of an infinite plenum. The slot velocities should be nearly constant over the full slot span. The appreciable flow variation indicates the fallacy in using slot velocity as the primary measurement. Any variation in local slot flows should be almost directly attributable to local variations in slot width. The known slot width variation of the test sample, approximately 0.0153 to 0.0178 cm (0.006 to 0.007in), was assumed to be distributed equally about an average slot width and the variation in local slot flow were predicted from the data discussed in Section 6.3.3.3. The resulting predicted slot flow variation was approximately  $\pm 9\%$ , which

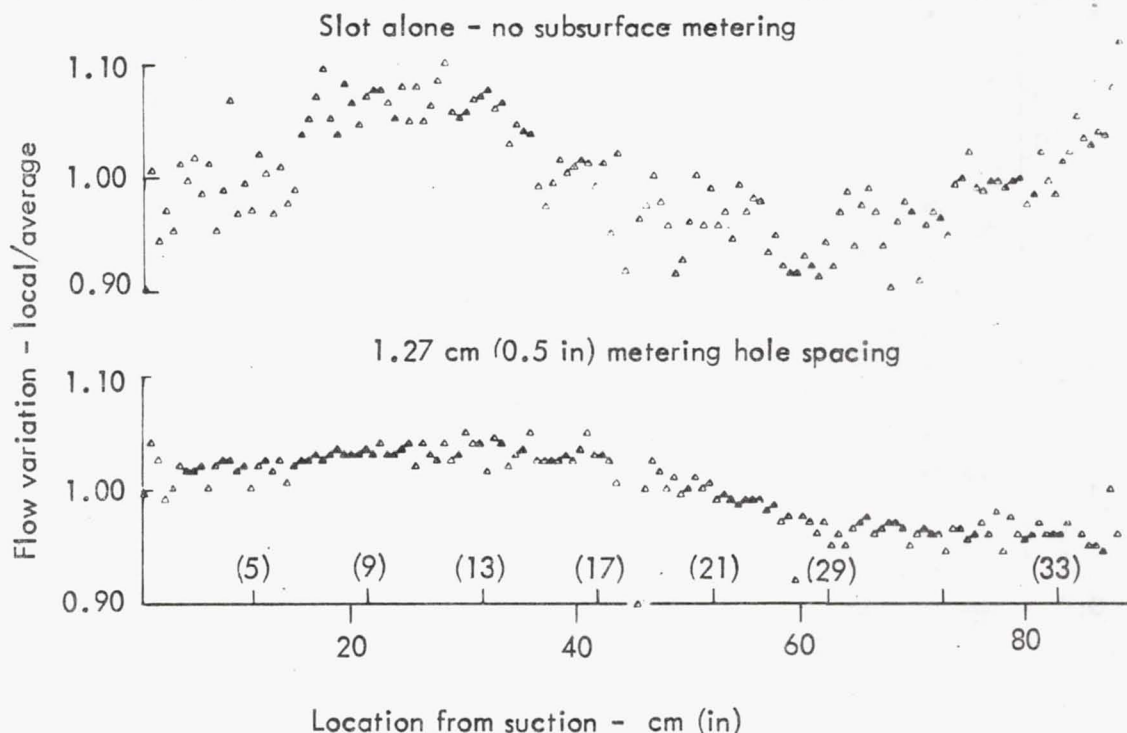


Figure 127. Effect of baseline metering configuration



compares favorably with the data shown on Figure 127. The slot alone data reflect a very localized and repeatable variation in slot flow superimposed on a more gradual variation in local average slot flows that extends over the full span of the slot. These flow variations may be considered indicative of similar trends in slot width variation. With the metering system placed under the slot, both the local variations and the more gradual variations in flow are reduced to about half of their unmetered amplitude. The more gradual variation in slot flows is still readily apparent in the metered data on Figure 127 and shows a range of about  $\pm 4\%$  but the local flow variations have been reduced to an acceptable level.

Typical results illustrating the progressive reduction in local flow variations between metering orifices as a result of reduced metering orifice pitch is shown in Figure 128. The localized effect of the 5.08 cm (2 in) metering orifice spacing may be seen to dominate the slot flow variations while the localized effect of the 2.54 cm (1 in) metering hole spacing is greatly suppressed and disappears altogether with the 1.27 cm (0.5 in) spacing.

A summary of the average flow variation between metering-holes is shown in Figure 129 as a function of slot Reynolds number for constant metering orifice pitch. This plot illustrates the acceptability of the current baseline design configuration in meeting a 1% flow variation requirement for

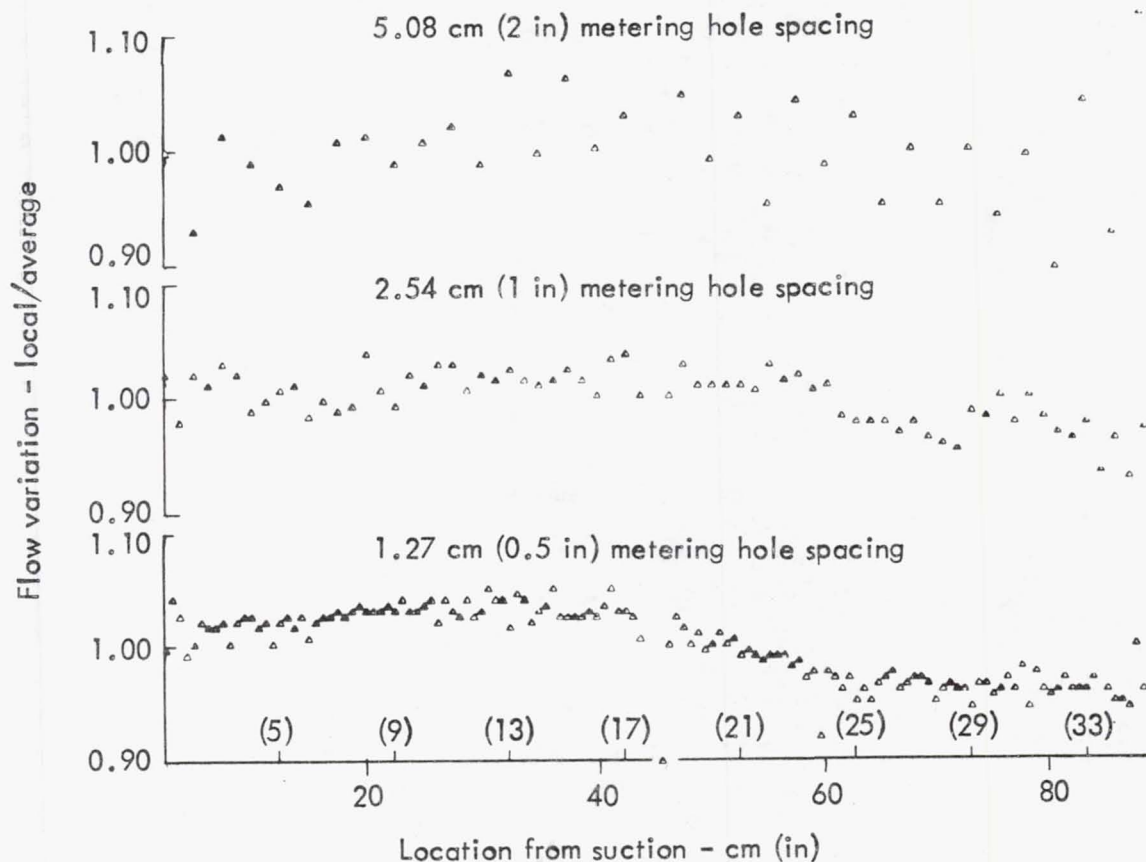


Figure 128. Effect of metering hole spacing on slot flow variations



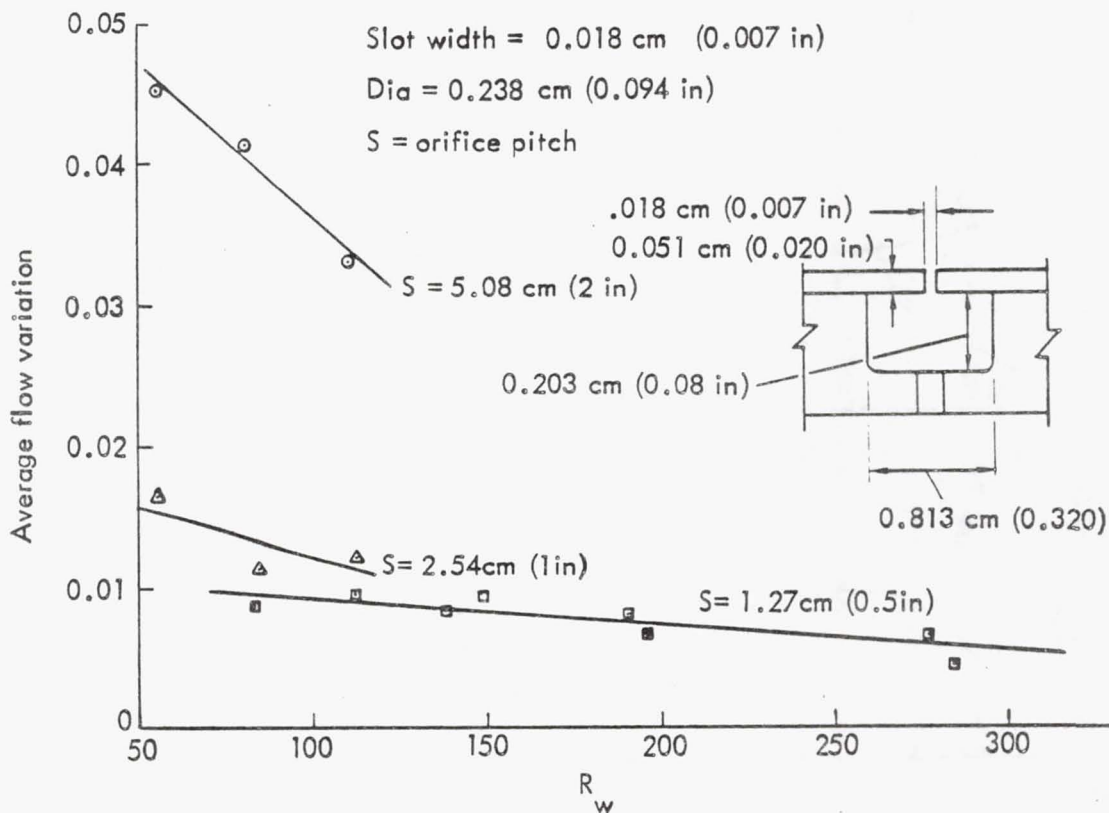


Figure 129. Slot flow variation summary

the range of slot Reynolds numbers tested. It should be noted that this is a  $\pm 1\%$  variation in slot flow which is a significantly more restrictive criteria than the recommended  $\pm 1\%$  variation in velocity since the flow limit includes variations due to slot width. When tested without metering, the slot would have met the  $\pm 1\%$  velocity limit but showed a  $\pm 9\%$  flow variation which the metering system satisfactorily suppressed.

The second phase of testing required measuring the relative pressure loss as a function of flow rate for each of the configurations.

The pressure loss across and mass flow through the test specimens were corrected to standard day sea level altitude for the slot and metering plate with orifice pitches of 5.08, 2.54 and 1.27 cm (2, 1 and 0.5 in). Comparison of the losses resulting from the slot/metering combination with the sum of the losses from the slot and metering components tested individually indicated an additional pressure loss or recovery of the slot/metering system shown in Figure 130. This is apparently a consequence of an interactive effect between the two components.

Slot and metering hole friction factors were evaluated for each of the individual components. It was interesting to note that there was little variation in metering hole friction factor data for the three metering hole configurations. This further supports the observation that the combined slot/metering effects shown in Figure 130 resulted from an interaction between the slot and metering hole flows.

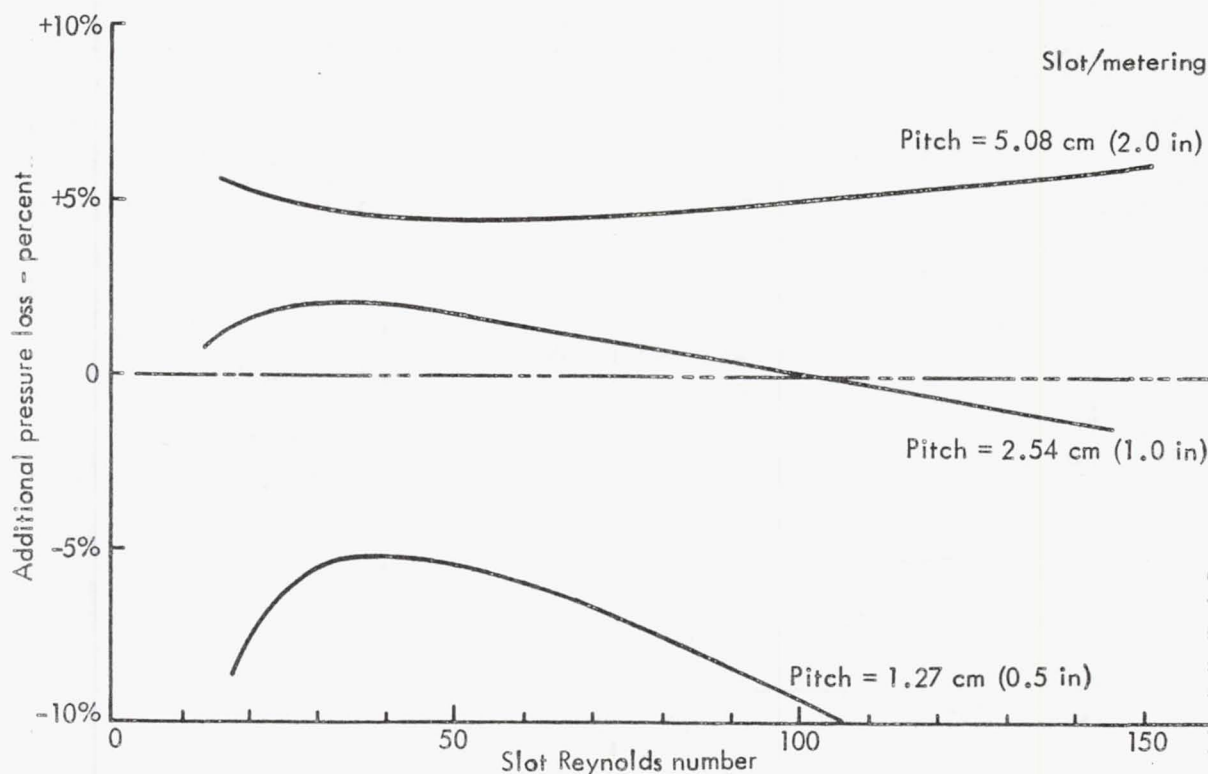


Figure 130. Pressure loss - comparison of slot/metering combination with summation of individual components

### Duct Acoustic Testing

Little is known about the acoustics of LFC duct components in terms of noise generation and transmission of noise through the slots into the free stream. An exploratory noise survey was conducted on the suction duct used in the preceding tests to acquire an improved understanding of the characteristics. The test objectives were to measure the noise internal and external to the duct for several slot/metering configurations over a range of slot Reynolds numbers, to identify and rank the contributing noise sources, and to determine slot noise transmission characteristics.

Acoustics tests were conducted over a range of slot Reynolds numbers from 0 to 290, which covers slot flow Mach numbers to approximately 0.07. In practice, the operating slot Reynolds number is expected to be in the range of 35 to 100. This corresponds to a slot flow Mach number range of approximately 0.01 to 0.03.

Measurements consisted of dB(C) overall level and, in selected cases, the associated octave band levels. Acoustic data were hand recorded in-situ. Duct internal data were acquired with a goose neck, attached to the sound level meter, feeding through a hole in the duct at the end opposite to the suction discharge. Duct external noise levels were acquired with a microphone 2.54 cm (1.0 in) above the slot. Noise measurements were also taken of the laboratory background noise and the noise entering the duct from the suction pump through the suction hose.

Possible noise sources contributing to the measured levels are the slot/metering system, duct flow including flowmeter and valves, the suction pump, and transmitted external ambient noise. The dB(C) measure of weighted overall sound pressure level was selected since it provides some attenuation of low-frequency noise which was dominated by the suction vacuum pump in these tests and is not of interest. Total overall dB(C) noise level data are summarized on Table 29 and the unweighted octave band data are shown on Figure 131. The following observations are made relative to the various noise sources:

- (1) Within the duct test rig, the dominant noise source is the slot/metering system. The suction pump and control valve generated low levels of internal duct noise. These tests were thus a study of the self noise of slot/metering systems.

TABLE 29. SUMMARY OF MEASURED NOISE LEVELS, dB(c)

Slot Reynolds number, $R_w$	<u>0</u>	<u>100</u>	<u>200</u>	<u>300</u>
(1) External ambient noise				
(a) Suction pump off			73	
(b) Suction pump on			79	
(2) Suction pump noise				
Noise radiated from disconnected suction pump hose, $r = 30.5$ cm (12 in) to side of hose				
		77	77	
(3) Duct internal noise				
(a) Slot alone	79	90-95		
(b) 2.54 cm (1 in) metering plate	80	89-94		
(c) 1.27 cm (1/2 in) metering plate	77	86-88	95-98	103-105
(4) Duct external noise				
(a) Slot alone	80	81		
(b) 2.54 cm (1 in) metering plate	82	81		
(c) 1.27 cm (1/2 in) metering plate	76	80	80	80



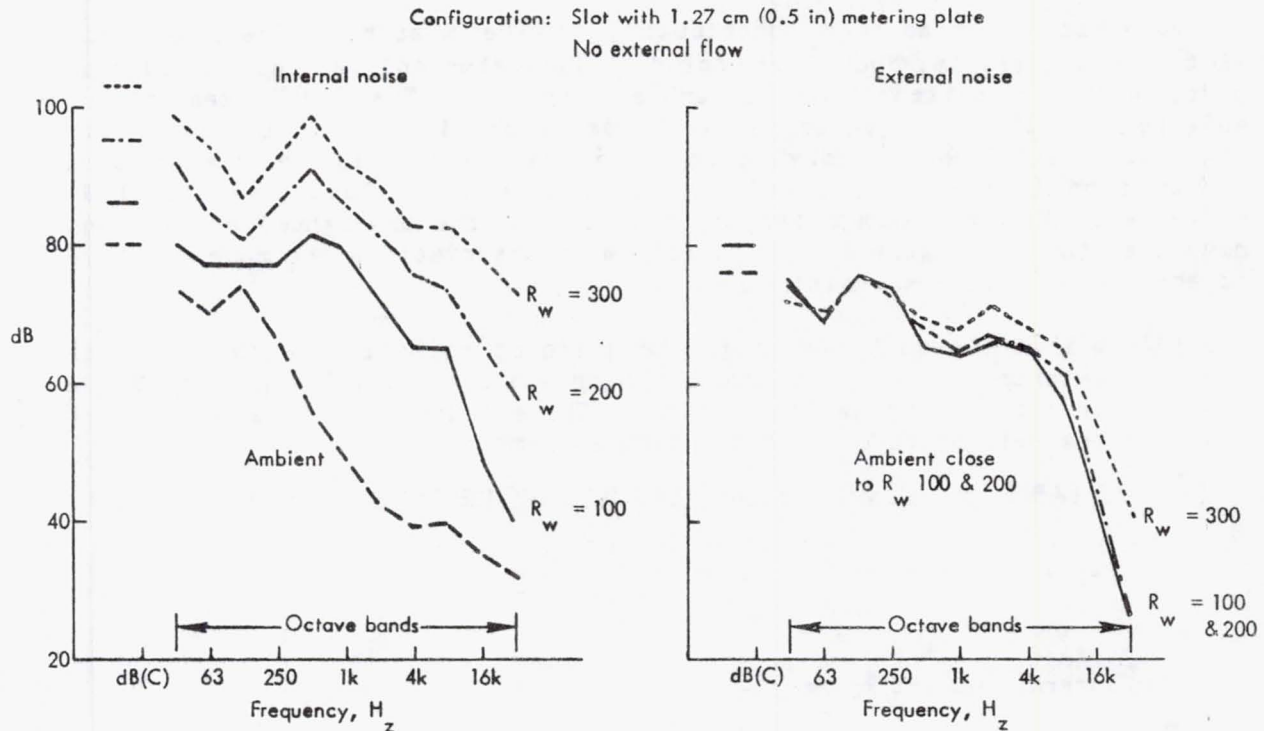


Figure 131. Duct internal and external octave band noise levels

- (2) Increasing suction (increasing slot Reynolds number) significantly increased noise within the duct, caused by the increased acoustic power output of the slot/metering system.
- (3) Within the duct, the noise levels were lower in the middle and higher at the end.
- (4) Internally, the noisiest configuration tested was the slot alone, addition of a metering plate reduced noise at the microphone.
- (5) Increasing internal noise did not increase slot external noise radiation except at an  $R_w$  of 290.
- (6) The self-noise of a slot/metering system is apparently not an important parameter in the selection of a slot/metering configuration. However, some designs may be better at suppressing noise originating from the suction pump and preventing feedback through the slot/metering system to the external surface.
- (7) In an actual LFC airplane the duct noise levels will probably be higher than measured in this test due to the suction compressor, which could be the dominant duct noise source.

#### 6.3.4 Suction Units

The suction system for the baseline configuration incorporates two interchangeable fuselage-mounted suction unit units, each powered by an independent gas turbine power unit. Each unit includes flow and pressure ratio capacity sufficient to pump half of the flow from each surface and dis-

charge the total pumped flow at the freestream flight velocity of Mach 0.8 at 40 000 ft altitude. Since the various laminarized surfaces have different surface pressures, it is necessary to design the suction pump to accommodate the various levels of inlet pressure while discharging all of the flow at the same pressure level.

#### 6.3.4.1 Suction Requirements

The suction requirements and external aerodynamics of the wing airfoil are consistent with the airfoil evolved in Section 6.1. These include wing surface  $C_p$  distribution, distributed suction requirements, and boundary layer characteristics for both the upper and lower surfaces.

The laminarized surfaces are as follows:

Wing upper	346.2 m <sup>2</sup> (3726 ft <sup>2</sup> )
Wing lower	318.7 m <sup>2</sup> (3430 ft <sup>2</sup> )
Horizontal tail - each surface	32.6 m <sup>2</sup> (351 ft <sup>2</sup> )
Vertical tail - total	81.2 m <sup>2</sup> (874 ft <sup>2</sup> )

The laminarized wing areas are the total for the airplane and include adjustments for 75% nominal chord laminarization, airfoil surface curvature, allowance for flap hinge fairings on the wing lower surface, and an adjustment to the wing surfaces to recognize the inclusion of leading edge suction with the upper surface suction. Empennage areas include adjustments for 65% nominal suction and airfoil surface curvature.

These areas, together with the  $C_p$  and distributed suction mass ratios were employed to define the total airplane suction profile shown in Figure 132. This figure illustrates the total suction flow and associated compression requirements arranged in the order of decreasing suction pump pressure ratio. The most stringent suction  $C_p$  values were taken for each surface and an allowance for 10% suction duct pressure loss was used in determining the required suction pressure ratios. The figure shows that 100% of the total flow must be compressed through a ratio of 1.92:1 or more, while 63.2% of the flow must be compressed through a ratio of at least 2.32:1, and 50.7% must be compressed through a ratio of 2.84:1.

#### 6.3.4.2 Suction Pump Comparisons

The most practical suction pump configuration for meeting these suction requirements is a compact axial flow compressor which incorporates a high-pressure compressor pumping the total flow with additional lower flow boost units integrally located on the inlet to raise the pressure of the low-pressure flows to the inlet pressure of the high-pressure compressor. Several possibilities exist for meeting these requirements, with various degrees of performance penalty traded off against system simplification, weight, and cost. Six configurations were evaluated but only three are included herein.

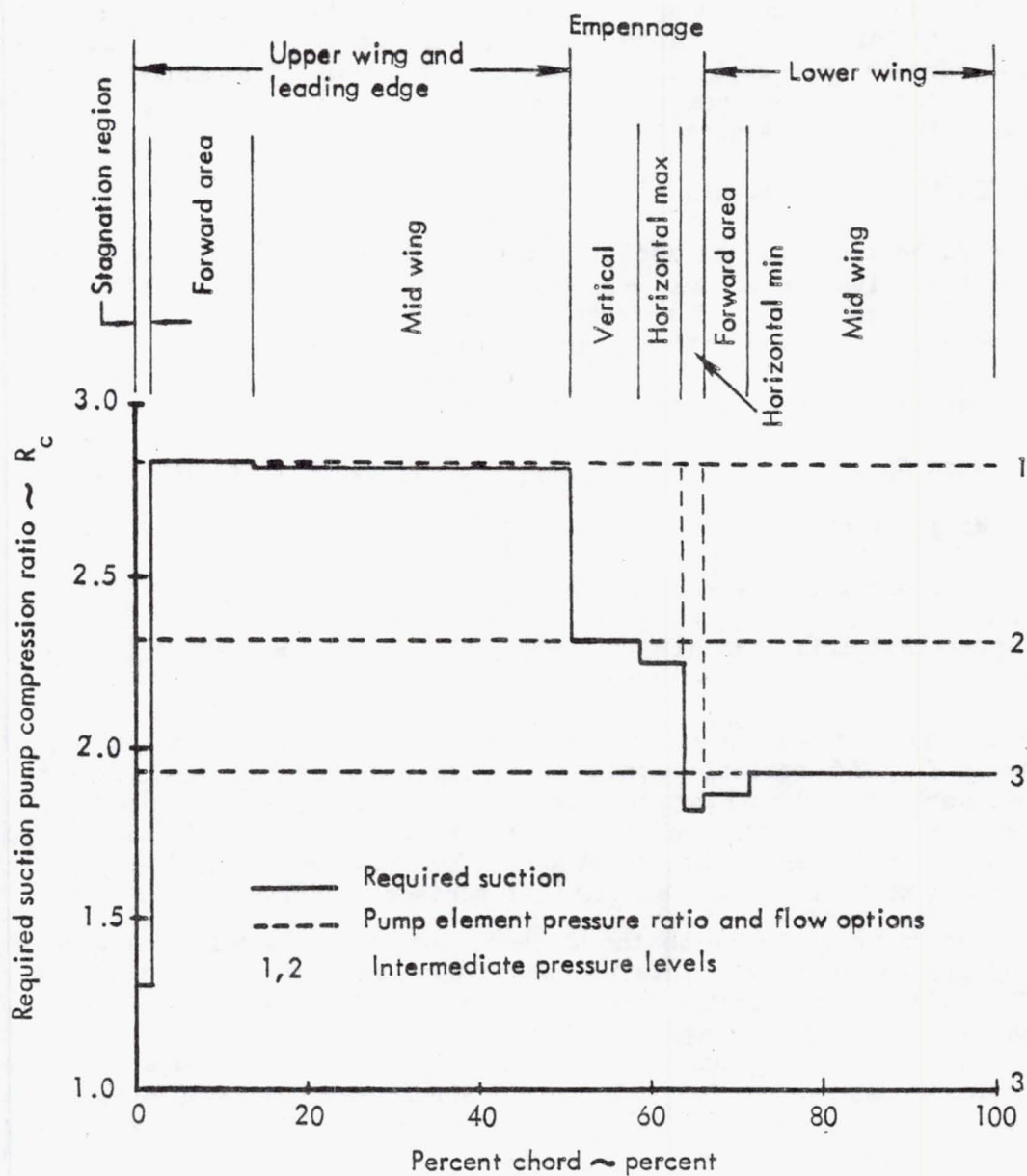


Figure 132. Suction requirement profile

#### Option I

The optimum theoretical performance can be achieved by a pump having two levels of boost compressors preceding the high-pressure compressor. This configuration is identified as Option I. This configuration includes a first boost compressor unit for the upper-wing suction flow. This flow is compressed to an intermediate pressure level by the first boost element. This flow then enters the intermediate boost unit together with the empennage flow bringing the flow of the second boost unit to about 66 percent of the total. The second boost unit compresses this combined flow to the pressure level of the flow from the lower-wing surface. It then enters the high-pressure compressor together with the flow from the lower-wing surface, bringing the entering flow to 100%, and the remaining required com-



pression takes place. The required drive power for this suction pump configuration was assessed for a cruise condition of 12 192m (40 000 ft) altitude and  $M = 0.8$ . This assessment assumed an efficiency of 86% for each suction pump component and also included an allowance for 5% deterioration in both suction unit flow and pressure ratio through the overhaul life of the unit. The drive power required, together with other particulars of this system, is shown in Table 30. Also shown in this table is the equivalent sea level static power requirement for the power unit at the aerodynamic surface  $C_D$  values corresponding to sea level at 0.8 Mach. It should be noted that assumption of static aerodynamic surface  $C_D$  values (i.e.,  $C_D = 0.0$ ) would be meaningless and would not illustrate the relative requirements for the suction power unit.

This suction pump configuration represents a near optimum insofar as theoretical drive power requirements are concerned. However, the dual-boost configuration of the pump is rather complex and adds cost, weight, and performance penalty to the pump because of the triple concentric inlets. Also, the necessity for bifurcations and integration of three inlet ducts requires a complex ducting configuration with attendant cost, weight, space, and pump inlet loss penalties. Some of the above considerations are included in the table.

TABLE 30. SUCTION UNIT COMPARISON

Option	I	V	VI
Number of boost compressors	2	1	0
Suction pump cruise power - Kw (HP)	344.5 (462)	357.2 (479)	408.7 (548)
Power increment relative to Opt 1 - %		+3.7	+18.6
Sea level static equivalent power* - Kw (HP)	1328.1 (1781)	1376.6 (1846)	1574.9 (2112)
Approximate airplane weight increase due to power increment** - %		+.18	+.93

\* Sea level static power of shaft engine that would provide power for suction pump at cruise.

\*\* Approximate weight increment associated with required power increment and includes additional fuel burned at cruise but does not include any increment for duct system weight.

## Option V

This configuration is a dual-duct system with the entire empennage flow ducted to the single boost element. This configuration resulted in a power penalty of only 3.7% relative to Option I, while possessing all the benefits of the two-duct system rather than the three-duct system of Option I. The excess pressure ratio capability of the boost element for pumping the empennage relieves some of the ducting constraints of the empennage. This is a benefit because of the potentially high losses in this ducting due to numerous turns, particularly those at the intersection of the horizontal T-tail with the vertical where the flow must be ducted through an articulated intersection. The airplane weight penalty due solely to the power increase is approximately 0.18% including increased cruise fuel consumption, as compared to Option I. This penalty would be partially offset by the weight savings associated with a simplified ducting system. The configuration also offers considerable cost, maintainability, and reliability benefits over Option I.

## Option VI

This configuration represents the ultimate in simplicity by eliminating the boost element entirely in a single-duct system. In this configuration all suction flow is manifolded and directly enters the single-element suction pump. The power penalty associated with this configuration is 18.6% relative to Option I. However, the benefits are considerable. This configuration would permit a more simplified and lighter-weight duct system throughout the span of the wing. The complex dual duct configuration at the wing root would be eliminated along with a number of valves, vents, and the bifurcated ducting at the pump inlet. This configuration would be much more compact and the volume of the suction unit installation could be greatly diminished. This would permit a reduction in the size and weight of the suction unit fairing. The airplane TOGW penalty due solely to the increased power requirement would amount to approximately 0.9% including the increased fuel burned during cruise but this could be reduced by the associated improvement in duct system pressure losses to the upper-wing suction air which determine the overall suction pump required pressure ratio. The remaining penalty may well be offset by the weight, cost, reliability, and maintainability benefits accruing from the greatly-simplified ducting system and it should not be eliminated from future consideration.

### 6.3.4.3 Suction Pump Selection

Option V was selected as the suction pump configuration for the baseline airplane. Option I has a slightly lower power requirement than Option V but requires a more complex, heavier, more costly, and less reliable and maintainable ducting system. Option VI evokes a significant penalty in power required but offers a great simplification to the ducting system with attendant reductions in weight, cost, maintainability, and reliability. These latter configurations are worthy of future consideration.



#### 6.3.4.4 Suction Unit Description

A rudimentary suction unit design was completed for the Option V configuration for the purpose of establishing conceptual size, weight, and general layout of the suction unit. While this analysis obviously lacks the refinements of an optimized design, it is reasonably accurate for satisfying the present requirements and serves to illustrate some of the required considerations. The suction pump for this unit is shown on Figure 133, which illustrates the unit partially sectioned. The suction pump consists of a forward frame, a two-stage low-pressure or boost element, a mid-frame, a four-stage high-pressure element, and a scroll diffuser. The forward frame serves as the attachment for the aircraft suction system low-pressure duct and houses boost element variable inlet guide vanes. These vanes provide a control for matching the boost element flow and pressure ratio with the high-pressure element inlet flow conditions under varying flight suction requirements. The two-stage boost element is sized to meet upper wing and empennage suction flow and pressure ratio requirements. The two stages operate at a modest pressure ratio compatible with the distorted inlet conditions that will undoubtedly exist with the suction flow. The mid-frame serves as the transition duct for the boost element exhaust flow to the inlet of the high pressure element. It also provides the introduction of the high-pressure suction flow into the high-pressure compressor. Variable inlet guide vanes are required in the high-pressure suction flow entry path for operation in conjunction with the boost element variable inlet guide vanes to assure a proper match between the boost and high-pressure elements.

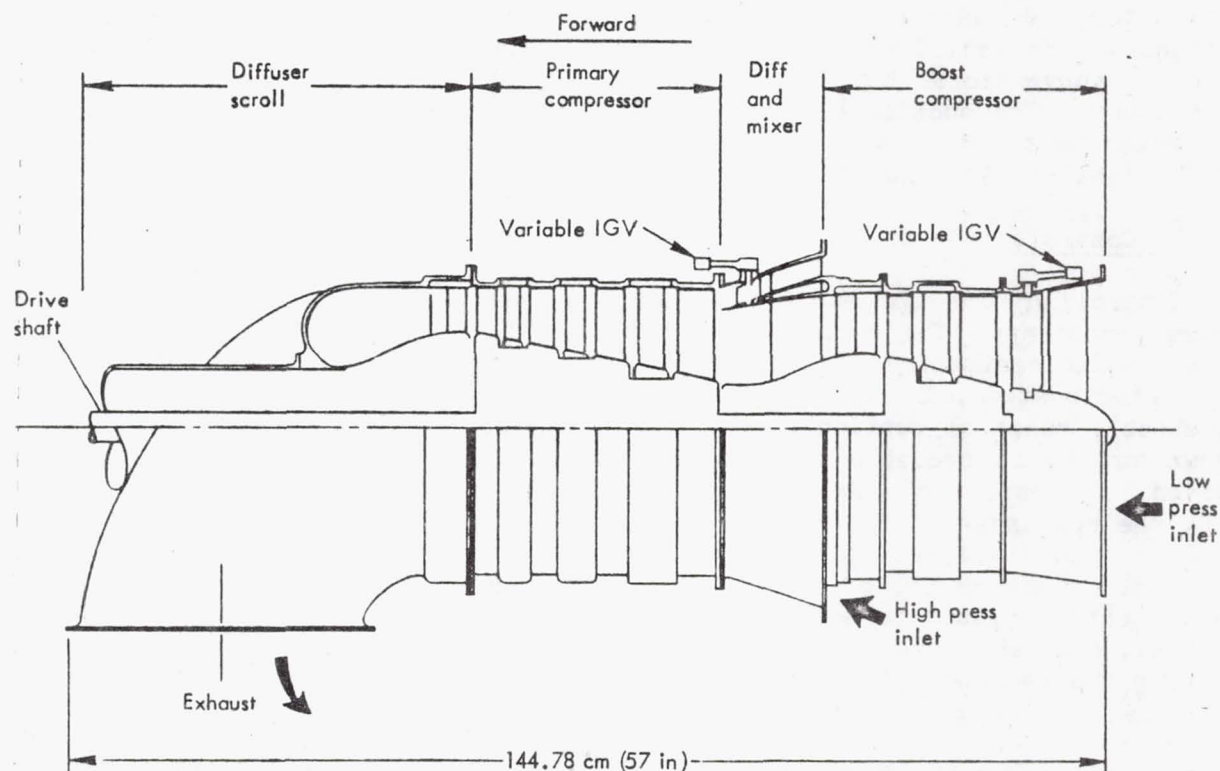


Figure 133. Suction pump



The high-pressure element is a four-stage unit of moderate stage loading. A three-stage unit would require stage loadings that are high but consistent with foreseeable practice for conventional engine compressors. However, the anticipated inlet distortions and mismatch to which this unit will be subjected dictate the use of a more conservative four-stage configuration. Both the boost and high-pressure elements operate on a common shaft.

The exhaust diffuser collects the discharge flow of the suction pump and turns it through  $1.571 \text{ rad}$  ( $90^\circ$ ), while reducing the flow velocity to  $0.3 \text{ Mach}$  and allowing the passage of the suction pump drive shaft axially through the center of the scroll. The flow thus exits the scroll in a round duct at a right angle to the axis of the suction pump. The diffuser/scroll also provides for a rigid mounting between the suction pump and drive unit. This includes a mounting for the drive shaft housing as well as an external truss structure to maintain shaft alignment and absorption of the torque between the suction pump and the power unit.

The suction pumps are driven by independent power units provided with ram inlets exhausting at essentially freestream velocity. The independent drive was adopted because it has no impact on the primary propulsion units and can therefore be independently sized. In previous studies, alternative systems were considered and include geared, bleed, and bleed/burn systems. All of these have a direct impact on the size, configuration and possibly location of the primary propulsion units and therefore interact with other airplane systems and configurations involved in trade considerations. Of these, only the bleed/burn drive system appeared to offer realistic benefits but these essentially disappeared when integrated into airplane performance. The penalties of the more complex systems led to their elimination. A conventional but advanced technology shaft engine was adopted for this study. The suction pump weight was evaluated at  $95.7 \text{ kg}$  ( $211 \text{ lb}$ ) and the power unit weight at  $196.4 \text{ kg}$  ( $433 \text{ lb}$ ), resulting in a total suction unit weight of  $292.1 \text{ kg}$  ( $644 \text{ lb}$ ).

#### 6.3.5 Controls

Control of the LFC suction system presents a number of complex and unique problems. The required suction flow levels and distributions for reliable laminarization are subject to the effects of production tolerances and deterioration, in addition to the variable flight conditions. The acceptable range of suction flow levels and distributions is not presently known but it is probable that much of this acceptable range will be required to negate the effects of production tolerances and deterioration, with the remainder of the range utilized to provide for limited variations in flight conditions. It is apparent that sufficient range is not likely to exist to absorb all of these influences over the entire flight spectrum and a control system to accommodate these variables would become extremely complex. In the interest of simplifying the control system, thereby improving the reliability and reducing the cost and maintenance, laminarization is applied only during the cruise portion of the mission and the system turned on only at the higher altitudes during climb. This approach also eliminates most of the system exposure to contamination that would result from operation in the terminal area and low altitude ranges.

With this approach, the major control of the suction flow becomes that of matching the requirements between start cruise and end cruise. An appreciable change in both level and distribution of wing surface  $C_p$  values occurs between these conditions, particularly in the differentials<sup>P</sup> between the upper and lower surfaces. The internal suction system pressures are dictated by these  $C_p$  values. In the selected suction pump configuration, variable inlet guide<sup>P</sup> vanes were used in both the low pressure and high pressure inlets. These vanes adjust the duct suction pressures to the varying upper and lower wing surface  $C_p$  values while maintaining desired suction flows and an acceptable match<sup>P</sup> between the primary and boost elements of the suction pump. This does not provide discrete control to accommodate the change in the chordwise  $C_p$  distributions. The suction system may be designed to minimize sensitivity to this change at the expense of increased suction system pressure losses. The allowable range in suction flows together with some compromises to the suction system will be utilized to accommodate this change. The suction pump variable inlet guide vanes are also capable of accommodating changes in suction system deterioration within limits. The variable vanes may be controlled automatically on the basis of low-pressure and high-pressure suction flows and pressures which may be monitored in the ducting system. Marginal ability to control these parameters according to a prescribed schedule would be an inflight indication of the requirement for system maintenance or cleaning. In the cruise mode, the suction power unit would also be controlled automatically to these same suction flow and pressure parameters to drive the pump at a speed commensurate with meeting the prescribed suction requirements.

The remaining control problems are primarily operational in nature and consist of:

- (1) Suction unit starting at both sea level static and altitude.
- (2) Unit failure in cruise.
- (3) Atmospheric conditions at cruise.
- (4) Sea-level static system checkout.

Starting the units at altitude will present some problem because the pressures at the suction pump inlet are appreciably below ambient. In the shut-down condition, a significant pressure ratio exists across the suction pump. This pressure ratio exceeds the capabilities of the suction pump until rotational speeds near design are achieved. This means that the suction pump would be stalled throughout the start range until near design speeds are attained during the start up. This is unacceptable due to power requirements and potential damage to the pump. To avoid this problem, valves are provided in the ducting system near the pump inlets to isolate the suction ducting and vent the pump inlet to ambient air during the start cycle, as shown on Figure 134. When the suction unit reaches a prescribed rotor speed, the vent valve will slowly close while the isolation valve slowly opens according to a prescribed schedule. This operation may be carried out either by an automatic system operated by a "start-run" switch or manually by the flight engineer.



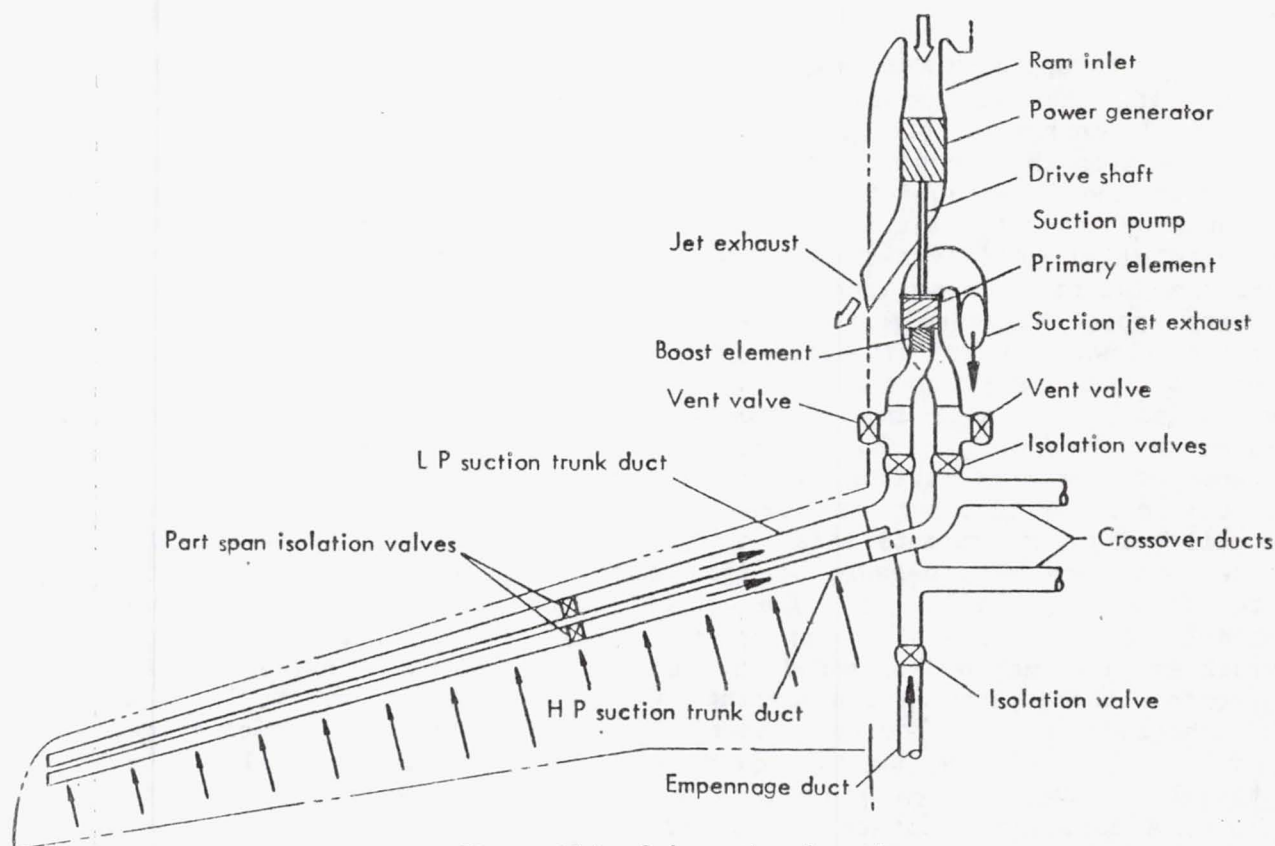


Figure 134. Schematic of suction system

In the event of an inflight suction unit failure, instrumentation at the suction pump inlet and discharge will immediately sense the failure and shut the unit down while simultaneously closing the isolation valves to that unit. After the isolation valves have closed, the valves located in the low- and high-pressure suction trunk ducts near the wing mid-semispan, shown in Figure 134 will also close, allowing only inboard wing suction. The empennage isolation valve will close simultaneously, eliminating empennage suction.

Incidence of rain and ice crystals in the cruise mode that would prevent laminarization may block the slots necessitating immediate shut down of the suction system to prevent pump stall as a result of airflow starvation. This would be accomplished through sensing an abrupt increase in pump pressure ratio, signaling interference with the suction flow ingestion, and automatically shutting the system down. Provision could be made for automatic re-start, or re-start could be the responsibility of the flight engineer. An incremental increase in primary propulsion engine thrust could be automatically accomplished to compensate for the temporary delaminarization.

A pre-flight suction system checkout must be accomplished at sea level static conditions prior to initiation of the flight. This may be accomplished by the flight engineer and would consist of a normal start with the suction unit rotor speed limited to a low value to minimize ingestion of contaminants to the suction system and prevent excessive noise in the terminal area. This start would duplicate the cruise start and valving sequence except for the reduced rotor speed. Since all wing surface  $C_p$



values are zero under static conditions, the high rotor speeds are not required. When the suction unit reaches the prescribed speed, suction system pressures and flows, pump pressure ratio, and pump and power unit operational parameters (i.e., oil pressure, turbine temperature, fuel flow, etc.) may be compared to prescribed limits. An adverse atmospheric condition would be simulated by a signal selected by the flight engineer to actuate the automatic shut-down sequence. It is expected that this ground check may be normally accomplished in a total time of less than 4 minutes.

Automation of these control systems does not appear to present any major problems and final selection of the level of automation would be at the discretion of the customer.

#### 6.4 LEADING-EDGE REGION CLEANING

Since the earliest consideration of applying laminar flow control to an operational aircraft, the potential problems attending leading-edge roughness due to insect contamination have been of continuing concern. The literature indicates that, while an appreciable amount of analytical effort has been expended and some wind-tunnel and flight testing of candidate concepts has been conducted, the effectiveness of a cleaning system compatible with the requirements of an operational LFC aircraft has not been demonstrated.

As a part of this study, the evaluation of candidate concepts resulted in the selection of a fluid dispersal system integrated into the leading edge to counter potential insect contamination and provide anti-icing protection for LFC aircraft proposed for the 1990 period. Wind-tunnel testing of a sub-scale leading-edge section was conducted to evaluate alternative configurations for fluid dispersal and the effectiveness of the fluid film in preventing insect accretion. This testing facilitated the selection of a conceptual design for the leading-edge section and demonstrated the effectiveness of the concept in preventing insect accretion at low speeds. Based on the results of this testing, a full-scale leading-edge section, sized for the mid-semispan region of aircraft in the JetStar/DC-9-10 class, was designed. This test section, incorporating functional cleaning and suction systems, was tested in the Lockheed-Georgia Company low-speed wind tunnel and demonstrated the effectiveness of the cleaning system design in preventing leading-edge contamination at speeds representative of the take-off/climb profile for LFC aircraft.

##### 6.4.1 Design Objectives

Throughout the evaluation, selection, and design of candidate leading-edge cleaning systems, the following requirements were placed on system design:

- (1) The system must be effective in preventing insect contamination of the leading-edge region at the highest anticipated insect densities.
- (2) The system must not prevent laminarization of the boundary layer.
- (3) The weight and cost penalties attending incorporation of the system should be minimized.

- (4) The system should involve no unusual maintenance procedures or requirements.

#### 6.4.2 Concept Evaluation

A data search of previously recorded work was accomplished to identify concepts worthy of additional consideration for the current study. To this list were added concepts developed during the course of the current study.

Following is a listing of concepts subjected to initial evaluations:

- (1) Natural erosion
- (2) Permanent coatings
- (3) Temporary coatings
  - o Soluble films
  - o Quasi-static liquid films
  - o Subliming materials
  - o Ice coatings
- (4) Continuously-flowing fluids
- (5) Protective covers
- (6) Incineration systems
- (7) Mechanical systems
  - o Armstrong-Whitworth wire scraper
  - o Armstrong-Whitworth moistened pad scraper
  - o Handley-Page discardable scraper
  - o Coleman's deflector plate
  - o Rotating leading-edge devices
  - o High-lift leading-edge devices
- (8) Restoration of laminar boundary layer

##### 6.4.2.1 Concept Description

Following is a description of each system listed above:

- (1) Natural erosion - Insect deposits tend to become brittle and have reduced adhesion characteristics when subjected to low temperature at high altitude. It has been proposed (Ref. 1) that this be-

havior in conjunction with the scouring action of airflow over the airfoil would reduce insect residue to acceptable heights. Tests reported in References 20-22 proved this concept to be feasible only at low aircraft climb speeds.

- (2) Permanent Coatings - Recent advances in materials technology has been proposed (Ref. 5) to yield a material for eliminating the insect contamination problem. Hydrophobic compounds, such as organosilicone rain-repellant coatings were also suggested for this purpose.
- (3) Temporary Coatings -
  - o Soluble Films - The principle embodied in the use of soluble films, such as glycerine and soap in methanol, is that a suitable viscous liquid is brushed or sprayed on the surface prior to flight (Ref. 23). Insects impacting the airfoil during flight become embedded in the film without counteracting the adhesion of the film. Subsequently, the liquid film and the embedded insects are removed by a solvent.
  - o Quasi-Static Liquid - An early proposal (Ref. 23) for elimination of insect deposits relied upon suitable liquids, such as silicone of various viscosities, being brushed or sprayed on the airfoil surface prior to flight. It was intended that the liquid would prevent adhesion of the insects to the surface and subsequently the insects would be carried over the trailing edge by the shearing force of the air on the liquid during flight.
  - o Subliming Materials - Volatile compounds such as camphor and naphthalene have been proposed, (Ref. 24) to prevent adhesion of insects to the surface. As the materials sublimed, the insect residue would be swept off the surface by the airflow.
  - o Ice Coatings - A thin layer of ice or frost around the leading edge has been suggested, (Ref. 24) wherein the residue of insects impacting the ice/frost layer would be removed as the ice abates in flight.
- (4) Continuously Flowing Fluids - It was postulated in References 23 and 25 that by keeping the airfoil wet with a continuously flowing fluid the insects debris would not congeal and adhere to the wing. Two methods have been proposed: (a) to force water through a spray nozzle to create a cloud in front of the wing, and (b) to seep low-velocity water through the surface to be carried aft over the airfoil by the airflow during flight.
- (5) Protective Covers - Sheets of paper, cloth, and light cardboard have been proposed (Ref. 26) as protective covers for leading edges during flight through altitudes of high insect density. Covers may be glued or taped to the surface and removed when the angle of attack is varied so that the airflow can remove the cover. Mechanical methods, such as traversing wires or knives, have also been proposed for cover removal.



- (6) Incineration Systems - This concept would provide heating elements inside the leading edge to raise the surface temperature above 260°C (500°F) to promote incineration/disintegration of the insect deposits.
- (7) Mechanical Systems -
- o Armstrong-Whitworth Wire Scraper - The scraper, described in References 27 and 28, has a light frame consisting of two spring steel arms which are curved to the shape of the airfoil leading edge. Tightly stretched between the aft tips of the arms is a piece of fine wire heavily spring-loaded to act as a scraper on the airfoil surface. The two arms are attached to a carrier plate at the leading edge, which is moved along a spanwise slot by an electric-motor-driven cable. The cable performs the secondary function of sealing the slot not occupied by the carrier plate. As the scraper traverses the leading edge, insect remains are sheared away by the fine wire bearing on the surface.
  - o Armstrong-Whitworth Moistened-Pad Scraper - This scraper is identical to the wire scraper except that the fine wire is replaced by a moist pad. As the carrier plate is traversed, the insect residue is loosened by the moisture and carried away on the pad. This system requires the addition of a water reservoir and supply system.
  - o Handley-Page Discardable Scraper - This device, described in Reference 26, is shaped much like those described above except that it is not driven mechanically. The scraper has an inclined vertical vane so that when the device is released from the side of the fuselage, the aerodynamic force exerted on the inclined vane drives the scraper along the leading edge. When reaching the wing-tip, the device flies off past the wing tip. This scraper has a dry felt pad for shearing insect residue from the surface.
  - o High-Lift Leading Edge Devices - Depending upon airport performance constraints imposed on the aircraft, it may be necessary to incorporate high-lift leading edge devices. In such cases, it may be theoretically advantageous for a leading edge device to serve the dual functions of contamination prevention and lift augmentation.
- (8) Restoration of Laminar Boundary Layer - This scheme, proposed in Reference 29, would incorporate a suction slot immediately aft of the contamination area. Wind-tunnel testing has shown that the laminar boundary layer could be re-established by removing the turbulent boundary layer reaching the slot, provided there are no unfavorable pressure gradients.

#### 6.4.2.2 Concept Selection

Lack of definitive test data presented a major obstacle in the rational

evaluation and selection of leading-edge cleaning concepts offering sufficient promise to justify additional investigation. All of the concepts described above have been investigated analytically and wind-tunnel testing has demonstrated the feasibility of several of the concepts over a limited range of operational parameters. With the exception of relying upon natural erosion, which has been shown to be ineffective when insects are impacted at takeoff speeds of current transports, (Ref. 25), all of the concepts analyzed detract from overall aircraft efficiency in that they increase weight and complexity, with attendant increases in both production and operating costs and a decrease in aircraft performance. Many of the concepts also impose potentially more severe penalties in the form of space requirements in the already constrained wing volume available in an LFC wing or in the generation of surface irregularities in the leading edge region to the extent that lower surface suction would be unattainable.

Based on these considerations, it is obvious that the concepts selected for further investigation should be those which require minimal perturbation of the aircraft configuration, while providing effective contamination control.

Following is a listing and summary evaluation of categories of concepts considered in order of increasing system complexity:

- (1) Natural Erosion - The flight tests described in Reference 25 demonstrated that natural erosion does not reduce the height of insect excrescence to an acceptable level.
- (2) Permanent Coatings - The flight tests of Reference 25 also indicated that currently available coating materials are not completely effective in preventing the accumulation of leading-edge contamination. However, the simplicity of this concept dictates that improved coatings be evaluated as they become available.
- (3) Temporary Coatings - The available literature indicates the absence of materials in the form of soluble films, quasi-static liquid films, or subliming materials to form effective temporary coatings for the prevention of leading-edge contamination. However, the use of a coating of ice or frost was shown to be effective (Ref. 24) and this concept should be considered a viable candidate for future development.
- (4) Continuously-Flowing Fluids - The continuously-flowing fluid concept was demonstrated to be effective in flight by the test data of Reference 25, and therefore is a promising concept for the prevention of leading-edge contamination.
- (5) Protective Covers - The use of protective covers is judged to be unacceptable in the current airline operational environment.
- (6) Incineration Systems - Calculations conducted in this study show that electrical power requirements are prohibitive for a system to effectively remove leading-edge contamination through incineration.



- (7) Mechanical Systems - Although a wide variety of mechanical systems have been proposed for the prevention or removal of leading-edge contamination, an acceptable configuration has not been demonstrated in flight. These systems are the most complex of those considered as potential candidates, and thus impose the greatest penalties on the aircraft. However, even considering such disadvantages, mechanical systems should not be eliminated from future consideration since the use of high-lift leading-edge devices may be an acceptable approach on future LFC transports with particularly stringent airport performance requirements.
- (8) Restoration of the Laminar Boundary Layer - Although insufficient data are available to permit the evaluation of this concept for application to the aircraft of the current study, systems based on this concept should be considered candidates for future investigations. However, in many cases, the energy required to laminarize a turbulent boundary layer is greater than that saved by the resultant reduction in skin friction.

On the basis of these evaluations, the following concepts were selected for further investigation during the subject study:

- (1) Continuously-flowing fluids
- (2) Ice Coatings
- (3) High-lift leading-edge devices

Detail design studies were accomplished for each of the concepts listed above. These design studies were carried to the depth required to develop component size and weight data required to determine the system weight penalty for incorporation in the LFC baseline airplane. Table 31 gives the weight comparisons of these systems.

Based on this weight comparison plus evaluation of each system from a maintenance standpoint and the availability of actual test data, the continuously-flowing liquid system was selected for use in the study aircraft.

#### 6.4.3 Testing

Design data necessary for integration of an efficient leading-edge washing system into an operational LFC transport were not available. It was also desired to use the same system to fulfill the requirements for de-icing. A similar concept has been used successfully on operational military and commercial aircraft for many years and some data are available for this application.

To obtain required design data and demonstrate the system concept, two tests were completed. A subscale exploratory test was conducted to evaluate various cleaning liquids, liquid injection surface configurations, governing characteristics of liquid distribution over the surface, and system capabilities for preventing insect accretion. A full-scale test was subsequently conducted to demonstrate the system with a full-scale distribution system and realistic insect impingement.



TABLE 31. WEIGHT COMPARISONS - CANDIDATE  
LEADING-EDGE CLEANING CONCEPTS

	System Weight	
	kg	(lb)
Continuously-flowing fluid washing	1540.4	(3 395)
Temporary ice coating		
o N <sub>2</sub> - Phase change	6872.5	(15 151)
o N <sub>2</sub> - Phase change with superheat	4417.2	(9 738)
o NH <sub>3</sub> - Phase change	4453.0	(9 817)
Mechanical leading-edge device	2100.2	(4 630)

Notes

- (1) Weights are for wing only
- (2) Weights are uncycled

#### 6.4.3.1 Subscale Wind-Tunnel Testing

An exploratory test was conducted in a low-speed wind tunnel on a constant radius representation of a full-scale leading edge. The objectives of this test were:

- o Evaluate flow properties of various liquid compositions and select a baseline liquid.
- o Evaluate the interactive effects of forces acting on the fluid including gravity, surface tension, viscosity, airfoil pressure distribution and boundary layer velocity.
- o Evaluate various liquid injection surface configurations.
- o Evaluate insect accretion prevention and removal capabilities and fluid film requirements.

#### Test Geometry

The wind-tunnel model for this testing was originally fabricated in an unswept configuration under Lockheed-funded activities. The model was modified to the swept configuration illustrated in Figure 135 and tested under this contract. The model consisted of a 15.24 cm (6 in) diameter

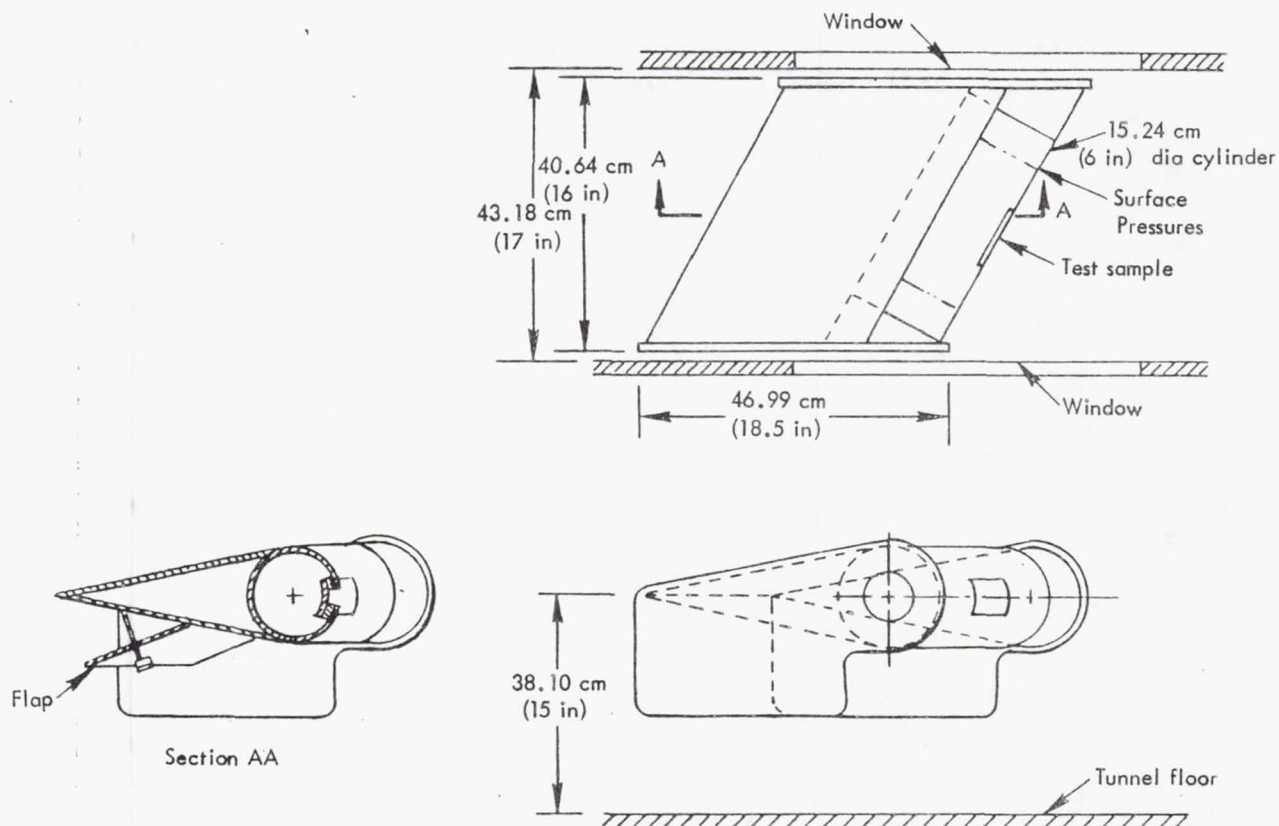


Figure 135. Subscale cleaning test configuration

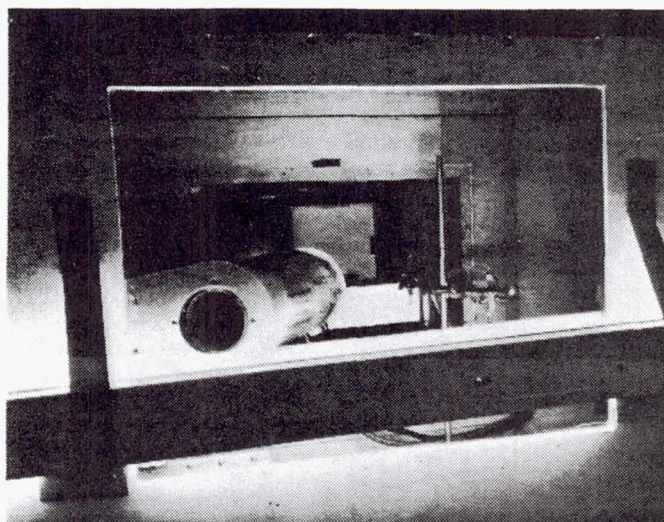
cylinder forming the leading edge with flat plate fairings tangent to the cylindrical surface. A recess was machined into the cylinder to form a chamber for injecting liquid on the surface. Internal piping connected the chamber to an external liquid reservoir. The front of this recess was provided with a recessed flange such that a 12.7 cm (5-in) long by 5.08 cm (2-in) circumferential surface test specimen could be flush bonded over the recess leaving a 10.16 cm (4-in) test length. The cylinder was mounted in the model so that it could be rotated to locate the test specimen in various positions on the upper, lower, or forward surfaces of the cylinder. An adjustable split flap was located on the lower surface of the flat plate fairing as illustrated on the figure. The rotation of the cylinder permitted introduction of the liquid at any point around the leading-edge surface while the flap permitted the movement of the stagnation point to locations around the lower forward quadrant of the leading edge. These two adjustments permitted isolated evaluation of the liquid flow coverage over the surface as a function of these two variables and the involved forces acting on the liquid.

The model was instrumented with static taps in circumferential rows around both ends of the cylinder slightly outside the test specimen for establishing the stagnation point and  $C_p$  distribution on the leading-edge surface. A 2.54 cm (1 in) grid was painted on the cylinder surface to aid in evaluating the fluid coverage.

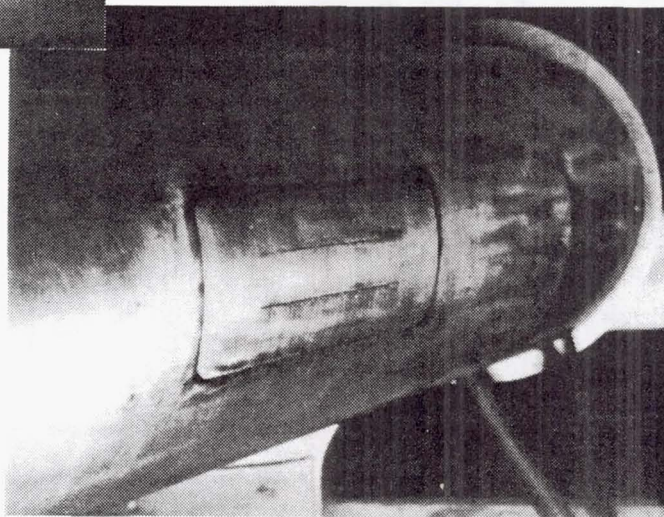


The model was mounted in a small wind tunnel and extended almost across the width of the tunnel as shown in Figure 136. The tunnel was provided with large windows in the sides and bottom affording a good view of the model. Lights were mounted above and below one of the windows and a camera mounted to view the model through the window to obtain photographic records of liquid coverage. Figure 136 illustrates the model mounted in the tunnel in (A). A close-up view of a two-slot test specimen mounted on the cylinder is shown in view (B). The wind tunnel has an ambient inlet through a bellmouth with straightening vanes and the flow is pulled through the tunnel by a blower exhausting to ambient. Tunnel velocities are infinitely controllable from 0 to  $526.7 \text{ N/m}^2$  (11 psf)  $q$  or about 30.5 m/sec (100 fps).

A liquid reservoir was mounted on a scale and pressurized through a regulator. An on/off valve was provided downstream of the reservoir. Flow was measured by timing an incremental weight of liquid flow from the reservoir. Internal liquid pressures were measured in the cylinder liquid chamber immediately inside the test specimen permitting determination of the liquid pressure differential across the specimen.



(A) Wind tunnel installation



(B) Test sample installation

Figure 136. Subscale cleaning test installation



## Cleaning Fluid Composition

The initial portion of the testing was conducted to evaluate various liquid mixes. Table 32 lists the liquid components that were tested and the approximate range of mixture percentages through which each was tested.

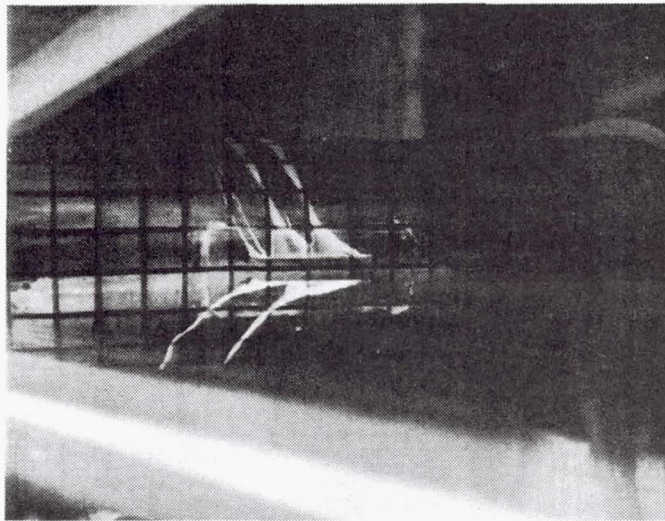
It was obvious from the outset that some form of dye was required to enhance the visual and photographic observation of the film coverage. Sodium fluorescene dye used with ultraviolet lighting produced far superior photographs and better visibility than either of the commercial food colorings tested.

Although the anti-icing requirement eliminated pure water as a cleaning liquid, primary liquid mixes of water and industrially pure ethylene glycol were tested ranging from pure water to pure glycol. None of these mixes were found to give satisfactory coverage because of the effects of surface tension. To reduce the surface tension, various amounts of several different wetting agents were tested individually as indicated on Table 32.

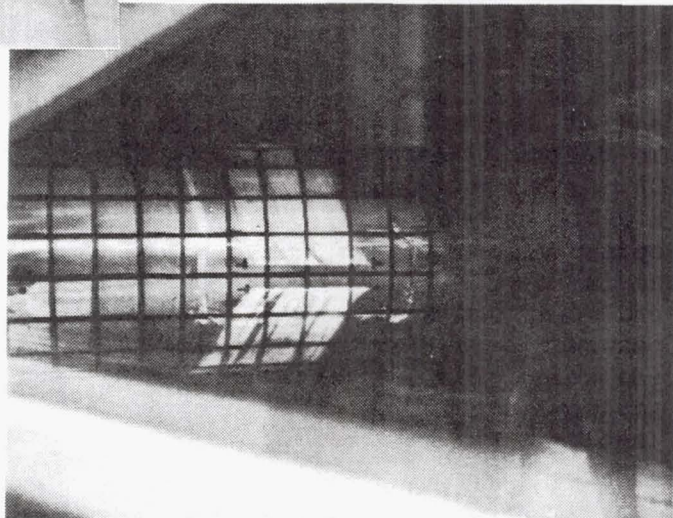
TABLE 32. CLEANING FLUID COMPOSITION

	<u>Component</u>	<u>Range</u>
Primary Liquid	Water	0 to 100%
	Glycol	0 to 100%
Wetting Agent	Ammonia Cleaning Agent	0 to 20%
	Soap	0 to 7%
	Alcohol	0 to 10%
	Tergitol	0 to 0.5%
Dye	Red Food Coloring	0 to 3%
	Green Food Coloring	0 to 3%
	Sodium Fluorescene	

Figure 137 illustrates the superior fluid coverage obtained by the addition of a 0.5% tergitol by volume to water with a small amount of fluorescene dye. In the examples shown, the tunnel  $q$  was  $478.8 \text{ N/m}^2$  (10 psf) approximately 102 km/hr (55 kn), with a liquid flow rate of 0.01018 kg/min/cm of slot (0.057 lb/min/in of slot). The test specimen illustrated is a two slot configuration with approximately 0.0127 cm (0.005 in) slots located 1.27 cm (0.5 in) apart. The slots were located above and below the forward centerline of the leading edge. The flap was deflected downward  $0.785 \text{ rad}$  ( $45^\circ$ ) which located the stagnation point very slightly below the lower slot. The aerodynamic forces acting upward on the liquid emanating from the upper slot significantly exceed the downward acting gravitational forces and the liquid flow is all upward over the top of the leading edge. Conversely the lower slot liquid flow is acted upon by greatly reduced aerodynamic forces and the downward acting gravitational force is slightly dominant resulting in a downward flow. The lack of a significant dominance of either upward or downward forces on the lower slot allows the liquid to form into rivulets. The example of water without a wetting agent illustrates that the flow from both the upper and lower slots, quickly coalesced into discrete rivulets, although generally leaving the slot as a film. When the wetting agent was added, the upper slot continued as a film over the upper surface and the tendency of the lower slot flow to coalesce into rivulets was greatly diminished.



(A) Water with fluorescene dye



(B) Water with fluorescene dye  
with 0.5% tergitol added

Figure 137. Fluid composition tests



Of the wetting agents tested, Tergitol proved to give the best surface film coverage without the foaming characteristics evidenced with the liquid soap and the ammonia cleaning agents. Only 0.5% Tergitol in the cleaning liquid mixture appeared to give maximum benefit from the Tergitol which was unequaled by up to 10% alcohol. Tergitol was selected as the wetting agent and was used for all subsequent tests.

Testing of various concentrations of ethylene glycol and water showed that with the Tergitol wetting agent added, there was little detectable difference in the fluid film characteristics with mixes ranging from 100% water to 100% glycol. The anti-icing requirement mandates that the glycol concentration be sufficient to not only prevent the mix from freezing but to lower the freezing point of the mix sufficiently to thaw ice on the surface. The establishment of a liquid composition that will satisfy the anti-icing requirement is not a part of the present study. Therefore a composition of 49.75% water, 49.75% ethylene glycol and 0.5% Tergitol with a trace of sodium fluoresceine dye was selected as representative for the present study and was used for all subsequent testing.

#### Fluid Coverage General Observations

After some preliminary testing, a test matrix was established for the injection surface samples that included three tunnel  $q$  values, 97.76, 293.3 and 488.8  $\text{N/m}^2$  (2, 6 and 10 psf). Flap deflections of 0, 0.785, and 1.047 rad ( $0^\circ$ ,  $45^\circ$  and  $60^\circ$ ) index settings were calibrated for  $C_p$  distribution and were found to produce stagnation lines of 0.017, -0.139, and -0.331 rad ( $+1^\circ$ ,  $-8^\circ$  and  $-19^\circ$ ) respectively measured around the cylinder surface from the forward horizontal axis. Aerodynamic analyses of the baseline airplane airfoil showed that this range of stagnation line travel was more than enough to encompass the range on the airplane through ground roll, rotation and climbout. These tunnel  $q$  values and stagnation line locations were used for testing all specimens.

The specimens were tested at various locations around the cylindrical leading-edge surface by rotating the cylinder. The range of angular locations varied for different specimens as their flow characteristics showed that testing in some locations was unwarranted. These locations ranged from 0.349 rad ( $20^\circ$ ) upward to 0.349 rad ( $20^\circ$ ) downward for the various specimens and all were tested in a minimum of 3 locations. In addition, all specimens were tested over a range of liquid flow rates. This range varied among the specimens depending on their individual characteristics.

Aside from the specific characteristics peculiar to each of the individual specimens, they all displayed similar fluid film characteristics that were dependent on the identified forces acting on the fluid. As would be expected, the quality of film coverage of the surface improved at higher flows and higher tunnel  $q$  values. At a tunnel  $q$  of 95.7  $\text{N/m}^2$  (2 psf), the liquid flow was nearly always downward with a strong tendency to form rivulets. This indicates that the dynamic forces were insufficient to overcome the gravitational force acting on the liquid and, in general, occurred regardless of the injection point location relative to the stagnation line or the quantity of liquid injected.

At a tunnel  $q = 287.3 \text{ N/m}^2$  (6 psf), the liquid flow could be either upward, downward or both depending on the location of the point of injection



relative to the stagnation line. If the liquid was injected on or below the stagnation line the liquid flow was downward and if  $0.175 \text{ rad } (10^\circ)$  or more above the stagnation line the flow was generally upward. When the liquid was injected between about  $0.087 \text{ rad } (5^\circ)$  and  $0.179 \text{ rad } (10^\circ)$  above the stagnation line and liquid could simultaneously flow both upward and downward. In general, the weaker the flow in a given direction, the greater the tendency to form rivulets. This dual direction flow characteristic was increased at higher liquid flow rates with a decrease in the tendency to form rivulets. This characteristic appeared to depend entirely on the relative location of the injection point to the stagnation line. Film coverage was generally good at tunnel  $q_0 = 287.3 \text{ N/m}^2$  (6 psf) except at low liquid flows or when injected between  $0^\circ$  and  $0.175 \text{ rad } (10^\circ)$  above the stagnation line with rivulets forming in both cases.

When tunnel  $q$  was increased to  $478.8 \text{ N/m}^2$  (10 psf), the flow characteristics were found to be quite similar to those observed with the tunnel  $q = 287.3 \text{ N/m}^2$  (6 psf). As would be expected, the aerodynamic forces had a general smoothing effect on the film coverage with a reduction in the tendency to form rivulets. A direct comparison between the two tunnel  $q$  values at the same injection point showed relatively little difference. However, in the range of injection point locations between  $0^\circ$  and  $0.175 \text{ rad } (10^\circ)$  above the stagnation line, differences became more pronounced. In cases where some upward flow occurred with strong tendencies to form rivulets at the lower  $q$ , the increase in  $q$  to  $478.8 \text{ N/m}^2$  (10 psf) increased the upward flow and the rivulets either disappeared or greatly diminished. In cases where the liquid flow was predominantly upward with some downward rivulets occurring at  $q = 287.3 \text{ N/m}^2$  (6 psf), the downward flow disappeared at the higher  $q$  and a reinforced and smoothed upward flow resulted.

### Surface Configurations

The testing from which the above general observations were drawn was conducted on six different surface configuration specimens as listed on Table 33.

These specimens all had a 12.7 cm (5 in) spanwise length along the surface of the leading-edge cylinder with a 5.08 cm (2 in) circumferential width. They were flush bonded into the surface of the cylinder. The bonding surface constituted the outer 1.27 cm (0.5 in) perimeter of the specimen leaving a 10.16 cm (4 in) by 2.54 cm (1 in) available active test area. In the case of the perforated and porous specimens, this entire 10.16 by 2.54 cm (4 in by 1 in) area was used for liquid injection but a 7.62 cm (3 in) slot length was used for all slot tests. It should be noted that the 2.54 cm (1 in) circumferential dimension of the active area constituted approximately  $0.332 \text{ rad } (19^\circ)$  around the surface of the cylinder.

The perforated specimen was a patterned matrix of  $0.00945 \text{ cm}$  ( $0.00372 \text{ in}$ ) nominal diameter electron beam drilled holes resulting in a 0.569% porosity or open area. Figure 138(B) illustrates the fluid flow from this perforated specimen at a tunnel  $q = 478.8 \text{ N/m}^2$  (10 psf). In this example, the liquid flow rate was  $0.0429 \text{ kg/min/cm}$  ( $0.24 \text{ lb/min/in}$ ) of active span. The figure illustrates a stagnation line location  $0.157 \text{ rad } (9^\circ)$  below the center of the test area locating the stagnation  $0.017 \text{ rad } (1^\circ)$  above the bottom of the test area. Most of the flow was injected well above the

TABLE 33. SURFACE TEST CONFIGURATIONS

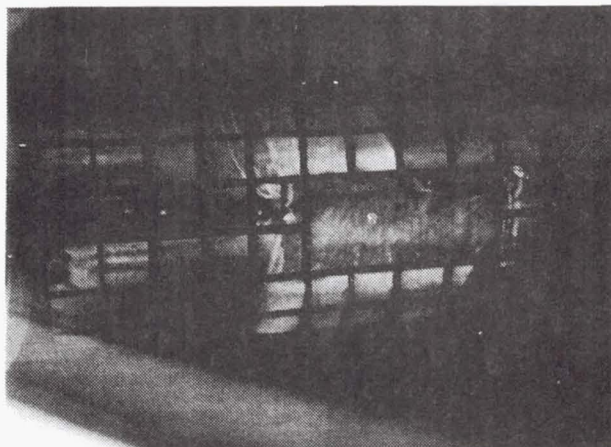
<u>Sample</u>	<u>Type</u>	<u>Porosity/Width</u>	<u>Notes</u>
A	Perforated	0.569%	.00945 cm (.00372 in) holes
B	Slot	0.0152 cm (0.006 in)	Sawed
C	Porous	6.3%	Rigimesh #1522 metal
D	Porous	2.2%	Rigimesh #1526 metal
E	Slot	0.00635 cm (0.0025 in)	Sawed
F	Double Slot	0.0127 cm* (0.005 in)*	Sawed

\*Two parallel slots 1.5875 cm (0.625 in) apart.

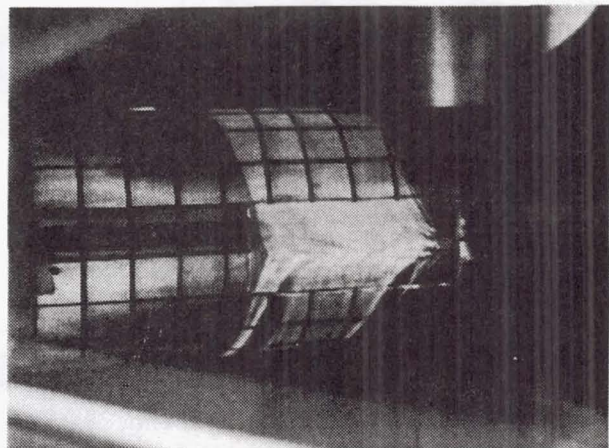
stagnation line and the flow was predominantly up with strong rivulet formations downward. Toward the right extremity of the flow coverage, discrete streams may be seen. These were apparently the result of the flow coalescing from groups of perforations which was characteristic of the perforated configuration at lower flows. When the stagnation line was raised higher onto the perforated surface, good coverage of the lower surface was observed. However when the flow was reduced to about 50% of the rate shown and at the stagnation line location shown, flow from the lower portion of the active area ceased and flow only issued from the upper portion of the area and flowed upward. This was the result of a very low liquid pressure differential across the perforated material and the internal liquid pressures were not sufficient to overcome the higher surface pressures near the stagnation line. It was felt that, while smaller discrete perforations may be drilled by the election beam proces, it was not likely that they could be made sufficiently small to overcome this pressure differential effect relative to the stagnation line pressures at airplane flight speeds. Although some of these characteristics could undoubtedly be overcome, the perforated configuration was rejected for this study.

Figure 138(A) illustrates one of the two porous surfaces tested. Both specimens tested were manufactured by Aircraft Porous Media Incorporated, a subsidiary of the Pall Corp. of Glen Cove, N.Y. The material is marketed under the trade name of Rigimesh and consists of two or more layers of high temperature woven metal mesh integrally sinter-bonded together. Various porosities are achieved by selecting the number of layers, the weave and the density of the weave. The samples tested included porosities equivalent to 6.3% and 2.2% open area, the latter being shown on the figure. In the case illustrated, tunnel  $q$  was  $478.8 \text{ N/m}^2$  (10 psf) and the stagnation line was coincident with the centerline of the active area of the specimen. The flow was  $0.0289 \text{ kg/min/cm}$  ( $0.162 \text{ lb/min/in}$ ) of active span. In general





(A) Porous



(B) Perforated

(C) Slot

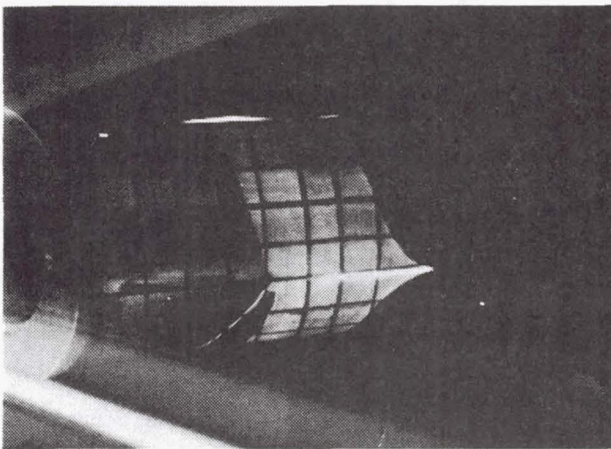


Figure 138. Surface test samples

this material behaved much the same as the perforated material, although at a much lower flow. The porous material did result in a more uniform liquid distribution without the streaking noted with the perforated material. However, when the stagnation line was lowered toward the bottom of the porous sample, rivulets formed similar to those illustrated for the perforated material. The high equivalent open area and lower flows of this example display again the problem associated with a low pressure differential across the material. Comparisons of the results of this specimen with the test results using the increased porosity specimen showed the benefits of lower equivalent open area. The pressure differential effects can undoubtedly be overcome by further decreases in equivalent open area, even at expected airplane flight conditions. However, the greatest difficulty in using this type of material is the necessity for a spanwise butt joint with the titanium skin in the critical leading-edge region where sensitivity to surface irregularities is greatest. A smooth joint between these two dissimilar surface materials would be particularly difficult to maintain in production. For this reason, this configuration was regarded as satisfactory but undesirable from the standpoint of manufacturing.



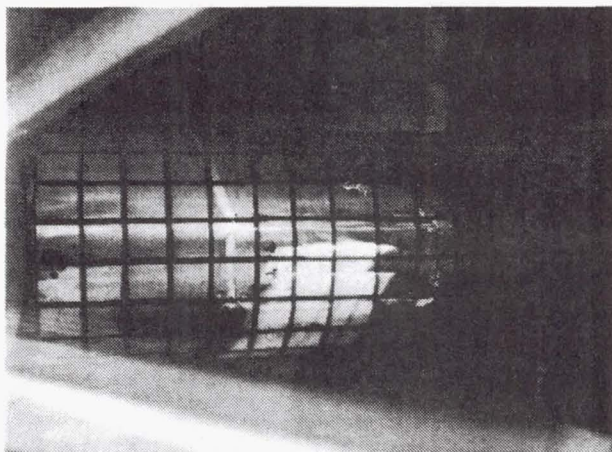
An example of a single slot is illustrated in Figure 138(C). This slot was nominally 0.0152 cm (0.006 in) wide but varied up to 0.0178 cm (0.007 in) at one end. The slot was located 0.175 rad ( $10^\circ$ ) below the forward centerline and the stagnation line<sub>2</sub> was approximately 0.087 rad ( $5^\circ$ ) below the slot; tunnel  $q$  was 478.8 N/m<sup>2</sup> (10 psf). The slot flow was 0.0193 kg/min/cm (0.108 lb/min/in) of slot span. This flow is less than 50% of the flow illustrated for the perforated sample in (B) and 30% less than the flow illustrated for the porous material in (A). The stagnation line location was selected to illustrate the quality of the surface films when the slot flow splits, passing both upward and downward, and to illustrate upward flow from a slot located on the lower surface. The coverage was good and continued to be good with significantly lower flows, lower tunnel velocities and at locations of 0.349 rad ( $20^\circ$ ) below the leading-edge. Admittedly, the stagnation line location was uniquely selected in this illustration.

Figure 137(B) provides a good illustration of the slot flows when the stagnation line is located further below the slot, 0.234 rad ( $13.4^\circ$ ) for the upper slot, and the fluid forms a good film coverage over the upper surface. The figure also shows a good example of slot flow when the stagnation line is only very slightly below the slot as is the case of the lower slot, downward rivulets of flow form from the slot. The combined flow from these two slots is approximately equal to that of the single slot illustrated in Figure 138(C). Therefore, the flow per slot in 137(B) is about half that from the single slot in 138(C) and poorer flow coverage from the lower slot results. When the stagnation line is located about 0.017 rad ( $1^\circ$ ) above the slot, the downward flow film appears much like the downward flow in Figure 138(C).

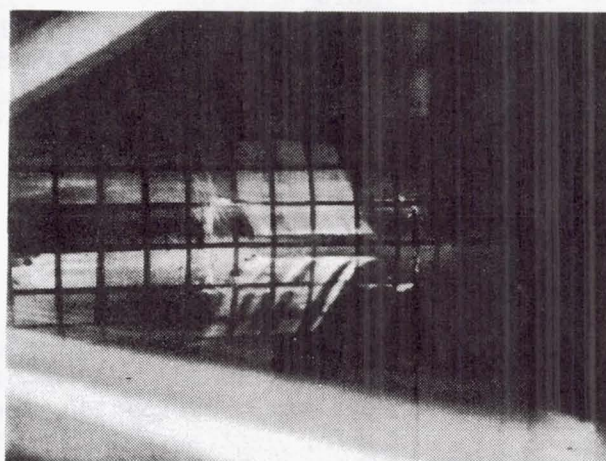
The slots in Figure 139 were both 0.0127 cm (0.005 in) wide and were spaced 1.588 cm (0.625 in) or 0.209 rad ( $12^\circ$ ) apart. As seen in Figure 137(B) there is no flow coverage between the two slots when the stagnation line falls only slightly below the lower slot. As the stagnation line falls farther below the slot, good film coverage occurs between the slots as well as on the upper surface. Conversely, as the stagnation line moves upward from that shown in Figure 137(B), good film coverage between the two slots does not result until the stagnation line reaches the vicinity of the upper slot and the upper slot flow splits both upward and downward. It is considered that the stagnation line transients involved in an airplane take-off and climbout would result in only momentary exposure of various spaces between multiple slots to a no-liquid-film condition. Figure 139 illustrates such a transient. The same slots of Figures 137 are shown at the same tunnel  $q$  and a slot flow of approximately 0.0177 kg/min/cm (0.099 lb/min/in) of slot. The slots are approximately centered on the leading-edge centerline. In Figure 139(A), the stagnation line is about 0.017 rad ( $1^\circ$ ) above the leading-edge centerline and both slots flow downward. As the stagnation line moves downward to 0.140 and 0.331 rad ( $8^\circ$  and  $19^\circ$ ) below the leading-edge centerline in Figure 139(B) and (C), respectively, the slot flow splits and then both flow upward successively.

The good film coverage provided by the slots coupled with the compatibility of the surface materials and the similarity to suction slots from a manufacturing standpoint led to the selection of slots for the baseline liquid film injection configuration. Slots could also provide both





(A) Stagnation point  
at 0.0175 rad (+1°)



(B) Stagnation point  
at -0.1396 rad (-8°)

(C) Stagnation point  
at -0.3316 rad (-19°)

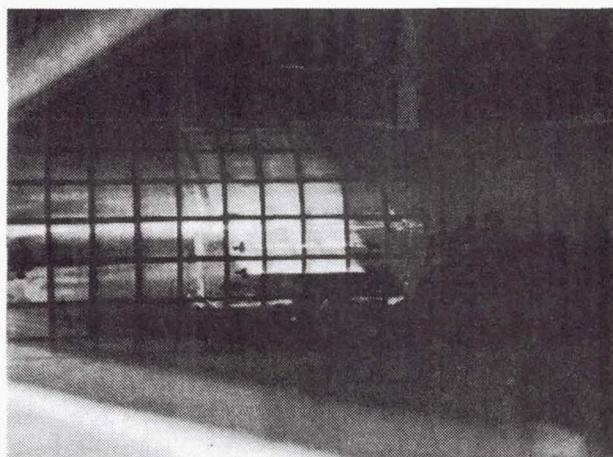


Figure 139. Effects of stagnation location

functions where both suction and cleaning liquid injection are required at the same location on the airfoil surface.

#### Insect Impingement

Insect accretion tests were performed with blowflies, blowfly larvae, houseflies, and fruit flies. The blowflies, which weigh more than seven times as much as houseflies, simulate the majority of moths which might be encountered at night. These insects were found to leave no accretion on a dry surface when injected 20.3 cm (8-in) upstream without any pre-injection velocity. When injected at a higher velocity, good examples of accretion were observed on a dry surface for all insects tested. At this increased injection velocity, it was determined that there was no observable accretion of fruit flies when there was any liquid film flowing over the surface. Blowflies, blowfly larvae and, to a lesser extent, houseflies were seen to accrete with the lowest liquid film coverages but the accretion was

entirely removed by the liquid film in less than approximately 3 sec. With higher liquid film flows, removal of the accretion was almost instantaneous.

It was observed that the leading edge surface remained wet for about 15 to 20 sec after the liquid flow was turned off. Tests were run in which the liquid flow was interrupted and insects were accreted on the wet surface with the film coverage then restored. Again the film flow removed the accretion. This demonstrated that stagnation line transients should influence the film coverage sufficiently to prevent accretion in the space between the slots where the film was momentarily interrupted during takeoff and climbout. This also suggests that a pulsing fluid film might be sufficient to prevent accretion at a greatly reduced total flow. This concept would require evaluation in actual flight test.

Limited tests were performed to determine whether the cleaning fluid could remove accretion that accumulated on a totally dry surface. It was found that the liquid film could not remove accretion from a totally dry surface even if the liquid was turned on almost immediately after the accretion took place.

#### 6.4.3.2 Full-Scale Wind-Tunnel Testing

The primary contractual objective of the leading-edge test article was to develop design and fabrication techniques, as discussed in Section 6.2.3. A secondary contractual objective was the demonstration of the leading-edge cleaning system on the article in a wind tunnel. To these objectives, a third, Lockheed-funded program, was added to evaluate the suction system characteristics.

The contractual test objective included the demonstration of the leading-edge cleaning system control of insect accretion and the determination of cleaning system effects on suction slot characteristics. The Lockheed-funded test objectives included determination of the suction system characteristics and the interactive effects between the suction system and the boundary layer.

#### LFC Systems Design

The design and fabrication objective required that both the cleaning system and suction system be designed to simulate an actual airplane application. Only minimal compromises were required to adapt this design to the wind-tunnel application. The suction surface design was defined by the procedures described in Section 6.3.2.1 and resulted in the nominal configuration dimensions shown in Tables 34 and 35 for the upper and lower surfaces, respectively.

This configuration included some compromises for manufacturing and structural capabilities and did not strictly adhere to the design criteria limits indicated in 6.3.2.1. One of the imposed structural limitations was that the slots should be no closer than 1.575 cm (0.62 in). This was a primary consideration in the location of the first few suction slots on both the upper and lower surfaces. The slot metering and ducting system was designed as described in Section 6.3.3.1. However, it was desired to



TABLE 34. NOMINAL LEADING EDGE SLOT GEOMETRY--  
UPPER SURFACE

Slot	$x/c$	Slot Width		Slot Spacing	
		cm	(in)	cm	(in)
U1	0.022	0.00686	(0.0027)	1.689	(0.665)
U2	0.030	0.00686	(0.0027)	1.575	(0.620)
U3	0.037	0.00686	(0.0027)	1.575	(0.620)
U4	0.046	0.00686	(0.0027)	1.654	(0.651)
U5	0.055	0.00686	(0.0027)	1.892	(0.745)
U6	0.069	0.00813	(0.0032)	2.705	(1.065)
U7	0.090	0.00940	(0.0037)	4.105	(1.616)
U8	0.126	0.01067	(0.0042)	6.919	(2.724)
U9	0.183	0.01448	(0.0057)	10.902	(4.292)

independently control and measure the suction flow through each of three spanwise segments of each slot. To obtain this control, it was necessary to individually duct each of these slot segment flows to the control room rather than meter them directly into the leading-edge trunk duct as described in Section 6.3.3.1.

Figure 140 is a schematic illustration of the suction system for one slot showing the three 40.64 cm (16-in) spanwise segments in the 121.9 cm (48-in) active suction test section. Although it is anticipated that the slot collector ducts in an actual airplane application will be uninterrupted, dams were located in the test panel every 40.64 cm (16-in) to isolate the segment flows. Each 40.64 cm (16 in) segment had 2 nipples installed in the slot collector duct which were connected by a T fitting to a common flexible tube leading to the control room. Segment control valves, a slot flow venturi and a slot control valve for each slot were mounted on a master suction control panel located in the control room. Suction lines from all slots were connected through a single shut-off valve to a roots blower suction pump system which was equipped with an automatically controlled inlet vent to prevent pump stalling. Instrumentation included the pressure and temperature measurements indicated in Table 36, which are keyed to the numbered locations on Figure 140.

TABLE 35. NOMINAL LEADING EDGE SLOT GEOMETRY--  
LOWER SURFACE

Slot	x/c	Slot Width		Slot Spacing	
		cm	(in)	cm	(in)
L1	0.020	0.00686	(0.0027)	1.575	(0.620)
L2	0.028	0.00686	(0.0027)	1.575	(0.620)
L3	0.035	0.00686	(0.0027)	1.575	(0.620)
L4	0.043	0.00686	(0.0027)	1.575	(0.620)
L5	0.051	0.00686	(0.0027)	1.575	(0.620)
L6	0.061	0.00813	(0.0032)	1.763	(0.694)
L7	0.071	0.00813	(0.0032)	2.159	(0.850)
L8	0.084	0.00813	(0.0032)	2.238	(0.881)
L9	0.101	0.00940	(0.0037)	3.345	(1.317)
L10	0.128	0.01067	(0.0042)	5.179	(2.039)
L11	0.183	0.01448	(0.0057)	10.366	(4.081)

TABLE 36. SUCTION SYSTEM INSTRUMENTATION

- (1) Slot collector duct segment pressure
- (2) Segment line pressure
- (3) Suction flow temperature
- (4) Slot flow venturi reference pressure
- (5) Slot flow venturi throat pressure

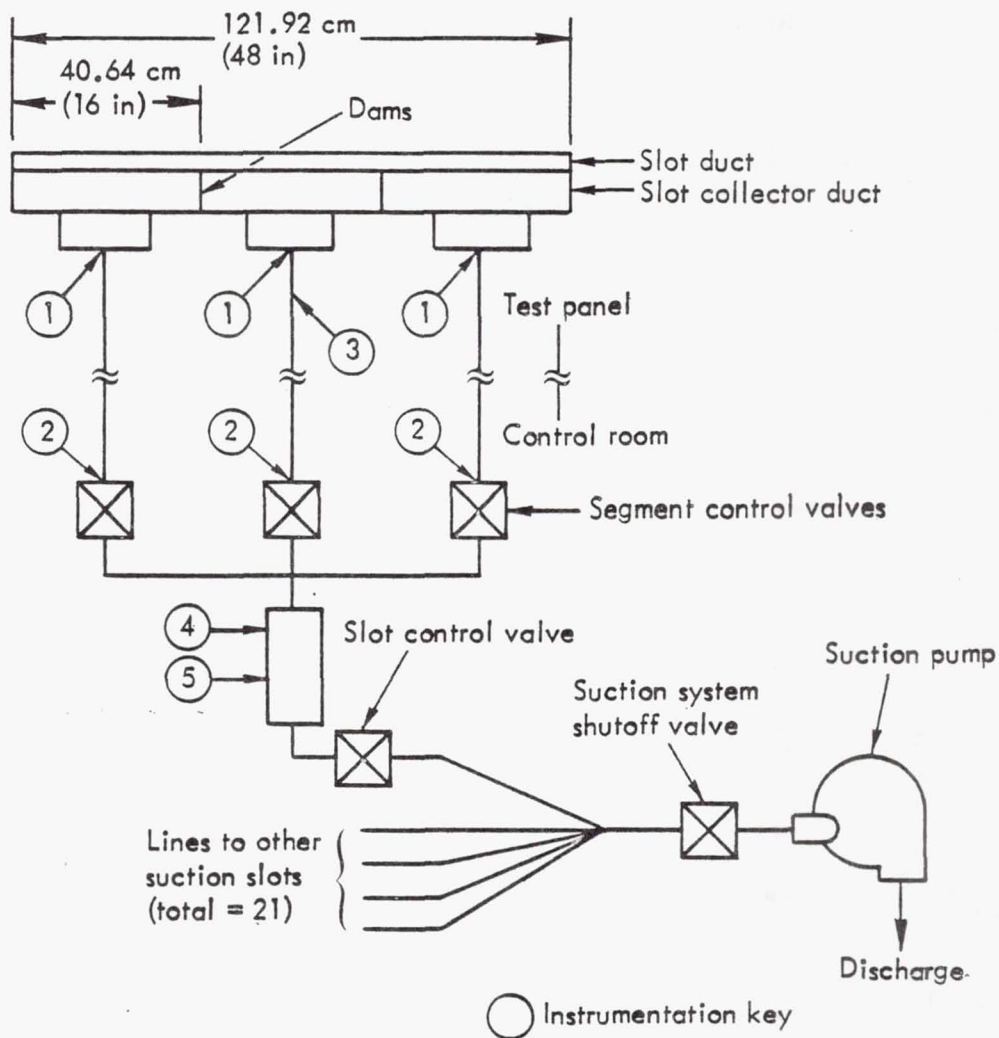


Figure 140. Slot suction system schematic

It was concluded that the results of the subscale cleaning test described in Section 6.4.3.1 would support the selection of a leading-edge cleaning system slot and slot duct of the same configuration as the suction slots. Analysis of the flows and pressure losses of the metering system and slot for the cleaning system application also supported this conclusion. Therefore, the cleaning slots, ducts and metering configuration were selected to be the same as the forward suction slots. An analysis of stagnation line movements around the leading edge during a takeoff and climbout indicated a stagnation line movement back to approximately 1.2% chord on the lower surface. Accordingly, slots were located such that there would always be at least one slot above and one slot below the stagnation line. The minimum slot spacing of 1.575 cm (0.62 in) noted previously was also selected. This resulted in the cleaning slot configuration shown in Table 37 and illustrated on Figure 141.

As in the case of the suction slots, it was desired to independently control and measure the liquid flow to each slot and control the flow to each of three segments of each slot. This system is illustrated



TABLE 37. LEADING EDGE SLOT GEOMETRY--CLEANING SYSTEM

Slot	x/c	Slot Width		Slot Spacing	
		cm	(in)	cm	(in)
W1	0.00023*	0.00686	(0.0027)	1.575	(0.620)
W2	0.00065	0.00686	(0.0027)	1.575	(0.620)
W3	0.00349	0.00686	(0.0027)	1.575	(0.620)
W4	0.00799	0.00686	(0.0027)	1.575	(0.620)
W5	0.01374	0.00686	(0.0027)	1.575	(0.620)

\*Located on upper surface

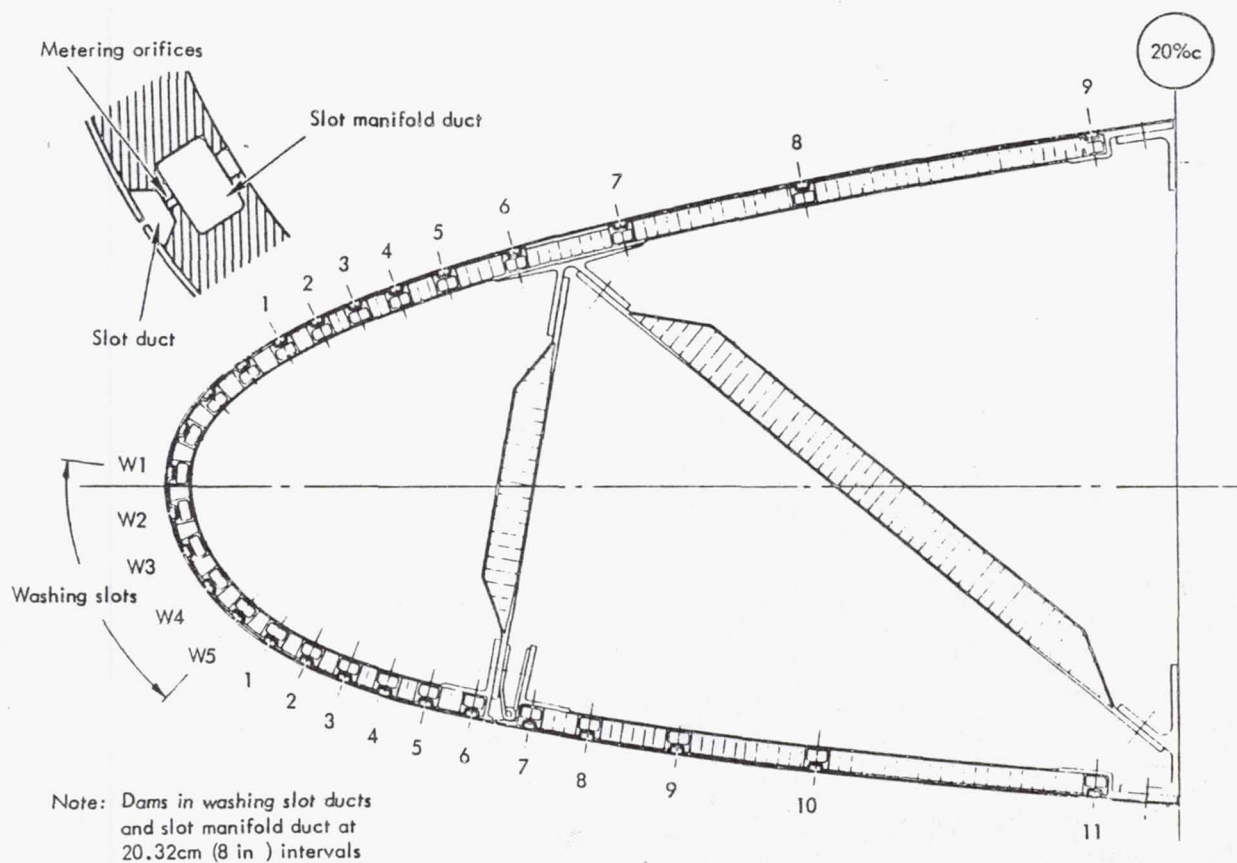


Figure 141. Cleaning slot configuration

schematically in Figure 142. It was also observed that at high pitch angles there is a tendency for the liquid in the slot and slot manifold ducts to flow toward the low end of the slot. This would result in excessive flow at the lower end of the slot with flow starvation at the upper end. A similar characteristic results during airplane acceleration due to the wing sweep with the excessive flow occurring at the most aft portions of the slot. To prevent this occurrence, dams were located at 20.32 cm (8-in) intervals in both the slot and slot metering ducts. A tendency would still exist in the upstream metering system to supply more flow to the lower/aft end of the slot. This was counteracted by the insertion of a high-pressure-drop restrictor in the liquid supply line to each 20.32 cm (8 in) segment. These were 2.54 (1 in) long segments of 0.1397 cm (0.055 in) inside diameter tubing. Each slot system was connected through a venturi meter and slot control valve. All slot lines were connected to a liquid reservoir through a common shutoff valve. The reservoir was pressurized by a compressed gas source through a regulator valve. The cleaning system was instrumented with the pressure and temperature measurements listed in Table 38 which are keyed to the numbered locations on Figure 142.

The test panel was mounted in a simulated airfoil section illustrated in Figure 143. The forward 35% of the full-scale chord airfoil was simulated. Beyond this point the airfoil was truncated, blending to a flat plate afterbody. The surface instrumentation locations are also shown on this figure for the keyed instrumentation listed in Table 39.

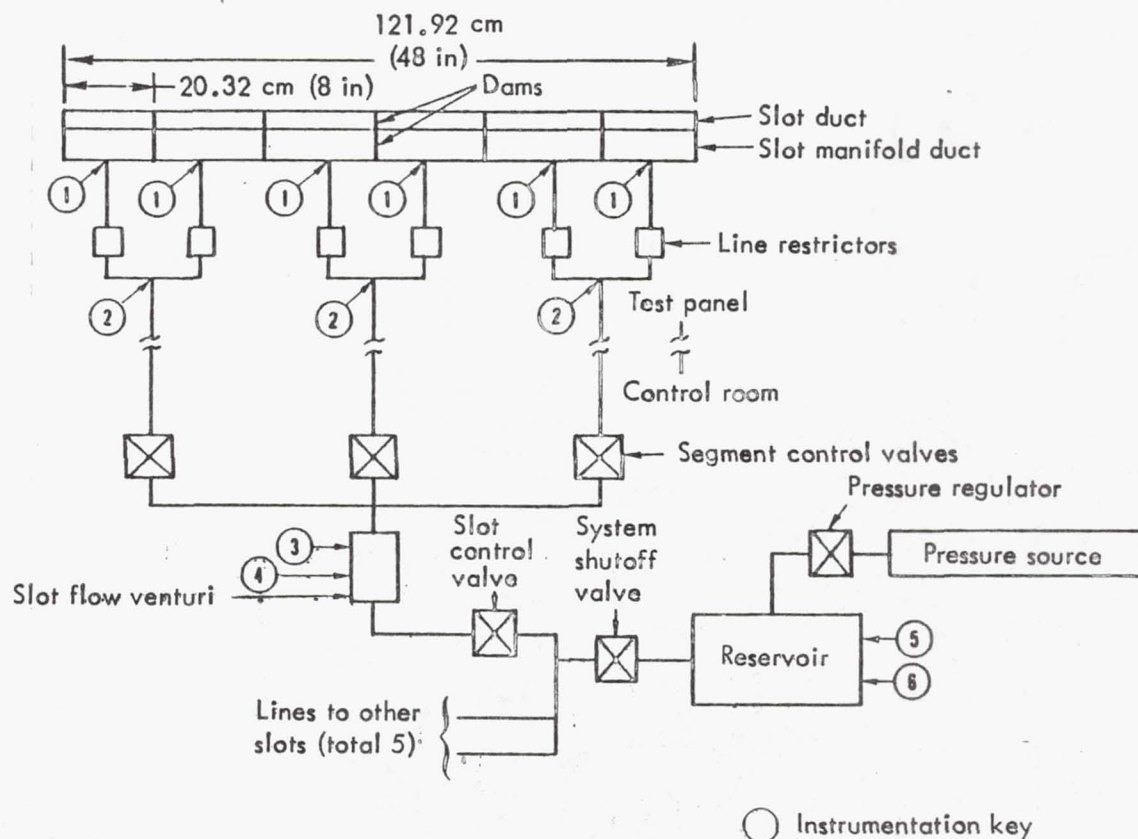


Figure 142. Slot cleaning system schematic

TABLE 38. CLEANING SYSTEM INSTRUMENTATION

- (1) Slot manifold duct pressures
- (2) Segment line pressure
- (3) Slot flow venturi reference pressure
- (4) Slot flow venturi throat pressure
- (5) Reservoir pressure
- (6) Reservoir temperature

Item 4 in the tabulation was a Preston probe rake that consisted of 24 probes located on 2.54 cm (1 in) centers and was mounted on the airfoil immediately behind and parallel to the test panel so that it sampled the flow over the test panel surface. All other surface instrumentation was permanently mounted on the surface in lines oriented  $0.175 \text{ rad}$  ( $10^\circ$ ) to the streamline direction in order to avoid any wake effects. The model airfoil was swept to  $0.436 \text{ rad}$  ( $25^\circ$ ) and large flat end plates were installed to eliminate end effects. The airfoil section was mounted in the Lockheed low speed wind tunnel on three pylons as shown in Figure 144 so that as the model was pitched up to high angles of attack the leading edge slope approximated that of a  $0.436 \text{ rad}$  ( $25^\circ$ ) swept airplane when rotated to the same attitude.

Figure 145 shows the insect injector that was suspended on a system of cables between the top and bottom of the wind tunnel about 4.57m (15 ft) upstream of the airfoil. The injector consisted of two 7.62 cm (3 in) flow-through tubes 50.8 cm (20 in) long mounted one over the other on 12.7 cm (5 in) centers. Toward the upstream end of each, a 2.54 cm (1 in) tube penetrated the 7.62 cm (3 in) tube at a  $0.785 \text{ rad}$  ( $45^\circ$ ) angle pointing downstream and extending slightly into the larger tube. From these 2.54 cm (1 in) tubes, flexible tubes led to hoppers located above the wind tunnel. During the testing, live but anesthetized insects were manually dropped into the hoppers at prescribed rates. The insects were then sucked into the tube where they accelerated to approximately tunnel velocity.

The Lockheed low-speed wind tunnel has a 7.12 by 4.95m (23.36 by 16.24 ft) test section with a continuously variable range of  $q$  values from 191.5 to 3830.4  $\text{N/m}^2$  (4 to 80 psf) or approximately 14.3 to 285 km/hr (7.7 to 154 kn). The tunnel is equipped for automatic data recording and on line data reduction.

#### Preliminary Testing

Prior to initiating wind-on testing, baseline data were recorded for the cleaning test. The suction system slot segment valves were adjusted to



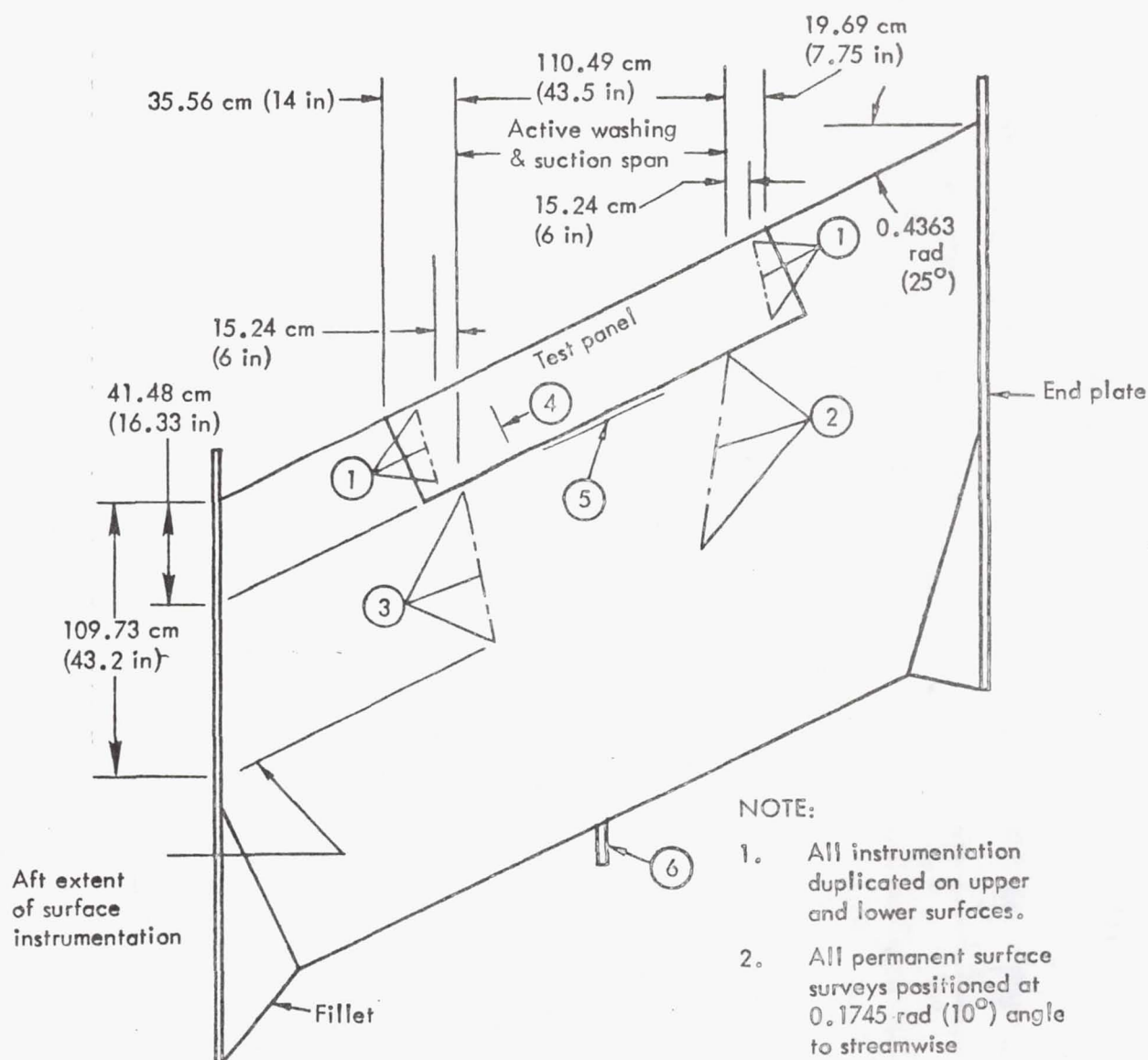


Figure 143. Model assembly

provide equal flow across the span of a slot. The slot flow control valves were then adjusted to produce nominal suction flow distribution level. Suction flow and pressure data were recorded.

$C_p$  distribution and stagnation line location data were recorded for a range of tunnel velocities up to the maximum and airfoil pitch angles for  $0^\circ$  up to approximately  $0.262 \text{ rad (} 15^\circ \text{)}$ . A tunnel transient test routine was established to best represent airplane takeoff and climbout within the wind tunnel limitations. The tunnel velocity was accelerated from approximately 65 to 259 km/hr (35 to 140 kn) in 75 sec at an airfoil angle of attack of  $0^\circ$  to simulate takeoff ground roll. The tunnel velocity was held constant while the airfoil angle of attack was increased to  $0.262 \text{ rad (} 15^\circ \text{)}$  in 15 sec. to simulate rotation and the tunnel velocity was then increased to 285 km/hr (154 kn) to simulate climbout. This sequence was used for subsequent transient tests.

TABLE 39. SURFACE INSTRUMENTATION

- (1) Surface static pressure taps at selected slots
- (2) Surface static pressure taps at 3.81 cm (1.5 in) intervals
- (3) Surface Preston probes and surface static pressure taps at alternate 3.81 cm (1.5 in) locations
- (4) Slot Preston probes on slot No. 5 and higher
- (5) Relocatable 24 Preston rake
- (6) Trailing edge B. L. rake pressures

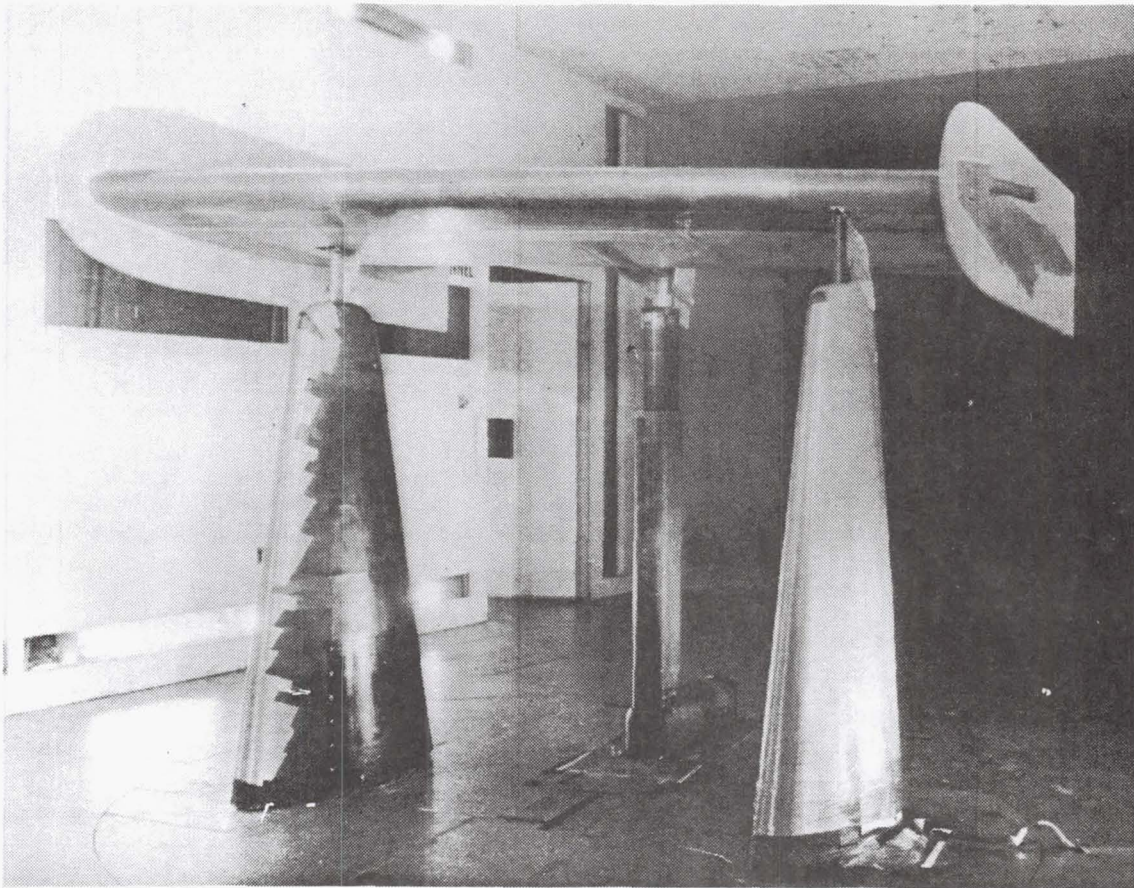


Figure 144. Installed wind tunnel model



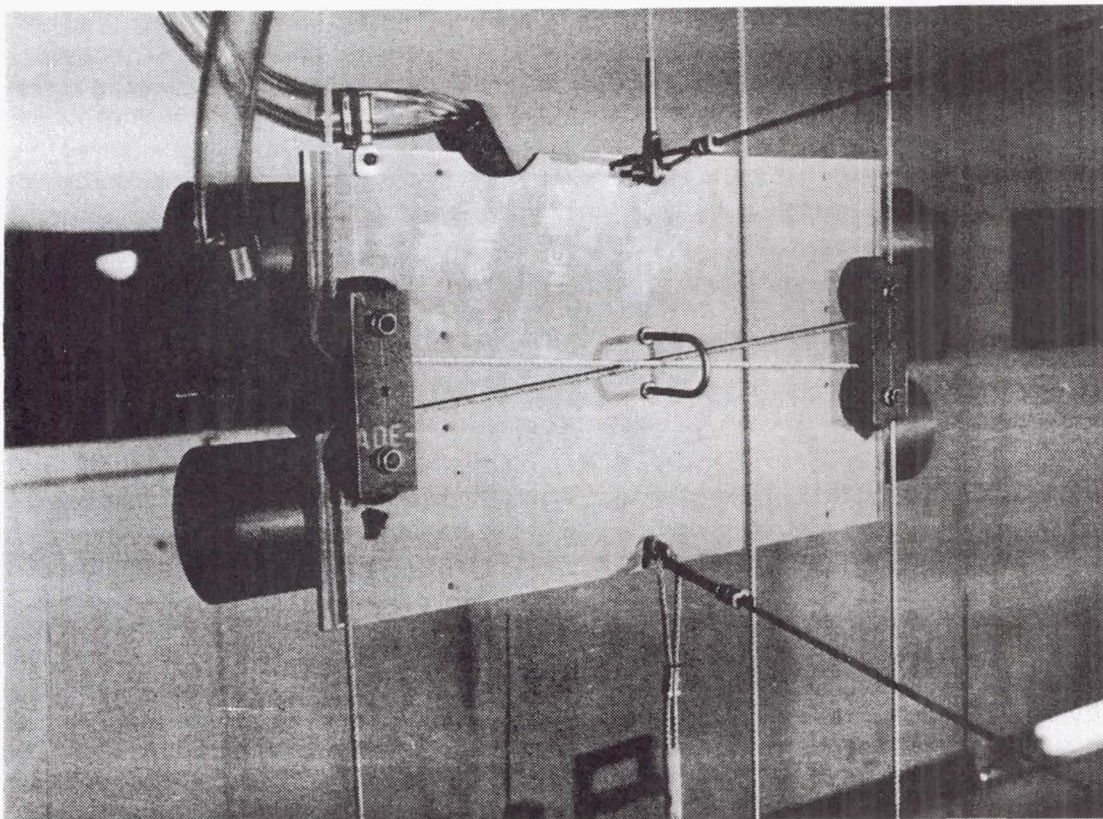


Figure 145. Insect injector

The Lockheed suction testing was conducted at this point in the program to preclude contamination from insect accretion or cleaning fluid.

#### Insect Accretion Pattern

Previous analysis had indicated that the insect injector would produce a dispersion of insects across approximately 0.6096m (2 ft) of the test panel span which was intended to be concentrated on the central 45.72 cm (18 in) slot segment. An allowance for a normal distribution of insects around a 45.72 cm (18 in) dispersion pattern was assumed along with an airplane takeoff profile. The highest insect distribution rate found in the literature was assumed for airborne insects as a function of altitude. This was reported in the 1939 researches of P. A. Glick (Ref. 30). The weight of airborne insects was assumed to follow the frequencies shown in Reference 31 that were reported by J. A. Freeman in 1945. These assumptions, together with the assumed airplane takeoff and climbout profile were used to determine a representative insect injection rate for test simulation. It was found that this would require a total of less than 10 insects in the dispersion pattern to simulate a complete airplane takeoff and climbout. Further, only one of these insects would be as large as a housefly, in fact the mass of a housefly is nearly seven times the average mass of a Freeman distribution. The previous subscale testing described in Section 6.4.3.1 indicated that the greatest demands on the cleaning system would be imposed by the impact of larger insects such as blowflies. Consequently, houseflies and blowflies were selected for the test.



Figure 146 illustrates the insect accretion of blowflies injected continuously during a simulated takeoff, climbout schedule on a totally dry surface. The blowfly injection frequency rate was 16 times that determined from the preceding assumptions and analysis to be required for a representative airplane takeoff and climbout. The blowflies injected in this test approached 800 times a representative weight. Insect accretion on the lower surface occurred during the portion of the run at  $0.262 \text{ rad}$  ( $15^\circ$ ) angle of attack and may be seen to extend back to 35% chord. Figure 147 shows a closeup of upper surface accretion for this same run. Evidence of insect accretion may be seen as far back as 5% chord on the upper surface. The extremely high concentration of impacts may be clearly seen in the stagnation region. Other insect accretion runs were made on a clean dry leading edge and an insect injection frequency 8 times that required for a typical takeoff, climbout was selected as providing a good demonstration without needlessly overloading the surface with insects. When blowflies were injected, this rate impacted approximately 400 times the mass of insects that would be representative of a typical takeoff. The injection frequency 8 times the typical rate was used for all further testing.

#### Cleaning Fluid Distribution

Initial tests were run to adjust the cleaning system and determine the liquid film coverage for a representative takeoff and climbout. It was found that a combination of difficulties precluded achieving design fluid film coverage of the lower surface. The most notable problems were with the non-production test plumbing contained inside the leading-edge test

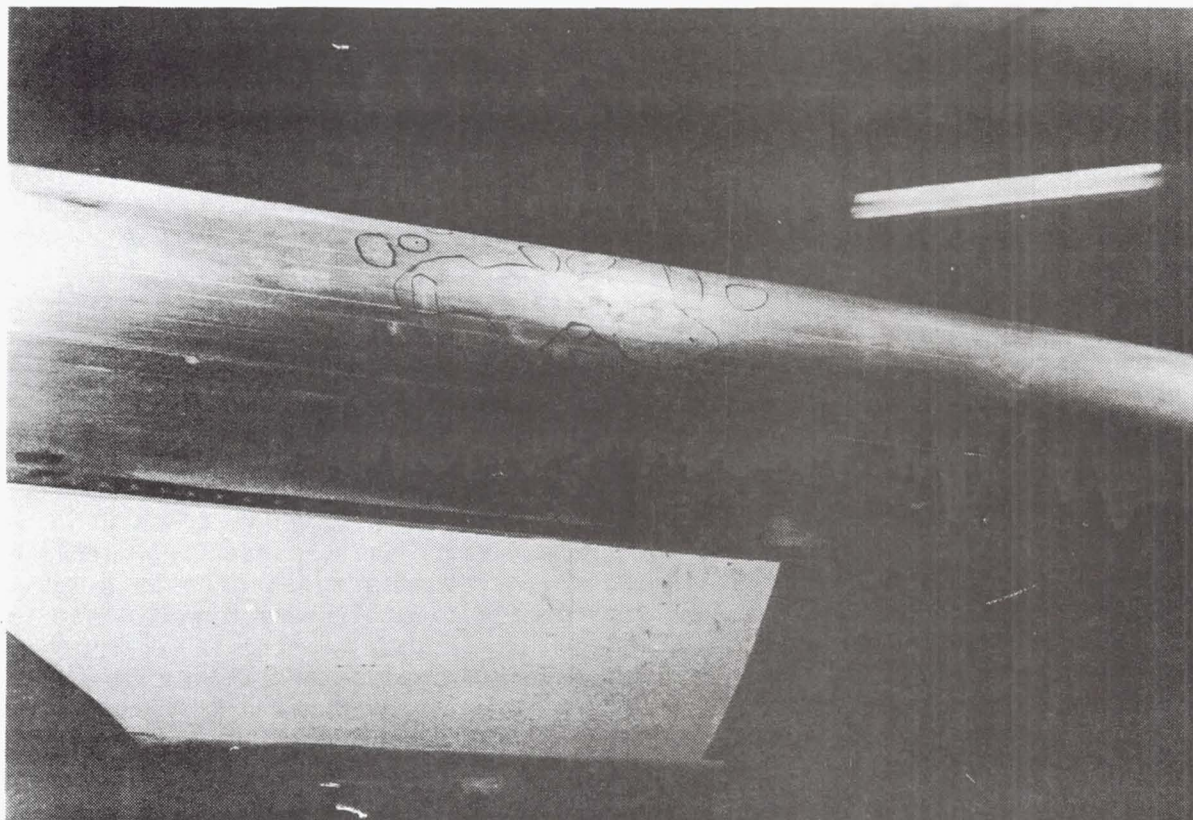


Figure 146. Dry leading edge accretion insect ratio = 16 run No. 34



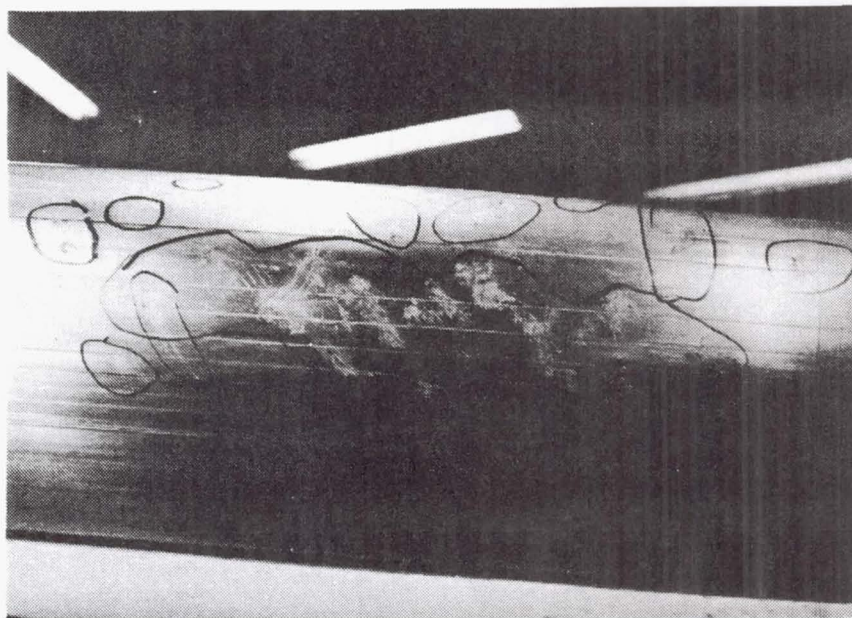


Figure 147. Dry leading edge accretion insect ratio = 16 run No. 34 closeup

panel. Numerous leaks in the internal plumbing systems of slots W3, W4 and W5 (see Figure 141) totally prevented use of slots W4 and W5. One outboard segment of slot W3 also leaked excessively and could not be used. It was also found that although slot number W3 had been cut with a nominal 0.00762 cm (0.003 in) saw, the central portion of the slot had closed up to less than 0.00127 cm (0.0005 in) after being cut. This virtually eliminated any liquid film coverage of the lower control portion of the leading edge where the insect impacts were concentrated at any appreciable angle of attack. It was also found that the average widths of slots W1 and W2 were wider than nominal, approximately 0.1143 and 0.0089 cm (0.0045 and 0.0035 in) respectively.

#### Cleaning System Demonstration

Because of the poor cleaning fluid distribution to the lower surface, testing at higher angles was limited. By setting the airfoil to  $-0.026$  rad ( $-1.5^\circ$ ), good liquid film coverage of both the upper and lower surface was obtained from slots W1 and W2 respectively. Figures 148 and 149 illustrate a run in which this angle was held constant while the tunnel velocity was increased from a  $q = 239.4$  N/m<sup>2</sup> (5 psf), to a  $q = 3830$  N/m<sup>2</sup> (80 psf) with approximately design cleaning flow rate from slots 1 and 2. Blowflies were injected continuously throughout the run at a frequency rate 8 times the representative level. Figure 148 shows the liquid flow film over the surfaces at the lower  $q$  while Figure 149 shows the liquid film at  $q = 3734.6$  N/m<sup>2</sup> (78 psf). At the higher tunnel  $q$ , the film is seen to be thinner and smoother than at the low-speed condition. Both upper and lower surface film coverages were good throughout the test run. The fluid film remained completely attached to the lower surfaces even at  $q = 239.4$  N/m<sup>2</sup> (5 psf) and at the  $-0.026$  rad ( $-1.5^\circ$ ) angle of attack, actually flowed upward toward the trailing edge. In no case throughout the test was the liquid seen to prematurely separate from the lower surface when the tunnel was turned on.



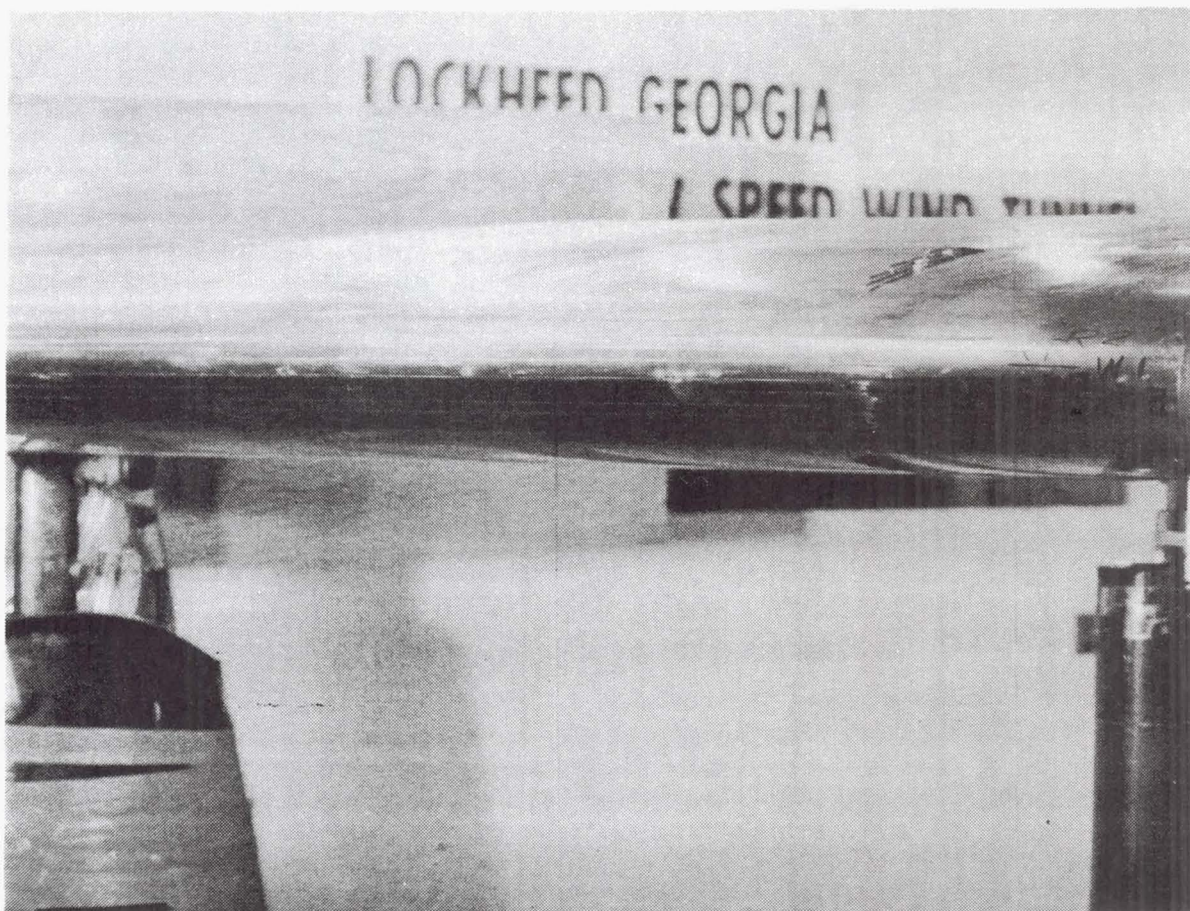


Figure 148. Test run No. 41,  $q = 239 \text{ N/m}^2$  ( $5 \text{ lb/ft}^2$ )  $\alpha = 0.262 \text{ rad}$  ( $15^\circ$ )

Approximately 80 blowflies had been injected at the time the Figure 149 photograph was taken. Two insect impacts can be seen in the original color photograph but are indistinguishable from other leading edge polish marks in the figure. These impacts were totally contained on the surface between slots W1 and W2, the area that had no liquid film coverage during the run. These were the only evidence of residual accretion found during close inspection following the run, even though insect mass flow rate had been extremely high.

Takeoff, climbout simulation runs were made in which the airfoil angle was increased to  $0.087 \text{ rad}$  ( $5^\circ$ ) with housefly injection. Even with the extremely deficient lower surface cleaning film flows there was only one instance of very questionable insect accretion. During the first part of these runs, slot W2 formed a film on the lower surfaces for approximately the first 75 sec. As the airfoil angle was increased to  $0.087 \text{ rad}$  ( $5^\circ$ ), the flow from W2 reversed direction and flowed over the upper surface. Apparently there was a sufficient residual film on the lower surface from slot W2 to prevent accretion from the houseflies. Numerous other runs were made at various flow rates and in which the airfoil angle was increased to  $0.105 \text{ rad}$  ( $6^\circ$ ). In no case during any of the test was residual accretion found on any surface that had been protected by design levels of cleaning fluid flow.



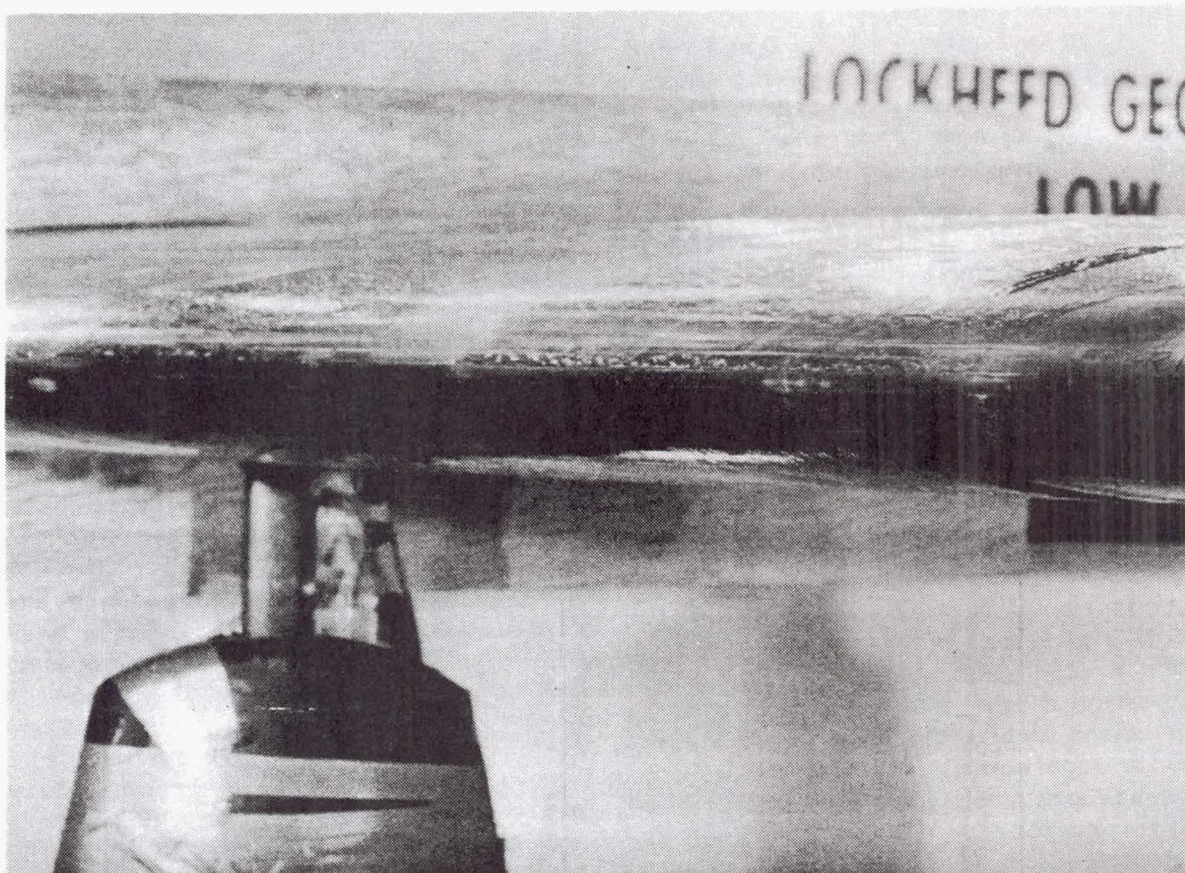


Figure 149. Test run No. 41,  $q = 3735 \text{ n/m}^2$  ( $78 \text{ lb/ft}^2$ )  $\alpha = 0.262 \text{ rad}$  ( $15^\circ$ )

It was also observed, in tests run with the airfoil pitched up to approximately  $0.262 \text{ rad}$  ( $15^\circ$ ), that good spanwise distribution of the cleaning liquid film was obtained from slots W1 and W2. There was no discernable evidence of excessive flow from the lower end of the slot or flow starvation at the upper end. This observation applies to all tunnel  $q$  values and cleaning liquid flow rates run at this angle. This appears to confirm the adequacy of the internal metering and distribution system to overcome the leading edge slope and acceleration effect on distribution.

Checks of the suction system following the cleaning liquid demonstrations disclosed that residual liquid partially blocked the slots. It was also found that much of the suction system internal pressure instrumentation, including the venturi flowmeters, had cleaning liquid in the lines. It was apparent that the slots must be either artificially purged or given sufficient time with external airflow for residual cleaning liquid to dry. It was also apparent that the suction system internal pressure instrumentation required artificial purging. This might be extended to include all surface pressure instrumentation in a flight test program where it cannot be protected during the cleaning tests as it was in the wind tunnel. It was also observed in the suction system testing that the open, unsucked leading-edge cleaning system slots did not prevent laminarization of the upper surface. A similar observation cannot be made relative to the lower surface. A poor lower surface hinge-line surface joint appeared to be the cause of failure to laminarize the lower surface.



## 6.5 AUXILIARY SYSTEMS INTEGRATION

The two unique LFC systems required for an LFC airplane are the suction system and the leading-edge system to prevent insect accretion. There would be obvious advantages from integrating either of these systems with any of the normal airplane auxiliary systems or using these systems to perform some additional beneficial functions. The suction system includes a suction pump or compressor and power unit and involves a significant amount of airflow. The possibilities of integrating all or some part of this system with the airplane environmental control system (ECS) or auxiliary power unit (APU) system are both obvious and enticing. Several variations of integrating these systems have been considered and in each case, basic mismatches or complexities appear to outweigh any advantages.

One system considered was the use of the suction airflow to supply the ECS requirements. There is sufficient suction air passing through one of the suction units to satisfy the ECS cruise requirements. However, the suction pump was selected to discharge the suction air at free stream velocity. The pump compresses the suction air sufficiently to increase the pressure from the low pressures of the wing surfaces, with the additional pressure losses of the suction and metering system, to the free stream total pressure conditions. This compression increases the temperature of the suction air at the cruise condition to  $331^{\circ}\text{K}$  ( $597^{\circ}\text{R}$ ). To meet the ECS pressurization and pressure loss requirements necessitates a further compression ratio of 3.5, or the same as free stream ram air would require. This compression of the ram air requires 428 kW (575 HP) while the additional compression of the suction air would require 588 kW (788 HP) due to the previously elevated temperature of the suction air,  $331^{\circ}\text{K}$  ( $597^{\circ}\text{R}$ ) versus  $251^{\circ}\text{R}$ ) for ram air at  $M = 0.8$  at 11 582m (38 000 ft). This is an increase of 37% in the power required to compress the suction air over that of ram air. Additionally, the still higher temperatures of the further compressed suction air would require more refrigeration and a larger refrigeration system than is required for a ram air system. The net thrust/drag of these two systems is the same. Several variations of this system were considered but all showed that there were no advantages and numerous penalties associated with use of suction air in the ECS system.

Similarly, several schemes were considered for using the suction unit, suction compressor, and power unit, in place of an APU. The suction pump pressure ratios are not compatible with the APU functional requirements. The additional compression requirements plus the requirements for 90 kVA electrical power precluded any advantages of using the suction pump. Using the suction pump power unit to drive a separate compressor and alternator would require an elaborate clutching system to declutch the suction pump and clutch in the APU compressor and alternator. In addition, the high pressure ratios and loading of the suction power unit would require extensive inlet and exhaust acoustic treatment to permit operation at the required power levels. These considerations, together with the weight, maintainability, and reliability problems associated with the clutching system appear to outweigh any possible advantages.

In Reference 5, use of suction air for takeoff thrust augmentation, blown flaps, etc. were considered and found to offer no advantages. In the current study, the airplane would not benefit significantly from either of

these arrangements. To date, the incompatibilities of the suction system with other airplane systems have precluded any advantageous integrations among those considered.

Integration of the leading-edge system to prevent insect accretion presented a more encouraging possibility. The leading-edge liquid film system for preventing insect accretion was found to be compatible with de-icing requirements and is similar to a system that has been successfully employed on operational airplanes for over twenty years. This integration was planned for the airplane and it was found that no basic modifications to the system were required for the de-icing function. The selected method of injecting the liquid film onto the surface, i.e. slots, provides yet another integration possibility. With very slight modification to the system, suction may be applied to the cleaning slots so that they can double as suction slots if this should prove beneficial for laminarization. These considerations are discussed elsewhere in this report.



## 7.0 CONFIGURATION SELECTION AND ASSESSMENT

The ultimate objective of this study is the integration of selected system concepts into the baseline configuration to form a final LFC transport configuration, and the subsequent comparison of this aircraft with a similarly-optimized turbulent transport. This section summarizes the operational considerations which must be included in the selection of design options and describes the selected LFC configuration and supporting systems. The characteristics of an advanced technology turbulent transport are summarized and two aircraft are compared on the basis of weight, cost, and fuel efficiency.

### 7.1 OPERATIONAL CONSIDERATIONS

#### 7.1.1 Airline Recommendations

During the course of this contract Lockheed carried on a dialogue with Delta Air Lines to ensure that practical operational considerations were accommodated in the 1993 LFC transport. The following comments establish the Delta position on pertinent aspects of a 1993 LFC transport.

- (1) Airlines are interested in new aircraft systems which provide a 20-25% fuel savings, particularly if fuel allocations were to be imposed. Any such system must be tried and proven prior to widespread airline acceptance.
- (2) Delta would require structural warranties on a 1993 LFC transport of 80 000 flight hours or 60 000 cycles without major repairs. They would expect a 99% mechanical dispatch reliability. Mechanical dispatch reliability, in this context, is defined as a percentage of revenue flights that depart within 15 min of schedule without incurring a delay or cancellation attributable to mechanical systems. Also, if the airplane could safely operate with LFC systems inoperative, Delta would allow revenue dispatch with the system inoperative. Performance warranties for the aircraft with LFC operative and without LFC would be required.
- (3) Along with dispatch reliability, Delta would require separate structural corrosion warranties and LFC system reliability warranties.
- (4) Delta would carry additional reserve fuel to account for the possibility of the hypothetical situation caused by LFC system failure at the midpoint of a 12 038 km (6500 n mi) flight. Such an occurrence would reduce the ultimate range by 1200 km (650 n mi) and increase fuel by approximately 12%. Final policy on operational procedures would be determined after the reliability of the system and its ability to function after a partial failure is determined.

- (5) Maintainability of the LFC system would be a primary concern during aircraft detail design and specification reviews during the airline procurement cycle. Mechanical and reliability aspects, rather than optimum performance, would be influencing factors. Less complex systems are preferred.
- (6) Allowable system deterioration prior to overhaul is traded off against overhaul expense. Normally, an airframe/engine combination performance degradation of 2%-5% is allowable prior to overhaul. However, in a fuel-critical environment, such a wide tolerance may not be acceptable.
- (7) Operationally, a completely automatic LFC system would be desirable. However, economics will govern the final decision at the time of system acquisition.
- (8) Delta prefers "on-condition" maintenance procedures using periodic ground checkout. In-flight performance monitoring would be considered. Use of airborne data acquisition devices is not desirable.
- (9) Flight-by-flight pre-takeoff checkout is not necessary, although the capability for such checkout should be available for those cases of maximum range flights in which block fuel and reserves are dependent on LFC.
- (10) Smoothness tolerances such as 0.015 cm (.006 in) for surface roughness, 0.015 cm (.006 in) downsteps, and 0.028 cm (.011 in) and 0.046 cm (.019 in) chordwise and spanwise gaps, respectively, would present serious problems due to maintenance time, probable cost of labor in 1990, and the probable skill levels available in 1990.
- (11) It would be necessary to allow maintenance personnel to walk on wing surfaces. Wing and empennage surface covers would not be desirable for ground protection of LFC surfaces. Use of a ground cart to provide reverse airflow to minimize ground contamination would not be desirable. The cost of owning and operating such equipment and the number of hours of required operation would negate considerable in-flight fuel savings. Cleaning of LFC aircraft leading edges prior to each flight would not be desirable from a maintenance cost standpoint.
- (12) Maintenance has overriding priority in Delta operational philosophy. They estimate that cost per maintenance manhour could conceivably reach \$25-\$30 per hour by the time fuel reaches \$0.53/l (\$2.00/gal).
- (13) They strongly recommend that all primary structure be readily accessible; this requirement is reinforced by recent study of 2,000 repair orders of which 65% were corrosion, fatigue, or damage items.



### 7.1.2 Ground Operations

Airline users of LFC aircraft will expect to maintain and handle this vehicle within the framework of their existing maintenance programs. While varying in details, airline maintenance programs are generally comprised of the following schedule inspections and intervals:

- o Post-flight/pre-flight - Each flight
- o A Check - Each 50 flight hours
- o C Check - Each 1000 flight hours
- o D Check - Each 8000 flight hours
- o Unscheduled - As required

Assimilation of LFC transports into fleet service will impact each of the above areas of maintenance.

#### 7.1.2.1 LFC Maintenance Requirements

Table 40 presents examples of LFC maintenance items which fall into the general categories listed above.

Elements of an LFC system can be categorized in two major areas: functional systems and surfaces and ducting. The functional systems, which include suction pumps, valves, and controls, are similar to systems currently being maintained by the airline users and thus present no unusual maintenance requirements.

The LFC surfaces with integral slots and ducting present unique maintenance requirements which airline operators have not previously encountered. These requirements result from the criticality of surface smoothness and cleanliness. New maintenance procedures for titanium covered, composite structure must be developed. Of particular importance are leading-edge panels which are more fragile than main box surfaces. Leading edges incur frequent, often unreported damage in current operations, but for LFC operations these surfaces will require immediate attention.

With proper procedural planning and training, it is expected that required LFC maintenance can be successfully folded into normal airline maintenance programs.

### 7.1.3 Flight Operation

Throughout the development of LFC transport aircraft, it is imperative that the minimization of operational differences between LFC and current turbulent transports be maintained as a continuing objective. Consequently, the investigations of this study have been directed toward the development of an aircraft for which flight operations differ little from those of the current airline fleet.



TABLE 40. LFC MAINTENANCE REQUIREMENTS

Periodic Maintenance (A, C, D Checks)

- o Inspection and testing of LFC ducting system - surfaces slots, metering holes and ducts--for proper flow, cleanliness, and smoothness
- o Inspection of pump installations for integrity of mounting, connections, and leakage
- o Operational check of safety items, such as the duct-installed sniffers to detect fuel leaks
- o Inspection and check-out of leading-edge cleaning system for proper flow characteristics
- o Inspection/verification of LFC monitoring system

Unscheduled Maintenance (as required)

- o Repair of damaged slots and slot ducts
- o Repair of trunk ducts
- o Repair/replacement of pumps and controls
- o Repair/replacement of cleaning system components
- o Repair/restoration of wing surfaces for smoothness and cleanliness

Servicing - Post-flight/Pre-flight

- o Inspection/cleaning of leading edge
- o Replenishment of leading-edge cleaning fluid
- o Replenishment of suction pump lubricant
- o Flushing/purging of suction system ducting

The LFC aircraft of this study are compatible with the air traffic control systems and the general operating environment envisioned for the post-1990 period. The aircraft are compatible with the international mission profile discussed in Section 5.1 and are capable of operating under pertinent FAA rules.

LFC aircraft will differ in flight operations in two areas:

- (1) Operation of LFC systems
- (2) Flight planning

#### 7.1.3.1 LFC System Operation

The in-flight operation of LFC aircraft of the current study differs from that of current transport aircraft primarily by the addition of two systems. A cleaning system is incorporated into the leading-edge region of the wings and empennage to prevent insect contamination, and a suction system is provided for laminarization of the same regions.

Operation of the leading-edge cleaning system is limited to ground operations above 46 km/hr (25 kn) and the initial portion of the climb phase. For a typical flight, the system would be turned on at the beginning of the takeoff roll and turned off when the aircraft reached 914 m (3000 ft).

The LFC suction system is designed to laminarize the wings and empennage over a limited flight envelope around the design cruise altitude. Thus, the suction pump would be started at an altitude above 6100 m (20 000 ft), operated throughout the cruise portion of the flight, and turned off at about the same altitude during the descent phase.

Both systems would be automated to the extent that actuation of a single control would be required for in-flight operations. Sensors in the trailing-edge region of the laminarized surfaces would be incorporated to provide a real-time indication of the state of the boundary layer.

#### 7.1.3.2 Flight Planning

Consistent with the procedures currently in use by the airlines, flight planning for LFC transports would be required for each flight leg. For each flight, it will be necessary to examine fuel requirements for combinations of primary engine/suction pump failures and establish reserves compatible with the most critical condition. While flight legs covering distances near the design range may require a reduction of the cargo payload, the LFC transport has adequate fuel volume to accommodate any fuel reserve requirement which may result.

Without a reduction of cargo payload, the requirements of FAR 121.645 are satisfied and adequate reserve fuel is carried to allow for loss of LFC due to weather phenomena during three percent of the mission cruise time. Allowances are also made for winds and fuel credibility as recommended in the mission definition study of Section 6.1. A 93 km/hr (50-kn) wind and a 2% fuel penalty account for these factors. The normal international

reserves ground rule of a 370 km (200 n mi) diversion distance was altered to include fuel for 6% of the design range to account for both alternate and track distance allowances. This produces a diversion distance of 722 km (390 n mi).

## 7.2 CONFIGURATION DEVELOPMENT

### 7.2.1 Configuration Variations

During this study, many design options presented themselves as possible candidates for incorporation into the baseline configuration defined in Section 5.3. During an earlier contract (Ref. 5), many of these same options were exercised to minimize block fuel. This contract identified Direct Operating Cost (DOC) as the optimizing parameter. Thus, these and other possible design and configuration variations were exercised to evaluate their impact on DOC.

Table 41 provides a listing of the options considered. In each case, the option was analyzed to assess the effect of the option on the total airplane. Figure 150 provides a graphic display of the DOC impact of the several configuration variations compared to the baseline LFC transport.

Figure 150 shows that none of the configuration variations resulted in a significant reduction in DOC. A majority of the candidates had the opposite effect. Thus, it is apparent that any configuration variation selected for incorporation into the final 1993 LFC transport would be chosen for reasons other than DOC, such as reduced block fuel, ease of aircraft maintenance, and manufacturing facility. Options 9, 12, and 14, in Table 41 have no discernable effect on DOC, thus should be considered for incorporation based on other considerations. A discussion of each and its disposition follows:

- (1) Option 9 - Laminarize the wing only to 75% on both surfaces. To forego laminarization of the empennage surfaces is attractive from both airframe cost and in-service maintenance standpoints in that significant dollar savings are offered. However, these savings are offset by the increase required in block fuel. Thus this option was not selected for incorporation due to the added fuel requirement.
- (2) Option 12 - Include trunk ducts in both leading and trailing edges. This configuration variation provides no fuel savings and it does increase the apparent complexity of the wing structure. While no cost increase could be identified, the option was not selected because of the added complexity with no offsetting improvement.
- (3) Option 14 - Alternate paths for wing box access. No benefits in block fuel nor in manufacturing and maintenance costs are identifiable. Since any lesser benefits could only be identified through in-depth detail study in a later design phase, this option was not incorporated.



TABLE 41. CONFIGURATION VARIATIONS

Option No.	Title	Baseline Aircraft	Variation
1	Alternate Structural Material	Graphite/Epoxy	Aluminum Plate
2	Alternate Structural Material	Graphite/Epoxy	Aluminum Laminate
3	Variation in Slot $R_N$	Variable-Based on Slot Design Criteria	$R_N = 35$
4	Variation in Slot $R_N$	Variable-Based on Slot Design Criteria	$R_N = 100$
5	Variation in Extent of Laminarization	75% Chord, Both Surfaces	25% Chord, Both Surfaces
6	Variation in Extent of Laminarization	75% Chord, Both Surfaces	50% Chord, Both Surfaces
7	Variation in Extent of Laminarization	75% Chord, Both Surfaces	90% Chord, Both Surfaces
8	Variation in Extent of Laminarization	75% Chord, Both Surfaces	90% Chord, Upper Only
9	Variation in LFC Capability	Wing and Tail	75% Chord, Wing Only
10	Alternate Suction Pump Location	Wing Root	At Wing Break
11	Alternate Suction Pump Location	Wing Root	In Aft Fuselage
12	Alternate Trunk Duct Location	Two in Leading Edge	One LE and one TE
13	Alternate Slot Duct Path	Spanwise/Chordwise	Spanwise to Root
14	Alternate Wing Access Means	Through Lower Surface	Through Rear Spar

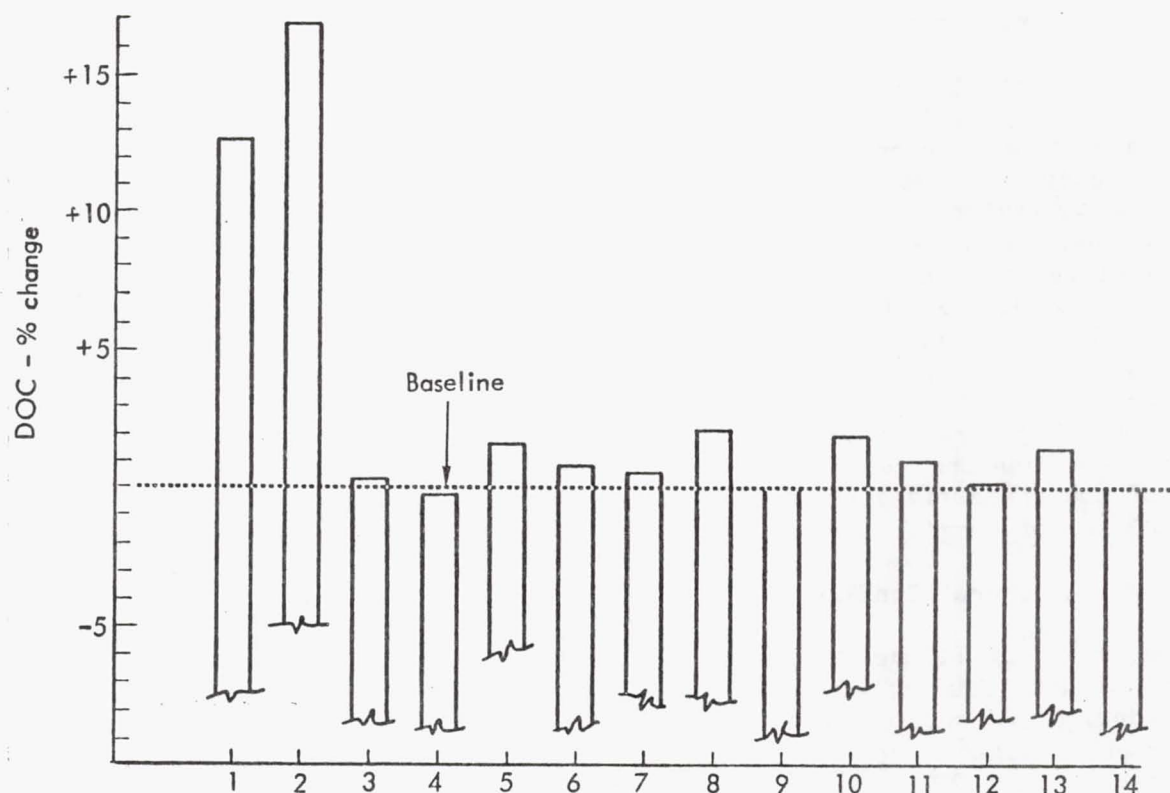


Figure 150. DOC comparison - configuration variations

### 7.2.2 Configuration Selection

In Section 5.3, a baseline LFC passenger transport for the 1993 time frame was defined to satisfy the requirements of the selected mission. This airplane was a 400 passenger low-wing, T-tail configuration with four aft-fuselage mounted engines, designed to cruise at  $M = 0.80$  at 11 582 m (38 000 ft).

Subsequent evaluation of alternative concepts and design options provided no justification for major changes in the baseline configuration. Therefore the final airplane is identical in general arrangement to the previously described baseline. Variations are limited to detail design refinements, a wing area change, operational procedure changes, various items affecting aircraft weight, and the addition of a leading-edge cleaning/de-icing system.

### 7.2.3 Configuration Definition

This section describes the selected LFC transport configuration, including aircraft systems and interfaces between basic aircraft and LFC systems. The details of the aerodynamic configuration, LFC surface design, and LFC systems characteristics are given in Section 6.0.

### 7.2.3.1 General Arrangement

The selected LFC configuration is shown in Figure 151. This airplane is a wide-body configuration designed to carry 402 passengers and their baggage over an intercontinental range of 12 038 km (6500 n mi) at  $M = 0.80$  with adequate fuel to account for adverse winds, intermittent LFC disruption due to atmospheric conditions at cruise altitude, and normal international fuel reserves. A typical cabin arrangement, shown in Figure 152, was developed for the basic purpose of sizing the fuselage. This arrangement accommodates a 10/90 passenger mix, with 40 in first class and 362 in tourist class cabins. Space allowances are made for galleys, lavatories, closets, cabin crew provisions, as well as rest areas for flight crew as dictated by FAR Part 121.485 for flight of more than 12 hours duration. Space for LD-3 cargo containers is provided forward of the wing box and aft of the main landing gear bay. A bulk cargo bay is also provided at the rear of the pressurized belly. These cargo bays will accommodate 16 874 kg (37 000 lb) of cargo.

### 7.2.3.2 Structural Configuration

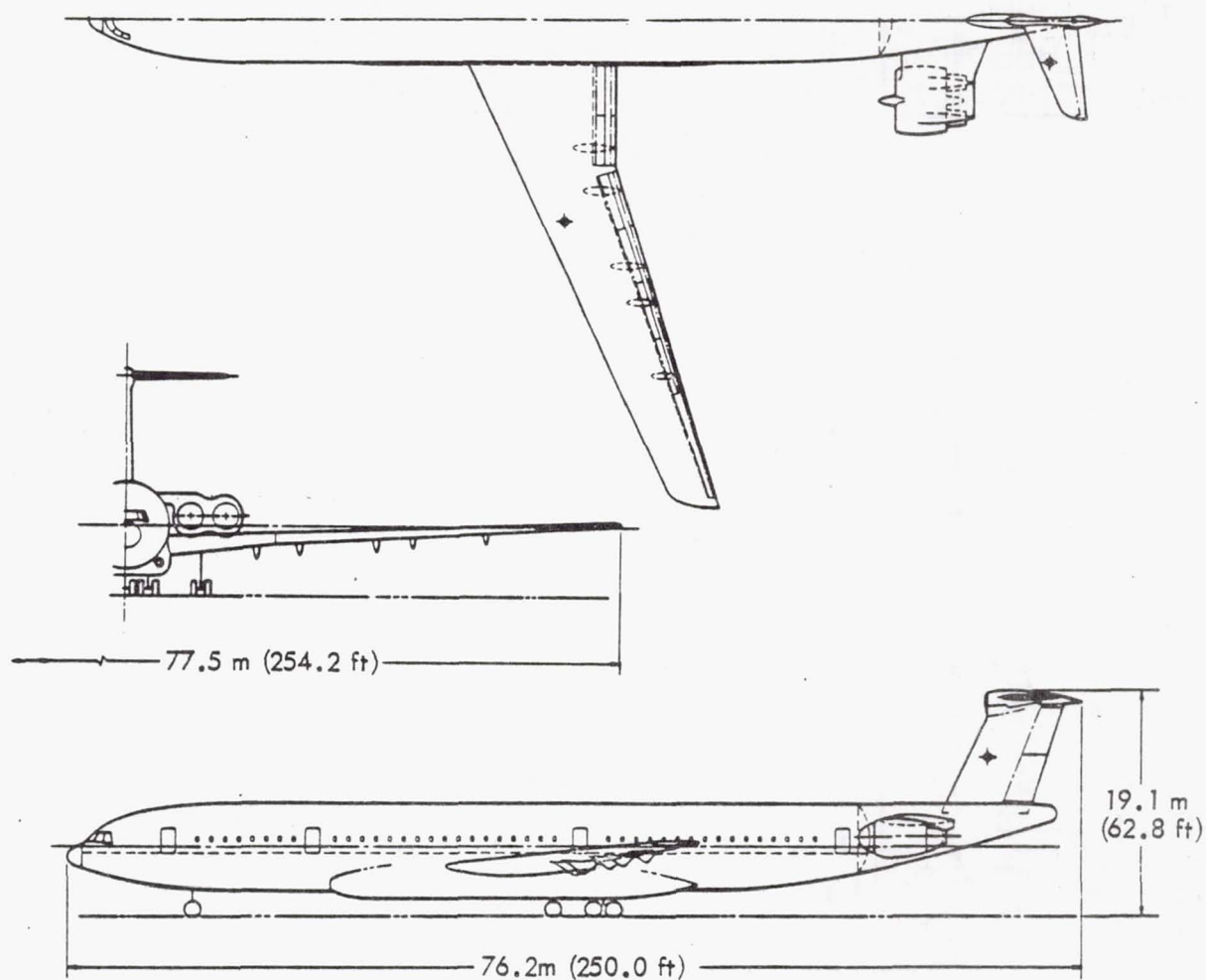
As shown in Figure 151, the baseline airplane is a low-wing T-tail monoplane with four aft-fuselage mounted propulsion engines. An independently-driven LFC suction unit is located in a fairing under each wing root as shown in Figures 153 and 154. The airplane and its power plants are designed to meet NPRM 75-37c proposed revisions to FAR Part 36. Fuel is carried in the wing including the wing center-section box.

The wing has a moderate sweep of .436 and  $(25^\circ)$  at the leading edge with an aspect ratio of 11.6. Full-span flaps, including drooped ailerons, provide the required airport performance. Leading-edge high-lift devices are not required. Partial span spoilers are incorporated as required. A structural arrangement of the wing is shown schematically in Figure 155. Small-chord secondary flaps shown in Figure 156, incorporated into the main flaps, provide upper surface pressure gradient and shock position control for off-design operation as well as serving as active controls to minimize structural requirements.

LFC suction capability is provided on both wing surfaces from 0 to 75% chord. A wing cross-sectional view, Figure 157, shows the hat-stiffened surface panels with the integrated surface slots and ducting. The removable nose cap incorporates a system of chordwise suction slots with sub-surface compartments incorporated to control the rapidly changing pressure gradients existing over the extreme leading-edge surface region. A combination de-icing, cleaning system is also incorporated in the leading edge region. This system is a pressurized liquid dispersal system providing the dual functions.

Figure 158 depicts schematically the structural arrangement of the empennage. In cross-section, the empennage components are constructed in similar fashion to the wing elements shown in Figure 157. LFC suction capability is provided on all four empennage surfaces from 0 to 65% chord. A liquid dispersal system for surface cleaning, similar to that described for the wing, is incorporated in both vertical and horizontal tail leading edges.





	Area	AR	Sweep	Taper
Wing (base)	491.7 m <sup>2</sup> (5293.0 ft <sup>2</sup> )	11.60	L.E. .436 rad (25°)	.350
Horizontal	50.2 m <sup>2</sup> (540.3 ft <sup>2</sup> )	5.00	1/4 Ch .349 rad (20°)	.400
Vertical	62.5 m <sup>2</sup> (672.6 ft <sup>2</sup> )	1.50	1/4 Ch .436 rad (25°)	.800
TOGW	268 624 kg (592 205 lb)			
Engine	149 kN (33 540 lb)			

Figure 151. General arrangement

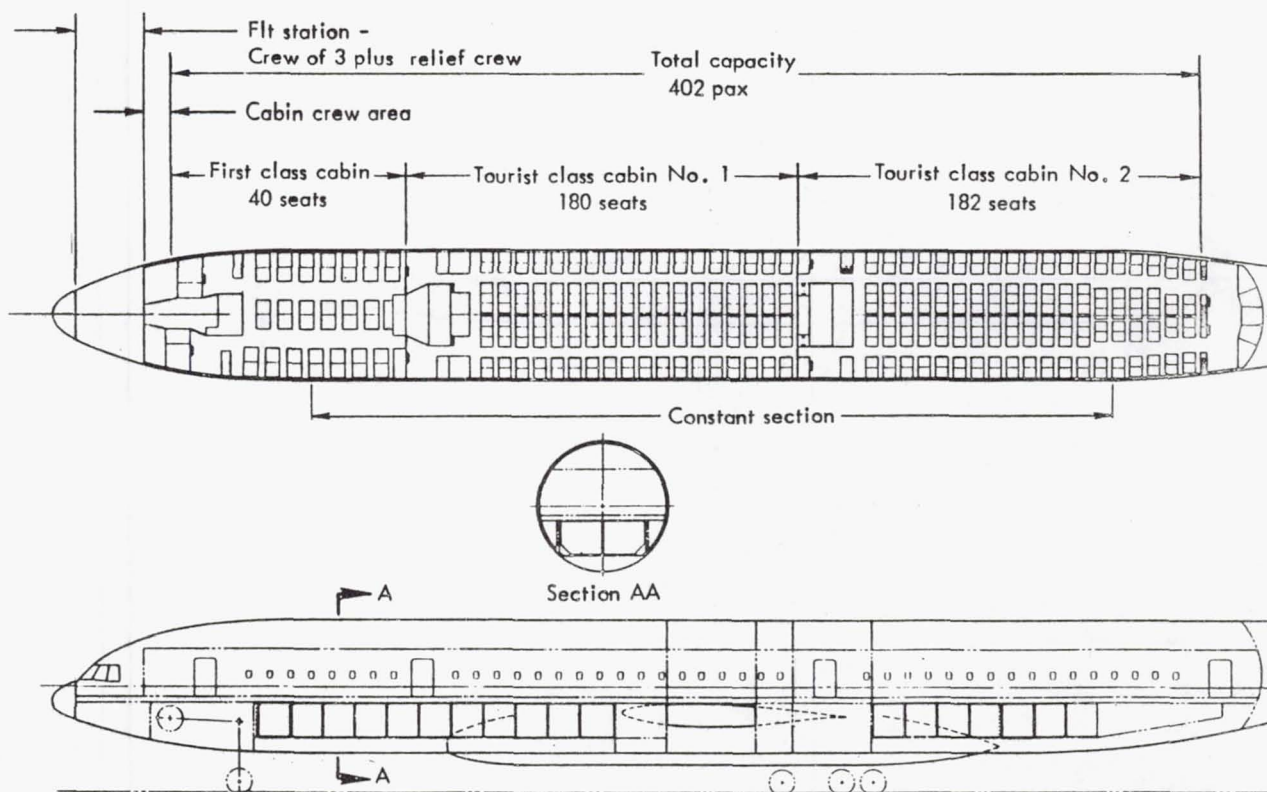


Figure 152. Inboard profile

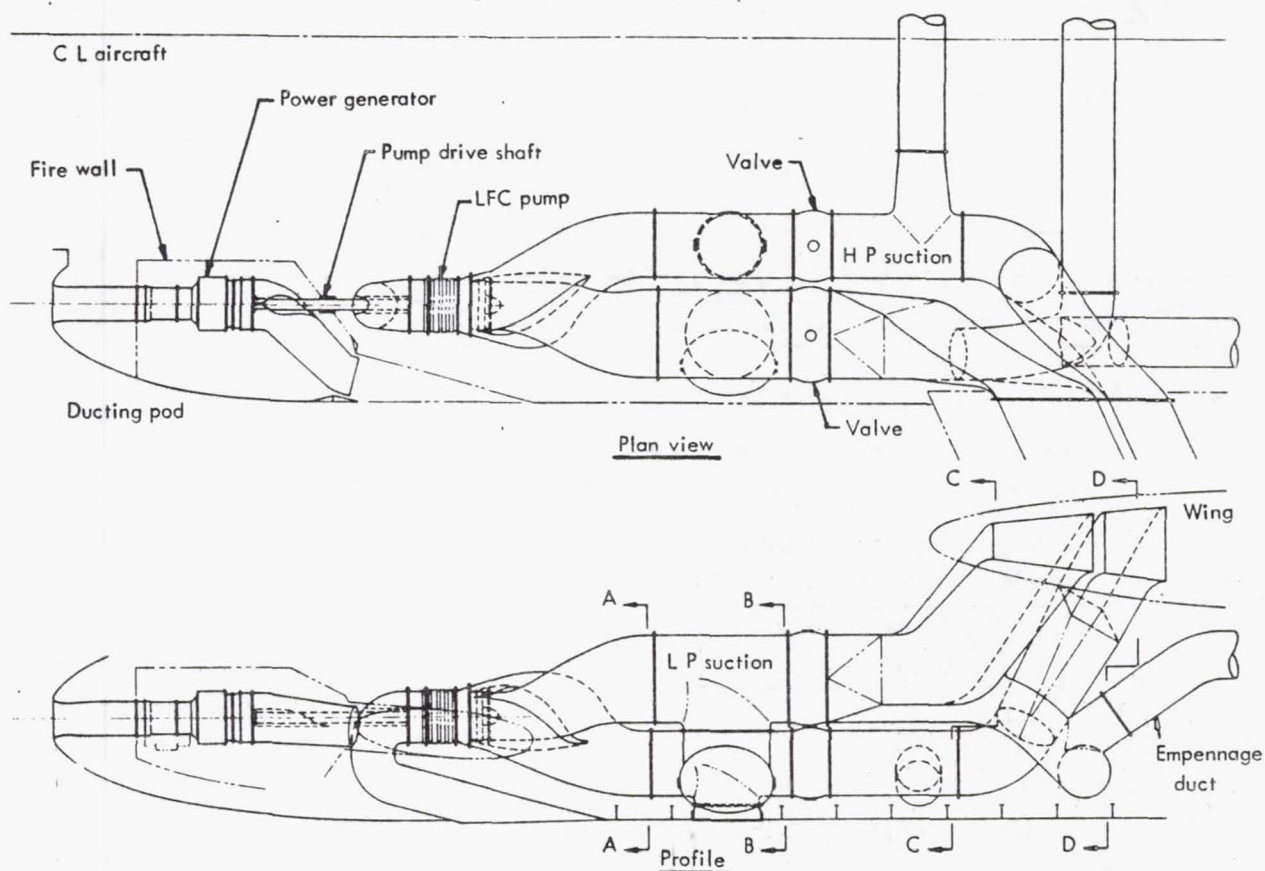


Figure 153. Ducting arrangement for fuselage-mounted LFC suction units

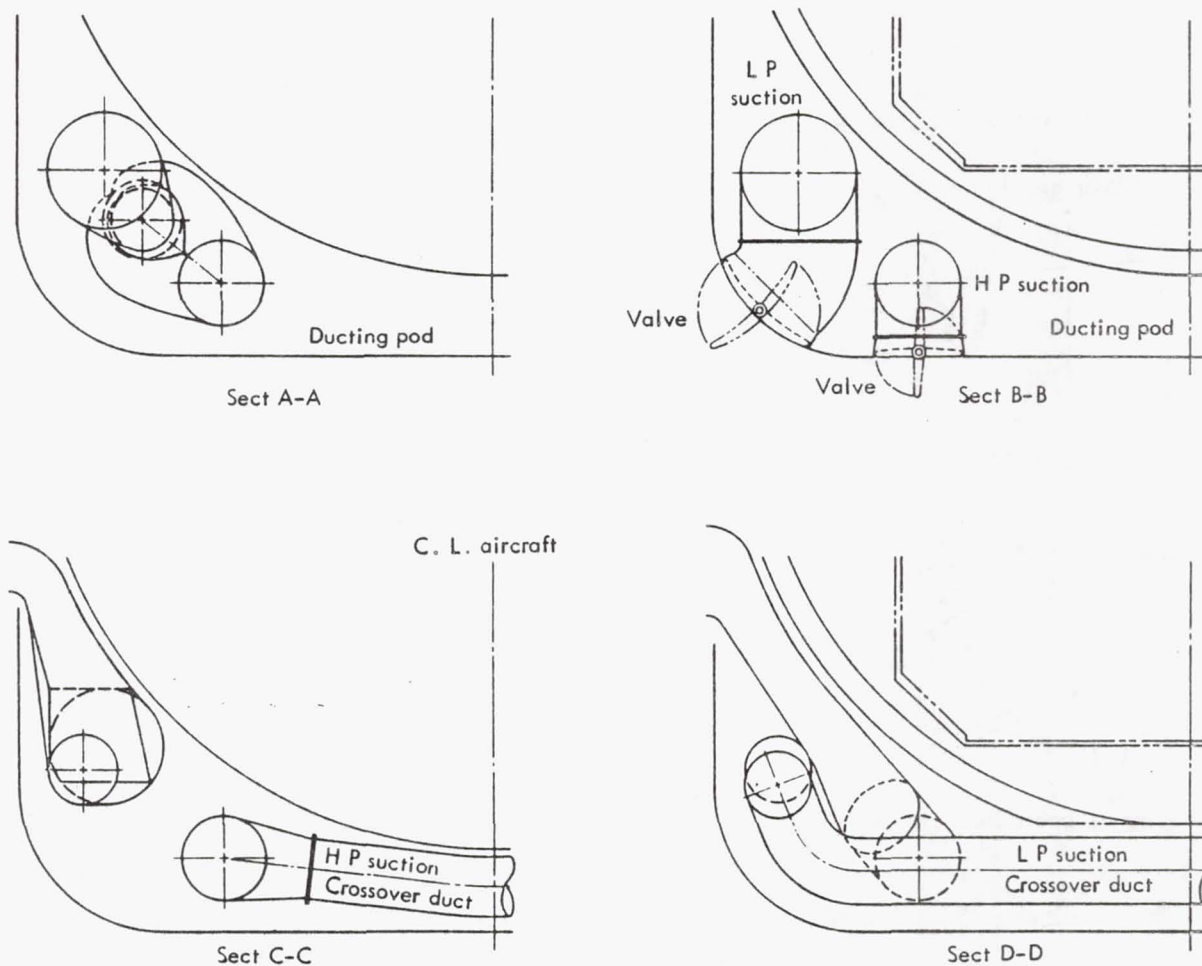


Figure 154. Ducting arrangement section cuts

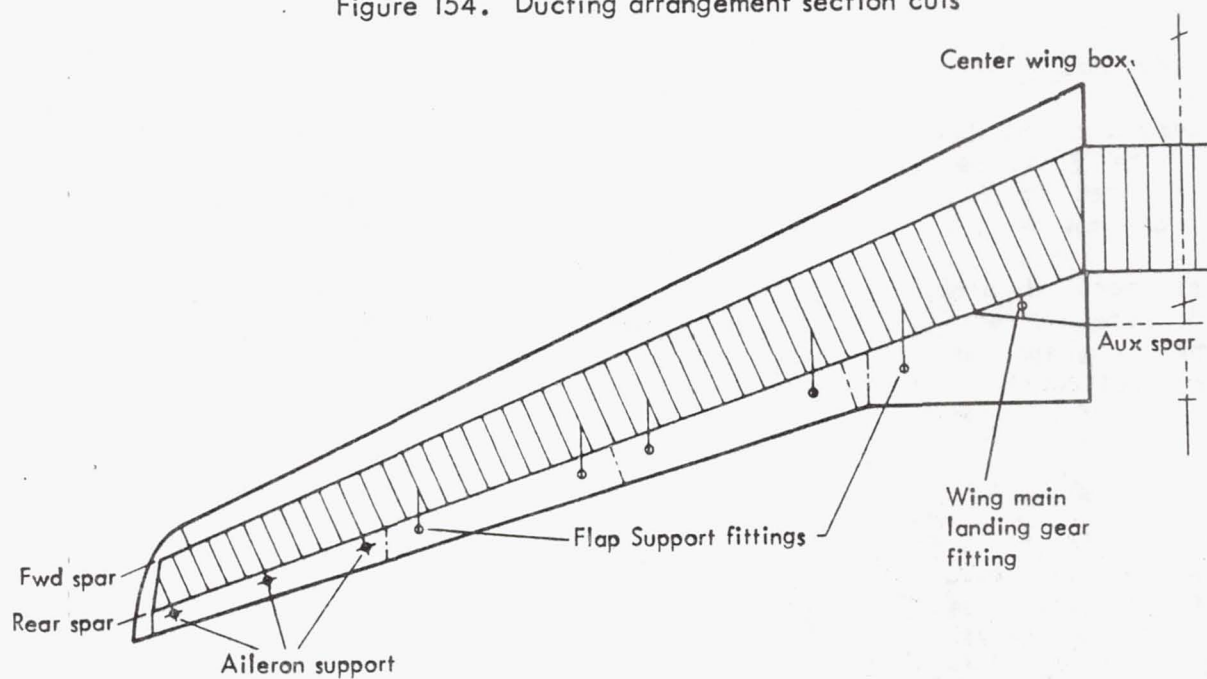


Figure 155. Wing structural arrangement



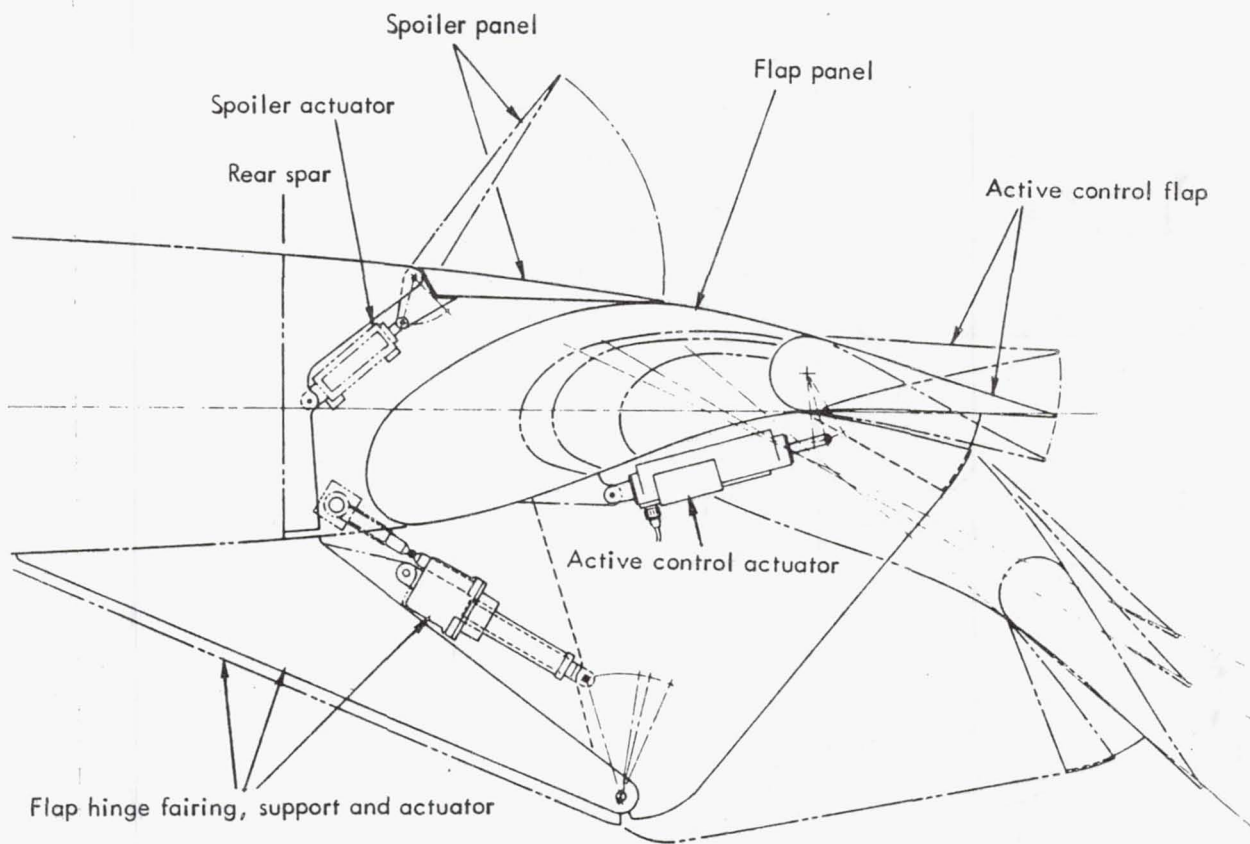


Figure 156. Trailing-edge flaps and spoiler arrangement

#### 7.2.3.3 Systems

Systems for the LFC aircraft logically fall into two distinct categories. The first category includes aircraft systems which are not directly affected by LFC, while the second category encompasses the systems required to provide LFC to the airplane.

Development of aircraft systems not impacted by LFC are beyond the scope of the current contract. Thus, the systems described in the following paragraphs are assumed to be representative of the state-of-the-art predicted to be available by 1990. Section 4.6 provides detailed descriptions of LFC-required systems.

#### Propulsion

The propulsion system is comprised of four engines with inlets, cowlings, exhaust ducting, thrust reversers and associated equipment. Two propulsion units, based on Pratt and Whitney STF 477 advanced engine technology, are siamese-podded, as shown in Figure 159, on either side of the aft fuselage. Gear boxes and accessories are located external to the fan case. The lower portions of the engine pod open for easy access to the engine and accessories.

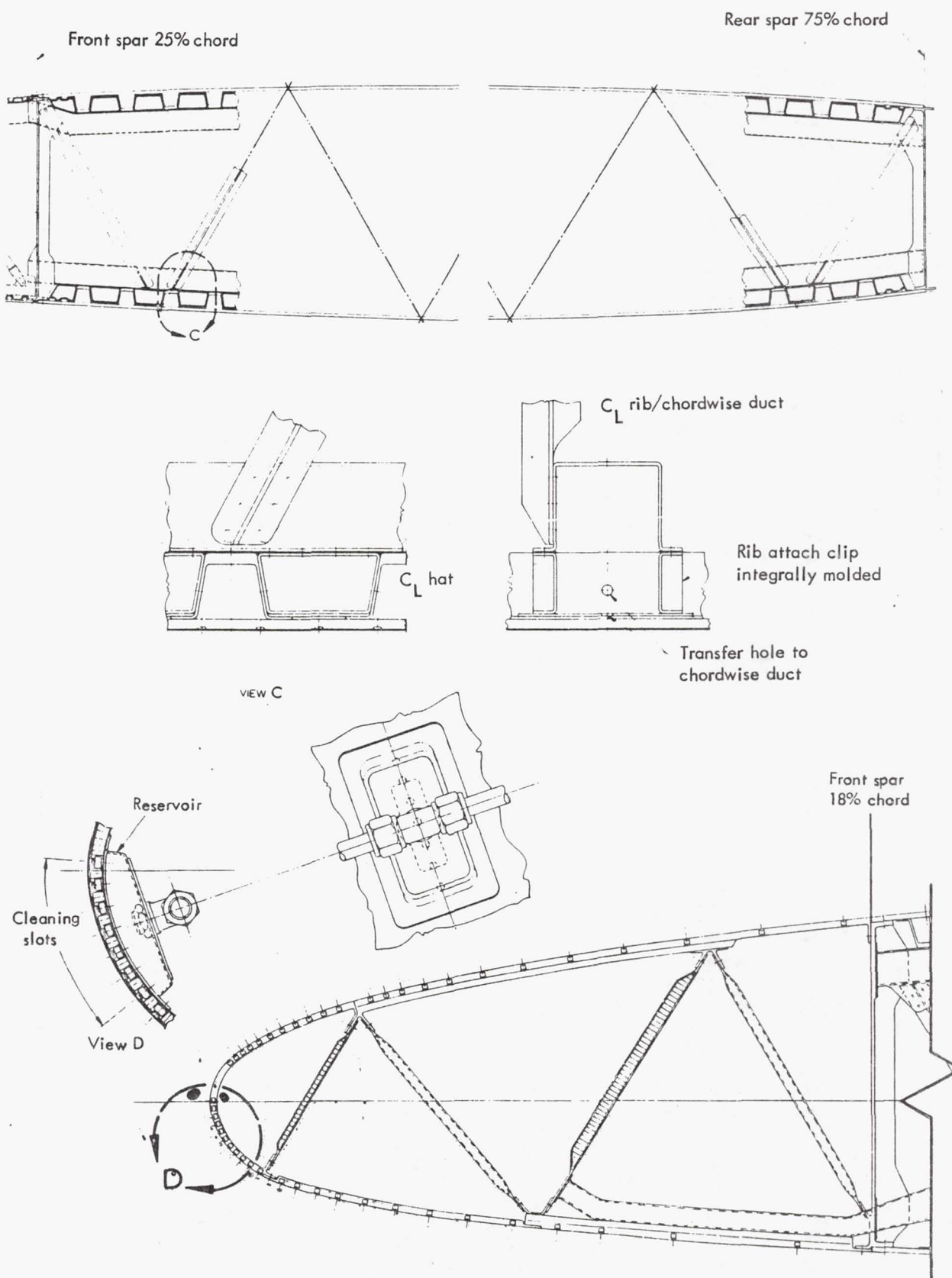


Figure 157. Wing cross-section

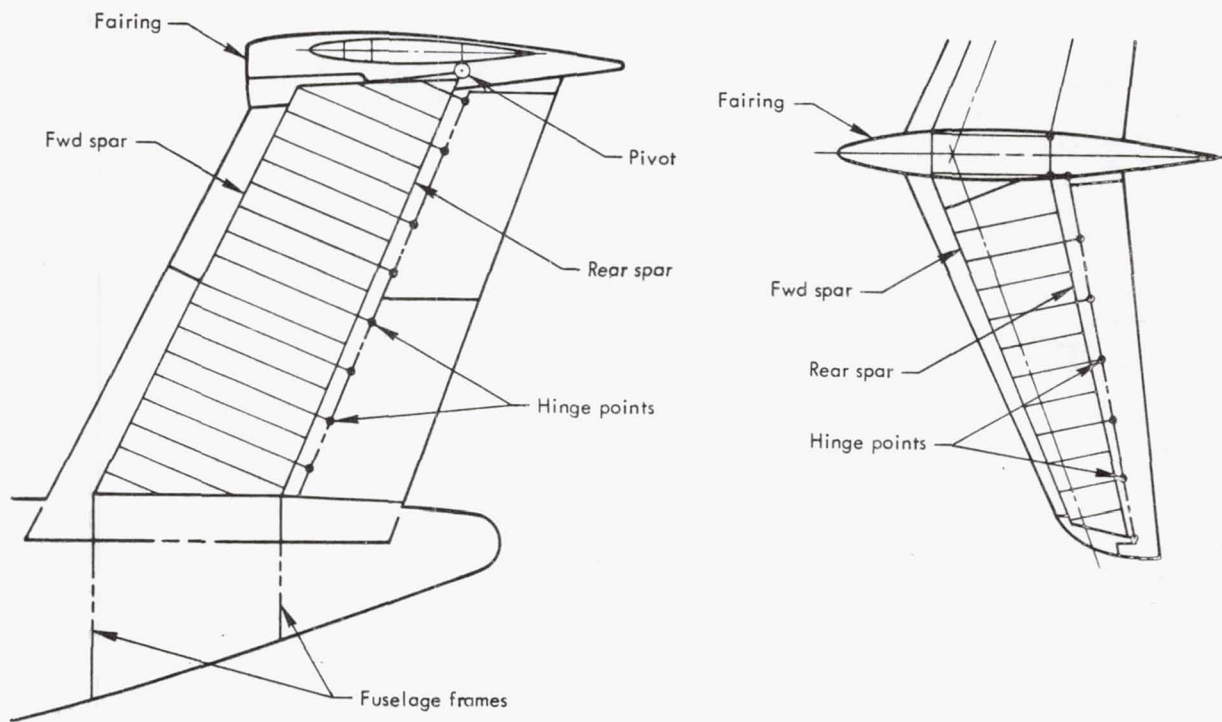


Figure 158. Empennage structural arrangement

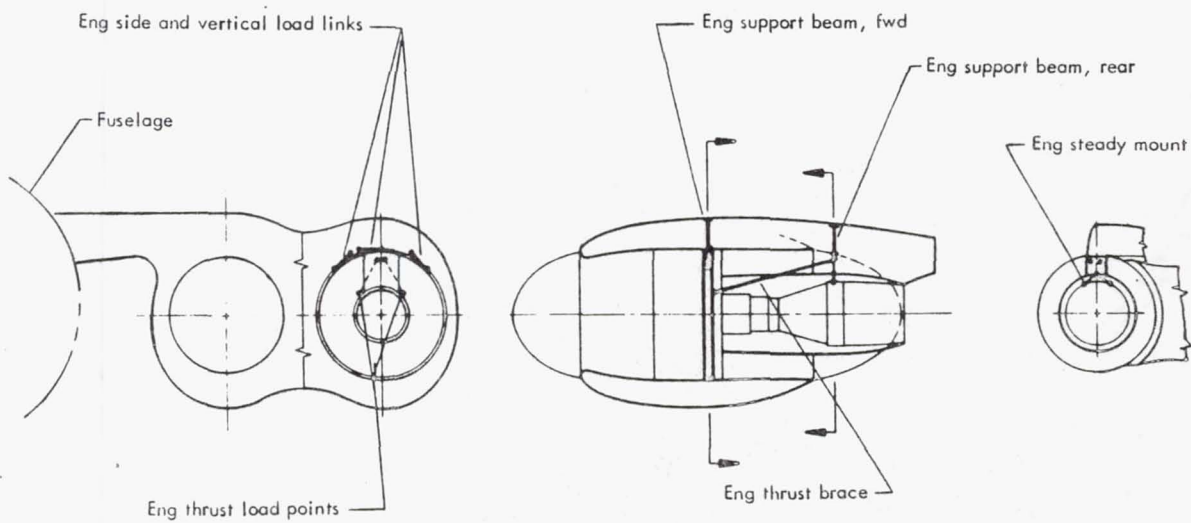


Figure 159. Power plant installation



## High Lift

The high-lift system consists of single-slot, hinged, full-span flaps. The extreme outboard portion of the flap is provided by "drooping" the aileron. The inboard flaps have a constant chord of 1.78m (5.83 ft), while outboard the flaps are 23% chord. The flaps are hydro-mechanically operated and controlled by a single pilot input. Flap position indication and a system to preclude asymmetrical operation are provided.

Built into the main flaps are 9.5%-chord secondary flaps over the entire span. The secondary flaps operate with the flaps in high-lift mode or separately from the flaps as part of the active control system described in Section 4.5. The secondary flaps are actuated in the active control mode by electro-hydraulic servo units controlled by the onboard fly-by-wire computer system.

## Flight Controls

The flight control system consists of controls for horizontal stabilizer and elevators, rudder, and drooped ailerons. The system is designed as a fly-by-wire (FBW) system with each primary control surface driven by multiple duplex (electro-hydraulic) on-line integrated servo units. The FBW system incorporates active control technology (ACT) which promises significant improvements in the efficiency of large transport aircraft.

The ACT system encompasses the following modes of control:

- o Relaxed Static Stability
- o Stability Augmentation System - all three axes
- o Maneuver Load Control
- o Gust Load Alleviation
- o Flutter Mode Control
- o Ride Control

The major improvements offered by the above systems are: minimum airframe weight with the attendant fuel savings or range increase, capability for automatic trouble-shooting, and smoother airplane ride characteristics.

The four-channel FBW system is controlled on each channel by an on-board digital computer. A digital system is mandated by the extensive complex signal processing, the flexibility required to accommodate the multi-mode control logic laws, and the redundancy required by an FBW system.

Geared elevators driven by the stabilizer, a double-hinged rudder, and outboard ailerons provide low-speed control. Ground-operable-only spoilers are provided for deployment during ground rollout or rejected takeoff. All

controls and instrumentation required for the operation of the airplane in the air and on the ground are located in the flight station. The on-board computers provide feedback for two hydro-mechanical units which provide the pilots with artificial feel in all three control axes.

### Landing Gear

The landing gear system is comprised of a two-wheel nose gear and a four-strut 12-wheel main gear. The main gear is configured as follows:

- o Two wing-mounted struts with two wheels each which retract inboard into the fuselage belly, as shown in Figure 160.
- o Two fuselage-mounted struts with four wheels each which retract forward into the belly, as shown in Figure 161.

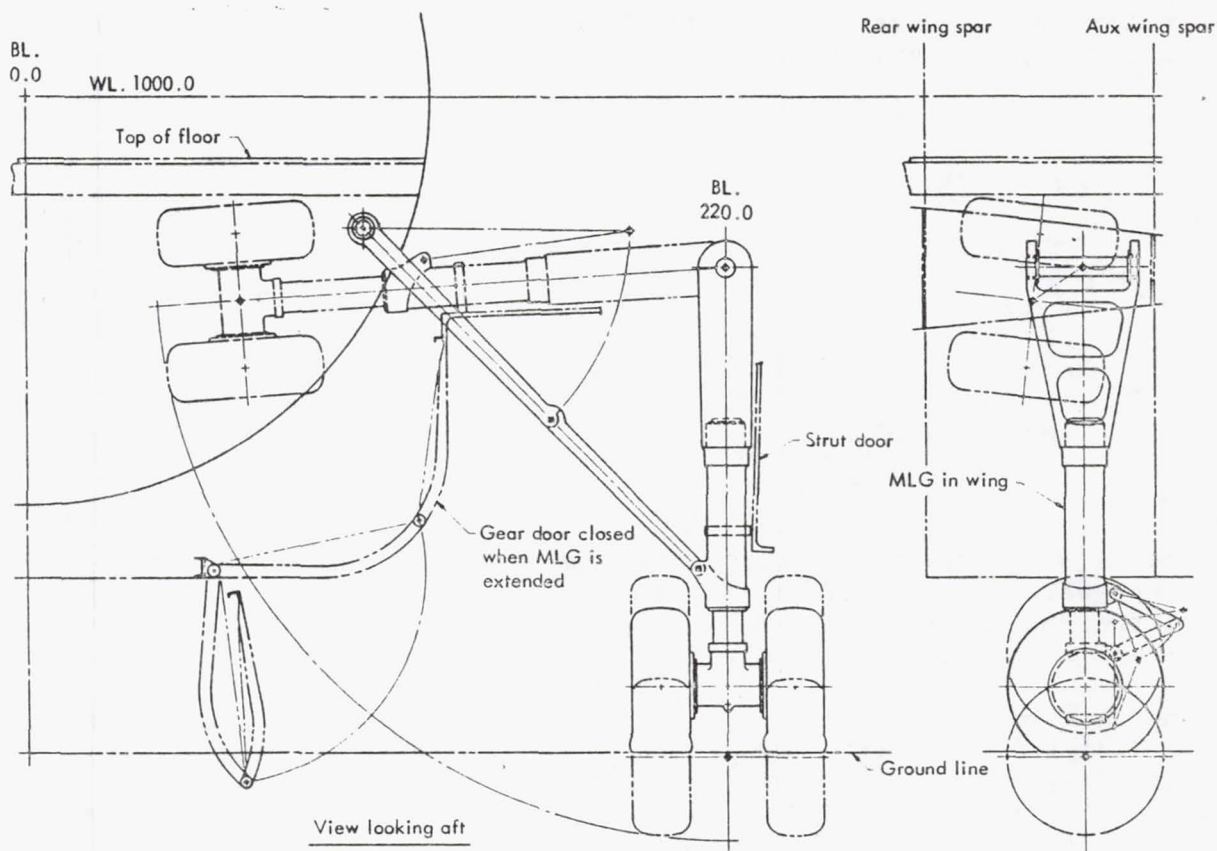


Figure 160. Wing-mounted main landing gear

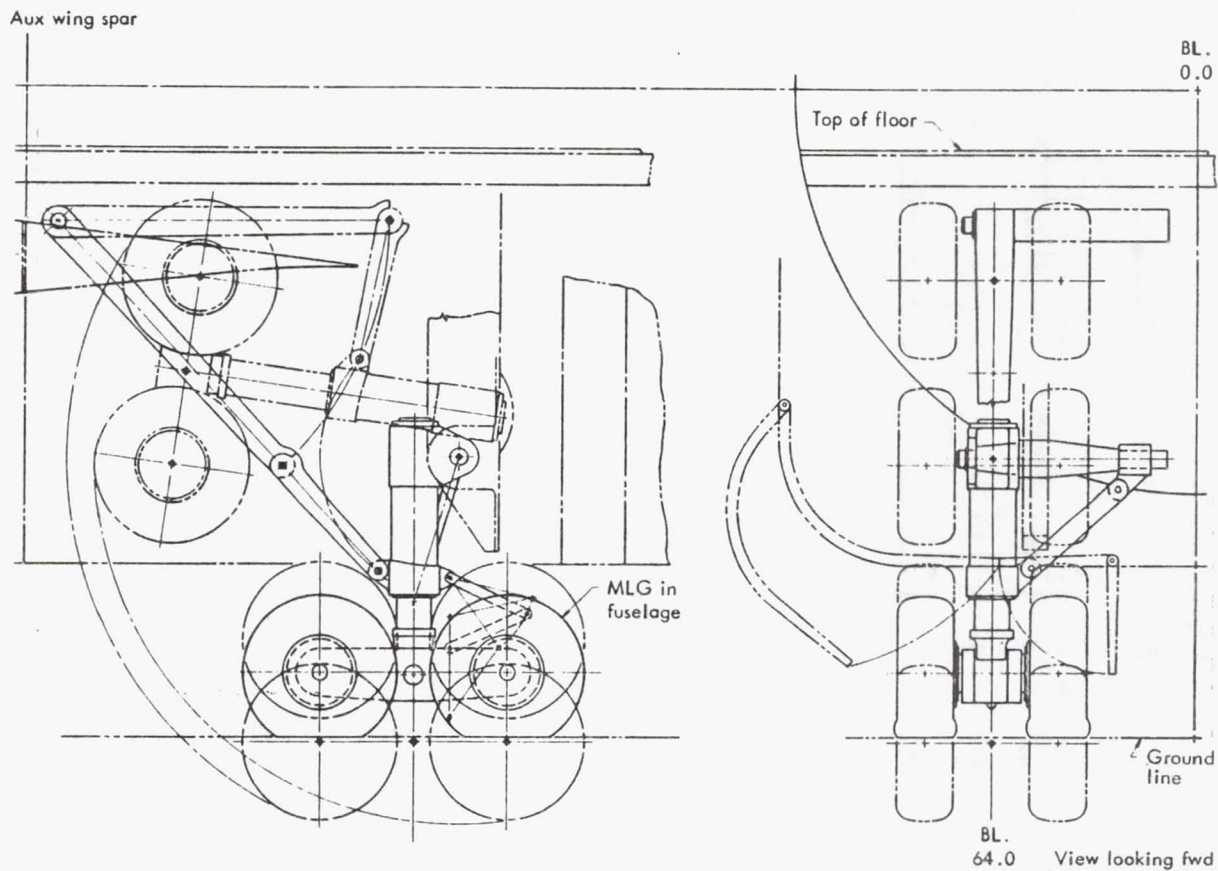


Figure 161. Fuselage-mounted main landing gear

The nose gear strut retracts forward into the belly. No form of directional steering or swivelling is employed on the main gears. Hydraulically powered nose gear steering controlled by the captain's handwheel is provided.

### Subsystems

The primary aircraft functional systems are separated into individual localized service centers throughout the airframe. There is a discrete service center for the hydraulic, environmental, electrical, electronic, and fuel systems. Each system maintains interface with the cockpit through necessary instrumentation and controls.

**Hydraulic** - The hydraulic system consists of four separate and independent systems, each system powered by two pumps. One pump is driven by a propulsion engine, and the other pump is driven by an air motor powered by engine bled air. An auxiliary system is powered by an APU while an emergency system pump is powered by a ram air turbine to provide inflight power in case of total engine failure. System operating pressure is anticipated to be in a higher range than used in current transports. A schematic of a conceptual hydraulic supply system is shown in Figure 162, while the hydraulic distribution system is shown schematically in Figure 163.



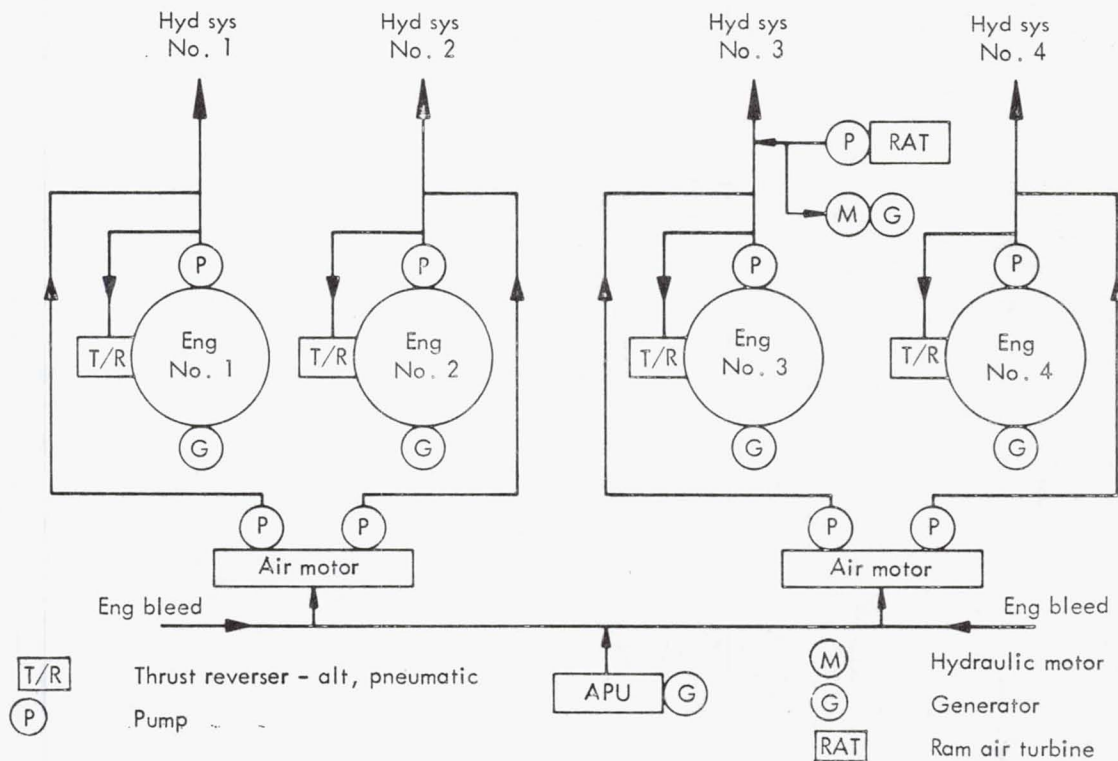


Figure 162. Schematic of hydraulic supply system

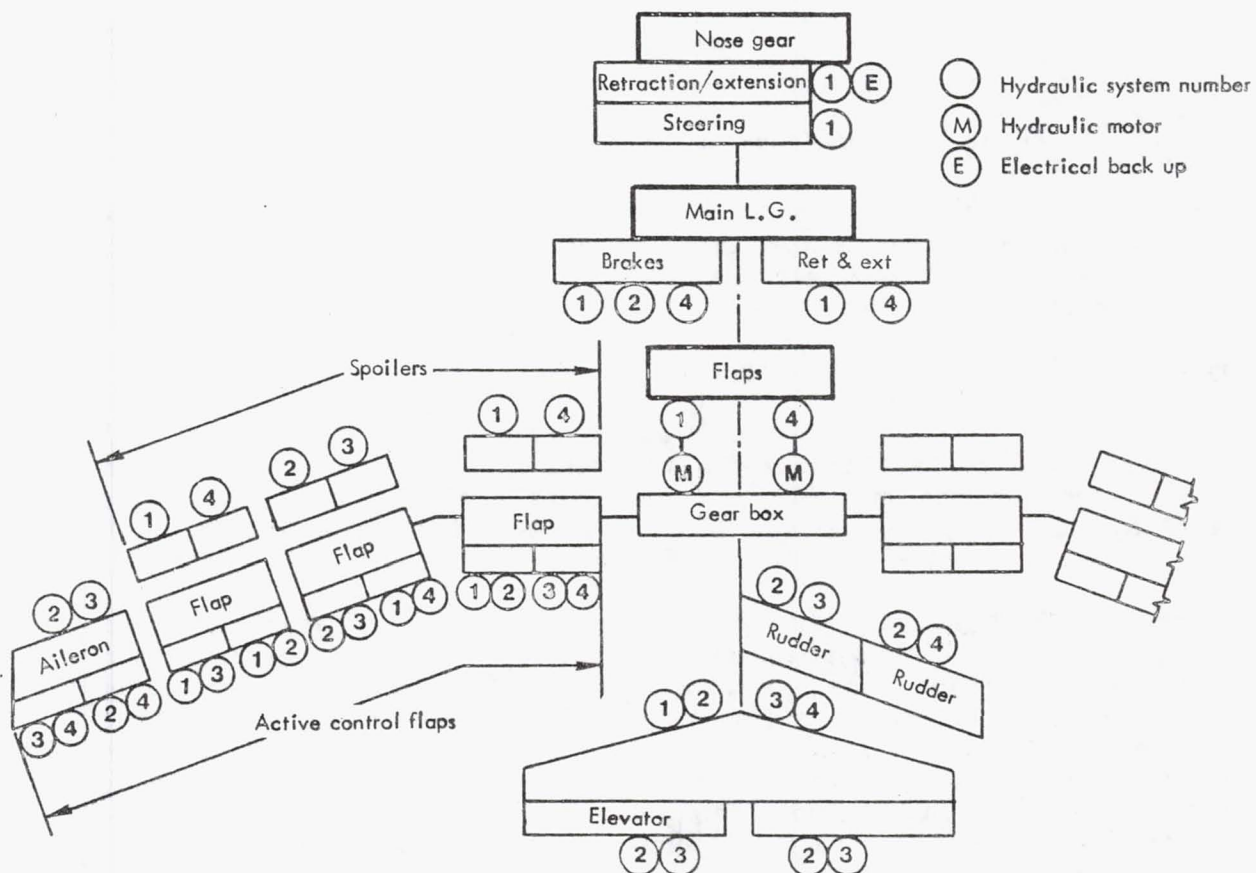


Figure 163. Schematic of hydraulic distribution

Environmental - The environmental system provides for passenger comfort during ground and inflight operations. The system consists of air-cycle refrigeration packs that condition compressed air extracted from all four propulsion engines to provide cabin ventilation and control of cabin temperature and pressure. An auxiliary power unit provides compressed air for ground air conditioning and can also provide supplemental air conditioning as required during takeoff, climb, descent, and landing.

The oxygen subsystem comprises the crew oxygen system and the passenger supplemental oxygen system. The systems are independent. The crew system is a low-pressure system providing flow to eight flight deck stations. Also included in the crew system is a portable cylinder providing free oxygen for emergency or first aid breathing. The passenger supplemental oxygen system comprises a series of chemical oxygen generators manifolded to drop-out masks at each passenger seat. Portable continuous flow units are also dispersed throughout the cabin to meet emergency conditions.

Electrical - Electrical power required for communications, navigation, passenger comfort, and other functional systems is provided by integrated constant-speed-drive, brushless AC generator units mounted on each engine. An auxiliary integrated-drive generator unit is mounted on the APU to provide ground electrical power and supplemental power in flight. An emergency generator unit driven by a hydraulic motor powered by the ram air turbine is provided.

Electronics - The electronics system comprises communications, navigation, passenger communications, and avionic flight controls required to operate a commercial passenger airplane over world-wide international routes.

Fuel - The fuel system is comprised of two main tanks and one auxiliary tank in each wing. An additional auxiliary tank is located in the center wing box within the fuselage. Each main tank feeds one main engine. LFC suction pump power units are fed from the center auxiliary tank. Fuel is transferred from the auxiliary tanks to the main tanks as required. A schematic of a conceptual fuel system is shown on Figure 164.

All fuel system components, including boost pumps, fuel probes, and fuel level control valves are removable from outside the lower wing surface. Access into the fuel cells for inspection, maintenance, and repair of wing structure and tanks is provided through access doors in the lower wing surface. Ground pressure fueling is accomplished from the main landing gear wheel well.

#### 7.2.4 Configuration Performance

##### 7.2.4.1 Mission Profile

The mission profile chosen for basic sizing of the configuration is defined by Figure 6. Since step-climb techniques cannot always be utilized because of air traffic control requirements, a constant cruise altitude of 11 582 m (38 000 ft) and cruise Mach number of 0.80 were chosen for missions presented. Requirements of FAR 121.645 are satisfied and, in addition, adequate reserve fuel is carried to allow for loss of LFC due to

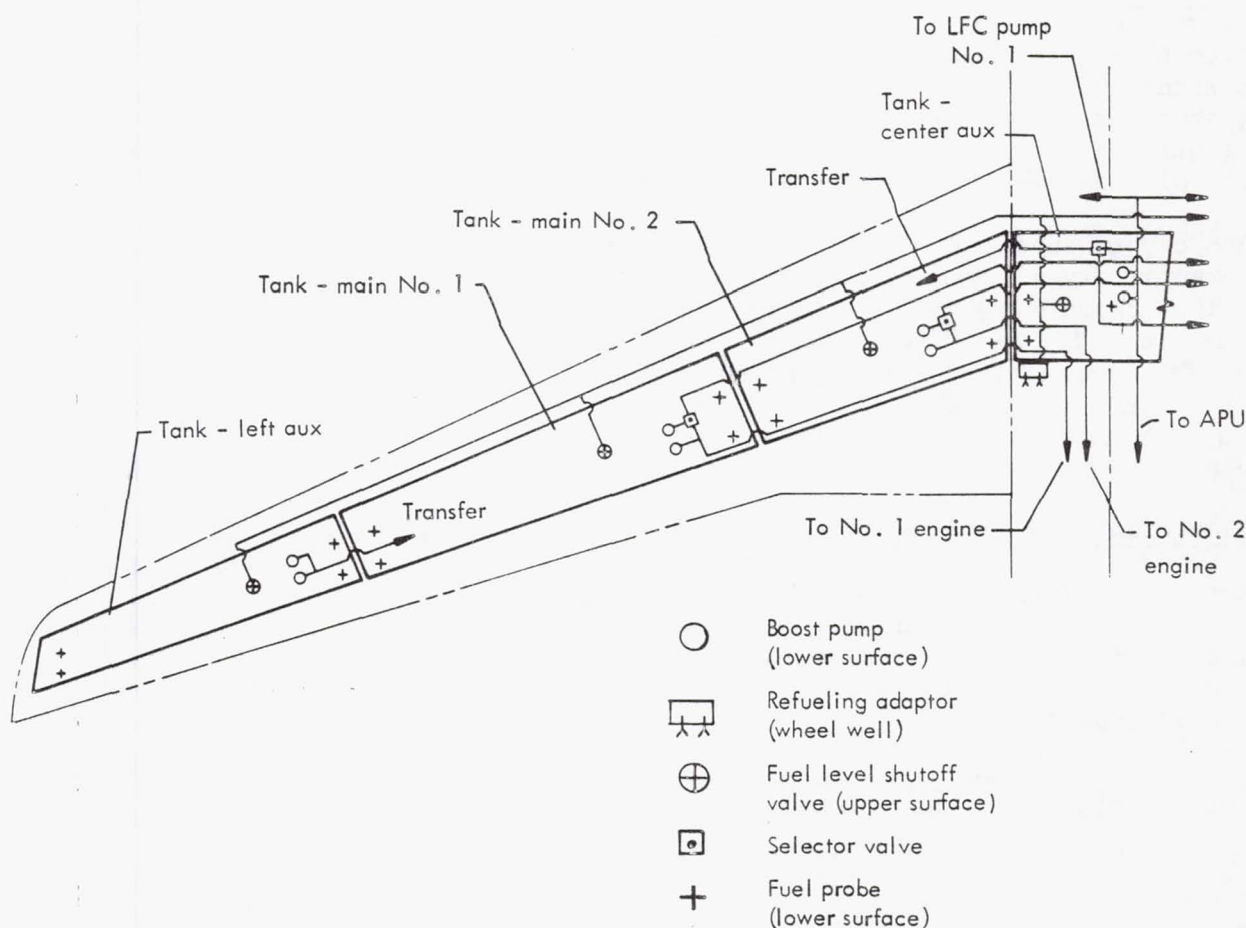


Figure 164. Schematic of aircraft fuel system

weather phenomena during three percent of the mission cruise time. Allowances are also made for winds and fuel tolerance as recommended in the mission definition study of Section 5.1. A 93 km/hr (50-kn) wind and a two percent fuel penalty account for these factors. The normal international reserves ground rule of a 370 km (200 n mi) diversion distance was altered on the basis of Section 5.1 to include fuel for six percent of the design range to account for both alternate and track distance allowances.

#### 7.2.4.2 Airport Performance

The full-span flaps and drooped ailerons described in Section 7.2.3 provide adequate maximum lift and lift/drag characteristics at a takeoff flap setting of 0.576 rad (33 deg) and landing flap setting of 0.873 rad (50 deg). These settings provide a  $C_{L_{Max}}$  of 2.18 for takeoff and 2.45 for landing. At maximum takeoff weight an engine-out second segment climb gradient of 0.03 is available during takeoff.

FAA field lengths were determined for the total range of aircraft gross weights and are presented in Figure 165. Landing results presented are for maximum braking and do not include use of thrust reversers. Ground operation of the spoilers was assumed.



### 7.2.4.3 Cruise Performance

Aircraft payload/range capabilities are summarized in Figure 166 for cruise at the design Mach number of 0.80 and altitude of 11 582 m (38 000 ft). Several mission points in the payload/range envelope were examined for comparison with the basic design point and are indicated by the circles labeled 1 through 6. Significant data for these missions are compared with the design point in Table 42.

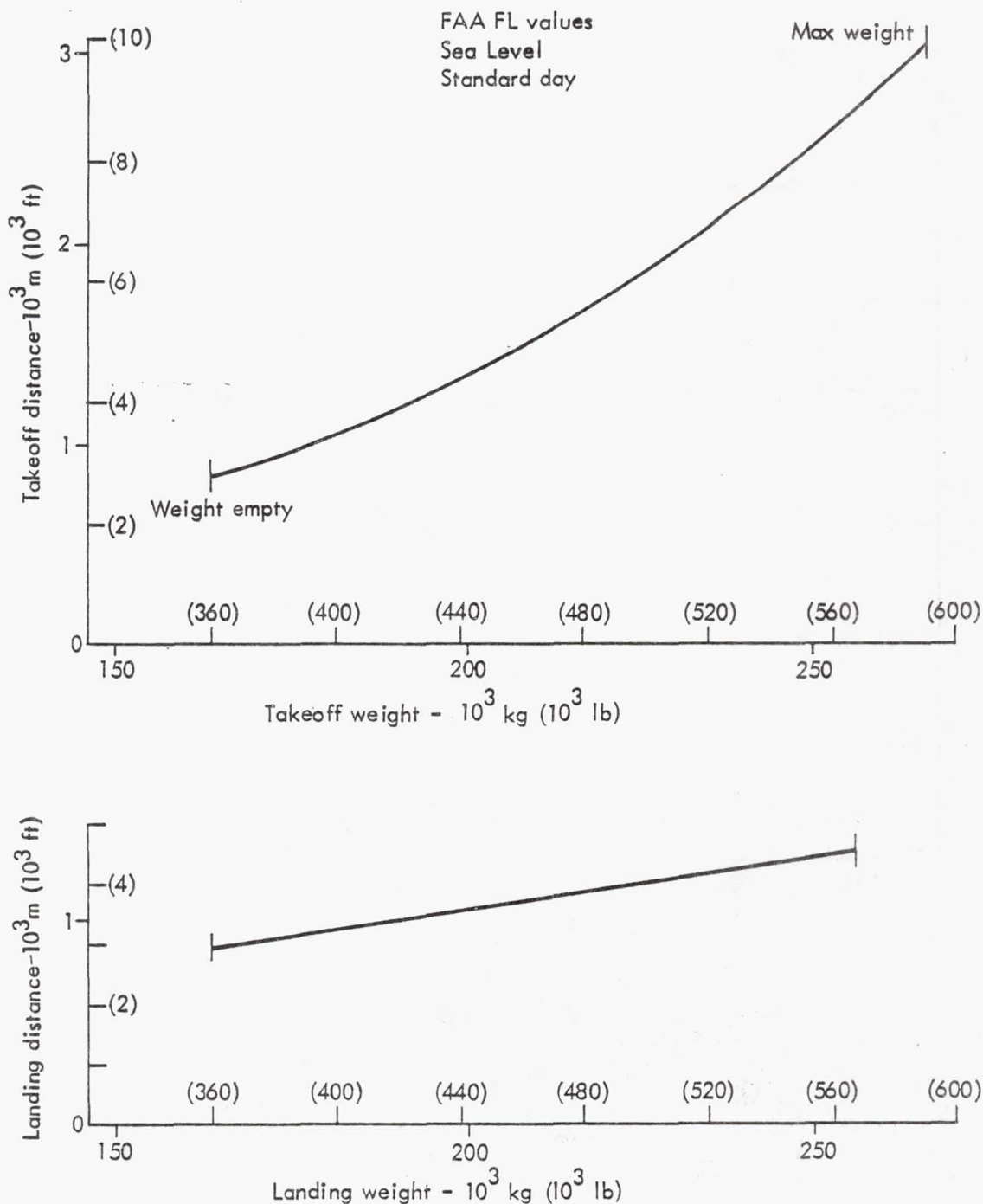


Figure 165. Airport performance

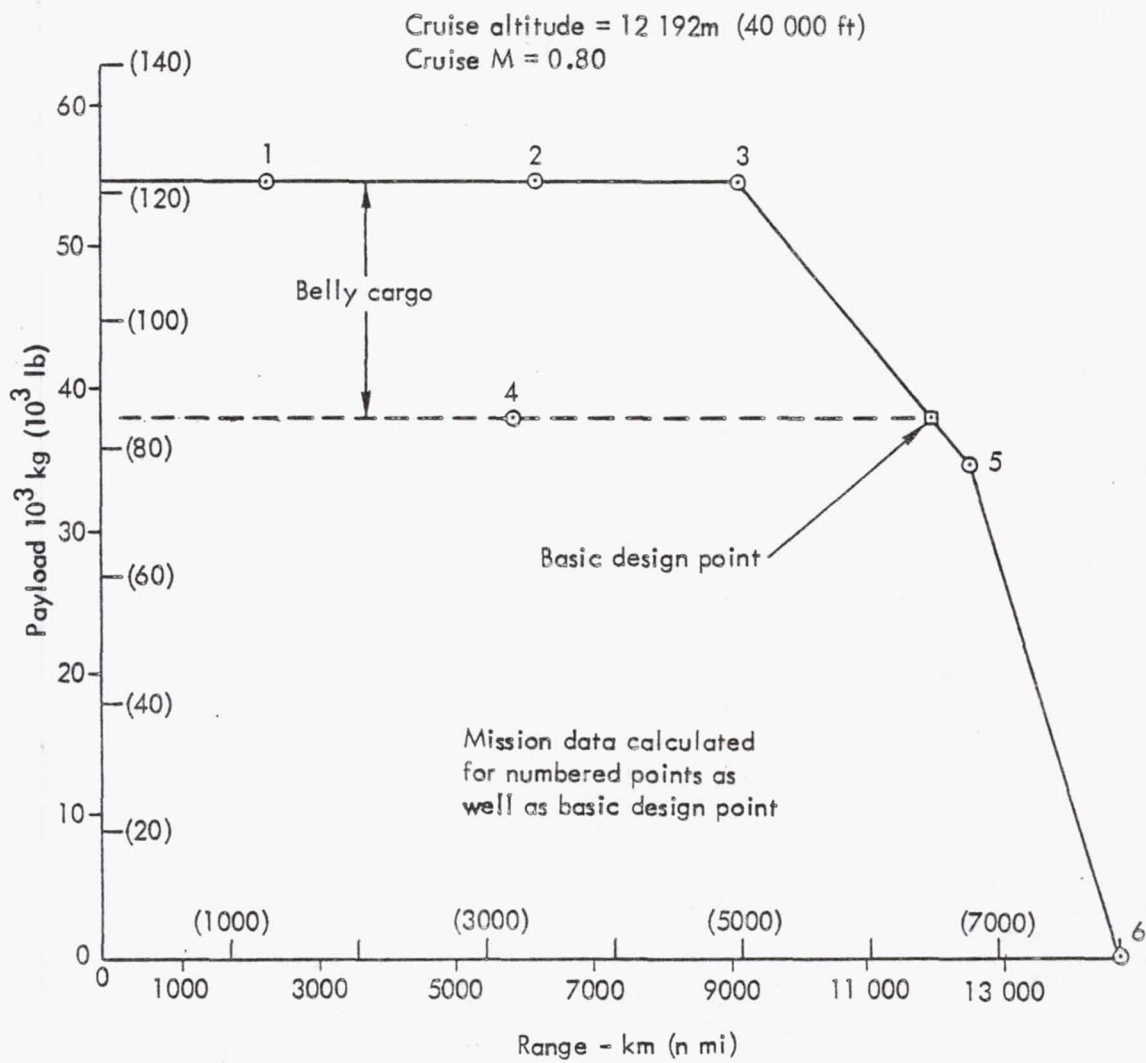


Figure 166. Payload/range

TABLE 42. PERFORMANCE FOR TYPICAL MISSIONS - LFC TRANSPORT

Cruise Altitude = 11 582 m (38 000 ft)

Cruise M = 0.80

Fuel Weight = .80 kg/l (6.70 lb/gal)

Mission No.	No. Passengers	Belly Cargo kg (lb)	Block Range km (n mi)	Block Time (hr)	Ramp Weight kg (lb)	Takeoff Distance m (ft)	Cruise Fuel Efficiency skm/l (snm/gal)	Average Fuel Efficiency skm/l (snm/gal)
*	400	0	12 049 (6 506)	16.20	268 624 (592 205)	3 050 (10 008)	50.3 (102.8)	47.1 (96.3)
1	400	16 874 (37 200)	2 445 (1 320)	3.50	216 435 (477 149)	1 615 (5 300)	55.0 (112.5)	44.1 (90.1)
2	400	16 874 (37 200)	6 312 (3 408)	8.62	244 764 (539 603)	2 323 (7 620)	51.3 (104.8)	46.2 (94.5)
3	400	16 874 (37 200)	9 277 (5 009)	12.54	268 624 (592 205)	3 050 (10 008)	49.0 (100.2)	45.2 (92.3)
4	400	0	6 026 (3 254)	8.23	232 162 (489 776)	2 045 (6 710)	54.8 (112.0)	49.6 (101.4)
5	366	0	12 601 (6 804)	16.93	268 204 (592 205)	3 050 (10 008)	46.2 (94.5)	43.4 (88.8)
6	0	0	14 716 (7 946)	19.71	235 038 (518 140)	2 054 (6 740)		

The cruise performance, as indicated by the fuel efficiency factor is very good for the aircraft even at low mission ranges. At ranges less than the 12 038 km (6500 n mi) design range, takeoff performance rapidly improves. At the stage length for direct operating cost (DOC) optimization (3254 n mi) takeoff field length is only 1740 m (5710 ft).

Sensitivity of range to intermittent loss of LFC was determined for the basic design point takeoff weight, payload, cruise speed and cruise altitude. Results of this sensitivity are given in Figure 167. With no intermittent loss of LFC, a range of 12 131 km (6550 n mi) may be attained. With LFC fuel flow continued, a range of 9630 km (5200 n mi) may be attained if the LFC system is lost for the entire mission.

A 50% loss of LFC would be similar to complete loss of LFC at the mid-point of the mission if no prior intermittent loss of LFC had been suffered. In this case, a range of 10 742 km (5800 n mi) is possible. By using the diversion distance fuel allowance, the remaining distance of only 1296 km (700 n mi) would have to be recovered through use of part of the normal 10% fuel reserves allowance to reach the original destination. Because more than 1482 km (800 n mi) range would be available through use of fuel reserves, some flexibility exists in establishing a revised flight plan. Because basic calculations have assumed a constant altitude and Mach number cruise, a larger loss of range may be recovered by revision of cruise mach number and altitude to slightly more fuel efficient values.



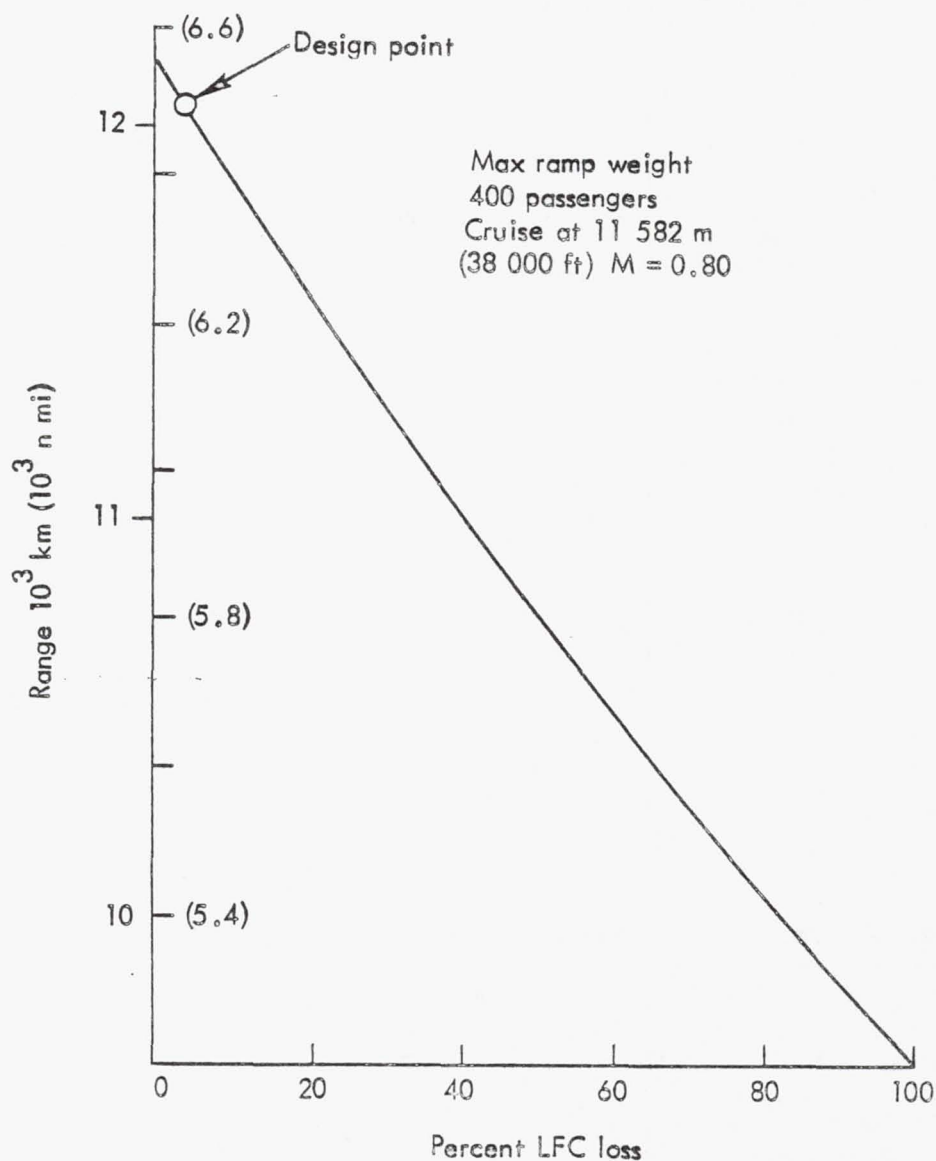


Figure 167. Range variation with loss of LFC system

### 7.3 TURBULENT CONFIGURATION

The contract required that a turbulent transport for the 1990 time period be developed to serve as a basis for comparison for the relative merits of LFC.

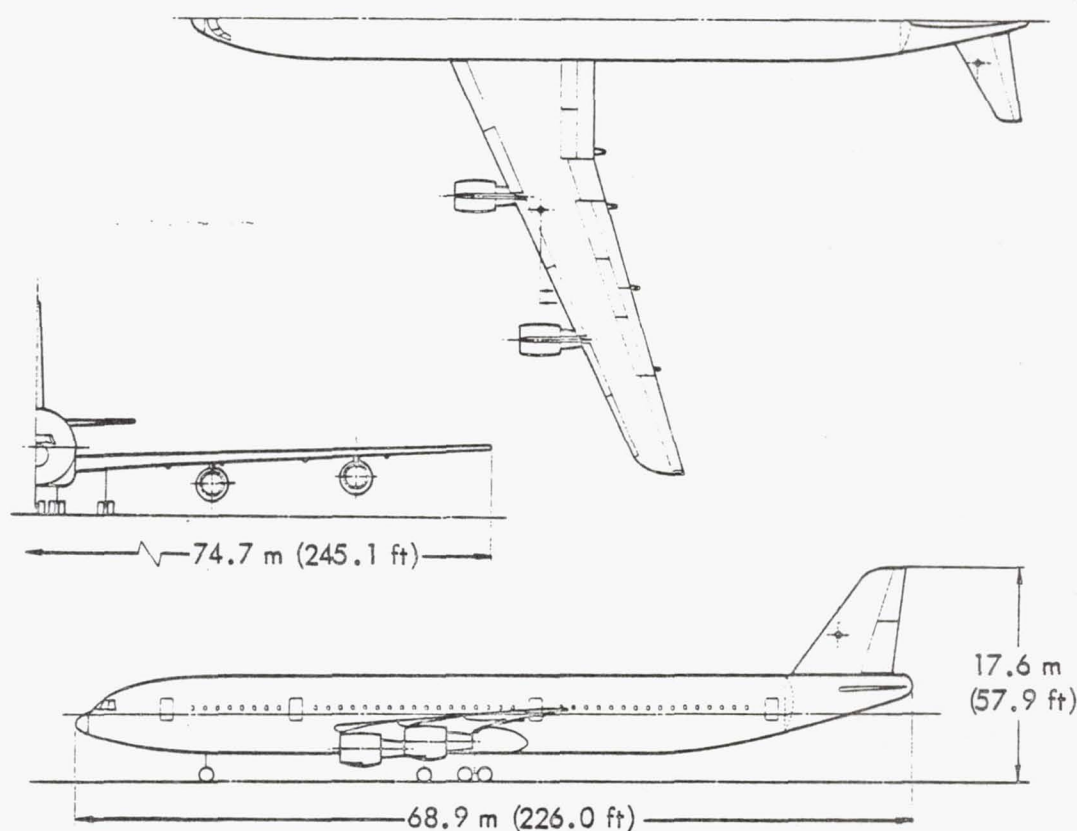
#### 7.3.1 Configuration Definition

Figure 168 shows a near-optimum turbulent transport configuration which incorporates the technology predicted to be available by 1990. The technology level assumed for the turbulent aircraft is identical to that assumed for the LFC configuration. Parametric analysis of operational and

geometrical parameters indicated a cruise altitude of 11 582 m (38 000 ft) and a cruise speed of  $M = 0.80$  to be near optimum for the specified mission.

The turbulent airplane is a wide-body, low-wing, low horizontal tail configuration with four wing-mounted engines. The wing has an aspect ratio of 11.0 and is swept  $.436$  rad ( $25^\circ$ ) at the leading edge. The high-lift system includes leading-edge slats and Fowler trailing-edge flaps.

The weight summary in Table 43, reflects the use of composite material technology in that the weight empty is considerably less than that of a current transport of the approximate passenger capability. The interior of the fuselage is identical to that described in Section 7.2.3 for the LFC transport.



	Area	AR	Sweep	Taper
Wing (base)	507.3 m <sup>2</sup> (5461 ft <sup>2</sup> )	11.00	L.E. .436 rad (25°)	.35
Horizontal	56.9 m <sup>2</sup> ( 613 ft <sup>2</sup> )	4.50	1/4 Ch .436 rad (25°)	.35
Vertical	55.8 m <sup>2</sup> ( 600.6 ft <sup>2</sup> )	1.60	1/4 Ch .524 rad (30°)	.35
TOGW	292 605 kg (645 073 lb)			
Engine	163 kN (33 799 lb) thrust ea			

Figure 168. Turbulent transport

TABLE 43. WEIGHT SUMMARY - TURBULENT AIRPLANE

	<u>kg</u>	<u>lb</u>
Structure	68 070	150 066
Propulsion System	15 079	33 243
Systems & Equipment	<u>31 376</u>	<u>69 170</u>
Weight Empty	114 524	252 478
Operating Equipment	<u>15 255</u>	<u>33 631</u>
Operating Weight	129 779	286 109
Pax Payload	<u>38 465</u>	<u>84 800</u>
Zero Fuel Weight	168 244	370 909
Fuel	124 361	274 164
L. E. Fluid	<u>-</u>	<u>-</u>
Gross Weight	292 605	645 073

### 7.3.2 Configuration Performance

#### 7.3.2.1 Mission Profile

The mission profile used in basic sizing of the turbulent configuration is identical to the profile used in sizing the LFC baseline. Complete compatibility of performance comparisons between the two aircraft concepts was thus assured. Allowances of fuel for wind, fuel tolerance, and diversion distance are identical to allowances for the LFC baseline. The reserve fuel to account for intermittent loss of LFC was not applicable to the turbulent baseline case.



### 7.3.2.2 Airport Performance

The high-lift system described in Section 7.3.1 provides adequate maximum lift and lift/drag characteristics at a takeoff flap setting of  $0.524 \text{ rad}$  ( $30^\circ$ ) and a landing flap setting of  $0.873 \text{ rad}$  ( $50^\circ$ ). These settings provide a  $C_{L_{\text{Max}}}$  of 2.34 for takeoff and 2.70 for landing. At maximum takeoff weight, an engine-out second segment climb gradient of 0.028 is available during takeoff.

FAA field lengths were determined for the range of aircraft gross weight and are presented in Figure 169. Landing results presented are for maximum braking and did not include use of thrust reversers. Ground operation of spoilers was assumed. Note the probable limitations due to minimum control speed considerations.

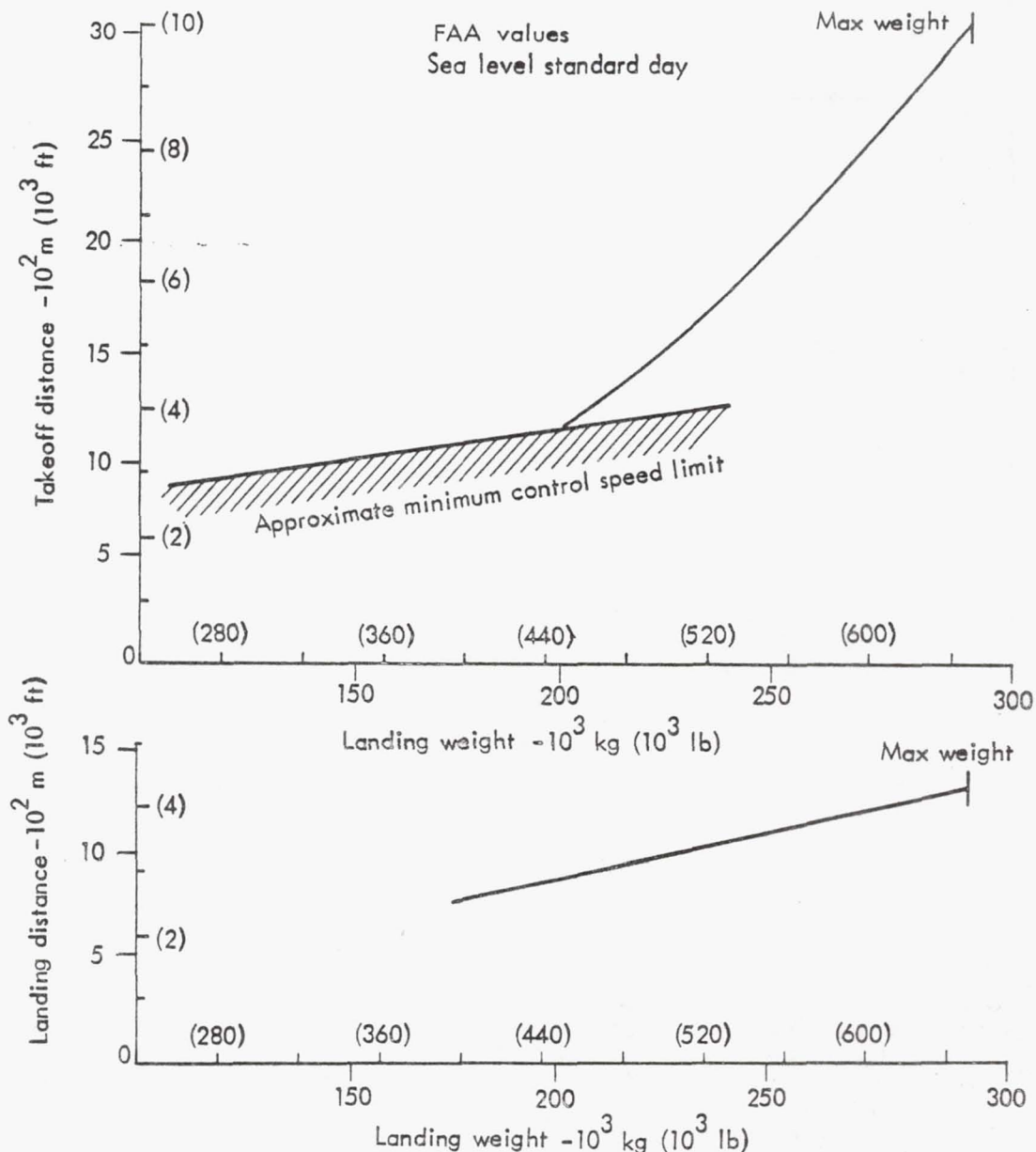


Figure 169. Turbulent baseline airport performance

### 7.3.2.3 Cruise Performance

Aircraft payload/range capabilities are summarized in Figure 170 for cruise at the design Mach number of 0.80 and altitude of 11 582 m (38 000 ft). Several mission points in the payload/range envelope were examined for comparison with the basic design point and are indicated by the circles labeled 1 through 6. Significant data for these missions are compared with the design point in Table 44.

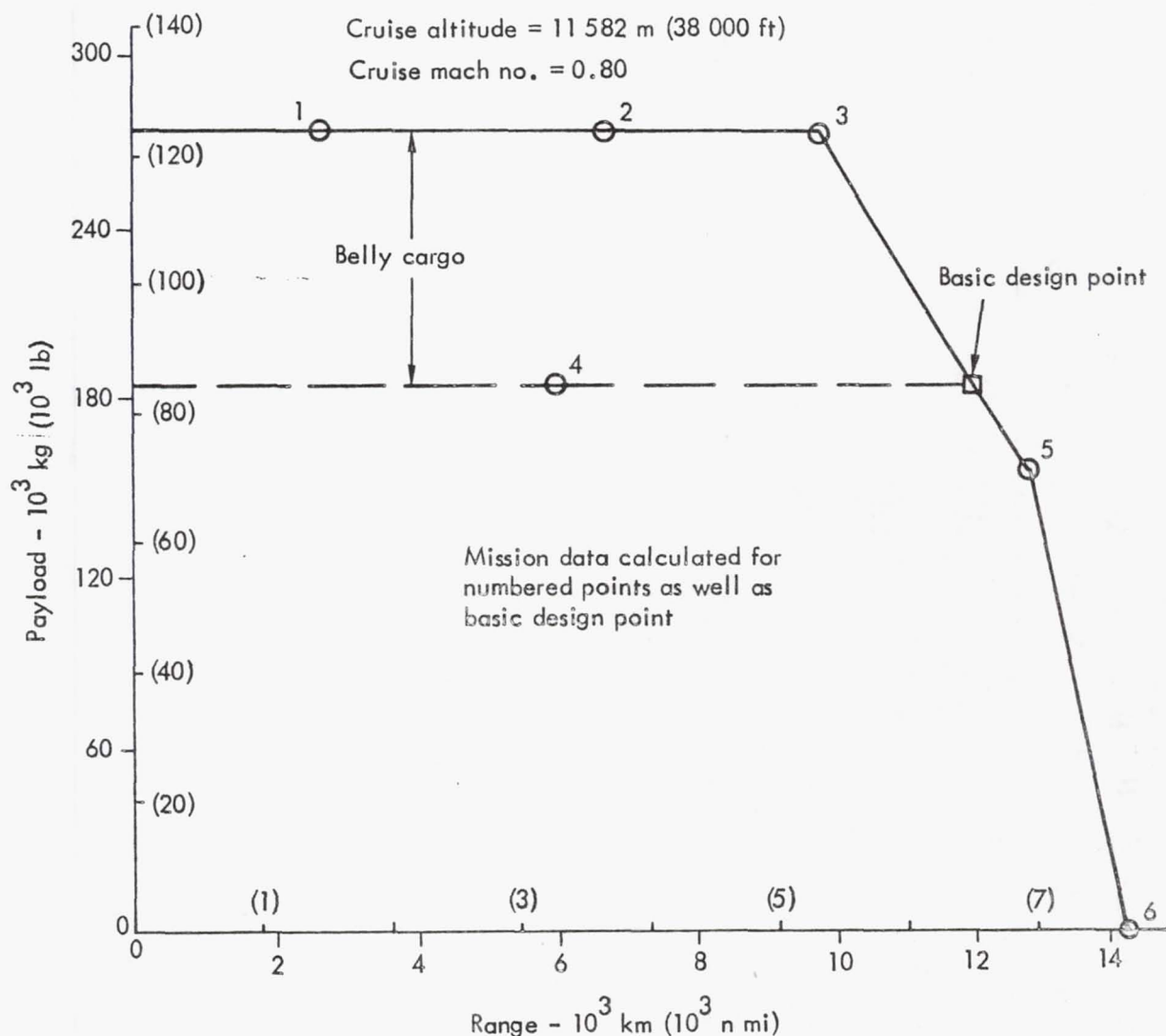


Figure 170. Turbulent baseline payload/range

TABLE 44. PERFORMANCE FOR TYPICAL MISSIONS - TURBULENT TRANSPORT

Cruise Altitude = 11 582 m (38 000 ft)

Cruise M = 0.80

Fuel Weight = .80 kg/l (6.70 lb/gal)

Mission No.	No. Passengers	Belly Cargo kg (lb)	Block Range km (n mi)	Block Time (hr)	Ramp Weight kg (lb)	Takeoff Distance m (ft)	Cruise Fuel Efficiency skm/l (snm/gal)	Average Fuel Efficiency skm/l (snm/gal)
*	400	0	12 038 (6 500)	16.20	292 605 (645 073)	3 051 (10 011)	38.5 (78.7)	36.9 (75.4)
1	400	16 874 (37 200)	2 719 (1 486)	3.91	222 863 (491 320)	1 417 (4 650)	41.6 (85.1)	36.5 (74.5)
2	400	16 874 (37 200)	6 784 (3 663)	9.24	260 607 (574 530)	2 210 (7 250)	39.4 (80.6)	36.9 (75.5)
3	400	16 874 (37 200)	9 864 (5 326)	13.32	292 605 (645 073)	3 051 (10 011)	37.6 (76.8)	35.8 (73.1)
4	400	0	6 088 (3 287)	8.32	233 298 (514 325)	1 945 (6 380)	42.0 (85.9)	39.3 (80.3)
5	335	0	12 864 (6 946)	17.29	292 605 (645 073)	3 051 (10 011)	32.5 (66.5)	31.3 (63.9)
6	0	0	14 246 (7 692)	19.10	260 358 (573 981)	1 954 (6 410)		



## 7.4 CONFIGURATION COMPARISON

Both the LFC and turbulent 1990 aircraft developed in this study represent near-optimum configurations for the defined mission. Thus, a valid comparison of the benefits provided by LFC is possible. As shown in Figure 171, there are several readily apparent configurational differences. The turbulent airplane is configured in the traditional form of current passenger transports with wing-mounted engines and a low-horizontal tail. High-lift devices for the turbulent airplane include leading-edge slats and modified Fowler trailing-edge flaps.

To provide a clean wing for maximum LFC efficiency, engines on the LFC configurations are mounted on the aft fuselage and the horizontal tail is in a T-configuration. There are no leading-edge devices included on this configuration to minimize wing surface discontinuities. LFC suction pumps are housed in pods beneath and extending forward of the wing roots. The aft fuselage of the LFC configuration is extended by 4.3 m (14 ft) to structurally accommodate the pylons which support the propulsion engines. The two fuselages are identical from the nose radome to the aft pressure bulkhead, providing accommodation for 402 passengers in a two-class cabin layout as shown in Figure 172. Cargo and baggage provisions are located in fore and aft lower holds.

### 7.4.1 General Characteristics

Both airplanes are designed to meet identical performance requirements, including cruise at  $M = 0.80$ , a maximum FAA takeoff field length of 3048 m (10 000 ft) and a maximum approach speed of 259 km/hr (140 kn). A comparison of the general characteristics of the two airplanes is shown in Table 45.

### 7.4.2 Weight

The weight summaries presented in Table 46 provide another comparison of the LFC and turbulent airplanes. It is significant to note that a savings of 21.7% in total fuel, block plus reserves, accrues to the laminar flow airplane, while the gross weight of the LFC airplane is 8.2% less than that of the turbulent configuration. Other items of interest tabulated in the weight comparison table illustrate the relatively small penalties imposed by LFC, such as the surface penalty of 2.4% of empty weight. This results from the efficiency of the integral-with-structure suction system which imposes a penalty of just  $3.5 \text{ kg/m}^2$  ( $0.71/\text{lb ft}^2$ ). The total weight of the entire LFC system, pumps, valves, ducts and surfaces, represents 4.4% of empty weight. Further, if the weight of the leading-edge cleaning fluid is added to the total LFC system weight, the entire penalty which can be attributed to LFC represents only 2.6% of gross weight. From these data, it can be seen that the effort expended during this contract study resulted in the design of a highly efficient LFC system.

### 7.4.3 Economics

An economic comparison of different types of airplanes is a less than precise exercise at best. In the current highly inflationary environment, the exercise becomes even less credible. However, the data shown in Table

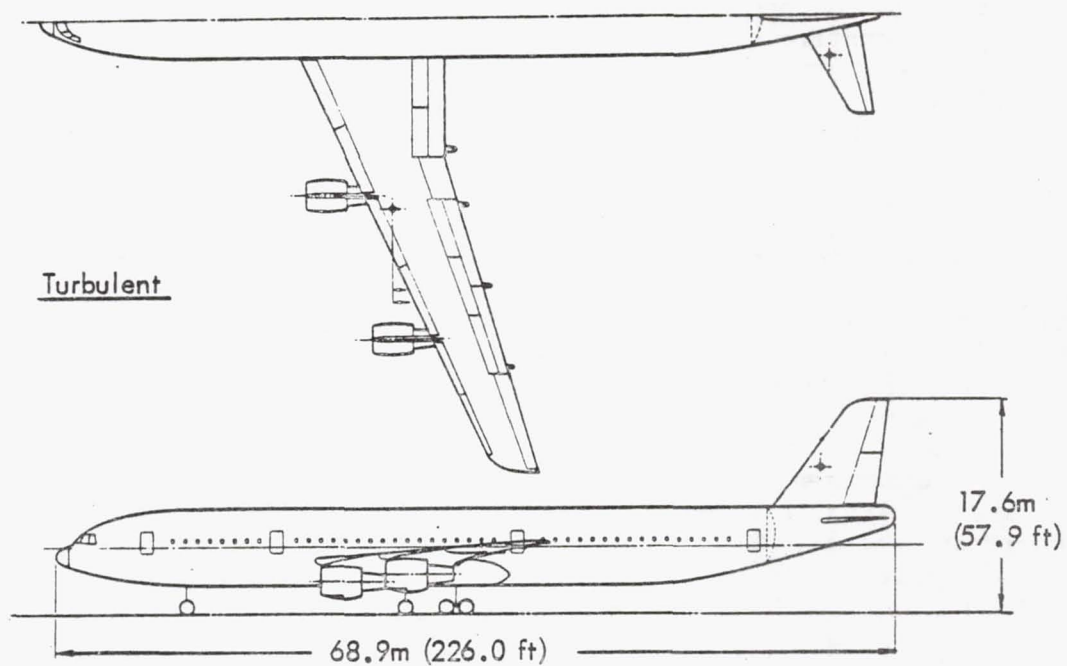
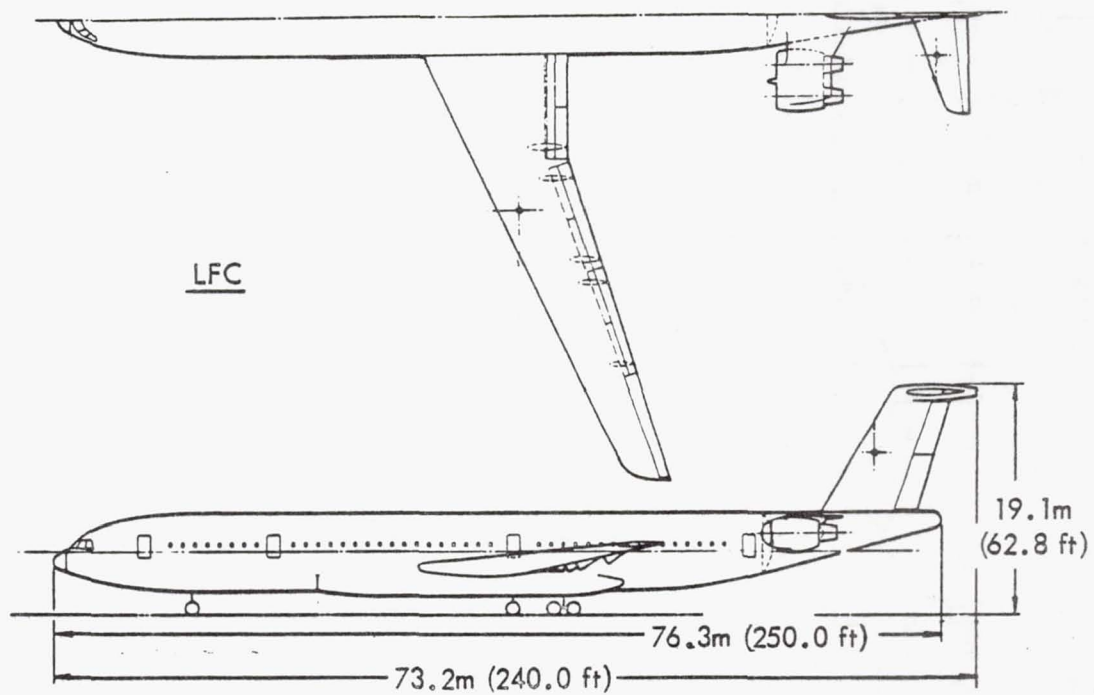


Figure 171. Configuration comparison

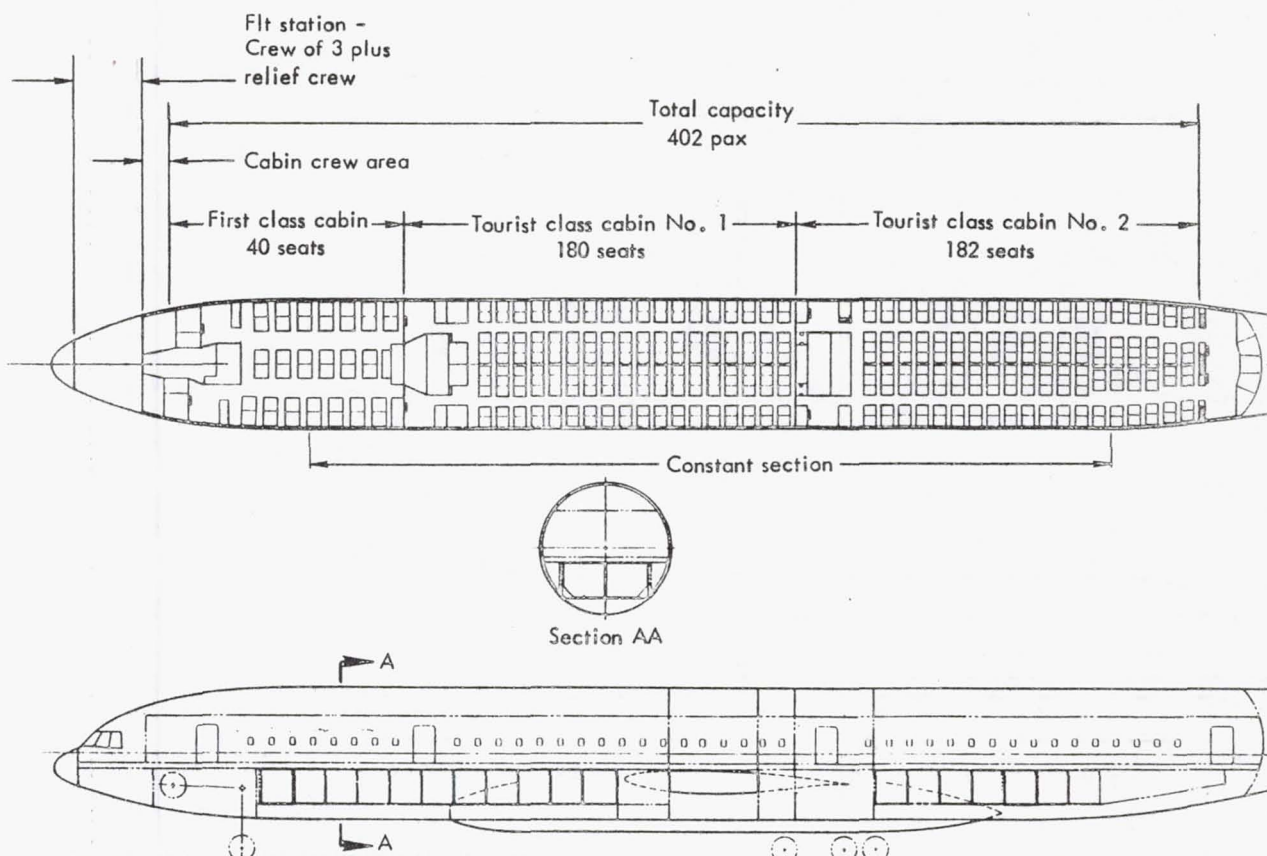


Figure 172. Interior arrangement

47 were developed on the basis of identical assumptions and are therefore useful for comparative evaluations. The data were computed using January 1, 1979 dollars for all DOC elements except fuel, which was computed at 12 cents/liter (45 cents/gal). This table shows that the DOC of the LFC and turbulent aircraft, in terms of total cost per flight and in cents per seat statute mile, are so close as to fall within the scatter of the computational methods.

For the LFC airplane, the 21.7% block fuel advantage offsets a 13% maintenance advantage and a 2% advantage in depreciation accruing to the turbulent airplane for a 6112 km (3300 n mi) flight. Similar cost computations for a 12 038 km (6500 n mi) flight shift the comparison in favor of the LFC aircraft, reflecting the growing advantage of LFC with increasing range.

It is recognized that during periods of high inflation all cost elements are increasing. However, fuel costs are rising more rapidly than other elements of the DOC formula. Figure 173 illustrates the impact of fuel cost escalation in terms of DOC in cents per seat kilometer (cents per seat statute mile). The crossover point beyond which DOC favors LFC, assuming all other costs to be constant, is 15 cents per liter (60 cents/gal) for the average stage length of 6112 km (3300 n mi). The current average carrier price for jet fuel is almost 26.4 cents per liter (\$1.00/gal). At this price, LFC provides a 4% DOC advantage. If fuel costs rise to 52.8 cents per liter (\$2.00/gal), a DOC advantage of 10% results from the application of LFC.



TABLE 45. GENERAL CHARACTERISTICS COMPARISON

	LFC		Turbulent	
Basic Wing Area, $m^2$ ( $ft^2$ )	491.7	(5 293)	507.3	(5 461)
AR		11.6		11.0
Sweep at L.E., rad (deg)	0.436	(25)	0.436	(25)
t/c		0.1128		0.0988
Wing Loading, $kg/m^2$ ( $lb/ft^2$ )	532.1	(109.0)	563.9	(115.5)
TOFL, m (ft)	3 050	(10 008)	3 051	(10 011)
Approach Speed, km/hr (kn)	253	(136.5)	249	(134.3)
Sea Level Static Thrust Each Engine, kN (lb)	149.2	(33 540)	163.6	(36 790)
Ramp Weight, kg (lb)	268 624	(592 205)	292 605	(645 073)
Block Fuel, kg (lb)	82 080	(180 953)	104 755	(230 942)
Maximum Ferry Range, km (n mi)	14 715	(7 946)	14 246	(7 692)
Total Suction, $m^2$ ( $ft^2$ )	811.2	(8 733)		

TABLE 46. WEIGHT COMPARISON

	LFC		Turbulent	
	kg	lb	kg	lb
Structure	69 611	153 465	68 070	150 066
LFC Surfaces	(2 820)	(6 218)		
Propulsion System	15 581	34 350	15 079	33 243
LFC Pumps	(597)	(1 318)		
LFC Ducts, etc.	(1 392)	(3 070)		
Systems & Equipment	30 745	67 779	31 375	69 170
LE Cleaning System	(325)	(716)		
Weight Empty	115 937	255 594	114 524	252 479
Operating Equipment	15 028	33 131	15 028	33 631
Operating Weight	130 965	288 725	129 552	286 110
Passenger Payload	38 465	84 800	38 465	84 800
Zero Fuel Weight	169 430	373 525	168 018	370 910
Fuel	97 392	214 711	124 360	274 163
LE Cleaning Fluid	1 800	3 968		
Gross Weight	268 622	592 204	292 378	645 073

LFC Surfaces = 2.4% of empty weight

LFC Total System = 4.4% of empty weight

LFC Surface =  $3.47 \text{ kg/m}^2$  ( $0.71 \text{ lb/ft}^2$ ) for laminarized area

TABLE 47. ECONOMIC COMPARISON

	<u>LFC</u>	<u>Turbulent</u>	<u>Δ%</u>
Flying Operations	10 695	11 885	-21.7
Direct Maintenance	8 994	7 932	+13.0
Depreciation	9 887	9 698	+ 2.0
Total DOC/Flight	29 566	29 515	+ 0.1
DOC			
¢/s km (¢/ssm)			
6112 km (3300 n mi)			
stage length	1.065 (1.973)	1.053 (1.950)	+ 0.1
DOC			
¢/s km (¢/ssm)			
12 038 km (6500 n mi)			
stage length	1.161 (2.150)	1.166 (2.160)	- 0.5
Fuel price = 11.8¢/l (45¢/gal)			
Costs in Jan. 1979 dollars			

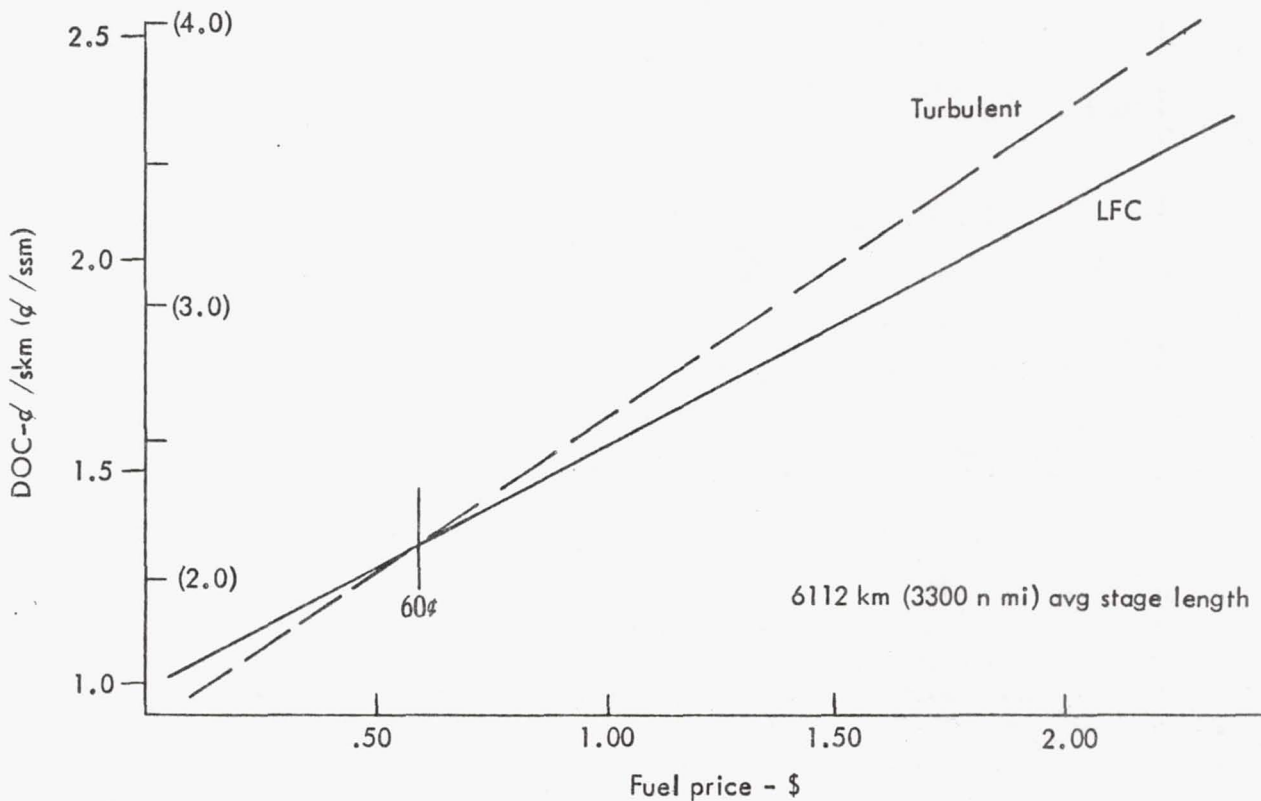


Figure 173. DOC vs fuel price



#### 7.4.4 Fuel Efficiency

Eliminating the vagaries of economics and recognizing future possibilities for jet fuel allocation measures, Figure 174 plots the potential advantages for LFC in terms of fuel efficiency in seat kilometers per liter (seat statute miles per gallon) versus stage length. Based on the data of Reference 32, the family of curves on the lower left represents the efficiencies of first- and second-generation jet transports in current service. The two circles represent current wide-body transports which are capable of long-range operations, and which are expected to be in operation well into the 1990's.

At the average stage length of 6114 km (3800 s mi), the LFC transport demonstrates an advantage in fuel efficiency of 91% and 28%, respectively, compared to the best of the current transports and the advanced technology turbulent aircraft. At 10 459 km (6500 s mi), the fuel efficiency of the LFC transport is greater than that of current transports by 255%. These data illustrate the dramatic potential offered by a fleet of LFC transports as we approach the 1990 time period.

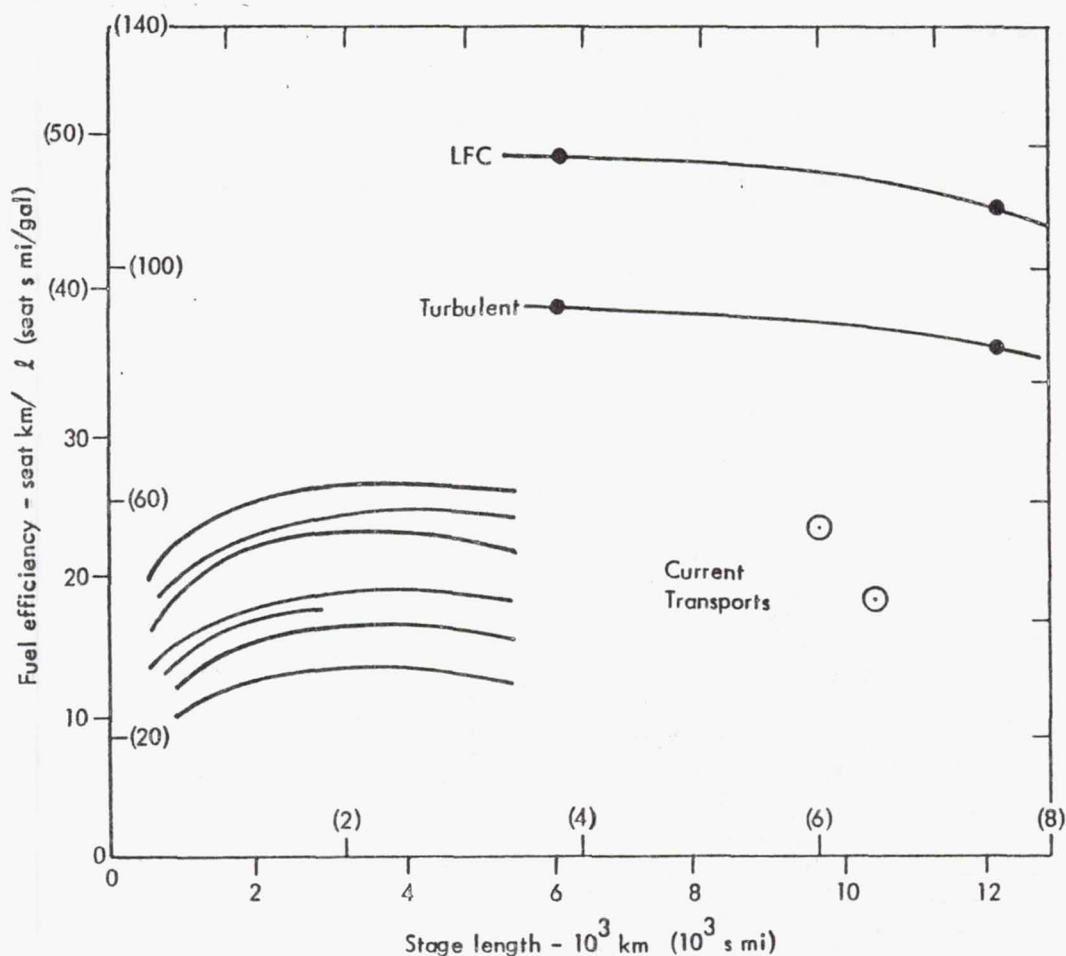


Figure 174. Fuel efficiency comparison

## 8.0 RECOMMENDED SUBSYSTEM DEVELOPMENT

Requirements for future development include the refinement of design criteria and methodology, the validation of current concepts, the continued development of manufacturing procedures, and the investigation of operational characteristics in flight. To a great extent, these requirements can be satisfied by the major programs currently included in the NASA LFC program plan. These programs are: (1) the NASA high-speed wind-tunnel program; (2) the JetStar leading-edge flight test program; (3) the LFC wing panel structural design and development program; and (4) the LFC validator flight test program.

As a part of the task devoted to the identification of future development requirements, studies were conducted which demonstrated the feasibility of using the NASA JetStar aircraft as a test bed for the evaluation of leading-edge cleaning concepts and established the feasibility of integrating the Lockheed LFC wing design into a DC-9-10 aircraft to form a LFC validator configuration. This section summarizes the results of those studies and outlines additional LFC technology development requirements.

### 8.1 LFC TEST BED DEVELOPMENT

The current NASA LFC Program Plan includes the flight validation of the LFC leading-edge concept described in Section 6.2.3, using an aircraft in the JetStar/DC-9-10 class as a test bed. This section summarizes the results of a study conducted to assess the feasibility of using the NASA Dryden JetStar aircraft as a test bed for the proposed flight validation. Included in the study is a definition of the leading-edge test section, an analysis of aerodynamic and structural considerations, a definition of aircraft modification/refurbishment requirements, and an evaluation of flight performance of the resultant configuration.

#### 8.1.1 Objectives

The overall objective of the Leading Edge Glove Flight Program is to demonstrate the effectiveness of LFC leading-edge systems under representative flight conditions. Specific objectives of the program are:

- (1) Install an operable LFC system in a segment of the leading edge of an aircraft.
- (2) Demonstrate the effectiveness of leading-edge cleaning/de-icing systems.
- (3) Achieve LFC in flight at conditions representative of commercial transport operations.
- (4) Examine systems performance from an operations and maintenance standpoint.

A further unspecified objective is to provide sufficient instrumentation to permit investigation of both suction and cleaning system design criteria. The configuration developed during this study provided such a capability.

The objective of the study summarized in this section was to evaluate the feasibility of using the JetStar aircraft as a test bed for the Leading Edge Glove Flight Program.

### 8.1.2 Configuration Description

Selection of a location for the leading-edge test section was based on achieving a chord length representative of a chord length existing on the Lockheed 1990 LFC transport and minimizing modifications to the aircraft and effects on aircraft performance. A location meeting these conditions is the area of the spar currently occupied by the external fuel tanks. The planform of the modified JetStar in Figure 175 shows the test section installed on the left wing and a dummy section to preserve aerodynamic symmetry installed on the right wing.

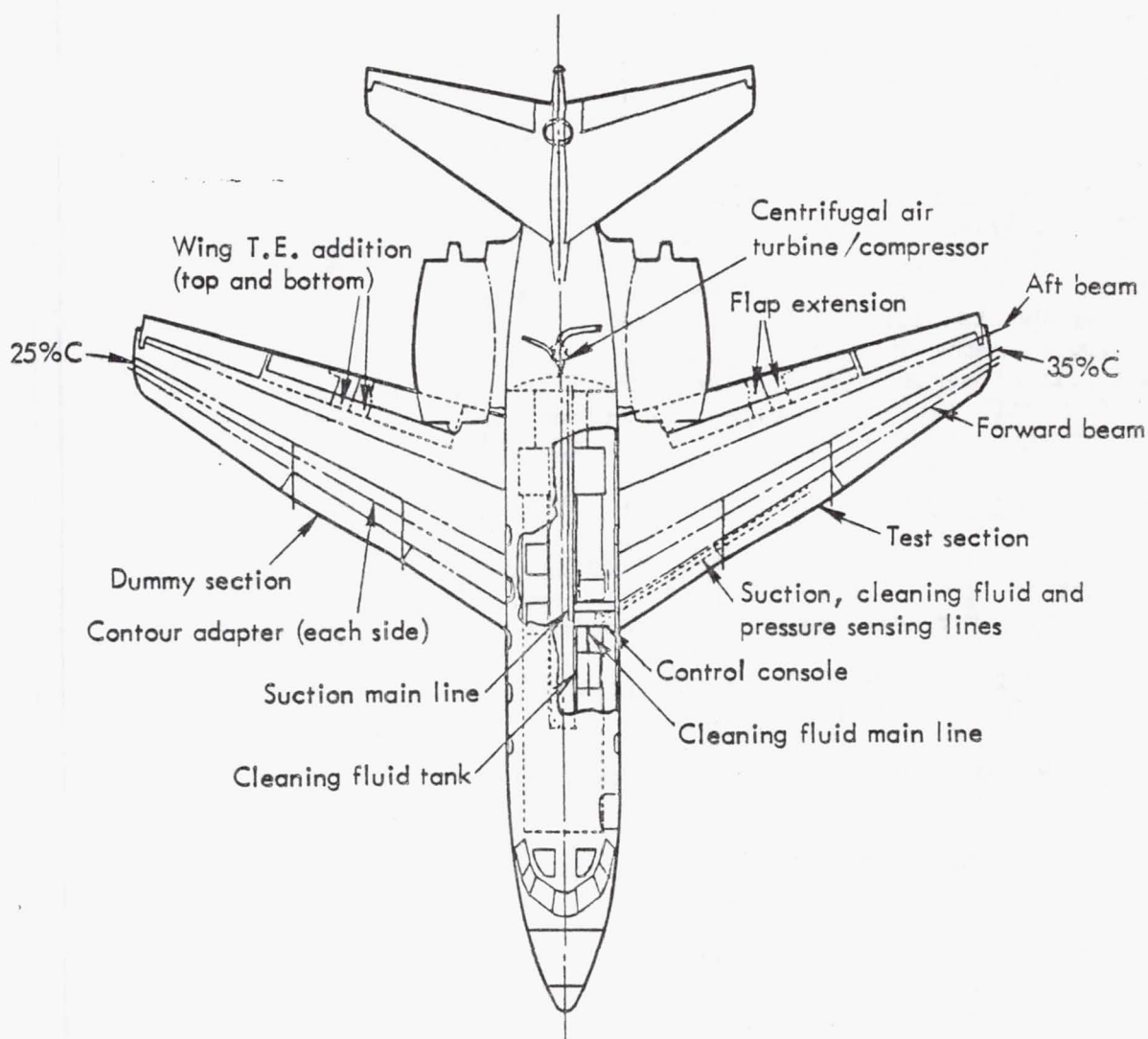


Figure 175. Plan view of modified JetStar



The inboard end of the section is at L.E. station 135.514, where an existing rib forms the outboard wall for the fuel cell. This L.E. station translates into W.S. 122.068. The outboard end of the test section falls on L.E. station 242.405, which is the outboard extremity of an existing leading-edge flap panel. This L.E. station translates into W.S. 205.278, which provides a test section span of 2.11 m (83.2 in). Connecting the points at these two wing stations provides a test section with a leading-edge sweep of 0.524 rad (30.01 deg) and a swept length of 2.44 m (96.09 in).

Figure 176 shows the proposed structural arrangement of the leading-edge section and the method of attachment and fairing to the basic JetStar wing. The section is fabricated in two panels, a fixed upper/nose panel and a hinged lower panel which provides access for maintenance and adjustment of the suction and cleaning systems. The substructure consists of two full-length diaphragms. These members provide support for the covers and form the boundaries of the upper and lower surface ducts on a full LFC wing. All leading-edge components are of sandwich construction and feature graphite/epoxy sheets and corrosion resistant aluminum honeycomb core. A thin gauge titanium skin, bonded to the surface panel outer face sheet, contains the required suction slots and also provides environmental protection for the composite structure.

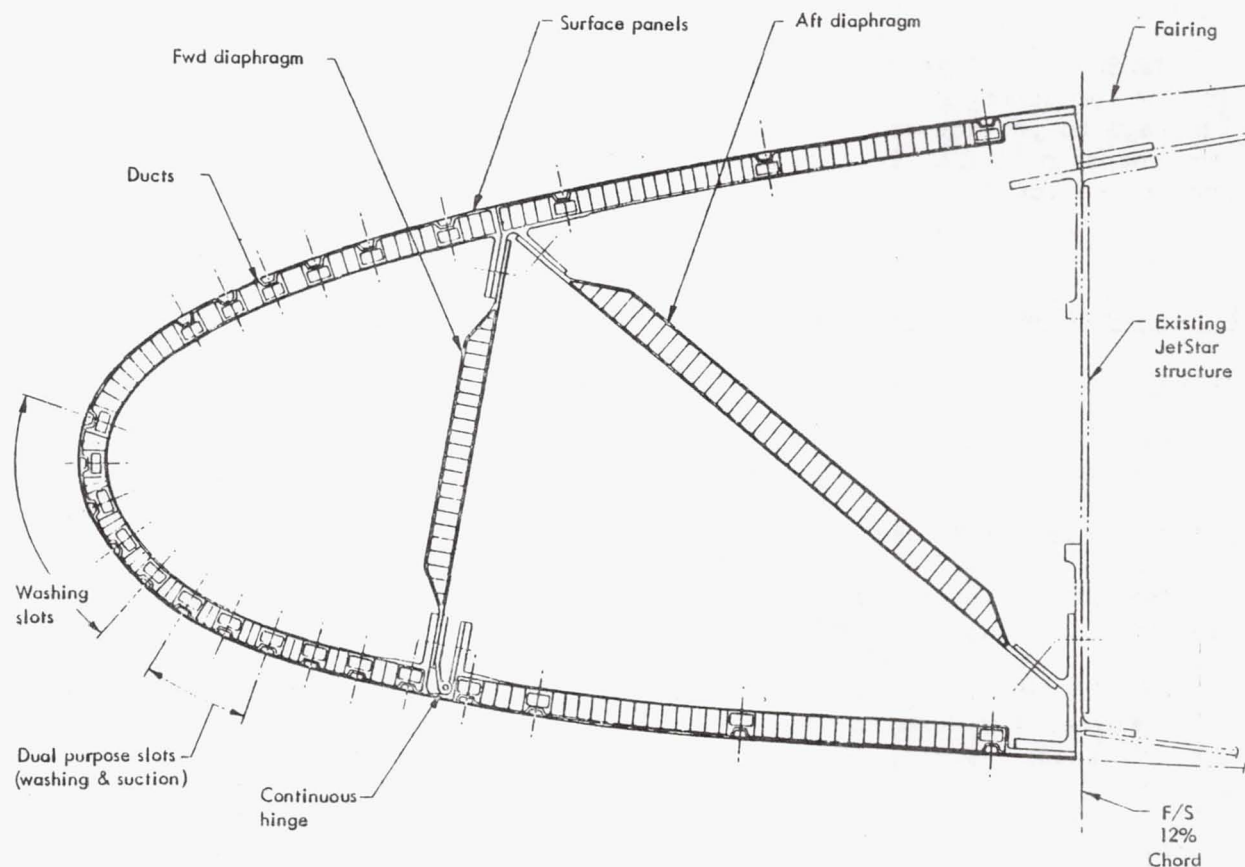


Figure 176. Structural design of leading-edge test section

The test section is isolated from the basic wing and blended into the existing wing contour through the use of appropriate fairings. Fairings are required in the areas between the test section and existing leading-edge structure. These panels are of built-up aluminum construction and mechanically attached to the wing.

The fairing panels required on the upper and lower surfaces to provide a smooth transition from the test section, and the entire fairing structure on the right hand wing, is fabricated of fiberglass and bonded to the wing box to prevent fastener penetration of the fuel tanks.

The aft boundary of the test section coincides with the existing JetStar 12%-chord front spar. The test section contour picks up the JetStar contour slope at 12% chord on the lower surface, while on the upper surface the new contour fairs to JetStar contour at approximately 35% chord. Fences or fairings are located at the section extremities. The upper surface contour change from 12% to 35% chord is effected with a light-weight add-on fairing.

Externally, the only other wing modification required is to fill in the gap in the trailing-edge flaps exposed by the removal of the fuel tank. Internally, the JetStar wing is modified to delete the fuel-carrying capability of the inboard leading edge to provide space for suction lines, fluid lines, and instrumentation leads.

JetStar fuselage modifications consist primarily of providing openings in the pressure shell at the juncture between the leading edge and the fuselage to provide entry for LFC services, providing space in the passenger compartment for instrumentation and controls, and making aft fuselage provisions for the suction pump and exhaust duct.

### 8.1.3 Leading Edge Test Section

#### 8.1.3.1 Structural Design

The leading-edge test section evaluated for the JetStar feasibility study is similar in shape and size to that described in Section 6.2.3.

#### 8.1.3.2 Suction System

The suction system ducting arrangement for a typical slot is illustrated schematically in Figure 177. The internal ducting of each slot is divided into two 76.2 cm (30 in) segments with individual ground adjustable valves located within the test section cavity to provide flexibility in the test program for limited spanwise suction flow adjustment. After passing through these valves, the total flow for each slot is collected into a single duct and routed to the fuselage, where an additional flight adjustable valve for each slot is located. This configuration provides flight capability for chordwise suction flow profile adjustment. Direct simultaneous comparison of two suction flow levels or distributions may be made by differential ground adjustment of the two 76.2 cm (30 in) segments of each slot prior to flight.

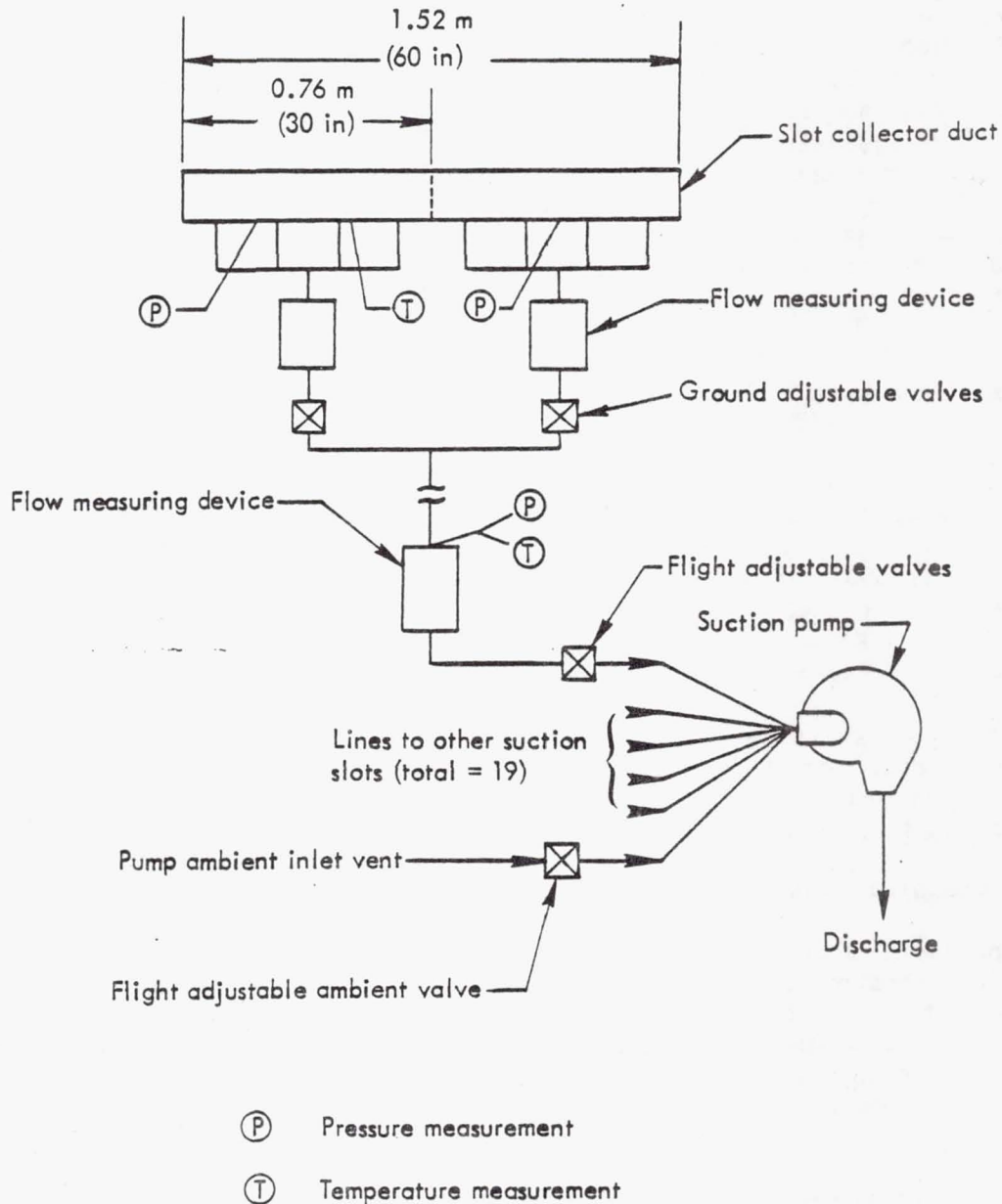


Figure 177. Schematic of slot suction system

To provide flexibility in testing, the flows were doubled for each suction slot and lines were sized accordingly. Adjustment to the suction system valving permits selection of the design suction levels and distributions as well as other distributions, including localized flows in excess of twice design flow level. Suction flow distributions and levels approximating those of the X-21A are within the system capability.



A design point suction flow rate of 0.019 kg/s (2.484 lb/min) is required for the leading-edge test section at the 12 192 m (40 000 ft) altitude, 0.80 Mach number cruise condition. With the assumption of a suction capability for twice the design suction flow rate and the pressure losses in the selected suction system and lines, this translates to a sea level standard day equivalent suction flow requirement of 0.39 kg/s (52.03 lb/min) at a pressure ratio of 2.1. A cursory survey of suitable and readily available suction units was made with the assistance of AiResearch Manufacturing Company. Largely on the basis of availability, reliability, cost, and adaptability, an AiResearch Model ATCU30 air turbine compressor was selected as a feasible unit for purposes of this study. This unit consists of a centrifugal compressor with an axial inlet and a radial discharge direct-coupled to an air turbine drive having a tangential inflow and an axial outflow. Compressor discharge air bled from the primary propulsion engines provides the turbine air supply.

This unit is greatly oversized for this application, having a rated flow of 1.74 kg/s (230 lb/min) at 50 000 rpm and a pressure ratio capability of 4.7. The unit can meet the required 2.1 pressure ratio at approximately 33 000 rpm but would require a minimum equivalent sea level flow rate of 0.68 kg/s (90 lb/min) in order to maintain a comfortable compressor stall margin. This necessitates an ambient vent for the pump inlet to supplement the flow from the leading-edge suction system.

Due to the excessive capabilities of this unit, it is fairly large, having an overall length of 49.83 cm (19.62 in) a height of 42.82 cm (16.86 in) with a dry weight of 58.9 kg (130.0 lb). This is compatible with installation in the JetStar in the space normally occupied by an APU.

#### 8.1.3.3 Cleaning System

The range of slot locations to assure adequate wetting of the leading edge is illustrated in Figure 178. A total of eight cleaning slots is available with five slots functioning only as cleaning slots and three slots performing a dual role as combination cleaning slots for takeoff and climb, and suction slots for cruise operation. It is anticipated that only selected slots would be used during different phases of the takeoff/climb cycle.

To conserve space in the crowded leading-edge region, each single 1.52 m (60 in) span of slot is supplied by fluid from the fuselage through a single supply line with the specific slot flow rate controlled by a flight adjustable valve. At the test section, this line is subdivided into two segments with ground adjustable flow valves, each supplying four collector duct chambers over a slot span of 76.2 cm (30 in).

Adequate valving is installed for switching the combination cleaning-suction slots between the cleaning mode for takeoff/climb and suction mode for cruise operation.

#### 8.1.3.4 Instrumentation

Testing the LFC system requires both internal suction system and external aerodynamic instrumentation. The internal suction system instrumen-

tation includes internal slot collector duct pressures, temperatures, and suction flow measurements for each 76.2 cm (30 in) segment of the slot. These instruments are all located in the leading-edge test section. Additional suction system pressures, temperatures, and suction flows are measured for each slot after the suction lines have entered the fuselage. External instrumentation includes surface static taps located at both the inboard and outboard ends of each slot at the same x/c as the slots. Surface boundary layer total pressures are measured at the aft edges of the leading-edge test section at 5.08 cm (2 in) spanwise intervals. The probes are configured so that they may be used to determine boundary layer laminarization and are also used to evaluate the presence of insect accretion during testing of the leading-edge cleaning system. These probes may also be pneumatically connected to microphones to obtain audible indication of the state of the boundary layer. Two flush microphones are included in the airfoil upper surface at the aft end of the leading-edge panel to measure impinging noise.

For the cleaning system, instrumentation is incorporated to record collector duct pressures in two typical chambers and temperatures in one of these chambers in each of the eight washing slots. Slot line pressure is measured in the fuselage, and the fluid reservoir pressure and temperature are monitored. The total flow rate to each individual cleaning slot and the flow distribution between each of 76.2 cm (30 in) span segments is measured.

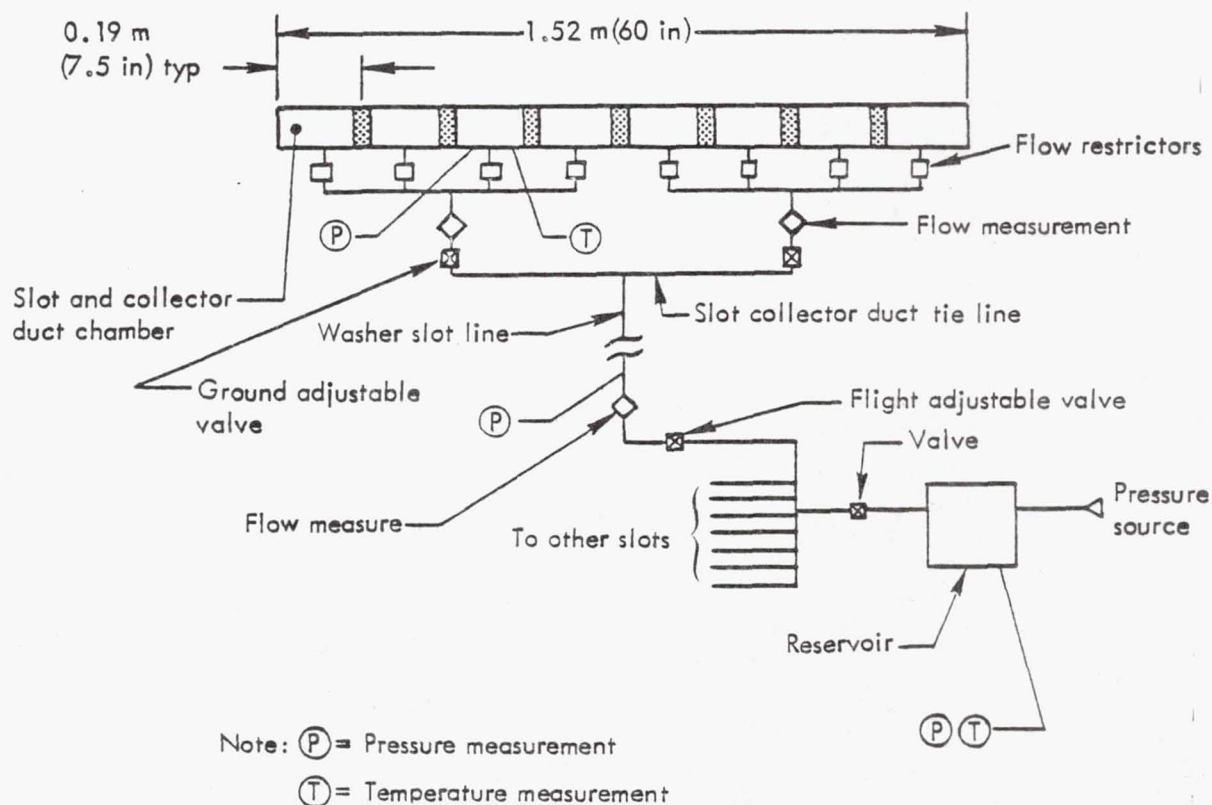


Figure 178. Schematic of cleaning system

#### 8.1.4 Aerodynamic Configuration

The loft panels for the JetStar wing and the location of the leading-edge test region are shown in Figure 179. The modification region extends from station 122.068 to 205.278. The planform projection of leading edge of the modified section matches the planform projection of the existing JetStar leading edge at these stations, producing a 0.524 rad (30 deg) leading-edge sweep for the test article modification area. The upper surface is tangent to the existing wing at approximately 35 percent chord. The simulation ends on the lower surface at the front spar location at 12 percent of the basic JetStar wing chord. At station 122.068 the modified contour has a moderate discontinuity, and at this station and at station 205.278, fairings smooth the modified section to the original JetStar contour.

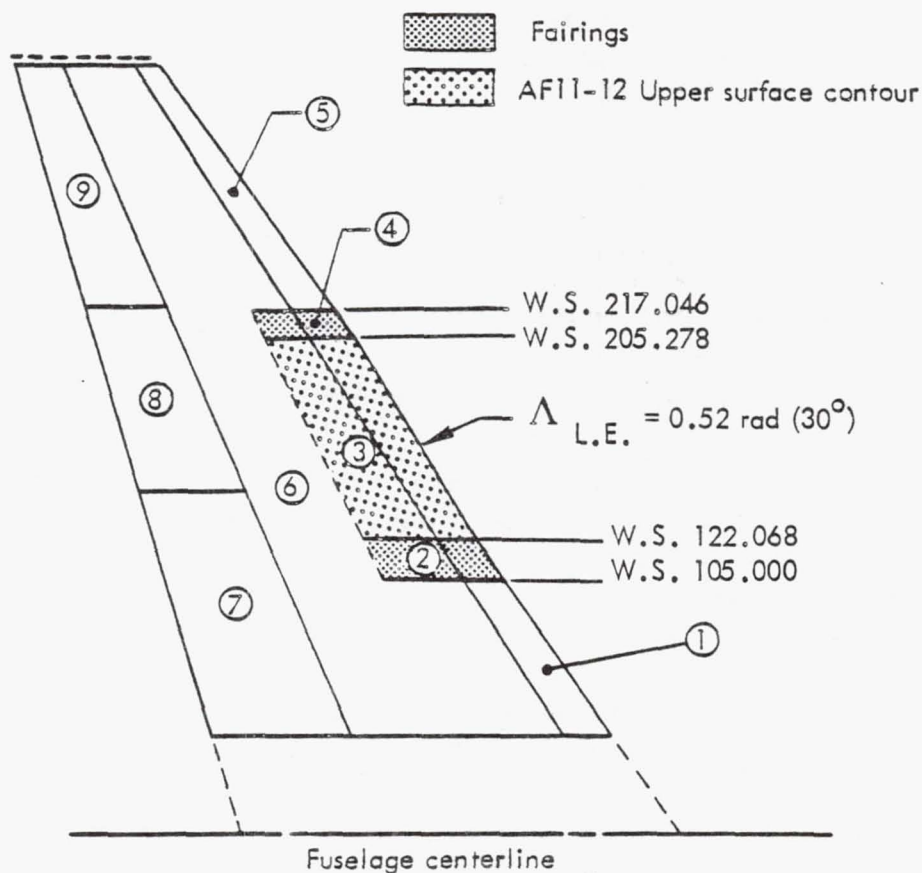


Figure 179. JetStar upper wing surface loft regions



In order to match the leading-edge sweep of the flight test section, a leading-edge sweep of 0.524 rad (30 deg) was used to factor a new stream-wise section from the airfoil developed in Section 6.1. The trailing-edge sweep used in the factoring was also 0.524 rad (30 deg), since only the leading-edge region is used on the JetStar wing. This section was put at 0.035 rad (2 deg) inclination relative to the basic JetStar wing and faired into the original JetStar contour at approximately 35 percent chord on the upper surface and at the front spar position on the lower surface. Stream-wise sections of the resultant airfoil are shown in Figure 180.

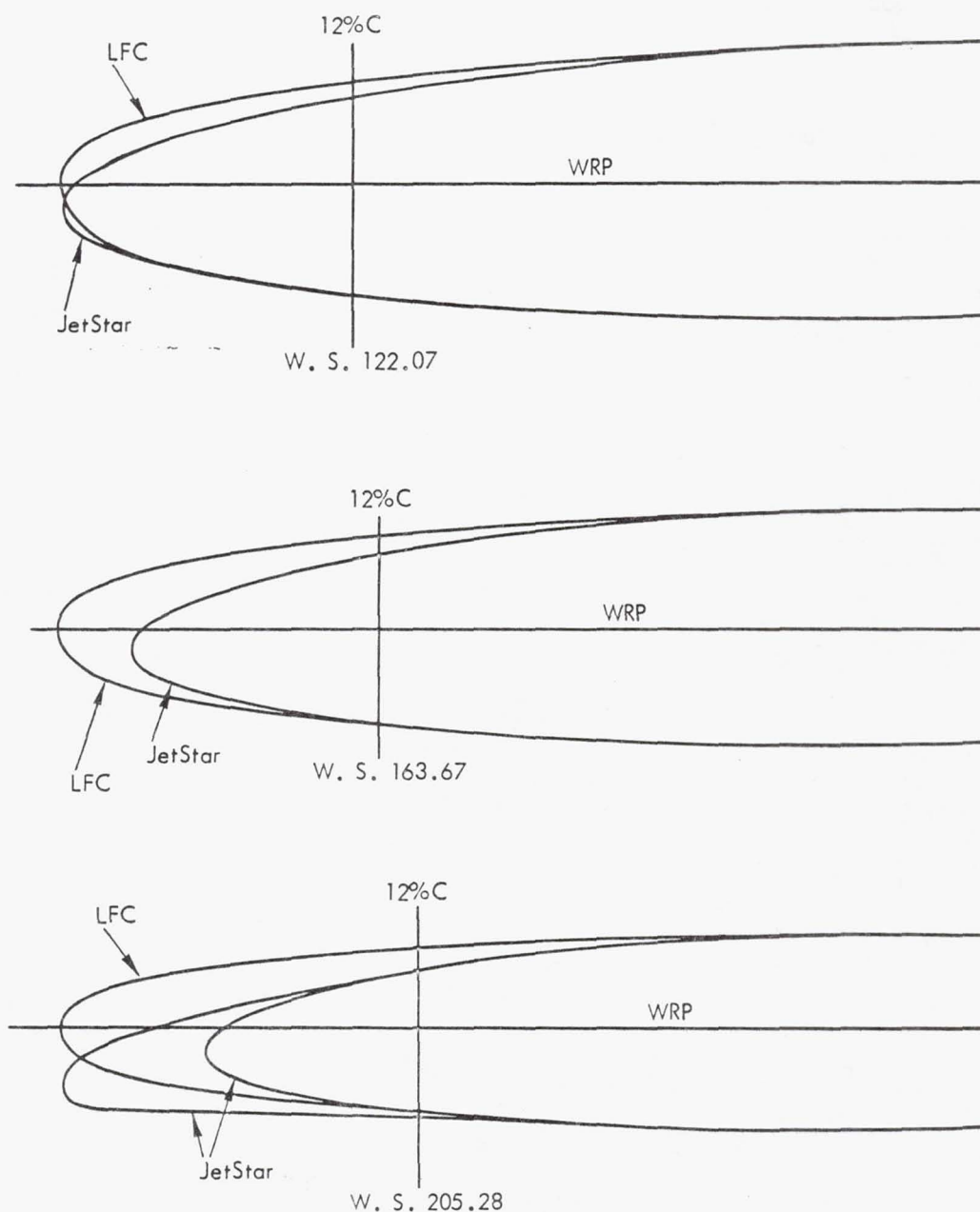


Figure 180. Streamwise airfoil sections

## 8.1.5 Structural Analysis

### 8.1.5.1 Flight Loads and Criteria

The removal of the external tanks results in a reduction in both the zero fuel weight and the fuel quantity available. In order to provide flight safety, the allowable maneuver load factor is reduced to 2.5g and speed placards are reduced for gust protection at altitudes below 6096 m (20 000 ft). These changes in weight and speed are shown in Table 48 and are compared to the original JetStar certified values. The structural design airspeeds are shown as a function of altitude in Figure 181.

TABLE 48. STRUCTURAL DESIGN CRITERIA

	<u>Current</u>		<u>Modified JetStar</u>	
Maximum zero fuel weight, kg (lb)	11 340	(25 000)	11 165	(24 614)
Maximum landing weight, kg (lb)	13 608	(30 000)	13 608	(30 000)
Maximum internal fuel weight, kg (lb)	4 649	(10 250)	4 511	(9 945)
Maximum external fuel weight, kg (lb)	3 434	(7 571)	0	0
Maximum flight weight, kg (lb)	18 562	(40 921)	15 422	(34 000)
Maximum ramp weight, kg (lb)	18 824	(41 500)	15 676	(34 559)
V <sub>C</sub> , km/hr(KEAS)	648	(350)M=.82	518	(280)M=.82
V <sub>D</sub> , km/hr(KEAS)	787	(425)M=.90	648	(350)M=.90
V <sub>B</sub> , km/hr(KEAS)	426	(230)M=.82	370	(200)M=.82
V <sub>F</sub> (landing),km/hr(KEAS)	330	(178)	315	(170)
V <sub>F</sub> (takeoff),km/hr(KEAS)	370	(200)	352	(190)
Maneuver load factors				
Clean at V <sub>C</sub>	3.0 and -1.0		2.5 and -1.0	
Clean at V <sub>D</sub>	3.0 and 0.0		2.5 and 0.0	
Dive brake extended				
At V <sub>C</sub>	3.0 and -1.0		2.5 and -1.0	
At V <sub>D</sub>	2.5 and 0.0		2.5 and 0.0	
Flaps extended	2.0 and 0.0		2.0 and 0.0	

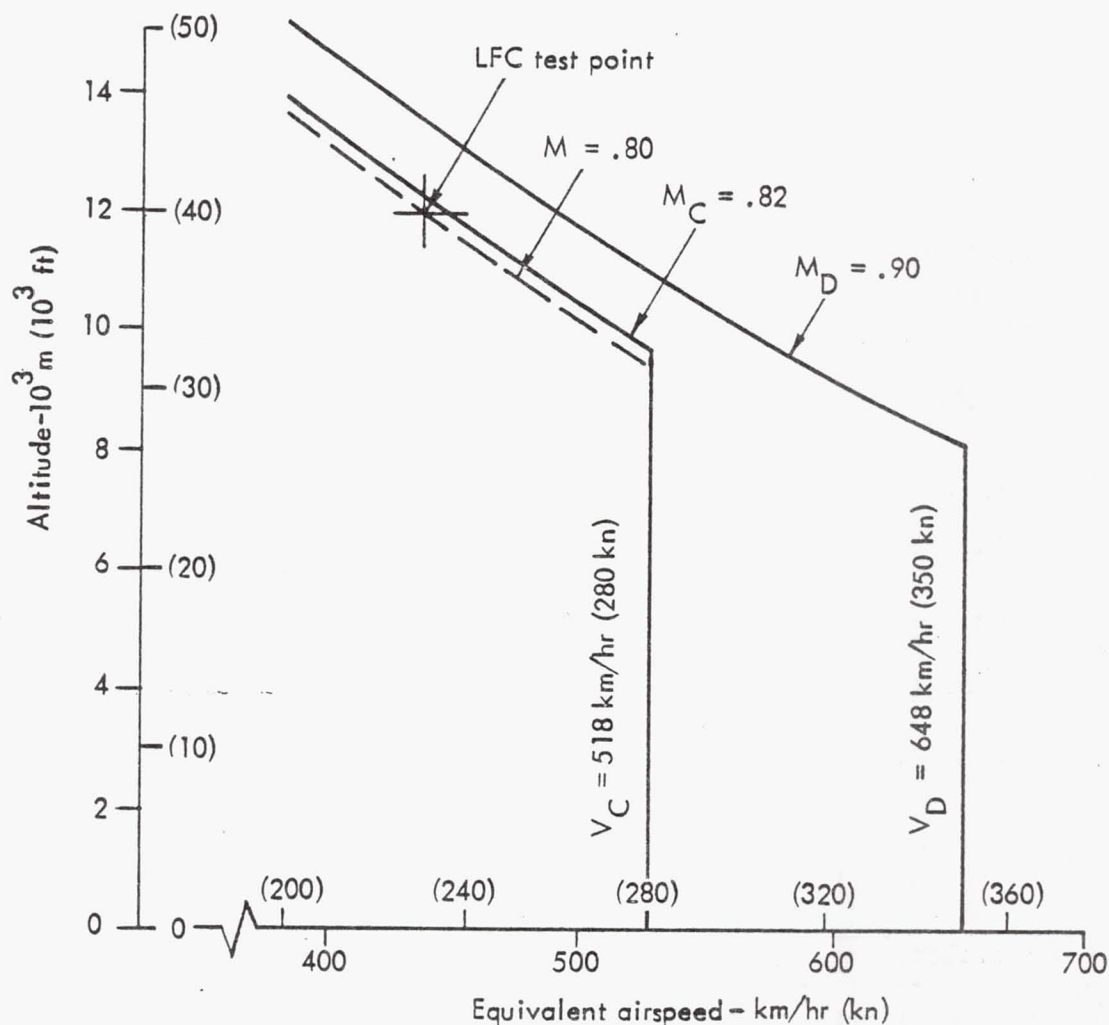


Figure 181. Structural design airspeeds vs altitude

#### 8.1.5.2 Flutter Considerations

A brief flutter appraisal was made of the LFC JetStar configuration. The modifications which have some potential for changing the flutter characteristics are: (1) the removal of the external fuel tanks, (2) the deletion of leading-edge fuel, and (3) the installation of the modified leading-edge sections. It was concluded that the modified aircraft will have wing flutter speeds in excess of 1.2 times the unmodified JetStar limit dive speed.

None of the proposed changes is expected to affect the empennage flutter speeds.

#### 8.1.5.3 Weight and Balance

The estimated weight empty of 21 500 lb for the modified JetStar is derived in Table 49.



TABLE 49. ESTIMATED WEIGHT EMPTY

	Weight	
	kg	lb
Basic weight	9 782	21 565
Oil (2) crew	182	401
Operating weight	9 964	21 966
Operating weight change		
LFC JetStar estimated changes	263	581
LFC JetStar operating weight	9 701	22 547
Less operating equipment, washing fluid	475	-1 047
LFC JetStar estimated weight empty	9 226	21 500

The feasibility assessment study indicated the cg location of 21% MAC with maximum tolerance on calculation of  $\pm 1\%$ . The aircraft is in balance and standard charts and limits prescribed in Flight Manuals apply.

#### 8.1.6 Performance Evaluation

The modification of the NASA JetStar to the LFC configuration includes the removal of the external fuel tanks, which produces the only significant effect on performance. Cruise drag is improved at the expense of fuel capacity. The modified aircraft is compatible with the desired test conditions of 0.8 Mach number at 12 192 m (40 000 ft) at the maximum weight for that altitude, which is approximately 9072 kg (20 000 lb). The time available at the test conditions is about 98 min. A slight improvement in the maximum lift coefficient is the only noticeable change in the flaps-down configuration.

##### 8.1.6.1 Speed/Altitude Capability

Maximum speed capability is presented in Figure 182, which includes angle of attack and Reynolds number information. These data are based on the use of maximum continuous power with normal plus LFC compressor bleed. The start cruise weight of 13 064 kg (28 800 lb) permits a Mach number of 0.798, essentially fulfilling the test condition requirement.

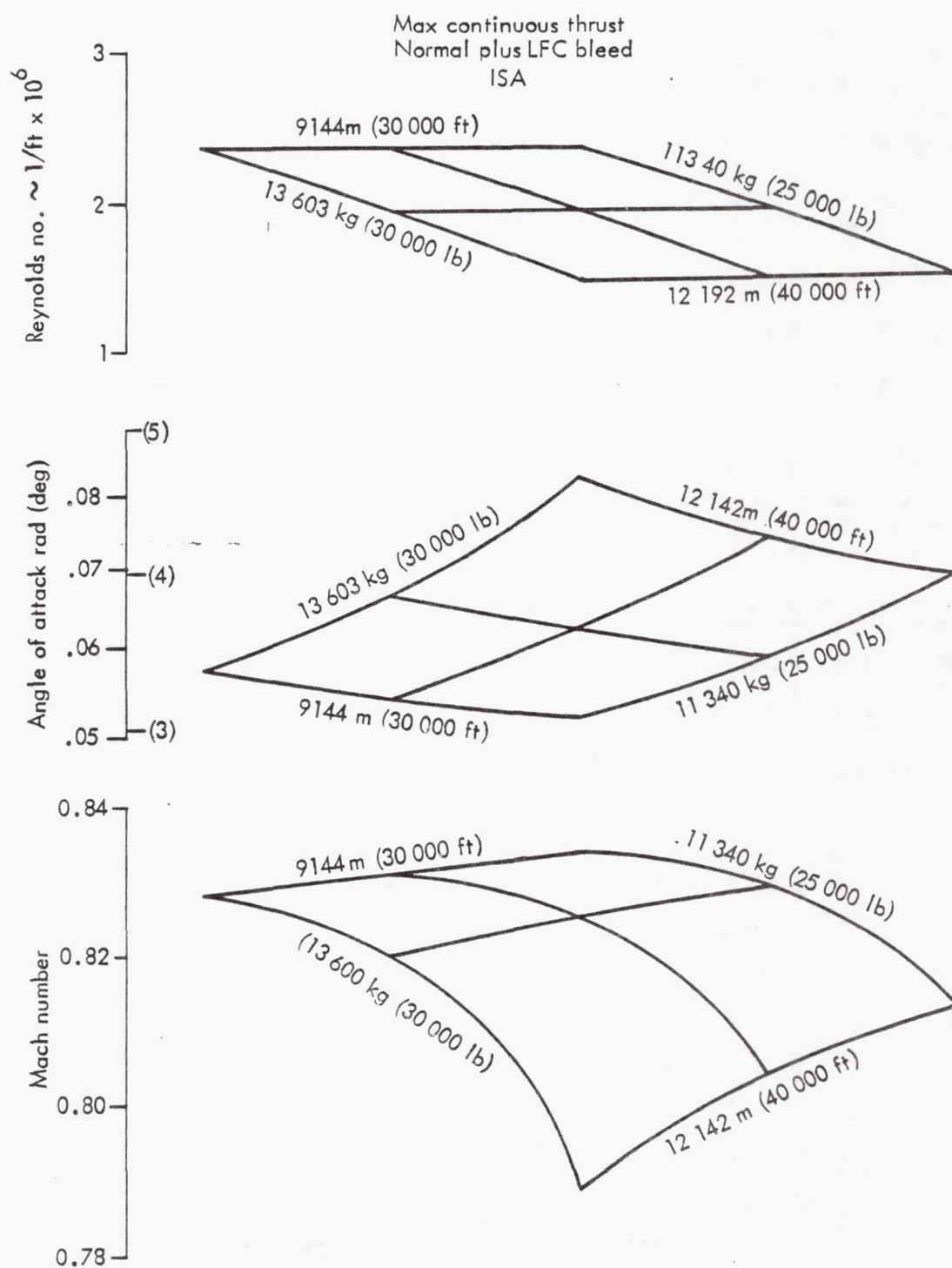


Figure 182. Maximum speed capability - modified JetStar

#### 8.1.6.2 Test Time

The operating weight empty of the LFC JetStar is estimated at 10 227 kg (22 547 lb). Available fuel is reduced to 4511 kg (9945 lb) due to the removal of the external tanks and elimination of the leading-edge tankage. This results in a maximum gross weight of 14 738 kg (32 492 lb). The following assumptions form the basis for calculating the test time available:

- (1) Warm-up and takeoff fuel equal to 5 min at maximum continuous power.
- (2) Enroute maximum speed climb.
- (3) Rapid descent.
- (4) Reserve fuel equivalent to 30 min loiter at sea level, maximum endurance.

Under the conditions discussed above, 98 min of operation are available at a Mach number of 0.8 at 12 192 km (40 000 ft). At long range cruise speed at 12 192 km (40 000 ft), the aircraft can operate for 116 min, while 2.2 hr are available at maximum endurance speeds at this altitude.

#### 8.1.7 Flight Test Program

The detailed planning required prior to the initiation of the flight test program is beyond the scope of the current feasibility study. The development of a detailed flight test plan will be a joint NASA/contractor activity to be conducted during the early phases of the Leading-Edge Glove Flight Program. However, following are the assumed objectives of the flight test program:

- (1) To demonstrate repetitive attainment of laminar flow on the leading-edge test panel at both design and off-design cruise conditions.
- (2) To demonstrate satisfactory operation of the leading-edge cleaning and de-icing systems.
- (3) To gather limited operational and maintainability data for the leading-edge test panel within the 100 flight hour constraint of the test program.

##### 8.1.7.1 Suction System Tests

To meet the first of the objectives, test procedures will be developed to determine the effects of Mach number and chord/unit Reynolds number on the extent of chordwise laminar flow, to determine suction distributions and levels which produce the maximum extent of laminar flow at various flight conditions, and evaluate the decay in laminarization due to uniform off-design suction levels.

These test procedures will be implemented by collecting data on suction



flow rate, surface pressure distributions, and chordwise extent of laminar flow on both the active test section on one wing and the nonactive section on the other wing simultaneously. A representative matrix of flight conditions includes three Mach numbers at each of three altitudes to provide data at three chord/unit Reynolds numbers. For each test flight, adjusting discrete slot suction levels and varying uniform suction levels will provide data from which to determine maximum extent of laminar flow and/or to locate the onset of transition in the laminar boundary layer.

A noise survey of the wing will be recorded for each flight to evaluate acoustical effects on the laminar boundary layer. Meteorological conditions at test altitudes will be monitored and recorded for each flight to provide additional data for use in the analysis of test results.

#### 8.1.7.2 Cleaning/De-icing System Tests

To meet the second objective, procedures will be developed to verify through which suction slots the liquid flow provides uniform surface coverage on the insect impingement zone to prevent insect accretion for takeoff, climb, and low-altitude loiter conditions. Various flow rates through these slots will be investigated and observed visually and photographically. Comparison of transition locations/extent of laminar flow will be made between washed and unwashed flight cycles to determine any degradation to the LFC system caused by insect accretion. Upon landing after each flight, a comparison of the functional test section and the dummy section will be made. All residue will be catalogued relative to surface location, photographed, and measured prior to surface cleaning for next flight preparation.

The visual and photographic observations of liquid flow coverage will suffice to judge the adequacy of the liquid system as a de-ice/anti-ice mechanism for an LFC wing.

#### 8.1.7.3 Operation and Maintenance Evaluation

Following the testing described above, optimum settings will be selected for the suction and cleaning systems to prepare the aircraft for accomplishing the final primary objective. During this phase, the aircraft will be flown to simulate operations into commercial airports. During these flights, operation of the test systems will be monitored through all modes of flight. All maintenance required will be catalogued as to type, frequency, and time to repair/replace components. From this data base, it will be possible to gain limited insight into the compatibility of LFC with commercial operation.

#### 8.1.8 Conclusions

The analysis conducted as a part of this study indicate that it is feasible to use the NASA JetStar as a test bed for flight validation of the Lockheed LFC leading-edge concept. Following are conclusions pertinent to specific elements of the feasibility assessment:

- (1) It is possible to integrate the leading-edge test section into the JetStar wing in a configuration which satisfies aerodynamic requirements for validation of the leading-edge systems.

- (2) The JetStar aircraft can be modified for installation of the leading-edge test section and required suction, cleaning, and instrumentation systems in a manner which permits restoration of the aircraft to original condition.
- (3) There are no structural problems attending the proposed modification. It is recommended that a reduction of flight speeds and load factors be observed for the modified aircraft.
- (4) Performance of the modified JetStar exceeds the specified nominal test conditions of  $M = 0.80$  at 12 192 m (40 000 ft).
- (5) There are no stability and control problems as a result of the proposed modification.
- (6) There are no safety-of-flight problems as a result of the proposed modification.

While development programs are required for both the leading-edge test section and the modified aircraft, the NASA JetStar is compatible with the requirements of the Leading-Edge Glove Flight Program.

## 8.2 VALIDATOR AIRCRAFT DEVELOPMENT

In order to fully establish the feasibility of LFC in a high utilization environment, a flight validation program closely approximating airline operations is required. A study was conducted to define and evaluate a representative LFC Validator Aircraft based on the integration of the Lockheed LFC wing concept described in Section 6.2 into a DC-9-10 aircraft.

### 8.2.1 Validator Program Objectives

This program has two major objectives:

- (1) To develop and evaluate an LFC validator aircraft configuration based on integrating an LFC wing concept of Lockheed design into a DC-9-10 aircraft.
- (2) To develop schedule and cost estimates for the validator aircraft program.

### 8.2.2 General Arrangement

The LFC validator aircraft, shown in Figure 183, is a DC-9-10 airplane modified to accept a new wing incorporating laminar flow control. The new wing duplicates in planform geometry the Lockheed LFC concept selected for the 1993 commercial transport and described in Section 6.2.

In general arrangement, the validator is a low-wing, T-tail, aft-fuselage-mounted two-engine transport with tricycle landing gear. In appearance it is not unlike the basic DC-9-10 from which it is developed.

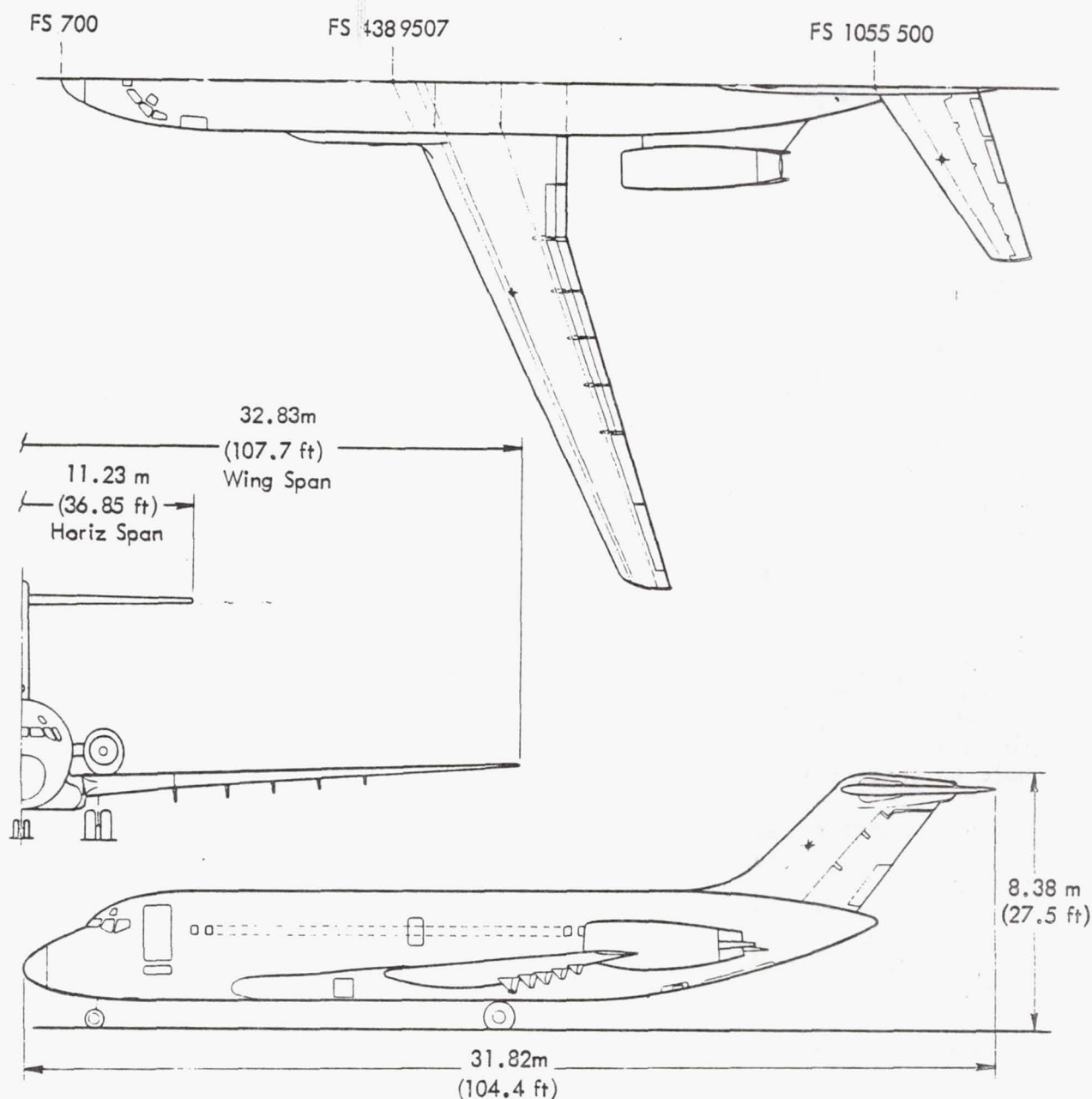


Figure 183. General arrangement - LFC validator/DC-9.

Readily noticeable differences are the increased wing span due to the higher aspect ratio and the fuselage/wing intersection pods housing LFC pumps. These pods are located beneath and extend well forward of the wing/fuselage fairing. Schematic details of the pod/pump installation are shown in Figure 184.

LFC capability is provided on both upper and lower wing surfaces to approximately 75% chord. The leading-edge cleaning/de-icing system duplicates the one selected by Lockheed for its 1993 LFC transport.



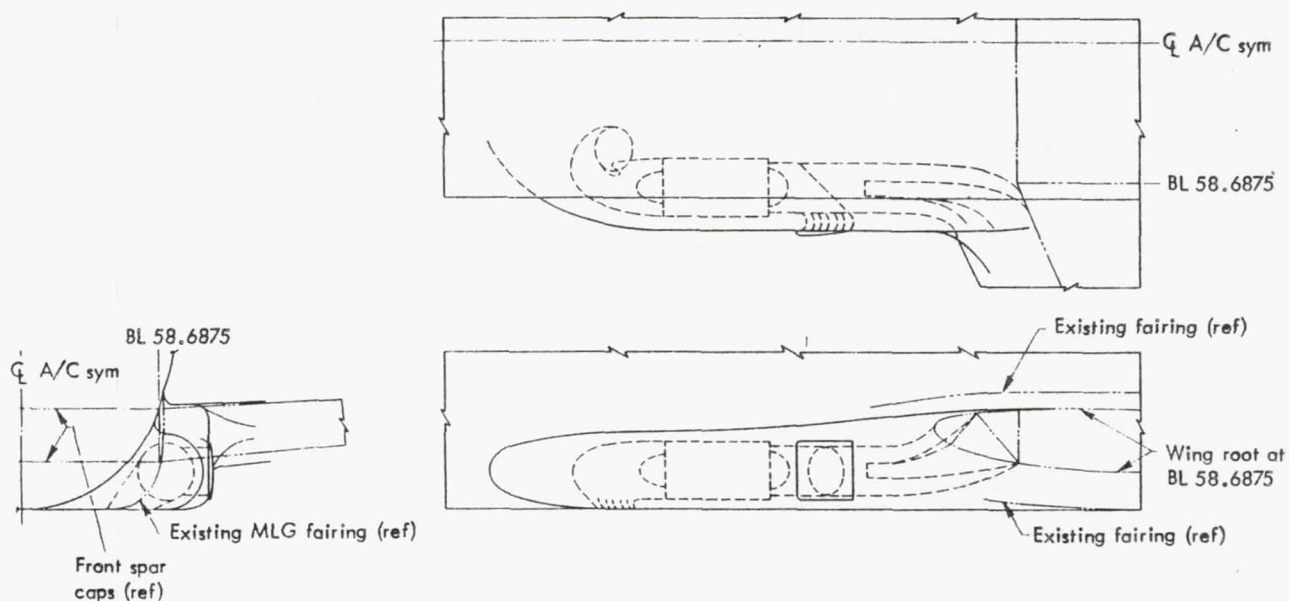


Figure 184. Schematic, LFC pump installation

Propulsion engine/nacelle packages are those furnished with the basic DC-9-10. No change in basic propulsion equipment is contemplated for the validator aircraft. Flaps, ailerons, and spoilers shown in Figure 183 are new, but are configured to provide flying qualities as similar as practicable to those presently existing in the DC-9-10.

The validator cabin is stripped of passenger amenities such as seats and galley to provide space for test equipment and ballast tanks. An LFC instrumentation console and on-board data recording equipment as required are located in the cabin. Test engineer and observer seats are installed in existing seat tracks to provide accommodation for personnel to monitor LFC system performance during the early phases of the LFC flight test program.

Aircraft systems and sub-systems generally duplicate those of the DC-9-10 aircraft.

### 8.2.3 Aerodynamic Configuration

The following general design requirements are of primary importance to the design of the validator wing:

- (1) Cruise Performance Requirements - The design must be capable of achieving cruise altitudes of 11 582 m (38 000 ft) and higher in order to have the capability of exploring unit Reynolds numbers consistent with future LFC aircraft. There must be sufficient cruise flight duration to permit efficient data collection relating to laminarization effectiveness.

- (2) Airport Performance Requirements - The validator design should have the capability of operating from airports with 1829 (6000) to 2438 m (8000 ft) runways in order to provide a choice of sites for simulating airline operations.
- (3) Geometric Requirements - In order to minimize the problems associated with mating a new validator wing to the DC-9-10 series fuselage, the root airfoil shape of the validator wing should be as compatible as possible with the DC-9 structural box at the root juncture. In addition, the DC-9 landing gear and structural fittings arrangement should be contained within the external contour of the new wing and permit good tie-in to the new box beam. Sufficient internal wing volume must be provided to accommodate LFC internal ducting and a reasonable fuel volume.
- (4) Wing Technology Level - The wing design will reflect, as much as practicable, the aerodynamic technology level of a 1993 design. An advanced supercritical or shock-free airfoil upper surface pressure distribution will be used with the chordwise extent of suction chosen to yield near the maximum drag benefit of LFC.

#### 8.2.3.1 Preliminary Design

The attainable revised DC-9 wing loading, and therefore lift coefficient, are considerably lower than the 1993 baseline values. Revisions to the shapes of the 1993 airfoil sections and wing planform shape and size options were investigated to derive an initial baseline wing.

#### Preliminary Airfoil Development

The preliminary validator airfoil section contours were defined by adding lower surface thickness to the baseline 1993 airfoil contours. The original and revised sections are shown in Figures 185 and 186.

The amount of thickness added to the wing was established by the attainable DC-9 cruise design lift coefficient of 0.36. The contour of the thickened section was established by the necessity for smooth isobars on the lower surface.

$$t/c = 11.93\% \text{ at } 31\% \text{ chord}$$

—— Original section  
----- DC-9 validator section

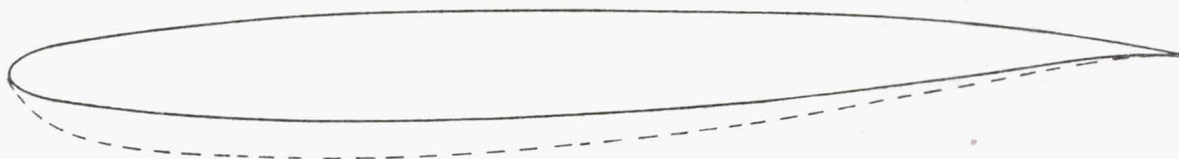


Figure 185. DC-9 validator root section development

$$t/c = 13.30\% \text{ AT } x/c = 45.1\%$$

———— Original section  
 ----- DC-9 validator section

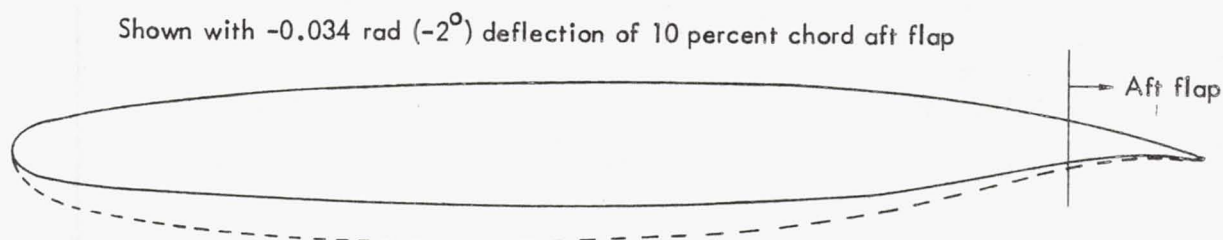


Figure 186. DC-9 validator outer wing section development

### Selection of Wing Planform and Size

Because of the requirement to mate with the original DC-9 fuselage, a relatively narrow range of wing areas is possible. Initial studies concentrated on wing areas of  $92.9 \text{ m}^2$  ( $1000 \text{ ft}^2$ ) to  $114.5 \text{ m}^2$  ( $1232 \text{ ft}^2$ ), with aspect ratios of 8.5 to 11.6. From these studies, a wing having the 1993 baseline aspect ratio of 11.6 and a wing area of  $92.9 \text{ m}^2$  ( $1000 \text{ ft}^2$ ) was selected. This wing planform is shown in Figure 187. Thickness ratios were initially chosen for this wing based on a design cruise lift coefficient of 0.36, which is compatible with a start-cruise wing loading of  $337 \text{ kg/m}^2$  ( $69 \text{ lb/ft}^2$ ) at  $M = 0.80$  at  $11\,582 \text{ m}$  ( $38\,000 \text{ ft}$ ). It was later determined through additional detailed design and analysis that an increase of the design cruise weight could be tolerated and therefore the final baseline validator wing was thinned to accept higher lift coefficients which are closer to the 1993 baseline design levels. The baseline wing loading is  $425 \text{ kg/m}^2$  ( $87 \text{ lb/ft}^2$ ) and design lift coefficient is 0.45.

#### 8.2.3.2 Wing Development

An initial conceptual wing was defined for use in configuration development. The upper surface of this initial wing matches the contours of the wing previously developed for the 1993 baseline. The lower surface has thickness increases as previously described.

The wing twist and aft flap schedules required to achieve the desired lift coefficient and acceptable pressure distributions are shown in Figures 188 and 189. The isometric pressure distribution of the resultant wing is shown in Figure 190.

#### 8.2.3.3 Stability and Control

Stability and control for the LFC validator was studied sufficiently to ensure that no major problems are introduced by the change from the basic Dc-9 wing to the validator wing.



#### 8.2.3.4 Boundary Layer Analysis

Boundary layer stability analysis was initially performed on a preliminary outer wing section at 40% wing semi-span. An aft flap deflection of 0.349 rad (2 deg) was chosen to match the 1993 airplane aft flap deflection at 40% semi-span. The Kaups/Cebeci laminar boundary code and Sally II stability code were used for the analysis.

For the initial boundary layer stability analysis, the 1993 airplane suction distribution was used. This resulted in a very stable laminar boundary layer on the upper surface, but the crossflow disturbance N-factors on the lower surface reached an unacceptably high value.

Wing sections from the initial wing were reduced in thickness by modifying the lower surface so that wing lift would be more representative of 1993 airplane. The 1993 airplane wing leading-edge contour on the lower surface is maintained to the maximum extent possible to produce leading-edge pressure gradients which will not require suction in the stagnation region.

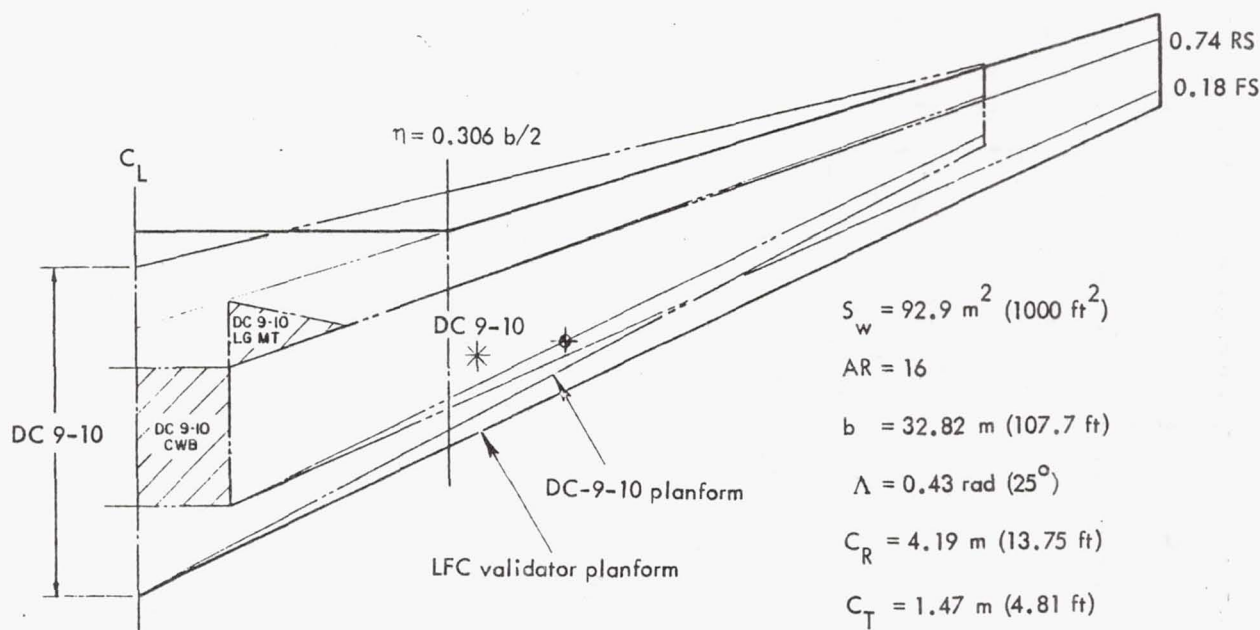


Figure 187. Wing planform

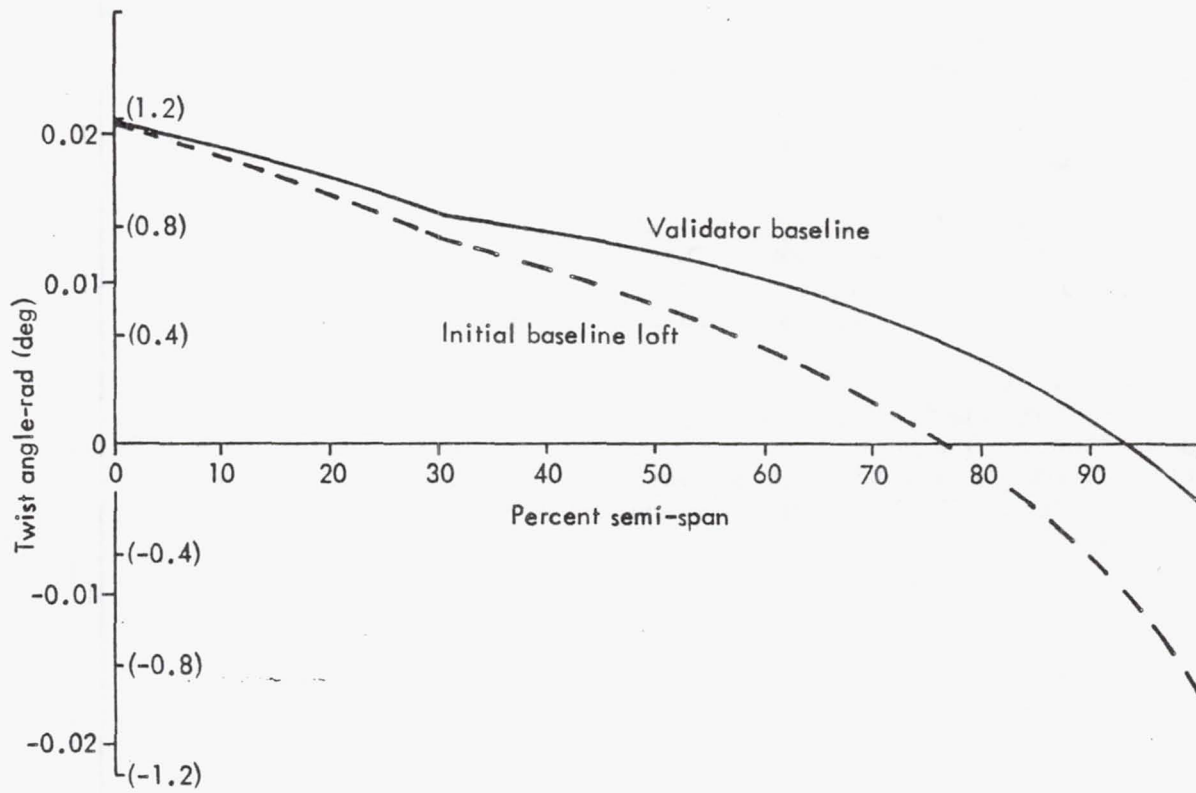


Figure 188. DC-9 LFC validator wing twist schedule

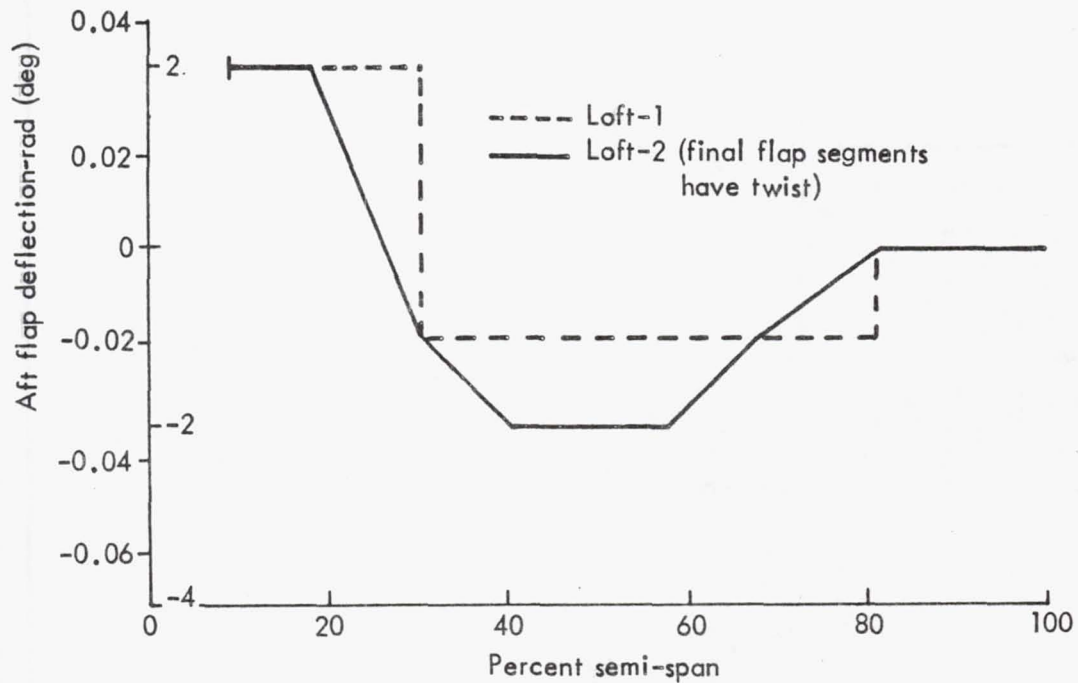


Figure 189. DC-9 LFC validator wing aft flap schedule

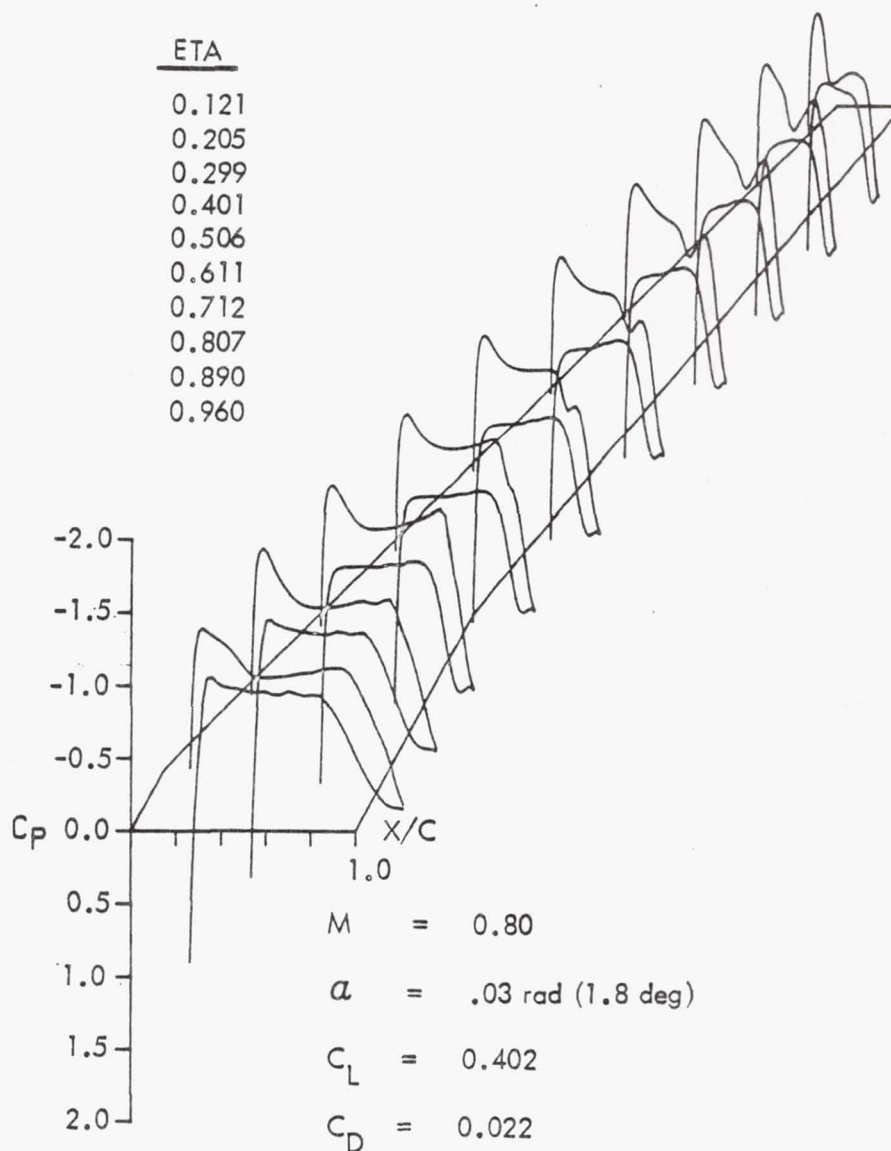


Figure 190. Transonic wing program isometric wing pressure distribution

The estimated suction distribution is presented as Figure 191. With the current baseline wing and this suction distribution, satisfactory laminar boundary layer stability can be achieved with better adherence to slot design criteria. Estimated crossflow N-factors are shown in Figure 192 for both the baseline validator and the initial validator outer wing airfoil section.



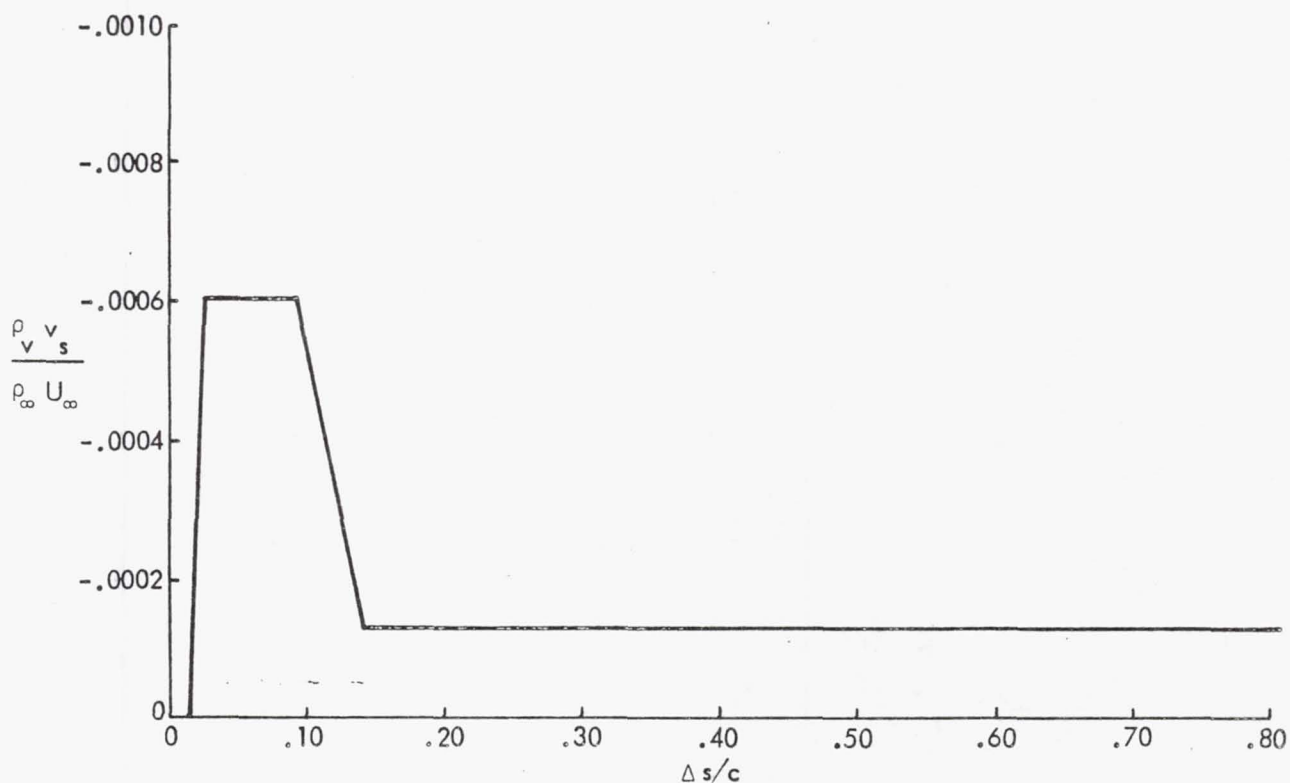


Figure 191. Baseline LFC suction distribution

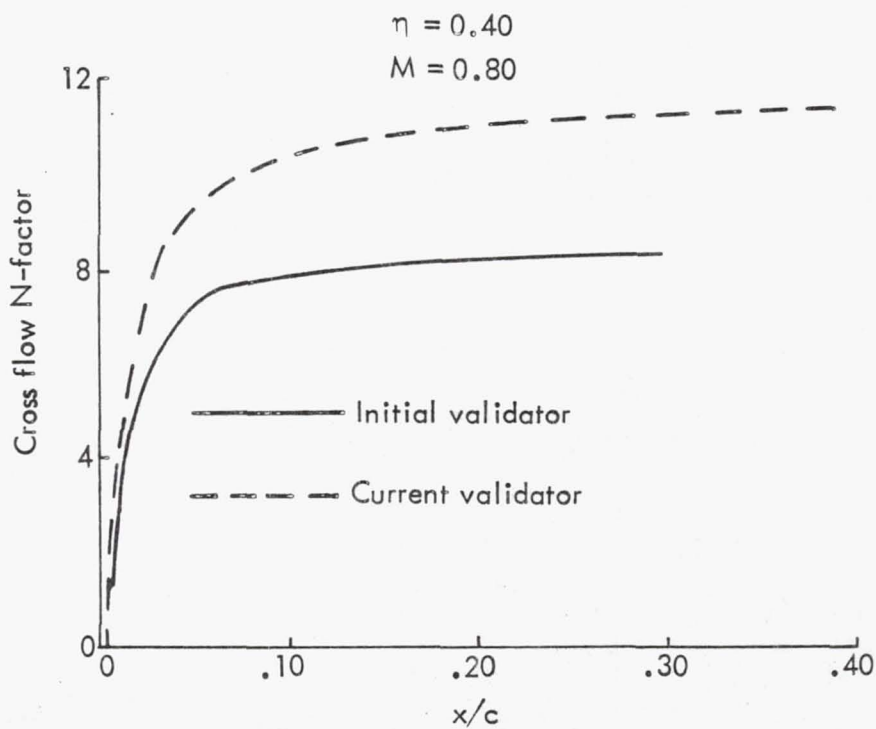


Figure 192. Current LFC validator lower surface crossflow disturbance N factors

## 8.2.4 Structural Configuration

### 8.2.4.1 Wing Structural Arrangement

The wing for the LFC validator aircraft is designed to be structurally and functionally representative of the Lockheed 1993 configuration. Particular emphasis is given to aerodynamic characteristics, structural configuration and materials, ducting arrangements, and cleaning/de-icing systems. A structural arrangement of the wing is shown in Figure 193. Certain characteristics of the 1993 aircraft, including aspect ratio, taper ratio, leading-edge sweep angle, and front spar locations, are duplicated. It is considered desirable to retain the existing DC-9 center wing spar locations to facilitate wing-to-fuselage attachment, thus the validator rear spar was positioned at 73.18% chord. The basic wing area is approximately  $92.9 \text{ m}^2$  ( $1000 \text{ ft}^2$ ) with suction capability provided on both upper and lower surfaces from 0 to 75% chord. Ribs are located on approximately 81.3 cm (32 in) centers to provide stability for the surface panels and are utilized as back-up structure for flap and aileron hinge fittings. Front and rear spars, which are one piece integrally molded assemblies, form the fuel tank boundaries and are mechanically attached to the upper and lower covers.

Wing box continuity is maintained across the fuselage through a mechanical splice of the left and right hand wings at the C/L aircraft centerline, duplicating DC-9 construction. Attachment to the fuselage is accomplished at the wing-fuselage intersection in a similar manner to that of the baseline aircraft.

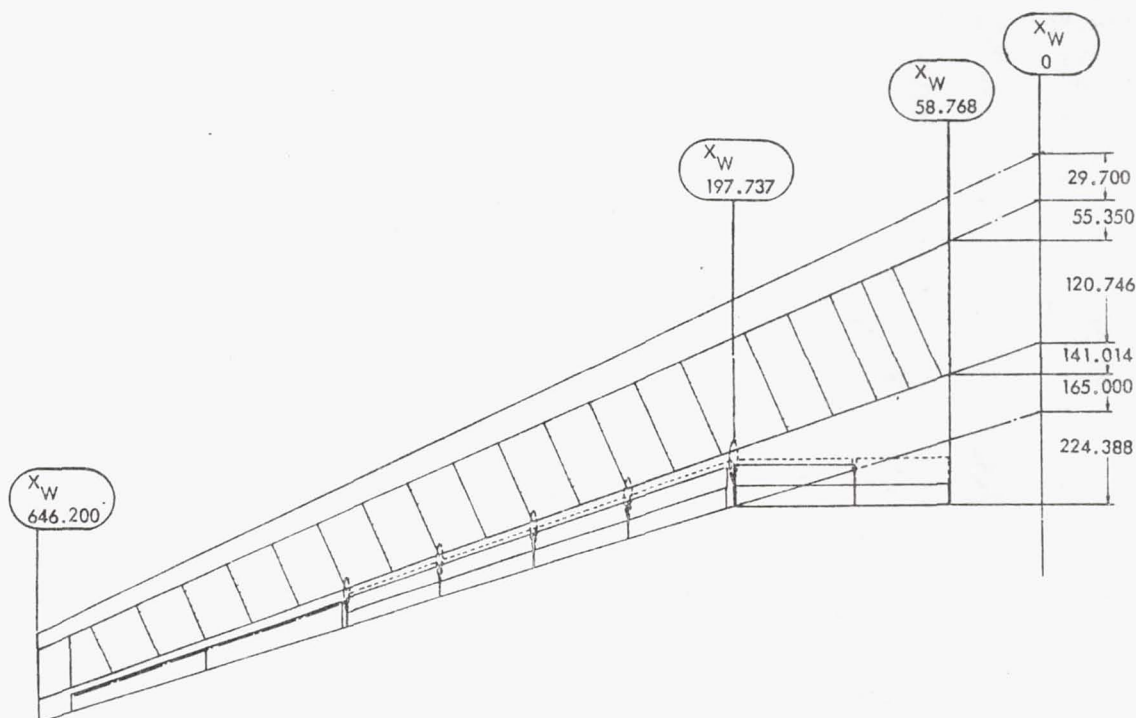


Figure 193. Wing structural arrangement

## Leading Edge

A predominant feature of this design concept is the integration of ducting systems into the major structural elements of the wing, as shown in Figure 194. This approach ensures a minimum weight structure as the spanwise and chordwise ducts are also load carrying members. Additional benefits are gained by utilizing the entire leading-edge cavity as the trunk duct for both upper and lower surface suction flow.

## Wing Surface Panels

The wing box upper and lower surface panels are fabricated as one piece assemblies which extend from the aircraft centerline to the wing tip. These panels consist of NARMCO 5208/T300 graphite/epoxy skins and hat section stiffeners which are cured separately and bonded.

A thin gauge titanium skin bonded to the entire outer surface, contains the required suction slots and provides protection against lightning strike and other environmental factors. Small ducts are molded into the graphite/epoxy skin panels immediately beneath the slots; metering holes transfer collected air into the hat-stiffener ducts. Second level metering occurs at each stiffener to rib intersection where holes in the stiffener sidewalls provide passageway to the rib cap ducts.

Skin stiffeners, which run parallel to the front beam, are spaced approximately 12.7 cm (5 in) apart and taper in thickness, together with the skin, to match the reduced level of loading toward the tip. At the wing-fuselage intersection, where outer wing sweepback originates, stiffeners are feathered out into a reinforced area of the skin, thus eliminating the necessity for a complicated stiffener splice between the constant section and tapered portions of the wing. This approach greatly simplifies attachment of the wing-fuselage bulkhead. Stiffener run-out at the rear beam is handled in a similar manner. Rib and stiffener spacing is coordinated to ensure that the run-out occurs at a rib intersections.

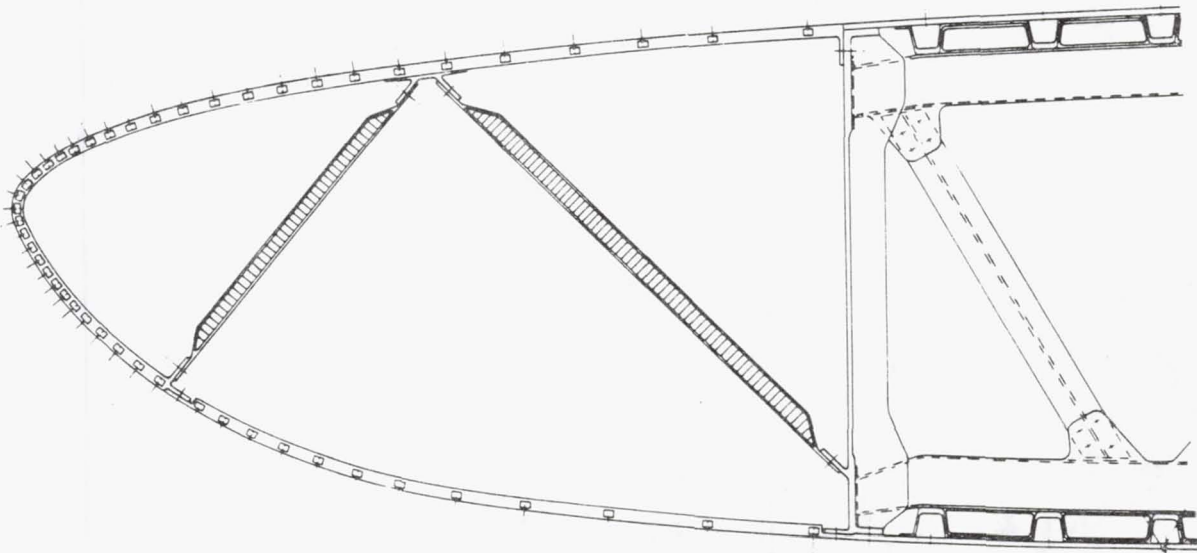


Figure 194, Leading edge



An adequate number of access holes is provided in the skin panels to allow access to the wing box for initial assembly and routine maintenance and inspection. Access panels/doors are located in the lower surface to preclude entry of foreign material, to facilitate access, to speed tank purge, and to reduce the necessity to walk on the upper slotted surfaces.

Upper and lower skins in the area of the main landing gear support structure are reinforced by titanium doublers co-cured into the wing skins. These doublers provide a load path to redistribute concentrated loads from the main landing gear support fitting into the wing box skins. The main landing gear support fitting and auxiliary spar members are similar to those used on the DC-9 basic wing.

#### 8.2.4.2 Design Criteria

FAR 25 structural design criteria are used for wing design for the LFC validator. The airspeed-altitude schedule shown in Figure 195 is derived using FAR 25. The following structural design weights are used:

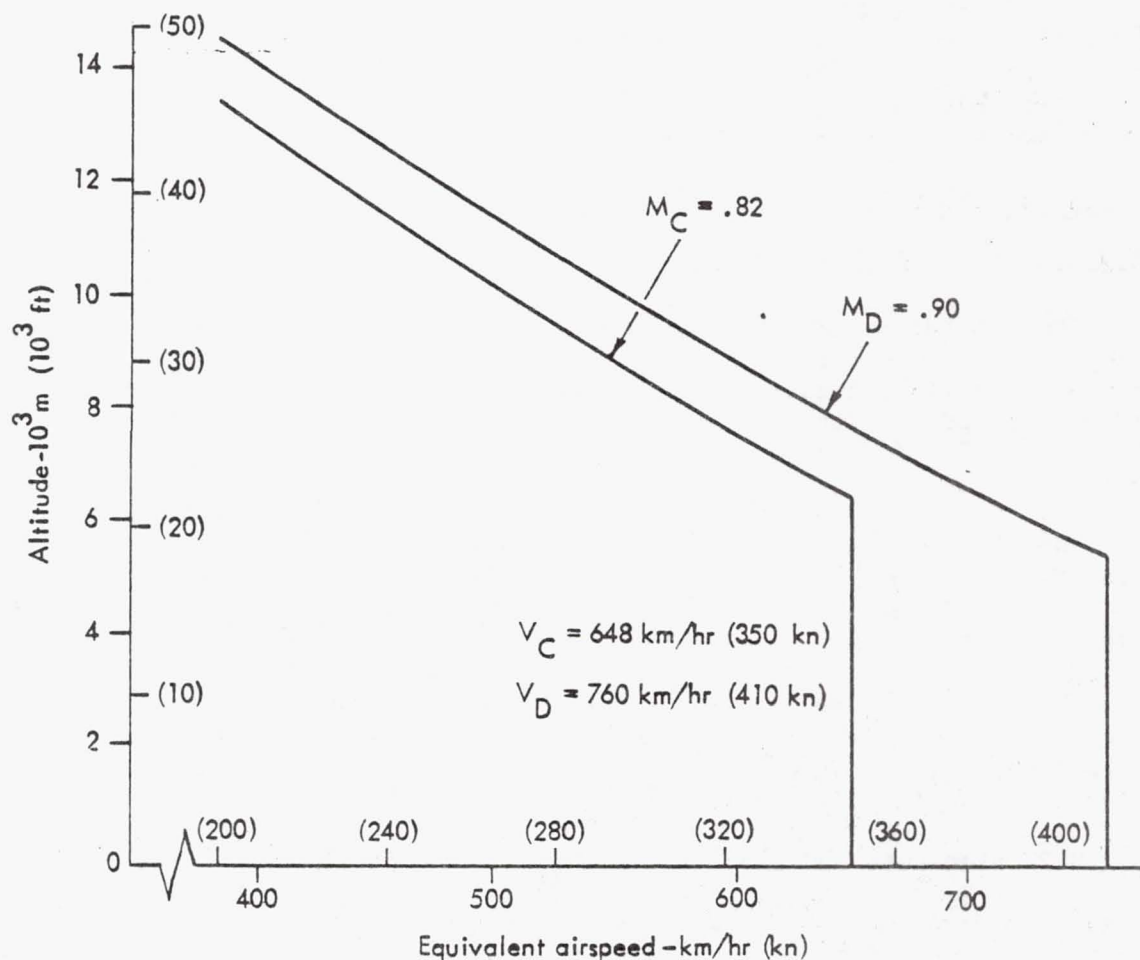


Figure 195. Structural design airspeeds vs altitude

(1) Gross weight = 41 142 kg (90 700 lb) including 10 433 kg (23 000 lb) of fuel

(2) Maximum zero fuel weight = 30 845 kg (68 000 lb)

The aircraft is designed for a 2.5g symmetric maneuver load condition in accordance with FAR 25.

#### 8.2.4.3 Weight and Balance

The baseline weights for the LFC validator airplane are taken from DC-9-10 typical weight data. Weight of the wing is calculated by a multiple station analysis program and adjusted in the primary and secondary structural areas by applying composite and advanced material weight technology factors considered to be the best predictions for 1990 design commitment. Other adjustments to the aircraft weight such as LFC engines and ducts and the leading-edge cleaning system and expendable fluids are estimated by methods developed specifically for these elements. A weight statement for the modified airplane is presented in Table 50.

The aircraft center of gravity is derived by starting from the manufacturer's empty weight and center of gravity supplied in the DC-9-10 weight and balance manual. The existing wing weight and center of gravity are also supplied. Modification changes are added to these starting points to arrive at the final configuration shown in Figure 196.

#### 8.2.5 Aircraft Systems

##### 8.2.5.1 Aileron Control System

The lateral control system for the validator is new from the side of body to the surfaces. The system, like that of the DC-9-10, is mechanical, cable controlled, designed so that no single failure shall result in loss of control of the aircraft under all operating conditions. Methods similar to those of the DC-9-10 are provided for adjustment and rigging of the aileron.

The LFC lateral control system is configured to use in-flight spoiler operation if required to supplement ailerons at all speeds. Trim tabs, similar to those of the DC-9-10, are provided as required to assure adequate lateral trim capability.

The spoiler system duplicates the capability of the DC-9-10 system in that it is common to the speed brake system as required and is available to supplement the ailerons for lateral control at all speeds, including approach and landing.

##### 8.2.5.2 High-Lift Systems

A trailing-edge flap system extending from side-of-body to approximately 69% semi-span is provided. Flap panels are constant chord to 30% semi-span and 25% chord in the outer wing panel. The flaps are simple externally hinged to provide chord extension. The system is hydraulically actuated, controlled by controls existing in the DC-9-10 flight station.

TABLE 50. WEIGHT STATEMENT

<u>Item</u>	<u>kg</u>	<u>lb</u>
Structure	(11 816)	(26 050)
Wing	3 674	8 100
Wing LFC-integral	426	940
Empennage	1 188	2 618
Fuselage	4 267	9 408
Landing Gear	1 657	3 653
Nacelle and Pylon	604	1 331
Propulsion	(4 946)	(10 903)
Power Plant	3 485	7 682
LFC Engines	582	1 284
LFC Miscellaneous	722	1 592
LFC Ducts	157	345
Systems and Equipment	(4 609)	(10 161)
APU	367	809
Surface Controls	591	1 304
Instruments	237	522
Hydraulics and Pneumatics	317	699
Electrical	811	1 787
Avionics	332	733
Furnishings	1 325	2 922
AC and AI	547	1 205
Anti-Ice Fluid	46	101
L.E. Clean or Anti-Ice System	36	79
Weight Empty	21 371	47 114
Operating Equipment	776	1 710
Operating Weight	22 147	48 824
Cargo	8 698	19 176
Zero Fuel Weight	30 845	68 000
Fuel	9 208	20 300
Expendable Fluids	1 089	2 400
Gross Weight	41 142	90 700



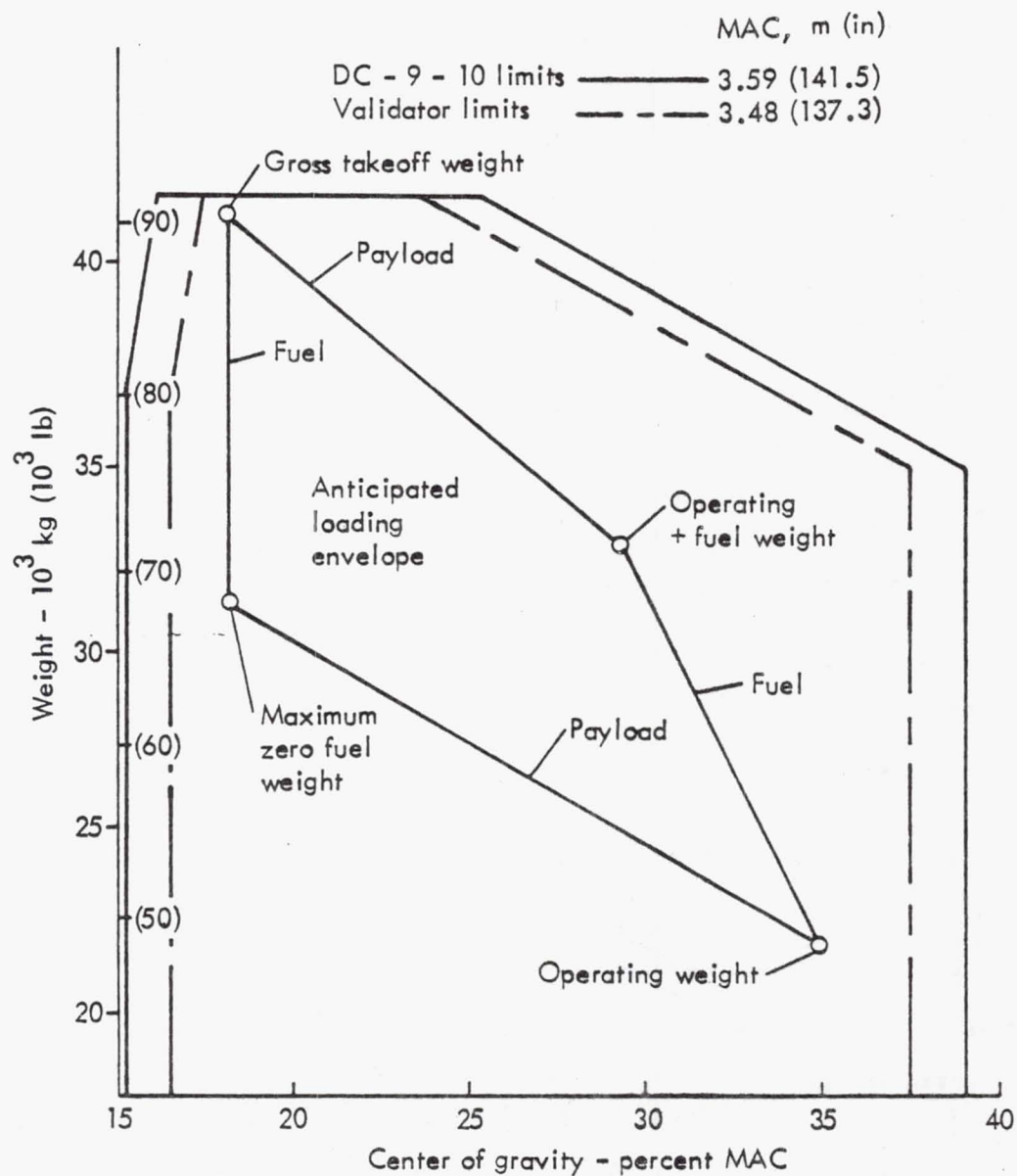


Figure 196. Center of gravity travel

#### 8.2.5.3 Propulsion

Primary propulsion for the validator aircraft, which consists of two Pratt & Whitney JT8D-7 engines, is unchanged. Validator airplane performance evaluations indicate that the JT8D-7 engine performance is more than adequate for the validator requirements.

#### 8.2.5.4 Landing Gear

The main landing gear for the validator aircraft is unchanged from the basic DC-9 landing gear. Since the gross weight and landing weight for the validator aircraft will be no higher than comparable weights for the DC-9, no landing gear modification is required. The LFC wing is configured to accommodate the DC-9 gear in all respects.

#### 8.2.5.5 Subsystems

Very little data were available concerning the details of DC-9 aircraft subsystems. However, this lack of information did not impose a serious constraint on the study since there are no changes of other than minor significance.

##### Fuel System

The fuel system duplicates the DC-9 system within the constraints imposed by the LFC wing design and geometry. Every effort is made to use DC-9 fuel system components such as pumps, probes, and valves through the expediency of recalibrating as required to retain compatibility with cockpit fuel system controls and gauging.

##### Electrical System

Electrical System demands peculiar to LFC are imposed by instrumentation, L.E. cleaning fluid pumps, and starting controls for the suction pumps. These added demands will be offset by the excess electrical power made available by deletion of normal passenger comfort systems.

##### Hydraulic System

No LFC peculiar demands are contemplated for the hydraulic systems. Normal hydraulic systems requirements, such as landing gear and flight controls, are duplicated by comparable systems in the validator.

##### Pneumatic System

An LFC-peculiar demand is imposed on the basic DC-9 pneumatic system due to the necessity to provide assistance for the wind-milling start cycle contemplated for the suction pumps. This starter assistance will momentarily require additional bleed from the propulsion units.

#### 8.2.6 LFC Systems

The suction and cleaning system configurations for the validator aircraft are identical to those for the 1993 aircraft, as are the airfoil shape and wing geometry used for calculation of suction requirements and for the definition of suction and cleaning system parameters. Therefore, for the same chord length, slot widths, slot spacing, ducting, and metering hole dimensions are identical to those of the 1993 configuration and are given in Sections 6.3 and 6.4.

Due to the lower total suction flow requirement of the validator as compared to the 1993 aircraft, the suction pump requirements for the validator are unique. Selection of suction units for the validator airplane is based on the assumption that, aside from meeting the suction flow and pressure ratio requirements, primary considerations are cost, reliability and minimum development requirements. Weight, efficiency, and dimensional size are considered to be of only secondary significance. Logically, these considerations are best met by making maximum use of existing hardware requiring minimum modification.

Analysis of the suction requirements indicated a cruise design absolute flow of 0.762 kg/sec (1.68 lb/sec) for each pump at 11 582 m (38 000 ft) and  $M = 0.80$ . This translates to a design equivalent sea level static inlet flow of 6.47 kg/sec (14.26 lb/sec) for each pump. If reasonable flow allowances are made for increased suction requirements to overcome noise effects, design deficiencies and uncertainties, manufacturing variations, and system deterioration, the required suction pump flow is 0.967 kg/sec (2.13 lb/sec) at cruise conditions. If additional allowances are made for pressure loss variations due to manufacturing variations, design deficiencies and uncertainties, and deterioration, the equivalent sea level static flow further increases to 10.68 kg/sec (23.54 lb/sec). To provide a significant margin for test flexibility, this value is selected for sizing each validator suction unit.

If all design conditions are met, the minimum suction pump pressure ratio required is 1.98, assuming minimum pump discharge velocity. If the air is to be discharged at free-stream relative velocity, a pressure ratio of 3.01 is required. If allowances are made for manufacturing and design deficiencies and deterioration, these required pressure ratios increase to 2.57 and 3.91 for minimum and free-stream relative discharge velocities, respectively.

Candidate compressors were evaluated from existing aircraft gas turbine engines. The feasibility and adaptability of the units for this application were explored, and the AVCO lycoming T55 turboshaft unit was selected for the validator aircraft. If minimum modifications are applied to this unit, case dimensions remain unchanged at a diameter of 70 cm (24 in) and a length of 1.12 m (44 in). Weight of the modified unit is approximately 290 kg (640 lb).

#### 8.2.7 Instrumentation

Instrumentation must provide data to verify satisfactory operation, quantify performance characteristics, and identify deficiencies of airfoil laminarization or of LFC systems. These broad objectives, coupled with the complex and unique nature of laminarization and LFC systems, dictates a system of instrumentation similar to that described in Section 8.1. Depending upon the results of investigations conducted prior to initiation of the validator program, some reduction of instrumentation may be possible. However, general requirements for in-flight instrumentation will remain unchanged.



### 8.2.8 Validator Performance

LFC validator performance is compatible with the requirements for both LFC system validation and operation from commercial airports. Validator cruise times and ranges are considerably greater than those of the basic DC-9.

#### 8.2.8.1 Airport Performance

Take-off and landing performance data are shown in Figure 197. Take-off performance for the DC-9-15 is included for comparison. The predicted airport performance for the LFC validator is comparable to that of the basic DC-9. Because of the increased wing span of the validator, 32.9 m (108 ft) versus 27.1 m (89 ft), second-segment climb on one engine is improved over the basic DC-9-10 series aircraft.

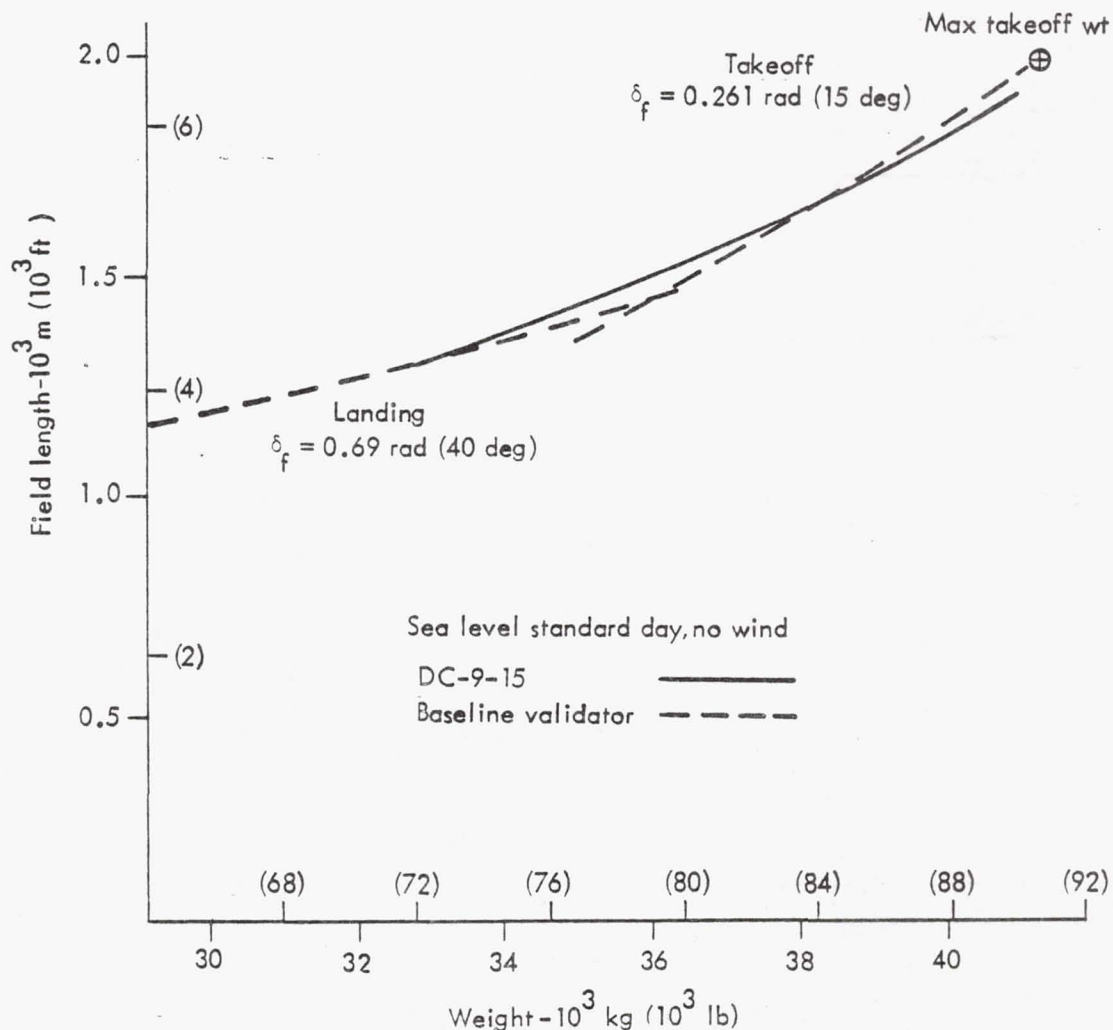


Figure 197. Takeoff field length comparison

### 8.2.8.2 Cruise Performance

Figure 198 presents a payload/range comparison of validator and the basic DC-9 aircraft. The increased capabilities of the validator are obvious. To illustrate the effect of LFC, the payload/range curve for the validator operating in a turbulent cruise mode is presented. At maximum payload, operation of LFC extends range by 833 km (450 n mi). The validator, operating in the turbulent mode at a payload of 3698 kg (19 176 lb), has a range advantage of 695 km (375 n mi) over the basic DC-9-15. This turbulent mode improvement accrues to the use of composite structures, advanced technology wing sections, greater wing span, and higher altitude cruise.

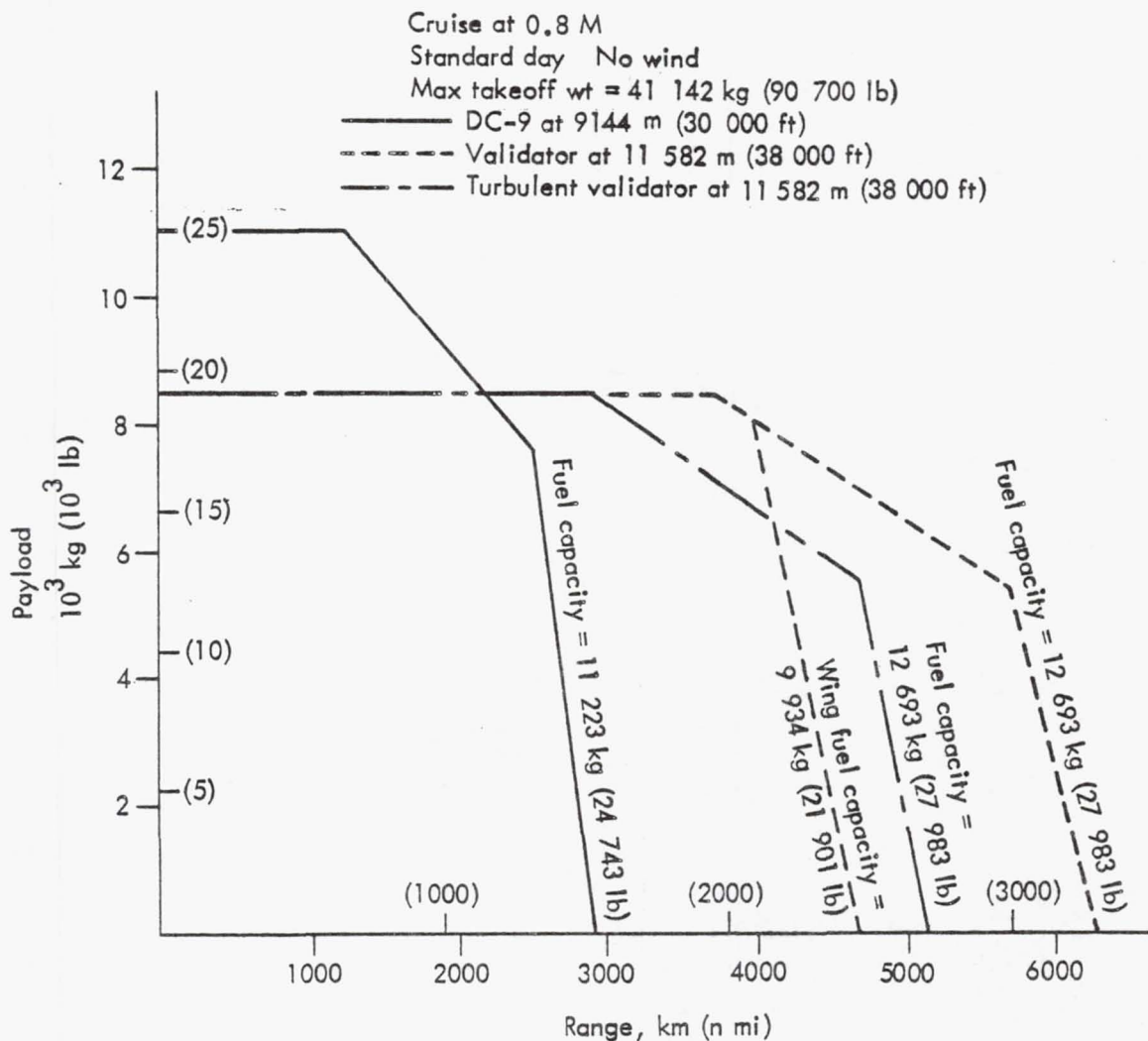


Figure 198. Payload-range comparison of DC-9-15 with various validator cases

### 8.2.9 Program Planning

The overall LFC validator aircraft program schedule is shown in Figure 199. Eighteen months are required for preliminary, wing, aircraft, and systems design. Concurrent with the design activity, wind tunnel, laboratory, and ground tests will be conducted to verify design data, functional operation of systems, and structural integrity. Manufacturing of the LFC wing, much of which is concurrent with final design activities and development testing, requires a total of 18 months. Modification of the aircraft and installation of the LFC wing is completed at the end of 30 months. After a 6-month airworthiness evaluation, the aircraft is released for the LFC flight test program. A total of 27 months is allowed for LFC system adjustment and calibration and the collection of operational data in the airline environment. The total duration of the program is 63 months.

### 8.2.10 ROM Cost Estimates

To facilitate subsequent program planning activities, ROM cost estimates for the LFC validator aircraft program are given in Table 51. These estimates are based on a combination of historical data generated in previous aircraft modification programs at the Lockheed-Georgia Company and an extrapolation of costs previously estimated for advanced composite technology programs.

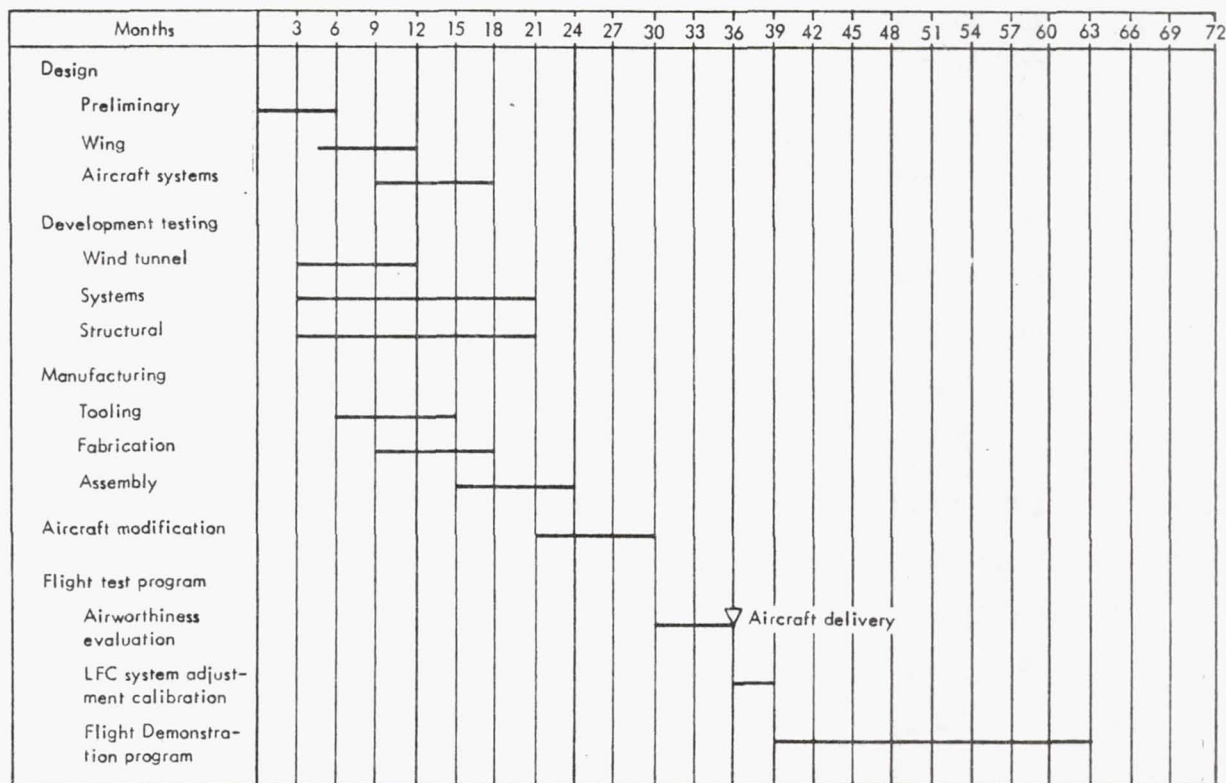


Figure 199. Program schedule - LFC validator aircraft



### 8.2.11 Conclusions

The analyses conducted as a part of this study provide a basis for the following conclusions:

- (1) It is possible to integrate the Lockheed LFC wing concept into the DC-9-10 aircraft to form a feasible validator aircraft configuration.
- (2) The performance of the resultant validator aircraft is in excess of that required to satisfy the objectives of the validator flight demonstration program.
- (3) Including design, development, fabrication, aircraft modification, and a representative flight demonstration program, the estimated cost of the LFC validator program is 190.6 million 1980 dollars.
- (4) Assuming that the accumulation of 4500 flight hours of simulated airline service over a period of 27 months is adequate to establish the operational feasibility of the validator, the estimated duration of the validator program is 63 months.

TABLE 51. ROM COST ESTIMATES - LFC VALIDATOR PROGRAM

Design	<u>\$ Millions</u>
Preliminary	20.0
Wing	76.0
Aircraft/Systems	9.0
	105.0
Development Testing	
Wind Tunnel	3.0
Systems/Structural	7.0
	10.0
Wing Manufacturing	50.0
Aircraft Modification	16.0
Flight Test Program	
Airworthiness Evaluation	2.5
LFC Systems Adjustment/Calibration	.3
Flight Demonstration Program	6.8
	9.6
TOTAL	<u>190.6</u>

### 8.3 ADVANCED DEVELOPMENT REQUIREMENTS

#### 8.3.1 Aerodynamics

The present 2-D pressure distribution code, the recently developed FLO 22 and FLO 27 codes, the tapered semi-infinite swept wing boundary layer code, and the 3-D stability code are useful and necessary computational tools in deriving a LFC 3-D swept-wing configuration. The basic design and analysis sequences originally conceived for external aerodynamics work are satisfactory. However, development of additional design and analysis tools is needed, particularly in the analysis of flow in the wing-root juncture, the tailoring of isobars, and the interfacing of individual computer codes into an integrated design and analysis framework.

Following are advanced development requirements resulting from external aerodynamics design and analysis work to date:

- (1) The current Cebeci boundary layer code should be revised to a discrete-suction code to permit approximate solutions for configurations with slots or bands of porosity. As a part of this work, the Lockheed-developed stagnation point location code should be incorporated as a subroutine and necessary computer code interfaces with the Transonic Airfoil Program (TAP) developed. In addition, Lockheed-developed codes should be added as subroutines so that slots conforming to various criteria can be automatically located on option.
- (2) Further detailed study of boundary layer growth and corresponding stability should be delayed until the discrete-suction boundary layer code is developed.
- (3) Additional sensitivity study of the effects of various design inputs on both crossflow and Tollmien-Schlichting instabilities should be accomplished using the improved boundary layer codes and the SALLY II stability code.
- (4) The feasibility of incorporating a combination of the Cebeci code and the Melnik code into the Transonic Airfoil Program should be determined.
- (5) The Carlson airfoil design program should be revised to incorporate automated procedures for relaxing input design pressures slightly to produce thin trailing edges for LFC airfoils.
- (6) The overall wing design and analysis methodology should be regularly updated to reflect the latest in computational codes for external flow, boundary layer flow, slot flow, stability, transition estimation, and other pertinent improvements. Particular attention should be directed toward establishing computer code interfaces and reducing design cost by developing improvements in computing efficiency for individual codes and reducing the number of design and analysis cycles necessary to achieve a satisfactory LFC wing configuration.

- (7) Stability codes incorporating the effects of noise should be supported, in addition to efforts currently directed toward determining non-linear and compressibility effects. Large-amplitude disturbance effects such as discrete slot suction should also be theoretically and experimentally investigated.

### 8.3.2 Structures and Materials

Major requirements for the development of LFC structure center around the use of advanced composite materials and characteristics peculiar to the fabrication of LFC surfaces. Included are the following:

- (1) In the development of composite LFC wings, additional effort is required in investigating the main landing gear support area, chordwise joints, access panels, and wing/fuselage joints.
- (2) Continued development of surface slotting procedures is required. Advances in laser and water jet techniques should be monitored to evaluate potential improvements leading to reduced slot widths and faster cutting rates.

In addition, a five-axis drive system should be developed for sawing slots. This system would track the slot and maintain exact saw-to-skin depth control reducing saw exposure to a minimum. Saw torque would be monitored and controlled by a microprocessor to allow stopping the saw prior to failure. After replacing a worn or broken saw, the computer system would return the saw to the exact spot where it stopped, with minimum disruption in slot.

- (3) In advanced materials development, powdered aluminum sheet materials should be considered as a candidate for the slotted outer surface. Powdered aluminum is corrosion resistant and no anodizing or corrosion protection would be required. Powdered titanium sheet material should be evaluated as a candidate for a porous outer skin.

### 8.3.3 LFC Systems

An area of significant risk in the design of an operational LFC aircraft is the tolerance of laminarization to variations in LFC system performance. Previous efforts in the area of achieving and demonstrating the performance advantage of LFC, culminating in the X-21A flight test program, were largely oriented to construction and testing in a research atmosphere with careful hand-tuning to achieve the desired level and distribution of suction in order to optimize LFC performance. The X-21A design included a large number of orifices and adjustable valves so that the suction flow profiles over the aerodynamic surfaces could be adjusted to achieve satisfactory LFC performance.

For an operational commercial airplane, economical production must be achieved through the adoption of a simplified system, compatible with large-scale production techniques and tolerances. Little or no adjustment of the suction system will be acceptable on individual airplanes. As a



consequence of these restrictions, suction flow profiles on new operational aircraft will reflect local chordwise and spanwise variations in suction flow from the optimum suction flows desired. These flow variations will influence the actual level of performance improvement available from LFC. It is therefore necessary to recognize the influence of these tolerances on LFC in the initial airplane suction system design.

The underlying theme of this study has been the orientation toward an operational production LFC airplane. To this end, manufacturability, cost, reliability, and maintainability are of prime importance. This study has underscored the impact of these considerations on the design and eventual degree of success achievable by an operational production airplane. These considerations have served to impose realistic limits and constraints on the design and configuration of the airfoil suction surface, metering, and ducting configurations. Production capabilities have imposed minimum limits on the width and spacing of slots and the diameter and spacing of metering holes. Fewer slots and metering holes of larger dimensions are obviously preferred from a production standpoint.

Not so obvious are the inherent advantages that accrue to the performance of the configuration of these dimensions are as large as possible. It is inevitable in any production design that some tolerance must be recognized. These tolerances apply to all elements in the suction surface, metering, and ducting system. If the system is designed to achieve the desired performance with the largest allowable nominal dimensions for these elements of the system, it follows that the system will be less sensitive to acceptable production tolerances.

Present manufacturing constraints, notably slot width and spacing, are such that the criteria limits set forth in the literature of the X-21 program in Reference 7 cannot be met in the leading-edge region for a nominal configuration. In some cases, it is impossible to simultaneously meet all of these criteria limits even without production constraints, because the criteria limits are mutually exclusive. Thus, any system design must violate some of the existing criteria limits with selections based on the judgment of the designer. When realistic production tolerances are superimposed on such a design, the effects on laminarization are totally unknown.

In this study, both analysis and testing have disclosed the wide variation in suction flow that results from very small variations in slot widths and slot metering. The effects of these flow variations are unknown, but if the design assumes that the prescribed suction flow is the minimum required for laminarization, the system must be designed for a higher nominal flow to allow for deviations that would reduce the flow. The flow would then be still higher when the deviations are in a direction to increase the suction flow. The effect of this increased flow on laminarization is also unknown.

These considerations serve to illustrate the dilemma and risk faced in the suction system design. A comprehensive parametric test is needed to explore the applicable criteria and their upper and lower limits as they affect laminarization. This testing should range from an exploration of the upper and lower limits of suction allowable to achieve laminarized flow

to an evaluation of the stability characteristics of various slot metering systems. The test should be oriented toward configurations that are more easily manufactured with low sensitivity to tolerances.

Initial testing may be accomplished in a small test facility where both suction surface and metering system configurations may be readily changed. Testing should be conducted on a relatively short length of laminarized surface with the primary emphasis placed on correlating test results with available analytical methods and design methodology. Testing should include variations in all suction system design criteria, with full exploration of both upper and lower limits. While it is recognized that all flight parameters cannot be properly simulated, sufficient simulations can be achieved to provide significant correlation with and verification of current methodology and indicate appropriate changes.

This testing would be very beneficial in reducing the risk of future programs which are largely restricted to single configurations. The results of such testing may also indicate further testing appropriate for the NACA high speed wind tunnel test.

#### 8.3.4 Leading-Edge Region Cleaning

The leading-edge cleaning system testing discussed in Section 6.4.4 has provided substantial verification of the system. The unfortunate difficulties with the injection of cleaning fluid on the lower surface prevented complete demonstration of the system but the test fully verified the concept. Reliance on transient characteristics of the stagnation line to intermittently alter the cleaning film flow to cover the area between some of the forward slots is the only facet of the design that was not fully demonstrated.

The adequacy of the cleaning fluid composition for the anti-icing function has not been evaluated. An analytical evaluation of the composition for this function is required and the composition requires alteration to satisfy this requirement. These analyses of the liquid composition should include consideration of the contamination characteristics and if possible improve the liquid composition from the standpoint of clearing the slots after the system is turned off. These refinements to the cleaning liquid composition should be completed before flight testing of the system.

The required cleaning liquid flow levels and distribution for both the prevention of insect accretion and for de-icing requires further evaluation and development. These evaluations may be carried out in the operational atmosphere of the flight test program.

#### 8.3.5 Aircraft Design

Previous design efforts have been directed toward providing LFC capability on wing surfaces, and have produced several viable concepts for providing efficient suction flow paths from the surface to the suction pump. These conceptual design studies considered maintainability and reliability in a broad sense, but the limited scope and budget available precluded the in-depth study and design required to evaluate the operational aspects of maintaining a fleet of LFC transports in a high-utilization en-



vironment. In general, direct maintenance costs and fuel costs represent comparable percentages of total direct costs. Thus, in order to maximize the benefits of LFC, maintenance costs attributable to LFC must be minimized.

It is expected that LFC transports entering fleet service will be integrated into a maintenance/overhaul schedule routine similar to that presently in general use by the major carriers. To allow LFC transports to be readily assimilated into general fleet service, the LFC systems must be designed with the same goals used for current conventional aircraft, including the use of proven, reliable components and designs, provision of generous access for inspection/replacement, and satisfying the requirement that 90% of all line replaceable units (LRU) be capable of replacement in 1 hr or less. Included in the LRU replacement time are opening and closing of access panels, attachment and removal of support equipment, and removal and installation of the LRU. Included in future maintenance requirements peculiar to LFC transports is the repair of composite/titanium surfaces and the protection, repair, and cleaning of slotted suction surfaces.

To demonstrate industry's capability to meet these requirements and establish the credibility of LFC among airline operators, more in-depth study and demonstration in reliability/maintainability is required. This can be accomplished in the flight test and flight validation programs planned by the NASA. The leading-edge flight test program will provide experience in maintaining smooth slotted surfaces and some insight into potential operational problems. The wing surface panel program will permit design effort in the detail design of access openings for inspections and maintenance, the development and verification of techniques for inspection of layered composite/titanium structure, and the development and validation of repair procedures for the same surfaces. The validator aircraft program will impose the requirement for implementation of the "design for maintainability" concept. The validator program, with its design, manufacture, test, and demonstration phases, will provide the ultimate proof of LFC as a viable technology for future transports. That program will demonstrate the compatibility of LFC with the real world of airline operations in which maintainability/reliability share equal importance with system performance if fuel or cost savings are to be realized in fleet usage.



## REFERENCES

1. Antonatos, P. P.: "Laminar Flow Control Concepts." Astronautics and Aeronautics, July, 1966.
2. Whites, R. C., Sudderth, R. W., and Wheldon, W. G.: "Flight Test Results of the Laminar Flow Control X-21 Airplane." Astronautics and Aeronautics, July, 1966.
3. Anon.: "Division Advisory Group Review - X-21A Program Summary." DAG 65-1-0, Northrop Corporation, Norair Division, 1965.
4. Anon.: "Report of Review Group on X-21A Laminar Flow Control Program." USAF Aeronautical Systems Division, November, 1965.
5. Sturgeon, R. F., et al: "Study of the Application of Advanced Technologies to Laminar-Flow Control Systems for Subsonic Transports." Vol. II, NASA CR-133949, prepared by the Lockheed-Georgia Company under Contract NAS1-13694, May, 1976.
6. NPRM 75-37C, "Noise Standards, Aircraft Type and Airworthiness Certification. Proposed Alternative Noise Reduction Stages and Acoustical Change Requirements for Subsonic Transport Category Large Airplanes, for Subsonic Turbojet Powered Airplanes and for Single Engine Transport Category Airplanes." Federal Register, Vol. 41 No. 209, Oct. 28, 1976.
7. Staff, LFC Engineering Section: "Final Report on LFC Aircraft Design Data, Laminar Flow Control Demonstration Program." NOR 67-136, Northrop Corporation, Norair Division, June, 1967.
8. Gray, D. E., et al: "Study of Turbofan Engines Designed for Low Energy Consumption." PWA-5318, NASA CR-135002, Pratt & Whitney Aircraft Div. of United Technologies Corp., April 1976.
9. Preliminary Performance and Installation Data for the STF-477 Turbofan Engine, Pratt & Whitney Aircraft Div. of United Technologies Corp., CDS-6. (Undated)
10. Nordstrom, K. E., Marsh, A. H., and Sargisson, D. F.: "Conceptual Design Study of Advanced Acoustic-Composite Nacelles." NASA CR-132703, Douglas Aircraft Co., McDonnell Douglas Corp., July 1975.
11. Lange, R. H., et al: "Study of the Application of Advanced Technologies to Long-Range Transport Aircraft." Vol. 1, NASA CR-112088, prepared by the Lockheed-Georgia Company under contract NAS1-10701, May 1972. CONFIDENTIAL.
12. Lange, R. H.: "Independent Research & Development Report for 1975 and Program Plan for 1976." Vol. I, LG76ER0033, prepared by the Lockheed-Georgia Company, March 1976.
13. Bauer, F., Garabedian, P., Korn, D., and Jameson, A., "Supercritical Wing Sections II, "Lecture Notes in Economics and Mathematical Systems, Vol. 108, Springer Verlag, N.Y., 1975.

14. Carlson, L. A., "Transonic Airfoil Flowfield Analysis Using Cartesian Coordinates," NASA CR-2577, August 1975.
15. Cebeci, T. and Kaups, K., "Compressible Laminar Boundary Layer with Suction on Swept and Tapered Wings," Journal of Aircraft, Vol. 14, No. 7, July 1977, pgs. 661-667.
16. Srokowski, Andrew J. and Orszag, Steven A., "Mass Flow Requirements for LFC Wing Design," Presented as paper 77-1222, AIAA Aircraft Systems and Technology Meetings, August 22-24, 1977, Seattle, Washington.
17. Stratford, B. S., "The Prediction of Separation of the Turbulent Boundary Layer." J. Fluid Mech., Vol. 5, Part 1, pp 1-16, January 1959.
18. Ballhaus, W. F., Bailey, F. R., and Frick, J., "Improved Computational Treatment of Transonic Flow About Swept Wings," NASA CP-2001, November 1976.
19. "Compendium of Minutes, Workshop on Laminar Flow Control." NASA Langley Research Center, April 6-7, 1976.
20. Johnson, D.: "Brief measurements of Insect Contamination on Aircraft Wings." Aeronautical Research Council Technical Report 14,999, May 1952.
21. Atkins, P. B.: "Wing Leading Edge Contamination by Insects." ARL (Australia) Flight Note No. 17, October 1951.
22. Coleman, W. S.: "Development of a Mechanical device for the Protection of Wings Against Insect Contamination." Blackburn and General Aircraft Limited, Note W. T. 128, February 1952.
23. Coleman, W. S.: "Wind-Tunnel Experiments on the Prevention of Insect Contamination by means of Soluble Films and by Liquids Discharged over the Surface." Blackburn and General Aircraft Limited, Note W. T. 131, July 1952.
24. Coleman, W. S.: "Roughness Due to Insects," in Boundary Layer and Flow Control - Its Principles and Application, Vol. 2, edited by G. V. Lachmann, Pergamon Press, 1961.
25. Peterson, J. B. Jr. and Fisher, D. F.: "Flight Investigation of Insect Contamination and its alleviation." NASA CP-2036, March 1978, NASA LaRC, Hampton, Va.
26. Lachmann, G. V.: "Aspects of Insect Contamination in Relation to Laminar-Flow Aircraft." C. P. No. 484, H.M.S.O., London 1960.
27. Beech, G. and Nicholas, W. M.: "A Mechanical Type of Scraper for Dealing with Insect Contamination of Aircraft Wings." Armstrong-Whitworth Aircraft Limited Report No. W. T. 53/18, July 1953.
28. Coleman, W. S.: "Note on the Blackburn and General Aircraft Wind-Tunnel Tests of the A.W.A. Fly Scraper." Report to the Boundary Layer Control Committee, B.L.C.C. Paper No. B 0142, H.M.S.O., London, 1953.

29. Cumming, R. W., Gregory, N. and Walker, W. S.: "An Investigation of the Use of an Auxiliary Slot to Re-establish Laminar Flow on Low-Drag Airfoils." R. & M. No. 2742, National Physical Laboratory, H.M.S.O., London, 1953.
30. Glick, P. A.: "The Distribution of Insects, Spiders and Mites in the Air." Tech. Bull. No. 673, U.S. Dept. Agriculture (1939)
31. Freeman, J. A.: "Studies in the Distribution of Insects by Aerial Currents." The Insect Propulation in the Air from Ground Level to 300 ft., J. An. Ecol., 14, 128-154 (1945)
32. Shevell, R. S.: "Technology, Efficiency, and Future Transport Aircraft." Astronautics and Aeronautics, September 1975.



1. Report No. NASA CR 159253		2. Government Accession No.		3. Recipient's Catalog No.	
4. Title and Subtitle EVALUATION OF LAMINAR FLOW CONTROL SYSTEM CONCEPTS FOR SUBSONIC COMMERCIAL TRANSPORT AIRCRAFT				5. Report Date September 1980	
				6. Performing Organization Code	
7. Author(s) R. F. Sturgeon, et al				8. Performing Organization Report No. LG80ERO150	
9. Performing Organization Name and Address LOCKHEED-GEORGIA COMPANY 86 South Cobb Drive Marietta, Georgia 30063				10. Work Unit No.	
				11. Contract or Grant No. NAS1-14631	
12. Sponsoring Agency Name and Address National Aeronautics and Space Administration Washington, D. C. 20546				13. Type of Report and Period Covered Contractor Report - Final	
				14. Sponsoring Agency Code	
15. Supplementary Notes Contract Monitors: D. B. Snow, A. L. Braslow, and M. C. Fischer NASA Langley Research Center					
16. Abstract A study was conducted to evaluate alternatives in the design of laminar flow control (LFC) subsonic commercial transport aircraft for operation in the 1990's period. Analyses were conducted to select mission parameters and define optimum aircraft configurational parameters for the selected mission, defined by a passenger payload of 400 and a design range of 12 038 km (6500 n mi). The baseline aircraft developed for this mission was used as a vehicle for the evaluation and development of alternative LFC system concepts. Alternatives were evaluated in the areas of aerodynamics, structures and materials, LFC systems, leading-edge region cleaning, and integration of auxiliary systems. Based on these evaluations, concepts in each area were selected for further development and testing and ultimate incorporation in the final study aircraft. Relative to a similarly-optimized advanced technology turbulent transport, the final LFC configuration is approximately equal in DOC but provides decreases of 8.2% in gross weight and 21.7% in fuel consumption.					
17. Key Words (Suggested by Author(s)) Fuel conservation  Laminar-flow control  Boundary-layer control  Drag reduction				18. Distribution Statement  Unclassified-Unlimited	
19. Security Classif. (of this report) Unclassified	20. Security Classif. (of this page) Unclassified		21. No. of Pages 316	22. Price*	